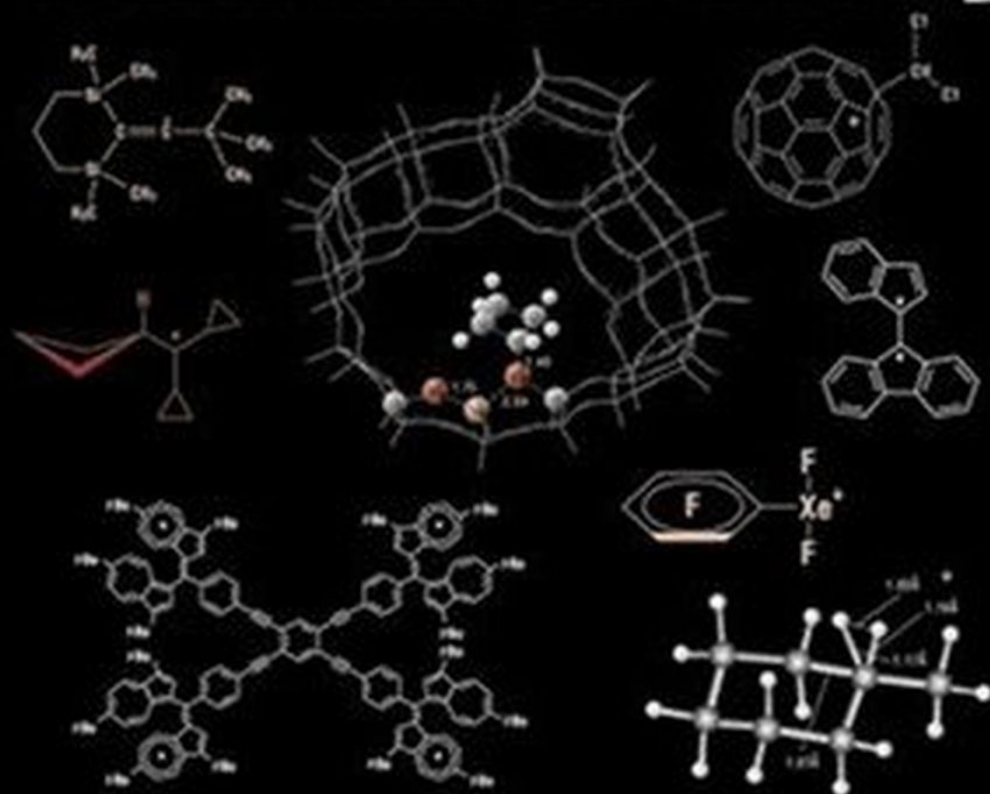


ACS SYMPOSIUM SERIES 965

Recent Developments in Carbocation and Onium Ion Chemistry



EDITED BY
Kenneth K. Laali

Recent Developments in Carbocation and Onium Ion Chemistry

ACS SYMPOSIUM SERIES **965**

Recent Developments in Carbocation and Onium Ion Chemistry

Kenneth K. Laali, Editor
Kent State University



American Chemical Society, Washington, DC



Library of Congress Cataloging-in-Publication Data

Recent developments in carbocation and onium ion chemistry / Kenneth K. Laali, editor.

p. cm.—(ACS symposium series ; 965)

Includes bibliographical references and index.

ISBN 13: 978-0-8412-7414-3 (alk. paper)

ISBN 10: 0-8412-7414-2 (alk. paper)

1. Carbocations. 2. Onium ions

I. Laali, Kenneth K.

QD305.C3R43 2007
541'.372—dc22

2006052660

The paper used in this publication meets the minimum requirements of American National Standard for Information Sciences—Permanence of Paper for Printed Library Materials, ANSI Z39.48–1984.

Copyright © 2007 American Chemical Society

Distributed by Oxford University Press

All Rights Reserved. Reprographic copying beyond that permitted by Sections 107 or 108 of the U.S. Copyright Act is allowed for internal use only, provided that a per-chapter fee of \$36.50 plus \$0.75 per page is paid to the Copyright Clearance Center, Inc., 222 Rosewood Drive, Danvers, MA 01923, USA. Republication or reproduction for sale of pages in this book is permitted only under license from ACS. Direct these and other permission requests to ACS Copyright Office, Publications Division, 1155 16th Street, N.W., Washington, DC 20036.

The citation of trade names and/or names of manufacturers in this publication is not to be construed as an endorsement or as approval by ACS of the commercial products or services referenced herein; nor should the mere reference herein to any drawing, specification, chemical process, or other data be regarded as a license or as a conveyance of any right or permission to the holder, reader, or any other person or corporation, to manufacture, reproduce, use, or sell any patented invention or copyrighted work that may in any way be related thereto. Registered names, trademarks, etc., used in this publication, even without specific indication thereof, are not to be considered unprotected by law.

PRINTED IN THE UNITED STATES OF AMERICA

Foreword

The volume is a valuable contribution to all chemists interested in the significant and broad area covering some of the most important reaction intermediates and their related chemistry. The editor and contributors are to be congratulated for their effort and valuable contribution.

George A Olah
USC Loker Institute

Contents

	Preface <i>Kenneth K. Laali</i>	xi-xiii
1	Experimental and Computational NMR Spectroscopic Investigation of Silyl-Substituted Carbocations <i>Hans-Ullrich Siehl</i>	1-31
2	Super-Stabilization of π -Conjugated Cations by Annulation to Bicyclic Frameworks <i>Koichi Komatsu</i>	32-50
3	Unusually Stable Vinyl Cations <i>Thomas Müller, Dominik Margraf, Yvonne Syha, Hamid Reza Nasiri, Christian Kaiser, Rita Maier, Bettine Boltre, Mark Juhasz, and Christopher A. Reed</i>	51-67
4	Vinyl Iodonium Salts as Precursors to Vinyl Cations <i>Tadashi Okuyama and Morifumi Fujita</i>	68-87
5	Generation of Alkylideneallyl Cations from Alkylidenecyclopropanone Acetals: Selectivity of Reaction with Nucleophiles <i>Morifumi Fujita and Tadashi Okuyama</i>	88-105
6	Conformational Studies of Cyclobutylmethyl Cations <i>V. Prakash Reddy, G. K. Surya Prakash, and Golam Rasul</i>	106-117
7	Persistent Organic Cationic Complexes: Structure and Reactivity <i>Gennady I. Borodkin and Vyacheslav G. Shubin</i>	118-143
8	Activation of Electrophilic Sites by Adjacent Cationic Groups <i>Douglas A. Klumpp</i>	144-159
9	Stabilized Carbocations as Redox Active Chromophores: Preparation of Electrochromic Materials Using Stabilized Carbocations <i>Shunji Ito, Koji Akimoto, and Noboru Morita</i>	160-183
10	Cation Pool Method and Cation Flow Method <i>Jun-ichi Yoshida</i>	131-138
11	Fluorenylidene and Indenylidene Dications: Insights about Antiaromaticity <i>Nancy S. Mills</i>	210-233
12	Generation, Stability, and Reactions of Alkylated Fullerene Cations <i>Toshikazu Kitagawa</i>	234-253

- 13 Carbocations on Surfaces: Formation of Bicyclobutonium Cation via Ionization of Cyclopropylcarbinyl Chloride over NaY Zeolite
Marcelo Franco, Nilton Rosenbach, Jr., W. Bruce Kover, and Claudio J. A. Mota 254-267
- 14 MO Calculations Involving μ -Hydrido Cation Intermediates Relevant to the Heptane to Toluene Dehydrocyclization Reaction
Ted S. Sorensen and Esther C. F. Yang 268-296
- 15 Theoretical Studies on Structure and Dynamics of Carbonium Ions
Pierre M. Esteves, Felipe P. Fleming, and André G. H. Barbosa 297-328
- 16 Quantum Chemical Studies of Carbocations from Oxidized Metabolites of Aza-Polycyclic Aromatic Hydrocarbons
Gabriela L. Borosky and Kenneth K. Laali 329-363
- 17 How Does Carbocation Stability Control the Beckmann Rearrangement Reaction?
Salai C. Ammal and Hiroshi Yamataka 364-374
- 18 Solvent Effects on the Chemistry of Bromonium and β -Bromocarbenium Ions as Reactive Intermediates
Cinzia Chiappe 375-393
- 19 Syntheses of the CFY_2^+ ($Y = Cl, Br$) and CX_3^+ ($X = Cl, Br, OTeF_5$) Cations Employing the Noble-Gas Oxidant, $XeOTeF_5^+Sb(OTeF_5)_6^-$
Hélène P. A. Mercier, Matthew D. Moran, and Gary J. Schrobilgen 394-427
- 20 Organoxenonium Salts: Synthesis by "Xenodeborylation", Reactivities, and NMR Spectroscopic Properties
H.-J. Frohn and V. V. Bardin 428-457
- 21 Halogen Transfer Reactions from bis-Amino Halonium Ions to Acceptor Olefins: Mechanism and Strategies for Chiral Halogenation
R. Stan Brown, Alexei A. Neverov, C. Tony Liu, and Christopher I. Maxwell 458-476
- 22 Synthesis of Phosphonium Salts by Metal-Catalyzed Addition Reaction
Mieko Arisawa and Masahiko Yamaguchi 477-492

Indexes

- Author Index 495
- Subject Index 497-528

Preface

In December of 2005, I organized a symposium entitled *Recent Developments in Carbocation and Onium Ion Chemistry* at Pacificchem in Hawaii, with Professors Ken Takeuchi (Kyoto University) and Andrew Bennet (Simon Fraser) acting as coorganizers from Japan and Canada, respectively. Twenty-four invited talks and twenty-two posters were presented. The symposium brought together an impressive group of leading experts and active researchers in the field, covering a broad spectrum of structural/mechanistic, synthetic/preparative, and theoretical/computational aspects, as well as creating an exciting and dynamic forum for highlighting current focus areas and trends.

Inspired by the success of the symposium, I subsequently agreed to take on editorship of this volume. Fortunately, the majority of the invited speakers at Pacificchem were able to participate in this project. In addition, I invited several other internationally recognized researchers who could not participate in the Hawaii symposium to also join the project, bringing the total number of contributions to 22 chapters.

Chapter 1 by H.-U. Siehl discusses parallel stable ion NMR spectroscopic and computational studies on various classes of silyl-substituted carbocations. Chapter 2 by K. Komatsu focuses on unusually stable π -conjugated carbocations that are formed as a result of annelation to bicyclic frameworks.

The focus of Chapters 3 and 4 is on vinyl cations. In Chapter 3, T. Müller et al. discuss the preparation, isolation, and characterization of unusually stable vinyl cations; whereas Chapter 4 by T. Okuyama and M. Fujita describes the generation and reactions of vinyl cations formed via solvolysis of vinyl iodonium salts.

Chapter 5 by M. Fujita and T. Okuyama examines the ring-opening reactions of alkylidenecyclopropanone acetals for solvolytic generation and trapping of alkylideneallyl cations (resonance hybrids of 1-vinyl-substituted vinyl cations). In Chapter 6 by V. P. Reddy et al. stable ion and computational studies of cyclobutylmethyl cations are discussed. In Chapter 7, G. I. Borodkin and V. G. Shubin discuss and

summarize more recent results from their laboratory on the NMR studies of long-lived carbocations and nitrosonium π -complexes.

Changing the emphasis to synthetic chemistry in superacid media, in Chapter 8, D. Klumpp examines the chemistry of dicationic electrophiles, demonstrating their enhanced reactivity via heteroatom protonation. In Chapter 9, S. Ito et al. explore the potential utility of stabilized carbocations for designing redox-active chromophores.

Focusing on the synthetic/preparative aspects, in Chapter 10 by J.-i. Yoshida, novel approaches to generation of *N*-acyliminium and alkoxy-carbenium ions are presented and their synthetic applications are discussed.

In Chapter 11 (the only chapter in the volume that focuses on persistent oxidation dications), N. S. Mills discusses the fluorenylidene dications and their antiaromatic character.

Recent progress in preparation and study of alkylated fullerene cations RC_{60}^+ and RC_{70}^+ as long-lived species are examined by T. Kitagawa in Chapter 12. Chapter 13 by C. J. A. Mota and co-workers examines the formation of the bicyclobutonium cation via cyclopropylcarbinyl chloride over solid acid catalysts.

The focus of the next four chapters (Chapters 14–17) is mainly on the theoretical/computational aspects. Chapter 14 by T. S. Sorensen and E. C. F. Yang examines the involvement of μ -hydrido cation intermediates in the context of the industrially important heptane to toluene dehydrocyclization process. Chapter 15 by P. M. Esteves et al. is devoted to theoretical studies of carbonium ions. Chapter 16 by G. L. Borosky and K. K. Laali presents a computational study on aza-PAH carbocations as models for the oxidized metabolites of Aza-PAHs. Chapter 17 by S. C. Ammal and H. Yamataka examines the borderline Beckmann rearrangement–fragmentation mechanism and explores the influence of carbocation stability on the reaction mechanism.

Chapter 18 by C. Chiappe focuses on the mechanism of bromination of alkenes, exploring the role of solvent on the formation of cyclic bromonium ion versus β -bromocarbenium ion, as key intermediates. In Chapter 19, H. P. A. Mercier et al. discuss the utility of a novel class of noble-gas onium salts as oxidants for generation and isolation of various trihalomethyl cation salts.

The remaining three chapters (Chapters 20–22) concentrate fully on onium ion chemistry. In Chapter 20, H.-J. Frohn and V. V. Bardin describe synthesis and multi-nuclear NMR studies of organoxenonium salts. Chapter 21 by R. S. Brown et al. focuses on the synthesis of chiral

amine-coordinated halonium salts and their potential utility in chiral halogenation. Finally, in Chapter 22, M. Arisawa and M. Yamaguchi discuss novel approaches to the synthesis of phosphonium salts via transition-metal catalyzed addition reactions.

Taken as a whole, the collection should serve as a reasonable representation of how the field is progressing and evolving and should serve as a model for gauging the current trends. It is hoped that the book can inspire the younger researchers who are still trying to find their niche and can be a useful source for students who are in the process of deciding whether or not to enter into this area. There is no doubt in my mind that much remains to be learned and that electrophilic chemistry and electron-deficient reactive intermediates will continue to play a pivotal role in structural/mechanistic and synthetic chemistry, both in the traditional sense and as applied to interdisciplinary areas.

A conference grant from the Army Research Office facilitated the organization of the Pacificchem Symposium. I should also thank many friends, colleagues, and collaborators who gave positive feedback and encouragement.

Kenneth K. Laali
Department of Chemistry
Kent State University
Kent, OH 44242
Email: klaali@kent.edu

Recent Developments in Carbocation and Onium Ion Chemistry

Chapter 1

Experimental and Computational NMR Spectroscopic Investigation of Silyl-Substituted Carbocations

Hans-Ullrich Siehl

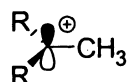
Division of Organic Chemistry I, University of Ulm, Albert-Einstein-Allee
11, D-89069 Ulm, Germany (ullrich.siehl@uni-ulm.de)

Organosilicon compounds are widely used in organic synthesis. The understanding of the structure and properties of the intermediates involved in their reactions is a prerequisite for further development and optimization of useful synthetic transformations involving silicon substituted compounds. Trialkylsilyl-substituted carbocations are particularly important as reactive intermediates in chemical reactions in polar media. Silicon substituted carbocations are however not generally accessible in superacid solutions. Due to the high affinity of silicon for fluorine and oxygen, the facile formation of five-coordinated Si-intermediates or transition states, and the polar nature of the carbon silicon bond ($C^{\delta-}-Si^{\delta+}$), the C–Si bond is prone to easy cleavage (1). Recently we have been successful in observing trialkylsilyl substituted carbocations as non-transient species in solution using suitable experimental methodology such as matrix co-condensation techniques and carefully controlled experimental conditions (2). A silyl substituent in the vicinity of a positively charged carbon interacts differently depending on the number of intervening bonds and the spatial arrangement (3). The effect of a silyl group directly attached to the C^+ carbon is called α -effect, a silicon two bonds away can give rise to a β -effect and silyl substituents separated by three bonds from the formally

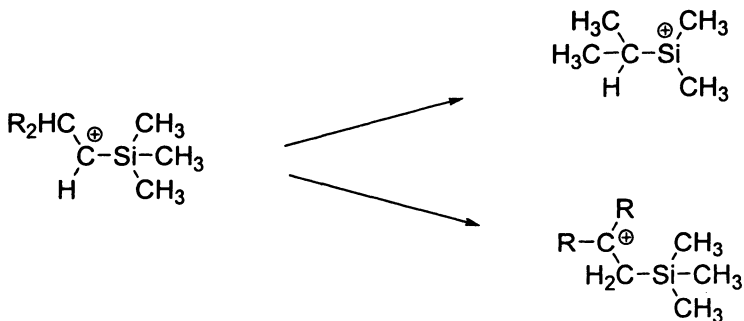
positively charged carbon may exhibit a γ -effect. A summary of our recent NMR spectroscopic investigations involving representative examples of α -, β - and γ -silyl substituted carbocations together with parallel computational studies of their structures and NMR properties is presented.

α -Silyl substituted Carbocations

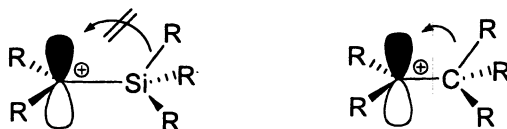
According to *ab initio* calculations, a silyl substituent stabilizes a directly attached positively charged carbon relative to a hydrogen but it destabilizes it as compared to a methyl substituent (4, 5, 6).



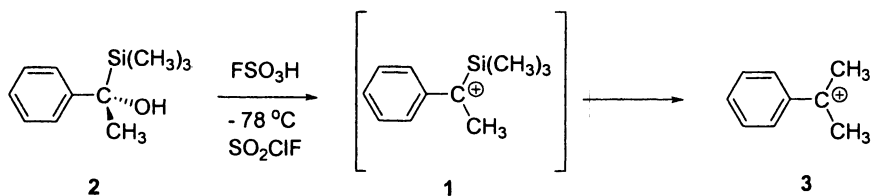
Gas-phase studies of α -silyl substituted carbenium ions show that these intermediates exist only in a very flat potential well (5, 7, 8, 9). They undergo fast 1,2-H or -alkyl shifts, producing the more stable silicenium or β -silyl substituted carbenium ions.



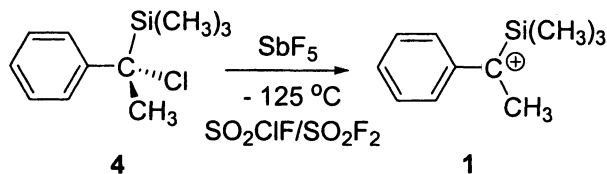
The destabilizing effect of a silyl group compared with an alkyl group in trivalent carbocations was explained by the weaker hyperconjugation of the Si-R σ -bond (R = alkyl) relative to a C-R σ -bond (R = H or alkyl) and by electrostatic repulsion between the adjacent positively charged cationic carbon and the electropositive silicon (10).



Early attempts to generate the 1-phenyl-1-(trimethylsilyl)ethyl cation **1** by ionization of the 1-phenyl-1-(trimethylsilyl)ethanol **2** with FSO_3H in SO_2ClF at -78°C were unsuccessful. Only the cumyl cation **3** was observed instead (11).



When 1-phenyl-1-trimethylsilyl ethylchloride **4** is reacted with SbF_5 under carefully controlled experimental conditions at -125°C , the 1-phenyl-1-(trimethylsilyl)ethyl cation **1** is generated exclusively as indicated by ^1H and ^{13}C (Figure 1) and ^{29}Si NMR spectra (12, 13, 14)



Due to the benzylic p - π resonance stabilization the $\text{C}^+ - \text{C}^{\text{ipso}}$ bond has partial double bond character and the ortho, ortho' and meta, meta' methine groups *syn* and *anti* to the silyl group are non-equivalent. The effect of the α -silyl group on the positive charge in benzyl cations can be estimated by comparison of the NMR spectroscopic data of the 1-phenyl-1-(trimethylsilyl)ethyl cation **1** with those for the 1-phenylethyl cation **5** (9) and the cumyl cation **3** (15, 16, 17) (Table 1).

The downfield shift of the resonance for the C^+ carbon of the 1-phenyl-1-(trimethylsilyl)ethyl cation **1** ($\delta = 231.28$ ppm) is noteworthy. This is likely to be the most deshielded shift of a benzyl cation carbon observed so far. The chemical shift of the C^+ carbon is however not a good measure of the relative charge in these type of benzyl cations because the trimethylsilyl substituent has a large deshielding effect on the chemical shift of an adjacent sp^2 -hybridized carbon. The para carbon chemical shift hence can be used to monitor the demand for delocalization of the positive charge into the aromatic ring. The chemical

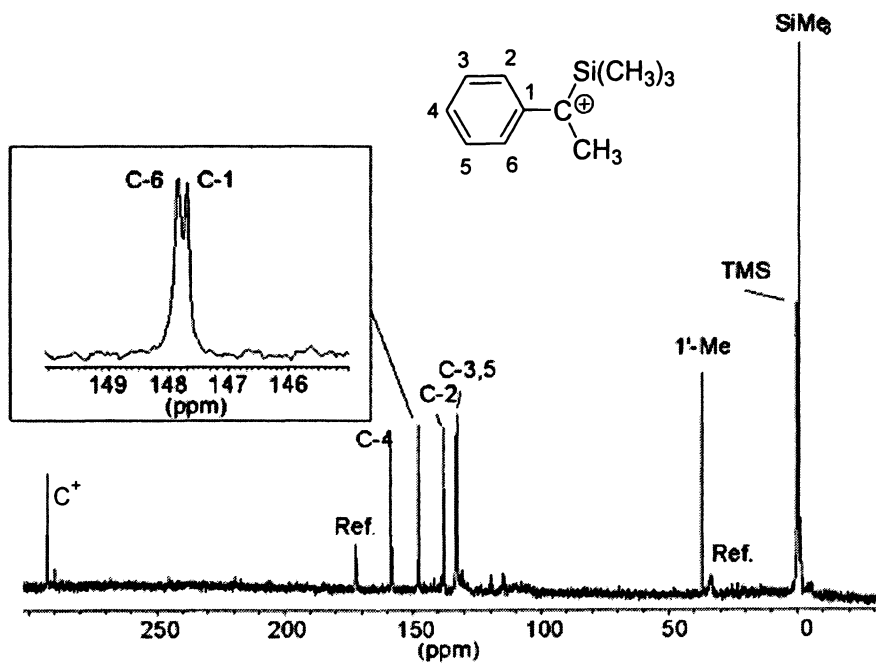


Figure 1 ^{13}C NMR spectrum of 1-phenyl-1-(trimethylsilyl)ethyl cation 1 in $\text{SO}_2\text{ClF}/\text{SO}_2\text{F}_2$ at -127°C , reference capillary CD_3COCl (12, 14)

Table 1. ^{13}C NMR chemical shifts (δ , ppm) for 1-phenyl-1-(trimethylsilyl)ethyl cation **1**, cumyl cation **3** and 1-phenylethyl cation **5** in $\text{SO}_2\text{ClF}/\text{SO}_2\text{F}_2$. (*14, 15, 16, 17*).

system	C^+	C_o	C_o'	C_m	C_m'	C_p	C	R
	231.28	155.36	144.14	134.25	134.01	161.92	141.91	28.05
5 ^a 	292.82	148.34 <i>anti</i> to Si	138.25 <i>syn</i>	133.59 <i>anti</i> to Si	133.07 <i>syn</i>	158.91	139.43	37.27 ^c -0.21 ^d
1 ^b 	255.85	142.22		132.96		156.14	140.25	33.46
3 ^a								

a) 63 MHz, at -117 °C in $\text{SO}_2\text{ClF}/\text{SO}_2\text{F}_2$, internal reference $\delta(\text{NMe}_4^+) = 55.65$ ppm.

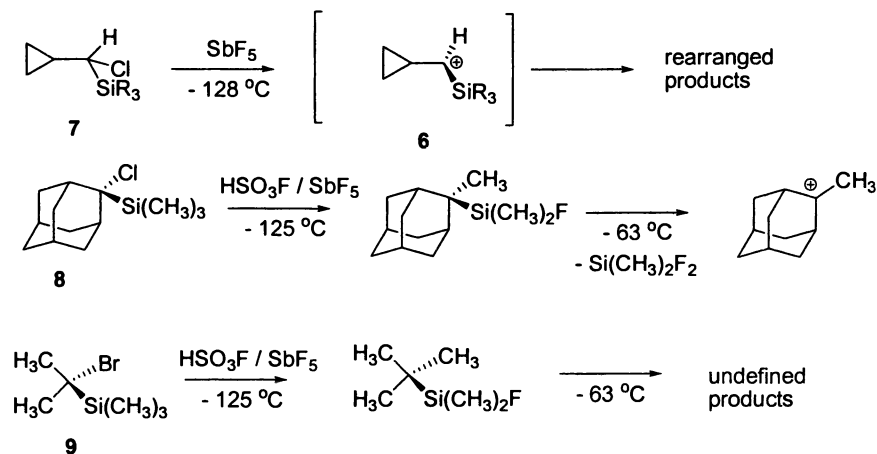
b) 100 MHz at -124 °C, internal reference $\delta(\text{CD}_2\text{Cl}_2) = 53.80$ ppm

c) C^+-CH_3

d) $\text{Si}-\text{CH}_3$

shift of the para carbon in the 1-phenyl-1-(trimethylsilyl)ethyl cation **1** ($\delta = 158.9$ ppm) is in between the value for the chemical shift of C_{para} in the 1-phenylethyl cation **5** ($\delta = 161.9$ ppm) and the cumyl cation **3** ($\delta = 156.7$ ppm). This shows that the α -trimethylsilyl group is stabilizing compared with an α -hydrogen, but destabilizing compared with an α -methyl group in this type of carbocations. These findings are in accord with earlier calculations on model systems, with solvolysis data and also with recent quantum chemical *ab initio* calculations of charge distribution in α -silyl substituted carbocations (**4**, **5**, **6**, **18**). The ^{29}Si NMR chemical shift ($\delta^{29}\text{Si} = 9.61$ ppm, $\text{SO}_2\text{ClF}/\text{SO}_2\text{F}_2$, -127 °C) is similar to that of the neutral progenitor, 1-phenyl-1-trimethylsilyl ethylchloride **4** ($\delta^{29}\text{Si} = 9.08$ ppm) indicating that charge delocalization to the silyl group is not important (**13**).

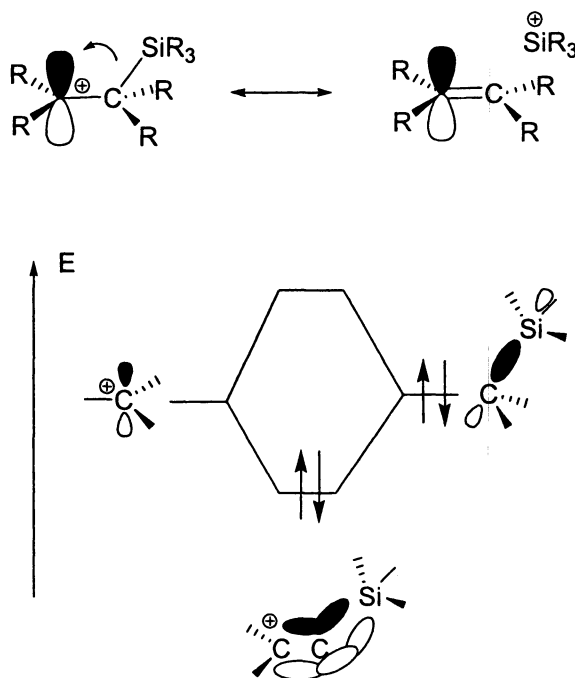
Other α -silyl substituted carbocations such as cyclopropyl substituted cations **6** or alkyl and cycloalkyl substituted α -silyl-carbocations could not be generated from the corresponding halides **7** - **9** using the superacids SbF_5 or $\text{FSO}_3\text{H}/\text{SbF}_5$ (1:1) as persistent species in $\text{SO}_2\text{ClF}/\text{SO}_2\text{F}_2$ solution, because silyl-group cleavage or rearrangements took place (**12**).



β -silyl substituted carbocations

The β -effect, the interaction of a β -carbon silicon σ -bond with the vacant p-orbital at the C^+ carbon, is called hyperconjugation i.e. the conjugation of the

vacant p-orbital with the remote σ -bond (6, 19) (Scheme 1). Calculations and experiments have shown that this effect is dependent on the dihedral angle between the vacant p-orbital and the interacting σ -bond.

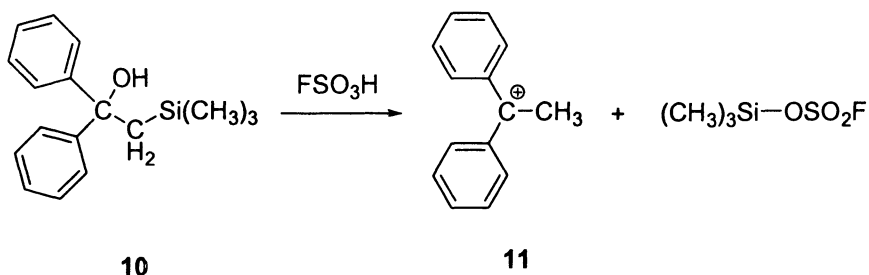


Scheme 1 Valence-bond- and MO-description of β -C-Si- σ -bond hyperconjugation

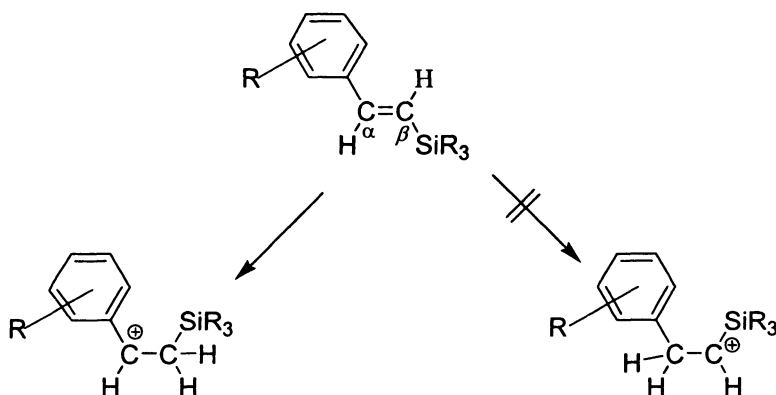
The β -silyl effect in benzyl cations

Early attempts to generate α -aryl- β -silyl substituted carbocations by ionization of 1,1-diphenyl-2-(trimethylsilyl)ethanol **10** using FSO_3H in SO_2ClF even at very low temperature of -140°C were unsuccessful (11). Only 1,1-diphenylethyl cation **11** and trimethylsilyl fluorosulfate, the products of β -silyl cleavage were observed.

The protonation of substituted styrenes generally leads to sequential oligomerization and polymerization reactions (3). Only when carefully



controlled experimental conditions are applied further reaction of the initially formed benzyl cation with the styrene progenitor can be suppressed. Protonation of 2-silyl substituted styrenes occurs in a regiospecific manner (Scheme 2). The β -silyl substituted benzyl cations with sterically bulky trialkylsilyl groups are accessible as persistent species in $\text{SO}_2\text{ClF}/\text{SO}_2\text{F}_2$ solution by protonation using superacids at low temperatures and can be characterized by ^1H - and ^{13}C - and ^{29}Si -NMR spectroscopy (13).



Scheme 2 Regiospecific formation of β -silyl substituted benzyl cations

The 1-phenyl-2-(triisopropylsilyl)ethyl cation **12** is formed by reaction of (*E*)-1-phenyl-2-(triisopropylsilyl)-ethene **13** with $\text{SbF}_5/\text{FSO}_3\text{H}$ (1:4) at -135°C (13).

The experimental ^1H , ^{13}C (Figure 2) and ^{29}Si - (Figure 3) NMR spectra show the exclusive formation of 1-phenyl-2-(triisopropylsilyl)ethyl cation **12** and give proof of its structure and conformation (13).

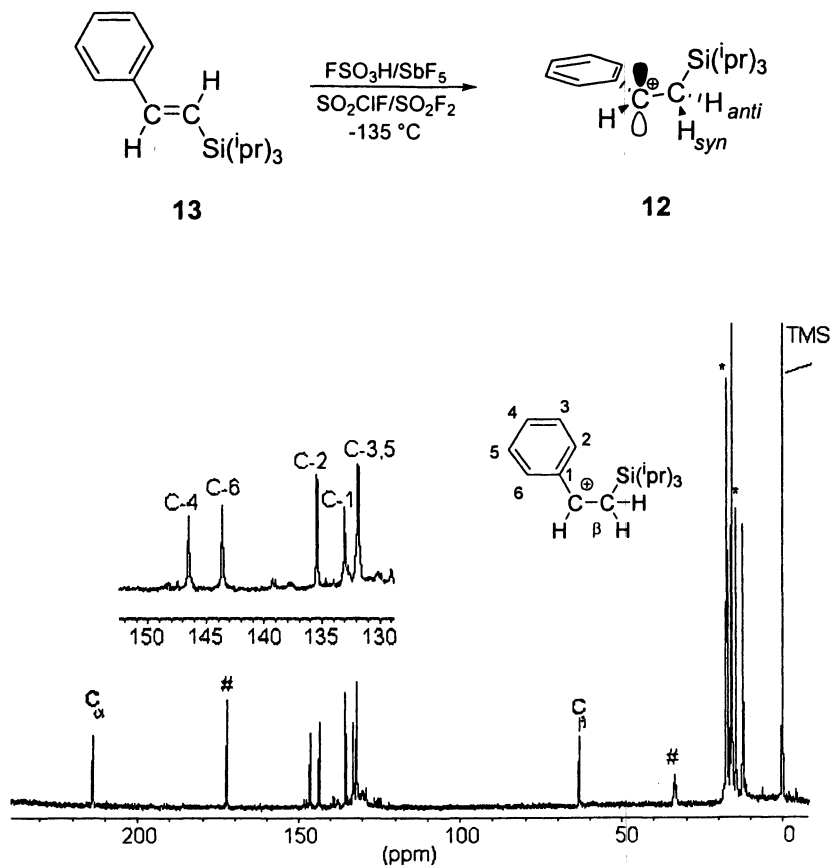


Figure 2 ^{13}C NMR spectrum of 1-phenyl-2-(triisopropylsilyl)ethyl cation **12** in $\text{SO}_2\text{ClF}/\text{SO}_2\text{F}_2$ at -123°C , # peaks of reference capillary CD_3COCl (**13**)

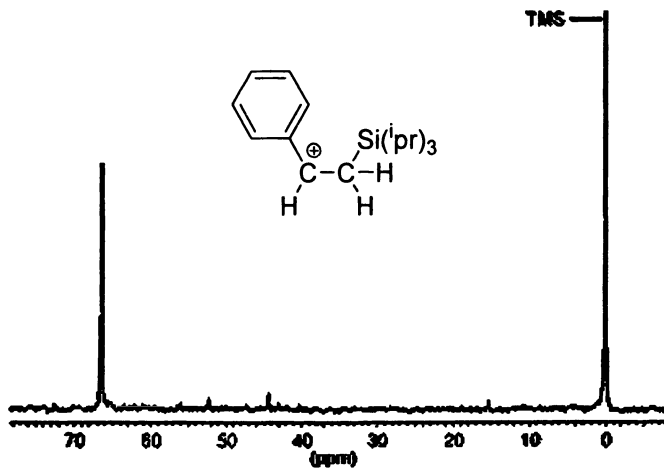


Figure 3 ^{29}Si NMR spectrum of 1-phenyl-2-(triisopropylsilyl)ethyl cation **12** in $\text{SO}_2\text{ClF}/\text{SO}_2\text{F}_2$ at $-123\text{ }^\circ\text{C}$ (**13**).

The ^{29}Si -NMR chemical shift of **12** ($\delta = 66.34$ ppm) is considerably deshielded as compared to the progenitor alkene **13** ($\delta = 0.14$ ppm), which is in accord with substantial β -Si-C-bond hyperconjugative delocalization of positive charge to silicon.

The structure of the 1-phenyl-2-(trimethylsilyl)ethyl cation (**14**), a close model cation for **12**, was optimized at B3LYP/6-31G(d)-level (*20*) (Figure 4). The positive charge in this type of carbocations is stabilized by aryl π -delocalization and hyperconjugative σ -bond interaction with the β -silyl group. The geometrical parameters confirm the efficient β -silyl stabilization. The $\text{C}_\alpha\text{-C}_\beta$ -bond is shortened and the $\text{C}_\beta\text{-Si}$ bond elongated, as expected for β -silyl hyperconjugative interaction. The quinoid distortion of the phenyl ring is less pronounced compared to analogous non-silyl substituted benzyl cations, the 1-phenyl-1-ethyl and the 1-phenyl-1-propyl cations which are models for the analogous benzyl cations with $\beta\text{-C-H}$ and $\beta\text{-C-C}$ hyperconjugation respectively. (*20*)

The NMR chemical shifts calculated (GIAO-DFT, B3LYP/6-311G(d,p)) for the optimized geometry (B3LYP/6-31G(d)) of the model cation **14** are in reasonable agreement with the experimentally observed ^{13}C NMR chemical shifts observed for **12**, considering the different alkyl substituted silyl groups in **12** ($\text{Si}(\text{iPr})_3$) and the model cation **14** (SiMe_3) (*20*).

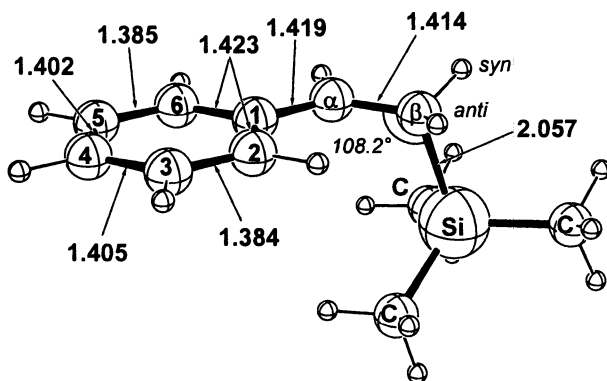
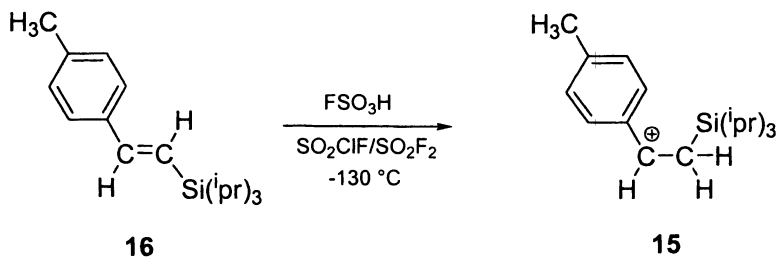


Figure 4 Geometry of 1-phenyl-2-(trimethylsilyl)ethyl cation (14)
(B3LYP/6-31G(d)) (20)

Likewise the 1-*p*-tolyl-2-(triisopropylsilyl)ethyl cation **15** is formed by protonation of (*E*)-1-*p*-tolyl-2-(triisopropylsilyl)ethene **16**. Cation **15** can be generated using less acidic conditions: FSO₃H without addition of SbF₅ is sufficient, while successful generation of **12** from **13** requires FSO₃H/SbF₅, the much stronger superacid, to prevent β-silyl cleavage (**13**).



Protonation of (*E*)-1-*p*-anisyl-2-(triisopropylsilyl)ethene **17** with FSO₃H in SO₂ClF/SO₂F₂ yields a mixture of *syn*- and *anti*-1-*p*-anisyl-2-(triisopropylsilyl)ethyl cations **18** (**13**, **21**).

Below about -120 °C the interconversion of the *syn* and *anti* isomers is slow on the NMR time scale (Fig 5). This renders the ortho, ortho' and meta, meta' positions in the two *anti*-**18** and *syn*-**18** isomers non-equivalent.

Two sets of four lines are observed, one for the C2 and C6 ortho and C3 and C5 meta carbons in the *anti*-isomer and another set with lower intensity for the C2' and C6' ortho and C3' and C5' meta carbons in the *syn*-isomer. Upon

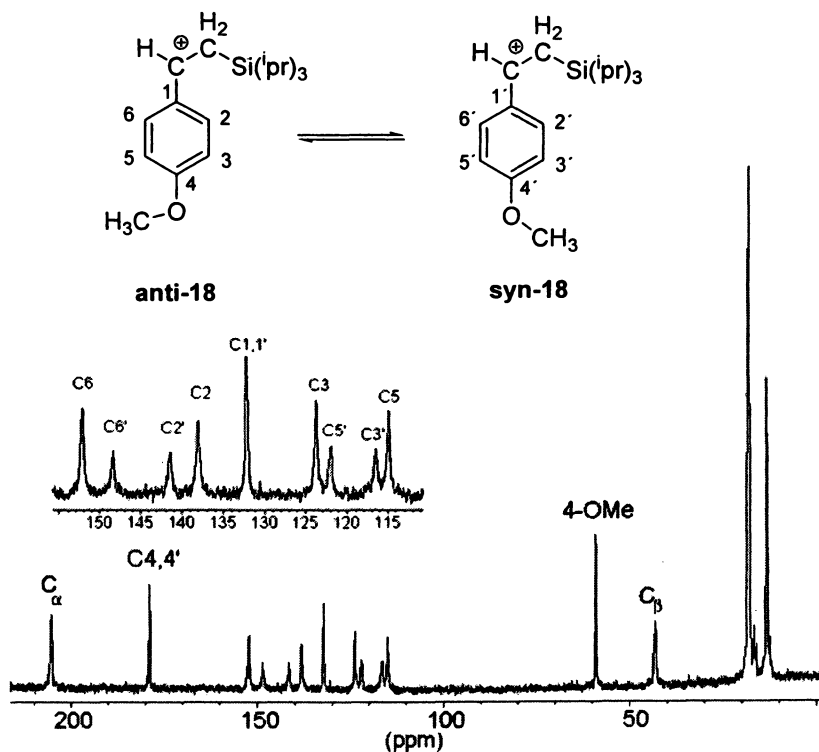
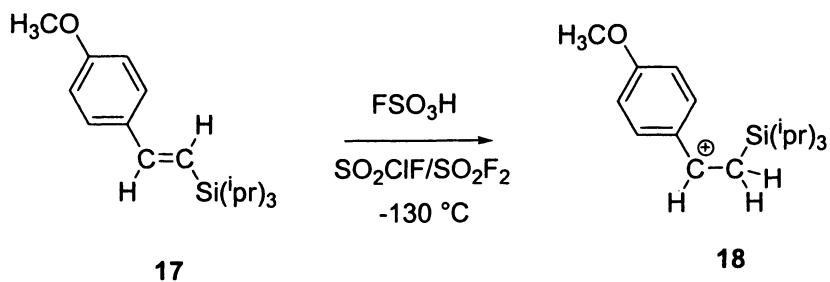
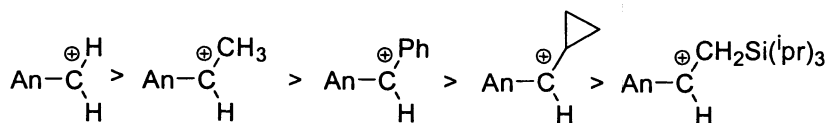


Figure 5 ^{13}C NMR spectrum of *syn*- and *anti*-1-*p*-anisyl-2-(triisopropylsilyl)ethyl cations **18** in $\text{SO}_2\text{ClF/SO}_2\text{F}_2$ at -126 °C (13).

warming above the coalescence temperature of about $-110\text{ }^{\circ}\text{C}$ four lines for the aromatic methine carbons with decreasing line-width are observable until decomposition takes place at about $-70\text{ }^{\circ}\text{C}$ (Figure 6). From the line shape analysis of the dynamic NMR spectra the energy barrier for the isomerization process is obtained as $\Delta G^{\ddagger} = 7.5\text{ kcal mol}^{-1}$ (13).

Quantum chemical calculations (B3LYP 6-31G(d) for a *syn*- and *anti*-1-*p*-anisyl-2-SiH₃-substituted ethyl cations **19** serve as close models for cations **18** showing that the *syn*-isomer of **19** is about 0.3 kcal mol^{-1} higher in energy than the *anti* isomer. The optimized transition state **19-Ts** for the *anti/syn*-isomerization of **19** is $10.3\text{ kcal mol}^{-1}$ higher in energy than the *anti*-isomer. In the transition state structure **19-Ts** the oxygen-methyl bond of the para-methoxy group is oriented perpendicular to the plane of the aryl ring and conjugation of the *p*-OCH₃ group with the aromatic π -system is not possible. The energy difference between the transition state **19-Ts** and the minimum structures of **19** is a measure of the barrier for the methoxy group rotation around the C4-oxygen bond. The calculated energy difference for the SiH₃-substituted model cation **19** is in satisfactory agreement with the experimentally determined energy barrier for **18** of $\Delta G^{\ddagger} = 7.5\text{ kcal mol}^{-1}$ ($-100\text{ }^{\circ}\text{C}$) (21, 22).

The energy barrier for rotation around the C^{para}-OCH₃ bond is a measure of the relative electron demand at the carbocation center. The better a β -substituent stabilizes the positive charge, the less delocalization of positive charge into the aryl ring is necessary, and thus the lower the barrier for the rotation of the para-methoxy group. The corresponding rotational barriers in the parent 1-*p*-anisylmethyl cation, the 1-*p*-anisylethyl cation, the 1-phenyl-1-*p*-anisylmethyl cation and the 1-cyclopropyl-1-*p*-anisylmethyl cation are $\Delta G^{\ddagger} = 12; 10.6; 8.9$ and 8 kcal mol^{-1} . The β -silyl stabilization in these type of benzyl cations is about as efficient as the effect of α -phenyl or α -cyclopropyl rings. This is in accord with a comparison of the ¹³C NMR chemical shifts of the para carbon in 1-*p*-anisylmethyl cations An-C⁺(H)R, with R=CH₃, CH₂CH₃ and CH₂Si(ⁱpr)₃, which are $\delta_{\text{C}^{\text{para}}} = 185.84\text{ ppm}, 181.93\text{ ppm}$ and 178.84 ppm respectively (13).



Scheme 3 Decreasing barrier for *p*-O-CH₃ group rotation in substituted *p*-anisyl cations

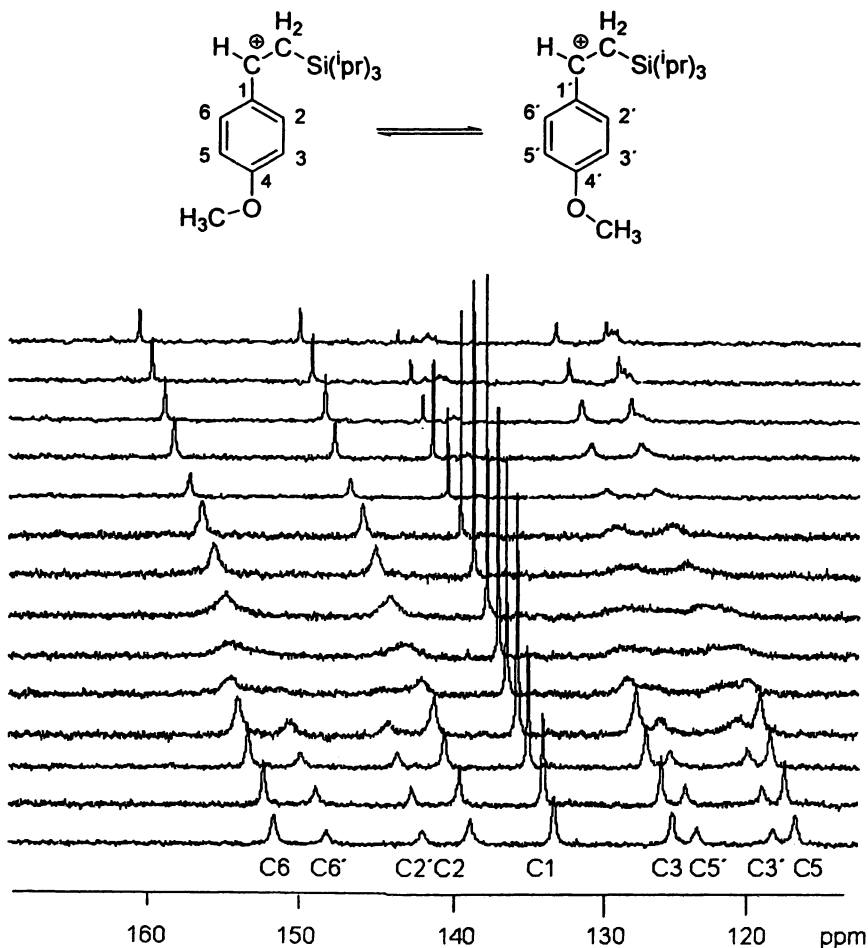
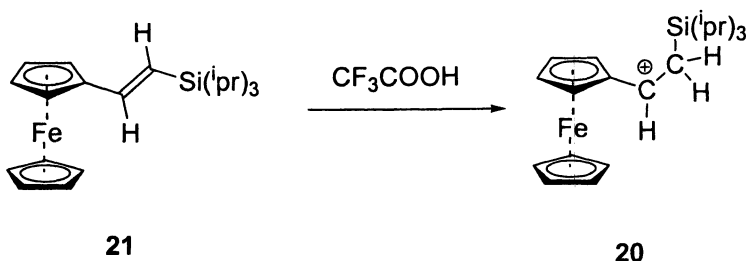


Figure 6 Temperature dependence ($-141\text{ }^{\circ}\text{C}$ (bottom trace) to $-71\text{ }^{\circ}\text{C}$ (top trace)) of ^{13}C NMR signals of the ortho and meta carbons of syn- and anti-1-p-anisyl-2-(triisopropylsilyl)ethyl cations **18** in $\text{SO}_2\text{ClF}/\text{SO}_2\text{F}_2$.

Calculations of the NMR chemical shifts for the B3LYP/6-31G(d) geometry of the *syn* and *ant*-1-*p*-anisyl-2-SiH₃-ethyl cation were performed with the GIAO-DFT method, using the BLYP functional with 6-31G(d) basis sets, the DFT/SCF hybrid method B3LYP with 6-31G(d,p) basis sets and the SOS-DFPT(IGLO) approach with PW91 functional and IGLO III basis sets. (22, 23, 24, 25, 26). The calculated NMR chemical shifts for the SiH₃-substituted model cation, although not in perfect agreement with experimental shifts of **14**, for all methods used, confirm the experimental assignment and allow unequivocal identification of the sets of NMR signals to the *syn* and *anti* isomeric cations respectively (21, 22).

The ferrocenyl group is a very good electron donor. The α -ferrocenyl β -silyl substituted carbocation **20** is accessible by protonation of (*E*)-1-ferrocenyl-2-(triisopropylsilyl)alkene **21** with trifluoroacetic acid in SO₂ClF at -95 °C (13, 22).

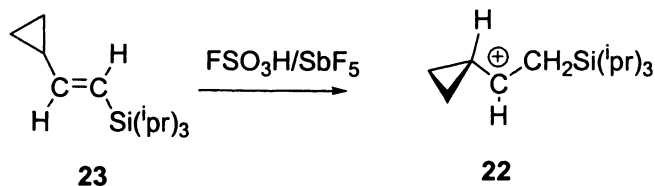


²⁹Si NMR spectroscopy is a suitable tool to monitor the electron demand in β -silylsubstituted carbocations and to compare the hyperconjugative delocalization of positive charge in a series of closely related β -silyl substituted carbocations with varying α -substituents. The ²⁹Si NMR chemical shifts in the α -phenyl- (**12**), α -(*p*-tolyl)- (**15**), α -(*p*-anisyl)- (**18**) and α -ferrocenyl- (**20**) substituted β -silylethyl cations are $\delta^{29}\text{Si} = 66.34, 56.92, 38.88$ and 23.48 ppm, respectively, decreasing regularly as expected on increasing the electron donating capability of the α -substituent.

The β -silyl effect in α -cyclopropyl substituted carbocations

(*E*)-1-cyclopropyl-2-(triisopropylsilyl)ethyl cation **22** (R = Si(^{*i*}pr)₃) can be generated by protonation of (*E*)-1-cyclopropyl-2-(triisopropylsilyl)ethene **23** (20, 27).

¹H and ¹³C NMR spectra and H,C-COSY 2D-NMR spectra of **22** allow full assignment of the structure and confirm the preferred *E*-conformation. The 400 MHz ¹H NMR spectrum of **22** shows spin-spin couplings with characteristic



$^3J_{(\text{HH})}$ coupling constants for the non-equivalent *syn*- and *anti*- oriented β -CH₂-hydrogens to the α -methine-hydrogen.

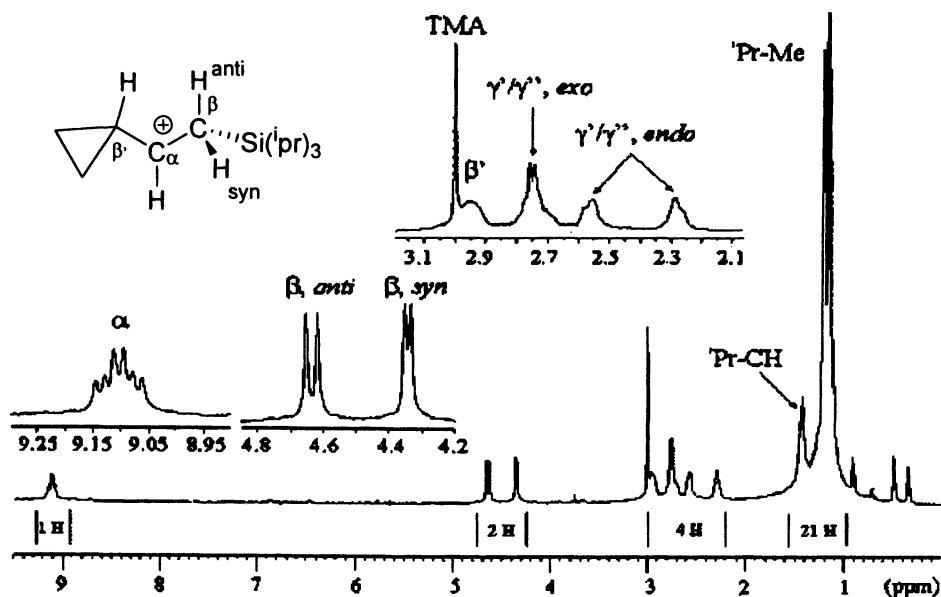


Figure 7 400 MHz ^1H NMR spectrum of *E*-1-cyclopropyl-2-(triisopropylsilyl)ethyl cation **22** in $\text{SO}_2\text{ClF}/\text{SO}_2\text{F}_2$ at -105°C (20).

The experimental $^3J_{(\text{HH})}$ spin-spin coupling constants for H_α , H_β , and $\text{H}_{\beta'}$ for the *E*-isomer **22** were quite satisfactorily reproduced ($\Delta = 0.1 - 1$ Hz) by calculations, using a finite perturbation method (FPT level (26), Perdew/IGLO-III at a MP2/6-31G(d) geometry for the model structure (*E*)-1-cyclopropyl-2-(trimethylsilyl)ethyl cation. The calculations confirm the *trans*-arrangement of H_α and H_β , the *syn/anti*-assignment and the *E*-conformation for the experimentally observed carbocation **22** (20, 27, 28). The (*E*)-1-cyclopropyl-2-

(triisopropylsilyl)ethyl cation **22** can be compared with the closely related α -aryl substituted carbocations **12**, **15** and **18**. The ^{29}Si NMR chemical shift of **22** ($\delta^{29}\text{Si} = 55.75$ ppm) indicates that the electron donating effect of an α -cyclopropyl substituent in this type of β -silyl substituted carbocations is somewhat better than the effect of the α -phenyl substituent in **12** ($\delta^{29}\text{Si} = 66.34$ ppm), comparable with the α -tolyl substituent in **15** ($\delta^{29}\text{Si} = 56.92$ ppm) and not as good as the α -anisyl substituent in **18** ($\delta^{29}\text{Si} = 38.88$ ppm) (20).

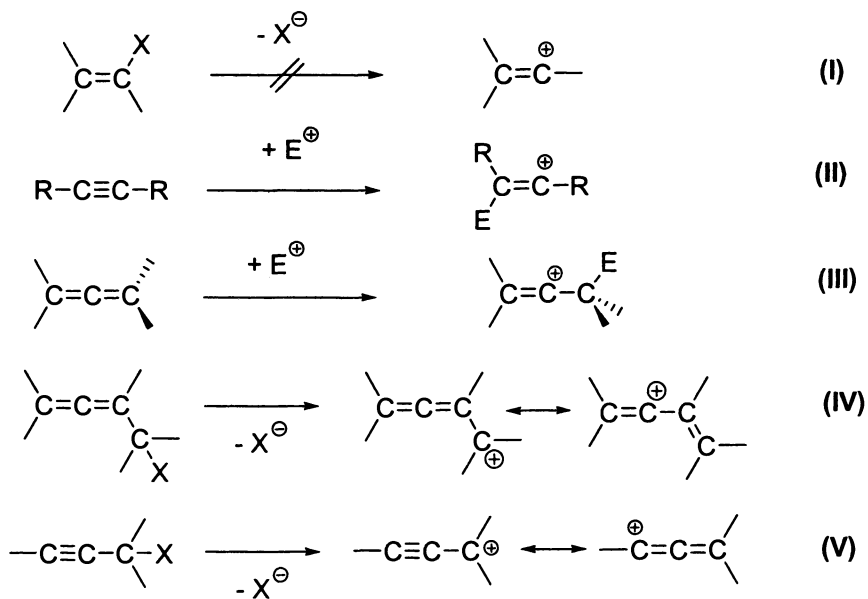
The β -silyl effect in vinyl cations

Vinyl cations (**23**) are disubstituted carbocations with an sp^2 -hybridized positively charged carbon with the vacant p-orbital at C_α and an orthogonal π -system of the C_α - C_β -double bond (29, 30, 31). All attempts to generate vinyl cations in superacid media by heterolytic cleavage of vinyl halides (Scheme 4, path I) have failed (32), including an alleged success (33), which was explicitly disproven (1, 32, 34). A number of vinyl cations including those with β -silyl substituents are accessible as persistent species in solution and were investigated by NMR spectroscopy (35, 36, 37). Principal pathways used in the author's laboratory for their generation are protonation or addition of other electrophiles to suitable precursor alkynes (Scheme 4, path II,) (1, 12, 13, 21, 34, 35, 36, 43, 38, 39, 40, 41, 42) or allenes (Scheme 4, path III) (12, 37, 44, 45, 46), under carefully controlled experimental conditions (2) which avoid cationic polymerization. We have reacted various allenylmethyl compounds (Scheme 4, path IV) (37, 47, 48, 49, 50) and alkynylmethyl compounds (Scheme 4, path V) (51) under superacidic conditions to undergo sp^3 -carbon-X bond cleavage to yield π -p-resonance stabilized vinyl cations.

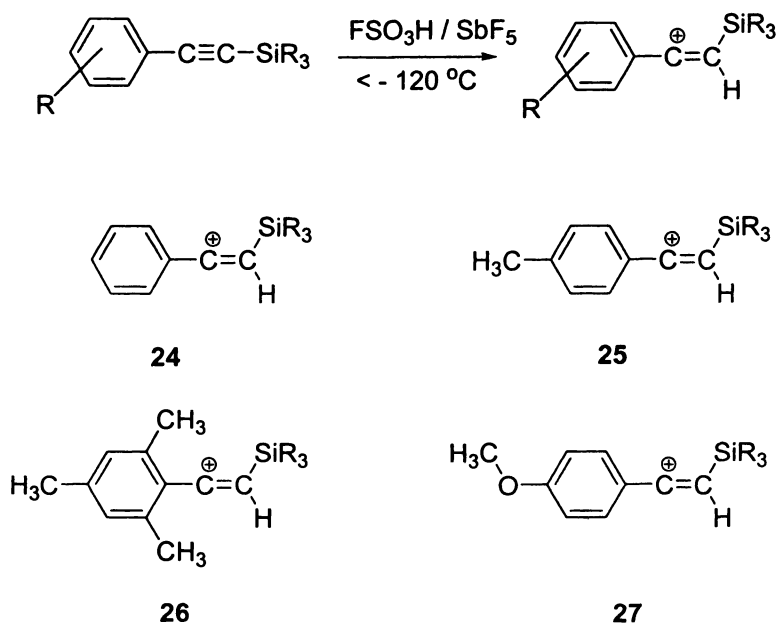


23

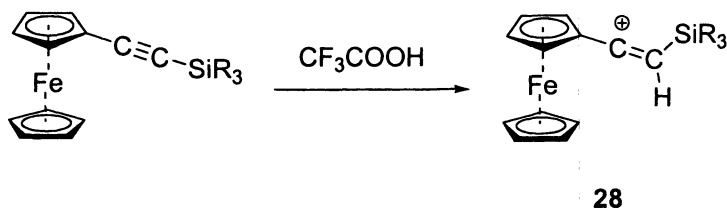
α -Phenyl- (**24**), α -tolyl- (**25**), α -mesityl- (**26**) and α -anisyl- (**27**), substituted β -silyl substituted vinyl cations are accessible in superacidic solution. Generally larger alkyl groups at silicon are required to prevent β -C-Si bond cleavage. The less electron donating the aryl substituent, the higher is the electron demand at silicon, and this leads to more facile β -cleavage.



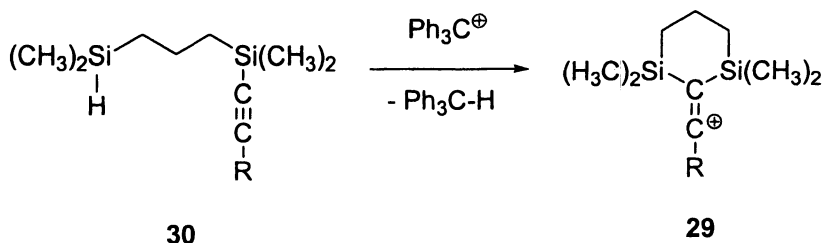
Scheme 4 principal reaction paths to generate vinyl cations



The generation of α -ferrocenyl- β -silyl substituted vinyl cations of type **28** does not require superacidic conditions, they can be generated by protonation of 1-ferrocenyl-2-trialkylsilyl alkynes with trifluoroacetic acid at room temperature. The SiR_3 -groups with larger alkyl substituents increase the lifetime of this type of carbocations.



Vinyl cations of type **28** with α -aryl or α -alkyl substituents and two β -silyl groups and with an anion of very low nucleophilicity can be generated at room temperature in non-coordinating solvents from **30** by a Si-H to C-H hydride transfer reaction. For **29** (R = t-butyl), an X-ray structure determination has been reported (43, 52, 53).



β -Silyl substituted dienyl cations

The β -silyl substituted vinyl cations **31** (R = CH_3 or H) are formed by reaction of the silyl substituted allenyl compounds **32** (R = H or CH_3 , X = OH or Cl) with SbF_5 at temperatures below -130°C (37).

The ^{13}C NMR spectrum of **31** (R = H) is shown in Figure 8. This is likely to be the smallest member of β -silyl substituted vinyl cations which can be generated and observed as persistent species in solution.

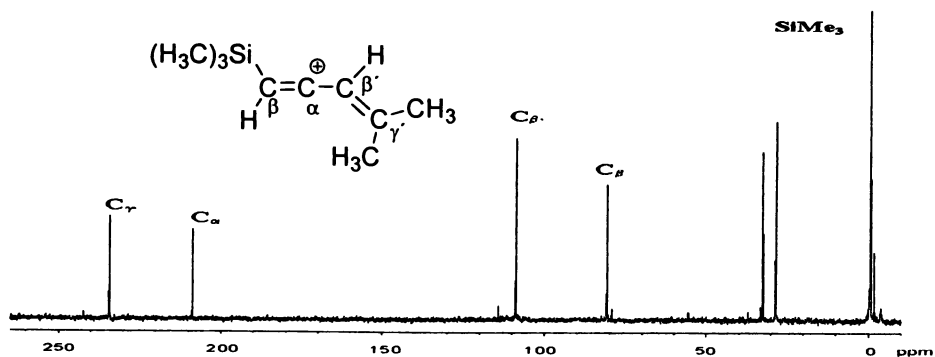
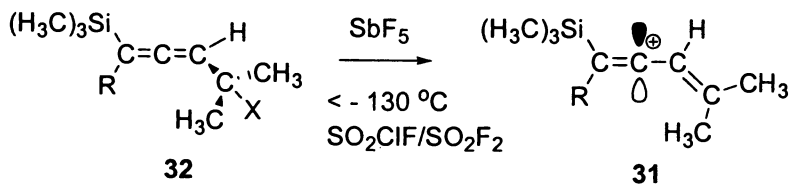
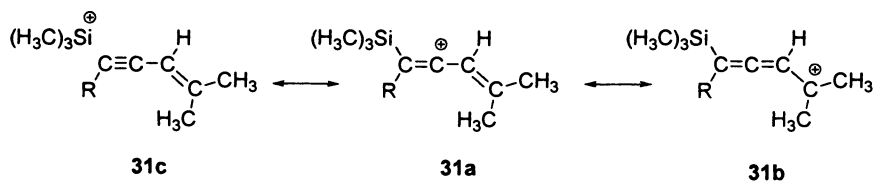


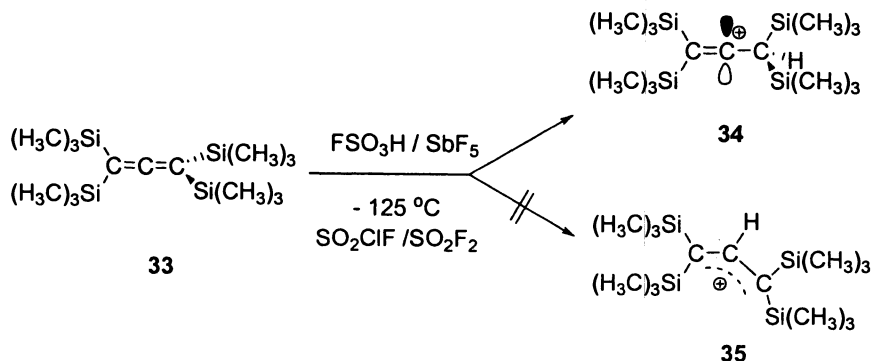
Figure 8 ^{13}C NMR spectrum of 1-trimethylsilyl-4-methyl-1,3-pentadien-2-yl cation **31** ($R = \text{H}$) in $\text{SO}_2\text{ClF}/\text{SO}_2\text{F}_2$ at -137°C (37).



The two positively charged carbons of the allyl moiety in **31** are less deshielded than the corresponding carbons in the analogous carbocation with a CH_3 instead of a SiMe_3 group. This indicates that the positive charge is delocalized away from the allylic system **31a** \leftrightarrow **31b** towards the β -trimethylsilyl group, as formally described by the hyperconjugative resonance structure **31c**

Protonation of Allenes

Protonation of tetrakis(trimethylsilyl)allene **33** with $\text{HSO}_3\text{F}/\text{SbF}_5$ (1:1) gives the 1,1,3,3-tetrakis(trimethylsilyl)-1-propen-2-yl cation **34**. The isomeric allyl cation **35** is not formed (12, 44).



In contrast, Allenes substituted only with alkyl or with alkyl and aryl groups are protonated with $\text{HSO}_3\text{F}/\text{SbF}_5$ at the central allene carbon to yield the corresponding allyl cations (**54**). The different reaction course followed by the silyl and alkyl substituted Allenes is fully consistent with the hyperconjugation model which predicts that a β -silyl group stabilizes a carbenium ion better than a β -alkyl group and with previous conclusions, that α -silyl substitution in carbocations is destabilizing relative to α -alkyl substitution. The ^{13}C NMR spectra of **34** show temperature dependent kinetic line broadening for the two silyl groups at the methine carbon. The rotation around the $\text{C}^+-\text{CH}(\text{SiMe}_3)_2$ bond is controlled by strong hyperconjugation with the β -silyl groups. IGLO/II calculations for model cations account for the strong shielding effect and confirmed nicely the experimentally observed dihedral-angle dependence of the β -silyl effect.

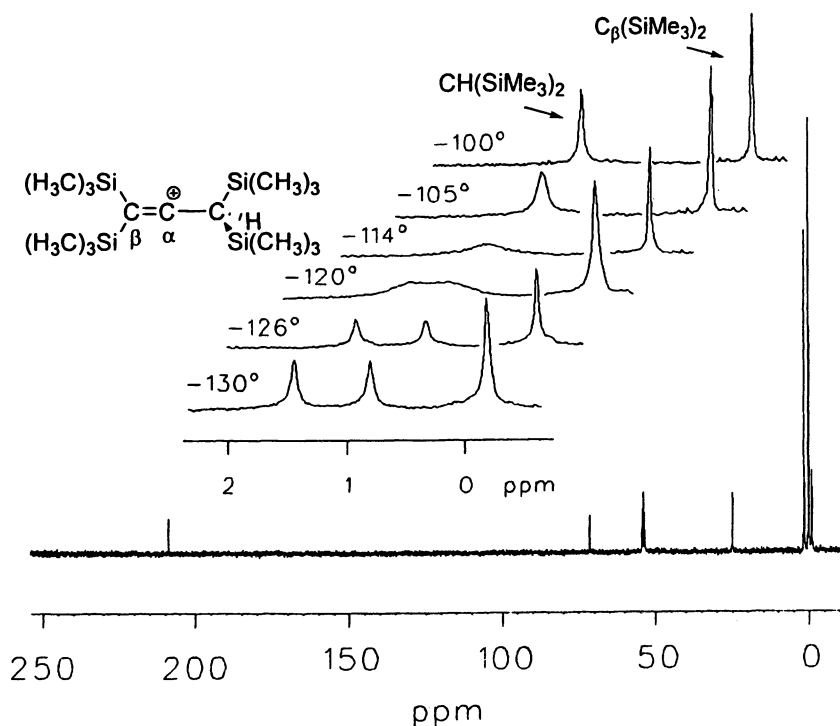
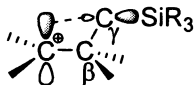


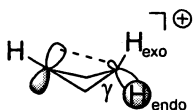
Figure 9 100.6 MHz ^{13}C NMR spectrum of **34** (-100°C , $\text{SO}_2\text{ClF} / \text{SO}_2\text{F}_2$, reference CD_2Cl_2 $\delta = 53.80$ ppm), inset: expanded region (2 to -0.5 ppm) showing the temperature dependence of the methine $\text{Si}(\text{CH}_3)_3$ signals (-130 to -100°C) (12, 44)

The γ -silyl effect in bicyclobutonium ions

The effect of a silyl-substituent at the carbon two bonds away from the formally positively charged carbon is called the γ -silyl effect. (55)



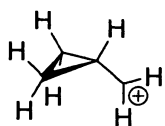
Bicyclobutonium ions, are bridged carbocations with a pentacoordinated γ -carbon which were first discussed as short lived intermediates in the solvolysis reaction of cyclopropylmethyl and cyclobutyl compounds (56, 57, 58, 59, 60, 61).



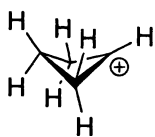
36

The cartoon-like drawing of the structure of the parent bicylobutonium ion $C_4H_7^+$ **36** is adopted from an ingenious forward-looking paper of Olah and coworkers in 1972, (61) long before routine ^{13}C -FT-NMR spectroscopy and routine *ab initio* quantum chemical calculations were available, which envisaged correctly the stabilization mode of the parent bicyclobutonium ion to arise from the interaction of the backside lobe of the C_γ - H_{endo} sp^3 orbital with the empty carbenium carbon p-orbital at C_α .

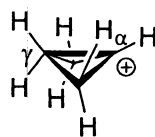
Experimental NMR spectroscopic investigations of the parent cation ($C_4H_7^+$) (62, 63), the 1-methyl substituted cation ($C_4H_6CH_3^+$) (64, 65, 66) and the 1- SiR_3 -substituted cation ($C_4H_6SiR_3^+$) (67, 68, 69, 70) revealed that the molecules in these systems have highly fluxional structures undergoing fast dynamic equilibria on a very flat potential energy surface. This prevented a direct spectroscopic characterization of a static bicyclobutonium ion structure in solution (71). The structures of lowest energy considered for the parent cation ($C_4H_7^+$) are, bisected cyclopropylmethyl cation **37**, a puckered cyclobutyl cation **38**, and the bicyclobutonium ion **39**, which has the same symmetry as **38** but with the additional bridging C_α - C_γ bond. The methylene hydrogens arranged *trans* to the methine hydrogen are labeled *endo* and the methylene hydrogens oriented *cis* to the methine hydrogen are designated *exo*. (63)



37



38

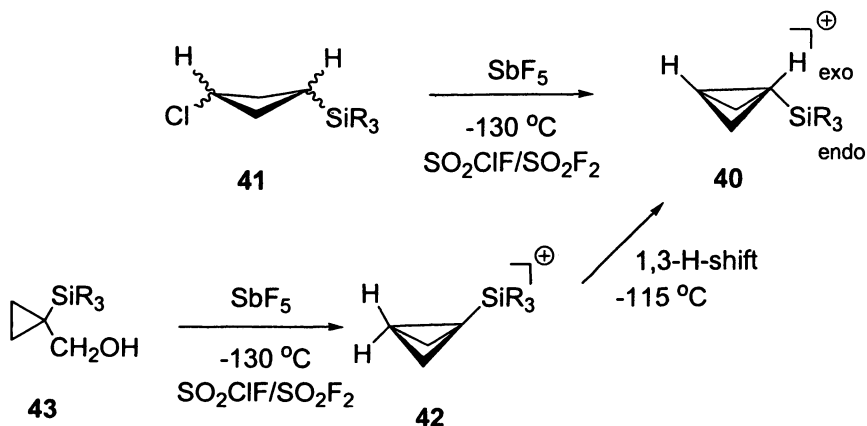


39

Only averaged chemical shifts and averaged coupling constants arising from a major and a minor isomer are experimentally accessible in solution. Quantum chemical calculations have confirmed the small energy differences in particular between structures **37** and **39** and a very low barriers for their rearrangements (72, 73, 74, 75). The averaged experimental NMR data obtained in solution cannot be correlated directly and unambiguously to calculated NMR chemical

shifts and NMR spin-spin coupling constants of static model structures, and consequently conflicting interpretations have been suggested.

We have used the stabilizing effect of a γ -silyl substituent to prepare a static bicyclobutonium ion in solution which could be characterized unambiguously by experimental and computational NMR spectroscopy. The *endo*-3-silyl-substituted bicyclobutonium ions **40** can be directly generated by ionization of 3-(trimethylsilyl)cyclobutyl chlorides **41** with SbF_5 . An indirect route to **40** is via a rearrangement of 1-silyl-substituted bicyclobutonium ions **42** generated from 1'-trialkylsilyl-cyclopropylmethanol **43**. Ionization of **43** at low temperatures leads to formation of the 1-trialkylsilyl bicyclobutonium cation **42**. Sterically bulky alkyl groups at silicon prevent cleavage of the silyl group at relatively higher temperatures. Controlled warming of **42** ($\text{SiR}_3 = \text{Si}(\text{Me})_2t\text{-Bu}$) up to -115°C leads to clean formation of the *endo*-3-silyl-substituted bicyclobutonium ion **40** ($\text{SiR}_3 = \text{Si}(\text{Me})_2t\text{-Bu}$). The rearrangement of **42** \rightarrow **40** occurs via a 1,3-hydride shift.



The 3-*endo*-(trialkylsilyl)bicyclobutonium ions **40** ($\text{SiR}_3 = \text{Si}(\text{Me})_3$ or $\text{Si}(\text{Me})_2t\text{-Bu}$) were characterized by one and two dimensional ^1H and ^{13}C NMR spectroscopy as static bicyclobutonium ions (Figure 10). The NMR spectra give unambiguous proof for the hyper-coordinated and puckered structure of bicyclobutonium ions. The ^{13}C NMR chemical shifts for C_α ($\delta = 101.7$ ppm) and the C_γ ($\delta = -18.7$ ppm) clearly exclude cyclopropylmethyl- and cyclobutyl-type cation-structures **37** and **38**. The extraordinary shielding of the pentacoordinated C_γ -carbon is particularly characteristic. In the ^1H NMR spectrum distinct *exo* and *endo* hydrogens at the methylene carbons show small *cis* and larger *trans* $^3J(\text{HH})$ couplings to H_α and H_γ . This excludes conformational averaging of the cyclobutyl ring and a planar ring structure and is only consistent with a bicyclobutane ring system, i. e. a puckered bicyclobutonium ion.

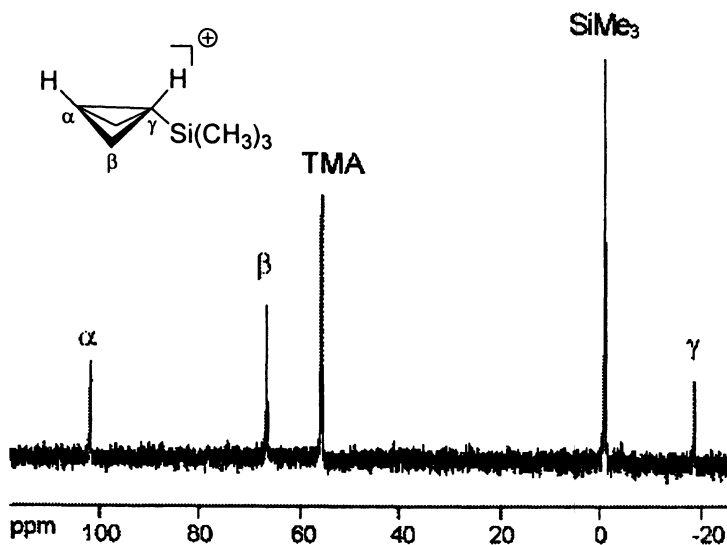


Figure 10: 100.6 MHz ^{13}C NMR spectrum of 3-endo-(trimethylsilyl)bicyclobutonium ion **40** ($\text{SiR}_3 = \text{Si}(\text{Me})_3$) in $\text{SO}_2\text{ClF}/\text{SO}_2\text{F}_2$ at -115°C , int. ref. TMA: $\delta(\text{N}(\text{Me})_4^+)$ = 55.65 ppm

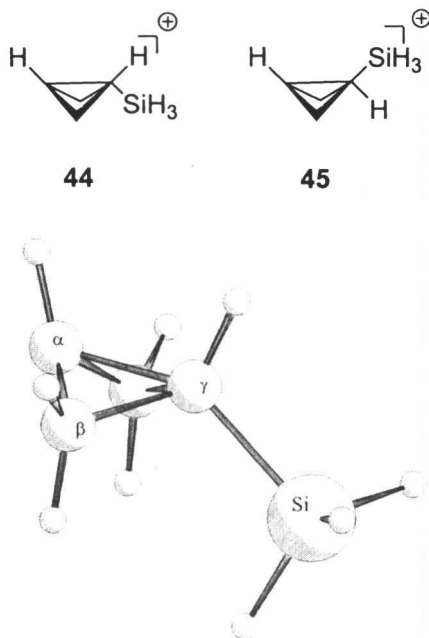


Figure 11: Structure of 3-endo-silylbicyclobutonium ion **44** (MP2/6-31G(d))

The endo-SiR₃ bicyclobutonium structure of cations **40** was confirmed by MP2/6-31G(d) calculations, which revealed that the model structure 3-endo-SiH₃-bicyclobutonium **44** (Figure 11) is an energy minimum, 7.9 kcal/mol lower in energy than the 3-exo-silylbicyclobutonium ion **45**, which is not an energy-minimum structure.

The interpretation of the NMR spectra and structure of the experimentally observed bicyclobutonium ions **40** is confirmed by a reasonably good agreement between the measured ¹³C and ¹H NMR chemical shifts and the calculated chemical shifts (GIAO-MP2/tzp/dz) of the MP2/6-31G(d) optimized structures of the model cations **44** and **45**. An unambiguous proof for the bridging and the stereochemical arrangement of the silyl substituent in the bicyclobutonium ions **40** is the transannular ³J(H,H) spin-spin coupling between H_α and H_γ. The 2D-H,H-COSY spectrum clearly shows the cross peaks between H_α (δ = 6.05 ppm) and H_γ (δ = 0.30 ppm) (Figure 12).

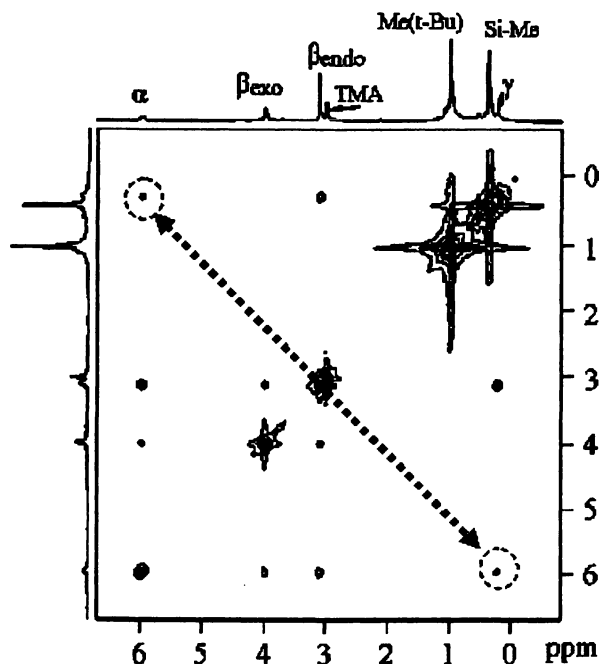


Figure 12: 2D-COSY-45 NMR spectrum (400,13 MHz) of 3-endo-silylbicyclobutonium ion **40** (SiR₃ = Si(Me)₂t-Bu) in SO₂ClF/SO₂F₂ at -112 °C, int. ref. TMA: δ(N(Me)₄⁺) = 55.65 ppm. Cross peaks between H_α and H_γ are labeled

The experimentally measured coupling constant $J(\text{H}_\alpha\text{H}_\gamma)_{\text{exp.}} = 5.5 \text{ Hz}$ is reproduced by calculations for the *endo*-silyl substituted model structure **44** using a finite perturbation level (FPT) (26) (Perdew/IGLO-III) approach $J(\text{H}_\alpha\text{H}_\gamma)_{\text{calc.}} = 5.9 \text{ Hz}$, whereas only 1.2 Hz is calculated for the $\text{H}_\alpha\text{H}_\gamma$ -coupling constant in the *exo*-silyl substituted model structure **45**. Finally the bonding orbital of the bridging C-C-bond between C_α and C_γ in these type of bicyclobutonium ions can be visualized by calculations of the natural bond orbitals (NBO's) (Figure 13).

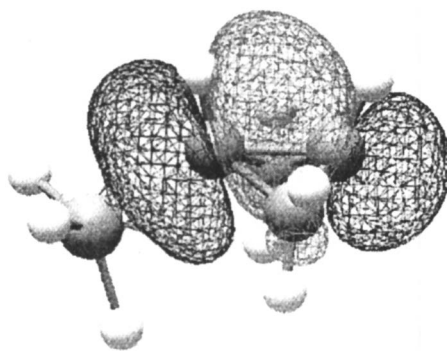


Figure 13: bonding orbital (NBO) showing the bridging bond between C_α and C_γ in the 3-*endo*-silylbicyclobutonium ion **44**.

Epilogue

Basic questions in physical organic chemistry have triggered the development of better tools and methods in chemistry. A fruitful interplay of experimental and computational methods has guided the further development of the field. Exploring the chemistry of carbocations by NMR spectroscopy in superacid solutions in combination with today's state-of-the-art quantum chemical calculations proved to be very successful, and serves as a shining example for close integration of experimental and computational methods in solving problems which are applicable to all areas of chemistry.

Silyl effects in carbocations which were predicted computationally and have been observed in the gas phase and in solvolysis reactions, have been proven by NMR spectroscopic investigation of long-lived silyl-substituted carbocations in

solution. Previously inaccessible vinyl cations could be generated using stabilizing silyl substituents. The hyperconjugational origin of the β -silyl-effect in carbocations has been directly demonstrated by dynamic NMR spectroscopy. Application of the silyl effect in conjunction with contemporary experimental and computational methodology could finally solve the structure of $C_4H_7^+$ cation (cyclopropylcarbinyl/bicyclobutonium cation), a problem which has been enigmatic for about half a century.

Reference

- (1) Siehl, H. - U.; Kaufmann, F.- P.; Hori K. *J. Am. Chem. Soc.* **1992**, *114*, 9343 - 9349.
- (2) for general methods to generate carbocations persistent in solution see: Lenoir, D.; Siehl, H.-U. In *Houben-Weyl Methoden der Organischen Chemie*; Hanack, M., Ed.; Thieme: Stuttgart, **1990**; Vol. E19c, pp 26 - 32.
- (3) for an older review on silyl-sibstituted carbocations see: Siehl, H.-U.; Müller, T. In *The chemistry of organosilicon compounds*; Rappoport, Z., Apeloig, Y., Eds.; John Wiley and Sons: New York, **1998**; Vol. 2; pp 595 - 701.
- (4) Apeloig, Y.; Arad, D. *J. Am. Chem. Soc.* **1985**, *107*, 5285 - 5286.
- (5) Apeloig, Y.; Karni, M.; Stanger, A.; Schwarz, H.; Drewello, T; Czekay, G. *J. Chem. Soc., Chem. Commun.* **1987**, 989 - 991.
- (6) Wierschke C.; Chandarasekhar J.; Joergensen W. J. *J. Am. Chem. Soc.* **1985**, *107*, 1496 - 1500.
- (7) Drewello, T.; Burgers, P. C.; Zummack, W.; Apeloig, Y.; Schwarz, H. *Organometallics* **1990**, *9*, 1161- 1165.
- (8) Hajdasz, D.; Squires, R. *J. Chem. Soc., Chem. Commun.* **1988**, 1212 - 1214.
- (9) Bakhtiar, R.; Holznagel, C. M.; Jacobson, D. B. *J. Am. Chem. Soc.* **1992**, *114*, 3227 - 3235.
- (10) Stang, P. J.; Ladika, M.; Apeloig, Y.; Stanger, A.; Schiavelli, M. D.; Hughey, M. R. *J. Am. Chem. Soc.* **1982**, *104*, 6852 - 6854.
- (11) Olah, G. A.; Berrier, A. L.; Field, L. D.; Prakash, G. K. S. *J. Am. Chem. Soc.* **1982**, *104*, 1349-1355.
- (12) Kaufmann, F.-P. Ph.D. thesis, University of Tübingen, Tübingen, **1992**.
- (13) Müller, B. Ph.D. thesis, University of Tübingen, Tübingen, **1995**.
- (14) Siehl, H.-U., Ulm., Apeloig, Y. Haifa, unpublished results
- (15) Olah, G. A.; Spear, R. J.; Forsyth, D. A. *J. Am. Chem. Soc.* **1977**, *99*, 2615- 2621.
- (16) Olah, G. A.; Westerman, P. W. *J. Am. Chem. Soc.* **1973**, *95*, 3706 - 3709.
- (17) Brown, H. C.; Periasamy, M.; Kelly, D. P.; Giansiracusa, J. J. *J. Org. Chem.* **1982**, *47*, 2089 - 2101.

- (18) Siehl, H.-U., Ulm, Karni, M.; Apeloig, Y., Haifa, unpublished results.
- (19) Ibrahim, M. R.; Jorgensen, W. J. *J. Am. Chem. Soc.* **1989**, *111*, 819 - 824.
- (20) Backes, A. C. Ph.D. thesis, University of Ulm, Ulm, **1999**.
- (21) Siehl, H.-U.; Müller, B.; Malkina, O. L. In *Organosilicon Chemistry III*; Auner, N.; Weis, J., Eds.; VCH: Weinheim, **1997**, S. 25 - 30.
- (22) Siehl, H.-U.; Ulm, unpublished results
- (23) Salahub, D.; Malkin, V. G.; Malkina, O. L. *deMon/MASTER-JMN*, **1994**, Université de Montreal, Quebec, Canada.
- (24) http://www.demon-software.com/public_html/index.html
- (25) Malkin, V. G.; Malkina, O. L.; Salahub, D. R. *Chem. Phys. Lett.* **1996**, *261*, 335- 345.
- (26) Malkin, V. G.; Malkina, O. L.; Casida, M. E.; Salahub, D. R. *J. Am. Chem. Soc.* **1994**, *116*, 5898 - 5908.
- (27) Siehl, H.-U.; Backes, A. C.; Malkina, O. L. in *Organosilicon Chemistry IV*; Eds.: Auner, N.; Weis, J. Wiley-VCH: Weinheim, **2000**, p. 150 -157.
- (28) Siehl, H.-U.; Vrcek, V. Calculation of NMR Parameters in Carbocation Chemistry in: *Calculation of NMR and EPR Parameters: Theory and Applications*, Kaupp, M.; Malkin, V. G.; Bühl, M., Eds.; Wiley-VCH: Weinheim, **2004**; Chapter 23, p. 373 - 397.
- (29) *Vinyl cations*; Stang, P. J.; Rappoport, Z.; Hanack, M.; Subramanian, L.R., Eds., Academic Press: New York, **1979**.
- (30) *Dicoordinated Carbocations*; Rappoport, Z.; Stang, P. J., Eds.; Wiley: Chichester, New York, **1997**.
- (31) Hanack, M.; Subramanian, L. R. In *Houben-Weyl Methoden der organischen Chemie*, Hanack M., Ed.; Thieme: Stuttgart, **1990**; Vol. E19c, p. 97 - 250.
- (32) Siehl, H.-U. Ph.D. thesis, University of Saarbrücken, Saarbrücken, **1977**.
- (33) Masamune, S.; Sakai, M.; Morio, K. *Can. J. Chem.* **1975**, *53*, 784-786.
- (34) Siehl, H.-U.; NMR Spectroscopic Characterisation, In *Dicoordinated Carbocations*; Rappoport, Z.; Stang, P., Eds.; Wiley: New York, **1997**; Chapter 5, p. 189 - 236.
- (35) Siehl, H.-U.; Excursions into Long-Lived Vinyl Cations: NMR Spectroscopic Characterization α -Aryl Vinyl Cations, In *Stable Carbocation Chemistry*; Prakash, G.K.S.; Schleyer, P. v. R., Eds.; Wiley: New York, **1997**; Chapter 5, p. 165 - 196.
- (36) Siehl, H.-U. *Pure and Appl. Chem.* **1995**, *67*, 769 - 775.
- (37) Müller, T. Ph.D. thesis, University of Tübingen, Tübingen, **1993**.
- (38) Koch, E. - W.; Siehl H.- U.; Hanack, M. *Tetrahedron Lett.*, **1985**, *26*, 1493 - 1496.
- (39) Siehl, H.-U.; Kaufmann, F.-P. *J. Am. Chem. Soc.* **1992**, *114*, 4937 - 4939.
- (40) Kaufmann, F.-P. Diploma thesis, University of Tübingen, Tübingen, **1990**.
- (41) Bertsch, K. Diploma thesis, University of Tübingen, Tübingen, **1987**.

- (42) Siehl, H.-U.; Müller, B.; Fuß M.; Tsuji Y In *Organosilicon Chemistry II*; Auner N.; Weis J., Eds.; VCH: Weinheim, 1996; p. 361 – 366.
- (43) Müller, T.; Lennartz, R.; Siehl, H.-U. *Angew. Chem.* **2000**, *112*, 3203-3206; *Angew. Chem. Int. Ed. Engl.* **2000**, *39*, 3074 - 3077.
- (44) Siehl, H.-U.; Kaufmann, F.-P.; Apeloig, Y.; Braude, V.; Danovich D.; Berndt, A.; Stamatis, N. *Angew. Chem.* **1991**, *103*, 1546 - 1549; *Angew. Chem., Int. Ed. Engl.*, **1991**, *30*, 1479 - 1482.
- (45) Siehl, H.-U.; Müller, T.; Gauss, J.; Buzek, P.; Schleyer, P.v.R. *J. Am. Chem. Soc.* **1994**, *116*, 6384 - 6387.
- (46) Stanton, J. F.; Gauss, J.; Siehl, H.-U. *Chem. Phys. Lett.* **1996**, *262*, 183 - 186.
- (47) Siehl, H.- U.; Mayr, H. *J. Am. Chem. Soc.* **1982**, *104*, 909 - 910.
- (48) Siehl, H.-U.; Koch, E.-W. *J. Org. Chem.* **1984**, *49*, 575 - 576.
- (49) Siehl, H.-U.; Müller, T.; Gauss, J. *J. Phys. Org. Chem.* **2003**, *16*, 577 - 581.
- (50) Siehl, H.-U.; Brixner, S. *J. Phys. Org. Chem.* **2004**, *17*, 1039 -1045.
- (51) Siehl, H.- U. *J. Chem. Soc. Chem. Commun.* **1984**, 635 - 636.
- (52) Müller, T.; Juhasz, M.; Reed, C. A. *Angew. Chem.* **2004** *116*, 1569 - 1572; *Angew. Chem., Int. Ed. Engl.*, **2004**, *43*, 1543 - 1546.
- (53) Müller, T.; Margraf, D.; Syha, Y. *J. Am. Chem. Soc.* **2005**, *127*, 10852 - 10860.
- (54) Pittman jr, C. U. *J. Chem. Soc. Chem. Commun.* **1969**, *2*, 122-123.
- (55) Shiner Jr., V. J.; Ensinger, M. W.; Rutkowske, R. D. *J. Am. Chem. Soc.* **1987**, *109*, 804 - 809.
- (56) *The nonclassical Ion Problem* Brown, H. C. with comments by Schleyer, p. V. R.; Plenum Press: New York, **1977**; Chapter 5, p. 69 - 82.
- (57) Olah, G. A.; Prakash Reddy, V. P.; Surya Prakash, G. K. *Chem. Rev.* **1992**, *92*, 69 - 95
- (58) Olah, G. A.; Sommer, J.; Prakash, S. G. K. *Superacids*, John Wiley; New York, **1985**.
- (59) Lenoir, D.; Siehl H.-U. In *Houben-Weyl Methoden der organischen Chemie, Carbokationen*; Hanack, M., Ed.; Thieme: Stuttgart, **1990**; Bd E19c, p. 413 - 414;
- (60) Siehl, H.-U.: Cyclobutyl, cyclobutyl-substituted and related carbocations In *The Chemistry of Cyclobutanes*; Rappoport, Z., Liebman, J. F., Eds.; John Wiley: New York, **2005**; Chapter 12, p. 521 - 548
- (61) Olah, G. A.; Jeuell, C. L.; Kelly, D. P.; Porter, R. D. *J. Am. Chem. Soc.* **1972**, *94*, 146 - 156.
- (62) Saunders, M.; Siehl, H. - U. *J. Am. Chem. Soc.* **1980**, *102*, 6868 - 6869.
- (63) Brittain, W. J.; Squillacote, M. E.; Roberts, J. D. *J. Am. Chem. Soc.* **1984**, *106*, 7280-7282.
- (64) Siehl, H.- U. *J. Am. Chem. Soc.* **1985**, *107*, 3390 - 3392.
- (65) Siehl, H. - U. In *Physical Organic Chemistry 1986*; Kobayashi, M., Ed.; Elsevier: Amsterdam, NL, 1987; p 25 - 32.

- (66) Saunders, M.; Krause, N. *J. Am. Chem. Soc.* **1988**, *110*, 8050 - 8052.
- (67) Siehl, H.-U.; Fuß, M.; Gauss, J. *J. Am. Chem. Soc.* **1995**, *117*, p. 5983 - 5991.
- (68) Siehl, H. -U; Fuss, M. *Silyl effects in hypercoordinated carbocations* IN . *Organosilicon Chemistry IV, From Molecules to Materials* Editors: Auner, N.; Weis, J. **2000**, Wiley-VCH: Weinheim, p. 140 – 149.
- (69) Fuß, Martin Ph.D. thesis, Universität Tübingen, Tübingen, **1997**
- (70) Siehl, H. -U.; Fuss, M. *Pure and Applied Chemistry* **1998**, *70*, 2015 - 2022.
- (71). Staral, J. S.; Yavari, I.; Roberts J. D.; Prakash, G. K. S.; Donovan, D. J.; Olah, G. A. *J. Am. Chem. Soc.* **1978**, *100*, 8016 - 8018.
- (72) Saunders, M.; Laidig, K. E.; Wiberg K. B.; Schleyer, P. v. R. *J. Am. Chem. Soc.* **1988**, *110*, 7652 - 7659.
- (73) Koch, W.; Liu B.; DeFrees, D. J. *J. Am. Chem. Soc.* **1988**, *110*, 7325 - 7328.
- (74) McKee, M. L. *J. Phys. Chem.* **1986**, *90*, 4908 - 4910.
- (75) Schleyer, P. v. R.; Maerker, C.; Buzek P.; Sieber, S. In *Stable Carbocation Chemistry*, Prakash, G. K. S. , Schleyer, P. v. R., Eds.; John Wiley & Sons Inc.: New York, **1997**; Chapter 2, p. 47 - 54.

Chapter 2

Super-Stabilization of π -Conjugated Cations by Annelation to Bicyclic Frameworks

Koichi Komatsu^{1,2}

¹Institute for Chemical Research, Kyoto University, Uji, Kyoto 611-0011,
Japan

²Current address: Department of Environmental and Biotechnological
Frontier Engineering, Fukui University of Technology, Gakuen,
Fukui 910-8505, Japan

As exemplified by the synthesis of the extraordinarily stable tropylium ion, the annelation of cyclic π -conjugated cations with rigid σ -framework, bicyclo[2.2.2]octene, has been found to be an effective method for creation of unusually stable cationic π -conjugated systems. By using this method, detailed X-ray crystallographic studies have been conducted for the monomeric radical-cation salts of hydrocarbons such as cyclooctatetraene and a series of benzenoid condensed aromatics and of sulfur containing compounds such as thiophene, dithiins, and oligothiophenes. Some of these species can be further oxidized to dications, and also undergo intriguing rearrangements to cationic species with novel structures. The results are well interpreted by the use of theoretical calculations.

Introduction

In addition to the well-known textbook concepts such as inductive effects, π - π and n - π conjugation effects, the σ - π conjugation (C-C hyperconjugation) phenomenon should also be an effective method for thermodynamic stabilization of π -conjugated carbocations. Such effects, however, are regarded to be rather weak to become a major factor for cation stabilization, except in such a special case as cyclopropyl conjugation, which is highly effective owing to a large p-character in the strained C-C single bonds. In this article, we wish to show that such σ - π conjugation effect exerted by strain-free C-C bonds typically of bicyclo[2.2.2]octene can become significant in cation stabilization when the effects are accumulated in properly constructed molecular structures (1,2,3). This effect together with the steric protection by the bicyclic frameworks is, in fact, quite advantageous, allowing the formation of a wide range of novel cyclic π -conjugated systems bearing positive charge, which could not have been realized by other means.

Bicyclo[2.2.2]octenotropylium Ions

This study originated in 1987, when we found that relatively strain-free bicyclic systems such as bicyclo[2.2.2]octene (abbreviated as BCO throughout the present article) can greatly stabilize a typical cyclic π -conjugated carbocation, the tropylium ion, as shown in Table I for several di-substituted derivatives (Figure 1) (4,5): here the pK_{R^+} value is taken as the criterion of thermodynamic stability of the carbocation; the values of reduction potential show a similar tendency. The stabilization effect of one BCO unit is shown to be much larger than that of two *t*-butyl groups and even comparable to the effects of two cyclopropyl groups (4).

This unexpectedly large stabilization effect of the bicyclo[2.2.2]octene moiety in cation 4 is ascribed to the σ - π conjugation of the empty 2p orbitals in the tropylium ring with C_α - C_β single bonds in the bicycloalkene unit, in addition to the inductive effect. Cation 5 has a more strained bicyclo[2.1.1]hexene unit, which was expected to exhibit a stronger σ - π conjugation effect, owing to the higher p-character in this bicyclic unit. However, the pK_{R^+} value was shown to be much smaller than that of 4. This is supposed to be due to a considerable

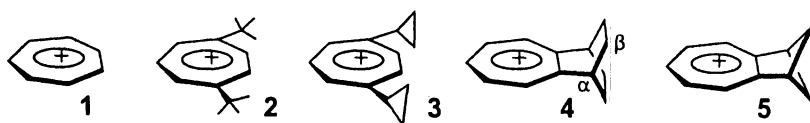


Figure 1. Typical di-substituted tropylium ions in Table I.

Table I. Values of pK_{R^+} and Reduction Potentials (E_{red}) for Disubstituted Tropylium Ions 1 – 5

<i>Cation</i>	$pK_{R^+}^a$	E_{red}^b
Unsubstituted tropylium ion (1) ^c	3.88	-0.51
1,4-Di- <i>t</i> -butyltropylium ion (2) ^c	5.42	-0.72
1,4-Dicyclopropyltropylium ion (3) ^c	7.63	-0.76
Bicyclo[2.2.2]octenotropylium ion (4) ^d	7.80	-0.765
Bicyclo[2.1.1]hexenotropylium ion (5) ^d	5.10	-0.71

^a Determined by direct UV-vis spectroscopic observation of the hydrolysis equilibrium in 50% aq MeCN.

^b Cathodic peak potential in V vs Ag/Ag⁺ measured in MeCN.

^c Ref. 4.

^d Ref. 5.

angle strain that is imposed to the seven-membered ring. This effect, which may be also called the Mills-Nixon effect, causes the homogeneous delocalization of a positive charge to become less effective in 5 (5).

This finding led us to prepare the tropylium ion fully annelated with the BCO units, that is, cation 6 (6). This cation exhibited the pK_{R^+} value of 13.0 in 50% MeCN, which is 9.12 pK unit (12.4 kcal/mol at 25 °C) greater than that of unsubstituted cation 1. The pK_{R^+} value of a hypothetical hexa-*t*-butyltropylium ion is estimated to be 8.5 by extrapolation of a linear correlation between the experimental pK_{R^+} value and the number of *t*-butyl group(s). If we assume that this stabilization is largely due to the inductive effect, the rest of the stabilization effect resulting from the σ - π conjugation effect in 6 could be estimated as 4.5 pK units, that is, 6.1 kcal/mol. More recently, tropylium ion 7 and triazulenylmethyl cation 8 having the pK_{R^+} values even larger than 6 are reported (7,8), and these constitute the most stable all-hydrocarbon cations known today (Figure 2).

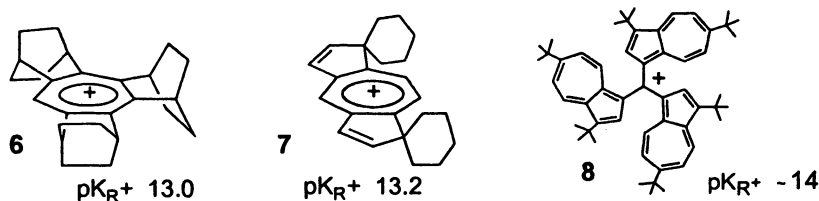


Figure 2. The most stable all-hydrocarbon carbocations with their pK_{R^+} values in 50% MeCN.

Tetrakis(bicyclo[2.2.2]octeno)cyclooctatetraene

Our success in super-stabilization of cation **6** led us to the preparation of a higher homologue, that is, cyclooctatetraene (COT), fully annelated with BCO units **9** (**9**). As compared with a large number of studies on its radical anion or dianions, the studies on the cationic species of COT have been quite limited. There have been only one study by Olah and Paquette on the substituted COT dication (**10**), which is a typical 6π Hückel aromatic system, and few sporadic studies on radical cations, which involve indirect spectral observations, such as electronic spectra in Freon matrix at low temperature (**11,12**) and constant-flow ESR study (**13**).

On the other hand, the HOMO level of COT **9** is raised due to the electronic effects of the BCO units to -4.87 eV (B3LYP/6-31G(d)//B3LYP/6-31G(d)) as compared with that of unsubstituted COT (-5.54 eV). This is reflected in the cyclic voltammogram, which exhibited two consecutive reversible oxidation waves at such low potentials as $+0.39$ V and $+1.14$ V vs Ag/Ag^+ in CH_2Cl_2 - $\text{CF}_3\text{CO}_2\text{H}$ - $(\text{CF}_3\text{CO})_2\text{O}$ (20:1:1) (**14**). In comparison, the parent COT only exhibits an irreversible oxidation peak at $+1.20$ V in acetonitrile. These results imply that the cationic species can be readily generated from COT **9**.

As expected, when one-electron oxidation was conducted on COT **9** with $\text{NO}^+\text{SbCl}_6^-$ in CH_2Cl_2 , the COT radical-cation salt, 9^+SbCl_6^- , was isolated for the first time, as air-stable dark-green crystals (Figure 3) (**15**). X-ray crystallography demonstrated that this radical cation has a tub-shaped eight-membered ring (Figure 4), as has been predicted theoretically (**16**). The molecular shape, including bent angles, is quite similar to that of the structure of the neutral molecule **9**, but the original double bond is elongated and the single bond shortened, reflecting the delocalization of the π -electronic system.

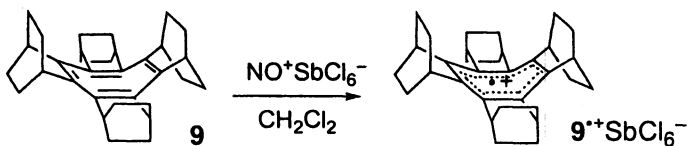


Figure 3. One-electron oxidation of BCO-COT **9**.

The radical cation 9^+ was further oxidized with SbF_5 to give the dication 9^{2+} , which is stable in CH_2Cl_2 (or CD_2Cl_2) at room temperature (**14**). This is much more stable than the previously reported sole examples of COT dications having two or four substituents 10^{2+} and 11^{2+} , which were observed only at low temperature (-78°C) in the SO_2ClF solution (**10**). The dication 9^{2+} exhibits only three ^{13}C NMR signals at δ 177.9, 41.0, and 23.9 ppm at room temperature, suggesting that the eight-membered ring might be planar. However, the signal

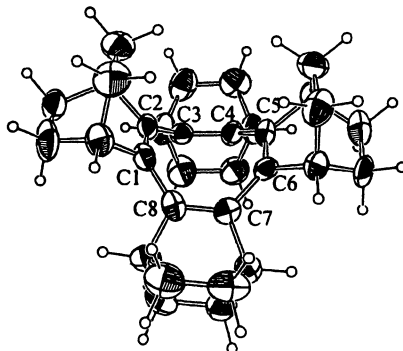


Figure 4. Molecular structure of radical cation salt 9^+SbCl_6^- (the anion is omitted for clarity). Selected bond lengths (Å) and angles (°) are: C1-C2, 1.389(10); C2-C3, 1.440(10); C3-C4, 1.356(10); C4-C5, 1.444(11); C5-C6, 1.377(10); C6-C7, 1.445(11); C7-C8, 1.338(11); C8-C1, 1.464 (10); C6-C7-C8, 126.1(7); C7-C8-C1, 127.9(7).

for the methylene carbon atoms of the ethano bridge was split into two signals at a low temperature ($-80\text{ }^\circ\text{C}$), indicating that the ground-state structure of this dication is in a tub form, which is undergoing rapid ring inversion with an energy barrier of $10.8\text{ kcal mol}^{-1}$ (Figure 5) (14).



Figure 5. COT dications 10^{2+} , 11^{2+} and ring inversion of dication 9^{2+} .

Condensed Aromatic Hydrocarbons Annulated with Bicyclo[2.2.2]octene Frameworks

We then focused our attention to the cationic species generated from a series of condensed aromatics fully annulated with BCO units. Newly synthesized naphthalene **12** (17), anthracene **13** (18), biphenylene **14** (19), and fluorene **15** (20) all underwent smooth one-electron oxidation by the use of 1.5

equivalents of SbCl_5 to give the SbCl_6^- salts of corresponding radical cations in high yields as deeply colored crystals, which are stable under air: deep-green for $12^{+\cdot}$ (λ_{max} (CH_2Cl_2) 690 and 761 nm), $13^{+\cdot}$ (λ_{max} 862 and 920 nm), and $15^{+\cdot}$ (absorption not measured), and deep-blue for $14^{+\cdot}$ (λ_{max} 563 and 608 nm). The most important point is that all these crystals of monomeric radical-cation salts are so stable as to allow the X-ray crystallography enabling the determination of their precise structures (Figure 7 and 8) (21). Here, we also urge the reader to refer to a series of significant studies by Kochi group, on monomeric and dimeric structures of methyl-substituted radical cations of naphthalene, biphenylene, and other aromatic compounds (22).

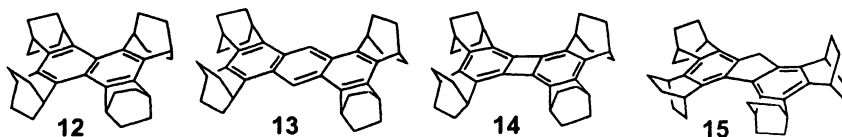


Figure 6. Naphthalene, anthracene, biphenylene, and fluorene annelated with BCO.

It was confirmed that the change in the π -bond lengths upon one-electron oxidation of 12–15 is systematically related to the coefficients of the relevant carbons' HOMO of the neutral molecules. The bonds with the bonding nature in the HOMO of the neutral molecules are elongated upon removal of one electron, and those with antibonding nature in HOMO are shortened.

It was also found that there is a tendency for characteristic changes in the averaged σ -bond lengths of the BCO frameworks involved in the σ - π conjugation. As shown in a simplified representation (Figure 9), the $\text{C}_{\text{Ar}}\text{-C}_{\alpha}$ bonds (*a* and *b*) should be antibonding in the HOMO of the neutral molecules, while the $\text{C}_{\alpha}\text{-C}_{\beta}$ bonds (*c* and *d*) should be bonding in nature. The bond lengths observed for the radical cations $12^{+\cdot}$ to $15^{+\cdot}$ and for the neutral precursors are shown in Table II. Here, it is seen that all of the $\text{C}_{\text{Ar}}\text{-C}_{\alpha}$ bonds are shortened (with an accidental exception for bond *a* in $14^{+\cdot}$), while all of the $\text{C}_{\alpha}\text{-C}_{\beta}$ bonds (*c* and *d*) are lengthened upon one-electron oxidation of the neutral molecules. Although the magnitudes are quite small, these systematic changes in σ -bond lengths can be taken as the experimental evidence for the presence of σ - π conjugation (C–C hyperconjugation) to stabilize these radical cations (21). A similar structural change in bond length has also been observed upon one-electron oxidation of adamantylideneadamantane and sesquihomoadamantene (23).

All these condensed aromatic hydrocarbons, naphthalene 12, anthracene 13, biphenylene 14, and fluorene 15, were found to undergo further two-electron

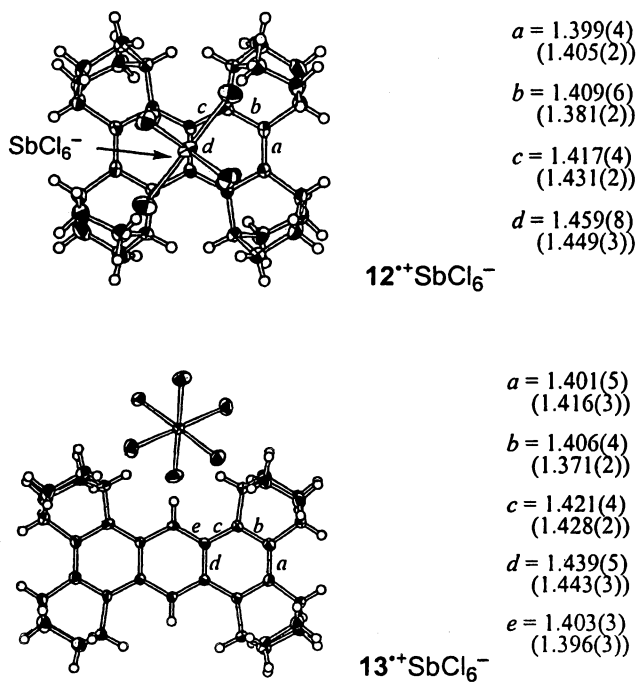


Figure 7. Molecular structures of 12⁺SbCl₆⁻ and 13⁺SbCl₆⁻ determined by X-ray crystallography, together with values of π -bond lengths in Å (those for neutral molecules in parentheses).

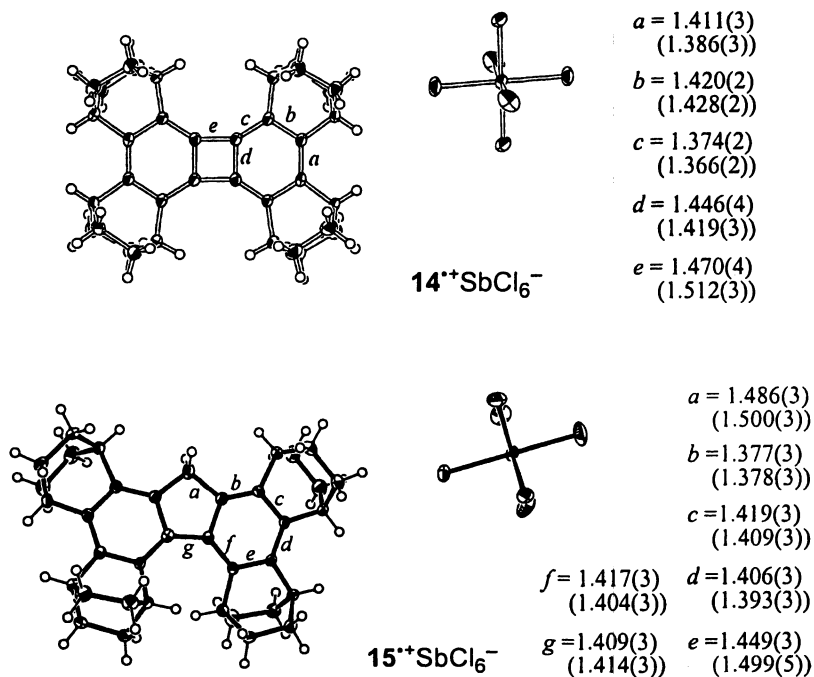


Figure 8. Molecular structures of 14^{+}SbCl_6^{-} and 15^{+}SbCl_6^{-} determined by X-ray crystallography, together with values of π -bond lengths in Å (those for neutral molecules in parentheses).

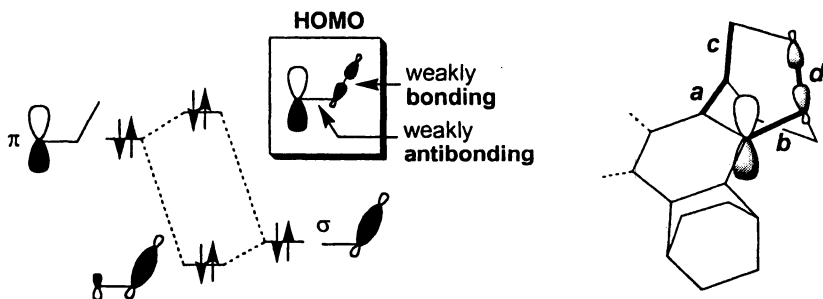


Figure 9. A simplified representation of the σ - π conjugation with a benzenoid π -system with BCO σ -bonds.

Table II. Bond Lengths (Å) of σ -Bonds in the BCO Units in **12 to **15** and in Radical-Cation Salts 12^{2+}SbCl_6^- to 15^{2+}SbCl_6^-**

<i>Compound</i>	<i>a</i>	<i>b</i>	<i>c</i>	<i>d</i>
12	1.518(2)	1.513(1)	1.537(2)	1.534(2)
12²⁺	1.508(5)	1.508(5)	1.541(4)	1.542(4)
13	1.510(2)	1.509(2)	1.531(2)	1.533(2)
13²⁺	1.496(4)	1.501(4)	1.544(3)	1.540(3)
14	1.498(2)	1.508(2)	1.533(2)	1.535(2)
14²⁺	1.505(2)	1.507(2)	1.545(2)	1.540(2)
15	1.508(2)	1.507(2)	1.543(2)	1.542(2)
15²⁺	1.505(4)	1.501(4)	1.547(5)	1.543(5)

^a Since there are two kinds of non-equivalent BCO groups in **15**, the values of the bond lengths are averaged for convenience.

oxidation to give corresponding dications by treatment with an excessive amount of SbF_5 or SbCl_5 in CD_2Cl_2 in a vacuum-sealed tube at low temperature (-78°C) (17,18,19,20). The dications were characterized by ^1H and ^{13}C NMR. It was shown that the ^1H NMR signals for the BCO units' bridgehead protons, which are located in the same plane as the π -systems, undergo upfield shift for **12** (10 π -electron) by 0.58 and 0.80 ppm and **13** (14 π -electron) by 0.54 and 0.27 ppm upon going from the neutral compounds to dications, reflecting the change from the Hückel aromatic $[4n+2]$ π systems to antiaromatic $[4n]$ π systems (21). Accordingly, the reverse tendency, i.e., downfield shift by 1.19 and 1.32 ppm, was observed for the 12 π -electron system **14** (24).

In the case of fluorene **15**, the ^{13}C NMR signal for C-2,7 of the dication exhibited a large down-field shift of 65 ppm (C-2,7; δ 202.7 ppm) as compared with neutral **15**, indicating the significant contribution of the quinoid structure such as $15^{2+}(\text{Q})$ (Figure 10) (20).

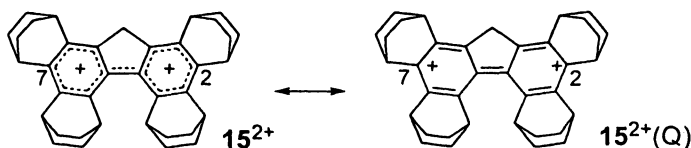


Figure 10. Resonance structure of dication 15^{2+} .

It was expected that a triphenylene derivative similarly annelated with BCO units **16** could also give a stable radical-cation salt. In fact, purple crystals were obtained from the solution of $16^{+\cdot}\text{SbCl}_6^-$ in CH_2Cl_2 . However, the X-ray crystallography (Figure 11) indicated that this is not the radical-cation salt but the spirocyclic arenium-ion salt 17^+SbCl_6^- (**25**). This resulting novel arenium ion salt is stable as a solid at room temperature for several months without any decomposition. This stability can be ascribed, in addition to the σ - π conjugation effect, to the spiro-conjugation effect of the fluorenyl unit, since theoretical calculations (B3LYP/6-31 G(d)) indicated that the coefficients of HOMO and LUMO are delocalized into both fluorene and arenium-ion moieties.

The transformation from the radical cation to arenium ion is proposed to proceed in the manner shown in Figure 12. Here, the release of strain, which is calculated to be 42.9 kcal/mol at the B3LYP/6-31G(d) level, accompanying the contraction of the central six-membered ring to the five-membered ring, is considered to be an important driving force for this rearrangement.

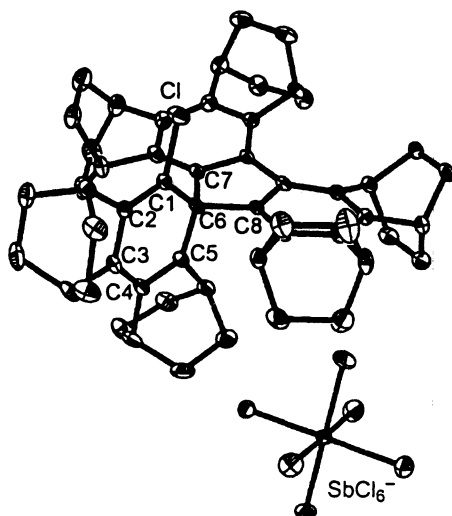


Figure 11. Molecular structure of arenium-ion salt 17^+SbCl_6^- . Hydrogen atoms are omitted for clarity. Selected bond lengths (\AA) and angles ($^\circ$) are: C1-C2, 1.363(4); C2-C3, 1.432(5); C3-C4, 1.394(5); C4-C5, 1.388(4); C5-C6, 1.475(5); C1-C6, 1.489(5); C1-Cl, 1.705(4); C6-C7, 1.545(5); C6-C8, 1.555(5); C7-C6-C8, 100.3(3).

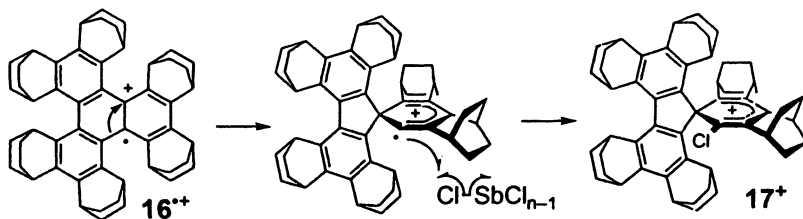


Figure 12. Possible mechanism for the transformation of radical cation $16^{+\bullet}$ to arenium cation 17^+ .

Sulfur-Containing Conjugated π -Systems Annulated with Bicyclo[2.2.2]octene Frameworks

Thiophene

The methodology for stabilization of π -conjugated cations by annulation with BCO units can be extended to other systems such as those containing sulfur atom(s). The most basic compound among such systems, thiophene **18**, was synthesized and was treated with 1.5 equivalents of either SbCl_5 or SbF_5 to give a yellow solution of radical-cation salt $18^{+\bullet}\text{SbX}_6^-$ ($\text{X} = \text{Cl}$ or F), which was identified by a five-line ESR signal ($a_{\text{H}} = 0.346$ mT, $g = 2.00215$) due to the coupling with four equivalent protons. This is in agreement with theoretical calculations indicating that the spin is localized mostly on the carbons at 2,5-positions (26). Although the single crystal was obtained and the X-ray crystallography showed its general structure as a salt, the precise structure can not be discussed because of too much disorder.

Reflecting the high spin density at the 2,5-positions, radical cation $18^{+\bullet}$ reacted with triplet oxygen smoothly in CH_2Cl_2 , possibly according to the mechanism shown in Figure 13, to give SbX_6^- ($\text{X} = \text{Cl}$ or F) as a novel proton-chelating cation 19^+ in 54 to 55% yield. The structure of 19^+SbF_6^- was unambiguously determined by X-ray crystallography as shown in Figure 14 (26). The salts, isolated as pale yellow crystals, were remarkably stable so that no decomposition was observed upon standing under air for several days. Among the NMR data of the cation 19^+ , it is noteworthy that the ^1H NMR signal of the chelated proton is observed at such a low field as 21.15 ppm. This is a good indication that the proton not only carries an almost full positive charge but is subjected to the strong deshielding effect of two carbonyl groups.

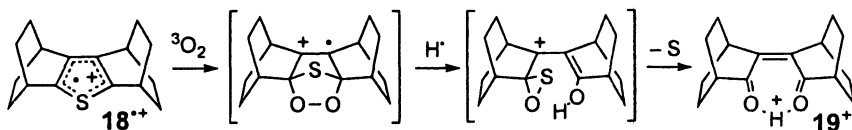


Figure 13. Possible mechanism for the transformation of 18^{2+} to 19^+ .

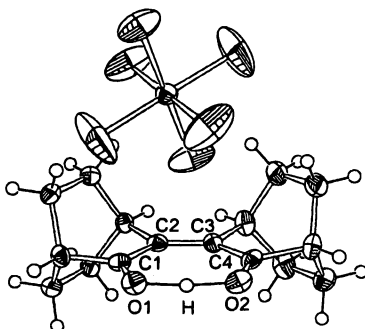


Figure 14. The X-ray structure of carbocation salt 19^+SbF_6^- . Selected bond lengths (Å) and angles (°) are: C1-C2, 1.489(4); C2-C3, 1.355(4); C3-C4, 1.480(4); C1-O1, 1.243(3); C4-O2, 1.252(3); O1-C1-C2, 126.4(3); C1-C2-C3, 126.2(3).

Dithiins

Dithiins are the six-membered π -conjugated systems containing two sulfur atoms at either 1,2- or 1,4-positions. Since they are 8π -electron systems isoelectronic to COT, the derivatives annelated with two BCO units, **20** and **21**, readily undergo two-electron oxidation with excessive SbF_5 in CH_2Cl_2 (or CD_2Cl_2) to give yellow solutions of the corresponding dications, 20^{2+} and 21^{2+} (Figure 15) (27,28). The aromatic character of the resulting 6 π -electron systems are clearly shown by nearly 2-ppm downfield shift of the ^1H NMR signal(s) for the BCO bridgehead protons, which are fixed at the same plane as the resulting aromatic π -systems.

The behavior of dithiins, highly characteristic of the annelation with BCO units, are demonstrated by the results of their one-electron oxidation as described below.

The one-electron oxidation of 1,2-dithiin **20** with 1.5 equivalent of SbCl_5 under vacuum at room temperature gave a bright yellow solution that exhibited a nine-line ESR signal. The optimized structure obtained by theoretical calculations (B3LYP/6-31G(d)) for the radical cation $20^{+\cdot}$ was the one with a

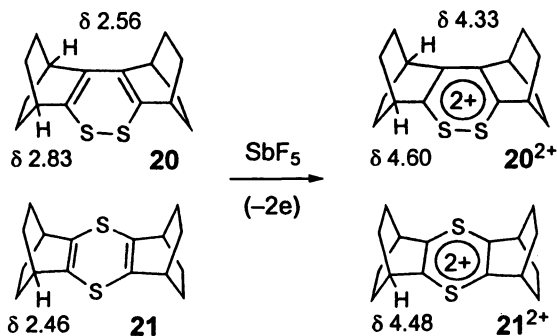


Figure 15. Two-electron oxidation of 1,2-dithiin **20** and 1,4-dithiin **21** with the ^1H NMR chemical shifts (ppm) of the bridgehead protons.

planar π -system. The ESR signal simulated using the spin densities at the two sets of four equivalent *anti*-protons of the BCO units reproduced the observed signal quite well (27).

Whereas the CH_2Cl_2 solution of $\mathbf{20}^{2+}$ in a low concentration (4×10^{-4} M) was quite stable, the radical cation was found to undergo an unexpected disproportionation reaction in a higher concentration (0.06 M). Thus, after about 5 min at room temperature, there were obtained thiophene **18** (29%), the 2-butene-1,4-dione derivative formed by deprotonation of cation $\mathbf{19}^+$ (23%), and orange-colored crystals identified as a SbCl_6^- salt of a radical cation having a novel 2,3,5,6-tetrathiabicyclo[2.2.2]oct-7-ene structure $\mathbf{22}^{2+}$ by X-ray crystallography (Figure 16) in 32% yield (27). This salt was remarkably stable and showed no decomposition upon standing under air for at least one week. The formation of this cation is considered to be a result of the reaction of disulfur, extruded upon disproportionation, with the 2,5-positions of the radical cation $\mathbf{20}^{2+}$.

In radical cation $\mathbf{22}^{2+}$, the two disulfide linkages are fixed in close proximity to each other. The averaged distance of $\text{S1}\cdots\text{S3}$ and $\text{S2}\cdots\text{S4}$ is 2.794(3) Å. This is much shorter than the sum of the van der Waals radii of a sulfur atom (3.70 Å), suggesting the presence of a strong transannular interaction between these sulfur atoms. The optimized structure of $\mathbf{22}^{2+}$ calculated at the UB3LYP/6-31G* level reproduced the observed structure fairly well, with the calculated distance of $\text{S1}\cdots\text{S3}$ and $\text{S2}\cdots\text{S4}$ being 2.923 Å. The calculation also indicated that spin and charge of radical cation $\mathbf{22}^{2+}$ are almost exclusively delocalized on four sulfur atoms: the spin and Mulliken charge on each of the four sulfur atoms are 0.229 and +0.258, respectively. This can account for the unusual stability of this novel cationic system.

The 1,4-dithiin annelated with two BCO units **21** also undergoes ready one-electron oxidation with 1.5 equivalents of SbF_5 in CH_2Cl_2 to give radical cation salt $\mathbf{21}^{2+}\text{SbF}_6^-$ in 67% yield as brown-colored single crystal, which was stable

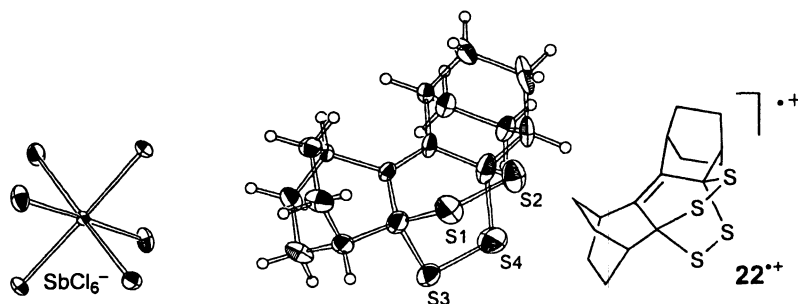


Figure 16. The molecular structure of the radical cation 22^+SbCl_6^- having a 2,3,5,6-tetrathiabicyclo[2.2.2]oct-7-ene structure, determined by X-ray crystallography.

under air without any decomposition after several days. The X-ray crystallography on this salt indicates that the dithiin ring is planar with marked shortening of the C–S bond as compared with that of neutral **21** as shown in Figure 17 (29).

A CH_2Cl_2 solution of 21^{++}SbF_6^- at a low concentration ($\sim 10^{-5}$ M) showed a nine-line ESR signal by coupling with eight equivalent *anti*-protons ($a_{\text{H}} = 0.08$ mT, $g = 2.0083$). In a higher concentration spectrum ($\sim 10^{-3}$ M), the hyperfine splitting was lost but the signal caused by $M_S = \pm 3/2$ of ^{33}S (natural isotopic abundance, 0.75%) became observable. The obtained value of a_{S} was 0.86 mT (29), which was smaller than that (0.92 mT) for thianthrene radical cation (23^{++}) (30). This result indicates that the spin density on the sulfur atom of 21^{++} is lower than that of 23^{++} and therefore the BCO units are even more effective than the fused benzene rings in delocalizing not only the positive charge but also spin density.

Oligothiophenes

Finally, it would be pertinent here to demonstrate that the present methodology of cation stabilization can be successfully applied to the preparation of a series of radical-cation salts and dication salts of oligothiophenes (2T, 3T, 4T, and 6T), fully annelated with BCO units, **24**, **25**, **26**, and **27** (Figure 18) (31,32).

The radical cations and dications of oligothiophene are important as models of polaron and bipolaron of the p-doped state of polythiophenes (33,34,35). However, detailed studies on the precise structures of these species are rather limited. The X-ray crystal structure of the radical-cation salt of terthiophene end-capped with phenyl groups (36,37) has been reported where the formation of so-called π -dimers was discussed in detail. In the case of BCO-annelated oligothiophenes **24**, such π - π interaction is inhibited by steric hindrance, and, as such, their properties are of great significance for investigation of cationic oligothiophenes as single molecules (38).

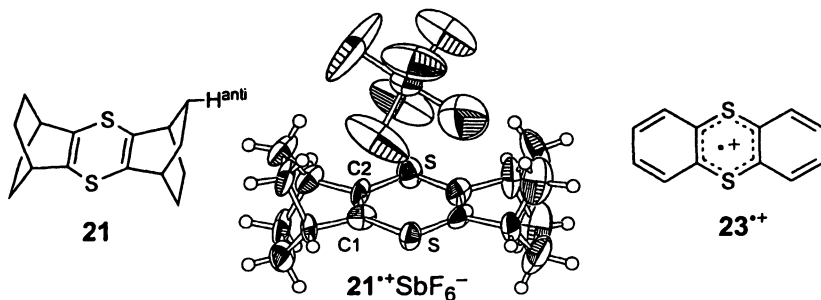


Figure 17. 1,4-Dithiin **21** and the molecular structure of its radical-cation salt **21⁺SbF₆⁻** determined by X-ray crystallography. The observed lengths (Å) of C1-S and C1-C2 in **21⁺SbF₆⁻** are 1.72(1) and 1.31(2) to be compared with 1.324(3) and 1.760(2) determined for neutral **21**, respectively. Also shown is the thianthrene radical cation **23⁺**.

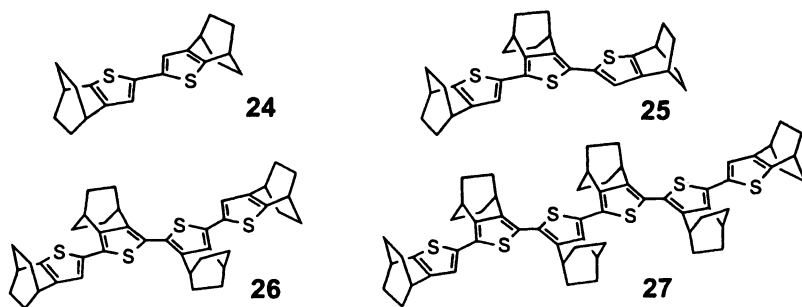


Figure 18. Oligothiophenes fully annelated with BCO units.

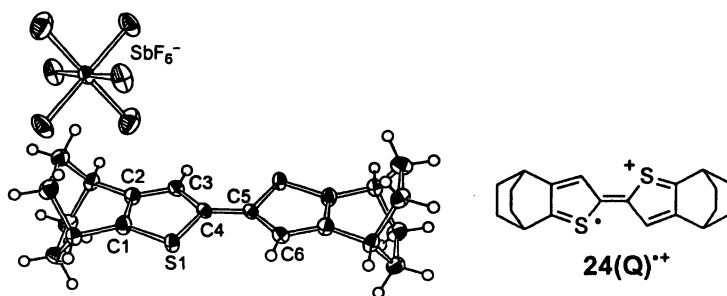


Figure 19. Molecular structure of the radical-cation salt **24⁺SbF₆⁻** (and representation of its quinoid form **24(Q)⁺**). Selected bond lengths (Å) and angles (°) are: S1-C1, 1.696(5); C1-C2, 1.408(6); C2-C3, 1.371(6); C3-C4, 1.403(6); C4-S1, 1.752(4); C4-C5, 1.398(8); C3-C4-C5-C6, 180.0.

As expected, one-electron oxidation of dimer **24** and timer **25** with one equivalent of $\text{NO}^+\text{SbF}_6^-$ in CH_2Cl_2 under vacuum took place smoothly and afforded single crystals of radical cation salts $\mathbf{24}^{+\cdot}\text{SbF}_6^-$ and $\mathbf{25}^{+\cdot}\text{SbF}_6^-$ as deep-green and deep-purple crystals in 61% and 73% yields, respectively (32). These crystals are so stable that they did not show any decomposition even after being left at room temperature under air for one month. The X-ray crystallography of the salt $\mathbf{24}^{+\cdot}\text{SbF}_6^-$ conducted for the first time for bithiophene, demonstrated that the π -system is completely planar with a significant contribution by the quinoid structure $\mathbf{24}(\text{Q})^{+\cdot}$ as shown in Figure 19 (32).

Similarly, the molecular structure was determined for timer $\mathbf{25}^{+\cdot}\text{SbF}_6^-$, which has the inter-ring bonds C4-C5 and C8-C9 with a little larger twisting (Figure 20) (32).

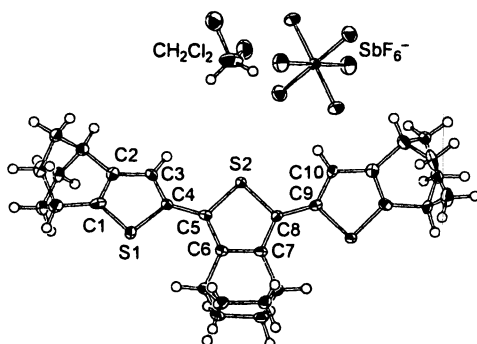


Figure 20. Molecular structure of the radical-cation salt $\mathbf{25}^{+\cdot}\text{SbF}_6^-$. Selected bond lengths (Å) and angles (°) are: S1-C1, 1.697(6); C1-C2, 1.394(9); C2-C3, 1.389(11); C3-C4, 1.390(11); C4-S1, 1.761(6); C4-C5, 1.421(9); C5-C6, 1.424(9); C6-C7, 1.389(9); C7-C8, 1.418(9); C8-S2, 1.747(6); S2-C5, 1.751(6); C8-C9, 1.436(9); C3-C4-C5-C6, $-155.5(8)$, C7-C8-C9-C10, $-149.4(8)$.

In the case of tetramer **26** and hexamer **27**, the similar treatment with two equivalents of $\text{NO}^+\text{SbF}_6^-$ afforded the corresponding dication salts $\mathbf{26}^{2+}\text{2SbF}_6^-$ and $\mathbf{27}^{2+}\text{2SbF}_6^-$ as dark green crystals with gold luster in 46% and 73% yield, respectively.

The X-ray crystallography, conducted for the first time for the dications of oligothiophenes, again indicated that the π -system of the terthiophene dication $\mathbf{26}^{2+}\text{2SbF}_6^-$ is completely planar with all the thiophene rings in *anti* conformation as shown in a side view in Figure 21 (a). This is quite similar to the case of the radical cation of the dimer $\mathbf{25}^{+\cdot}$ probably because the amount of positive charge per one thiophene ring is the same in both cases. In contrast, the planarity decreases in the sexithiophene dication $\mathbf{27}^{2+}\text{2SbF}_6^-$ as shown by the side view of the X-ray structure in Figure 21 (b). Upon comparison of the C-C bond length in the π -system of dication $\mathbf{27}^{2+}$, $\text{C}_\alpha\text{-C}_\beta$ bonds (1.370(14) and 1.393(14) Å) in the terminal thiophene ring were found to be shorter than the

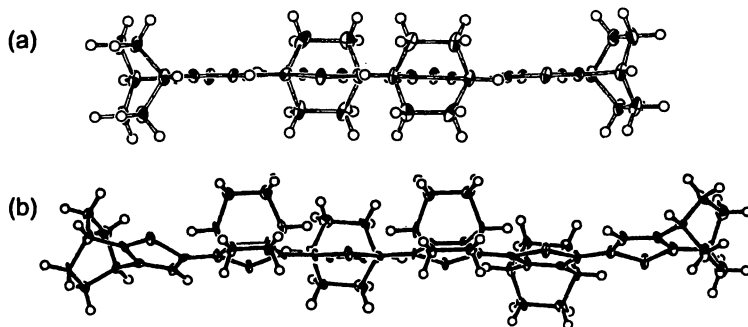


Figure 21. Molecular structures (side views) of (a) dication salt 26^{2+}SbF_6^- and (b) dication salt 27^{2+}SbF_6^- . The anions are omitted for clarity.

$\text{C}_\beta\text{-C}_\beta$ bond (1.419(14) Å) while the former become longer than the latter in the rings closer to the center of the molecule. This indicates that the electronic structure of the terminal rings is closer to that of neutral thiophene, while the quinoidal character becomes greater in the rings closer to the central position.

Summary

It has been found that the structural modification of various cyclic π -conjugated systems by full annelation with BCO (bicyclo[2.2.2]octene) units is remarkably effective in stabilization of the cationic systems derived therefrom. Thus, the cationic species, which could not be prepared by any other method have been realized by this methodology and even characterized by X-ray crystallography. Among these are hydrocarbon π -systems such as condensed aromatics and COT as well as the sulfur-containing systems such as thiophene, dithiins, and oligothiophenes. Results of the present work have revealed that the σ - π interaction (C-C hyperconjugation), which has been considered as a relatively weak interaction because of generally large separation of energy levels between the relevant σ - and π -molecular orbitals, can actually exert significant contribution to stabilize the cationic species, if the interacting σ -bonds are rigidly fixed in a desirable arrangement. This result would be useful for the design and creation of yet unknown cationic species for further fundamental and application oriented studies.

References

1. Komatsu, K. *Bull. Chem. Soc. Jpn. (Accounts)* **2001**, *74*, 407.
2. Komatsu K.; Nishinaga, T. *Synlett*, **2005**, 187.

3. Komatsu, K. *Pure & Appl. Chem.* **2006**, *78*, 685.
4. Komatsu, K.; Takeuchi, K.; Arima, M.; Waki, Y.; Shirai, S.; Okamoto, K. *Bull. Chem. Soc. Jpn.* **1982**, *55*, 3257.
5. Komatsu, K.; Akamatsu, H.; Okamoto, K. *Tetrahedron Lett.* **1987**, *28*, 5889.
6. Komatsu, K.; Akamatsu, H.; Junbu, Y.; Okamoto, K. *J. Am. Chem. Soc.* **1988**, *110*, 633.
7. Oda, M.; Kainuma, H.; Uchiyama, T.; Miyatake, R.; Kuroda, S. *Tetrahedron*, **2003**, *59*, 2831.
8. Ito, S.; Morita, N.; Asao, T. *Bull. Chem. Soc. Jpn.* **1995**, *68*, 1409.
9. Komatsu, K.; Nishinaga, T.; Aonuma, S.; Hirosawa, C.; Takeuchi, K.; Lindner, H. J.; Richter, J. *Tetrahedron Lett.*, **1991**, *32*, 6767.
10. Olah, G. A.; Staral, J. S.; Liang, G.; Paquette, L. A.; Melega, W. P.; Carmody, M. J. *J. Am. Chem. Soc.* **1977**, *99*, 3349.
11. Shida, T.; Iwata, S. *J. Am. Chem. Soc.* **1973**, *95*, 3473.
12. Dai, S.; Wang, J. T.; Williams, F. *J. Am. Chem. Soc.* **1990**, *112*, 2837.
13. Dessau, R. M. *J. Am. Chem. Soc.* **1970**, *92*, 6356.
14. Nishinaga, T.; Komatsu, K.; Sugita, N. *Chem. Commun.* **1994**, 2319.
15. Nishinaga, T.; Komatsu, K.; Sugita, N.; Lindner, H. J.; Richter, J. *J. Am. Chem. Soc.* **1993**, *115*, 11642.
16. Dewar, M. J. S.; Harget, A.; Haselbach, E. *J. Am. Chem. Soc.* **1969**, *91*, 7521.
17. Matsuura, A.; Nishinaga, T.; Komatsu, K. *Tetrahedron Lett.* **1999**, *40*, 123.
18. Matsuura, A.; Nishinaga, T.; Komatsu, K. *Tetrahedron Lett.* **1997**, *38*, 3427.
19. Matsuura, A.; Nishinaga, T.; Komatsu, K. *Tetrahedron Lett.* **1997**, *38*, 4125.
20. Nishinaga, T.; Inoue, R.; Matsuura, A.; Komatsu, K. *Org. Lett.*, **2002**, *4*, 4117.
21. Matsuura, A.; Nishinaga, T.; Komatsu, K. *J. Am. Chem. Soc.* **2000**, *122*, 10007.
22. Kochi, J. K.; Rathore, R.; Le Maguères, P. *J. Org. Chem.* **2000**, *65*, 6826, and the references cited therein.
23. Rathore, R.; Lindeman, S. V.; Zhu, C.-J.; Schleyer, P. v. R.; Kochi, J. K. *J. Org. Chem.* **2002**, *67*, 5106.
24. Matsuura, A. Ph.D. thesis, Kyoto University, Kyoto, Japan. 2001.
25. Nishinaga, T.; Inoue, R.; Matsuura, A.; Komatsu, K. *Org. Lett.*, **2002**, *4*, 1435.
26. Wakamiya, A.; Nishinaga, T.; Komatsu, K. *Chem. Commun.* **2002**, 1192.
27. Wakamiya, A.; Nishinaga, T.; Komatsu, K. *J. Am. Chem. Soc.* **2002**, *124*, 15038.
28. Nishinaga, T.; Wakamiya, A.; Komatsu, K. *Chem. Commun.* **1999**, 777.
29. Nishinaga, T.; Wakamiya, A.; Komatsu, K. *Tetrahedron Lett.* **1999**, *40*, 4375.

30. Sullivan, P. D. *J. Am. Chem. Soc.* **1968**, *90*, 3618.
31. Wakamiya, A.; Yamazaki, D.; Nishinaga, T.; Kitagawa, T.; Komatsu, K. *J. Org. Chem.* **2003**, *68*, 8305.
32. Nishinaga, T.; Wakamiya, A.; Yamazaki, D.; Komatsu, K. *J. Am. Chem. Soc.* **2004**, *126*, 3163.
33. Hotta, S. In *Handbook of Organic Conductive Molecules and Polymers*; Nalwa, H. S., Ed.; Wiley: Chichester, 1997; Vol. 2, Chapter 8.
34. Bäuerle, P. In *Electronic Materials: The Oligomeric Approach*; Mullen, K., Wegner, G., Eds.; Wiley-VCH: Weinheim, 1998; Chapter 2.
35. *Handbook of Oligo- and Polythiophenes*; Fichou, D., Ed.; Wiley-VCH: Weinheim 1999.
36. Graf, D. D.; Campbell, J. P.; Mann, K. R.; Miller, L. L. *J. Am. Chem. Soc.* **1996**, *118*, 5480.
37. Graf, D. D.; Duan, R. G.; Campbell, J. P.; Miller, L. L.; Mann, K. R. *J. Am. Chem. Soc.* **1997**, *119*, 5888.
38. Nishinaga, T.; Komatsu, K. *Org. Biomol. Chem. (Perspective)*, **2005**, *3*, 561.

Chapter 3

Unusually Stable Vinyl Cations

Thomas Müller¹, Dominik Margraf², Yvonne Syha²,
Hamid Reza Nasiri², Christian Kaiser², Rita Maier²,
Bettine Boltres², Mark Juhasz³, and Christopher A. Reed³

¹Institut für Reine und Angewandte Chemie der Carl von Ossietzky,
Universität Oldenburg, D-26211 Oldenburg, Germany

²Institut für Anorganische und Analytische Chemie der Goethe, Universität
Frankfurt, D-60439 Frankfurt/Main, Germany

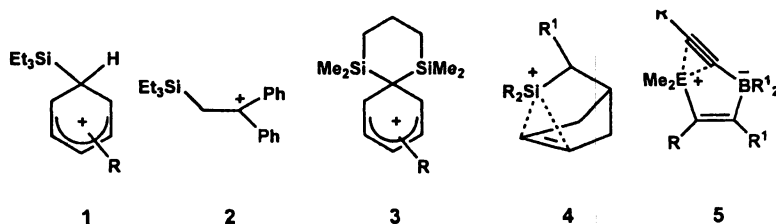
³Department of Chemistry, University of California,
Riverside, CA 92521-0403

Recent results on the chemistry of persistent vinyl cations are summarized. β , β -Disilyl-substituted vinyl cations were synthesized by intramolecular addition of transient silylium ions to alkynes. The vinyl cations are stable at ambient temperature and were isolated in the form of their tetrakis(pentafluorophenyl)borate and hexabromocboranate salts. The vinyl cations were characterized by IR and NMR spectroscopy and by X-ray crystallography. The experimental results for the α -alkyl- and α -aryl-substituted vinyl cations confirm their Y-shape structures, consisting of a linear dicoordinated, formally positively charged α -carbon atom and a trigonal planar coordinated β -carbon atom. In addition, the spectroscopic data clearly indicate the consequences of, β -silyl hyperconjugation in these vinyl cations. Scope and limitations of the synthetic approach to vinyl cations via addition of silylium ions to C \equiv C triple bonds are discussed.

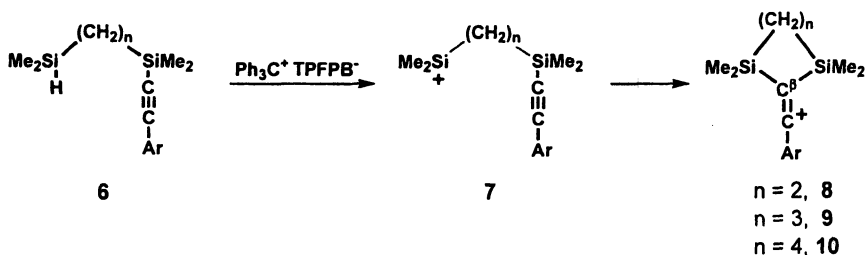
Introduction

Vinyl cations (*1*), the dicoordinated unsaturated analogues of trivalent carbenium ions, were first detected by Grob and coworkers in the early 1960s in solvolysis reactions of α -arylvinyl halides. (*2, 3*) In the 1970s, numerous investigations established vinyl cations as transient intermediates in solvolysis reactions of activated alkenyl halides (*4, 5*), and of alkenes bearing superleaving groups like the triflate, nonaflate or phenyliodonio groups. (*6-8*) Similarly, the addition of electrophiles to alkynes and allenes was shown to proceed via vinyl cations. (*9*) A landmark in the chemistry of stable vinyl cations was their direct NMR detection under superacidic reaction conditions at temperatures below $-100\text{ }^{\circ}\text{C}$, which was achieved in the early 1990s by Siehl and co-workers. In combination with quantum mechanical computations, their work provided important information concerning structures and the electronic properties of persistent vinyl cations. (*10-18*) The major drawback of this conventional approach via superacids, like $\text{FSO}_3\text{H/SbF}_5$, is the high oxidation potential and the reactivity of the applied Lewis acid, SbF_5 , which leads in the case of vinyl cations to rearranged products or decomposition at temperatures higher than -100°C . (*16, 18*) In the case of silyl-substituted carbocations, the omnipresence of sources for fluoride ions in the superacidic reaction media leads to facile desilylation. (*10-15*) Although, this was ingeniously used for the generation of silicon free carbocations, (*12*) the thermodynamic stabilization by the β -silyl group, however, was lost.

On the other hand, the progress in silylium ion chemistry led to a new route for the synthesis of stable carbocations in arene solvents. (*19-21*) The reaction of transient silylium ions with arenes in the presence of weakly coordinating anions leads to the formation of silylated arenium ions of type **1** which in one case was also structurally characterized. (*22-24*), see also (*25-27*)) These arenium ions **1** were used to transfer a trialkylsilylium ion equivalent to alkenes which results in the formation of stable β -silyl-substituted carbocations such as **2**. (*28-30*) Similarly, in the intramolecular reaction of transient silylium ions with distant aryl groups bissilylated arenium ions of type **3** are formed and with the $\text{C}=\text{C}$ double bond in cyclopentenylmethyl derivatives silanorbornyl cations **4** are formed. (*31, 32*) The carbocations formed in these reactions are stable at ambient temperatures in solution with arenes and could be isolated in many cases as salts of weakly coordinating anions such as tetrakis(pentafluorophenyl) borate (TPFPB). In particular, no desilylation occurs in the absence of nucleophiles. That this general reaction scheme can be in principle extended to the synthesis of stable vinyl cations was demonstrated previously by Wrackmeyer and co-workers. This group synthesized the interesting zwitterions **5**, and the X-ray analysis revealed an intriguing structure in which trivalent stannylum and plumbylum ions are stabilized by intramolecular side-on coordination to $\text{C}\equiv\text{C}$ triple bonds. (*33, 34*) Alternatively, these ions can be regarded as stannyl- or plumbyl-substituted vinyl cations.



On the basis of these results we embarked on a systematic study on the synthesis of vinyl cations by intramolecular addition of transient silylium ions to $C\equiv C$ -triple bonds using alkynyl substituted disila alkanes **6** as precursors.⁽³⁵⁻³⁷⁾ In a hydride transfer reaction with trityl cation the alkynes **6** are transformed into the reactive silylium ions **7**. Under essentially non-nucleophilic reaction conditions, i.e. in the presence of only weakly coordinating anions and using aromatic hydrocarbons as solvents, the preferred reaction channel for cations **7** is the intramolecular addition of the positively charged silicon atom to the $C\equiv C$ triple bond which results in the formation of vinyl cations **8-10** (Scheme 1).



Ar = phenyl (a), tolyl (b), 4-ethylphenyl (c), 2,4-dimethylphenyl (d), 2,5-dimethylphenyl (e), 3,5-dimethyl-phenyl (f), p-biphenyl (g), 2-fluorophenyl (h), 3-fluorophenyl (i), 4-fluorophenyl (k), 4-chlorophenyl (l).

Scheme 1. Synthesis of aryl-substituted vinyl cations 8-10

Results and Discussion

Synthesis and Spectroscopic Characterization

A series of α -aryl-substituted vinyl cations were synthesized at ambient temperatures according to the reactions summarized in Scheme 1.^(35, 37) In all cases the hydride transfer reaction proceeded rapidly at room temperature and the resulting vinyl cation TFPFB salts were isolated as red to brown oils or

glassy amorphous solids in high yields. The TFPFB salts of the vinyl cations are not soluble in hydrocarbons, and they form liquid clathrates with aromatic hydrocarbons. Clathrates prepared from benzene- d_6 or toluene- d_8 were used for NMR investigations. The high concentrations of the vinyl cations in the clathrate allow a fast and detailed characterization of the vinyl cations. As a typical example demonstrating the quality of the obtained spectra, the ^{13}C NMR of the salt **9b**•TFPFB in toluene at 283 K is shown in Figure 1 and characteristic NMR parameters of the aryl-substituted vinyl cations **8-10** are summarized in Table 1.

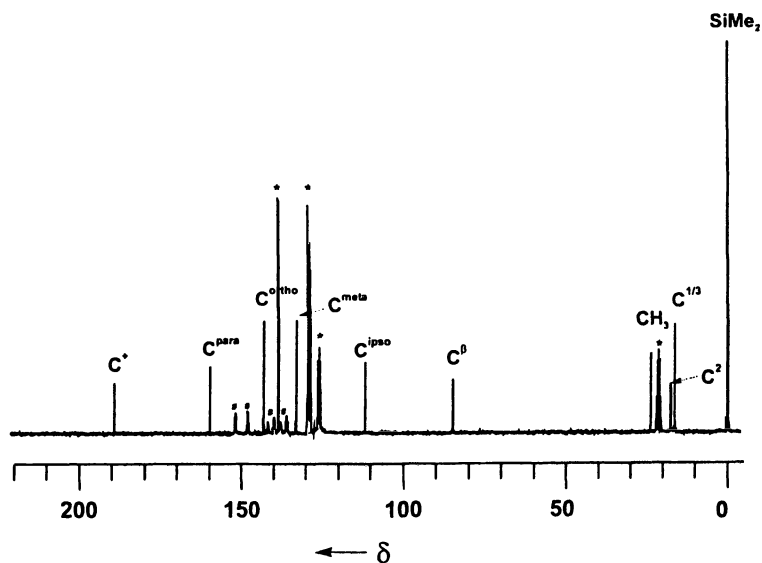


Figure 1. 62.9 MHz ^{13}C NMR spectra of the salt **9b**•TFPFB in toluene- d_8 at 273K (# TFPFB anion, * toluene- d_8).

The obtained ^{13}C and ^{29}Si NMR data do not vary significantly with the solvent as long as aromatic hydrocarbons are used. That is the maximum solvent effect on ^{13}C NMR chemical shift, $\Delta\delta^{13}\text{C}^{\text{solv}}$, for cation **9a** is $\Delta\delta^{13}\text{C}^{\text{solv}} = 0.5$ when the solvent is changed from benzene to toluene and the position of the ^{29}Si resonance remains even unchanged. This indicates negligible interaction between the cation and solvent molecules, in particular no Wheland-type intermediates are formed. (38) Solvents other than aromatic hydrocarbons are however reactive towards vinyl cations **8-10** (see below).

The $\text{C}^\beta=\text{C}^+$ unit of vinyl cations **8-10** is readily identified by the low-field resonance of the positively charged C^+ carbon atom at $\delta^{13}\text{C} = 178.1 - 189.2$ and

that of the trigonal carbon atom C^β at $\delta^{13}\text{C} = 83.3 - 89.0$. These ^{13}C NMR chemical shifts are characteristic for the bonding situation expected for a $\text{C}=\text{C}$ double bond formed from a positively charged sp -hybridized, linear coordinated carbon atom and a second sp^2 -hybridized trigonal carbon center. Similar ^{13}C NMR chemical shifts were reported previously for related β -silyl-substituted vinyl cations in superacidic media at temperatures below -100°C .^(11, 12) Of similar diagnostic value for the $\text{C}^\beta=\text{C}^+$ aryl linkage is the relatively high field shifted ^{13}C NMR resonance of the carbon atom C^{ipso} at $\delta^{13}\text{C} = 104.0 - 115.2$. These ^{13}C NMR signals appear at even lower frequencies than in the precursor alkynes.

Table 1. Characteristic NMR parameter of vinyl cations. (35-37)

<i>cpd</i>	$\delta^{13}\text{C}(C^\alpha)$	$\delta^{13}\text{C}(C^\beta)$	$\delta^{13}\text{C}(C^{\text{ipso}})$	$\delta^{29}\text{Si}$	$\Delta\delta^{29}\text{Si}$	$^1J(\text{CSi})$ (Hz)
8a	181.8	84.4	114.7	58.9		
8b	184.3	84.3	111.6	55.7		
9a	185.5	84.1	113.7	22.8	39.2	18.2
9b	189.2	84.7	111.5	20.1	36.6	19.8
9c	187.9	84.2	110.9	20.1	37.2	20.2
9d	187.6	87.0	111.0	19.0	36.1	20.7
9e	186.5	86.6	113.9	20.4	37.4	19.5
9f	187.9	83.3	113.6	20.6	37.7	18.8
9g	187.9	84.9	111.7	20.5	37.3	19.5
9h	178.1	89.9	104.0	24.9	41.2	16.6
9i	182.0	84.7	115.2	25.0	41.4	17.2
9k	184.8	84.8	110.3	22.1	38.4	18.8
9l	184.3	85.3	111.8	23.0	39.6	18.4
10a	188.5	86.2	113.5	30.1		
21	184.8	77.7	-	24.1		
20	202.4	75.3	-	29.1		

The symmetric structure of the formed vinyl cations is indicated by the presence of only one ^{29}Si NMR signal. The silicon atoms in vinyl cations **8**, **9** and **10** are deshielded compared to the starting alkynyl silane, the actual position of the ^{29}Si resonance, however, strongly depends on the ring size. The silicon atoms in the five membered ring cations **8** are strongly deshielded ($\delta^{29}\text{Si} = 55.7$ (**8b**), 58.9 (**8a**)), while ^{29}Si resonances of the six- and seven-membered ring cations **9** and **10** appear at significantly higher field ($\delta^{29}\text{Si} = 30.1$ (**10a**), $\delta^{29}\text{Si} = 19.0$ -25.0 (**9a-l**), see Table 1). This difference can be attributed at least in part to the increased ring strain in the five-membered ring compounds **8** compared with

the 1,3-disilacyclohexane-, **9**, and 1,3-disilacycloheptane compounds **10**. Similar deshielding effects on $\delta^{29}\text{Si}$ NMR chemical shifts have been previously described for neutral 1,3-disilacyclopentanes in comparison to 1,3-disilacyclohexanes.(38)

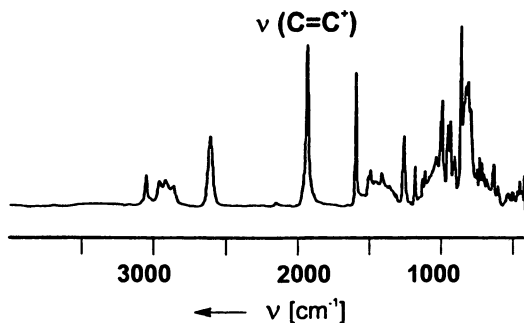


Figure 2. FT-IR spectra of the salt **9b**•[CB₁₁H₆Br₆].

Vinyl cation salts of the brominated carborane [CB₁₁H₆Br₆]⁻ (**40**) are less soluble in aromatic hydrocarbons, but have advantages in crystallization experiments. Figure 2 shows the IR spectra of the salt **9b**•[CB₁₁H₆Br₆]. The most prominent feature is a very intense band at $\tilde{\nu} = 1935\text{ cm}^{-1}$, which is assigned to the C^β=C⁺- stretching vibration. This IR band is stronger than regular C=C stretch vibrations and its position is strongly shifted to higher energy, which indicates a bond order for the C^β=C⁺ bond in cation **9b** larger than 2.

The characterization of the vinyl cations **8-10** is supported by quantum mechanical computations of structure and of the NMR chemical shifts at the GIAO/B3LYP/6-311G(2d,p)//B3LYP/6-31G(d) level of theory.(41-48) The computations predict for the α -aryl-substituted vinyl cations classical Y-shaped structures. Figure 3 shows the computed structure of the phenyl-substituted vinyl cation **8a** as a typical example. The sp-hybridization of the positively charged carbon atom C⁺ is indicated by a bond angle $\alpha(\text{C}^{\beta}\text{C}^+\text{C}^{\text{ipso}})$ near to 180° ($\alpha(\text{C}^{\beta}\text{C}^+\text{C}^{\text{ipso}}) = 179.7^\circ$) and the very short C^β=C⁺ double bond lengths ($r(\text{C}^{\beta}=\text{C}^+) = 125.5\text{ pm}$), which is actually closer to a C≡C triple bond. Long C^β-Si bonds ($r(\text{C}^{\beta}\text{-Si}) = 198.0\text{ pm}$), which exceed regular single bond lengths between sp²-hybridized carbon atoms and tetracoordinated silicon atoms by ca 10 pm, suggest considerable interaction between the σ (Si-C) bond and the empty 2p orbital at the carbon atom C⁺.

The phenyl substituent in cation **8a** is oriented almost perpendicular to the plane spanned by the two silicon atoms and the C^β atom. This ground state conformation provides maximum overlap between the empty 2p orbital at

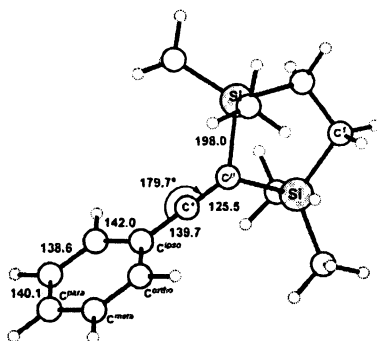


Figure 3. Computed structure of vinyl cation **8a**. (B3LYP/6-31G(d), bond lengths in picometer).

carbon atom C^+ and the π -type orbitals of the aryl substituent. This interaction is also indicated by the short C^+-C^{ipso} single bond length ($r(C^+-C^{ipso}) = 139.7$ pm).

The validity of theoretical structures is frequently established by comparing the computed NMR chemical shifts with experimental data.^(49,50) The agreement between the calculated ^{29}Si NMR chemical shifts, $\delta^{29}\text{Si}^{calc}$, and the experimental data for the vinyl cations **9** is good, that is the maximal deviation $\Delta\delta^{29}\text{Si}$ of $\delta^{29}\text{Si}^{calc}$ is +4.1. Notably, the agreement for the five-membered and seven-membered ring cations **8** and **10** is less satisfactory with $\Delta\delta^{29}\text{Si}^{calc} = 10.6 - 11.9$ and 8.5 . Similarly, the computed ^{13}C NMR chemical shifts for the tri- and di-coordinated carbon atoms of vinyl cations **8-10** are found to be too large with $\Delta\delta^{13}\text{C}^{calc} = 2.5 - 21.0$. However, in both cases experimental and calculated NMR chemical shifts are linearly correlated (see Figures 4, 5).

This indicates that the deviations are due to systematic errors, for example deficiencies of the applied methods and basis sets. DFT-based methods, such as GIAO/DFT calculations are known to overestimate paramagnetic contributions to the chemical shielding. This results, for critical cases with small HOMO/LUMO separations, in overly deshielded computed chemical shifts. Notorious examples for these deficiencies are ^{29}Si or ^{13}C NMR chemical shift computations of silylenes, silylium ions or dienyl cations.⁽⁵¹⁻⁵⁴⁾ Taking into account the deficiencies of the applied method, and bearing in mind very reasonable correlations shown in Figures 4 and 5, the computational results do support the structural characterization of the synthesized vinyl cations.

The unusual position of the $C^\beta=C^+$ stretching vibration in the IR spectra of **9b** $\cdot[\text{CB}_{11}\text{H}_6\text{Br}_6]$ is in agreement with the results from quantum mechanical calculations. A frequency calculation at the B3LYP/6-31G(d) level of theory

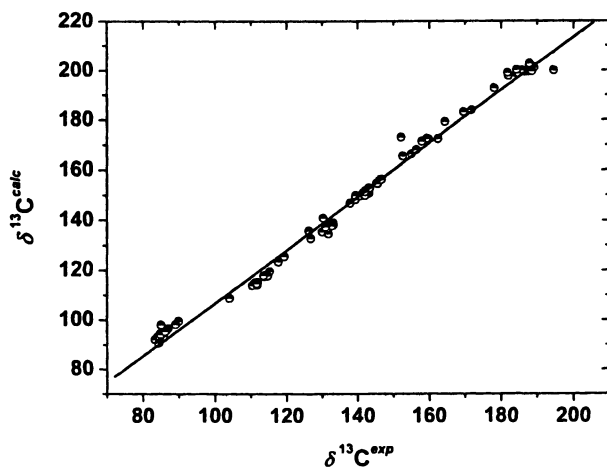


Figure 4. Correlation between calculated ($\delta^{13}\text{C}^{\text{calc}}$) and experimental ^{13}C NMR chemical shift ($\delta^{13}\text{C}^{\text{exp}}$) for vinyl cations 8-10. The correlation is given by the following equation: $\delta^{13}\text{C}^{\text{calc}} = (0.0 \pm 1.3) + (1.067 \pm 0.010) \delta^{13}\text{C}^{\text{exp}}$, $R = 0.996$, $SD = 3.06$, 96 data points. Only di- and tricoordinated carbon atoms are included in the correlation.

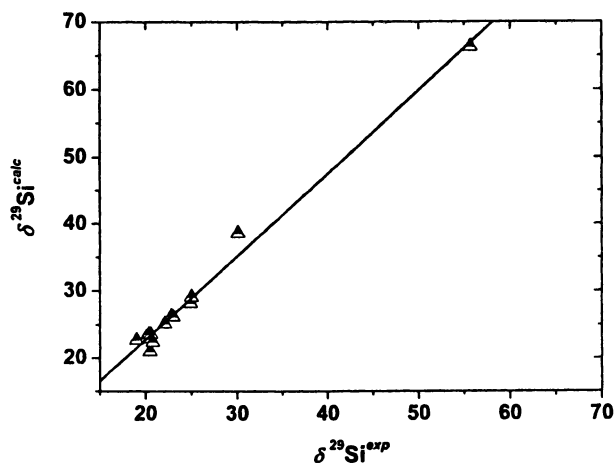


Figure 5. Correlation between calculated ($\delta^{29}\text{Si}^{\text{calc}}$) and experimental ^{29}Si NMR chemical shift ($\delta^{29}\text{Si}^{\text{exp}}$) for the cations 8-10. The correlation is given by the following equation: $\delta^{29}\text{Si}^{\text{calc}} = (-2.0 \pm 0.8) + (1.238 \pm 0.027) \delta^{29}\text{Si}^{\text{exp}}$, $R = 0.996$, $SD = 1.28$, 15 data points.

predicts a very strong IR absorption at $\tilde{\nu} = 1930 \text{ cm}^{-1}$ for the $\text{C}^{\beta}=\text{C}^{+}$ stretch, which is in close agreement with the experimental value at $\tilde{\nu} = 1935 \text{ cm}^{-1}$ (see Figure 2).(55)

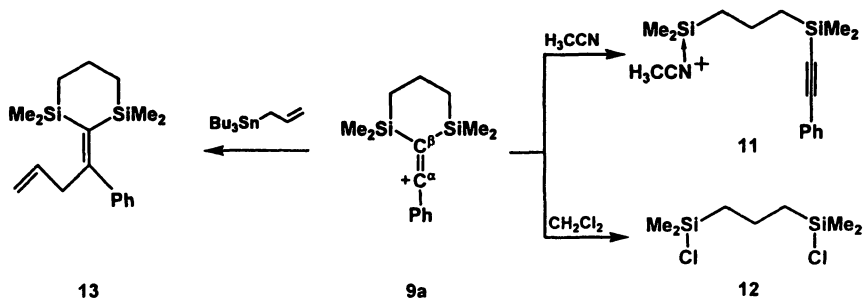
Stability and Reactivity

The unusual stability of TFPFB salts of vinyl cations **8** – **10** stems from both thermodynamic and kinetic factors. In the former, thermodynamic stabilization is gained via the two β -silyl substituents and by the presence of a strongly electron donating aryl substituent attached to C^{+} . According to quantum mechanical computations at the B3LYP/6-31G(d)//B3LYP/6-31G(d), the vinyl cation **9a** is only by 7.1 kJ mol^{-1} less stable than trityl cation.(35) Kinetic stabilization of the vinyl cations originates from the essentially non-nucleophilic reaction conditions which are guaranteed by the application of the weakly coordinating TFPFB anion and the use of aromatic hydrocarbons as solvents. The importance of the reaction conditions is demonstrated by selected reactions of vinyl cation **9a** summarized in Scheme 2. Addition of acetonitrile to a toluene solution of cation **9a** at room temperature results in the formation of silylated nitrilium ions **11**(35) With methylene chloride a fast fragmentation reaction occurs even at temperatures as low as -50°C and the disilylchloride **12** was detected by NMR spectroscopy as the final product.(37) In general, attack by nucleophiles occurs at the silicon atom which yields a ring opened product. An exception is the π -nucleophile tri-*n*-butylallyl tin, which reacted with vinyl cation **9a** via a C-allylation reaction to give the 1,4-diene **13**.

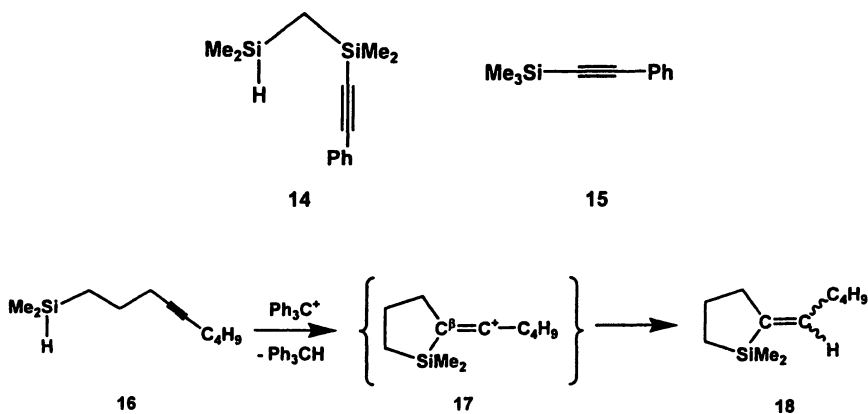
Limitations of the Method

Interestingly, reaction of alkynyl disilane **14** with trityl cation did not result in the formation of stable vinyl cations. Obviously, the formation of the four-membered disilacyclobutane ring is unfavorable. Similarly, treatment of alkyne **15** with the pre-formed triethylsilylarenium ion **1** derived from toluene did not give the expected intramolecular transfer of the silylium ion to the triple bond. Instead, only a complex product mixture was obtained.

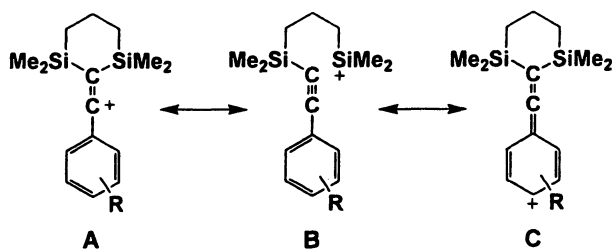
Not only the ring size but also the number of stabilizing silyl groups in the β -position is essential for the stability of the vinyl cations. Thus, reaction of alkyne **16** with tityl cation gave both stereoisomers of alkenylsilane **18** as the only products in 80-85% isolated yield (Scheme 3). This result suggests, that the generated β -silyl-substituted vinyl cation intermediate **17** did not persist under the applied reaction conditions but underwent a second hydride transfer with the formation of compound **18**.



Scheme 2. Reactivity of vinyl cation 9a.



Scheme 3. Reaction of alkyne 16 with trityl cation



Scheme 4. Resonance structures of vinyl cations 9.

σ -Delocalization versus π -Conjugation in Vinyl Cations (37)

The stabilization mechanism operating in aryl-substituted vinyl cations such as **9** can be qualitatively depicted by the Lewis resonance structures **A-C** (Scheme 4). There is hyperconjugation between the σ -C ^{β} -Si bond and the empty 2p-orbital of the carbon atom C ^{α} which is described by the no-bond resonance structure **B**. In addition, π -delocalization between the aryl ring and the C ^{α} carbon atom is indicated by structures such as **C**.

Vinyl cations **9** are therefore well suited to study the interplay between σ -delocalization and π -resonance. In particular, the question as to whether the extent of β -silyl hyperconjugation in vinyl cations **9** depends on the electron demand at the electron deficient C ^{α} atom can be investigated in detail. An important factor which controls the charge distribution in vinyl cations **9** is the electron donating ability of the aryl groups. Modifications of the resonance effects transmitted by the aryl ring which are quantified by Brown's σ_R^+ constants of the ring substituents will greatly influence the electron density at C ^{α} and thus the effect on the σ -Si-C ^{β} -delocalization can be studied.(56, 57)

Two NMR spectroscopic parameters in vinyl cations **9** indicate the occurrence of σ -delocalization as described by the canonical resonance structure **B**. That is, a significant low-field shift of the ²⁹Si NMR resonance upon ionization of the alkynyl silanes **6** ($n = 3$) is detected (See Figure 6), which suggests a considerable build-up of positive charge at the silicon atoms. In addition, the resonance structure **B** implies a decrease in the bond order of the C ^{β} -Si bond. In agreement, the ¹ J (C ^{β} Si) coupling constant detected for cations **9** (¹ J (C ^{β} Si) = 16.6 – 24.6 Hz, for an example, see Figure 7) are significantly smaller than regular coupling constants found usually between sp²-hybridized carbon atoms and tetra substituted silicon atoms (¹ J (=CSi) \approx 60 Hz).(58) Both NMR spectroscopic parameters are influenced by the different substituents at the aryl ring. Furthermore, a plot of the σ_R^+ constants for the eight *meta* and *para* substituents in vinyl cations **9a-c**, **f**, **g**, and **i-l** versus the deshielding $\Delta\delta^{29}\text{Si}$ indicates a correlation between these parameters. The deshielding $\Delta\delta^{29}\text{Si}$ increases with decreasing π -electron donating ability of the aryl substituent (see Figure 8a) and also the coupling constant ¹ J (C ^{β} Si) is reduced with decreasing π -donating ability of the aryl substituent (see Figure 8b). Both correlations suggest that hyperconjugation in vinyl cations **9** as shown by the resonance structure **B** (Scheme 4) becomes more important as the π -stabilization of the aryl substituent is diminished. This interpretation of the experimental data implies that the contribution of β -SiC hyperconjugation to the overall thermodynamic stability of vinyl cations is not constant, but is determined by the electron demand at the electron deficient dicoordinated carbon atom.

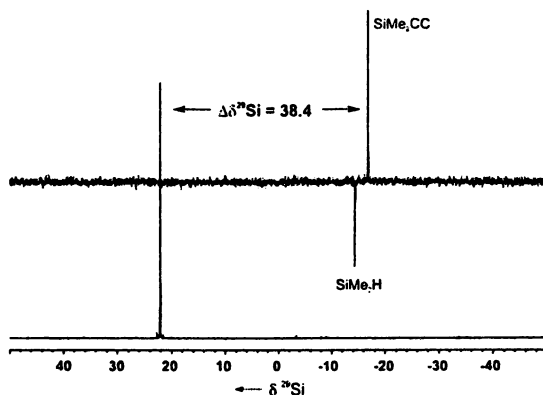


Figure 6. ^{29}Si NMR INEPT spectra of alkyne **6k** ($n = 3$) (upper trace) and of cation **9k** (lower trace) which demonstrate the low field shift of the ^{29}Si NMR resonance $\Delta\delta^{29}\text{Si}$ upon ionization.

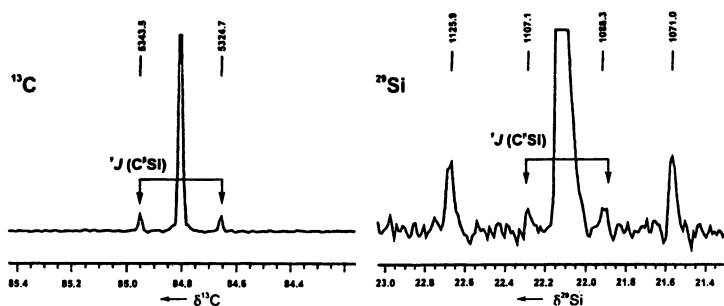


Figure 7. The 62.90 MHz ^{13}C NMR (left) and 49.69 MHz ^{29}Si NMR (right) spectra of **9k** in benzene- d_6 at 30 °C, which show the reduced $^1J(\text{C}^\beta\text{Si})$ coupling constant (Hz), (Reproduced from reference 37. Copyright 2005 American Chemical Society.)

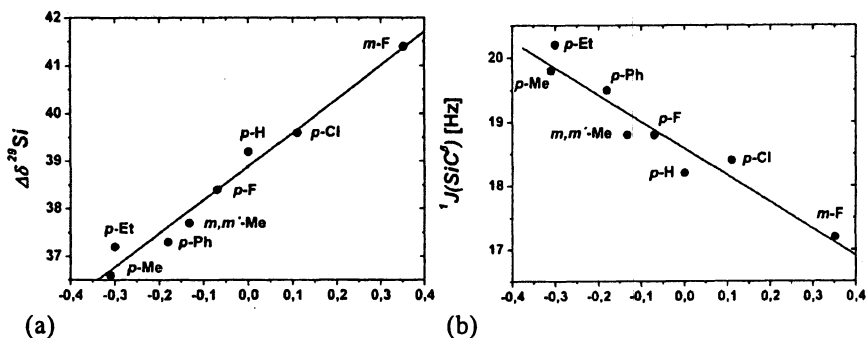
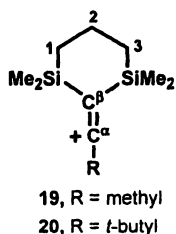


Figure 8. (a) Plot of σ^+ versus $\Delta\delta^{29}\text{Si}$ for vinyl cations **9a-c,f,g,i-l**. (b) Plot of σ^+ versus $^1J(\text{C}^{13}\text{Si})$ for vinyl cations **9a-c,f,g,i-l**. (Reproduced from reference 37. Copyright 2005 American Chemical Society.)

Alkyl Substituted Vinyl Cations (35, 36)

Stabilization of the vinyl cations **8-10** by aryl substituents is important but even substituents without strong resonance effects provide adequate stabilization to allow the synthesis of persistent vinyl cations at ambient temperature. This is demonstrated by the synthesis and isolation of the salts of alkyl-substituted vinyl cations **19** and **20**, and their characteristic NMR parameters are summarized in Table 1.



In solution, the TFPB salt of the methyl-substituted vinyl cation **19** has only limited stability. Decomposition into unidentified products took place during several days. In contrast, the steric and electronic effects provided by the *t*-butyl substituent confer indefinite stability to the vinyl cation **20** in the absence of nucleophiles. That is, according to the NMR experiments, a solution of **20**•TFPB in benzene showed no sign of decomposition even after weeks at room temperature. With the carborane anion $[\text{CB}_{11}\text{H}_6\text{Br}_6]$ suitable crystals for

X-ray analysis were obtained from 1,2-dichlorobenzene.(36) Figure 9 shows the molecular structure of vinyl cation **20** in the salt $20^+[\text{CB}_{11}\text{H}_6\text{Br}_6]^-$. As previously predicted by computations (59, 60) and deduced from ^{13}C NMR chemical shift parameters (10, 35), the vinyl cation is linear around the positively charged carbon atom C^+ ($\alpha(\text{C}^\beta\text{-C}^+\text{-C}^\alpha) = 178.8^\circ$), which suggests a sp -hybridization for C^+ . As a consequence the $\text{C}^\beta\text{=C}^+$ double bond is unusually short ($r(\text{C}^\beta\text{=C}^+) = 125.5$ pm) and approaches the bond length for a normal $\text{C}\equiv\text{C}$ triple bond. A quite remarkable feature of vinyl cation **20** are the very long $\text{C}^\beta\text{-Si}$ bond lengths ($r(\text{C}^\beta\text{=Si}^1) = 194.6$ pm and $r(\text{C}^\beta\text{=Si}^2) = 198.4$ pm). This bond elongation as compared to regular sp^2 carbon silicon bond lengths provides experimental evidence for the interaction of the $\sigma(\text{C}^\beta\text{Si})$ bond with the empty 2p orbital at the carbon atom C^+ . The NMR data indicate that vinyl cation **20** is symmetric in solution, whereas in the solid state the two silicon atoms are clearly different. The SiC^β bond lengths are markedly different and also the $\text{SiC}^\beta\text{C}^+$ bond angles can be clearly distinguished (see Figure 9). The more acute bond angle is linked to the longer SiC^β bond. This fact suggests more pronounced σ -delocalization for this β -silyl group. Density functional computations at the hybrid density B3LYP level and wave function based MP2 calculations for vinyl cation **20** predict equilibrium structures for **20** (see Figure 10) which are not only close to each other but are also very near to the experimentally determined structure. In particular, the unsymmetrical grouping of the silicon atoms around the $\text{C}=\text{C}^+$ unit is found also in the theoretical structures. This provides evidence that this arrangement is a result of an intrinsic bonding situation in cation **20** and is not a consequence of crystal lattice or similar intermolecular interactions in the condensed phase.

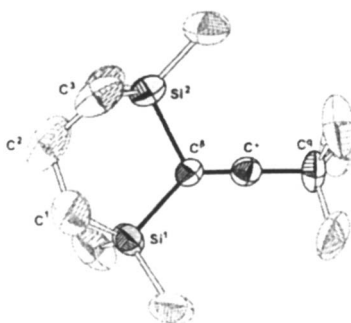


*Figure 9. Molecular structure of cation **20** in the salt $20^+[\text{CB}_{11}\text{H}_6\text{Br}_6]^-$. Thermal ellipsoids are drawn at the 50% probability level. Important bond lengths [in picometer] and bond angles [$^\circ$]: $\text{C}^\beta\text{-C}^+ = 122.1$, $\text{C}^+\text{-C}^\alpha = 145.2$, $\text{Si}^2\text{-C}^\beta = 198.4$, $\text{Si}^1\text{-C}^\beta = 194.6$; $\text{C}^\beta\text{-C}^\alpha\text{-C}^+ = 178.8$, $\text{Si}^2\text{-C}^\beta\text{-C}^+ = 115.5$, $\text{Si}^1\text{-C}^\beta\text{-C}^+ = 133.0$. (Reproduced with permission from reference 36. Copyright 2004, VCH- Wiley.)*

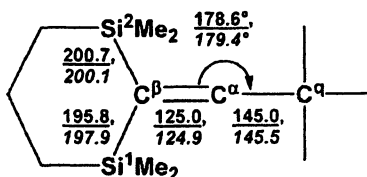


Figure 10. Computed structure of vinyl cation 20 (underlined MP2/6-31G(d), italic B3LYP/6-31G(d)). Additional bond angles: $\text{Si}^2\text{-C}^\beta\text{-C}^+$ = 112.3, 118.0; $\text{Si}^1\text{-C}^\beta\text{-C}^+$ = 133.5, 127.6.

Conclusion

Aryl- and alkyl-substituted vinyl cations **8-10**, **19**, **20** have been synthesized by treatment of alkynyl silanes with trityl cation in the presence of TPFPB as counter ion in aromatic hydrocarbons as solvents. The vinyl cation salts have been isolated and characterized by NMR and IR spectroscopy and in the case of **20** \cdot [CB₁₁H₆Br₆] also by an X-ray structure analysis. The experimental investigations are supported by the results of quantum mechanical computations of structure, energy and the NMR parameters. Although vinyl cations **8-10**, **19**, **20** are thermodynamically stabilized by two β -silyl groups, the kinetic stabilization provided by the essentially non-nucleophilic reaction conditions is important. The synthesized vinyl cations are highly reactive, and attack of nucleophiles occurs in most cases at the silicon atoms. Consequences of σ -delocalization in vinyl cations **8-10**, **19**, **20** are apparent from their spectroscopic data and also from the molecular structure of vinyl cation **20**. The interplay between σ -delocalization and π -conjugation was studied in detail for vinyl cations **9**. A Hammett-type analysis for eight *para*- and *meta*-substituted vinyl cations **9** indicates that σ -delocalization in vinyl cations depends on the electron demand at the dicoordinated positively charged carbon atom C^+ . Electron donating aryl substituents at C^+ are found to reduce the extent of $\text{Si-C}^\beta\text{-C}^+$ hyperconjugation, while electron withdrawing substituents at the aryl group increase the effects of σ -delocalization from the silyl groups.

Acknowledgement

This work was supported by the Deutsche Forschungsgemeinschaft (DFG) and by the German Israeli Foundation (GIF).

References

1. For a recent monograph on vinyl cations: *Dicoordinated Carbocations*; Rappoport, Z., Stang, P. J., Eds.; Wiley: New York, NY, 1997.
2. Grob, C. A.; Csapilla, J.; Cseh, G. *Helv. Chim. Acta* **1964**, *47*, 1590.
3. Grob, C. A. In ref. 1, p 1-7.
4. Hanack, M. *Acc. Chem. Res.* **1976**, *9*, 364.
5. Kitamura, T.; Taniguchi, H.; Tsuno, Y. In ref 1, p 321-376.
6. Stang, P. J.; Summerville, R. *J. Am. Chem. Soc.* **1969**, *91*, 4600.
7. Subramanian, L. R.; Hanack, M. *Chem. Ber.* **1972**, *105*, 1465.
8. Okuyama, T.; Takino, T.; Sueda, T.; Ochiai *J. Am. Chem. Soc.* **1995**, *117*, 3360.
9. Lucchini, V.; Modena, G.; Pasquato, L. In ref. 1, p 237-320.
10. Siehl, H-U. In ref. 1, p 189-236.
11. Kaufmann, F-P.; Siehl, H-U. *J. Am. Chem. Soc.* **1992**, *114*, 4937.
12. Siehl, H-U.; Kaufmann, F-P.; Hori, K. *J. Am. Chem. Soc.* **1992**, *114*, 9343.
13. Siehl, H-U. *Pure Appl. Chem.* **1995**, *67*, 769.
14. Siehl, H-U. In *Stable Carbocation Chemistry*; Prakash, G. K. S., Schleyer, P. v. R., Eds.; Wiley: New York, 1997; p 165.
15. Siehl, H-U.; Kaufmann, F-P.; Apeloig, Y.; Braude, V.; Danovich, D.; Berndt, A.; Stamatis, N. *Angew. Chem.* **1991**, *30*, 1479.
16. Siehl, H-U.; Muller, T.; Gauss, J.; Buzek, P.; Schleyer, P. v. R. *J. Am. Chem. Soc.* **1994**, *116*, 6384.
17. Stanton, J. F., Gauss, J., Siehl, H-U. *Chem. Phys. Lett.* **1996**, *262*, 183.
18. Siehl, H-U.; Müller, T.; Gauss, J. *J Phys. Org. Chem.* **2003**, *16*, 577.
19. Müller, T. *Adv. Organomet. Chem.* **2005**, *53*, 155.
20. Lickiss, P. D. In *The Chemistry of Organosilicon Compounds Vol. 2*; Rappoport, Z., Apeloig, Y., Eds.: Wiley, 1998, p. 557-594.
21. Maerker, C.; Schleyer, P. v. R. In *The Chemistry of Organosilicon Compounds Vol. 2*; Rappoport, Z., Apeloig, Y., Eds.: Wiley, 1998, p. 513-556.
22. Lambert, J. B.; Zhang, S. *J. Chem. Soc. Chem. Commun.* **1993**, 383.
23. Lambert, J. B.; Zhang, S.; Stern C. L.; Huffman, J. C. *Science* **1993**, *260*, 1917.
24. Lambert, J. B.; Zhang, S.; Stern C. L.; Ciro, S. M. *Organometallics* **1994**, *13*, 2430.
25. Schleyer, P. v. R.; Buzek, P.; Müller, T.; Apeloig, Y.; Siehl, H-U. *Angew. Chem.* **1993**, *32*, 1471.
26. Pauling, L. *Science* **1994**, *263*, 983.
27. Olah, G. A.; Rasul, G.; Buchholz, H.; Li, X.-Y.; Sandford, G.; Prakash, G. K. S. *Science* **1994**, *263*, 983.
28. Lambert, J. B.; Zhao, Y. *J. Am. Chem. Soc.* **1996**, *118*, 7867.
29. Lambert, J. B.; Zhao, Y.; Wu, H. *J. Org. Chem.* **1999**, *64*, 2729.

30. Lambert, J. B.; Liu, C.; Kouliev, T. *J. Phys. Org. Chem.*, **2002**, *15*, 667.
31. Meyer, R.; Lennartz, D.; Muller, T. *Chem.-Eur. J* **2002**, *8*, 3203.
32. Müller, T.; Bauch, C.; Ostermeier, M.; Bolte, M.; Auner, N. *J. Am. Chem. Soc.* **2003**, *125*, 2158.
33. Wrackmeyer, B.; Kundler, S.; Milius, W.; Boese, R. *Chem. Ber.* **1994**, *127*, 333.
34. Wrackmeyer, B.; Kehr, G.; Boese, R. *Angew. Chem.* **1991**, *30*, 1370.
35. Müller, T.; Meyer, R.; Lennartz, D. Siehl, H-U. *Angew. Chem.* **2000**, *39*, 3074.
36. Müller, T.; Juhasz, M.; Reed, C. A. *Angew. Chem.* **2004**, *43*, 1543.
37. Müller, T.; Margraf, D.; Syha Y. *J. Am. Chem. Soc.* **2005**, *127*, 10852.
38. In the case of silylium ions the formation of Wheland-type intermediates is shown by appreciable solvent effects on the ^{29}Si NMR chemical shifts.
39. Seyferth, D.; Friedrich, H. *Z. f. Naturforsch B* **1994**, *49*, 1818.
40. Reed, C. A. *Acc. Chem. Res.* **1998**, *31*, 33.
41. All computations were done with Gaussian 03 revision B.03; Gaussian Inc.: Pittsburgh PA 2003.
42. Ditchfield, R. *Mol. Phys.* **1974**, *27*, 789.
43. Wolinski, K.; Hilton, J. F.; Pulay, P. *J. Am. Chem. Soc.* **1982**, *104*, 5667.
44. Cheeseman, J.; Trucks, G. W.; Keith, T. A.; Frisch M. *J. Chem. Phys.* **1996**, *104*, 5497.
45. Becke, A. D. *Phys. Rev.* **1988**, *A38*, 3098.
46. Lee, C., Yang, W.; Parr, R. G. *Phys. Rev. B*, **1988**, *37*, 785.
47. Becke, A. D. *J. Chem. Phys.* **1993**, *98*, 5648.
48. Johnson, B. G.; Gill, P. M. W.; Pople, J. A. *J. Chem. Phys.* **1993**, *98*, 5612.
49. Schleyer, P. v. R.; Maerker C. *Pure Appl. Chem.* **1995**, *67*, 755.
50. Siehl, H-U., Vrećek, V. In *Calculation of NMR and EPR Parameter*, Kaupp, M.; Malkin, V. G.; Bühl, M. Eds.; Wiley-VCH: Weinheim Germany 2004.
51. Müller, T. *J. Organomet. Chem.* **2003**, *686*, 251.
52. Lee, G.-H., West, R., Müller, T. *J. Am. Chem. Soc.* **2003**, *125*, 8114.
53. Müller, T.; Zhao, Y.; Lambert, J. B. *Organometallics* **1998**, *17*, 278.
54. Siehl, H-U.; Müller, T.; Gauss, J. *J. Phys. Org. Chem.* **2003**, *16*, 577.
55. The computed frequency of $\tilde{\nu} = 2004 \text{ cm}^{-1}$ is scaled by the global scaling factor of 0.963 suggested by Rauhut and Pulay. Rauhut, G.; Pulay, P. *J. Phys. Chem.* **1995**, *99*, 3093.
56. Hansch, C; Leo, A.; Taft, R. *Chem. Rev.* **1991**, *91*, 165.
57. Brown, H. C.; Okamoto, Y. *J. Am. Chem. Soc.* **1958**, *80*, 4979.
58. Lambert, J. B.; Shawl, C. E.; Basso, E. *Can. J. Chem.* **2000**, *78*, 1441.
59. Sustmann, R.; Williams, J. E.; Dewar, M. J. S.; Allen, L. C.; Schleyer, P. v. R. *J. Am. Chem. Soc.* **1969**, *91*, 5360.
60. For a review: Apeloig, Y.; Müller, T. In ref. 1, Ch. 2, p 9-104.

Chapter 4

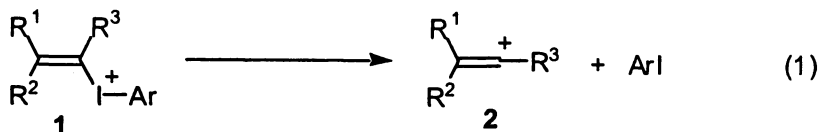
Vinyl Iodonium Salts as Precursors to Vinyl Cations

Tadashi Okuyama and Morifumi Fujita

Graduate School of Material Science, Himeji Institute of Technology,
University of Hyogo, Kamigori, Hyogo 678-1297, Japan

General reactivities of vinyl iodonium salts are summarized, and reactions of cyclohexenyl, 1-alkenyl, styryl, and 2,2-disubstituted vinyl iodonium salts are discussed in relation to possible formation of vinyl cation intermediates. Primary vinyl cation cannot be generated thermally but rearrangement via neighboring group participation often occurs. Photosolvolysis to give primary vinyl cation is also discussed.

Vinyl iodonium salts **1** are reactive due to the high leaving ability of the positive iodine group, and the stability is inversely dependent on the stability of the carbocation **2** formed upon departure of the iodonio group (eq 1).¹

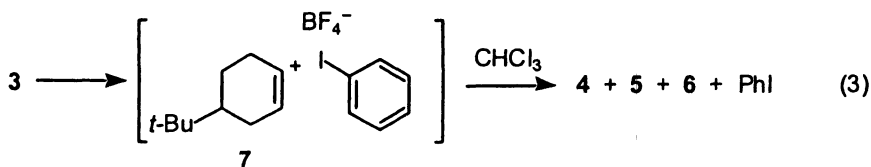
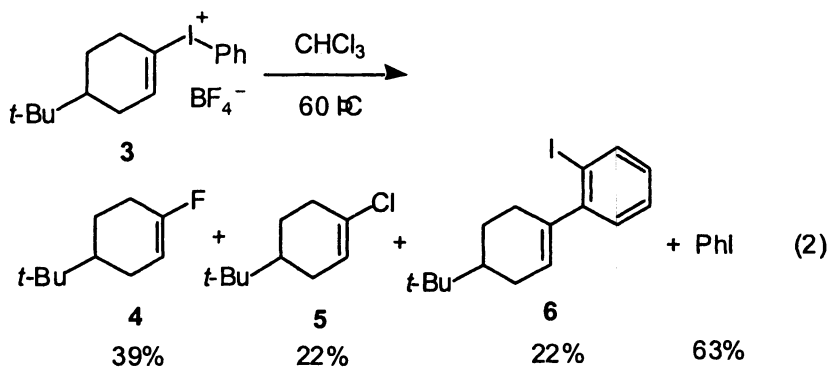


Primary vinyl iodonium compounds (**1**, $\text{R}^3 = \text{H}$) are readily prepared as stable salts, but secondary analogs (**1**, $\text{R}^3 = \text{alkyl}$) cannot be isolated without the presence of electron-accepting moieties. Cyclopent-1-enyl iodonium salt is very stable and poorly reactive toward bases and nucleophiles, while cyclohept-1-enyl

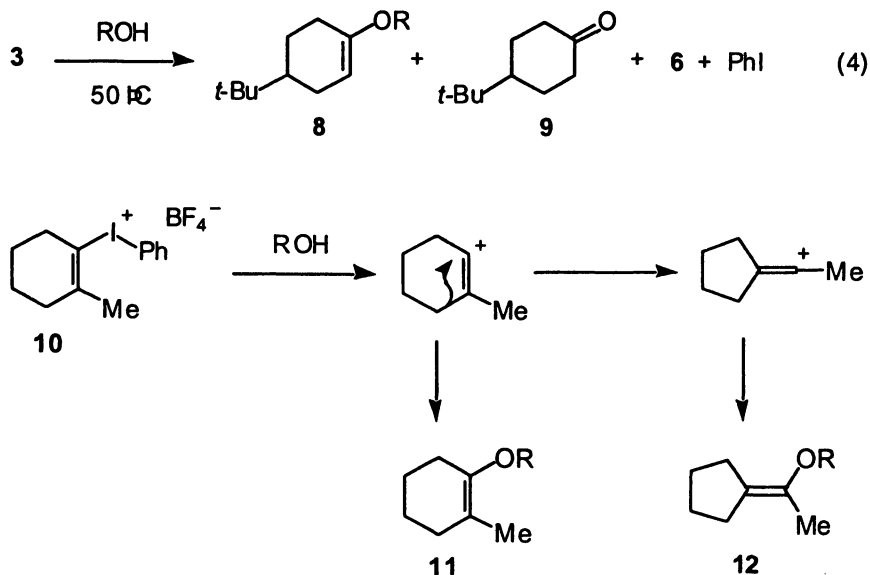
iodonium salt can only be isolated at low temperature and has a short lifetime. Cyclohex-1-enyl iodonium salt can be isolated easily and is moderately reactive at room temperature. Relative stabilities of cycloalkenyl iodonium salts are ascribed to the angle strain at the positive carbon of the cyclic vinylic cations: the positive carbon of the vinyl cation is linear and of sp -hybridization (1).²

Reactions of Cyclohex-1-enyl Iodonium Salt

When 4-*t*-butylcyclohex-1-enyl(phenyl)iodonium tetrafluoroborate (3) is heated at 60 °C in chloroform, 1-fluorocyclohexene 4, 1-chlorocyclohexene 5 and 1-(*o*-iodophenyl)cyclohexene 6 are formed with accompanying iodobenzene leaving group (eq 2).³ These three substitution products are best accounted for by formation of an ion pair involving cyclohexenyl cation 7. The cyclohexenyl cation 7 formed picks up fluoride from tetrafluoroborate and chloride from chloroform solvent, and recombines with the iodobenzene generated (eq 3). This kind of reactions with a counteranion and solvent are characteristic of unstable carbocations and are known in the case of phenyl cation generated from the diazonium salt in the Schiemann-type reaction.⁴



Reactions of **3** in alcoholic and aqueous solvents result in a normal solvolysis product **8** (and cyclohexanone **9**) as well as the recombination product **6** (eq 4).⁵ This is again rationalized by an ion-pair mechanism. 2-Methylcyclohex-1-enyl(phenyl)iodonium tetrafluoroborate (**10**) undergoes solvolysis about 250 times as fast as **3**, and gives some rearranged product **12** in accord with the S_N1 solvolysis mechanism (Scheme 1).



Scheme 1. Solvolysis of 2-methylcyclohex-1-enyl iodonium salt 10.

Kinetic measurements also show that the solvolysis is of the S_N1-type: small solvent polarity effects were found in the correlation with the ionizing power parameter Y_{OTs} , with a small m value of 0.12, characteristic of a reaction of a cationic substrate to give a cationic product. Furthermore, the rate data show that the leaving group ability of the phenyliodonio group is about 10^6 times as great as triflate or 10^{12} -fold higher than iodide.⁵

These results show that cyclohexenyl iodonium salt readily gives cyclohexenyl cation under poorly nucleophilic/basic conditions. When a stronger nucleophile like bromide is added to the solution of **3**, 1-bromocyclohexene **13** is formed as a main product (eq 5). It is noteworthy here that the rate of the reaction is strongly retarded by the added bromide salt as a nucleophilic reagent (Figure 1), although bromide does react with the substrate to give substitution product **13**.⁶

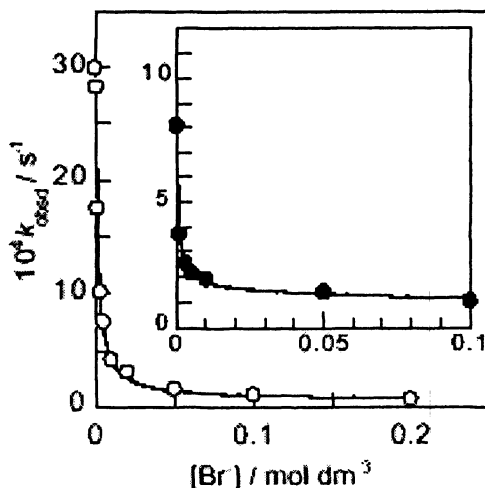
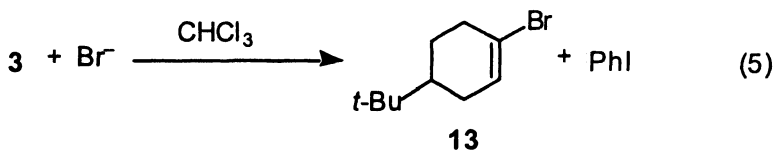
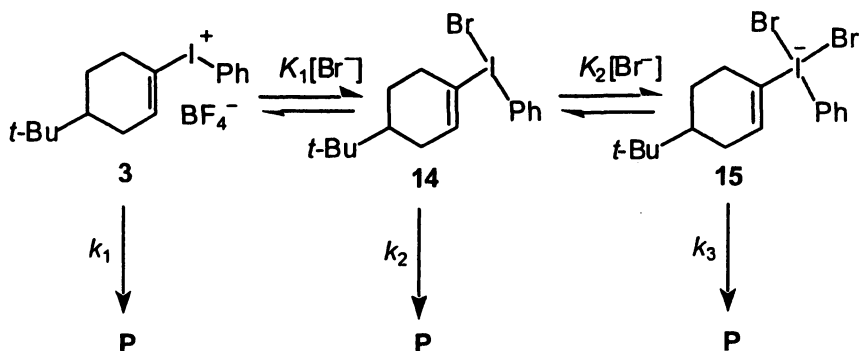


Figure 1. Observed rate constants for the reaction of the *p*-chloro derivative of 3 with bromide ion in chloroform (open circles) and acetonitrile (inset, closed circles) at 50 °C.

This behavior can be rationalized by the formation of a hypervalent adduct, iodane 14 (Scheme 2). Although a solution of vinylidonium tetrafluoroborate has no absorption above 250 nm in the UV spectrum, a new absorption develops at the longer wavelength on addition of halide ion.^{6,7} This new absorption gradually decreases following pseudo-first-order kinetics to give the rate constant for the reaction. The initial absorbances A_0 at 270 nm and the observed rate constants k_{obsd} for the reaction of the *p*-chloro derivative of 3 with bromide ion are plotted against bromide concentration in Figure 2.⁶ The saturation curve for A_0 is compatible with equilibrium formation of the adduct 14, while the decreasing curve for k_{obsd} is rationalized by the slower reaction of 14 than the free iodonium ion 3. The curves are simulated according to Scheme 2 and the equilibrium and kinetic parameters are summarized in Table I.



Scheme 2. Equilibrium formation of the hypervalent adducts of the iodonium ion with bromide and their reactions.

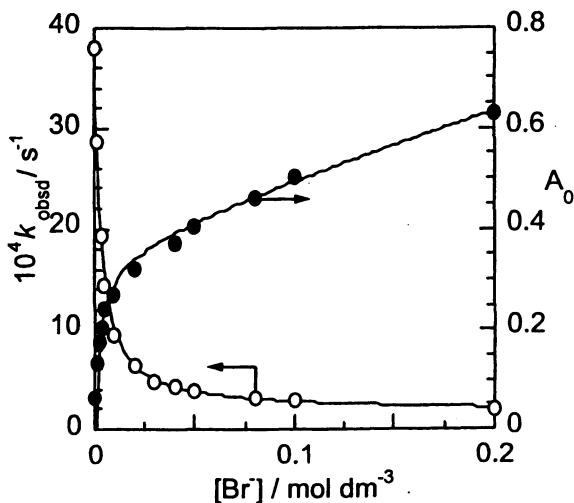


Figure 2. Initial absorbance (closed circles) at 270 nm and observed rate constants (open circles) for the reaction of 3 in acetonitrile at 60 °C in the presence of tetrabutylammonium bromide at the ionic strength of 0.20.

Table I. Kinetic Parameters for the Reaction of the *p*-Chloro Derivative of 3 in the Presence of Tetrabutylammonium Bromide^a

	MeOH	MeCN ^b	CHCl ₃	MeCN ^c
$K_1/\text{mol}^{-1}\text{dm}^3$	5.0	690 (370)	1600	7160
$K_2/\text{mol}^{-1}\text{dm}^3$	~0	~0 (0.7)	3.3	15.1
$10^4 k_1/\text{s}^{-1}$	6.8	30 (40)	8.1	(0.30) ^d
$10^4 k_2/\text{s}^{-1}$	~0	0.6 (2)	1.5	(0.028) ^d
K_1/k_2	large	50 (20)	5.4	(11) ^d

^a Reactions were carried out at 50 °C and the ionic strength of 0.20 mol dm⁻³ in methanol and acetonitrile or 0.10 mol dm⁻³ in chloroform maintained with Bu₄NClO₄.

^b Values in parentheses are those obtained for the reaction of 3 at 60 °C.

^c Data for the reaction of dec-1-enyl(phenyl)iodonium tetrafluoroborate (15) with chloride at 25 °C and the ionic strength of 0.10 mol dm⁻³.

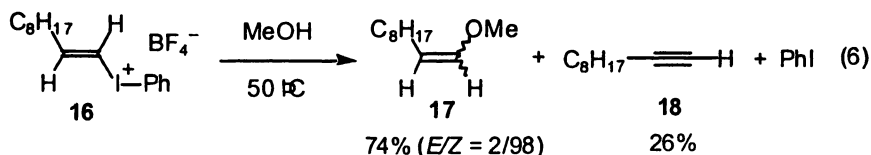
^d Second-order rate constant in mol dm⁻³s⁻¹ for the S_N2 reaction.

The reactions involved are unimolecular, and the cyclohexenyl derivative 3 undergoes solely the spontaneous heterolysis while both spontaneous heterolysis and ligand coupling occur with the iodane 14. The relative contributions of the two reactions of 14 depend on the solvent polarity. The results summarized in Table I show that the iodonium ion and the counteranion are in equilibrium with the hypervalent adduct, λ³-iodane. The equilibrium constants depend on the identity of the anion and the solvent employed, and the iodane is less reactive than the free iodonium ion as the k_1/k_2 ratios demonstrate. Spontaneous heterolysis of 3 occurs more than 100 times as fast as that of the adduct 14 as observed in methanol; the leaving ability of the iodonio group is lowered by association by more than 100 times.

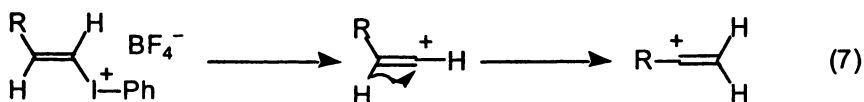
Chirality Probe for Primary Vinyl Cation

Formation of vinyl cation was first demonstrated in the solvolysis of 1-arylvinyl halide in 1960s,⁸ and then 1-alkylvinyl substrates was found to undergo S_N1 solvolysis when triflate was used as a leaving group.⁹ To observe the less stable carbocationic intermediate, the better leaving group was employed. Primary vinylic cation carrying no substituent at the positive carbon is still less stable, and we need a still better leaving group. A highly reactive iodonium substrate is a good candidate for this purpose. A simple 1-alkenyl iodonium salt, dec-1-enyl(phenyl)iodonium tetrafluoroborate (16), was subjected to thermal reaction in hydroxylic solvents.¹⁰ The solvolysis occurs at 50 °C as readily as

that of cyclohexenyl analog **3**. However, the reaction rate depends on the nucleophilicity of the solvent but not in its ionizing power. Furthermore, the substitution product **17** is predominantly that of inversion of configuration as observed, e.g., in methanol (eq 6).



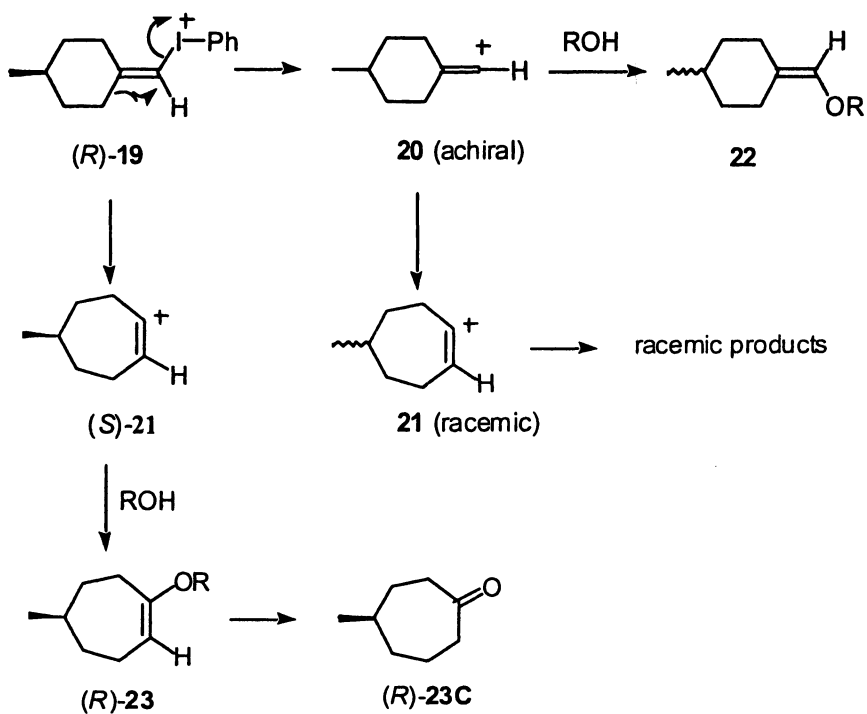
These results can be explained by an S_N2 mechanism, which can occur both by in-plane and out-of-plane attacks.¹¹ No sign of formation of the primary 1-alkenyl cation was detected. If it were formed, the facile 1,2-hydride shift to give the more stable secondary vinyl cation should have been observed (eq 7).



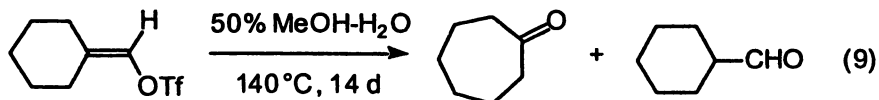
However, there still remained strong arguments that the results could be explained if a short-lived tight ion pair intermediate was involved. We employed a chirality probe approach to search for intermediacy of the primary vinyl cation. A 4-substituted cyclohexylidenemethyl structure has a molecular chirality if the terminal sp² carbon is unsymmetrically substituted, while the corresponding vinyl cation has a plane of symmetry and achiral due to the linearity of the positive carbon, as illustrated in Scheme 3. Optically active 4-methylcyclohexylidenemethyl(phenyl)iodonium tetrafluoroborate (**19**) gives achiral primary vinyl cation **20** on direct heterolysis, but it can give optically active secondary cation **21** via σ-bond participation (Scheme 3). Cation **21** can also be formed by rearrangement of the initially formed **20**. However, the cation **21** formed in this manner should be racemic. So, the rearranged products formed from **21** should be optically active or racemic depending on whether **20** is involved or not.¹²

Optically active **19** was prepared, and solvolysis products obtained in various solvents were examined. The rearranged product **23** was always the main product and the chirality of the substrate **19** was completely transferred to the product **23** in all solvents employed, ranging from ethanol to HFIP (1,1,1,3,3,3-hexafluoropropan-2-ol).¹² Typical results are shown in eq 8.

A similar vinylic cation was once claimed to be formed during the solvolysis of cyclohexylidenemethyl triflate in aqueous methanol at 140 °C (eq 9),¹³ but this reaction could occur via participation and S_N2-type reaction. Solvolysis of the optically active 4-methyl-substituted triflate under the same reaction conditions took place with complete retention of the optical purity.¹⁴



Scheme 3. Chirality probe approach to search for primary vinyl cation.



It should be noted here that racemization should have been observed, if the racemization of cation **21** via 1,2-hydride shift (eq 10) occurred during the reaction even though the primary cation **20** was not involved. The barrier to this rearrangement should be high enough as the theoretical calculations suggest (Figure 3). This is in contrast to the fact that the acyclic analog has essentially no barrier to rearrangement (see below).

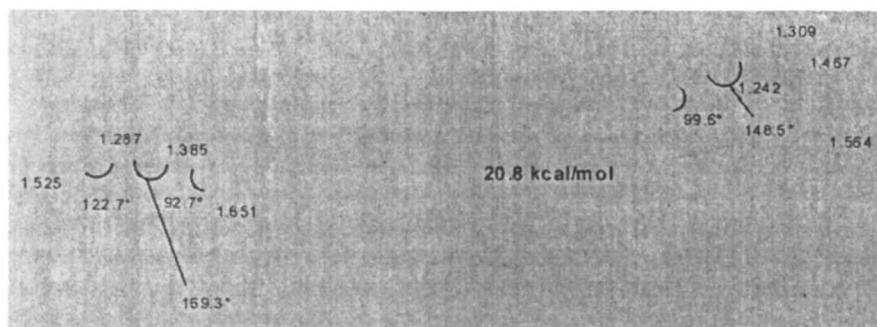
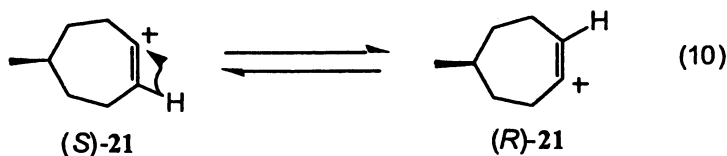
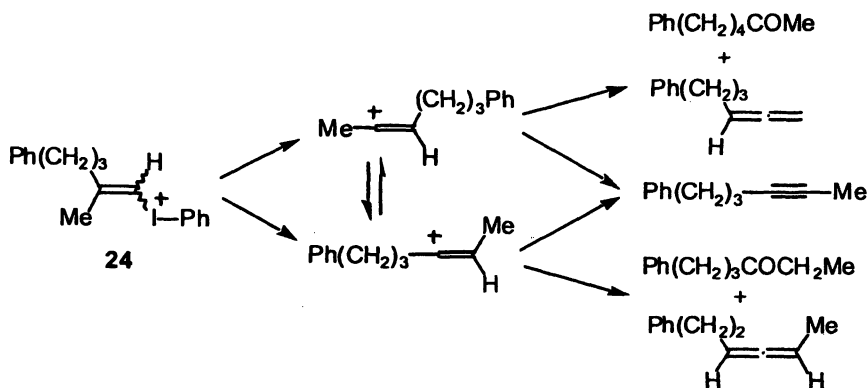


Figure 3. Calculated free energy barrier for 1,2-hydride shift of cyclohept-1-enyl cation and the optimized structures (MP2/6-31 G(d)).^{12b}

Neighboring Group Participation

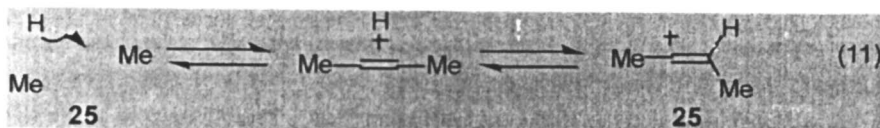
Although formation of primary vinyl cation was disproved by the chirality probe approach, a vinyl cationic intermediate can be generated from a primary substrate via participation if a more stable cation could result. Unsymmetrically substituted 2,2-dialkylvinyl iodonium salt **24** gave mainly rearranged products on solvolysis.¹⁵ The products involve those of the 1,2-shift of either of the alkyl groups on the β position (Scheme 4). Those formed from migration of the alkyl

group *trans* to the leaving iodonio group are somewhat more predominant but not significantly. The diversity of the solvolysis products can be explained by participation of the *trans* alkyl group to form one of the secondary vinyl cations, but the 1,2-hydride shift to give the isomeric secondary cation is very fast. Those two secondary vinylic cation intermediates give rise to a variety of substitution and elimination products. The primary vinyl cation may not be formed.



Scheme 4. Rearrangement in solvolysis of 2,2-dialkylvinyl iodonium salt.

A model calculation was carried out for the degenerate 1,2-hydride shift of 1,2-dimethylvinyl cation 25 (eq 11) at the level of MP2/6-31G(d).¹⁵ As illustrated in Figure 4, a hydrogen-bridged structure is more stable than the normal open structure in the gas-phase calculation, although the solution structure could be the latter open form. The barrier to the hydride shift is very low. It is also noticeable that the C-C-C angle at the vinylic carbons of the hydrogen-bridged form is nearly 180°: the intermediate state for the 1,2-hydride shift looks like a proton-coordinated acetylene. We found a considerable barrier to the 1,2-hydride shift of cycloheptenyl cation as mentioned above (Figure 3). This barrier for the cyclic vinyl cation may be derived from the angle strain at the positive carbons in the transition state, which is similar to the hydrogen-bridged form.



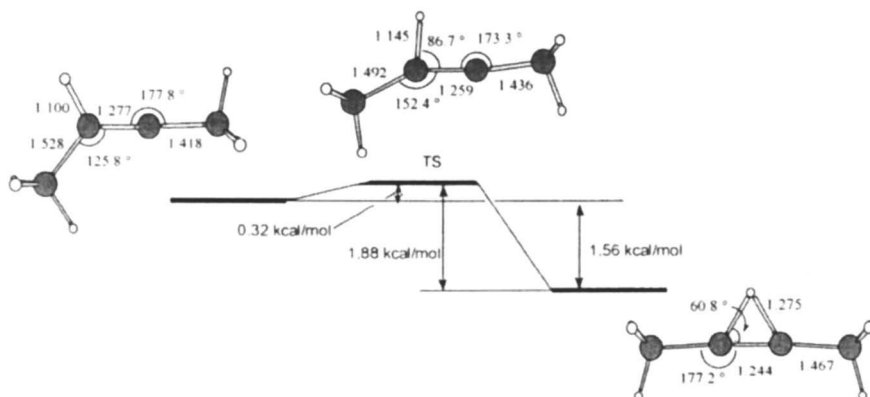
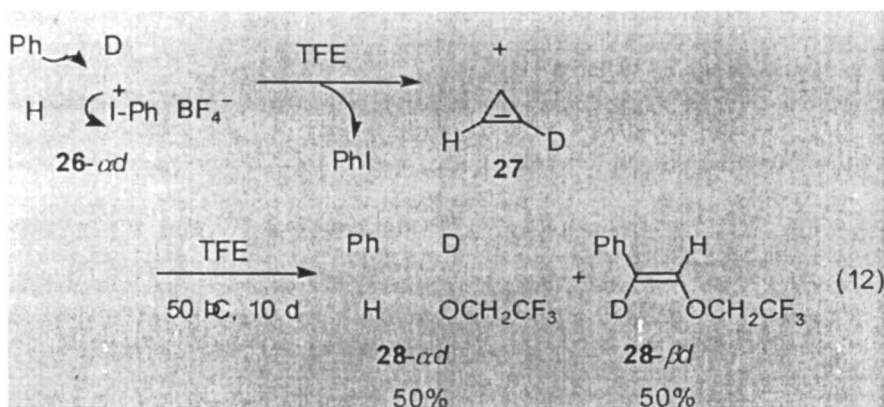
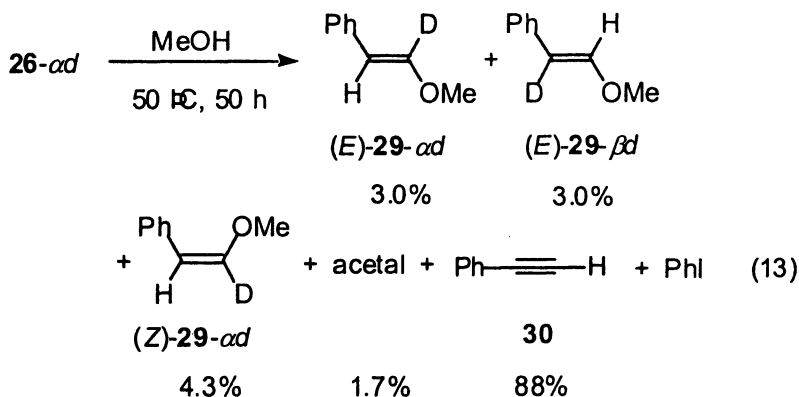


Figure 4. Free energy barrier for the 1,2-hydride shift of 1,2-dimethylvinyl cation (**25**) calculated at MP2/6-31G(d).

Interesting results concerning phenyl group participation were observed with (*E*)-styryl(phenyl)iodonium tetrafluoroborate (**26**) using a deuterated substrate (eq 12)¹⁶ When **26-*ad*** was heated in trifluoroethanol (TFE) at 60 °C, slow reaction gave the *E* isomer of substitution product **28** quantitatively, but the deuterium was completely scrambled between the α and β positions. This strongly indicates that a symmetrical intermediate is involved during the reaction and the most reasonable one is vinylenebenzenium ion (**27**) formed by phenyl participation. This intermediate also explain the exclusive formation of the retained (*E*)-**28**.



Methanolysis of **26-*ad*** gave mainly the product of α -elimination, phenylethyne (**30**), but a small amount of substitution product **29** was also obtained (eq 13).^{16b} The deuterium distributions in the isomeric products (*E*)-**29** and (*Z*)-**29** are very interesting and shed light on the reaction mechanisms for their formation. Due to the basicity of methanol, the main reaction path becomes α -elimination. The deuterium is completely scrambled in the *E* isomer of **29**, as observed in the products of trifluoroethanolysis. In contrast, the *Z* isomer of **29**, the product of inversion, retains the deuterium at the original *a* position. The best interpretation is that (*E*)-**29** is formed via phenyl participation while (*Z*)-**29** is produced via the in-plane S_N2 reaction.



Since participation should occur *trans* relative to the leaving group due to the stereoelectronic effects, the substrate geometry must affect the outcome. Reactions of stereoisomeric 2-phenylprop-1-enyl(phenyl)iodonium tetrafluoroborate (**31**) were thus examined.¹⁷ The solvolysis rate for the *E* isomer is much greater than that for the *Z* isomer (4000 times in TFE); the phenyl group is more effectively assisting the departure of the leaving group than the methyl group. This reactivity is contrasting to that observed in the reaction with base (α -elimination) where (*Z*)-**31** is about 3 times more reactive than (*E*)-**31**. Solvolysis products, however, involve those of migration of both phenyl and methyl groups as shown in eq 14. Product distributions in reactions of (*E*)-**31** and (*Z*)-**31** in methanol and TFE at 60 °C are summarized in Table II.¹⁷

As illustrated in Scheme 5, (*E*)-**31** directly gives cation **37** via phenyl participation, while (*Z*)-**31** provides **38** more slowly via methyl participation. Cation **37** can further rearrange to more stable **38** by 1,2-hydride shift, but **38** cannot isomerize to less stable **37**. As a result, (*E*)-**31** can afford not only **33**, **35**, and **36** but also **34**, but (*Z*)-**31** only gives **34** and **35** depending on the nucleophilicity of the solvent. The unrearranged product **32** is formed via inversion only from (*Z*)-**31** in a more nucleophilic solvent. This must result directly from the S_N2 reaction of (*Z*)-**31**.

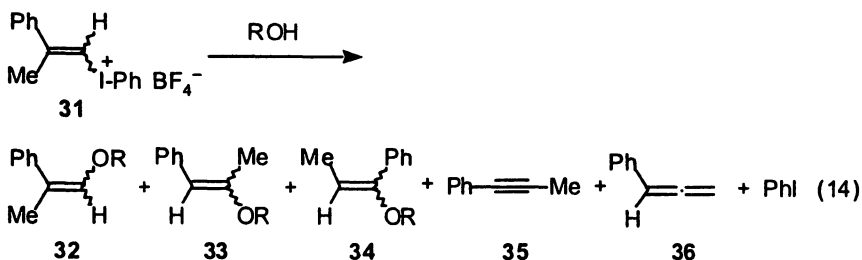
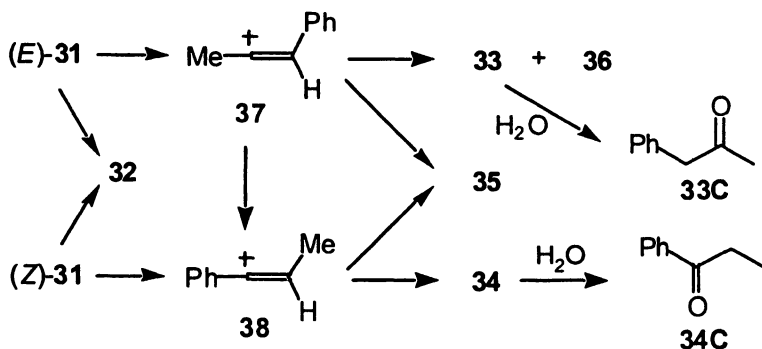


Table II. Product Distributions (in percent Yields) in the Solvolysis of 31^a

Subst.	Solv.	time (h)	32(<i>E/Z</i>) ^b	33(<i>E/Z</i>) ^b	34	35	36	PhI
(<i>E</i>)-31	MeOH	1	0	29(15/0)	0	28	30	97
(<i>Z</i>)-31	MeOH	95	5.8(5.8/0)	0	4.9	81	0	87
(<i>E</i>)-31	TFE	0.5	0	20	11	17	6.4	85
(<i>Z</i>)-31	TFE	170	0	0	14	6.7	0	22

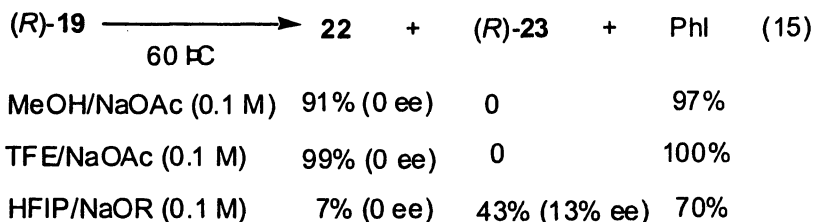
^a At 60 °C. ^b Total yields of the enol ether and the hydrolyzed carbonyl derivative with the isomer yields of *E/Z* enol ethers in parentheses.



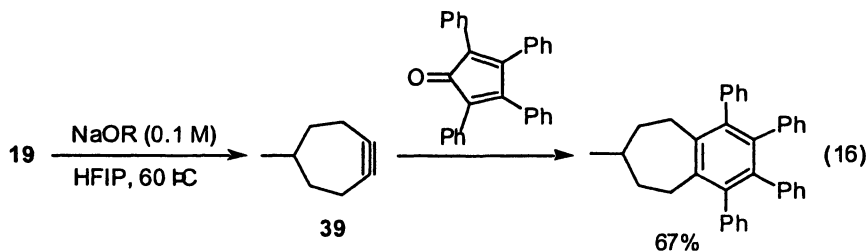
Scheme 5. Solvolysis of (E)- and (Z)-31.

Participation and Elimination

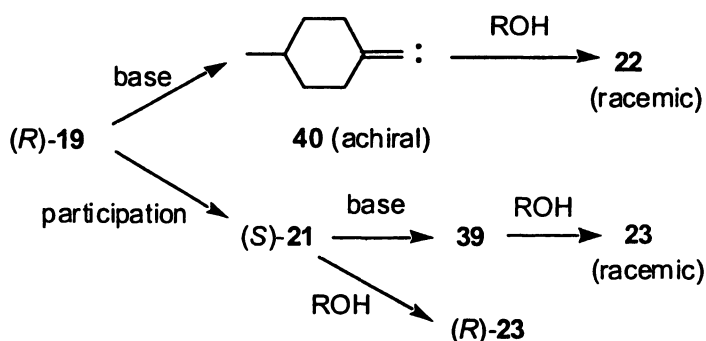
As discussed in the preceding section, primary vinylic iodonium salts undergo rearrangement via participation if this leads to a more stable vinylic cation. However, a more facile reaction, α -elimination (or S_N2 reaction), competes with the rearrangement when some base (or nucleophile) can operate. Even neutral methanol solvent is basic enough to induce α -elimination (and some S_N2 reaction), as observed with the styryl derivative **26** (eq 13). The chiral substrate **19** also undergoes some α -elimination to give largely racemized unrearranged product **22** (eq 8). That is, competition between the participation (leading to rearrangement) and the α -elimination depends on the basicity of the reaction medium. In the presence of acetate as a base in methanol, **22** was obtained exclusively from **19**, and racemization occurred (eq 15). This is also the case for the reaction in TFE (eq 15).^{12b,18}



In a still less basic solvent, HFIP, a considerable amount of the rearranged product **23** was obtained even in the presence of base. Interestingly, compound **23** obtained was largely racemized, although **23** was the exclusive product and retained the optical purity of the substrate in a neutral HFIP without added base.¹² So, the racemization cannot be ascribed to the intermediate formation of the primary cation **20**. Trapping experiments support the formation of cycloheptyne **39** as an intermediate (eq 16).¹⁸



Under more basic conditions, α -elimination predominates and insertion of the carbene **40** to the solvent gives racemic **22**. Non-basic and poorly nucleophilic conditions allow neighboring group participation to form the rearranged substitution product **23** with complete chirality transfer. The participation can be considered as an intramolecular nucleophilic substitution, and does occur only when it is preferable to the external reactions. Under slightly basic conditions with bases in HFIP, participation is allowed, and the weak base can react with the more electrophilic vinylic cation **21** (but not with the iodonium ion **19**). A suitably controlled basicity can result in the formation of cycloalkyne **39**, which is symmetrical and leads to racemization. These reactivities are illustrated in Scheme 6.

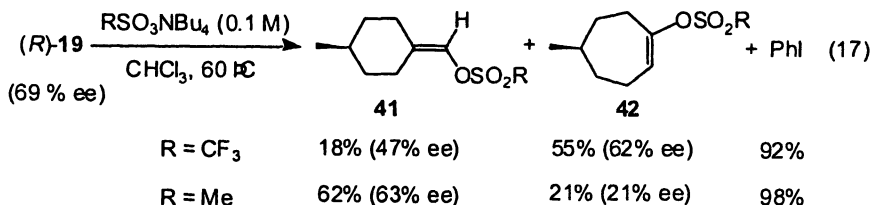


Scheme 6. Competition between participation and base/nucleophile.

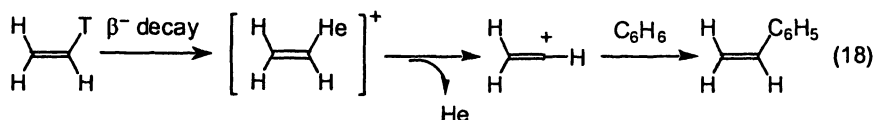
Similar observations were found in the reaction of **19** with sulfonates in chloroform.¹⁹ Triflate gave mainly the rearranged product that retained the optical purity mostly if not completely. In contrast, mesylate (methanesulfonate) gave mainly the optically active unrearranged substitution product **41** probably mainly via S_N2 reaction, while accompanying rearranged product **42** was largely racemized (eq 17). Trapping experiments again showed formation of cycloheptyne **39** in the mesylate reaction. The difference in selectivity of triflate and mesylate may arise in two steps: the nucleophilicity (in this case) works in the first step, while basic and nucleophilic competition operates in the second step. Low nucleophilicity (and basicity) of triflate allows more participation and the nucleophilic reactivity predominates toward the cation **21** in the second step. Mesylate only allows partial rearrangement in the first step in competition with S_N2 , but the basicity predominates in the second step.

Photosolvolysis

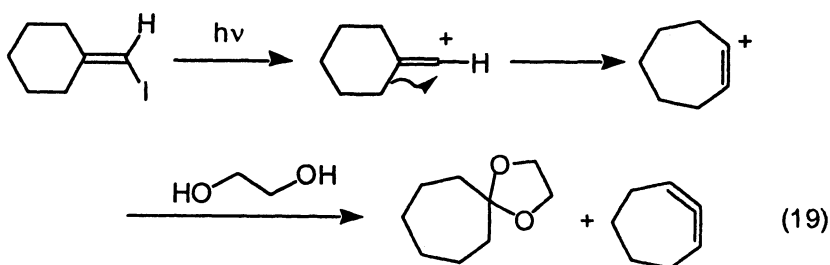
Primary vinyl cation cannot be generated thermally from the iodonium salts as described above. However, parent vinyl cation could be generated from the



precursor bearing the extreme leaving group helium which is generated by nuclear decay of tritium (³H, half-life, 12.25 years). That is, tritioethene was left in a benzene solution for a year, and formation of styrene, a Friedel-Crafts product from vinyl cation, was detected (eq 19).²⁰



The leaving group ability of halides in electronically excited vinyl halides should be greatly enhanced as compared to the ground-state molecules. This makes photolysis of vinyl halides a good entry to vinyl cations.²¹ Many vinyl bromides and iodides were subjected to photochemical reaction, and the rearranged products were observed. Formation of the primary vinyl cations is usually assumed and rearrangement to the more stable secondary cations is proposed without any definitive evidence. For example, cyclohexylidenemethyl iodide gives ring-expanded substitution and elimination products (eq 19).²²



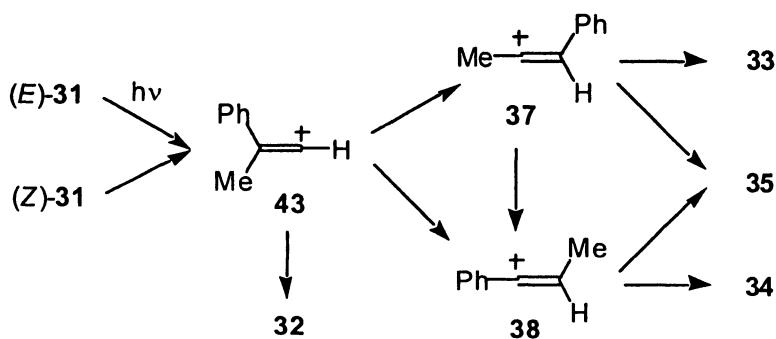
Photosolvolysis of some vinyl iodonium substrates can be compared with thermal solvolysis of the same substrates. Photochemical reaction of (*E*)- and (*Z*)-2-phenylprop-1-enyl(phenyl)iodonium tetrafluoroborate (**31**) in methanol and TFE gave products of heterolytic cleavage of vinylic C-I bond as summarized in Table III (for the product structures see eq 14.¹⁷ In contrast to

the corresponding thermal reaction (Table II), product distribution is not affected much by the geometrical structure of **31**. This points to the formation of a common intermediate, the primary vinyl cation **43**, from both (*E*)-**31** and (*Z*)-**31**. This cation gives unrearranged product **32**, and rearranges to the more stable cations, **37** and **38**, which in turn give **33**, **34**, and **35** (Scheme 7). In thermal reaction, the rearranged cations, **37** and **38**, should form directly from **31** via participation of the group *trans* to the leaving group (Scheme 5), and thus product distribution is greatly affected by the geometry of the substrate.

Table III. Product Distributions (in percent Yields) in Photosolvolysis of (*E*)- and (*Z*)-31** in Methanol and TFE at 20 °C**

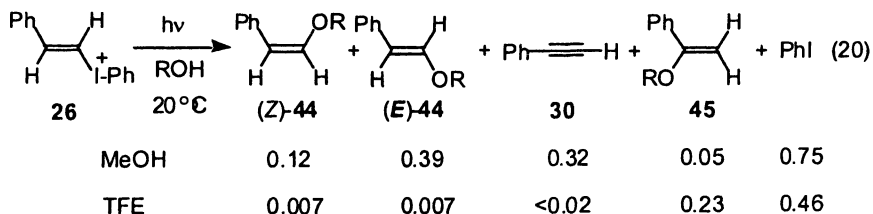
<i>Subst.</i>	<i>Solv.</i>	32 (<i>E/Z</i>) ^a	33 (<i>E/Z</i>) ^a	34 (<i>E/Z</i>) ^a	35	<i>PhI</i>
(<i>E</i>)- 31	MeOH	47.5(34.1/13.4)	6.5(6.5/0)	16.8(8.2/8.6)	15.3	66.3
(<i>Z</i>)- 31	MeOH	53.3(14.8/38.5)	7.5(7.5/0)	22.3(10.8/11.5)	16.7	71.5
(<i>E</i>)- 31	TFE	0	46.9(32.6/4.4)	46.8	<2	81
(<i>Z</i>)- 31	TFE	0	15.2(11.0/2.2)	64.5	<2	70

^a Total yields of the enol ether and the hydrolyzed carbonyl derivative with isomer yields of *E/Z* enol ether in parentheses.

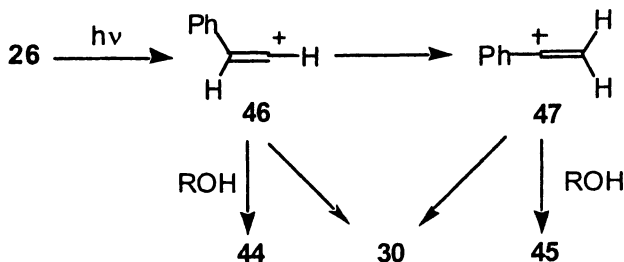


*Scheme 7. Photosolvolysis of (*E*)- and (*Z*)-**31**.*

Photosolvolysis of (*E*)-styryl iodonium salt **26** also gave product distributions quite different from those obtained in thermal solvolysis.^{16,23} Quantum yields for the formation of photoproducts formed via heterolytic cleavage of the vinylic C-I bond of **26** in methanol and TFE at 20 °C are given in eq 20.²³



In contrast to the thermal solvolysis, a rearranged enol ether **45** (and also the hydrolysis product, acetophenone) is formed in addition to the unrearranged product **44**. The rearrangement is more apparent in less nucleophilic TFE. The results are best accounted for by heterolysis to give the open primary styryl cation **46** (Scheme 8). This cation gives products of substitution **44** and elimination **30** by reaction with the solvent. Alternatively, **46** can rearrange to the α -phenyl vinyl cation **47** via 1,2-hydride shift, which gives rise to **45** and **30**.



Scheme 8. Photosolvolysis of **26**.

Comparisons of product distributions in thermal and photochemical solvolyses show that the primary vinyl cation is not involved in thermolysis but is formed photochemically. The chirality probe approach using optically active 4-methylcyclohexylidene(methyl(aryl)iodonium tetrafluoroborate **19** was applied to the photosolvolysis.²⁴ The rearranged product 4-methylcycloheptanone retained some optical activity, but the enantiomeric product in slight excess has a different structure depending on the iodoarene leaving group ArI of the substrate. The results indicate that the primary vinyl cation involved is not in a free, dissociated achiral form.

Cyclohexenyl and cyclopentenyl iodonium tetrafluoroborates were also photolyzed in methanol. Ring-strained five-membered cyclic vinyl cation could be generated photochemically as well as the six-membered cyclic vinyl cation.²⁵

In conclusion, vinyl iodonium salts are excellent pregenerators for vinylic cations due to high nucleofugality of the iodonio group (about 10^6 -fold of triflate), although they are in equilibrium with the less reactive hypervalent

adduct with the counterion. Primary vinyl cation cannot be generated thermally but rearrangement occurs readily via participation if a more stable vinylic cation results. Photo-excited state of vinyl iodonium salts can effectively provide primary vinyl cations without participation.

References

1. Recent reviews on vinyl iodonium salts: Zhdankin, V. V.; Stang, P. J. *Chem. Rev.* **2002**, *102*, 2523–2584. Stang, P. J. *J. Org. Chem.* **2003**, *68*, 2997–3008. Ochiai, M. *Hypervalent Iodine Chemistry*; Wirth, T., Ed.; Springer: Berlin, 2003; pp 5–68.
2. A recent review on vinyl cations: Rappoport, Z.; Stang, P. J. Eds.; *Dicoordinated Carbocations*, John Wiley & Sons: Chichester, 1997.
3. Okuyama, T.; Fujita, M.; Gronheid, R.; Lodder, G. *Tetrahedron Lett.* **2000**, *41*, 5125–5129.
4. Swain, G.; Rogers, R.J. *J. Am. Chem. Soc.* **1975**, *97*, 799.
5. Okuyama, T.; Takino, T.; Sueda, T.; Ochiai, M. *J. Am. Chem. Soc.* **1995**, *117*, 3360–3367.
6. Okuyama, T.; Imamura, S.; Fujita, M. *J. Org. Chem.* **2006**, *71*, 1609–1613.
7. (a) Okuyama, T.; Takino, T.; Sato, K.; Ochiai, M. *J. Am. Chem. Soc.* **1998**, *120*, 2275–2282. (b) Okuyama, T.; Takino, T.; Sato, K.; Oshima, K.; Imamura, S.; Yamataka, H.; Asano, T.; Ochiai, M. *Bull. Chem. Soc. Jpn* **1998**, *71*, 243–257.
8. Grob, C.A.; Cseh, G. *Helv. Chim. Acta*, **1964**, *47*, 194
9. Stang, P.J. *Acc. Chem. Res.* **1978**, *11*, 107–114.
10. Okuyama, T.; Imamura, S.; Ishida, Y. *Bull. Chem. Soc. Jpn* **2001**, *74*, 543–548.
11. Okuyama, T.; Lodder, G. *Adv. Phys. Org. Chem.* **2002**, *37*, 1–56.
12. (a) Fujita, M.; Sakanishi, Y.; Okuyama, T. *J. Am. Chem. Soc.* **2000**, *122*, 8787–8788. (b) Fujita, M.; Sakanishi, Y.; Nishii, M.; Yamataka, H.; Okuyama, T. *J. Org. Chem.* **2002**, *67*, 8130–8137.
13. Hanack, M.; Märkl, R.; Martinez, A. G. *Chem. Ber.* **1982**, *115*, 772–782.
14. Fujita, M.; Yamamoto, A.; Sugimura, T.; Okuyama, T. *Chem. Lett.* **2001**, 806–807;
15. Okuyama, T.; Yamataka, H.; Ochiai, M. *Bull. Chem. Soc. Jpn* **1999**, *72*, 2761–2769.
16. (a) Okuyama, T.; Ochiai, M. *J. Am. Chem. Soc.* **1997**, *119*, 4785–4786. (b) Okuyama, T.; Ishida, Y.; Ochiai, M. *Bull. Chem. Soc. Jpn* **1999**, *72*, 163–170.
17. Gronheid, R.; Lodder, G.; Ochiai, M.; Sueda, T.; Okuyama, T. *J. Am. Chem. Soc.* **2001**, *123*, 8760–8765.
18. Fujita, M.; Ihara, K.; Kim, W.H.; Okuyama, T. *Bull. Chem. Soc. Jpn* **2003**, *76*, 1849–1855.

19. (a) Fujita, M.; Sakanishi, Y.; Okuyama, T. *J. Am. Chem. Soc.* **2001**, *123*, 9190–9191. (b) Fujita, M.; Sakanishi, Y.; Nishii, M.; Okuyama, T. *J. Org. Chem.* **2002**, *67*, 8138–8146.
20. Fornarini, S.; Speranza, M. *Tetrahedron Lett.*, **1984**, *25*, 869–872; *J. Am. Chem. Soc.* **1989**, *111*, 7402–7407.
21. Lodder, G., *Dicoordinated Carbocations*, Rappoport, Z.; Stang, P. J., Eds.; John Wiley & Sons: Chichester, **1997**; pp. 377–431.
22. Kropp, P.J.; McNeely, S.A.; Davis, R.D. *J. Am. Chem. Soc.* **1983**, *105*, 6907–6915.
23. Gronheid, R.; Lodder, G.; Okuyama, T. *J. Org Chem.* **2002**, *67*, 693–702.
24. Fujita, M.; Furutani, M.; Okuyama, T. *Tetrahedron Lett.* **2002**, *43*, 8579–8581.
25. Slegt, M.; Gronheid, R.; van der Vlugt, D.; Ochiai, M.; Okuyama, T.; Zuilhof, H.; Overkleeft, H.S.; Lodder, G. *J. Org Chem.* **2006**, *71*, 2227–2235.

Chapter 5

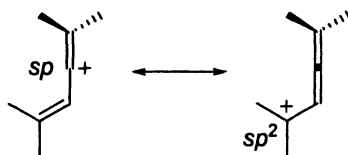
Generation of Alkylideneallyl Cations from Alkylidenecyclopropanone Acetals: Selectivity of Reaction with Nucleophiles

Morifumi Fujita and Tadashi Okuyama

Graduate School of Material Science, Himeji Institute of Technology,
University of Hyogo, Kamigori, Hyogo 678-1297, Japan

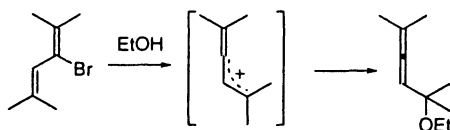
Ring opening reaction of alkylidenecyclopropanone acetals readily proceeds in the presence of Lewis or Brønsted acids to produce 1-alkylidene-2-oxyallyl cation, which is provided for the reaction with nucleophiles such as chloride, alcohols, siloxyalkenes, and furans. The reaction of this cation with the carbon nucleophiles gives products of [4 + 3] and [3 + 2] cycloaddition as well as those of nucleophilic addition. The modes of addition reactions are controlled by the oxy group of the cation and by the reaction conditions including solvent.

Alkylideneallyl cations can be described as resonance hybrids of 1-vinyl-substituted vinyl cations and allenylmethyl cations, and thus contain two reactive sites (the sp - and sp^2 -hybridized carbons) for nucleophilic addition (Scheme 1) (1,2). Hybridization affects the electronic and steric character of these reaction sites. The electronic property was deduced from the ^{13}C NMR chemical shifts of alkylideneallyl cations measured under superacidic conditions (3) and also from the charge distribution calculated (4). The charge distributions are affected by substituents on the cation: the sp^2 carbon is more positive than the sp carbon when two methyl groups are introduced at the sp^2 carbon.

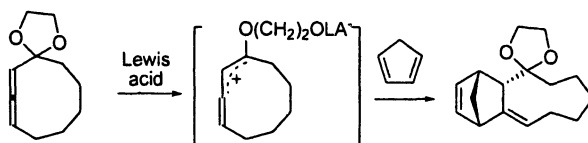


Scheme 1. Resonance structure of alkylideneallyl cation.

Some reactions via intermediate alkylideneallyl cations have been reported. Solvolysis of 3-bromo-2,5-dimethyl-2,4-hexadiene in ethanol at 100 °C for 80 min gives 5-ethoxy-2,5-dimethyl-2,3-hexadiene in quantitative yield (Scheme 2) (5). This indicates that ethanol selectively attacks the sp^2 carbon of the intermediate alkylideneallyl cation. A similar selectivity has been observed in the solvolysis of 2,3-dienyl alcohols (6), and is in agreement with the charge distribution. A cycloaddition reaction via an alkylideneallyl cation intermediate has been reported as illustrated in Scheme 3 (7).



Scheme 2. Solvolysis of vinyl bromide via an alkylideneallyl cation.

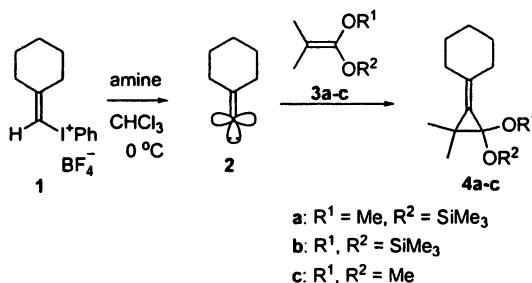


Scheme 3. [4 + 2] Cycloaddition of an alkylideneallyl cation.

We have recently developed a novel method for the generation of alkylideneallyl cations from alkylidenecyclopropanone acetals (8, 9). This method provides a nice opportunity to examine the selectivity of reactions of the ambident cation with various nucleophiles including siloxyalkenes (10) and furans (11). The reaction of the cation with the carbon nucleophiles gives [4 + 3] and [3 + 2] cycloaddition products as well as simple nucleophilic addition products. These results are summarized in this chapter.

Preparation of Alkylidenecyclopropanone Acetals

Alkylidenecyclopropanone acetals **4** are readily available from the reaction of alkylidenemethyliodonium salt **1** and ketene acetals **3** in the presence of an amine base such as triethylamine and 1,5-diazabicyclo[4.3.0]non-5-ene (Scheme 4). The alkylidenemethyliodonium salt **1** readily gives the corresponding alkylidenecarbene **2** (*12*) in the presence of amine in an aprotic solvent owing to the high acidity of the α -hydrogen (*13*), and the excellent nucleofugality (*14*) of the positive iodonio group. Addition of **2** to **3a–c** gives the cyclopropane compounds **4a–c**.



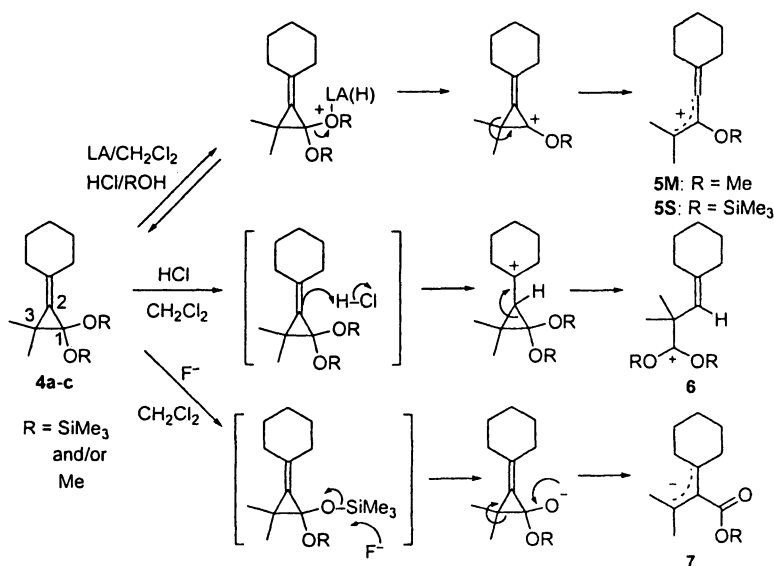
Scheme 4. Preparation of alkylidenecyclopropanone acetals.

Ring Opening of Alkylidenecyclopropanone Acetals

Alkylidenecyclopropanone acetal **4** is a suitable precursor for generation of 1-alkylidene-2-oxyallyl cation **5M** or **5S** via ring opening at the C2–C3 bond of the cyclopropane ring (Scheme 5). To find suitable conditions for generation of the cation, reactions of **4a–c** were examined under varied conditions. Reaction with Lewis acid (TiCl₄ and SnCl₄) in dichloromethane proceeds at –78 °C to give 1-alkylidene-2-oxyallyl cation intermediate **5M** or **5S**. Hydrogen chloride also promotes the ring opening reactions of **4a–c**, but the regioselectivity of ring opening depends on the solvent. Thus, the reaction in 1,1,1,3,3,3-hexafluoropropan-2-ol (HFIP) selectively gave the desired allylic cation via the C2–C3 bond cleavage, while the reaction in dichloromethane resulted in the ring opening at the C1–C2 bond to give **6**. Another mode of bond cleavage at the C1–C3 bond is affected by fluoride ion, leading to an allylic anion **7**.

The regioselectivity of ring opening of **4a–c** is successfully controlled by the choice of reaction conditions. Lewis acid in dichloromethane and hydrogen chloride in alcohol are suitable conditions for generation of an alkylideneallyl cation, which was employed for studying its reactivity with nucleophiles such as

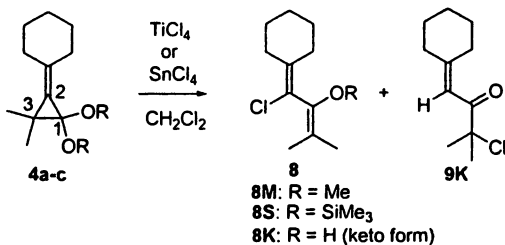
chloride, methanol, siloxyalkenes, and furans. The mechanistic details of the regioselectivity of ring opening of **4a–c** will be mentioned in the following section.



Scheme 5. Regioselective ring opening of alkylidenecyclopropanone acetal.

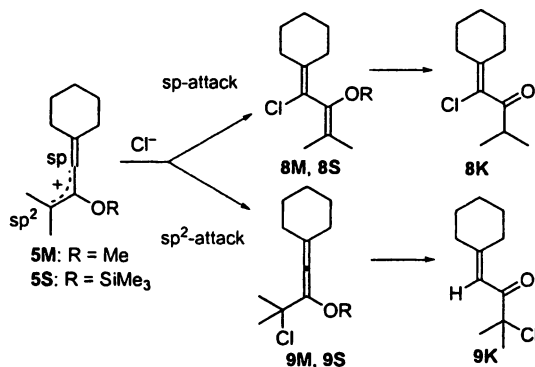
Reaction with Lewis Acid

Reactions of **4a–c** with a Lewis acid, TiCl₄ or SnCl₄, were carried out in dichloromethane at 0 and –78 °C to yield the chlorinated products, **8** and **9** (Table I) (**8**). These products are the result of selective C2–C3 bond cleavage of the cyclopropane ring. The reaction is rationalized by a mechanism involving an alkydeneallyl cation intermediate **5**, which is trapped by chloride ion at the sp and sp² carbons to give **8** and **9**, respectively (Scheme 6). The Lewis acid-mediated ring opening reaction of **4a–c** is initiated by cleavage of the acetal. For the unsymmetrical acetal **4a**, there are two possibilities for acetal cleavage, namely siloxide elimination and methoxide elimination (Scheme 7). The former gives methoxy allyl cation **5M** and the latter gives the siloxyallyl cation **5S**. Product distribution of the reaction of **4a** (**8M** as a major product and no **8S**) indicates preferential formation of the methoxy-substituted allyl cation **5M** via siloxide elimination. This is consistent with the higher leaving ability of trimethylsiloxy group relative to methoxy group and furthermore the siloxy oxygen is more basic to promote its departure via acid coordination.

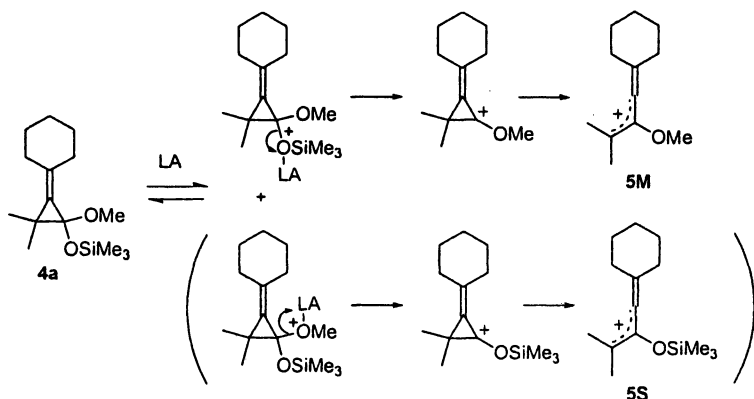
Table I. Reaction of 4a–c with Lewis Acid^a

Sub.	Acid	Temp. (°C)	Yield (%)			
			8M	8S	8K	9K
4a	TiCl ₄	0	51	0	16	29
4a	TiCl ₄	-78	82	0	0	6
4a	SnCl ₄	0	85	0	0	0
4a	SnCl ₄	-78	98	0	0	0
4b	TiCl ₄	0	0	63	13	24
4b	TiCl ₄	-78	0	92	0	8
4b	SnCl ₄	-78	0	95	5	0
4c	SnCl ₄	0	69	0	0	0

^a In dichloromethane.



Scheme 6. Lewis acid-mediated reaction via alkylideneallyl cation.

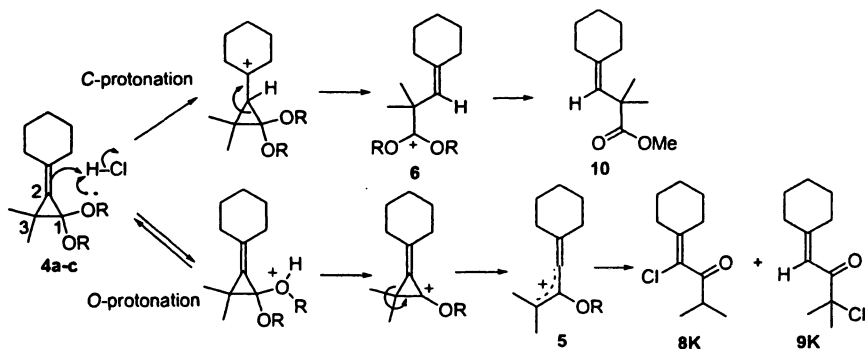


Scheme 7. Selectivity of acetal cleavage.

The product ratio of **8/9** reflects the regioselectivity of nucleophilic attack at the allylideneallyl cation **5** which has two electrophilic centers, the sp and sp^2 carbons. Exclusive formation of **8** is observed in the reaction of **4a–c** with SnCl_4 , but the TiCl_4 -induced reaction also gives **9K** as well as **8**. The reaction at lower temperature provided more **8**. This tendency is observed for the reactions of **4a** and **4b**, which proceed via **5M** and **5S**, respectively. The positive charge is distributed mainly at the sp and sp^2 carbons of the allylic cation **5**, and the methyl groups stabilize the positive charge at the sp^2 position. Formation of a smaller amount of **9K** cannot be explained by the charge distributions in the allylic cation **5**. Addition of chloride to the sp^2 carbon gives a tertiary allenylmethyl chloride (**9M** or **9S**), which can readily regenerate **5**. However, decreasing yield of **8** at higher temperature is contrary to the exception from the thermodynamic stability of **8**. Similar regioselectivity of the chloride addition to **5** was also observed in the HCl -mediated reaction of **4a–c** (see below). Although the temperature-dependent product distributions are not consistent with the reversibility of the sp^2 addition or thermodynamic control of the product formation, any other reasonable interpretation cannot be proposed of this regioselectivity.

Reaction with Hydrogen Chloride

Reaction of **4a–c** with hydrogen chloride was carried out at room temperature in various solvents including dichloromethane, diethyl ether, tetrahydrofuran, acetonitrile, DMF, and 1,1,1,3,3,3-hexafluoropropan-2-ol (HFIP). The ring opening of **4a–c** readily proceeded to give the ester **10** as well as chloride substitution products, **8K** and **9K**, as shown in Scheme 8 (**9**). Product yields are dependent on the solvent, as summarized in Table II. Ester **10**



Scheme 8. Reaction with hydrogen chloride.

Table II. Reaction of 4a–c with Hydrogen Chloride^a

Sub.	Solvent	Yield (%)			
		8K	9K	10	10/(8K+9K)
4a	CH ₂ Cl ₂	0	0	82	>99/1
4a	Et ₂ O	19	2	59	73/27
4a	MeCN	22	9	37	55/45
4a	DMF	48	3	18	26/74
4a	HFIP	77	0	0	<1/99
4b ^b	CH ₂ Cl ₂	8	0	77	91/9
4b ^b	Et ₂ O	8	2	64	87/13
4b ^b	MeCN	40	9	42	46/54
4b ^b	DMF	71	4	5	6/94
4b ^b	HFIP	85	0	0	<1/99
4c	CH ₂ Cl ₂	0	0	98	>99/1
4c	Et ₂ O	0	0	60	>99/1
4c	MeCN	0	9	82	90/10
4c	DMF	0	0	98	>99/1
4c	HFIP	69	0	0	<1/99

^a Reaction was carried out at rt in the presence of HCl (0.1 M). ^b The reaction mixture was worked-up with methanol containing sulfuric acid in order to analyze silyl ester and/or carboxylic acid as the methyl ester 10. No 10 was detected before the work-up.

is formed via cleavage of the C1-C2 bond of **4a-c**, while the chloride products **8K** and **9K** result from cleavage of the C2-C3 bond. For **4a** and **4b**, the regioselectivity $10/(8K+9K)$ was gradually changed as a function of the solvent employed; the content of **10** seems to decrease with increasing polarity of the solvent. The reaction of **4c** gave **10** as a major product, except for the reaction in HFIP.

The formation of **10** may be initiated by protonation of the olefinic carbon giving the cyclopropyl-stabilized cation which undergoes cleavage at the C1-C2 bond to form the dioxy-stabilized carbocation **6**. This cation finally gives rise to ester **10** (Scheme 8). A similar regioselective bond cleavage was observed in the ring-opening reactions of 1-alkoxy-2-cyclohexylidene cyclopropanes (*15*). The ring opening initiated by protonation at the carbon-carbon double bond is well known for the acid-mediated reaction of simple alkylidene cyclopropanes (*16*).

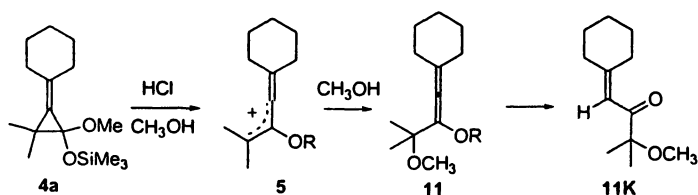
The product ratio of **8K/9K** is similar to that of the Lewis acid-mediated reaction of **4a-c**. These products of the C2-C3 bond cleavage (**8K** and **9K**) may be formed via alkylideneallyl cation intermediate, which is formed by the oxygen protonation of **4**. Thus, the product ratio of $10/(8K + 9K)$ is controlled by the protonations at the olefinic carbon and at the acetal oxygen of **4**.

Rate-determining protonation of the carbon must be followed by rapid ring opening, while oxygen protonation must take place reversibly and the ensuing acetal cleavage should be rate determining (*17*). These mechanisms of carbon and oxygen protonations can be differentiated by the kinetic isotope effect: the rate-determining carbon protonation should be decelerated by deuterium acid while the equilibrium protonation should be facilitated. Indeed, the reaction with deuterium chloride gave a lower yield of **8** than that observed in the reaction with hydrogen chloride in accord with these considerations. The product ratio of $10/(8K + 9K)$ decreased from 36/64 to 24/76 when DCl was employed instead of HCl for the reaction of **4a** in acetonitrile containing 1% H₂O (*9*). Compared with the dimethyl acetal substrate **4c**, the siloxy substrates **4a** and **4b** have a higher tendency for C2-C3 bond cleavage via oxygen protonation. This is in agreement with preferential elimination of siloxide as compared to methoxide during the Lewis acid-mediated reaction of **4a**.

The reactions in a non-basic aprotic solvent CH₂Cl₂ provided solely **10**, the product of carbon protonation, while those carried out in an acidic protic solvent HFIP give exclusively **8K**, the product of oxygen protonation. The equilibrium protonation may be favored in a protic solvent having abundant protons available. In other basic solvents, the proton donor involved in the reaction should be the conjugate acid of the solvent, and many factors may delicately control the selectivity of the reaction.

An alkylideneallyl cation intermediate **5** was effectively formed in alcoholic solvent during the HCl-mediated reaction of **4a-c**. Reaction of **4a** in methanol also gave **11K** (Scheme 9). When the reaction was carried out in CD₃OD,

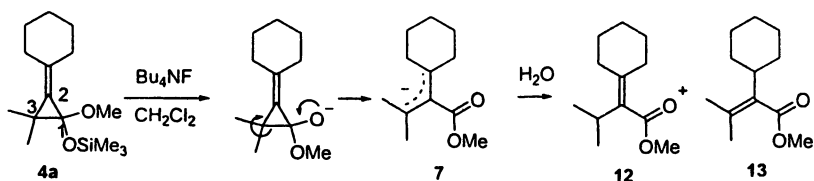
deuterium was incorporated at the vinylic position of **11K**, and **11K** contained the labeled methoxy CD₃O group. This is consistent with a reaction mechanism involving nucleophilic addition of methanol to **5**, formed by a proton-induced siloxide elimination process. The original methoxy group must be removed during acid-induced cleavage of the initially formed enol ether product **11**. Selective nucleophilic addition at the sp² position of **5** is that expected from the charge distribution in **5**, but differs from the regioselectivity of chloride addition.



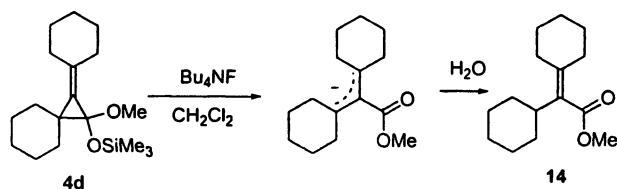
Scheme 9. Reaction of alkylideneallyl cation with methanol.

Reaction with Fluoride Ion

The reaction of **4a** with tetrabutylammonium fluoride in CH₂Cl₂ at ambient temperature gave a 1:1 mixture of esters **12** and **13** (Scheme 10), showing that ring cleavage occurs at the C1–C3 bond. Reaction of **4a** with fluoride ion must be initiated by elimination of the silyl group to give the oxy anion. Cleavage of the C1–C3 bond of this first-formed anion then opens the ring selectively to give the allylic anion **7**, which is protonated to yield a mixture of unsaturated esters, **12** and **13** (Scheme 10). The fluoride-initiated ring opening reaction of spiro substrate **4d** gave a single product **14** in 95% yield because of the symmetrical structure of the allylic anion intermediate (Scheme 11).



Scheme 10. Reaction with fluoride ion.

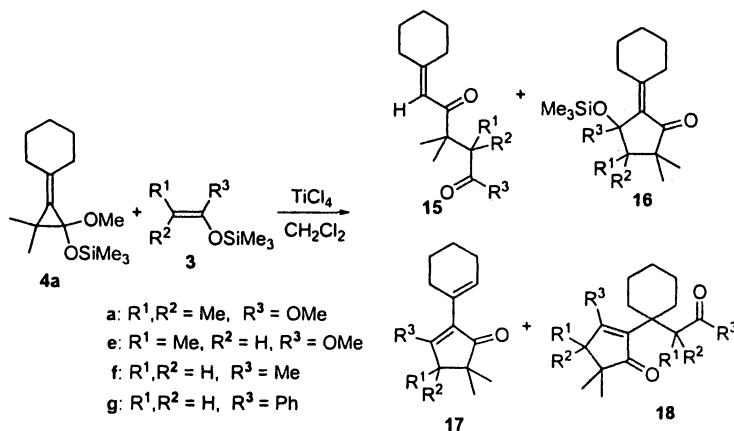


Scheme 11. Reaction of symmetrical allyl anion.

Reaction with Siloxyalkenes

Reaction of **4a** with TiCl_4 was carried out in the presence of siloxyalkene **3** as nucleophile and the results are summarized in Table III. In the reaction with ketene silyl acetals **3a** and **3e** at -78°C , γ -ketoesters **15a** and **15e** were obtained instead of chloride product **8** which is a major product in the absence of **3**. Formation of product **15** is likely to result from trapping of alkylideneallyl cation **5** with **3** at the sp^2 carbon. In contrast, the reactions with silyl enol ethers **3f** and **3g** gave no acyclic product **15**, but gave cyclopentanone derivatives **16–18**. The product distribution depends on the mode of addition of TiCl_4 (entries 4–7).

Table III. Reaction of **4a** with Siloxyalkene^a



Entry	3 ^b	$[\text{TiCl}_4]$ (mmol)	Yield (%)			
			15	16	17	18
1	3a (0.70)	0.14	90	0	0	0
2 ^c	3a (0.50)	0.70	0	0	41	0
3	3e (1.0)	0.41	81	0	0	0
4	3f (0.35)	0.15	0	73	9	6
5	3f (0.35)	0.075+0.075 ^d	0	28	3	38
6	3f (0.50)	0.075+0.15 ^d	0	0	0	75
7	3f (0.20)	0.11+0.11 ^d	0	0	62	0
8	3g (0.35)	0.15	0	63	0	0

^a In dichloromethane (10 mL) containing **4a** (0.1 mmol) at -78°C for 5 min.

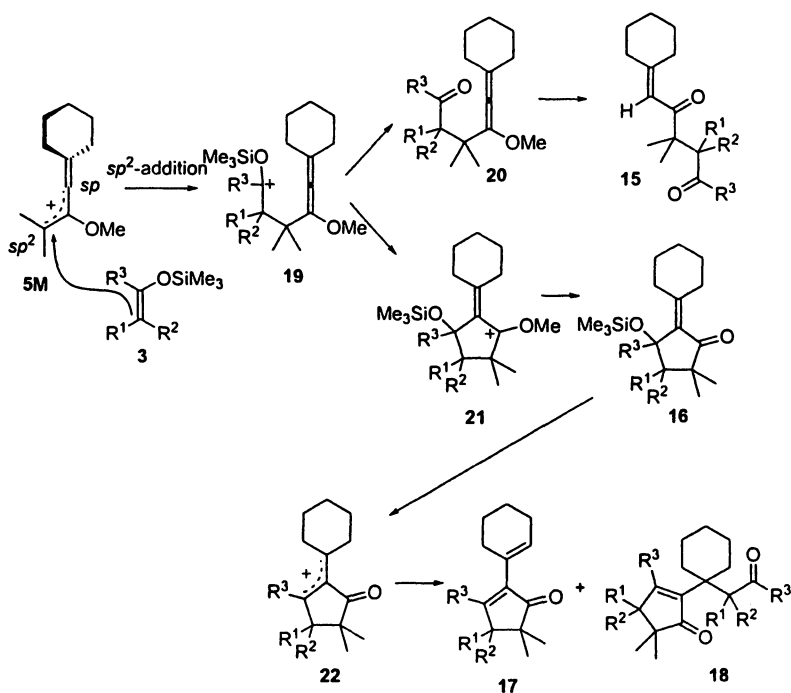
^b The values in parentheses are the amount of **3** (mmol).

^c Reaction was carried out at 0°C .

^d TiCl_4 was added twice. The second was after 5 min of the first.

Further addition of TiCl_4 decreased the yield of siloxycyclopentanone **16f**, accompanied by an increase of the double addition product **18f**. Use of a small amount of **3f** gave cyclopentenone **17f** (entry 7). These results suggest that **17** and **18** are secondary products derived from **16**. To confirm the secondary reactions, the isolated **16f** was subjected to the same reaction conditions. Treatment of **16f** with TiCl_4 gave **17f**, and those in the presence of **3f** gave **18f** as expected.

A plausible mechanism for the reactions of alkylideneallyl cation **5** with siloxyalkenes **3** is illustrated in Scheme 12. The cation **5M** generated from **4a** is



Scheme 12. A plausible mechanism for reaction with siloxyalkene.

trapped by siloxyalkene **3** at the sp^2 position to give the carbocation intermediate **19** which is stabilized by the oxy group(s). Desilylation of **19** results in the formation of acyclic adduct **15** via **20**, while intramolecular cyclization of **19** gives the cycloadduct **16**. If the stepwise $[3 + 2]$ cycloaddition were initiated by the addition at the sp carbon of **5**, a different regioisomer of the cycloadduct should have been obtained. Thus, all the products **15–18** stem from nucleophilic attack at the sp^2 carbon of **5**. The regioselective addition at the sp^2 carbon of **5** is compatible with its charge distribution estimated from calculations. Regio-

selectivity is not affected by the steric effect of the siloxyalkenes employed, and the reaction with dimethylketene silyl acetal **3a** allows for a smooth connection of the two contiguous quaternary carbon centers (18).

The reaction with silyl enol ethers **3f** and **3g** gave only the [3 + 2] cycloadducts in comparison with effective formation of acyclic adduct **15** in the reaction with ketene silyl acetals **3a** and **3e** at lower reaction temperature. This can be explained by the reactivity of cationic intermediates **19**: the intermediates from **3f** and **3g** are more reactive owing to lower stabilization by the oxy group than those from **3a** and **3e**, and react with the internal allene more efficiently to give the cycloadduct(s). Cyclic product **17a** could be obtained at higher temperature via the reaction of **3a** (entry 2).

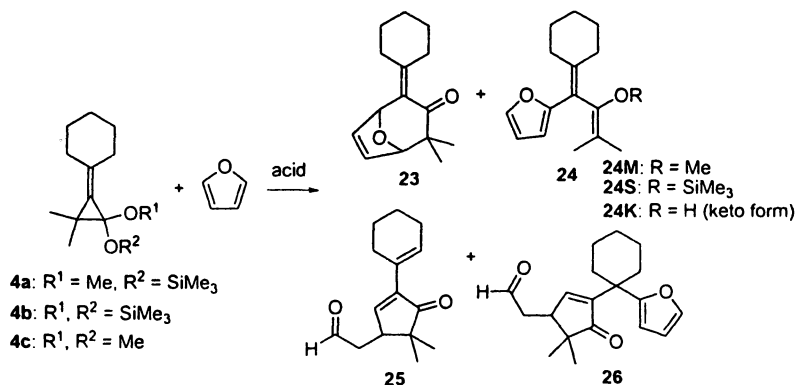
Reaction with Furans

Cyclohexylidenecyclopropanone acetal **4a–c** was treated with TiCl_4 at -78 °C in dichloromethane in the presence of furan to give adducts of furan, **23** and **24** (Table IV). All products formed result from C2–C3 bond cleavage in **4a–c**, and are rationalized by a reaction mechanism including alkylideneallyl cation intermediate **5**. The reactions of **4a** and **4c** preferentially gave a furanyl product **24** (entries 1, 2, and 6) in contrast to preferential formation of [4 + 3] cycloadduct **23** in the reaction of the disilyl acetal substrate **4b** (entries 3 and 4). The reaction also took place by using SnCl_4 (entry 5).

Reaction of **4a** with furan also proceeds in HFIP containing hydrogen chloride at 0 °C to yield a cyclopentenone product **26** as well as the products obtained in the reaction with Lewis acid, **23** and **24** (entries 7–9). The formation of cyclopentenone product **26** did not occur when less than one equivalent of furan was employed; a simple cyclopentenone product **25** was obtained instead (entry 7). Addition of THF also retarded the formation of **26** in the reaction in HFIP as solvent with an increasing yield of **25** (entry 10). Preferential formation of the [4 + 3] cycloadduct **23** was observed without formation of **26** in the reaction of **4b** in HFIP (entries 11 and 12) as was observed with Lewis acid in dichloromethane (entries 3–5). Reaction of **4c** in HFIP gave **26** (entry 13), with a product distribution similar to that of **4a** in HFIP.

Product distribution in the reaction of **4** with furan depends on the reaction conditions as well as on the oxy group of the acetal substrates **4a–c**. The diverse products formed in the reaction of **4a–c** with furan are rationalized by the reaction pathways illustrated in Scheme 13. All products arise from nucleophilic addition of furan to alkylideneallyl cation intermediate **5M** (**5S**), which is generated by acid-mediated ring opening of cyclopropanone acetals **4a–c** (Scheme 5). The [4 + 3] cycloadduct **23** is simply formed via **27**, and the furanyl

Table IV. Reaction of 4a–c with Furan



Entry	Sub.	[furan] (mM)	Acid	Yield (%)			
				23	24 ^a	25	26
1 ^b	4a	30	TiCl ₄	5	44(93/7/0)	0	0
2 ^b	4a	200	TiCl ₄	11	49(90/10/0)	0	0
3 ^b	4b	TiCl ₄	44	7(0/0/100)	0	0	0
4 ^b	4b	100	TiCl ₄	52	7(0/0/100)	0	0
5 ^b	4b	100	SnCl ₄	70	4(0/24/76)	0	0
6 ^b	4c	14	TiCl ₄	0	56(81/0/19)	0	0
7 ^c	4a	6	HCl	4	6(0/0/100)	26	0
8 ^c	4a	15	HCl	5	13(0/0/100)	0	43
9 ^c	4a	100	HCl	0	0	0	44
10 ^{c,d}	4a	100	HCl	0	66(0/0/100)	0	0
11 ^c	4b	15	HCl	76	0	0	0
12 ^c	4b	100	HCl	67	0	0	0
13 ^c	4c	100	HCl	0	0	0	75

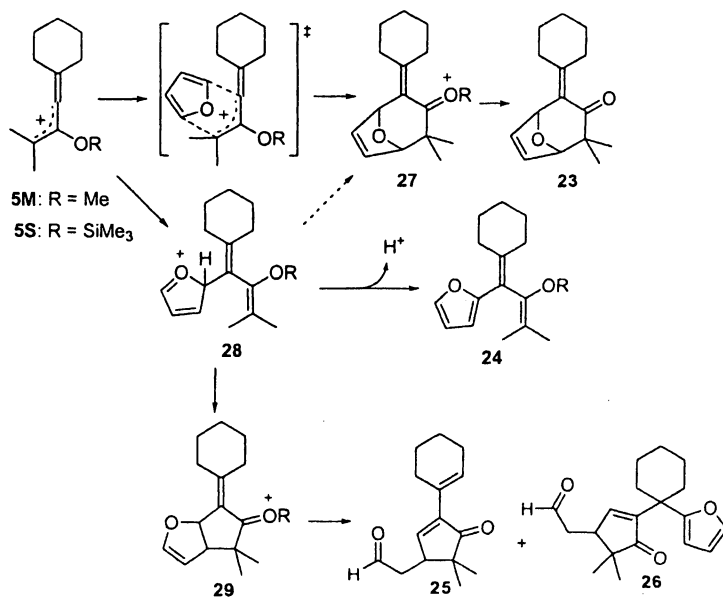
^a Values in parentheses are the ratio of 24M/24S/24K.

^b Reaction of 4 (7 mM) was carried out at -78 °C for 30 min in dichloromethane containing furan and Lewis acid (14 mM).

^c Reaction of 4a–c (7 mM) was carried out at 0 °C for 5 min in HFIP containing furan and HCl (20 mM).

^d In the presence of THF (10% v/v).

product **24** by deprotonation of **28**. The cyclopentenone structure of **25** and **26** may be formed via **29** which is in turn formed via a [3 + 2] cycloaddition of **5** with furan.

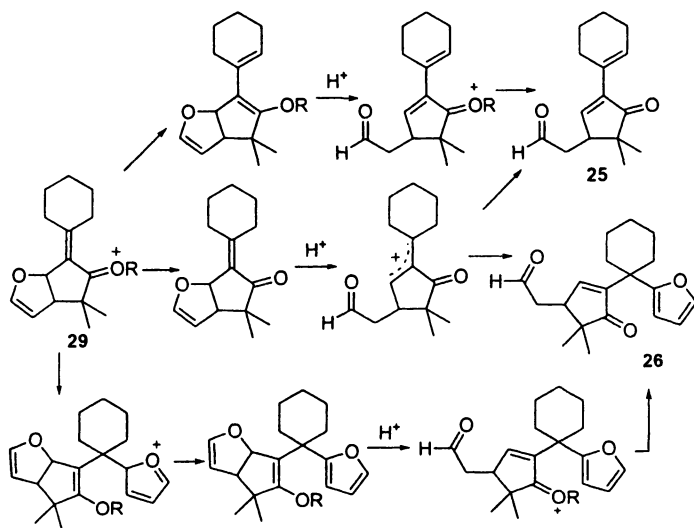


Scheme 13. Possible pathways for the reaction with furan.

Reaction of **4b** preferentially gave the [4 + 3] cycloadduct **23** in both HFIP and dichloromethane solvents, while only a small amount of **23** was obtained in the reactions of **4a** and **4c**. Thus, the product distribution depends on the reaction conditions including solvent. The contrasting tendency of the product distribution may be ascribed to the difference in the oxy group of the alkylideneallyl cation intermediate: methyl acetals **4a** and **4c** give the methoxy-substituted cation **5M**, while the disilyl acetal **4b** gives the siloxy cation **5S**. Preferential formation of the methoxy-substituted allylic cation **5M** from the unsymmetrical acetal **4a** is rationalized taking into account higher basicity of trimethylsiloxy relative to methoxy group (see also entries 1 and 2). The [4 + 3] intermediate **27** is possibly formed mainly via a concerted pathway, if not solely: a stepwise pathway via **28** may also be possible (19). Preferential formation of the [4 + 3] cycloadduct **23** from **4b** was independent of the solvent employed for the reaction in comparison with solvent-dependent product distribution of the reactions of **4a** and **4c**, which may proceed mainly via **28**. The lack of solvent effect is reasonable for the concerted pathway of the [4 + 3] cycloaddition of furan and **5S** derived from **4b**. Competition between the concerted reaction of the siloxy cation **5S** and the stepwise process for the methoxy cation **5M** could lead to varied product distributions that depend on the oxy groups of the

substrates **4a–c** and on the reaction conditions including solvent. Theoretical and stereochemical studies for the cycloadditions of 2-oxyallyl cation with dienes indicate that an electron-donating 2-oxy group decreases the electrophilicity of the cation, thus favoring a concerted mechanism (*19a*, *20*). The effect of the oxy group of 2-oxyallyl cations agrees well with the difference between the methoxy and siloxy-substituted alkylideneallyl cations (**5M** and **5S**).

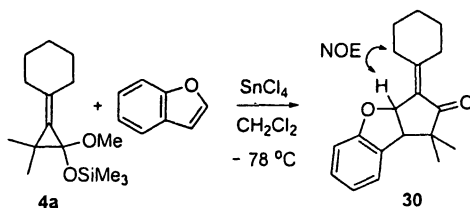
Solvent-dependency of product distribution in the reactions of **4a** and **4c** is rationalized by the reaction pathways originating from cation **28** (*21*). Acidic HFIP solvent retards the deprotonation from **28**, thus promoting internal cyclization to give **29**. Tetrahydrofuran acts as a base to promote the deprotonation of **28** to yield **24** in HFIP (entry 10). An excess amount of furan acts as a nucleophile toward **29** to yield the double addition product **26**, but does not act as a base due to its lower basicity. Use of a smaller amount of furan provides a single addition product **25** instead of the double addition product **26**. Formation of these two products may result from [3 + 2] cycloaddition of **5** with furan, followed by acid-mediated ring opening of the furan ring to give formylmethylcyclopentenones (**25** and **26**) as illustrated in Scheme 14.



Scheme 14. Possible Pathways Leading to 25 and 26.

To obtain further insight into the [3 + 2] cycloaddition of alkylideneallyl cation **5**, the reaction with 2,3-benzofuran was carried out as shown in Scheme 15. The reaction of **4a** gave a simple [3 + 2] cycloadduct **30** as a single regioisomer in 76 % isolated yield. The regioisomeric structure of **30** confirmed by NOE measurements is well compatible with the cyclic structure of **29**. These

results are consistent with a mechanism whereby nucleophilic addition of furan selectively proceeds at the sp carbon of the alkylideneallyl cation **5** to yield **24**, **25**, and **26** via **28**. The selective addition of furan at the sp carbon of **5** is in contrast to the sp^2 addition observed in the reaction with siloxyalkenes and with methanol. Although reasons for the regioselective addition at the sp carbon are not clear, the frontier orbital interactions between furan and allyl cation may control the regioselectivity because the sp selectivity is not compatible with the electronic and steric advantages of the sp^2 addition of nucleophile to **5**.



Scheme 15. Reaction with benzofuran.

Alkylideneallyl Cation Reaction Selectivity

Alkylideneallyl cation intermediate **5** was effectively generated by ring opening reaction of alkylidenecyclopropanone acetals **4a–c**. Lewis acid in dichloromethane and hydrogen chloride in HFIP are suitable conditions for generation of the cation and its trapping with various nucleophiles. Regioselectivity of nucleophilic addition to the cation depends on the type of nucleophiles. Methanol and siloxyalkenes selectively attack the sp^2 carbon of the alkylideneallyl cation, while chloride ion and furans attack the sp carbon. The sp^2 carbon is more positive than the sp carbon, and the vacant orbital at the sp carbon is partially shielded by the cyclohexane ring. That is, electronic and steric characters should simply promote addition to the sp^2 carbon. Interaction of frontier orbitals may be involved in the sp addition.

Modes of cycloaddition of alkylideneallyl cation are also controlled by the reaction conditions. [4 + 3] Cycloaddition occurs in the reaction with furan. The [4 + 3] cycloaddition with furan was observed for the siloxy-substituted allyl cation **5S**, but not for the methoxy-substituted allyl cation **5M**. The lower electrophilicity of **5S** may prefer the concerted pathway of [4 + 3] cycloaddition in competition with the stepwise pathway to yield a [3 + 2] cycloadduct and an electrophilic substitution product.

The [3 + 2] cycloaddition of furan proceeds in the reaction of **5M** in protic solvent (HFIP), where deprotonation from the initially formed intermediate **28** does not take place and intramolecular cyclization predominates in the termi-

nation, yielding electrophilic substitution product **24**. The [3 + 2] cycloaddition of siloxyalkene also competes with desilylation of **19**. These [3 + 2] cycloadditions take place when a stepwise nucleophilic addition to **5** occurs and subsequent internal cyclization predominates in the termination step, giving rise to substitution product.

References

1. Apeloig, Y.; Müller, T. In *Dicoordinated Carbocations*; Rappoport, Z., Stang, P. J. Eds.; John Wiley & Sons: Chichester, 1997; Chapter 2.
2. Siehl, H.-U. In *Dicoordinated Carbocations*; Rappoport, Z., Stang, P. J. Eds.; John Wiley & Sons: Chichester, 1997; Chapter 5.
3. For example, see: (a) Siehl, H.-U.; Mayr, H. *J. Am. Chem. Soc.* **1982**, *104*, 909–910. (b) Siehl, H.-U.; Koch, E.-W. *J. Org. Chem.* **1984**, *49*, 575–576.
4. For recent examples, see: (a) Siehl, H.-U.; Brixner, S. *J. Phys. Org. Chem.* **2004**, *17*, 1039–1045. (b) Siehl, H.-U.; Müller, T.; Gauss, J. *J. Phys. Org. Chem.* **2003**, *16*, 577–581.
5. Grob, C. A.; Spaar, R. *Helv. Chim. Acta* **1970**, *53*, 2119–2129.
6. (a) Olsson, L.-I.; Claesson, A.; Bogentoft, C. *Acta Chem. Scand.* **1973**, *27*, 1629–1636. (b) Gelin, R.; Gelin, S.; Albrand, M. *Bull. Soc. Chim. France* **1972**, 720–723.
7. Gassman, P. G.; Lottes, A. C. *Tetrahedron Lett.* **1991**, *32*, 6473–6476.
8. Fujita, M.; Fujiwara, K.; Mouri, H.; Kazekami, Y.; Okuyama, T. *Tetrahedron Lett.* **2004**, *45*, 8023–8026.
9. Fujita, M.; Hanagiri, S.; Okuyama, T. *Tetrahedron Lett.* **2006**, *47*, 4145–4148.
10. Fujita, M.; Fujiwara, K.; Okuyama, T.; *Chem. Lett.* **2006**, *35*, 382–383.
11. Fujita, M.; Oshima, M.; Okuno, S.; Sugimura, T.; Okuyama, T. *Org. Lett.* **2006**, *8*, 4113–4116.
12. For a review, see: Stang, P. J. *Chem. Rev.* **1978**, *78*, 383–405.
13. (a) Ochiai, M.; Takaoka, Y.; Nagao, Y. *J. Am. Chem. Soc.* **1988**, *110*, 6565–6566. (b) Ochiai, M.; Uemura, K.; Masaki, Y. *J. Am. Chem. Soc.* **1993**, *115*, 2528–2529. (c) Ochiai, M.; Sueda, T.; Uemura, K. Masaki, Y. *J. Org. Chem.* **1995**, *60*, 2624–2626. (d) Sueda, T.; Nagaoka, T.; Goto, S.; Ochiai, M. *J. Am. Chem. Soc.* **1996**, *118*, 10141–10149. (e) Okuyama, T.; Imamura, S.; Ishida, Y. *Bull. Chem. Soc. Jpn.* **2001**, *74*, 543–548.
14. Okuyama, T.; Takino, T.; Sato, K.; Ochiai, M. *J. Am. Chem. Soc.* **1995**, *117*, 3360–3367.
15. (a) Newman, M. S.; Fraunfelder, J. *J. Org. Chem.* **1974**, *39*, 251–252. (b) Newman, M. S.; Zwan, M. C. V. *J. Org. Chem.* **1974**, *39*, 1186–1189.
16. For recent examples, see: (a) Siriwardana, A. I.; Nakamura, I.; Yamamoto, Y. *Tetrahedron Lett.* **2003**, *44*, 985–987. (b) Huang, J.-W.; Shi, M. *Tetrahedron* **2004**, *60*, 2057–2062. (c) Huang, J.-W.; Shi, M. *Synlett* **2004**,

- 2343–2346. (d) Xu, G.-C.; Ma, M.; Liu, L.-P.; Shi, M. *Synlett* **2005**, 1869–1872. (e) Wang, B.-Y.; Jiang, R.-S.; Li, J.; Shi, M. *Eur. J. Org. Chem.* **2005**, 4002–4008. (f) Ikeda, H.; Nomura, T.; Akiyama, K.; Oshima, M.; Roth, H. D.; Tero-Kubota, S.; Miyashi, T. *J. Am. Chem. Soc.* **2005**, *127*, 14497–14504.
17. Stewart, R. *The Proton: Applications to Organic Chemistry*; Academic Press: Orlando, 1985; pp 251–305.
18. For example, see: Klein, H.; Mayr, H. *Angew. Chem. Int. Ed. Engl.* **1981**, *20*, 1027–1029.
19. Recent reviews of [4 + 3] cycloaddition, see: (a) Rigby, J. H.; Pigge, F. C. *Org. React.* **1997**, *51*, 351–478. (b) Harmata, M.; Rashatasakhon, P. *Tetrahedron* **2003**, *59*, 2371–2395. (c) Harmata, M. *Acc. Chem. Res.* **2001**, *34*, 595–605. (d) Hoffmann, H. M. R. *Angew. Chem. Int. Ed. Engl.* **1984**, *23*, 1–19.
20. (a) Cramer, C. J.; Barrows, S. E. *J. Phys. Org. Chem.* **2000**, *13*, 176–186. (b) Cramer, C. J.; Barrows, S. E. *J. Org. Chem.* **1998**, *63*, 5523–5532.
21. (a) Solvent effects on the reaction of 2-oxyallyl cation with furans have been reported (*21b*). (b) Shimizu, N.; Tanaka, M.; Tsuno, Y. *J. Am. Chem. Soc.* **1982**, *104*, 1330–1340.

Chapter 6

Conformational Studies of Cyclobutylmethyl Cations

V. Prakash Reddy¹, G. K. Surya Prakash², and Golam Rasul²

¹Department of Chemistry, University of Missouri at Rolla,
Rolla, MO 65409

²Loker Hydrocarbon Research Institute and Department of Chemistry,
University of Southern California, Los Angeles, CA 90089

α,α -Dicyclopropylcyclobutylmethyl cation is a unique cyclobutylmethyl cation, which is stabilized by neighboring cyclopropyl groups. It is persistent up to $-40\text{ }^{\circ}\text{C}$ in superacidic medium. The primary and secondary cyclobutylmethyl cations, however, are still elusive species. α,α -Dicyclopropylcyclobutylmethyl cation adopts a bisected conformation as shown by the variable temperature dynamic ^{13}C NMR spectroscopy, in conjunction with density functional theoretical (DFT) calculations. DFT calculations for α,α -dimethylcyclobutylmethyl cation, and *endo*- and *exo*- α -methylcyclobutylmethyl cations show that these carbocations also exist as bisected conformers. Primary cyclobutylmethyl cation, on the other hand, spontaneously collapses to cyclopentyl cation at B3LYP/6-311+G* level.

Introduction

Stabilization due to neighboring group participation of carbocationic intermediates in small ring compounds, especially those involving cyclopropylmethyl cations is well documented in the early solvolytic studies. The bent 'banana-shaped' cyclopropyl ring C-C bonds are sterically well positioned for the stabilization of the adjacent carbocationic center so that dramatic rate accelerations were observed in the solvolyses of cyclopropylmethyl tosylates. The structure of parent cyclopropylmethyl cation has been under intense scrutiny over many years and is now well established, by ultra-low temperature ^{13}C NMR and high level ab-initio theoretical calculations among other techniques, that it exists as degenerately equilibrating, σ -delocalized bicyclobutonium ions, having a pentacoordinated carbon, in equilibrium with a minor amount of the bisected cyclopropylmethyl cation (Figure 1).¹⁻⁸

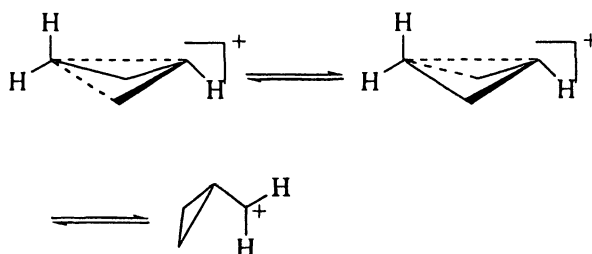


Figure 1. Equilibrating bicyclobutonium ions and bisected cyclopropylmethyl cations.

Although not as strained as the cyclopropylmethyl cation, the corresponding homologous cyclobutylmethyl cation is relatively strained, and the cyclobutyl ring exists as boat-shaped puckered conformation to relieve some of the ring strain. Thus cyclobutylmethyl cations are expected to show substantial neighboring group stabilization of the adjacent carbocationic centers.⁹ In this chapter, we outline our recent progress on ^{13}C NMR and DFT theoretical studies on the nature of the cyclobutylmethyl cations. Prominent earlier work by others, based mostly on solvolytic studies, is also outlined from a historical perspective.

Solvolytic Generation of Cyclobutylmethyl Cations

Early solvolytic studies by Winstein and coworkers clearly established the anchimeric assistance provided by the neighboring cyclobutyl ring in the

solvolysis of the cyclobutylmethyl cations.⁹ Thus, solvolysis of nopinyl brosylate, a bicyclic analogue of the parent cyclobutylmethyl cation resulted in the formation of the products resulting from ring-expansion rearrangements: 7,7-dimethyl-2-norbomanol, 2,2-dimethyl-2-norbomanol, and 4,4-dimethyl-2-norbomanol (Figure 2). Further, kinetics of acetolysis of 1-cyclobutylethyl brosylate and dicyclobutylmethyl brosylate showed rate accelerations attributable to the neighboring group participation of the cyclobutyl ring(s). The combined kinetic and product studies led to the postulation of a nonclassical σ -bridged cyclobutylmethyl cation as an intermediate in these reactions.⁹

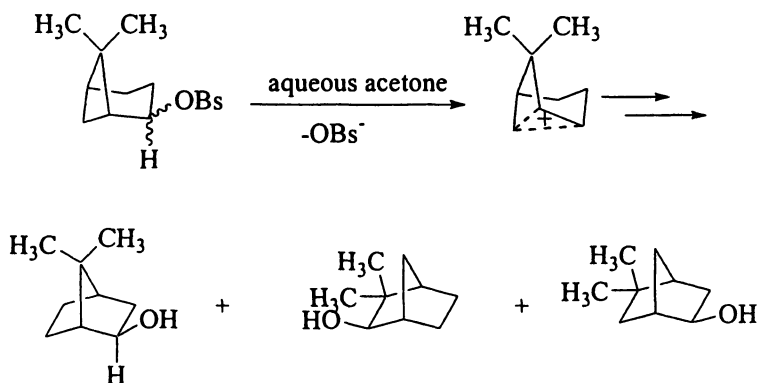


Figure 2. Product distribution from the solvolysis of nopinyl brosylate, a cyclobutylmethyl substrate.

Dauben and coworkers observed unusual rate accelerations and ring-expansion rearrangements in the solvolysis of bicyclo[2.2.0]hexane-1-methyl *p*-nitrobenzoate, in agreement with Winstein's proposed nonclassical cyclobutylmethyl cations (Figure 3).¹⁰ Thus, the rate of the solvolysis of bicyclo[2.2.0]hexane-1-methyl *p*-nitrobenzoate is 7×10^6 times faster than that of the corresponding extrapolated rate for neopentyl derivative. The lack of scrambling of the ¹⁸O label in the solvolysis of the ¹⁸O-labeled bicyclo[2.2.0]hexane-1-methyl *p*-nitrobenzoate confirmed the involvement to a significant degree of σ -participation from the neighboring cyclobutyl ring.¹¹

Brown-Hammett correlation of 1-aryl-1-cyclobutylethyl *p*-nitrobenzoate gave a ρ^+ value of -3.94 which is more positive than that of a model compound, 1-aryl-1,2-dimethylpropyl *p*-nitrobenzoate ($\rho^+ = -4.65$), which indicates substantial neighboring group participation of the cyclobutyl ring even in tertiary carbocationic systems.¹² Solvent effects on the kinetics of the solvolysis

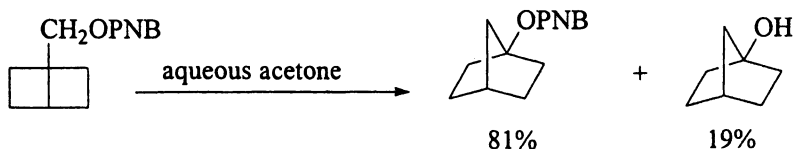


Figure 3. Products of solvolysis of bicyclo[2.2.0] hexane-1-methyl *p*-nitrobenzoate.

of the cyclobutylmethyl systems also show evidence for the σ -bridged cyclobutylmethyl cationic system.^{13,14}

Ring expansion rearrangement was also observed in the solvolysis of the *endo*- and *exo*- bicyclo[2.1.1]hexane-5-methyl tosylates. Interestingly, the *exo*- isomer gives 96% of the rearranged product, presumably going through the nonclassical cyclobutylmethyl cation. The reaction of *endo*- isomer presumably involves predominantly the S_N2 pathway (k_s) (Figure 4).

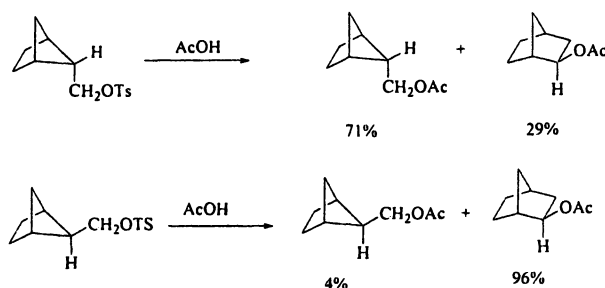


Figure 4. Products of acetolysis of bicyclo[2.1.1]hexane-5-methyl tosylates.

Gajewski has demonstrated stereochemical integrity (retention of configuration) in the ring expansion rearrangements in the solvolysis reactions of *cis*- or *trans*-2-methylcyclobutylmethyl brosylates (Figure 5).¹⁶ Thus, acetolysis of *trans*-2-methylcyclobutylmethyl brosylate gives predominantly *trans*-3-methylcyclopentyl brosylate, as the intermediate product, through internal ion pair return of the nonclassical 2-methylcyclobutylmethyl cation. The predominant product of the acetolysis reaction is *cis*-3-methylcyclopentyl acetate, which arises through solvent assisted pathway (k_s) of the rearranged brosylate. Coates and coworkers showed that the cyclobutylmethyl carbocations, and the accompanying ring expansion-rearrangements, are involved in diterpene biosynthesis.¹⁷

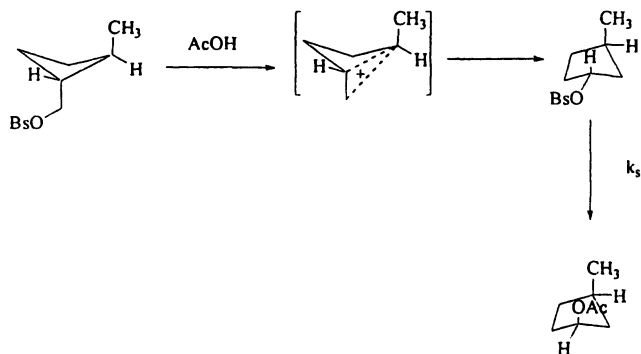


Figure 5. Stereoselective rearrangement in the acetolysis of *trans*-2-methylcyclobutylmethyl brosylate.

Stable Ion Studies of Cyclobutylmethyl Cations

Cyclobutylmethyl Cation

Several attempts at generation of persistent cyclobutylmethyl cations in superacidic media were not successful. Thus, ionizing cyclobutylmethyl chloride using SbF_5 in sulfuryl chloride fluoride (SO_2ClF) clearly gave the cyclopentyl cation due to the ring-expansion rearrangement.¹⁸ This result is also in accord with early solvolysis studies of Wiberg and coworkers, showing that cyclopentyl acetate is the predominant product (99%) of the acetolysis of cyclobutylmethyl tosylate. In order to characterize the nature of the primary cyclobutylmethyl cation, we carried out density functional theory calculations. At B3LYP/6-311+G* level, the primary cyclobutylmethyl cation is not a minimum on the potential energy surface, and it spontaneously rearranged to the cyclopentyl cation.¹⁸

Ionization of cyclobutylmethanol using SbF_5 in SO_2ClF at -78°C gives Lewis acid-base complex, whereas upon further warming it undergoes deep-seated dimerization/rearrangements to give the 1-bicyclo[4.4.0]dec-1-yl cation (Figure 6), which is in rapid degenerate equilibrium as shown by its ^{13}C NMR spectrum.¹⁸

Secondary Cyclobutylmethyl Cations

Ionization of the secondary substrates such as 1-cyclobutylethanol, cyclobutylphenylmethanol, and cyclobutylcyclopropylmethanol, in all cases,

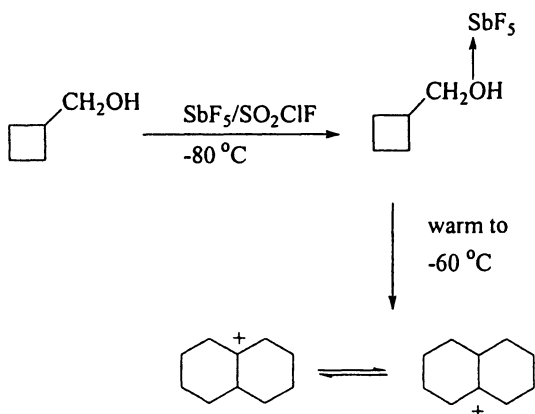


Figure 6. Formation of 1-bicyclo[4.4.0]dec-1-yl cation from the ionization of cyclobutylmethanol.

provided the corresponding alkyl/phenyl substituted cyclopentyl cations (Figure 7).¹⁸ However, our DFT theoretical studies suggest that unlike the primary cyclobutylmethyl cation, the secondary α -methylcyclobutylmethyl cations are minima on the potential energy surface, and may be observable under appropriate conditions.

It should be noted that analogous secondary α -methylcyclopropylmethyl cations are observable species in superacidic media at low temperatures.²¹ Observation of the secondary cyclopropylmethyl carbocations under superacidic conditions indicates the superior charge delocalization into the cyclopropyl ring as compared to the cyclobutyl ring.

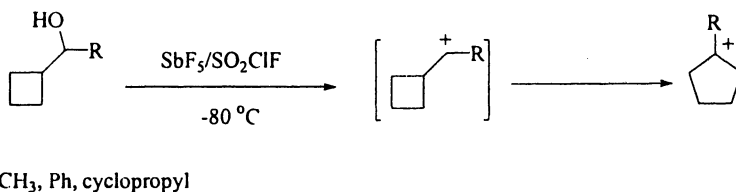


Figure 7. Formation of cyclopentyl cations from the ionization of secondary cyclobutylmethanols.

The secondary, α -methylcyclobutylmethyl cation shows an unsymmetrically delocalized nonclassical type of intermediate at B3LYP/6-311+G* level.¹⁹ The

endo conformer is more stable than the *exo* conformer by 1.7 kcal/mol at this level.

The σ -delocalization from the cyclobutyl C-C bond is relatively more advanced in the *endo* isomer than that of the *exo* isomer as shown by the C₄-C₅ bond distances: The C₄-C₅ bond length for the *endo* isomer (1.890 Å) is considerably shorter than that of the *exo* isomer (1.980 Å). In the *endo* isomer, the C₁-C₄ (1.872 Å) and C₄-C₅ bonds (1.890 Å) are almost equal. Due to this unsymmetrical nonclassical charge delocalization, the C₁-C₂ bond (1.519 Å) is relatively shorter than that of the C₃-C₄ or C₂-C₃ bonds (1.551 Å and 1.541 Å). Similarly the *exo* isomer also has significantly elongated C₁-C₄ bond (1.818 Å) and relatively shortened C₁-C₂ bond (1.522 Å). Thus the *endo* conformer involves relatively more nonclassical stabilization as compared to that of the *exo* isomer.

Tertiary Cyclobutylmethyl Cations

Ionization of the *cx,cx*-dimethylcyclobutylmethanol in superacidic media similarly gives the ring-expanded carbocation, 1,2-dimethylcyclopentyl cation

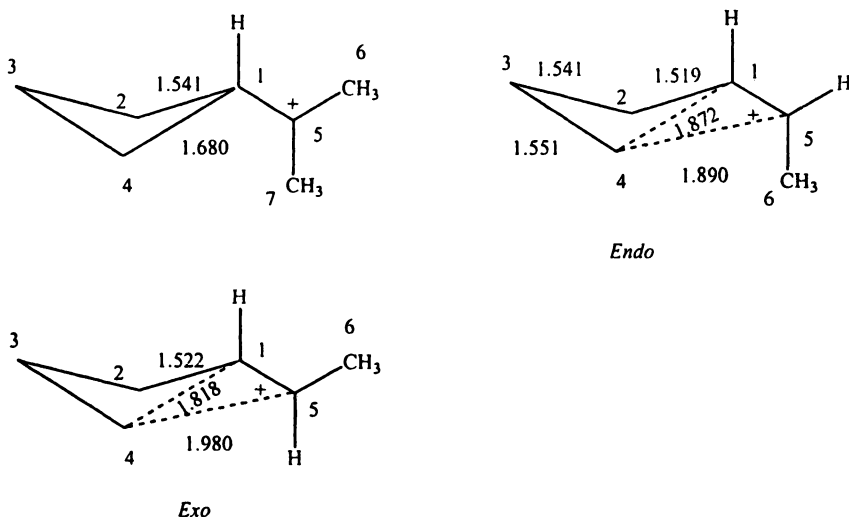


Figure 8. Structures of α, α -dimethylcyclobutylmethyl cation, and *endo*- and *exo*- α -methylcyclobutylmethyl cations, with selected bond distances (Å; at B3LYP/6-311+G*).

(Figure 9).¹⁸ DFT studies, however, indicate that the tertiary α,α -dimethylcyclobutylmethyl cation is a minimum on the potential surface, with substantial charge delocalization into the neighboring cyclobutyl ring (*vide infra*).

Apparently, the stabilization afforded by the methyl groups attached to carbocation center is not sufficient to prevent the ring expansion rearrangement involving the adjacent cyclobutyl ring. Neighboring cyclopropyl group is comparable to, and slightly more effective, in stabilizing the carbocationic centers as compared to the phenyl group. Thus cyclopropyl group is a preferred substituent for suppressing the ring expansion rearrangement of the incipient cyclobutylmethyl carbocations.

By choosing cyclopropyl groups as the α -substituents, a tertiary cyclobutylmethyl cation, α,α -dicyclopropylcyclobutylmethyl cation, was indeed obtained as a persistent carbocation in superacidic medium (Figure 10), without formation of any products corresponding to ring expansion rearrangements. This carbocation is sufficiently stable at low temperatures, from $-80\text{ }^{\circ}\text{C}$ to $-40\text{ }^{\circ}\text{C}$, so that we were able to carry out dynamic NMR studies, which showed a rotational barrier of $11.0 \pm 0.5\text{ kcal/mol}$ (at $-40\text{ }^{\circ}\text{C}$) for the free-rotation across $\text{C}_1\text{-C}^+$ bond. From these dynamic NMR studies it is evident that the cyclobutyldicyclopropylmethyl cation exists as the bisected conformation. Of particular significance, the C_α ($\delta^{13}\text{C}$ 39.6) and $\text{C}_{\alpha'}$ ($\delta^{13}\text{C}$ 32.2) as well as C_β ($\delta^{13}\text{C}$ 36.6) and $\text{C}_{\beta'}$ ($\delta^{13}\text{C}$ 31.5) carbons showed distinct signals in the ^{13}C NMR spectrum, confirming its bisected nature.¹⁸ The C_α and $\text{C}_{\alpha'}$ (as well as C_β and $\text{C}_{\beta'}$) signals would be expected to be identical in the perpendicular conformation.

DFT Studies of α,α -Dicyclopropylcyclobutylmethyl Cation

At the B3LYP/6-31G* and B3LYP/6-311+G* levels the perpendicular conformation of α,α -dicyclopropylcyclobutylmethyl cation is not a mini-

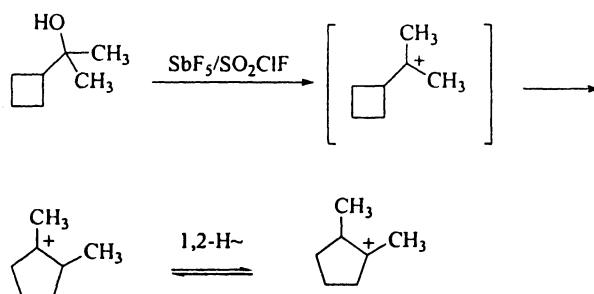


Figure 9. Formation of 1,2-dimethylcyclopentyl cation from the ionization of α,α -dimethylcyclobutylmethanol.

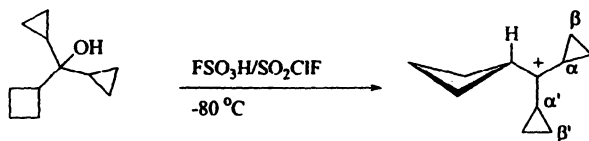


Figure 10. Preparation of α, α -dicyclopropylcyclobutylmethyl cation in $\text{FSO}_3\text{H}/\text{SO}_2\text{ClF}$.

imum on the potential energy surface, and the bisected conformation was obtained as the global minimum. ^{13}C NMR chemical shifts obtained at IGLO and later at GIAO methods,¹⁹ are in reasonable agreement with that of the experiment. Applying a scaling factor of 0.97 to the GIAO chemical shifts, as suggested by Siehl and coworkers,²⁰ gave $\delta^{13}\text{C}$ 276.5 for the carbocation center which is in close agreement with that of the experimental value ($\Delta\delta^{13}\text{C} = 0.6$).

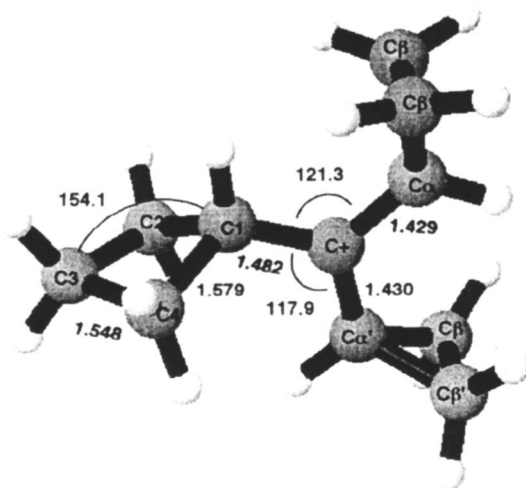


Figure 11. DFT (at B3LYP/6-311+G*) optimized structure of α, α -dicyclopropylcyclobutylmethyl cation, with selected bond distances and bond angles

The structural parameters for the C_s symmetric bisected conformation obtained at B3LYP/6-311+G* are similar to those obtained at B3LYP/6-31G* level. At B3LYP/6-311+G* level, C1-C2 bond slightly elongated (1.579 Å) as

compared to that of the C2-C3 bond (1.548 Å).¹⁹ The C⁺-C_α bond length (1.430 Å) is essentially similar to that of the C⁺-C_α bond (1.429 Å). These bonds are relatively shorter as compared to that of cyclobutyl C₁-C⁺ bond (1.482 Å). The cyclobutyl ring is puckered with a bending angle of 154.1°, and the carbocation adopts a propeller shaped conformation to relieve steric strain and to maximize the electronic stabilization of the carbocationic center. The DFT calculations thus show substantial charge delocalization into the cyclobutyl ring.

Rotational Barrier for α,α-Dicyclopropylcyclobutylmethyl Cation

The α,α-dicyclopropylcyclobutylmethyl cation was shown to exist in the bisected conformation by its ¹³C NMR spectrum at -80 °C. The assignments of the chemical shifts were confirmed by IGLO and GIAO calculations. In the ¹³C NMR spectra, at -80 °C, the cyclopropyl methine (C_α and C_{α'}) and methylene (C_β and C_{β'}) carbons show distinct chemical shifts (δ¹³C). In the bisected conformation, the C_α and C_{α'}, methine carbons (as well as the C_β and C_{β'}, methylene carbons) are diastereotopic and therefore distinct absorptions are expected in its ¹³C NMR spectra. The alternative perpendicular conformation would be expected to have identical chemical shifts for the C_α and C_{α'}, as well as those of C_β and C_{β'}. Thus, the α,α-dicyclopropylcyclobutylmethyl cation exists in the bisected conformation. Upon warming the solution to -40 °C, the cyclopropyl methine and methylene absorptions merged into the baseline, based on which a free energy of activation for the rotation across the C₁-C⁺ bond was estimated as 11.0 ± 0.5 kcal/mol.¹⁸

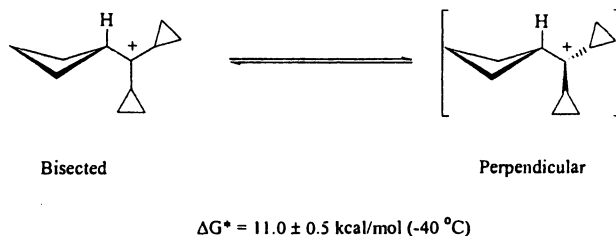


Figure 12. Estimation of the rotational barrier for the interconversion of bisected and perpendicular conformations of the α,α-dicyclopropylcyclobutylmethyl cation.

DFT Studies of α,α -Dimethylcyclobutylmethyl Cation

The α,α -dimethylcyclobutylmethyl cation is a minimum on the potential energy surface at B3LYP/6-311+G* level. At this level of calculation, we have identified the unsymmetrically charge delocalized bisected conformer as the only minimum (global minimum).¹⁹ It shows relatively more extensive charge delocalization into the adjacent cyclobutyl ring, as compared to that of the α,α -dicyclopropylcyclobutylmethyl cation. The C₁-C₄ bond is relatively elongated (1.680) as compared to C₁-C₂ (1.541 Å) (Figure 8). Further, the C₁-C⁺ bond (1.427 Å) is also relatively shorter as compared to the α,α -dicyclopropylcyclobutylmethyl cation (1.482 Å), indicating more charge delocalization into the cyclobutyl ring in the relatively less stable α,α -dimethylcyclobutyl cation. However, it should be mentioned that both of these carbocations are predominantly classical in nature, although they involve significant charge delocalization into the cyclobutyl rings.

Conclusions and Outlook

Cyclobutylmethyl cations, in their bisected forms, have unique stabilization due to charge delocalization into the neighboring cyclobutyl rings. The relatively strained cyclobutyl ring, especially in bisected conformation, is well positioned to stabilize the adjacent carbocation centers. The neighboring group participation provided by the cyclobutyl ring, although relatively smaller than that of the related cyclopropylmethyl cations, is substantially involved in the stabilization of secondary and tertiary cyclobutylmethyl cations, as shown by early solvolytic studies, and more directly by our ¹³C NMR and DFT theoretical studies. Based on DFT theoretical calculations as well as solvolytic evidence it may be possible to obtain even the secondary cyclobutylmethyl carbocations as persistent species in superacids under ultra-low temperature conditions for selected systems.

Acknowledgement

We are grateful to Professor George A. Olah for his encouragement and support. Support of our work by the National Science Foundation and donors of the American Chemical Society Petroleum Research Fund (PRF No. 39643-AC; to V.P.R.) is gratefully acknowledged.

References

1. Olah, G. A.; Reddy, V. P.; Prakash, G. K. S. *Chem. Rev.* **1992**, *92*, 69, and references therein.

2. Lenoir, D.; Siehl, H.-U., In *Houben-Weyl Methoden der Organischen Chemie*, Stuttgart, Germany, 1990; Vol. E19c, pp 413, and references therein.
3. Staral, J. S.; Yavari, I.; Roberts, J. D.; Prakash, G. K. S.; Donovan, D. J.; Olah, G. A. *J. Am. Chem. Soc.* **1990**, *100*, 8016.
4. Yannoni, C. S.; Myhre, P. C.; Webb, G. G. *J. Am. Chem. Soc.* **1990**, *112*, 8992.
5. Koch, W.; Liu, B.; DeFrees, D. J. *J. Am. Chem. Soc.* **1988**, *110*, 7325.
6. Olah, G. A.; Kelly, D. P.; Juell, C. L.; Porter, R. D. *J. Am. Chem. Soc.* **1970**, *92*, 2544.
7. Saunders, M.; Siehl, H.-U. *J. Am. Chem. Soc.* **1980**, *102*, 6868.
8. Siehl, H.-U.; Fuss, M.; Gauss, J. *J. Am. Chem. Soc.* **1995**, *117*, 5983.
9. Winstein, S.; Holness, N. J. *J. Am. Chem. Soc.* **1955**, *77*, 3054.
10. Dauben, W. G.; Chitwood, J. L.; Scherer, K. V. *J. Am. Chem. Soc.* **1968**, *90*, 1014.
11. Dauben, W. G.; Chitwood, J. L. *J. Am. Chem. Soc.* **1969**, *34*, 726.
12. Peters, E. N. *J. Org. Chem.* **1977**, *42*, 3015.
13. Roberts, D. D. *J. Org. Chem.* **1984**, *49*, 2521, and references therein.
14. Roberts, D. D. *J. Org. Chem.* **1982**, *47*, 561.
15. Wiberg, K. B.; Lorry, B. R. *J. Am. Chem. Soc.* **1963**, *85*, 3188.
16. Gajewski, J. J. *Tetrahedron Lett.* **1970**, 1189.
17. Coates, R. M. *J. Org. Chem.* **1987**, *52*, 2065.
18. Prakash, G. K. S.; Reddy, V. P.; Rasul, G.; Casanova, J.; Olah, G. A. *J. Am. Chem. Soc.* **1998**, *120*, 13362.
19. Reddy, V. P.; Rasul, G. unpublished results.
20. Vreck, V.; Kronja, O.; Siehl, H.-U. *J. Chem. Soc., Perkin Trans. 2*, **1999**, 1317.
21. Olah, G. A.; Kelly, D. P.; Juell, C. L.; Porter, R. D. *J. Am. Chem. Soc.* **1970**, *92*, 2544. Olah, G. A.; Donovan, D. J.; Prakash, G. K. S. *Tetrahedron Lett.* **1978**, *48*, 4779. Olah, G. A.; Liang, G.; Babiak, K. A.; Morgan, T. K., Jr., Murray, R. K., Jr. *J. Am. Chem. Soc.* **1978**, *98*, 576. Olah, G. A.; Prakash, G. K. S.; Rawda, T. N. *J. Org. Chem.* **1980**, *45*, 965.

Chapter 7

Persistent Organic Cationic Complexes: Structure and Reactivity

Gennady I. Borodkin and Vyacheslav G. Shubin

Vorozhtsov Novosibirsk Institute of Organic Chemistry, Russian Academy
of Sciences, Siberian Division, Siberia, Russia

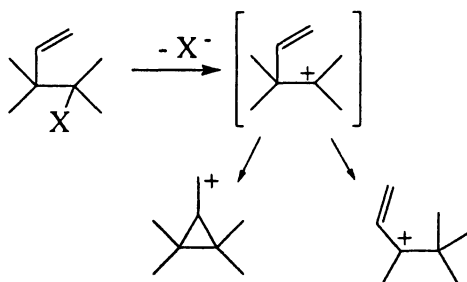
Recent results obtained by the authors and their co-workers in the field of organic cationic complexes generated under stable ion conditions are discussed. Complexes with C- and N-centered electrophiles are considered.

Cationic complexes are key intermediates in a great variety of organic transformations such as isomerizations, rearrangements, addition reactions, aromatic substitutions, polymerization and others. Long-lived cationic complexes are important structural models for these intermediates. Studies of such complexes by modern physical methods provide valuable insight regarding their structure and reactivity.

There are numerous publications on the chemistry of long-lived cationic complexes; see, for example (1-10). Most of our recent results in this area have been published in Russian and are probably not easily accessible to most foreign researchers. It was for this reason that we enthusiastically accepted the invitation made by Prof. Ken Laali to contribute a brief review summarizing our recent studies on the structure and reactivity of long-lived cationic organic complexes. We limit this account to the data obtained after 2000 but include some earlier unpublished results that were not included in our earlier reviews (5, 11).

Complexes with C-Centered Electrophiles

Cationic σ -complexes formed via unsaturated organic compounds with C-centered electrophilic sites: viz carbocations, have been under study for many years (1-6, 10). However, until recently long-lived carbocations having a vinyl group in the β -position relative to carbocationic center were unknown. Attempts to generate such complexes failed. Ionization of potential precursors to the long-lived β -vinyl-substituted carbocations in the aliphatic series led to formation of isomeric allyl and cyclopropylcarbiny l cations due to effective interaction between the developing carbocation center and the vinyl group (12-16) (Scheme 1), *cf.* ref. (17).



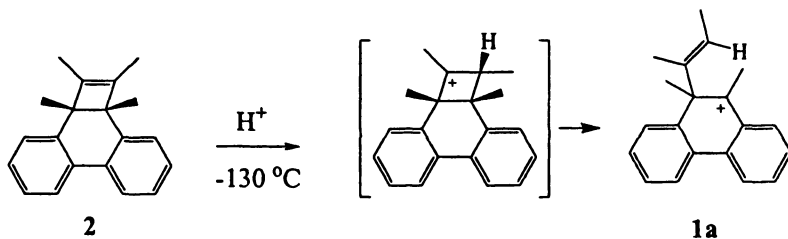
Scheme 1

A similar pattern had been observed earlier with β -phenyl-substituted carbocations. Relative migration ability of phenyl and substituted phenyl groups were determined for the first time, not by focusing on carbocations formed via aliphatic series as structural models, but rather by studying 9-aryl-9,10-dimethylphenanthrenium ions (18, 19).

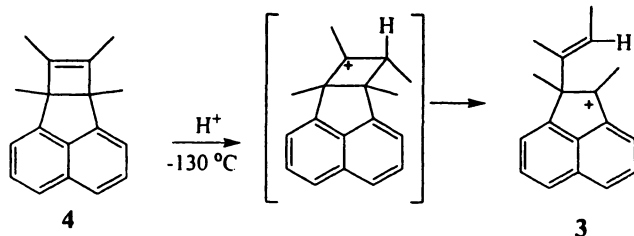
The authors succeeded in preparing (20-25) a series of long-lived carbocations bearing vinyl and related groups in the β -position to the carbocationic center (1a-d, 3). Their structures were confirmed by ^1H and ^{13}C NMR spectroscopy. These cations can be considered as σ -complexes of C-centered electrophilic agents, namely vinyl and methyl-substituted vinyl cations derived from 9,10-dimethylphenanthrene and 1,2-dimethylacenaphthylene, respectively. Quite naturally, they had not been prepared by electrophilic vinyl-

ation reaction because that approach would have resulted in a mixture of products, with vinyl groups in the aromatic rings being predominant.

The first carbocation in this series – (*cis*-1,2-dimethylvinyl)-9,10-dimethylphenanthrenium ion (**1a**) was formed as a result of rearrangement of 1,2,2a,10b-tetramethyl-2a,10b-dihydrocyclobuta[*l*]phenanthrene (**2**) in super-acids (Scheme 2). Analogously, (*cis*-1,2-dimethylvinyl)-1,2-dimethyl-acenaphthylenium ion (**3**) was generated by rearrangement of 6b,7,8,8a-tetramethyl-6b,8a-dihydrocyclobuta[*a*]acenaphthylene (**4**) in $\text{FSO}_3\text{H}\text{-SO}_2\text{ClF}$ at low temperature (Scheme 3).



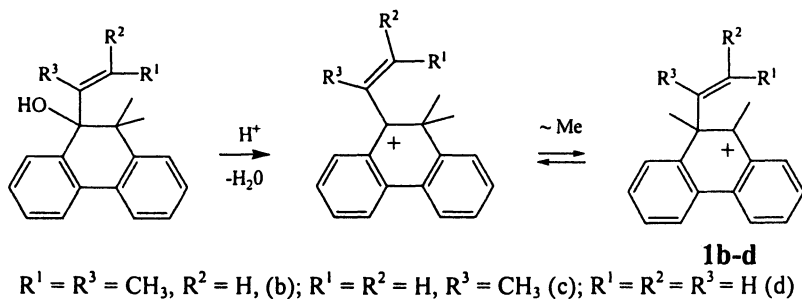
Scheme 2



Scheme 3

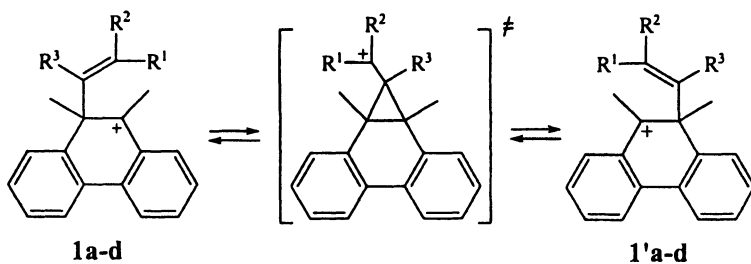
Other carbocations in this series were generated by dehydration of the corresponding carbinols in superacids at low temperatures, followed by 1,2-methyl shifts (Scheme 4).

It has been found by NMR that carbocations **1a-d** and **3** are prone to undergo degenerate rearrangements [automerization reactions (26)] via 1,2-shifts of the vinyl and the methyl-substituted vinyl groups (Schemes 5, 6), with

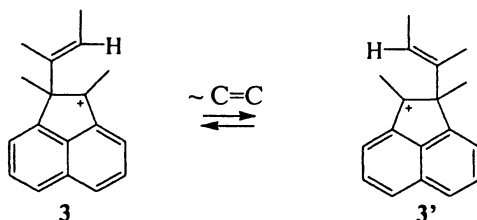


Scheme 4

the unsubstituted vinyl and the *cis*-1-methyl-1-propenyl groups migrating more rapidly than other hydrocarbon migrants, *cf.* ref. (17) [data on migration ability of the latter are given in monograph (5)]. To the best of our knowledge, degenerate rearrangement of cation **1a** (20) is the first example for a 1,2-vinyl migration in a long-lived carbocation.



Scheme 5



Scheme 6

It was determined by dynamic NMR that the rates of degenerate rearrangement for long-lived cations **1b,c** (24, 25) are unexpectedly much lower than those of cations **1a,d** (Table I), i.e. migration ability for 1-methyl-1-vinyl- and *trans*-1-methyl-1-propenyl groups is substantially lower than that of vinyl and *cis*-1-methyl-1-propenyl groups. For example, in passing from cation **1a** having *cis*-1-methyl-1-propenyl group to **1b** having *trans*-1-methyl-1-propenyl group, rearrangement rate decreases 10^5 times. It is noteworthy that the rate of migration of *trans*-1-methyl-1-propenyl group is close to that of 1-methyl-1-vinyl group, despite the presence of a methyl group in the β -position in the former.

Table 1. Rates of 1,2-shifts of vinyl groups in cations 1a-d

<i>Ion</i>	k (s^{-1}) ^a	T ($^{\circ}C$)	ΔG^{\ddagger} (kJ/mol)	
$k_{.103\ ^{\circ}C}$ (s^{-1}) ^b				
1a	1.0×10^5	-120	22	6×10^5
1b	40	-88	39	4
1c	12	-102	37	10
1d	1.1×10^5	-103	24	1×10^5

^a Experimental values. ^b Calculated from the Eyring equation.

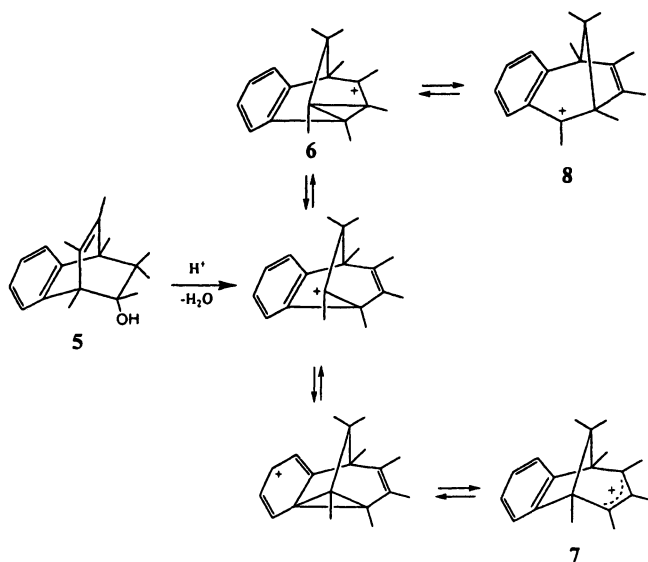
The reasons for such retardation effects were disclosed by quantum chemical calculations. Analysis of geometric characteristics for the initial and transition states of the rearrangements obtained by DFT method with the use of PRIRODA program (27, 28) showed that unfavorable steric interactions in transition states of the rearrangements of cations **1b,c** were responsible for the retardation effects (25).

Rearrangements of long-lived carbocations formed via *endo*-9-hydroxy-1,8,9,10,10,11,12-heptamethyltricyclo[6.2.2.0^{2,7}]dodeca-2(7),3,5,11-tetraene (**5**) in FSO₃H-SO₂ClF-CD₂Cl₂ at low temperature ($-95\ ^{\circ}C$) were studied by ¹H and

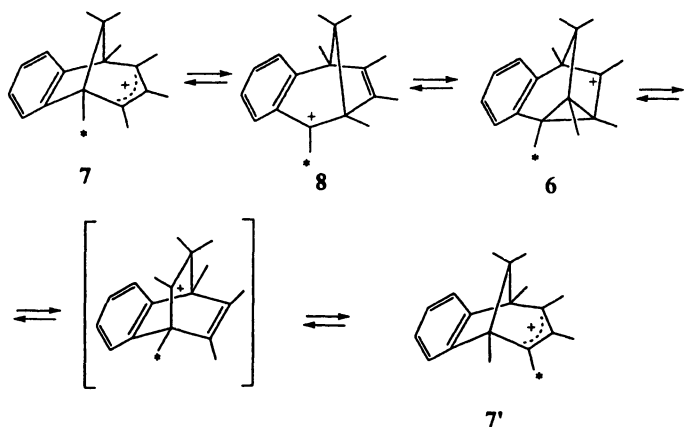
^{13}C NMR spectroscopy (29). Carbocation **6** was found to be involved in a rapid interconversion with cations **7** and **8** (Scheme 7).

This conclusion is in accord with the results of MINDO/3 quantum-chemical calculations. Cation **7** is also prone to undergo a rather slow degenerate rearrangement by 1,2-bridge shift (ΔG^\ddagger is about 60 kJ/mol) (Scheme 8). This rearrangement was probed via ^2H NMR spectroscopy, when the 9- CD_3 -analog of carbinol **5** was used as precursor for carbocation generation. At -50°C cations **6-8** transform firstly into 1,1,2,3,3a,4,8b-heptamethyl-1,3a,8b-trihydrobenzopentalenium ion (**9**) and then (partially) into 1,1,2,3,4,4,8b-heptamethyl-1,4,8b-trihydrobenzopentalenium ion (**10**) (Scheme 9).

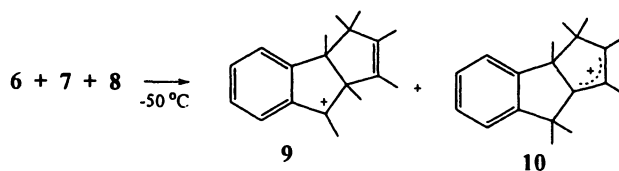
Cations **9** and **10** are also formed on dissolution of alcohol **5** in $\text{CF}_3\text{SO}_3\text{H}$ at -20°C . Their signals rapidly disappear from the ^1H NMR spectrum of the resulting solution, and a new set of signals appears which corresponds to 1,2,3,3a,4,4,8b-heptamethyl-3a,4,8b-trihydrobenzopentalenium ion (**11**). A possible mechanism for this transformation is outlined in Scheme 10.



Scheme 7

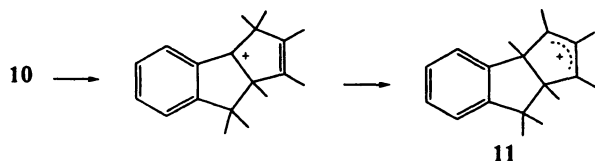


Scheme 8



Scheme 9

Thus, the rearrangements of bicyclo[3.2.1]octadienyl carbocations having a fused benzene ring are generally analogous to those occurring in structurally related cations with isolated double bond (30). Unlike the latter, which migrates from one position in the cation to another, the *ortho*-phenylene fragment retains its position in all carbocations involved.



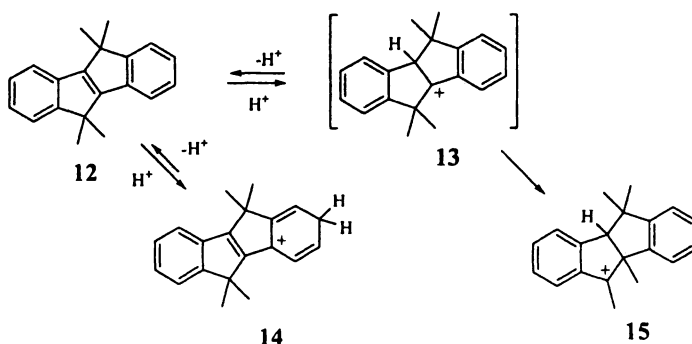
Scheme 10

Chemical behavior of polycyclic aromatic hydrocarbons (PAHs) and their derivatives in superacidic media continues to attract increased interest (2, 5, 11,

31), as they serve in particular as models for biological electrophiles formed via their oxidized metabolites, and because many classes of PAHs and their substituted derivatives exhibit mutagenic and/or carcinogenic properties (31).

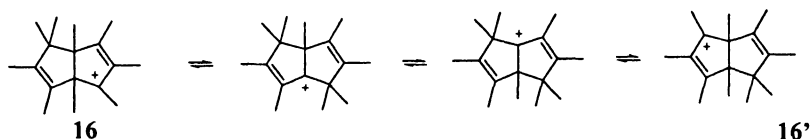
Among polycyclic hydrocarbons, there is a considerable interest in poorly studied compounds having a benzopentalene skeleton. The presence of a fused aromatic ring is expected to restrict possible rearrangements, therefore ensuring relatively high regioselectivity.

As mentioned above, persistent carbocation **9** underwent rearrangement into cation **10** which rearranged further into cation **11**. To reveal general relations/factors governing cationic rearrangements in benzopentalene derivatives, the behavior of 5,5,10,10-tetramethyl-5,10-dihydroindeno[2,1-*a*]indene (**12**) in superacids was studied (32). It had been expected that hydrocarbon **12** would transform into the long-lived 5,5,10,10-tetramethyl-4b,5,9b,10-tetrahydroindeno[2,1-*a*]inden-4b-yl cation (**13**). However, ^1H and ^{13}C NMR data showed that hydrocarbon **12** transformed firstly into isomeric ion **14** which transformed further into cation **15** (Scheme 11).



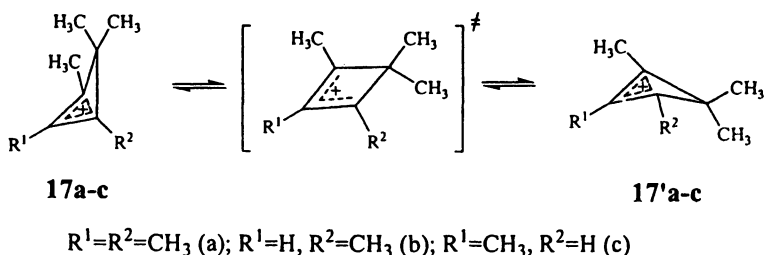
Scheme 11

The results obtained in combination with the data on the transformations of cations **9-11**, led to the conclusion that 1,2-shifts of methyl groups occur readily in carbocations having a pentalene fragment. On the basis of the data obtained for rearrangements of such carbocations, an alternative mechanism has been proposed (32) for the rearrangement of structurally related carbocation **16** having a bicyclo[3.3.0]octane skeleton described in (33) (Scheme 12).



Scheme 12

Cyclobutenyl carbocations have been under study in our laboratory for some years (11). In (34), unusually strong temperature dependence of ^{13}C chemical shifts (up to 0.077 ppm/K) was observed for long-lived cations **17a-c**. The authors suggested that this resulted from a very low inversion barrier for the four-membered ring (Scheme 13).



Scheme 13

Complexes with N-Centered Electrophiles

Nitrosonium Complexes

Among complexes of organic compounds with N-centered electrophiles, a special position is occupied by the nitrosonium complexes. Interest in these complexes has not diminished over the years as they are intermediates in several important organic reactions, such as nitrosation of aromatic compounds (35),

nitrosohalogenation of olefins (36, 37), and others (8). Recently this interest has amplified due to a unique role for NO molecule in subtle biochemical processes proceeding in vivo (38-41). It is proposed that NO^+ and certain molecules capable of generating it, are involved in the mechanism of neurotoxic and neuroprotective actions of NO (42,43) (*cf.* refs. (44-46), and also participate in cross-linking of DNA (47, 48).

Nitrosonium Complexes with Two-Electron Ligands

Until recently experimental data on structure of complexes of olefins with the nitrosonium cation were lacking. Attempts to prepare nitrosonium complexes of ethylene and 2,3-dimethyl-2-butene by the interaction thereof with NO^+BF_4 failed (49). The authors of (49) succeeded in preparation of a complex of adamantylideneadamantane with NO^+ cation, but they could not make a choice between a dynamic σ -complex and a static π -complex. Authors of (50) succeeded in preparation of nitrosonium complex of 2,3-dimethyl-2-butene. A detailed analysis of the structure of this complex was performed with the use of ^1H and ^{13}C NMR spectroscopy, including isotope perturbation, *ab initio* (HF/6-31G*) and *IGLO* calculations. The calculations predict two type of complexes – of C_{2v} symmetry (18) and symmetry which is close to C_s (19), *cf.* ref. (51) (Figure 1). In these complexes, the distances between N atom and C=C bond are 1.22 and 2.18 Å, respectively, with bonding energies of 93.7 and 117.6 kJ/mol. The chemical shift for C^2 and C^3 (190.2 ppm) is much closer to those obtained by *IGLO(DZ)* for complex 19 (183.4 and 189.8 ppm, respectively) than to that for complex 18 (67.2 ppm).

Equivalency of C^2 and C^3 atoms and the carbon atoms of methyl groups observed in ^{13}C NMR spectrum of complex 19 may stem from fast inversion at the N atom or rotation of the NO group around the axis crossing the N atom and perpendicular to the $\text{C}^2 - \text{C}^3$ bond and rapid migration of this group from one side of the molecule to another (Scheme 14).

Nitrosonium complexes 20a-d of 1-R-2-methylacenaphthylenes 21a-d (Scheme 15) can be considered as complexes with two-electron ligands, as unlike complexes of other polycyclic aromatic compounds (8, 52), nitrosonium

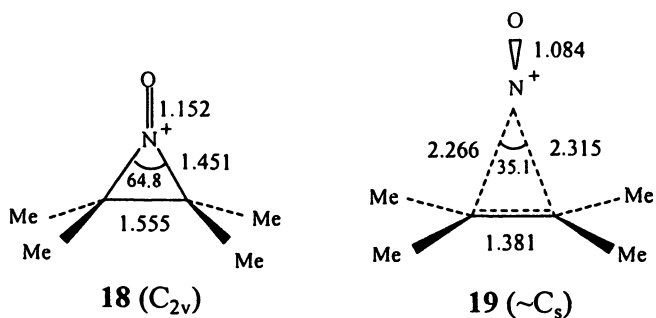
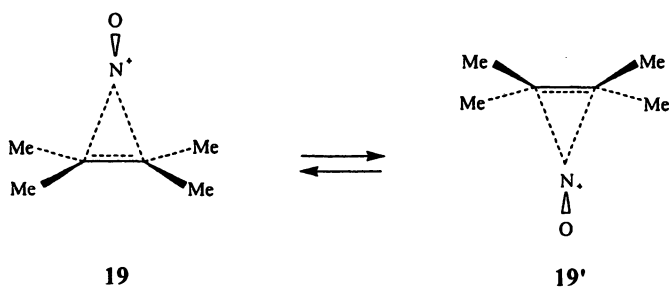
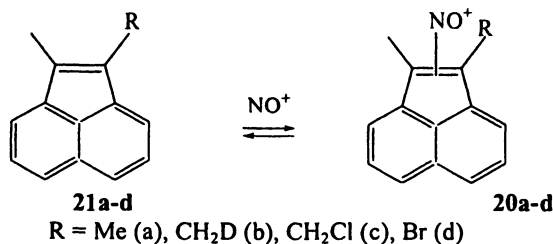


Figure 1. Schematic representation of the nitrosonium complexes of 2,3-dimethyl-2-butene. Distances are in angstroms and angles are in degrees, the values correspond to the HF/6-31G* optimized structures.



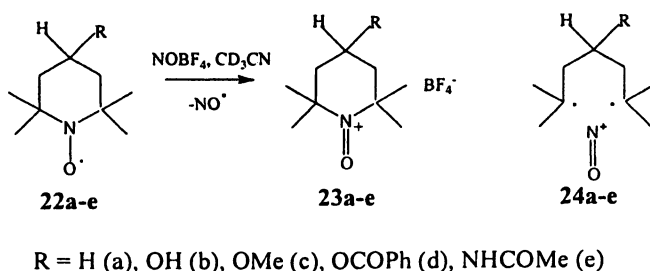
Scheme 14



Scheme 15

cation is bonded not to aromatic system, but to the $C^1=C^2$ bond (**53**). This was determined by ^1H , ^{13}C and ^{15}N NMR spectroscopy with the use of isotope perturbation.

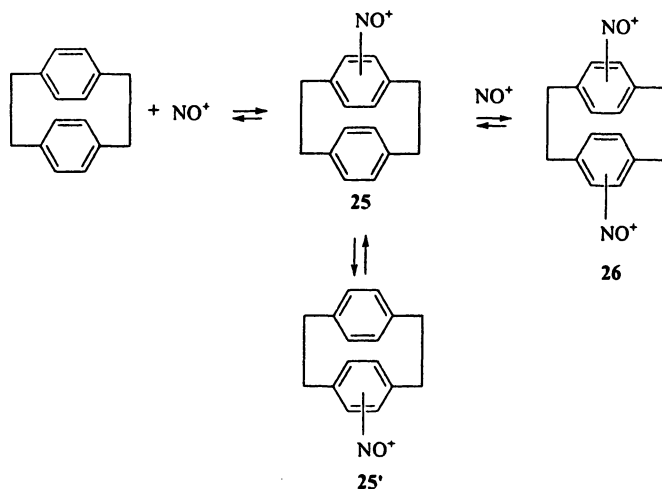
It is known that the nitronium cation is a strong oxidant (**54**). In (**55**) it was found by multinuclear NMR (^1H , ^{13}C , ^{19}F and ^{14}N) that the interaction of nitronium tetrafluoroborate with 2,2,6,6-tetramethyl-4-R-piperidine-1-oxyl radicals **22a-e** resulted in formation of 4-R-2,2,6,6-tetramethylpiperidine-1-oxoammonium tetrafluoroborates (Scheme 16). Cations **23a-e** could be classified as nitronium complexes of biradicals **24a-e**.



Scheme 16

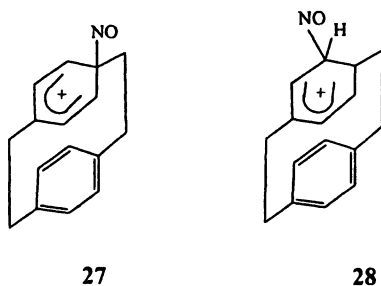
Nitronium Complexes of [2.2]paracyclophane

To date the structure and reactivity of numerous complexes derived from aromatic compounds and nitronium cation have been studied (8, 56-63). However, relatively few studies are available on the nitronium complexes of cyclophanes (5, 57, 59, 61, 62), *cf.* ref. (63). The interaction of [2.2]paracyclophane with nitronium tetrachloroaluminate was studied by ^1H and ^{13}C NMR spectroscopy using deuterium isotope perturbation technique (64). It was found that the resulting nitronium complexes containing one (**25**) or two NO groups (**26**) are involved in fast interconversion (on the NMR time scale) (Scheme 17).



Scheme 17

Quantum chemical DFT calculations (3Z basis set) indicate greater stability of η_2 single-charged π -complexes as compared to σ -complexes corresponding to the addition of NO^+ cation at the *ipso*- or *ortho*-positions (27 and 28 respectively). The formation of the singly-charged π -complex (25) is energetically more favorable than that of a doubly-charged π -complex (26).



The affinity of [2.2]paracyclophane for nitrosonium cation is much greater than that of *para*-xylene, presumably owing to stacking interaction between the aromatic rings in the π -complex. Low isotope effect on the aromatic carbon

signals observed for the nitrosonium complex of 4-deuterio[2.2]paracyclophane [δ (-50 °C) \approx 0.3 ppm, *cf.* refs. (65-71)] testifies against a mechanism with considerable involvement of the σ -complexes **27** and **28**.

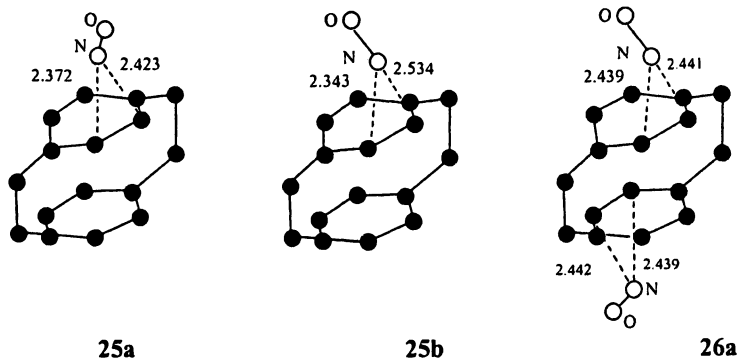


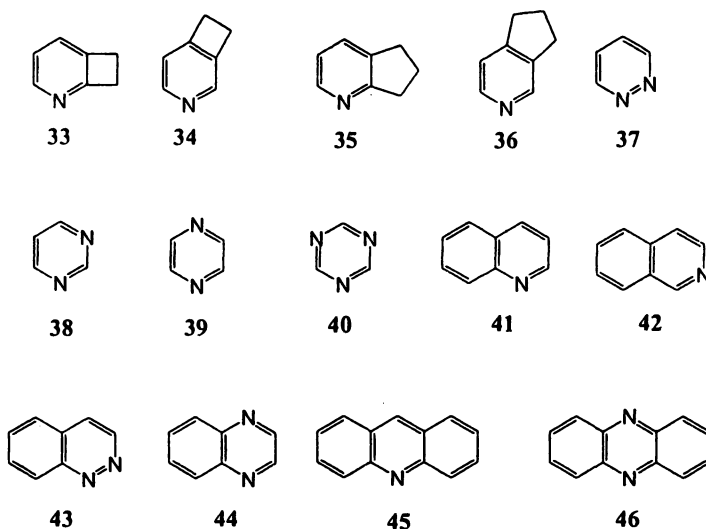
Figure 2. Optimized structures of the nitrosonium complexes of [2.2]paracyclophane at DFT/3Z. Distances are in angstroms.

Among singly-charged π -complexes optimized by the DFT method, π -complex **25a** is energetically most favored, its optimized geometry is similar to those obtained by X-ray diffraction method for nitrosonium complex of methyl-substituted benzene derivatives (58, 72, 73). Complexes of this type are characterized by angular orientation of the NO group with respect to benzene ring plane, sp^2 hybridization of the aromatic carbon atoms, and long bonds between the NO nitrogen and the nearest carbon atoms of the aromatic ring (2.0–2.5 Å).

Nitrosonium Complexes of N-heteroaromatic Compounds

Data pertaining to affinity of organic N-bases towards nitrosonium cation are numerous (74-80), however, those for N-heteroaromatic compounds are limited (77-80).

In (81) affinities of the following N-heteroaromatic compounds towards nitrosonium cation have been calculated by AM1 and *ab initio* methods: C₅H₅N (**29**), 2-XC₅H₄N (**29a-j**) [X = Me (a), Et (b), CF₃ (c), CN (d), MeO (e), MeS (f), Br (g), Cl (h), F (i), NH₂ (j)], 3-XC₅H₄N (**30a-k**) [X = Me (a), CF₃ (b), Ac (c), PhCO (d), OH (e), MeO (f), MeS (g), Br (h), Cl (i), F (j), NH₂ (k)], 4-XC₅H₄N (**31a-l**) [X = Me (a), 4-Et (b), CH=CH₂ (c), Ph (d), CF₃ (e), MeO (f), MeS (g), Br (h), Cl (i), F (j), NH₂ (k), NO₂ (l)], XYC₅H₃N (**32a-i**) [X = 2-Me, Y = 3-Me (a); X = 2-Me, Y = 4-Me (b); X = 2-Me, Y = 5-Me (c); X = 2-Me, Y = 6-Me (d); X = 3-Me, Y = 4-Me (e); X = 3-Me, Y = 5-Me (f); X = 2-Cl, Y = 4-Me (g); X = 2-Cl, Y = 6-Me (h); X = 2-Cl, Y = 6-MeO (i)], **33-46**.



The best agreements between the calculated and experimental affinities of the N-heteroaromatic compounds toward nitrosonium cation (A_{NO^+}) are observed by use of AM1 and *ab initio* with split polarizing [HF/6-31G (2d), 6-31G (2d, p), 6-31G (3d)] or diffuse functions [HF/(6-31G+(d), 6-31G++(d), 6-31G+(d, p) and 6-31G++(d, p)]. It has been found that A_{NO^+} value increases with decreasing

number of nitrogen atoms in a cycle, increasing donor character of substituents, and also by the presence of ring annelation.

Approximately linear relationships between the calculated A_{NO^+} values (kJ/mol) and σ - or σ^+ -constants, or values of total charge on the NO group of complex q_{NO^+} were found for the 3- and 4-substituted pyridines (81):

$$\begin{array}{lll} A_{\text{NO}^+} = (177.1 \pm 2.5) - (94.8 \pm 7.6) \sigma & r = -0.936, & s = 11.2 \\ A_{\text{NO}^+} = (163.9 \pm 2.6) - (63.2 \pm 5.3) \sigma^+ & r = -0.942, & s = 11.5 \\ A_{\text{NO}^+} = (327 \pm 14) - (960 \pm 81) q_{\text{NO}^+} & r = -0.933, & s = 11.6 \end{array}$$

A linear relationship between calculated A_{NO^+} values and experimental values of proton affinity (PA) for N-heteroaromatic compounds was also established (Figure 3). The points 1-4 (compounds 32h, 46, 32d and 31d respectively) have been excluded from the statistical treatment, $r = 0.969$].

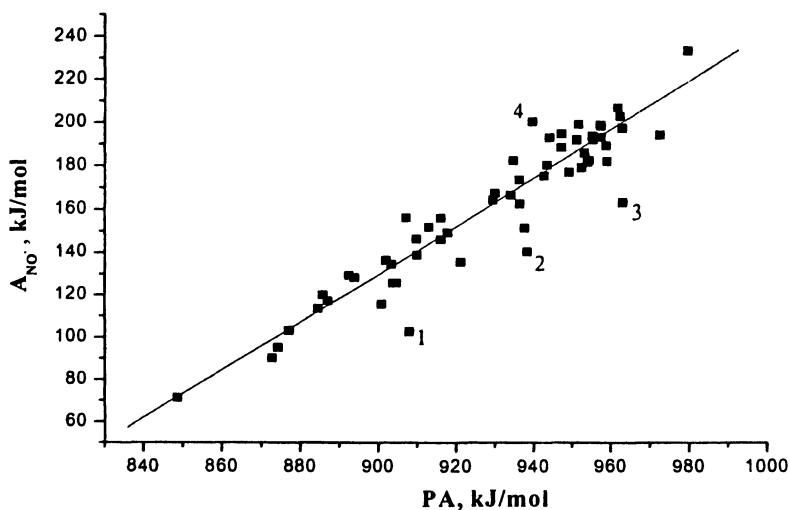
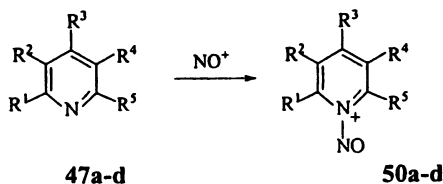


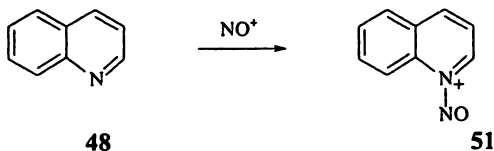
Figure 3. Correlation between the affinity of N-heteroaromatic compounds for NO^+ cation (A_{NO^+}) and proton affinity (PA).

Interaction of pyridine and its derivatives (**47a-d**), as well as of quinoline (**48**) and pyrimidine derivatives (**49a,b**) with NO^+BF_4^- in $(\text{CD}_3)_2\text{SO}$ at 20°C or $\text{NO}^+\text{AlCl}_4^-$ in SO_2 at -60°C results in formation of complexes **50a-d**, **51**, and **52a,b**, respectively (Schemes 18-20). Their structures have been confirmed by ^1H and ^{13}C NMR spectroscopy (82-84).

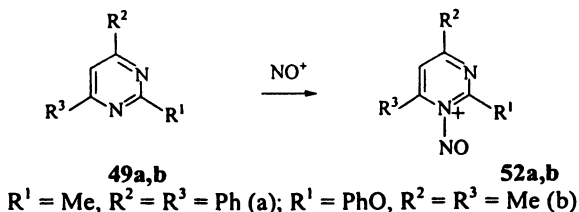


$\text{R}^1=\text{R}^2=\text{R}^3=\text{R}^4=\text{R}^5=\text{H}$ (a); $\text{R}^1=\text{R}^3=\text{R}^4=\text{R}^5=\text{H}$, $\text{R}^2=\text{CH}_3$ (b); $\text{R}^1=\text{R}^2=\text{R}^4=\text{R}^5=\text{H}$, $\text{R}^3=\text{CHO}$ (c); $\text{R}^1=\text{R}^3=\text{R}^5=\text{CH}_3$, $\text{R}^2=\text{R}^4=\text{H}$ (d)

Scheme 18

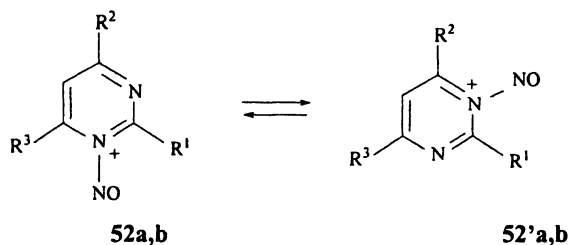


Scheme 19

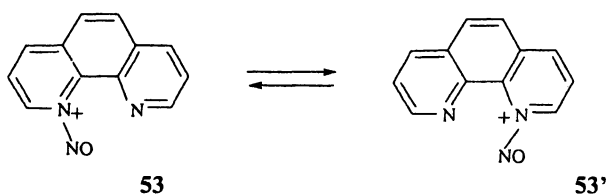


Scheme 20

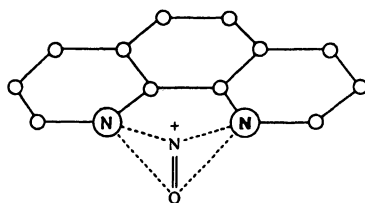
NMR spectra show that complexes **52a,b** undergo fast degenerate rearrangement proceeding by intra- and/or intermolecular transfer of NO group (Scheme 21).

*Scheme 21*

Analogous rearrangement is also observed for the nitrosonium complex of 1,10-phenanthroline (**53**) (Scheme 22) (82-85).

*Scheme 22*

In the solid state formation of a symmetric static complex **54** is favorable (86,87).

**54**

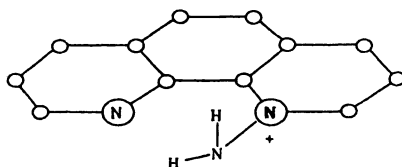
A distinctive feature of the complex is the NO group position between the two nitrogen atoms of phenanthroline skeleton, and so the complex may be regarded

as belonging to a bidentate type. The distances from the N atom of the NO group to the nitrogens of the skeleton are approximately equal (2.3 Å) and are considerably shorter than the average intermolecular contacts of the pair of nitrogen atoms N[⋯]N (3.00 Å) (88). In the crystal two types of cations are present where the NO groups are oriented at angles 54° and 61° with respect to phenanthroline plane, and the length of N–O bonds is close to that in the NO⁺ cation. The quantum chemical AM1 calculations suggest that the most stable structure is an asymmetrical n-complex 53 (85). *Ab initio* calculations HF/6-31G also indicate an asymmetrical structure to be preferred (87). Analysis of the Hessian reveals that at constraint by symmetry in the framework of point group C_s at HF/6-31G*, the symmetrical complex is a local minimum on the potential energy surface (PES). Optimization, taking into account electron correlation (method MP2/6-31G), leads to a local minimum with a virtually symmetrical structure 54. Apparently the structure of the asymmetrical complex is not a minimum in the framework of MP2/6-31G method. The binding energy between cation NO⁺ and phenanthroline in the symmetrical complex (A_{NO⁺}) is fairly large and depends on the chosen approximation. All versions of *ab initio* calculations result in close geometrical parameters for the symmetrical complex 54 that are similar to the experimental data obtained by X-ray diffraction method.

Nitrenium Complexes

Nitrenium cation is an extremely unstable species (89-91). That is why nitrenium complexes are usually prepared by the interaction of organic compounds with some sources of nitrenium cation (91, 92). Thus, the interaction of O-mesityl-sulfonylhydroxylamine with 1,10-phenanthroline results in the formation of 1-amino-1,10-phenanthrolium mesitylenesulfonate (93-99). The structure of this salt has been confirmed by ¹H and ¹³C NMR spectroscopy (93,

94, 96-99) and by X-ray diffraction method (94, 95, 97). In contrast to complex 54, complex 55 is a monodentate in the crystalline state.

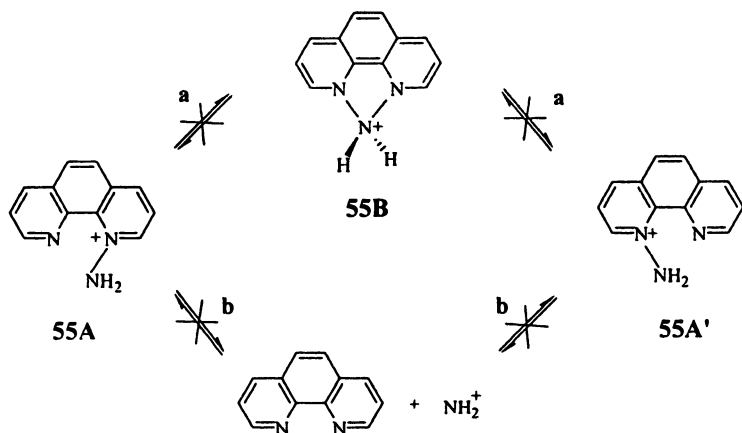


55

The N^1-NH_2 bond length [1.403(3) Å] is between $N(sp^2)-N(sp^3)$ (1.420 Å) and $N(sp^2)-N(sp^2)$ bonds (1.401 Å) (100). The distance between nitrogen atoms $N^{10} \cdots N(NH_2)$ [2.689(4) Å] is much less than the average value of intermolecular contact of nitrogen atoms pair 3.00 Å (88). The $N-NH_2$ fragment has a pyramidal structure, the nitrogen atom of NH_2 group lying in the plane of phenanthroline skeleton. The 1H NMR spectra show that the asymmetrical structure of cation 55 is retained in going to solution (97). Quantum-chemical calculations by the AM1 method and *ab initio* (HF/6-31G, HF/6-31G*, MP2/6-31G) give geometric parameters for the cation that are similar to those determined experimentally.

No dynamic processes involving intra- or intermolecular transfer of the NH_2 group was observed by NMR spectroscopy up to 100 °C (Scheme 23). 1-Amino-1,10-phenanthroline cation does not react with 4-methylpyridine and 4-methyl-1,10-phenanthroline with a transfer of the amino group, and it fails to react with mesitylene and anthracene even at elevated temperature.

Upon reaction of O-mesitylsulfonylhydroxylamine with X-1,10-phenanthrolines (56a-d) in CH_2Cl_2 the respective isomeric cations (55a-d) and (57a,e-g) were formed (Scheme 24) (99), and their structures were confirmed by 1H and ^{13}C NMR spectroscopy.



Scheme 23



Scheme 24

The ratio of isomeric cations **55** and **57** strongly depends on the nature of X substituent. Donor substituents increase electron density on the neighboring nitrogen atom in the same ring and favor addition of the amino group at that nitrogen atom; therefore, the fraction of the corresponding isomer is larger. However, no quantitative correlation between the ratio of isomers **55** and **57** and the difference in the charges on the N¹ and N¹⁰ atoms in the initial azine, calculated by the AM1 method has been found. This may be interpreted in terms of the mechanism with a late transition state, according to which the ratio of isomeric ions is determined by their relative stabilities. Thus, linear correlations between the logarithms of the ratio of ions **55** and **57** and the differences in $\Delta\Delta H_f$ and ΔE values for these ions calculated by AM1 and B3LYP/6-31G(dp) methods, respectively, have been observed (98, 99):

$$\lg ([55]/[57]) = (-0.11 \pm 0.06) - (0.084 \pm 0.015) \Delta\Delta H_f, r = -0.971, s = 0.13$$

$$\lg ([55]/[57]) = (0.03 \pm 0.06) - (0.065 \pm 0.010) \Delta E, r = -0.964, s = 0.11$$

Conclusion

By employing modern physical methods and quantum-chemical calculations, a significant body of data concerning the structure and reactivity of organic cationic complexes has been accumulated during the past decade and further studies on this dynamic area of organic chemistry are currently underway in our laboratory.

Acknowledgements

We are grateful to our co-workers who have carried out a large portion of the work described herein and whose names appear in the references. We are also grateful to the Russian Foundation for Basic Research and to the Russian Academy of Sciences (project N 06-03-32406 and program N 5.1.9, respectively) for financial support

References

1. Vogel, P. *Carbocation Chemistry*; Elsevier: Amsterdam, Holland, 1985.
2. Olah, G.A.; Prakash, G.K.S.; Sommer, J. *Superacids*; Wiley-Interscience: New York, 1985.
3. Borodkin, G.I.; Shubin, V.G. *Russ. Chem. Rev.* **1995**, *64*, 627.
4. *Stable Carbocation Chemistry*; Prakash, G.K.S.; Schleyer, P.v.R., Eds.; J. Wiley & Sons, Inc.: New York, 1997.
5. Borodkin, G.I.; Shubin, V.G. *Chemistry Reviews*; Vol'pin, M.E., Ed.; 1999; vol. 24, part 2, p 1.
6. *Onium Ions*. Olah, G.A.; Laali, K.K.; Wang, Q.; Prakash, G.K.S. Eds.; J. Wiley & Sons, Inc., New York, 1998.
7. Borodkin, G.I.; Shubin, V.G. *Russ. J. Org. Chem.* **2000**, *36*, 455.
8. Borodkin, G.I.; Shubin, V.G. *Russ. Chem. Rev.* **2001**, *70*, 211.
9. *Modern Arene Chemistry*, Astruc, D., Ed.; Wiley-VCH Verlag: Weinheim, Germany, 2002; p 435.
10. *Carbocation Chemistry*. Olah, G.A.; Prakash, G.K.S. Eds.; J. Wiley & Sons, Inc.: Hoboken, NJ, 2004.

11. Shubin, V.G.; Borodkin G.I. In *Carbocation Chemistry*; Olah, G.A.; Prakash, G.K.S., Eds.; John Wiley & Sons, Inc.: Hoboken, NJ, 2004; p 125.
12. Mayr, H.; Olah, G.A. *J. Am. Chem. Soc.* **1977**, *99*, 510.
13. Zefirov, N.S.; Davydova, A.F.; Yur'ev, Yu. K. *Zh. Obshch. Khim.* **1966**, *36*, 1217.
14. Thomas, A.F. *Chem. Commun.* **1970**, 1054.
15. Bly, R.S.; Swindell, R.T. *J. Org. Chem.* **1965**, *30*, 10.
16. Miller, J.A.; Ullah, G.M. *Chem. Commun.* **1982**, 874.
17. Marx, J.N.; Hahn, Y.-S. P. *J. Org. Chem.* **1988**, *53*, 2866.
18. Shubin, V.G.; Korchagina, D.V.; Borodkin, G.I.; Derendyaev, B.G.; Koptuyug, V.A. *Zh. Org. Khim.* **1973**, *9*, 1031.
19. Shubin, V.G.; Korchagina, D.V.; Derendyaev, B.G.; Borodkin, G.I.; Koptuyug, V.A. *Zh. Org. Khim.* **1973**, *9*, 1041.
20. Bushmelev, V.A.; Genaev, A.M.; Shubin, V.G. *Russ. Chem. Bull.* **2004**, *53*, 2886.
21. Bushmelev, V.A.; Genaev, A.M.; Shubin, V.G. *Russ. J. Org. Chem.* **2004**, *40*, 966.
22. Bushmelev, V.A.; Genaev, A.M.; Shubin, V.G. *Russ. J. Org. Chem.* **2006**, *42*, 100.
23. Bushmelev, V.A.; Genaev, A.M.; Shubin, V.G. *Russ. J. Org. Chem.* **2006**, *42*, 220.
24. Artamoshkin, V.G.; Bushmelev, V.A.; Genaev, A.M.; Shubin, V.G. *Mendeleev Commun.* **2006**, 112.
25. Artamoshkin, V.G.; Bushmelev, V.A.; Genaev, A.M.; Shubin, V.G. *Russ. J. Org. Chem.*, in press.
26. Balaban, A.T.; Fărcașiu, D. *J. Am. Chem. Soc.*, **1967**, *89*, 1958.
27. Laikov, D.N. *Chem. Phys. Lett.* **1997**, *281*, 151.
28. Laikov, D.N.; Ustynyuk, Yu. A. *Izv. AN. Ser. Khim.* **2005**, 804.
29. Genaev, A. M.; Mamatyuk, V.I.; Sal'nikov, G.E.; Shakirov, M.M.; Shubin, V.G. *Russ. J. Org. Chem.* **2000**, *36*, 1268.
30. Hart, H.; Kuzuya, M. *J. Am. Chem. Soc.*, **1976**, *98*, 1551.
31. Laali, K.K. *Chem. Rev.* **1996**, *96*, 1873; Laali, K.K. In *Carbocation Chemistry*; Olah, G.A.; Prakash, G.K.S., Eds.; John Wiley & Sons, Inc.: Hoboken, NJ, **2004**; p 237.
32. Genaev, A.M.; Sal'nikov, G.E.; Shubin, V.G. *Russ. J. Org. Chem.* **2001**, *37*, 1255.
33. Hart, H.; Kuzuya, M. *J. Am. Chem. Soc.*, **1976**, *98*, 1545.
34. Salnikov, G.E.; Genaev, A.M.; Mamatyuk, V.I. *Mendeleev Commun.* **2003**, 48.
35. Williams, D.L.H. *Nitrosation*. Cambridge Univ. Press: Cambridge, UK, 1988.
36. Kadzyscas, P.P.; Zefirov, N.S. *Usp. Khim.* **1968**, *37*, 1243.
37. De la Mare, P.B.D.; Bolton, R. *Electrophilic Additions to Unsaturated Systems*. Elsevier Scient. Publ. Co. Amsterdam, Holland, 1982; p 247.

38. Murad, F. *Angew. Chem., Int. Ed. Engl.* **1999**, *38*, 1856.
39. Furchgott, R.F. *Angew. Chem., Int. Ed. Engl.* **1999**, *38*, 1870.
40. Ignarro, L.J. *Angew. Chem., Int. Ed. Engl.* **1999**, *38*, 1882.
41. Patel, R.P.; McAndrew, J.; Sellak, H.; White, C.R.; Jo, H.; Freeman, B.A.; Darley-Usmar, V.M. *Biochim. Biophys. Acta*, **1999**, *1411*, 385.
42. Lipton, S.A.; Choi, Y.-B.; Pan, Z.-H.; Lei, S.Z.; Chen, H.-S.V.; Sucher, N.J.; Loscalzo, J.; Singel, D.J.; Stamler, J.S. *Nature (London)*. **1993**, *364*, 626.
43. Stamler, J.S.; Singel, D.J.; Loscalzo, J. *Science (Washington, D.C.)*. **1992**, *258*, 1898.
44. Butler, A.R.; Flitney, F.W.; Williams, D.L.H. *Trends Pharmacol. Sci.*, **1995**, *16*, 18.
45. De Groote, M.A.; Testerman, T.; Xu, Y.; Stauffer, G.; Fang, F.C. *Science (Washington, D.C.)*. **1996**, *272*, 414.
46. Hughes, M.N. *Biochim. Biophys. Acta*. **1999**, *1411*, 263.
47. Kirchner, J.J.; Sigurdsson, S.T.; Hopkins, P.B. *J. Am. Chem. Soc.*, **1992**, *114*, 4021.
48. Elcock, A.H.; Lyne, P.D.; Mulholland, A.J.; Nandra, A.; Richards, W.G. *J. Am. Chem. Soc.* **1995**, *117*, 4706.
49. Olah, G.A.; Schilling, P.; Westerman, P.W.; Lin, H.C. *J. Am. Chem. Soc.* **1974**, *96*, 3581.
50. Borodkin, G.I.; Elanov, I.R.; Genae, A.M.; Shakirov, M.M.; Shubin, V.G. *Mendeleev Commun.*, **1999**, 83.
51. Raghavachari, K.; Reents, W.D.; Haddon, R.C. *J. Comput. Chem.* **1986**, *7*, 265.
52. Rosokha, S.V.; Kochi, J.K. *New J. Chem.* **2002**, *26*, 851.
53. Borodkin, G.I.; Elanov, I.R.; Shakirov, M.M.; Shubin, V.G. *Zh. Org. Khim.* **1991**, *27*, 889.
54. Ebersson, L.; Radner, F. *Acc. Chem. Res.* **1987**, *20*, 53.
55. Borodkin, G.I.; Elanov, I.R.; Shakirov, M.M.; Shubin, V.G. *Russ. J. Org. Chem.* **2003**, *39*, 1144.
56. Borodkin, G.I.; Elanov, I.R.; Shubin, V.G. *The 13th IUPAC Conference on Physical Organic Chemistry, August 25-29, 1996, Incheon, Korea, Abstracts*, p 243.
57. Rathore, R.; Lindeman, S.V.; Rao, K.S.S.P.; Sun, D.; Kochi, J.K. *Angew. Chem. Int. Ed. Engl.* **2000**, *39*, 2123.
58. Rosokha, S.V.; Lindeman, S.V.; Kochi, J.K. *J. Chem. Soc. Perkin Trans. 2*. **2002**, 1468.
59. Zyryanov, G.V.; Kang, Y.; Stamp, S.P.; Rudkevich, D.M. *Chem. Commun.* **2002**, 2792.
60. Gwaltney, S.R.; Rosokha, S.V.; Head-Gordon, M.; Kochi, J.K. *J. Am. Chem. Soc.*, **2003**, *125*, 3273.
61. Rosokha, S.V.; Lindeman, S.V.; Rathore, R.; Kochi, J.K. *J. Org. Chem.*, **2003**, *68*, 3947.

62. Zyryanov, G.V.; Rudkevich, D.M. *J. Am. Chem. Soc.* **2004**, *126*, 4264.
63. Laali, K.K.; Borodkin, G.I. *J. Chem. Soc., Perkin Trans. 2.* **2002**, 953.
64. Borodkin, G.I.; Elanov, I.R.; Andreev, R.V.; Shakirov, M.M.; Shubin, V.G. *Russ. J. Org. Chem.* **2006**, *42*, 406.
65. Borodkin, G.I.; Elanov, I.R.; Shakirov, M.M.; Shubin, V.G. *Izv. AN SSSR, Ser. Khim.*, **1992**, 2104.
66. Borodkin G.I., Elanov I.R., Shakirov M.M., Shubin V.G. *J. Phys. Org. Chem.* **1993**, *6*, 153.
67. *Rearrangements in Ground and Excited States*; De Mayo P., Ed.; Acad. Press: New York, 1980, Vol. 1, p 1.
68. Saunders, M.; Kronja, O. In *Carbocation Chemistry*. Olah, G.A. Prakash, G.K.S., Eds.; J. Wiley & Sons: Hoboken, NJ, 2004, p 213.
69. Hansen P.E. *Annual Reports on NMR Spectroscopy*. Acad. Press: London, 1983, Vol. 15, p 105.
70. Siehl H-U. *Adv. Phys. Org. Chem.* Acad. Press: London, 1987, Vol. 23, p 63.
71. Borodkin G.I., Elanov I.R., Podryvanov V.A., Shakirov M.M., Shubin V.G. *J. Am. Chem. Soc.* **1995**, *117*, 12863.
72. Borodkin, G.I.; Nagi, Sh.M.; Gatilov, Yu.V.; Mamatyuk, V.I.; Mudrakovskii, I.L.; Shubin, V.G. *Dokl. AN SSSR*, **1986**, *288*, 1364.
73. Brownstein, S.; Gabe, F.; Lee, F.; Piotrowski, A. *Can. J. Chem.*, **1986**, *64*, 1661.
74. Kulkarni, S.A.; Pundlik, S.S. *Chem. Phys. Lett.* **1995**, *245*, 143.
75. Aschi, M.; Grandinetti, F. *Chem. Phys. Lett.* **1997**, *267*, 98.
76. Torday, L. L.; Santillán, M.B.; Ciuffo, G.M.; Jauregui, E.A.; Pataricza, J. Papp J.G.; Csizmadia, I.G. *J. Mol. Struct. (Theochem)*, **1999**, *465*, 69.
77. Borodkin, G.I.; Shubin, V.G. *Book of Abstracts of the International Conference "Reaction Mechanisms and Organic Intermediates"*, Saint-Petersburg, **2001**, 88.
78. Andreev, R.V.; Borodkin, G.I.; Shubin, V.G. *Book of Abstracts of the 2nd International Conference on Natural Products and Physiologically Active Substances (ICNPAS-2004) and 3rd EuroAsian Heterocyclic Meeting "Heterocycles in Organic and Combinatorial Chemistry" (EAHM-2004)*, Novosibirsk, Russia, September 12-17, 2004, p 131.
79. Andreev, R.V.; Borodkin, G.I.; Shubin, V.G. *Materials of the International Conference of Students and Post-Graduates on Basic Sciences "LOMONOSOV-200"*, Moscow, April 12-15, 2005, p 133.
80. Cacace, F.; de Petris, G.; Pepi, F. *Proc. Natl. Acad. Sci. USA.* **1997**, *94*, 3507.
81. Andreev, R.V.; Borodkin, G.I.; Shubin, V.G. *Russ. J. Org. Chem.*, in press.
82. Borodkin, G.I.; Shubin, V.G.; Andreev, R.V. *Book of Abstracts of the International Conference on Reactive Intermediates and Reaction Mechanisms*. Ascona, Switzerland, 1998, p 38.

83. Borodkin, G.I.; Andreev, R.V.; Elanov, I.R.; Shubin, V.G. *Book of Abstracts of the 7th European Symposium on Organic Reactivity*. Ulm, Germany, 1999, p 136.
84. Andreev, R.V.; Borodkin, G.I.; Shubin, V.G. *Book of Abstracts of the Youth School on Organic Chemistry*. Ekaterinburg, Russia, 1999, p 65.
85. Andreev, R.V.; Borodkin, G.I.; Shubin, V.G. *Russ. J. Org. Chem.*, **2001**, 37-144.
86. Andreev, R.V.; Borodkin, G.I.; Gatilov, Yu.V.; Shubin, V.G. *Russ. Chem. Bull.*, **2001**, 50, 2477.
87. Andreev, R.V.; Borodkin, G.I.; Gatilov, Yu.V.; Shubin, V.G. *Russ. J. Org. Chem.*, **2002**, 38, 845.
88. Zefirov, Yu.V.; Zorkii, P.M. *Zh. Strukt. Khim.* **1976**, 17, 994.
89. McClelland, R.A. *Tetrahedron*, **1996**, 52, 6823.
90. Falvey, D.E. *J. Phys. Org. Chem.* **1999**, 12, 589.
91. Borodkin, G.I.; Shubin, V.G. *Russ. J. Org. Chem.* **2005**, 41, 473.
92. Tamura, Y.; Minamikawa, J.; Ikeda, M. *Synthesis*, **1977**, 1.
93. Takeuchi H., Hayakawa S., Tanahashi T., Kobayashi A., Adachi T., Higuchi D. *J. Chem. Soc., Perkin Trans. 2.* **1991**, 847.
94. Andreev, R.V.; Borodkin, G.I.; Gatilov, Yu.V.; Shubin, V.G. *Materials of the Russian Scientific Youth Conference "Under the Badge Σ "*, Omsk, Russia, **2003**, p 48.
95. Andreev, R.V.; Borodkin, G.I.; Gatilov, Yu.V.; Shubin, V.G. *Book of Abstracts of the 4th Russian Conference for Young Scientists "Contemporary Problems of Theoretical and Experimental Chemistry"*, Saratov, Russia, **2003**, p 51.
96. Andreev, R.V.; Borodkin, G.I.; Vorob'ev, A. Yu.; Shakirov, M.M.; Shubin, V.G. *Book of Abstracts of the 7th Scientific School-Conference on Organic Chemistry*, Ekaterinburg, Russia, **2004**, p 125.
97. Andreev, R.V.; Borodkin, G.I.; Gatilov, Yu.V.; Shakirov, M.M.; Shubin, V.G. *Russ. J. Org. Chem.*, **2004**, 40, 567.
98. Andreev, R.V.; Borodkin, G.I.; Shakirov, M.M.; Shubin, V.G. *Book of Abstracts of the 2nd International Conference on Natural Products and Physiologically Active Substances (ICNPAS-2004) and 3rd EuroAsian Heterocyclic Meeting "Heterocycles in Organic and Combinatorial Chemistry" (EAHM-2004)*, Novosibirsk, Russia, September 12-17, 2004, p 132.
99. Andreev, R.V.; Borodkin, G.I.; Shakirov, M.M.; Shubin, V.G. *Russ. J. Org. Chem.* **2004**, 40, 1379.
100. Allen, F.H.; Kennard, D.; Watson, D.G. *J. Chem. Soc. Perkin Trans. 2 (Suppl.)*. **1987**, S1.

Chapter 8

Activation of Electrophilic Sites by Adjacent Cationic Groups

Douglas A. Klumpp

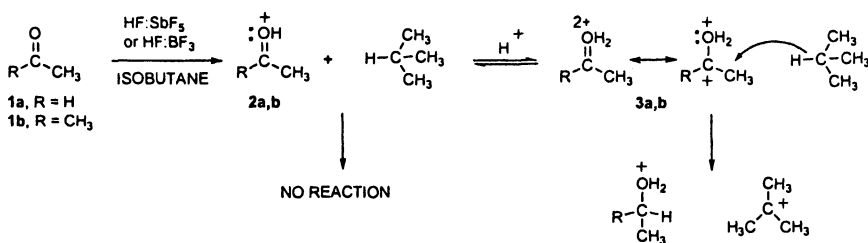
Department of Chemistry and Biochemistry, Northern Illinois University,
DeKalb, IL 60115

This chapter describes our studies of electrophilic systems having adjacent, stable cationic centers. We have shown in a wide variety of systems that stable cationic centers (i.e., ammonium, pyridinium, and phosphonium groups) can enhance the reactivities of some electrophiles. This enhanced reactivity is evident by reactions with weak nucleophiles, but may also involve unusual rearrangements or regiochemistry in the conversions. Using this chemistry, reactive dicationic systems can be generated and studied.

Introduction

In the 1970s, Brouwer and Kifflin reported the reactions of saturated hydrocarbons with aliphatic aldehydes and ketones in superacidic media.¹ Analysis of the products from these reactions suggested that the protonated aldehydes and ketones (carboxonium ions) were reacting at the carbon-hydrogen σ -bonds of the alkanes. This was a surprising observation because carboxonium

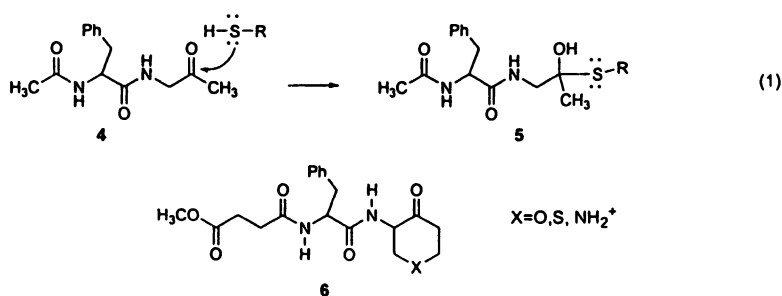
ions are not particularly strong electrophiles and alkanes are extremely weak nucleophiles. Soon after this report, Olah noted that there is no reaction between carboxonium ions and alkanes in aprotic solvents such as CH_2Cl_2 or nitromethane. To explain this dichotomy, Olah proposed the concept of superelectrophilic activation in which the carboxonium ion (**2a,b**) is protosolvated in the superacid to generate the doubly electron-deficient species (**3a,b**, Scheme 1).^{2,3} The diprotonated species (**3a,b**), or superelectrophiles, possess enhanced electrophilic reactivities due to their dipositive charge and they are capable of reacting with the weak nucleophile, *iso*-butane. The enhanced reactivities of nitronium salts in superacid were also explained in this seminal paper,² that being a result of superelectrophilic activation.



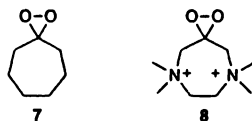
Scheme 1. Proposed mechanism for the superacid-catalyzed hydride transfer involving isobutene.

Since Olah's initial proposal, there have been many reports of superelectrophilic systems and reactions.³ Several superelectrophiles have been directly observed in the condensed phase by NMR techniques³ and in the gas-phase by mass-spectroscopy methods.⁴ Superelectrophilic activation is thought to be involved in some enzyme-catalyzed transformations and it is the basis for a number of synthetically useful transformations.⁵ Application of superelectrophilic chemistry has also been demonstrated in the efficient preparation of gasoline oxygenates and other industrially important feedstock chemicals.³ In our research, we have studied systems in which a stable cationic center is adjacent to an electrophilic site. We reasoned that stable cationic sites in dicationic systems would provide electrostatic and inductive effects similar to those in superelectrophiles. Like the superelectrophilic systems, dicationic systems having a stable positive charge can exhibit reactivities that greatly exceed that of related monocationic species. Moreover, incorporation of stable cationic sites can provide reactive, dicationic systems that are generated under more mildly acidic conditions than superelectrophiles. The resulting dicationic electrophiles are often readily observed by spectroscopic techniques.

Other research groups have studied the effects of cationic groups on electrophilic reactivities. For example, Seto and co-workers sought to design more highly electrophilic protease inhibitors.⁶ Compound **4** is a known protease inhibitor and its activity is thought to arise from the formation of the thio-hemiketal adduct (**5**). It is the electrophilic character of the ketone carbonyl group that gives compound **4** its biological activity as a protease inhibitor. In order to increase the electrophilic character of the carbonyl group, a series of derivatives (**6**) were prepared and tested for their protease inhibitor activity. Although the piperidone derivative was shown to be the most highly electrophilic compound in the series (established by measurements of the equilibrium concentrations of the *gem*-diol adducts in H₂O), its biological activity

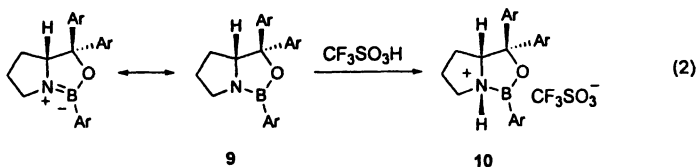


was poor. The cationic nitrogen does enhance the electrophilic character of the carbonyl, but it also adversely affects drug binding to the protease active site. Denmark and coworkers have studied dioxirane epoxidations and attempted to enhance the electrophilic reactivities of these reagents using ammonium groups.⁷ For example, the two dioxiranes were studied (**7-8**) and the cationic system (**8**) was shown to have increased reactivity in the electrophilic epoxidation of olefins (shown by the uptake of oxone). The Corey group has been using the chiral Lewis acid (**10**) in a number of asymmetric synthetic methodologies.⁸ This

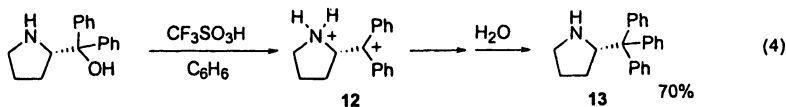
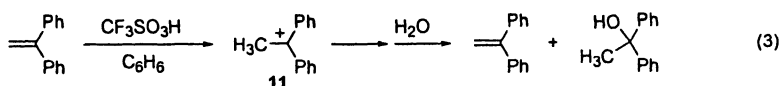


catalyst has been shown to be much more reactive than the neutral species **9**. Not only does protonation create a positive charge center adjacent to the Lewis acid site in **10** (eq 2), but it also prevents the π -bonding interaction between the nitrogen lone pair and empty orbital on boron, an interaction that decreases the

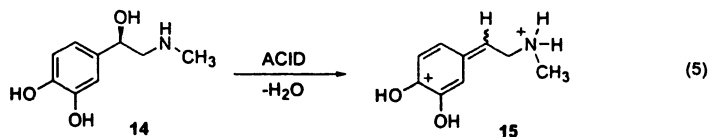
Lewis acidity of the boron. In each of the above examples, it is shown that a stable positive charge can enhance electrophilic reactivities. In a similar respect, it is also well known that positive charge centers can increase the acidities of protons on neighboring groups.



Much of our research has involved the use of dicationic electrophiles in reactions with very weak nucleophiles, such as non-activated arenes and alkanes. By comparison to similar monocationic electrophiles, we have been able to show the extent of electrophilic activation by adjacent cationic centers. For example, carbocations show an increased reactivity with a nearby cationic charge (eqs 3-4).⁹ When 1,1-diphenylethene is reacted with superacidic $\text{CF}_3\text{SO}_3\text{H}$

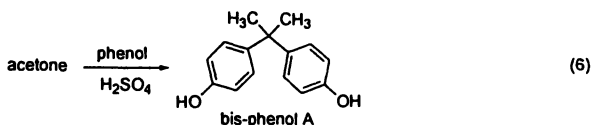


(triflic acid) in the presence of benzene, no phenylated product is isolated from the reaction. This is due to the effective stabilization of the 1,1-diphenylethyl cation (**11**). In contrast, reaction of the proline derivative under the same conditions leads to the formation of the phenylated product (**13**) in reasonably good yield (eq 4). This indicates that the cationic group activates the adjacent carbocationic center in dication **12** and thus the electrophilic center reacts with benzene. In this study, a variety of amino-alcohols were shown to react readily with benzene in the presence of superacid. Although only a few superelectrophiles have been directly observed by spectroscopic methods in the condensed phase, several of the amino-alcohols were studied in $\text{FSO}_3\text{H-SbF}_5\text{-SO}_2\text{ClF}$ and the dicationic products were visible by low temperature NMR, including the chiral dication **12** (derived from (L)-proline; at this level of acidity, it is assumed that there is no deprotonation at the stereocenter). Spectroscopic studies showed that under conditions of strong acidity, compounds

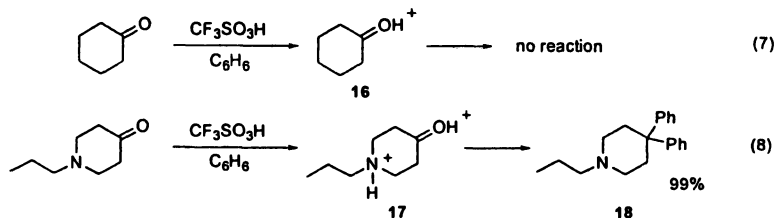


such as adrenaline (epinephrine, **14**) can form dicationic electrophilic species (eq 5).

We have found several examples in which adjacent cationic charge centers are shown to activate carboxonium electrophiles. A convenient method for studying this activation is through the use of the hydroxyalkylation reaction, a commercially important, acid-catalyzed condensation of aldehydes and ketones with arenes.¹⁰ It is used for example in the synthesis of bis-phenol A from acetone and phenol (eq 6). While protonated acetone is able to react with activated arenes like phenol, it is not capable of reacting with less nucleophilic



aromatic compounds, like benzene or chlorobenzene. Similarly when cyclohexanone is reacted with $\text{CF}_3\text{SO}_3\text{H}$ and benzene, no products are formed by the reaction with benzene (a small amount of the acid-catalyzed Aldol condensation product is obtained however; eq 7). However when piperidones are reacted with benzene under similar conditions, the condensation products (i.e. **18**) are formed in high yields (eq 8).¹¹ In this conversion, the ring nitrogen

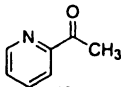
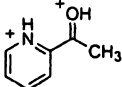
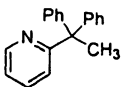
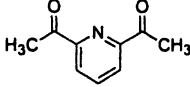
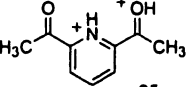
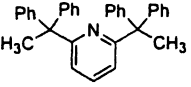
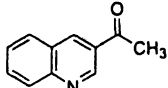
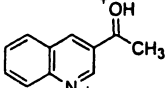
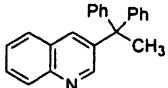
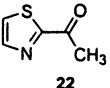
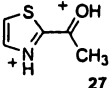
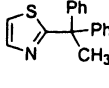
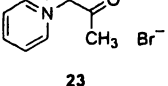
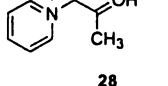
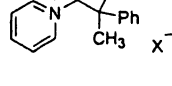


is protonated and this leads to the dicationic intermediate **17**. The dicationic intermediate (**17**) exhibits an enhanced electrophilic reactivity compared to the protonated cyclohexanone (**16**), and consequently there is a reaction with benzene.

Like the piperidones, a wide variety of *N*-heterocyclic aromatic compounds show an ability to activate electrophilic functional groups. It is known that acetophenone is completely protonated in $\text{CF}_3\text{SO}_3\text{H}$, however in the presence of benzene there is no hydroxyalkylation (condensation) reaction.¹² On the other

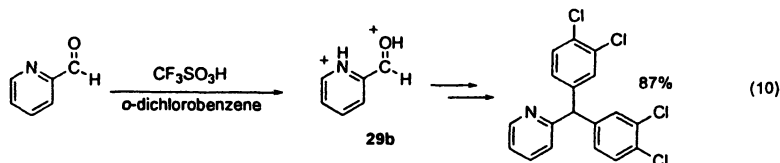
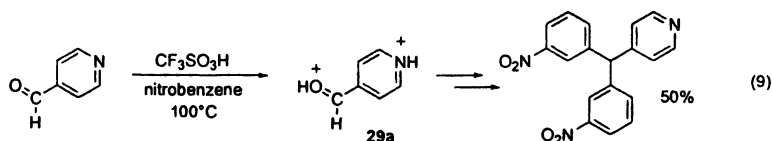
hand, acetyl-substituted *N*-heterocyclic aromatic compounds (**19-22**) and *N*-acetylpyridine (**23**) condense with benzene in good yields (Table 1).¹³ The dicationic intermediates (**24-28**) are proposed as intermediates in the reactions. In a similar respect, the pyridinecarboxaldehydes are shown to produce extremely

Table 1. Products, intermediates, and yields from the reactions of substituted heterocycles (19-23) with CF₃SO₃H and C₆H₆.

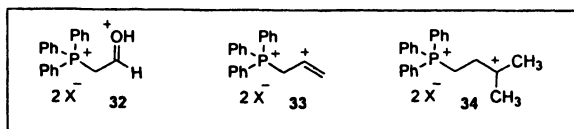
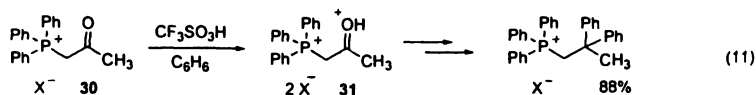
Acetyl-substituted Heterocycles	Proposed Dicationic Intermediates	Products	Yields
 19	 24		93%
 20	 25		90%
 21	 26		80%
 22	 27		75%
 23 Br ⁻	 28	 X ⁻	92%

reactive electrophilic species in superacidic solution.¹⁴ While benzaldehyde is unreactive to nitrobenzene or dichlorobenzene in superacid-promoted condensations, the isomeric pyridinecarboxaldehydes condense unreasonably good yields (eqs 9-10). Diprotonated intermediates (**29a-b**) are proposed for the conversions, both of which have been directly observed by low temperature NMR from FSO₃H-SbF₅-SO₂ClF solution. Dication **29a** has also been shown recently to react with saturated hydrocarbons.

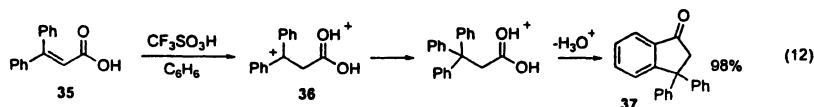
The phosphonium cationic center is well known for its ability to stabilize adjacent anionic centers (i.e. Wittig reagents), however we have shown it to be capable of activating (or destabilizing) cationic electrophilic sites.¹⁵ As noted



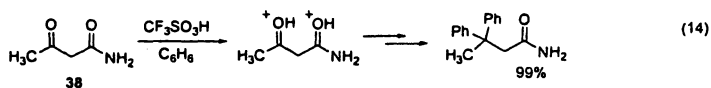
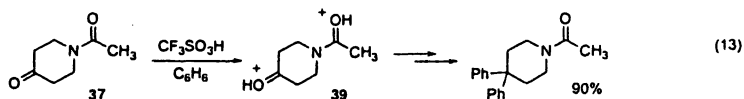
above, protonated aliphatic ketones generally are not reactive towards benzene. In contrast, the phosphonium derivative **30** readily forms the dicationic species (**31**) in superacid which condenses with benzene in high yield (eq 11). Dication **31** has been directly observed by low temperature ^{13}C NMR experiments, with the carboxonium ^{13}C signal found at 239 ppm. Other phosphonium-based dications were studied, including the phosphonium-carboxonium, phosphonium-vinyl, and the phosphonium-carbenium dications (**32-34**). Each of these dications is shown to react with benzene.



Protonated amides and carboxylic acids have also been shown to activate adjacent electrophilic centers. Although protonated carboxylic acids and amides are not typically considered stable cationic groups, in superacidic media they can be readily generated and many have been observed by spectroscopic studies.¹⁶ As an example of electrophilic activation by a protonated carboxylic acid, β -phenylcinnamic acid (**35**) is diprotonated in superacid to give the dication (**36**, observable by NMR) which then reacts with benzene and gives the indanone (**37**) in good yield (eq 12).¹⁷ It is known that the 1,1-diphenylethyl

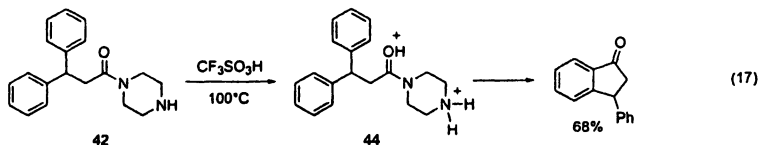
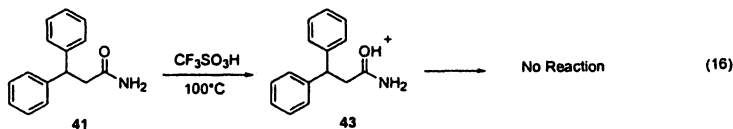
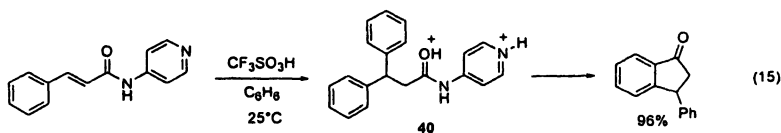


cation (11, eq 3) is unreactive towards benzene, so the carbocationic center in **36** is activated by the adjacent carboxonium group. Likewise, amides (**37** and **38**) condense with benzene in high yield (eqs 13-14).¹⁸ Since the analogous protonated (monocationic) ketones (**16** and protonated acetone) do not give condensation products from reactions with benzene, this is evidence that the



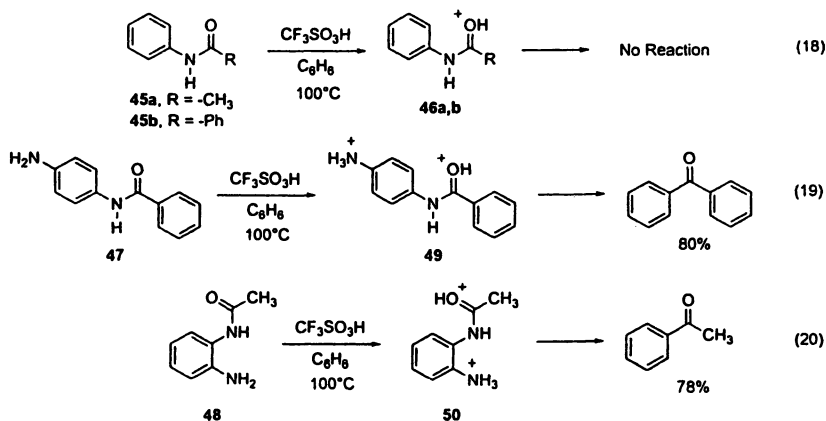
protonated amide groups enhance the electrophilic reactivities of the adjacent carboxonium ions. Dication **39** has also been directly observed by low temperature ¹³C NMR using Olah's stable ion technique (FSO₃H-SbF₅-SO₂ClF, -50°C).

Acyl-transfer reactions are some of the most important conversions in organic chemistry and biochemistry. Recent work has shown that adjacent cationic groups can also activate amides in acyl-transfer reactions. Friedel-Crafts acylations are known to proceed well with carboxylic acids, acid chlorides (and other halides), and acid anhydrides, but there are virtually no examples of acylations with simple amides.¹⁹ During studies related to unsaturated amides, we observed a cyclization reaction that is essentially an intramolecular acyl-transfer reaction involving an amide (eq 15). The indanone product is formed by a cyclization involving the dicationic species (**40**). To examine this further, the related amides **41** and **42** were studied in superacid promoted conversions (eqs 16-17). It was found that amide **42** leads to the indanone product while **41**

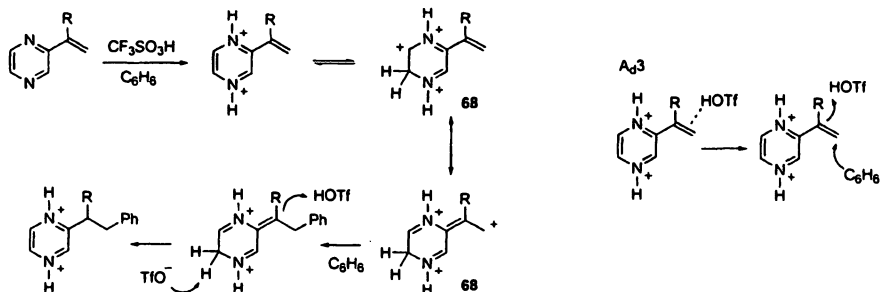


gives no indanone. These results are consistent with the formation of the dicationic species (44), which shows enhanced electrophilic reactivity of the protonated amide group when compared to the related monocation (43).

Besides the intramolecular acyl-transfer reactions, electrophilic activation is shown to occur with intermolecular Friedel-Craft-type reactions.¹⁸ When the simple amides (45a,b) are reacted in the presence of superacid, the monoprotonated species (46a,b) is unreactive towards benzene (eq 18). Although in the case of 45b a trace amount of benzophenone is detected as a product, more than 95% of the starting amides 45a,b are isolated upon workup. In contrast, amides 47 and 48 give the acyl-transfer products in good yields (eqs 19-20). It was proposed that dications 49-50 are formed in the superacidic solution. The results indicate that protonated amino-groups can activate the adjacent (protonated) amide-groups in acyl-transfer reactions.

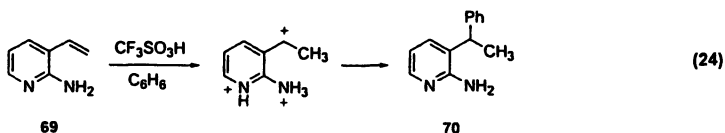


The above results clearly demonstrate that the reactivities of electrophilic centers can be enhanced by adjacent positive charge. We have also found several interesting examples suggesting that positive charge centers can influence the regiochemistry of nucleophilic attack. There are two reported examples of superelectrophilic species undergoing nucleophilic attack at the less-substituted positions of olefins (eqs 21-22).²⁰ In these reactions, diprotonated species 51 and 52 are likely involved, both of which have a considerable amount of positive charge located on the terminal carbon. Our studies have found a remarkable difference between vinylpyridine (53) and vinylpyrazine (54).²¹ The vinylpyridine gives the expected Markovnikov-type addition product (eq 23), while the vinylpyrazine gives an apparent anti-Markovnikov addition product (61, Table 2). Remarkably, the 2-propenyl and α -styryl substituted pyrazines (55-56) also give the anti-Markovnikov-type of



Scheme 2. Proposed mechanisms for the anti-Markovnikov addition reactions.

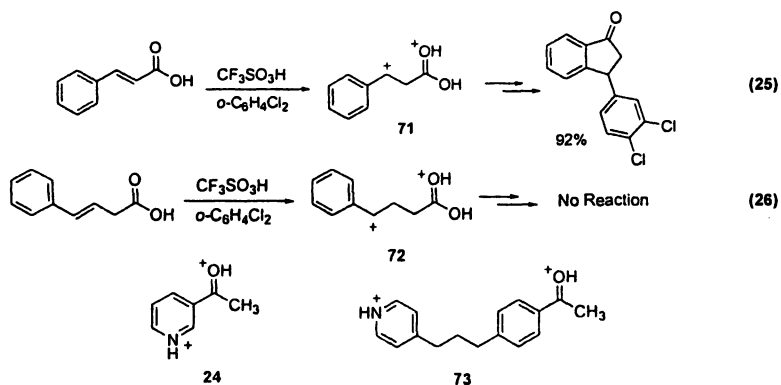
superelectrophiles **51** and **52**, intermediate **68** can lead to positive charge formation on the terminal carbon. Nucleophilic attack then occurs at the less substituted position. An alternative mechanism can also be proposed involving an A_d^3 mechanism. Interestingly when the aminopyridine (**69**) is reacted with CF_3SO_3H and C_6H_6 , the Markovnikov addition product (**70**) is formed (eq 24).²²



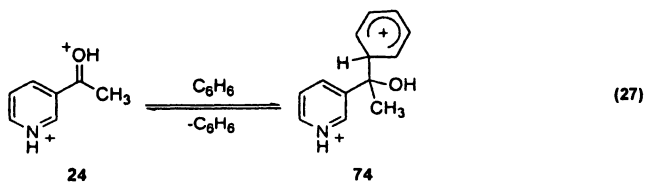
This may suggest that fully conjugated charge centers are an important aspect in directing nucleophilic attack to the terminal carbon. Thus, the superacid promoted reactions of the olefinic pyrazines (and related systems) may be viewed as the superelectrophilic version of Michael addition.

It has been known for many years that dicationic species exhibit increasing stability with increasing distance between the charge centers. In a similar respect, we have found that the distance between charge centers to be an important consideration in the activation of electrophiles. For example, the carboxonium-carbenium dications **71-72** have both been generated in superacid, but only **71** is sufficiently electrophilic to react with the deactivated arene, *o*-dichlorobenzene (eqs 25-26). Dication **71** reacts with the *o*-dichlorobenzene and cyclizes to the indanone product in good yield. With the increasing distance between charge centers however, dication **72** does not react with, *o*-dichlorobenzene. In a similar vein, diprotonated acetylpyridine **24** condenses with benzene (Table 1), but the charge-separated species **73** does not.¹³

A variety of examples are presented above showing electrophilic activation by adjacent cationic charge centers. This activation is thought to involve both

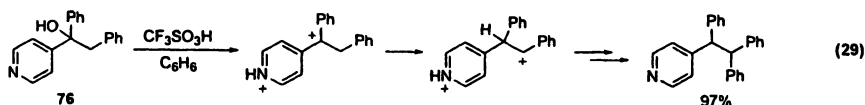
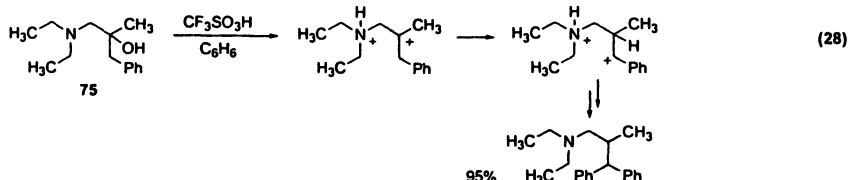


electrostatic and inductive effects and it is similar to superelectrophilic activation studied by the Olah group and others.³ In this regard, it has been noted that superelectrophiles possess a diminishing amount of neighboring group stabilization of the electron deficient site(s) on an ion. The same can be said about many of the activated, dicationic electrophiles. For example in the case of **24**, the pyridinium group is less capable of donating electron density to the carboxonium group, compared to the phenyl group of acetophenone. The smaller amount of neighboring group stabilization in **24** leads to a more reactive electrophilic carboxonium ion. Consistent with this concept, recent computational studies have shown that dicationic species like **24** possess LUMOs significantly below the HOMO of benzene.²³ In addition, the reactions of dicationic systems often lead to transition states and intermediates with increasing charge separation. In the reaction of **24**, the first intermediate σ -complex is produced as a charge-delocalized species (**74**) with widely separated positive charge centers (eq 27). The increasing charge separation may provide a

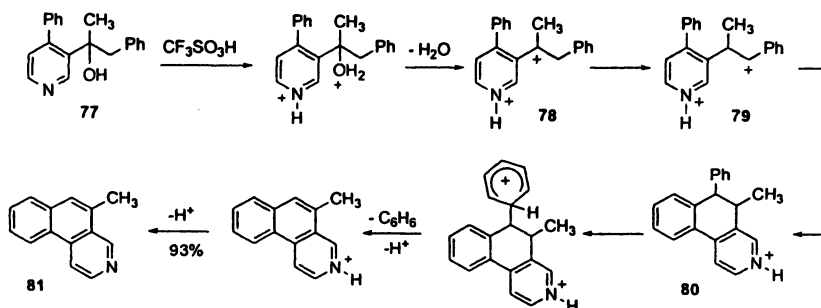


significant energetic driving force in the formation of the activated complex and σ -complex. In gas-phase studies of dicationic species, it has been shown that dicationic species can react with neutral molecules and that formation of the initial encounter complex can be quite exothermic.²⁴ Some of this stabilization involves movement of positive charge from the dication to the neutral molecule, and in a similar respect, this may be an important aspect in the chemistry of the dicationic electrophiles that we have studied.

The importance of charge-charge separation as a driving force in chemical conversions was demonstrated in the superacid-promoted reactions amino-alcohols and related systems.²⁵ For example, we found that the reactions of alcohols **75-76** lead to dicationic intermediates that undergo charge migration prior to reaction with benzene (eqs 28-29). In the case of **76**, charge migration



is clearly driven by an increasing distance between the charge centers. When charge migration is followed by a cyclization step, an efficient synthesis of aza-polycyclic aromatic compounds can be achieved (Scheme 3). A wide variety of aza-polycyclic aromatic compounds have been prepared using this chemistry. It is proposed that charge migration occurs (**78** \rightarrow **79**) and this is followed by a cyclization step. Cyclization of dication **79** leads to intermediate **80**. Under superacidic conditions, the phenyl group undergoes *ipso*-protonation and elimination of benzene gives the aza-polycyclic aromatic compound (**81**).



Scheme 3. Conversion and proposed mechanism for the superacid promoted conversion of compound **77** to 5-Methyl-benzo[*f*]isoquinoline (**81**).

Similar reactions of been described leading to benz[e]imidazoles, benz[g]indazoles, and benz[f]isoquinolines.

In summary, we have shown that stable cationic charge centers can significantly enhance the reactivities of adjacent electrophilic centers. Most of the studied systems involve reactive dicationic electrophiles. A number of the reactive dications have been directly observed by low temperature NMR. Along with their clear structural similarities to superelectrophiles, these dicationic systems are likewise capable of reacting with very weak nucleophiles. Utilization of these reactive intermediates has led to the development of several new synthetic methodologies, while studies of their reactivities have revealed interesting structure-activity relationships. Based on the results from our work and that of others, it seems likely that similar modes of activation will be discovered in biochemical systems (perhaps in biocatalytic roles) in the years to come.

References

1. (a) Brouwer, D. M.; Kiffen, A. A. Hydride Transfer Reactions II. Hydride Transfer from Alkanes to Methyloxocarbonium Ion. *Recl. Trav Chim. Pays-Bas* **1973**, *92*, 689-697. (b) Brouwer, D. M.; Kiffen, A. A. Hydride Transfer Reactions III. Rates of Hydride Transfer from Isobutane to Hydroxycarbonium Ions. *Recl. Trav Chim. Pays-Bas* **1973**, *92*, 809-813.
2. Olah, G. A.; Germain, A.; Lin, H. C.; Forsyth, D. Electrophilic reactions at Single Bonds. XVIII.¹ Indication of Protosolvated de facto Substituting Agents in the Reactions of Alkanes with Acetylium and Nitronium Ions in Superacidic Media. *J. Am. Chem. Soc.* **1975**, *97*, 2928-2929.
3. (a) Olah, G. A. Superelectrophiles. *Angew. Chem. Int. Ed. Engl.* **1993**, *32*, 767-922. (b) Olah, G. A.; Klumpp, D. A. Superelectrophilic Activation. *Accts. Chem. Res.* **2004**, *37*, 211-220.
4. Weiske, T.; Koch, W.; Schwarz, H. Experimental Evidence for the Existence of the Protonitronium Dication (HONO^{2+}) in the Gas Phase and ab Initio Molecular Orbital Calculations of Its Potential Energy Surface. *J. Am. Chem. Soc.* **1993**, *115*, 6312-6316.
5. (a) Berkessel, A.; Thauer, R. K. On the Mechanism of Catalysis by a Metal-Free Hydrogenase from Methogenic Archaea: Enzymatic Transformation of H_2 without a Metal and Its Analogy to the Chemistry of Alkanes in Superacid. *Angew. Chem. Int. Ed. Engl.* **1995**, *34*, 2247-2250. (b) Olah, G. A.; Prakash, G. K. S.; Mathew, T.; Marinez, E. R. Superacid-Catalyzed Selective Formylation-Rearrangement of Isoalkanes with Carbon Monoxide to Branched Ketones. *Angew. Chem., Int. Ed. Engl.* **2000**, *39*, 2547-2548. (c) Olah, G. A.; Török, B.; Joschek, J. P.; Bucsi, I.; Esteves, P. M.; Rasul,

- G.; Prakash, G. K. S. Efficient Chemoselective Carboxylation of Aromatics to Arylcarboxylic Acids with Superelectrophilically Activated Carbon Dioxide-Al₂Cl₆/Al System. *J. Am. Chem. Soc.* **2002**, *124*, 11379-11391. (d) Klumpp, D. A.; Rendy, R.; McElrea, A. Superacid Catalyzed Ring-opening Reactions Involving 2-Oxazolines and the Role of Superelectrophilic Intermediates. *Tetrahedron Lett.* **2004**, *45*, 7959-7961.
6. Conroy, J. L.; Sanders, T. C.; Seto, C. T. Using Electrostatic Field Effect to Design a New Class of Inhibitors for Cysteine Proteases. *J. Am. Chem. Soc.* **1997**, *119*, 4285-4291.
 7. Denmark, S. E.; Wu, Z. 6-Oxo-1,1,4,4-Tetramethyl-1,4-diazepinium Salts. A New Class of Catalysts for Efficient Epoxidation of Olefins with Oxone. *J. Org. Chem.* **1998**, *63*, 2810-2811.
 8. Corey, E. J.; Shibata, T.; Lee, T. W. Asymmetric Diels-Alder Reactions Catalyzed by a Triflic Acid Activated Chiral Oxazaborolidine. *J. Am. Chem. Soc.* **2002**, *124*, 3808-3809.
 9. Klumpp, D. A.; Aguirre, S. L.; Sanchez, Jr., G. V.; de Leon, S. J. Reactions of Amino Alcohols in Superacid: The Direct Observation of Dicationic Intermediates and Their Application in Synthesis. *Org. Lett.* **2001**, *3*, 2781-2784.
 10. (a) Hofmann, J. E.; Schriesheim, A. in *Friedel-Crafts and Related Reaction*; Olah, G. A., Ed.; Wiley: New York, NY, 1964; Vol. 2, pp 597-640. (b) March, J. *Advanced Organic Chemistry*, 4th Ed; Wiley: New York, NY, 1992; pp 548-549.
 11. Klumpp, D. A.; Garza, M.; Jones, A.; Mendoza, S. Synthesis of Aryl-Substituted Piperidines by Superacid Activation of Piperidones. *J. Org. Chem.* **1999**, *64*, 6702-6705.
 12. Ohwada, T.; Yamagata, N.; Shudo, K. Friedel-Crafts-Type Reactions Involving Di- and Tricationic Species. Onium-Allyl Dications and O,O-Diprotonated *aci*-Nito Species Bearing a Protonated Carbonyl Group. *J. Am. Chem. Soc.* **1991**, *113*, 1364-1373.
 13. Klumpp, D. A.; Garza, G.; Sanchez, G. V.; Lau, S.; DeLeon, S. Electrophilic Activation of Acetyl-Substituted Heteroaromatic Compounds. *J. Org. Chem.* **2000**, *65*, 8997-9000.
 14. (a) Klumpp, D. A.; Lau, S. 3-Pyridinecarboxaldehyde: A Model System for Superelectrophilic Activation and the Observation of a Diprotonated Electrophile. *J. Org. Chem.* **1999**, *64*, 7309-7311. (b) Klumpp, D. A.; Zhang, Y.; Kindelin, P. J.; Lau, S. *Tetrahedron*, **2006**, in press.
 15. Zhang, Y.; Aguirre, S. A.; Klumpp, D. A. Reactive, Dicationic Electrophiles: Electrophilic Activation Involving the Phosphonium Group. *Tetrahedron Lett.* **2002**, *43*, 6837-6840.
 16. Olah, G. A.; Laali, K. K.; Wang, Q.; Prakash, G. K. S. *Onium Ions*; Wiley: New York, NY, 1998

17. Rendy, R.; Zhang, Y.; McElrea, A.; Gomez, A.; Klumpp, D. A. Superacid-Catalyzed Reactions of Cinnamic Acids and the Role of Superelectrophiles. *J. Org. Chem.* **2004**, *69*, 2340-2347.
18. Klumpp, D. A.; Rendy, R.; Zhang, Y.; Gomez, A.; McElrea, A. Dicationic Intermediates Involving Protonated Amides: Dual Modes of Reactivity Including the Acylation of Arenes. *Org. Lett.* **2004**, *6*, 1789-1792.
19. (a) Gore, P. H. in *Friedel-Crafts and Related Reaction*; Olah, G. A., Ed.; Wiley: New York, NY, 1964; Vol. 3, pp 16-32. (b) Carey, F. A.; Sundberg, R.J. *Advanced Organic Chemistry, 4th Ed., Part B: Reactions and Synthesis*; Kluwer Academic/Plenum Publishers: New York, NY, 2001, pp 699-711.
20. Prakash, G. K. S.; Yan, P.; Török, B.; Olah, G. A. Superacidic Trifluoromethane Acid-Induced Cycli-Acylation of Aromatics. *Catal. Lett.* **2003**, *87*, 109-112.
21. Zhang, Y.; Briski, J.; Zhang, Y.; Rendy, R.; Klumpp, D. A. Superacid-Catalyzed Reactions of Olefinic Pyrazines: an Example of Anti-Markovnikov Addition Involving Superelectrophiles. *Org. Lett.* **2005**, *7*, 2505-2508.
22. Zhang, Y. Ph.D. Dissertation, Northern Illinois University, DeKalb, IL, 2006.
23. Koltunov, K. Y.; Prakash, G. K. S.; Rasul, G.; Olah, G. A. Reactions of 5-, 6-, 7-, 8-Hydroxyquinoline and 5-Hydroxyisoquinoline with Benzene and cyclohexane in Superacids. *J. Org. Chem.* **2002**, *67*, 4330-4336.
24. Roithova, J.; Schröder, D. Bond-Forming Reactions of Molecular Dications as a New Route to Polyaromatic Hydrocarbons. *J. Am. Chem. Soc.* **2006**, *128*, 4208-4209.
25. Li, A.; Kindelin, P. J.; Klumpp, D. A. Charge Migration in Dicationic Electrophiles and Its Application to the Synthesis of Aza-polycyclic Aromatic Compounds. *Org. Lett.* **2006**, *8*, 1233-1236.

Chapter 9

Stabilized Carbocations as Redox Active Chromophores: Preparation of Electrochromic Materials Using Stabilized Carbocations

Shunji Ito¹, Koji Akimoto¹, and Noboru Morita²

¹Department of Frontier Materials Chemistry, Hirosaki University,
Hirosaki 036–8561, Japan

²Department of Chemistry, Tohoku University, Sendai 980–8578, Japan

A new structural principle for the preparation of polyelectrochromic materials with high thermodynamic stability is proposed. The system consists of either one or two polymethine dyes as end group(s). Because of their high thermodynamic stability, di(1-azulenyl)methyl cation salts were employed as redox active polymethine dye for the construction of such systems. The scope of novel polyelectrochromic materials preparation, taking full advantage of di(1-azulenyl)methyl cation unit as building block, and the new structural principles to enable the design of polyelectrochromic systems is demonstrated by several examples.

Electrochromism is observed in reversible redox systems, which exhibit significant color changes in different oxidation states. Violenes, whose general structure is represented in Figure 1, are typical examples that exhibit electrochromism (1).

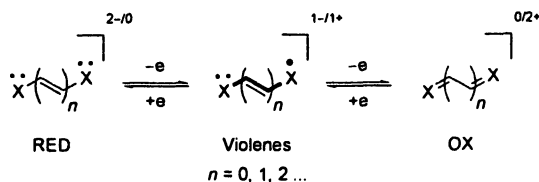


Figure 1. General structure of violene.

Violene is constructed by a conjugated chain with two redox active chromophores. It is classified as two types (see Figure 2). As noted from the position of the end groups, one type is separated by an aromatic core and the other is located inside a cyclic π -system. In both cases, the colored species in this system are the radical ionic states. Thus, in general, the violene system does not show high redox stability (2).

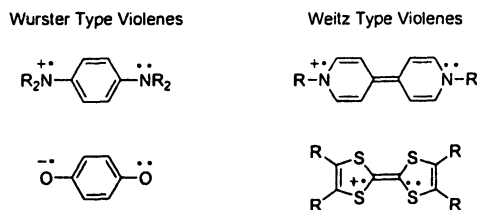


Figure 2. Two types of violene structures.

Violene–Cyanine Hybrid

Stabilization of the redox cycle is relatively important in construction of potentially useful electrochromic materials, because the molecules needed for application require high redox-stability. Recently, S. Hünig et al. proposed the concept of violene–cyanine hybrid to produce stabilized organic electrochromic materials (3). The hybrid is constructed by a violene-type redox system containing delocalized closed-shell polymethine dyes as end groups. The hybrid is expected to exhibit the color of a cyanine dye, by an overall two-electron

transfer as illustrated with the general structure in Figure 3. Contrary to the violene-type redox system, both the colored and the discolored species consist of closed shell systems. Therefore, the hybrid improves the persistency of the redox cycle. However, the hybrid does not exhibit multiple color changes which is important for the construction of polyelectrochromic materials.

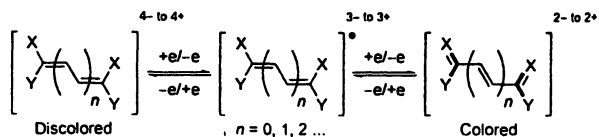


Figure 3. General structure of Hünig's violene-cyanine hybrid. One or two of the moieties $X=C-Y$ represent cyanines, oxonols, or merocyanines.

Wurster Type Violene-Cyanine Hybrid

Because of the polyolefinic structure in the violene unit core, the general structure proposed by S. Hünig et al. should be constructed on the basis of Weitz type violene. If we design the hybrid from the Wurster type violene, the color will be changed between the quinoid color and the cyanine color (Figure 4). For the construction of the new hybrid system, illustrated in Figure 4, it should be very important to select highly colored cyanine end groups with high redox stability.

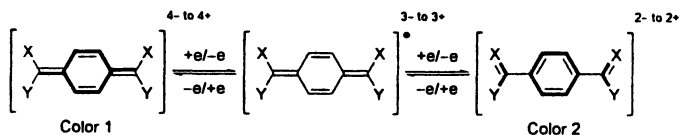


Figure 4. Wurster type violene-cyanine hybrid.

Azulene-Substituted Methyl Cations

Azulene ($C_{10}H_8$) has attracted the interest of many research groups over the years due to its unusual properties as well as its attractive blue color. The azulene system has the tendency to stabilize cations, as well as anions, owing to its remarkable polarizability (4). Indeed, the pK_R^+ value for the cyclopro-

penylium ion 1^+ substituted by three guaiazulene moieties is reported to be over 10.0 (Figure 5) (5).

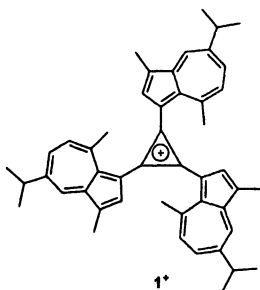


Figure 5. The cyclopropenylium ion 1^+ substituted by three guaiazulene moieties.

We have reported the synthesis of a series of azulene-substituted methyl cations, i.e., tri(1-azulenyl)methyl, di(1-azulenyl)phenylmethyl, and (1-azulenyl)diphenylmethyl cations ($2a^+$, $3a^+$, and $4a^+$) (Figure 6) (6). In order to examine substituent effects on the azulene rings and to enhance their stabilities, a series of the cations ($2b-d^+$, $3b-d^+$, and $4b-d^+$) bearing *tert*-butyl groups on each azulene ring were also synthesized (7).

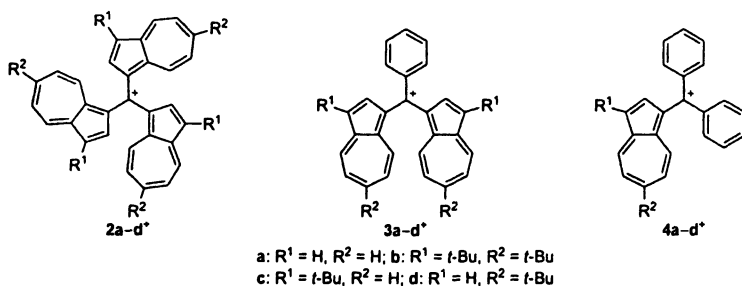


Figure 6. Azulene-substituted methyl cations.

Preparation of Azulene-Substituted Methyl Cations

Azulene-substituted methyl cations were prepared as illustrated in Figure 7. The hydro derivatives ($7a-d$) became good precursors for the methyl cations. These derivatives were readily obtained by the reaction of azulenes $6a-d$ with 1-formyl compounds $5a-d$ under acidic conditions. The synthesis of the tri(1-

azulenyl)methyl cations ($2a-d^+$) was accomplished by hydride abstraction with DDQ, followed by addition of aqueous HPF_6 to exchange the counter anion. This afforded the corresponding carbocations as hexafluorophosphate salts as deep colored powders in good yield.

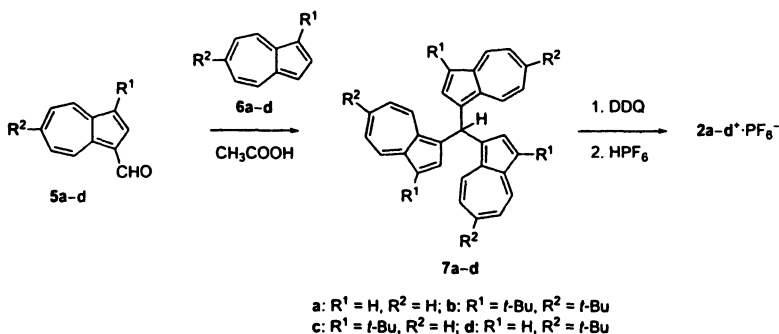


Figure 7. Preparation of the azulene-substituted methyl cation salts $2a-d^+ PF_6^-$

Thermodynamic Stability

As a measure of their thermodynamic stability, the pK_R^+ values for the carbocation salts were determined spectrophotometrically in a buffer solution prepared in aqueous solution of acetonitrile. The K_R^+ scale is defined by the equilibrium constant for the reaction of a carbocation with water molecule ($K_R^+ = [ROH][H_3O^+]/[R^+]$). Therefore, the larger pK_R^+ index indicates higher stability for the carbocation. However, the neutralization of these cations was not completely reversible. This is attributable to instability of the neutralized products. The instability of the neutralized products should arise from production of unstable polyolefinic substructure by attack of the base at the aromatic core.

The pK_R^+ value for the parent tri(1-azulenyl)methyl cation ($2a^+$) is 11.3. Hydrocarbon-based carbocations, which comprise only of carbon and hydrogen, are generally very reactive species. Some extremely stable hydrocarbon carbocations, which exist even under basic conditions, were reported in the literature (8). However, most of these examples are cyclic cations, such as cyclopropenylum or tropylium ions (Figure 8). The tropylium ion 8^+ annelated to three bicyclo[2.2.2]octane units is one of the most stable hydrocarbon-based carbocation ever reported (9).

Stabilization by the introduction of bulky *tert*-butyl groups into the azulene rings should be attributable to not only their steric and inductive electronic effects but also C–C hyperconjugative effects induced by the σ -bond of the *tert*-butyl groups. The pK_R^+ value of 14.3 for methyl cation **2b**⁺ with six *tert*-butyl groups is the highest value ever reported for a methyl cation substituted with only hydrocarbon groups.

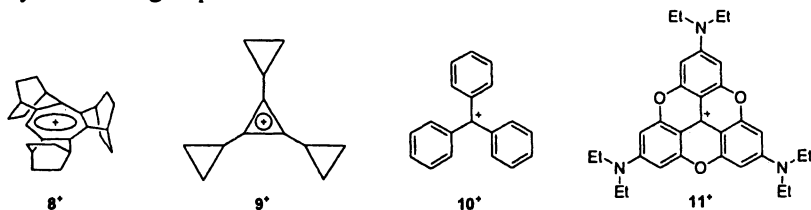


Figure 8. Some stabilized carbocations.

Triphenylmethyl cation (**10**⁺) is effectively stabilized by electron donating substituents. B. W. Laursen et al. reported the highly stable carbocation **11**⁺ with a pK_R^+ value of 19.7 (10). Recently, they reported a similar carbocation with a much higher pK_R^+ value (23.7) (11). In our continuing efforts to prepare extremely stable carbocations, we have investigated the effect of introduction of electron donating substituents into each azulenyl group.

Stabilization of Azulenylmethyl Cations by Electron Donating Substituents

The methoxy substituents on each azulenyl ring stabilized the carbocation effectively (12). The reaction of 6-methoxyazulene (**13**) with 6-methoxyazulene-1-carbaldehyde (**12**) in acetic acid did not afford the condensation product **14** under the reaction conditions. However, a high-pressure reaction (10 kbar) afforded the desired hydro derivative **14** in 6% yield. Synthesis of the cation **15**⁺ was accomplished by hydride abstraction from the hydro derivative **14** (Figure 9).

As expected, the cation **15**⁺ exhibited high stability. In fact, its exact pK_R^+ value could not be determined by the earlier method due to its high stability. The pK_R^+ value for **15**⁺PF₆ was well beyond 14.0. Consequently, the combination of 1-azulenyl groups with methoxy substituents stabilized the methyl cation effectively.

Preparation of the dimethylamino derivative **20**⁺ is shown in Figure 10 (13). The bromine substituents in cation **19**⁺ were readily replaced by secondary

amines to give the desired cation 20^+ . High-pressure reaction (10 kbar) was also required for the preparation of the precursor **18**. After the generation of cation 19^+ with DDQ, treatment with dimethylamine afforded the desired tris-(dimethylamino)-substituted methyl cation 20^+ in 18% yield.

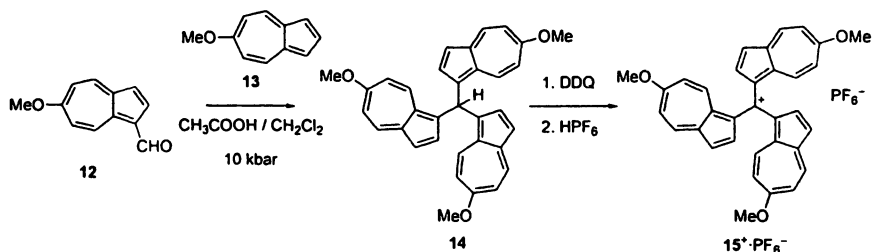


Figure 9. Preparation of trimethoxy-substituted azulenylmethyl cation salt $15^+ \cdot PF_6^-$.

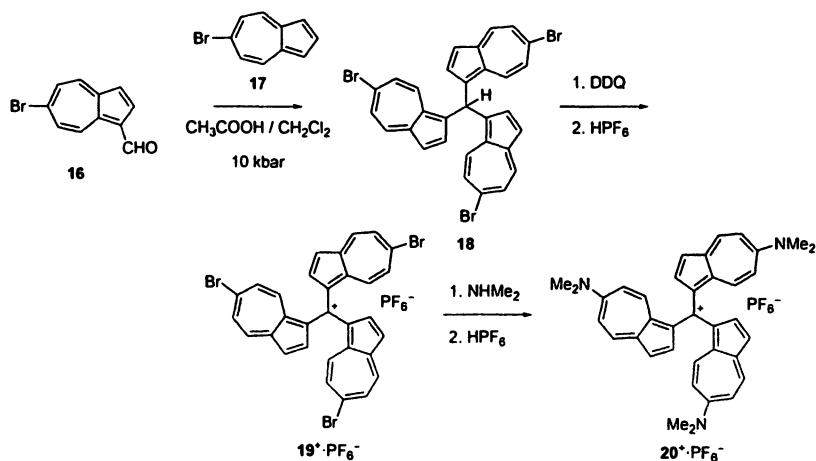


Figure 10. Preparation of dimethylamino-substituted azulenylmethyl cation salt $20^+ \cdot PF_6^-$.

The exact pK_R^+ value for 20^+ could also not be determined by the earlier method. Therefore, dimethyl sulfoxide (DMSO)-water-tetramethylammonium hydroxide (0.011 M) system was used for the measurement. The H_- scale (Hammett acidity scale) for the system ranges from 12 in water up to 26.2 in

99.6 mol% DMSO/water (14). The value for the cation salt 20^+ was determined to be 24.3. This value is extremely high for a methyl cation. The unusually high stability of the methyl cation is attributable to the dipolar structure of the azulene rings in addition to contribution by three dimethylamino groups.

Absorption Spectra and Redox Behavior

Figure 11 shows the UV-vis spectrum of parent $2a^+$ in acetonitrile along with those of 6-methoxy- and 6-dimethylamino analogues (15^+ and 20^+). These cations showed strong absorptions in the visible region. The absorption maxima are little influenced by the electron-donating substituents, but the coefficient tends to increase by the substitution.

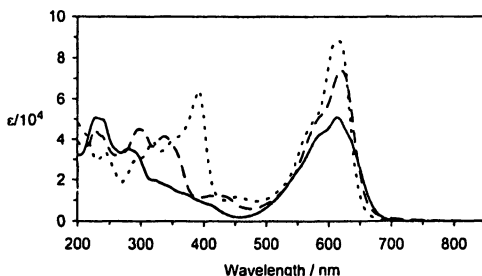


Figure 11. UV-vis spectrum for the parent cation $2a^+$ (solid line) in acetonitrile along with those of 6-methoxy- and 6-dimethylamino derivatives (15^+ ; broken line and 20^+ ; dotted line) (Adapted from reference 13. Copyright 1999.)

Table I summarizes the pK_R^+ values and redox potentials for the tri(1-azulenyl)methyl cations. The oxidation exhibited a barely separate two-step, two-electron oxidation wave. This wave is ascribed to the oxidation of two azulene rings to generate a tricationic species. The reduction showed a one-electron wave, which is ascribed to the formation of a neutral radical.

In spite of their high pK_R^+ values, the methyl cations have less negative reduction potentials as compared to those of the cyclic cations; e.g., -1.12 V for the tropylium ion 8^+ and -2.20 V for cyclopropenium ion 9^+ (8). Presence of *tert*-butyl groups in cations $2b-d^+$ increased the reversibility of both reduction and oxidation waves. The most negative reduction potential in the dimethylamino derivative 20^+ reflects its high electrochemical stability.

Table I. pK_R^+ Values and Redox Potentials for the Azulenylmethyl Cations

<i>sample</i>	pK_R^+ value	E_1^{red}	E_1^{ox}	E_2^{ox}
2a⁺	11.3	-0.78	+0.98	+1.07
2b⁺	14.3	-0.91	+0.84	+0.95
2c⁺	13.3	-0.83	+0.82	+0.99
2d⁺	13.7	-0.85	+0.92	+1.03
15⁺	>14.0	-0.88	+0.90	+0.98
20⁺	24.3	-1.26	+0.50	+0.64

Wurster-Type Violenne–Cyanine Hybrid

The methyl cations stabilized by the 1-azulenyl substituents showed high thermodynamic stabilities. A strong absorption exists in the visible region owing to the contribution of their cyanine substructure. The original definition of the cyanine is a polymethine dye constructed from iminium ion and amine units. Thus, the methine units in the cyanine system should be odd numbers. This is in contrast to the violene system, which is composed of an even number of methine units. We would call the charged conjugated π -electron system composed by an odd number of methine units also cyanine. The azulenylmethyl cations also exhibited facile redox activities, despite their high thermodynamic stability. Thus, di(1-azulenyl)methylm units should be good candidates for the construction of new hybrid systems as polymethine end groups.

Dication Composed of *p*-Phenylene Spacer

The dication **21²⁺** composed of two methylm units connected to a *p*-phenylene spacer would be a candidate for new Wurster type violene–cyanine hybrid (Figure 12) (**15**). The reaction of four molar amounts of azulene **6b** with terephthalaldehyde yielded the hydro precursor. Synthesis of the dication **21²⁺** was accomplished by hydride abstraction with DDQ in almost quantitative yield. The dication **21²⁺** was expected to show destabilization, but instead it exhibited high thermodynamic stability just like the corresponding monocation **3b⁺**.

The dication **21²⁺** exhibited a reduction wave upon CV at a less negative potential than that of **3b⁺**. This wave corresponds to a one-step, two-electron reduction of **21²⁺**. In the electronic spectra, dication **21²⁺** also showed strong absorption in the visible region. The extinction coefficients for the dication was almost twice as large as those of monocations. The deep-blue color of the

solution of 21^{2+} changed to brown during electrochemical reduction. Absence of the isosbestic point during the electrochemical reduction is indicative of instability of the fully reduced species **21**. Chemical reduction of 21^{2+} with Zn powder also did not afford satisfactory results.

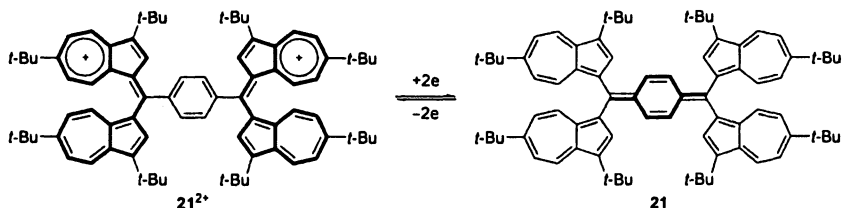


Figure 12. Wurster type violene–cyanine hybrid composed of two methylium units connected via a *p*-phenylene spacer.

The combination of the di(1-azulenyl)methylium units produced dicationic species with high stabilities. However, transformation of the dication 21^{2+} to the quinoid compound **21** as a Wurster type violene–cyanine hybrid was not achieved due to the instability of the reduced species.

Dication Composed of Thiophenediyl and Thienothiophenediyl Spacer

Thiophene and thienothiophene units have been frequently used in thienoquinoid or condensed forms in the design of new molecular architecture (16). Incorporation of the thiophene or thienothiophene unit as a π -bridge linker could stabilize the quinoidal structure in the reduced forms (Figures 13 and 14). These two-types of new dications (22^{2+} and 23^{2+}) stabilize the presumed two-electron reduction state by contribution of the thienoquinoid substructures (**22** and **23**) instead of the quinoidal form in the dication 21^{2+} (17).

Dications 22^{2+} and 23^{2+} were synthesized by hydride abstraction reaction of the corresponding hydro derivatives as stable dark-brown powder. The pK_R^+ values for these dications are also extremely high for doubly-charged systems (22^{2+} ; 11.7 and 23^{2+} ; 11.7). The electrochemical reduction of 22^{2+} and 23^{2+} exhibited a reduction wave at less negative potentials than that of dication 21^{2+} . This wave corresponds to the reduction of two cation units by a one-step, two-electron reduction to form thienoquinoid products. Chemical reduction of 22^{2+} and 23^{2+} afforded the closed-shell thienoquinoid compounds (**22** and **23**), which exhibited high electron-donating ability. The formation of the closed-shell molecules is in contrast with the result from reduction of dication 21^{2+} connected via a *p*-phenylenediyl spacer.

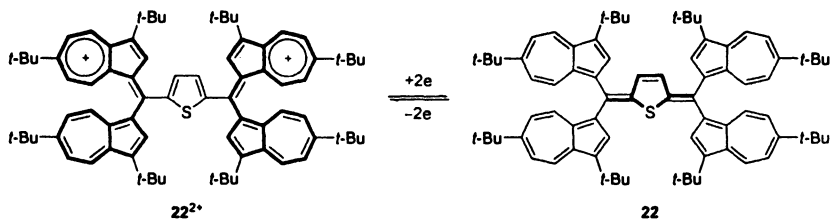


Figure 13. Wurster type violene–cyanine hybrid composed of two methylium units connected via a thiophenediyl spacer.

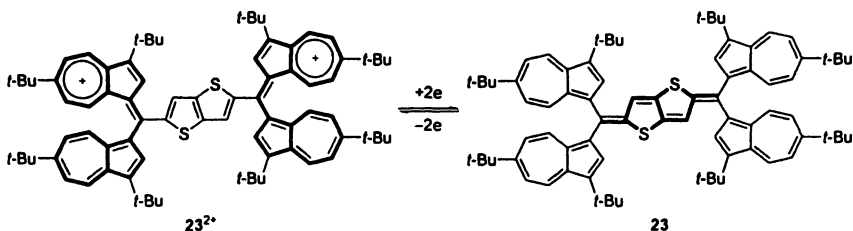


Figure 14. Wurster type violene–cyanine hybrid composed of two methylium units connected via a thienothiophenediyl spacer.

When the UV–vis spectra of dications 22^{2+} and 23^{2+} were measured under the reduction conditions, strong absorptions in the visible region gradually decreased as shown in Figure 15. This change is accompanied by an increase in the new band of the thienoquinoid products (**22** and **23**). The color of the solution changed from deep-green to violet and blue, respectively, during the electrochemical reduction. The development of new absorptions in the visible region is in contrast to the result obtained with dication 21^{2+} .

We have established the conversion between the two colored species by electrochemical reaction utilizing the concept of a Wurster type violene–cyanine hybrid. Dications 22^{2+} and 23^{2+} showed significant changes in their absorption spectra in different oxidation states. Therefore, dications 22^{2+} and 23^{2+} could function as new violene–cyanine hybrids, in which the four end groups (X and Y) in the general structure are azulenes (Figure 4).

Cyanine–Cyanine Hybrid

Two color changes could be induced by the violene–cyanine hybrid designed from the Wurster type violene. However, the multiple color changes

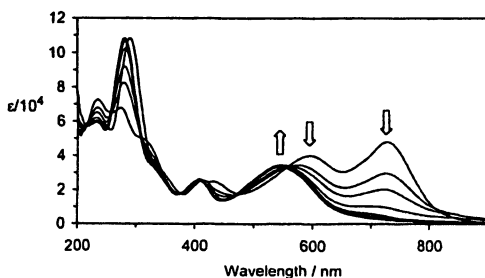


Figure 15. Continuous change in visible spectrum of the dication 22^{2+} under electrochemical reduction conditions (Adapted from reference 17. Copyright 2001.)

would be difficult to derive from the violene–cyanine hybrid system. To achieve multiple color changes, we designed a redox system from cyanine-based polymethine dye (18). The cyanine dye, itself does not possess good electrochemical properties. However, if either one or two end groups could be replaced by another cyanine unit, the hybrid should exhibit redox activities with multiple color changes.

Cyanine–Cyanine Hybrid with a Cyanine Unit at One Terminus

The general structure with a cyanine unit at one terminus is represented in Figure 16. Two-electron transfer of the hybrid system produces another cyanine substructure via neutral radical state. In this case, a two-step redox reaction is expected, because the neutral radical state is stabilized by the *capto-dative* substituents effect (19). Therefore, three colored states will be achieved by the hybrid system. We call this system a cyanine–cyanine hybrid.

Di(1-azulenyl)(6-azulenyl)methyl cation (24^+) represented in Figure 17 exemplifies the cyanine–cyanine hybrid (20). Di(1-azulenyl)methyl cation unit in 24^+ acts as a cyanine terminal group. The tropylium substructure stabilizes the cationic state (24^+). Reduction of 24^+ should afford the neutral radical 24^\bullet , which is stabilized by *capto-dative* substitution effect, because 24^\bullet is substituted with azulenes in the donor and acceptor positions. The anionic state (24^-) is also stabilized by contribution of the cyclopentadienide substructure, which should exhibit the third color change in this system.

The tri(azulenyl)methane derivative 24^+ including a 6-azulenyl group was prepared by the reaction of azulene **6b** with diethyl 6-formylazulene-1,3-dicarboxylate. Synthesis of 24^+ was accomplished by hydride abstraction with DDQ. Cation 24^+ was isolated as a hexafluorophosphate salt by treatment with aqueous HPF_6 . The new salt is a stable, deep-green colored crystals, that can be

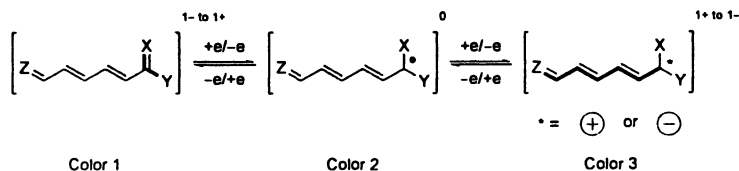


Figure 16. General structure of the cyanine–cyanine hybrid with a cyanine unit at the one terminus.

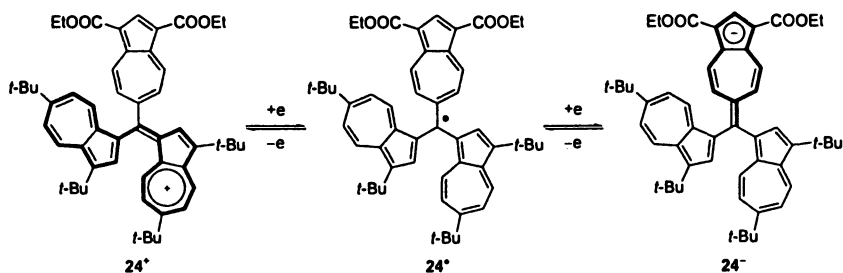


Figure 17. Di(1-azulenyl)(6-azulenyl)methyl cation (24^+) as the first example of the cyanine–cyanine hybrid exhibiting three-primary color changes.

stored in the crystalline state, despite the fact that 24^+ is substituted at the electron-withdrawing position of azulene ring. Cation 24^+ exhibited some destabilization as compared to parent tri(1-azulenyl)methyl cation ($2a^+$). However, cation 24^+ still exhibits a large pK_R^+ value (10.1).

Electrochromic Behavior of Cation 24^+

Cation 24^+ showed strong absorption in visible region, as did the parent tri(1-azulenyl)methyl cation ($2a^+$). The longest wavelength absorption showed an appreciable bathochromic shift as compared to that of $2a^+$. As expected, the CV exhibited two reversible reduction waves (-0.56 V and -0.73 V), which correspond to two single-electron transfers. The less negative second reduction potential, as compared to parent tri(1-azulenyl)methyl cation ($2a^+$), corresponds to an increase in electron affinity of the cation due to the 6-azulenyl substituent.

When UV–vis spectra of the cation 24^+ were measured under the electrochemical reduction conditions, a new absorption in the visible region gradually developed as shown in Figure 18. The color of the solution changed from deep-green to deep-blue during electrochemical reduction. On further

reduction, the new blue band in the visible region gradually decreased accompanied by change of color to deep-red. The reverse oxidation of the red-colored solution regenerated the deep-green colored cation 24^+ .

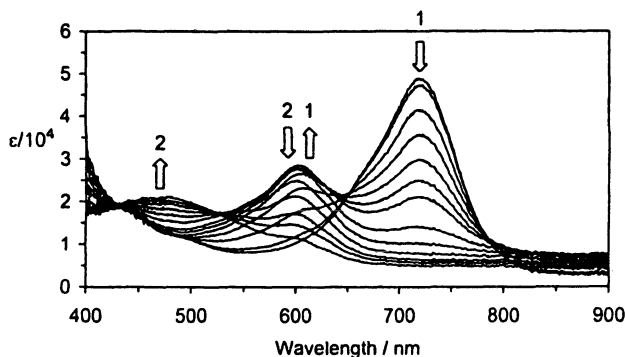


Figure 18. Continuous change in the visible spectrum of 24^+ under electrochemical reduction conditions (Adapted from reference 20. Copyright 2003.)

Di(1-azulenyl)(6-azulenyl)methyl cation (24^+) prepared as a candidate for a cyanine–cyanine hybrid system with a cyanine unit at one terminus exhibited high stability with large pK_R^+ values, although the cation was connected through the electron-withdrawing position of the azulene ring. It was found to possess a two-stage reduction property with a small numerical sum of the first and the second reduction potentials. It is noteworthy that depending on the charge state this compound exhibits three primary colors, deep-green for monocation 24^+ , deep-blue for neutral radical 24^\bullet , and red for anion 24^- .

Tetracation Salts as Novel Cyanine–Cyanine Hybrid System

We utilize the redox system from the cyanine-based hybrid for a two-electron transfer process. The core cyanine unit is constructed by an odd number of polymethine chains. Therefore, when both end groups in the cyanine dye are replaced by the cyanine substructures, a defect in the conjugation will be induced in the core cyanine unit (Figure 19). This system should also represent redox properties with color changes. However, such defect should decrease the redox stability. We proposed that by connecting two such units to a viologen chain, we could improve the redox stability. Therefore, the general structure for the next hybrid system takes shape as illustrated in Figure 20. For this reason, the system in Figure 20 should be called a viologen–cyanine–cyanine hybrid as illustrated in Figure 21. However, we also call this system, a cyanine–cyanine hybrid, since the colored cyanine substructure is converted into another cyanine

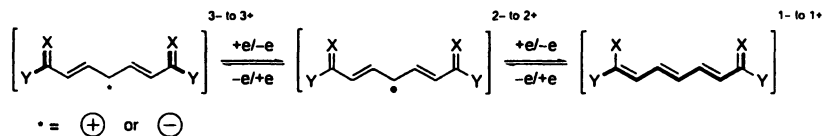


Figure 19. General structure for the cyanine–cyanine hybrid with a cyanine unit at the both termini.

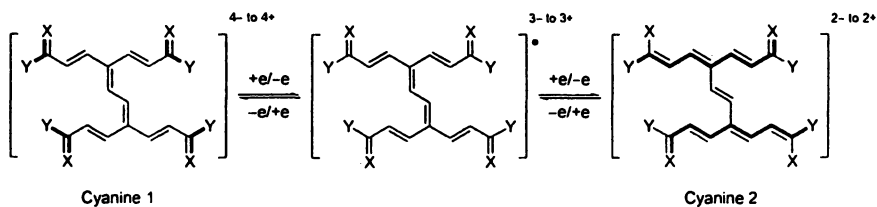


Figure 20. Improved structure for the cyanine–cyanine hybrid with a cyanine unit at both termini

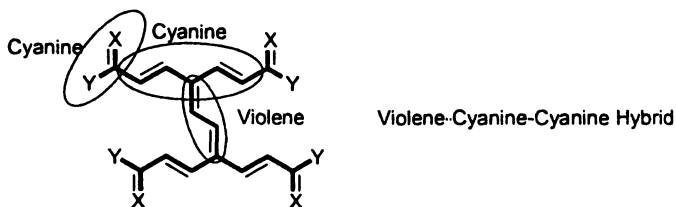


Figure 21. Schematic representation of the cyanine–cyanine hybrid with a cyanine unit at both termini

substructure by an overall two electron transfer process. Both colored species should be closed shell systems, from which higher stability is also to be expected.

The First Tetracation Utilized in a Cyanine–Cyanine Hybrid

For the central violene π -system, we chose benzene with acetylene spacers for decreasing steric hindrance between the large cationic centers. Therefore, the tetracation 25^{4+} salt was designed as a first example for a hybrid with a cyanine unit at the both termini (21). As illustrated in Figure 22, tetracation 25^{4+} exemplifies a new hybrid system, which produces another cyanine substructure 25^{2+} by two-electron transfer. In this case, overall, four electron transfer should afford a fully neutralized species such as a neutral diradical.

Preparation of the precursor of the tetracation salt was accomplished by a simple one-pot reaction involving repeated Pd-catalyzed alkynylation of the ethynyl-substituted di(1-azulenyl)phenylmethane derivative with tetraiodobenzene under Sonogashira–Hagihara conditions. The reaction with four molar amounts of DDQ, followed by treatment with aqueous HPF_6 yielded the tetracation 25^{4+} as a tetrakis(hexafluorophosphate) salt. In order to examine the effect of hybrid structure on 25^{4+} , a series of di- and monocations (26^{2+} and 27^+) were also synthesized utilizing a similar procedure. Dication 26^{2+} is a typical example for a violene–cyanine hybrid in which two polymethine substructures are connected to the violene like core (Figure 23). Monocation 27^+ could be considered as the parent compound for the multi-charged tetracation (Figure 24).

Carbocations having more than four cationic centers are rare species, and very few have been isolated as isolable salts. A tetrahedrally-arrayed tetracation, which was stable only at low temperature was generated by G. A. Olah et al. in 1995 (22). Recently, R. Rathore et al. prepared isolable tetra- and hexatriyl cations utilizing tetraphenylmethane and hexaphenylbenzene as platforms (23). Tetracation 25^{4+} is one of the new multi-charged methylium compounds with considerable high stability.

In the case of tetracation 25^{4+} four cationic units were neutralized at pH 8.7. This value corresponds to an average between the $\text{p}K_{\text{R}}^{4+}$ value of the tetracation and $\text{p}K_{\text{R}}^+$ value of the partially neutralized monocation. The $\text{p}K_{\text{R}}^+$ value of dication 26^{2+} was determined to be 10.8. The $\text{p}K_{\text{R}}^+$ value of monocation 27^+ (12.3) is almost equal to that of di(1-azulenyl)phenylmethyl cation ($3b^+$). Thus, tetracation 25^{4+} is even more destabilized than the mono- and dications (27^+ and 26^{2+}). This indicates the existence of some interaction among the cationic centers.

The electrochemical reduction of monocation 27^+ exhibited a reversible wave at -0.70 V upon CV due to the formation of a neutral radical. Although the $\text{p}K_{\text{R}}^+$ values decrease by increasing the cationic units, the reduction potentials for the tetra- and dications (25^{4+} and 26^{2+}) are almost equal to that of 27^+ . The CV waves of 25^{4+} and 26^{2+} exhibit more current, as compared with that of 27^+ at the same concentration. Therefore, the first reduction wave of 25^{4+} and 26^{2+} is

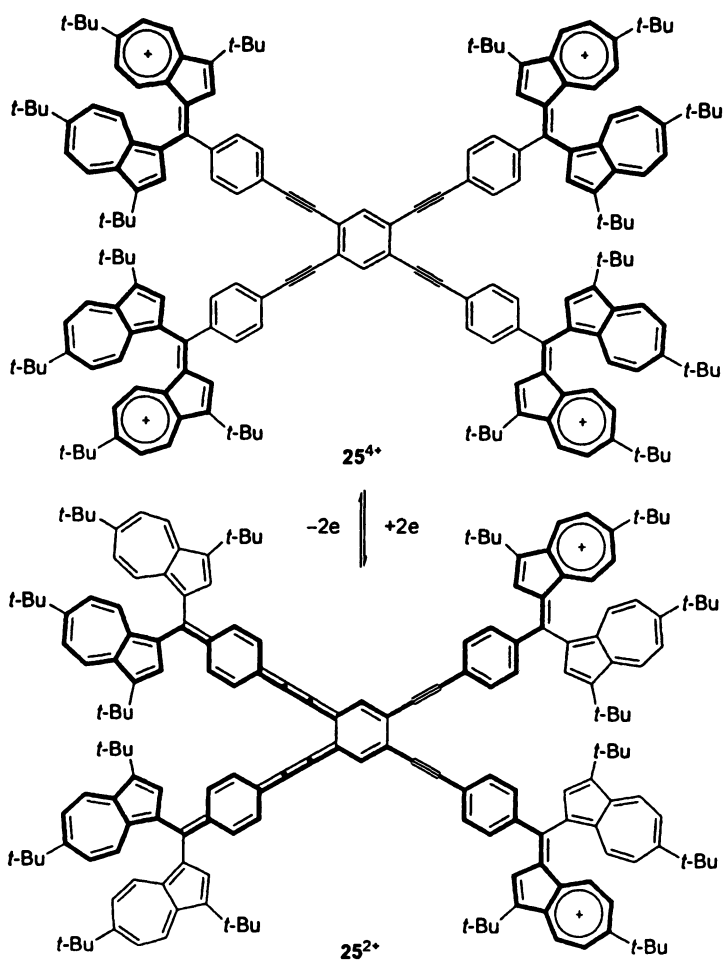


Figure 22. The tetracation 25^{4+} designed as the first example of a cyanine-cyanine hybrid with cyanine units at the both termini.

attributed to four- and two-electron transfer in one step to generate a neutral species.

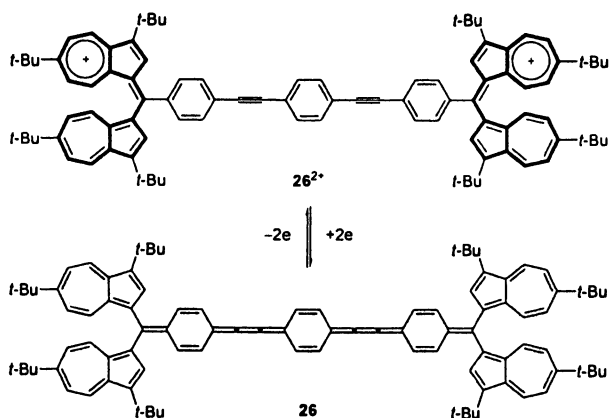


Figure 23. The dication 26^{2+} designed as a typical example for the violene–cyanine hybrid.

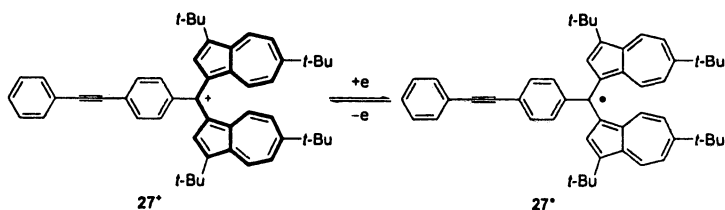


Figure 24. The monocation 27^+ designed as parent compound for the multi-charged tetracation.

As expected by their polymethine substructures, these polycations showed characteristic charge-transfer absorption in visible region. The extinction coefficients for dication 26^{2+} and tetracation 25^{4+} are approximately twice and four times, as large as that of monocation 27^+ respectively. Figure 25 shows the spectroelectrograms of 25^{4+} under the electrochemical reduction conditions. The strong absorption in the visible region for 25^{4+} gradually decreased under electrochemical reduction conditions as shown in Figure 25. The color of the solution changed from dark-green to yellow during the electrochemical reduction. Absence of an isosbestic point suggests the instability of the fully

reduced species. Reverse oxidation of the pale-colored solution did not regenerate the spectrum of 25^{4+} completely (ca. 30%), although good reversibility was observed upon CV. The spectral changes for the mono- and dication (27^+ and 26^{2+}) are rather comparable with those of 25^{4+} . Thus, change of color of the solution should correspond to the formation of an unstable radical species via multiple-electron transfer.

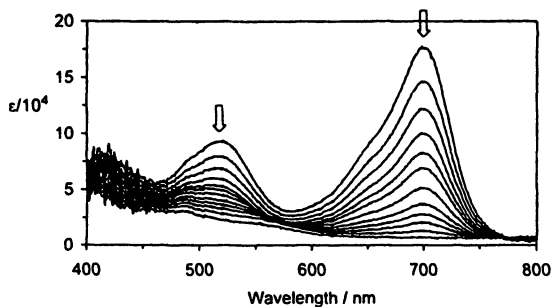


Figure 25. Continuous changes in the visible spectrum of tetracation 25^{4+} under electrochemical reduction conditions.

We have therefore been able to prepare the highly stable tetracation 25^{4+} salt despite the presence of four positive charges in the structure. However, this first example for a cyanine–cyanine hybrid with cyanine units at both two termini did not demonstrate the presumed multiple color changes during electrochemical reduction. However, the tetracation 25^{4+} exhibited multiple-electron transfer as a function of the substituted di(1-azulenyl)methylm units and also showed color change during the electrochemical reduction.

The Second Tetracation Connected to Thienylacetylene Spacers

We considered that formation of the thienoquinoid forms during the redox reaction might improve the reversibility and the redox interaction among the cationic units. Therefore, the redox properties of the tetracation 28^{4+} connected via a benzene unit with thienylacetylene spacers were examined (21). Incorporation of the thiophene as a π -bridge linker should stabilize the quinoidal structure in the reduced forms and improve the redox interaction among the cationic units, as demonstrated in dication 22^{2+} (Figure 26).

Preparation of the tetracation 28^{4+} was accomplished by hydride abstraction from the corresponding tetrahydro-derivative in the same way as preparation of

the tetracation 25^{4+} . A series of di- and monocations (29^{2+} and 30^+) were also synthesized to compare their redox properties (Figure 27).

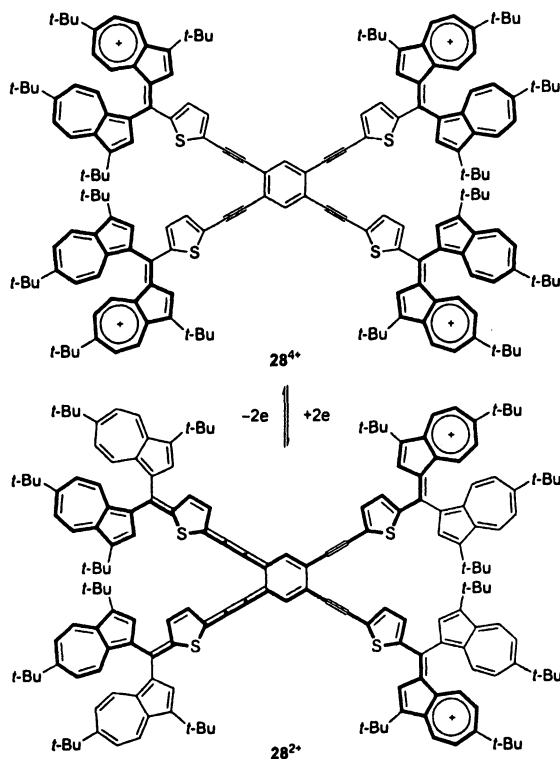


Figure 26. The tetracation 28^{4+} connected via benzene to thierylacetylene spacers in order to increase redox interaction among the cationic units.

In contrast to the stabilizing ability of the 2-thienyl substituent, these cations (28^{4+} , 29^{2+} , and 30^+) were less stable than the corresponding polycations connected via the phenylethynyl spacers. All cationic units up to tetracations were similarly reduced in one step upon CV. In these cases, the presumed redox interaction among the cationic units was also small. The first reduction potentials of 28^{4+} , 29^{2+} , and 30^+ were slightly less negative as compared to those of polycations connected via phenylethynyl spacers. This indicates that electrochemical destabilization of the methyl cations by thienyl substituents is similar to the results based on the pK_R^+ values.

UV-vis spectra of these cations (28^{4+} , 29^{2+} , and 30^+) in the visible region were characterized by two strong absorption bands, although the polycations

connected with phenylethynyl spacers exhibited an absorption band in this region. The spectroelectrograms of 28^{4+} are shown in Figure 28. In this case, as before we were not able to obtain any evidence for the formation of a colored cyanine-type structure in the two-electron reduction. Low reversibility in the reductions of 28^{4+} , 29^{2+} , and 30^{+} suggests the formation of neutral radical species in the presumed reduction products.

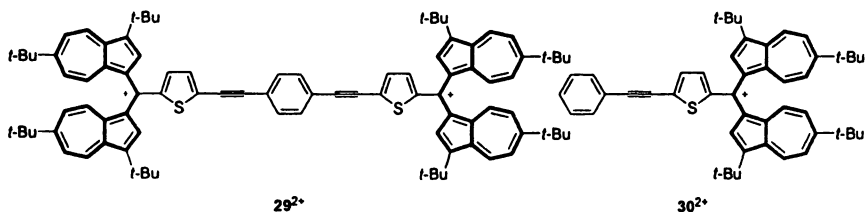


Figure 27. The di- and monocations (29^{2+} and 30^{+}) synthesized to compare their redox properties.

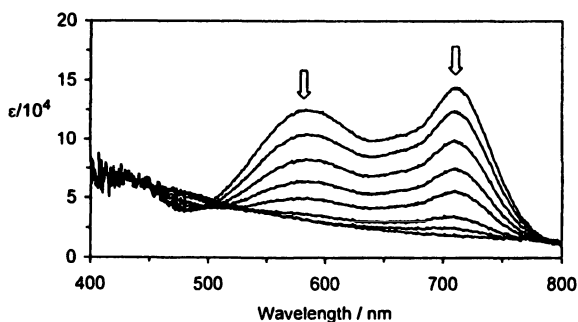


Figure 28. Continuous changes in the visible spectrum of 28^{4+} under electrochemical reduction conditions.

The Third Tetracation Incorporating an Anthraquinodimethane Unit

The electrochemical behavior was not ideal for the presumed cyanine–cyanine hybrid, probably due to the less effective electrochemical interaction among the positive charges. This should be attributable to the disadvantage of conjugation of the positively charged units by the central benzene ring.

Therefore, the tetracation 31^{4+} incorporated with an anthraquinodimethane unit, should improve the redox interaction among the cationic units, via aromatization in a two-electron reduced state (Figure 29) (24).

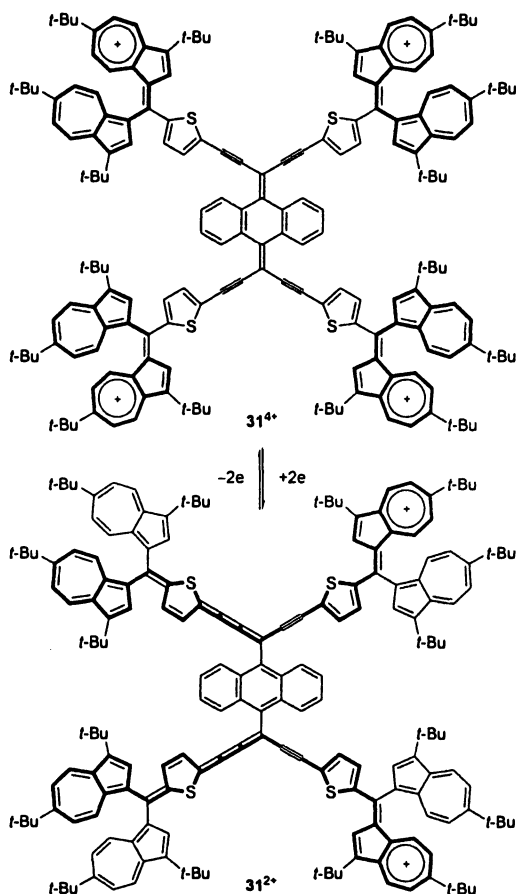


Figure 29. The tetracation 31^{4+} designed to improve the redox interaction among cationic units.

Synthesis of the tetracation 31^{4+} was accomplished by hydride abstraction on the corresponding tetrahydro derivative, analogous to other tetracations. CV and DPV measurements demonstrated that tetracation 31^{4+} exhibits a two-step reduction as presumed for a cyanine–cyanine hybrid. This indicates that the redox interaction among the four cationic units is increased by the anthraquinodimethane core.

In this case, however, we also could not obtain any evidence for the formation of a colored cyanine-type structure 31^{2+} in the two-electron reduction. Low reversibility for the electrochemical reduction suggests the formation of unstable, fully neutralized, species such as a neutral diradical in the presumed reduction products under the conditions of the visible spectral measurements.

The tetracation 31^{2+} exhibited the idealized electrochemical behavior upon CV and DPV, although the redox interaction among the cation units was still small. Additionally, tetracation 31^{4+} , synthesized as a representative for the cyanine–cyanine hybrid, also did not exhibit the presumed multiple-color change during electrochemical reduction.

Summary

Synthesis of novel polyelectrochromic materials with the new structural motif utilizing stabilized carbocations has been demonstrated by several examples. The Wurster type violene–cyanine hybrid systems (22^{2+} and 23^{2+}) exhibit the presumed two color changes. The new cyanine–cyanine hybrid system (24^+) with a cyanine unit at the one terminus exhibits three color changes.

The synthesized tetracations (25^{4+} , 28^{4+} , and 31^{4+}), did not show the presumed multiple color changes during electrochemical reduction. However, these tetracation salts are highly stable in spite of their tetracationic structure. They exhibit multiple-electron transfer as a function of the substitution of the di(1-azulenyl)methylum units and significant color change during electrochemical reduction.

So far, we have not succeeded in obtaining a good example for a new cyanine–cyanine hybrid system with a cyanine unit at the both termini. However, the use of di(1-azulenyl)methylum units as stabilized redox active polymethine units is effective because of their high stability and presence of strong absorption in the visible region through their redox activity.

References

1. Monk, P. M. S.; Mortimer, R. J.; Rosseinsky, D. R. *Electrochromism: Fundamentals and Applications*; VCH: Weinheim, Germany, 1995.
2. Deuchert, K.; Hünig, S. *Angew. Chem. Int. Ed. Engl.* **1978**, *17*, 875-886.
3. (a) Hünig, S.; Kemmer, M.; Wenner, H.; Perepichka, I. F.; Bäuerle, P.; Emge, A.; Gescheid, G. *Chem. Eur. J.* **1999**, *5*, 1969-1973. (b) Hünig, S.; Kemmer, M.; Wenner, H.; Barbosa, F.; Gescheidt, G.; Perepichka, I. F.; Bäuerle, P.; Emge, A.; Peters, K. *Chem. Eur. J.* **2000**, *6*, 2618-2632. (c) Hünig, S.; Perepichka, I. F.; Kemmer, M.; Wenner, H.; Bäuerle, P.; Emge, A. *Tetrahedron* **2000**, *56*, 4203-4211.

4. Zeller, K.-P. Azulene. In *Houben-Weyl; Methoden der Organischen Chemie*, 4th ed.; Kropf, H., Ed.; Georg Thieme: Stuttgart, Germany, 1985; Vol. V, Part 2c, pp 127-418.
5. Agranat, I.; Aharon-Shalom, E. *J. Org. Chem.* **1976**, *41*, 2379-2383.
6. Ito, S.; Morita, N.; Asao, T. *Tetrahedron Lett.* **1991**, *32*, 773-776.
7. Ito, S.; Morita, N.; Asao, T. *Bull. Chem. Soc. Jpn.* **1995**, *68*, 1409-1436.
8. Okamoto, K.; Takeuchi, K.; Kitagawa, T. *Advances in Physical Organic Chemistry*, **1995**, *30*, 173-221.
9. Komatsu, K.; Akamatsu, H.; Jinbu, Y.; Okamoto, K. *J. Am. Chem. Soc.*, **1988**, *110*, 633-634.
10. Laursen, B. W.; Krebs, F. C.; Nielsen, M. F.; Bechgaard, K.; Christensen, J. B.; Harrit, N. *J. Am. Chem. Soc.* **1998**, *120*, 12255-12263.
11. Laursen, B. W.; Krebs, F. C. *Chem. Eur. J.* **2001**, *7*, 1773-1783.
12. Ito, S.; Kikuchi, S.; Morita, N.; Asao, T. *Bull. Chem. Soc. Jpn.* **1999**, *72*, 839-849.
13. Ito, S.; Kikuchi, S.; Morita, N.; Asao, T. *J. Org. Chem.* **1999**, *64*, 5815-5821.
14. Dolman, D.; Stewart, R. *Can. J. Chem.* **1967**, *45*, 911-924.
15. Ito, S.; Morita, N.; Asao, T. *Bull. Chem. Soc. Jpn.* **2000**, *73*, 1865-1874.
16. See e.g., (a) Takahashi, K.; Nihira, T. *Tetrahedron Lett.* **1989**, *30*, 5903-5906. (b) Takahashi, K.; Nihira, T.; Tomitani, K. *J. Chem. Soc., Chem. Commun.* **1993**, 1617-1619.
17. Ito, S.; Kikuchi, S.; Okujima, T.; Morita, N.; Asao, T. *J. Org. Chem.* **2001**, *66*, 2470-2479.
18. Ito, S.; Morita, N.; Kubo, T. *J. Syn. Org. Chem.* **2004**, *62*, 766-777.
19. (a) Stella, L.; Janousek, Z.; Merényi, R.; Viehe, H. G. *Angew. Chem. Int. Ed. Engl.* **1978**, *17*, 691-692. (b) Viehe, H. G.; Merényi, R.; Stella, L.; Janousek, Z. *Angew. Chem. Int. Ed. Engl.* **1979**, *18*, 917-932. (c) Viehe, H. G.; Janousek, Z.; Merényi, R. *Acc. Chem. Res.* **1985**, *18*, 148-154.
20. Ito, S.; Kubo, T.; Morita, N.; Ikoma, T.; Tero-Kubota, S.; Tajiri, A. *J. Org. Chem.* **2003**, *68*, 9753-9762.
21. Ito, S.; Akimoto, K.; Kawakami, J.; Tajiri, A.; Shoji, T.; Satake, H.; Morita N. to be published.
22. (a) Head, N. J.; Prakash, G. K. S.; Bashir-Hashemi, A.; Olah, G. A. *J. Am. Chem. Soc.* **1995**, *117*, 12005-12006. (b) Heagy, M. D.; Wang, Q.; Olah, G. A.; Prakash, G. K. S. *J. Org. Chem.* **1995**, *60*, 7351-7354.
23. Rathore, R.; Bums, C. L.; Guzei, I. A. *J. Org. Chem.* **2004**, *69*, 1524-1530.
24. Ito, S.; Sasaki, S.; Kawakami, J.; Tajiri, A.; Morita N. to be published.

Chapter 10

Cation Pool Method and Cation Flow Method

Jun-ichi Yoshida

Department of Synthetic Chemistry and Biological Chemistry, Graduate
School of Engineering, Kyoto University, Kyoto 615-8510, Japan

In the cation pool method organic cations are generated by electrochemical oxidation and are accumulated in a solution. In the next step, a suitable nucleophile is added to the thus-generated solution of the cation. In the cation flow method organic cations are generated by electrochemical oxidation using a microflow cell. The cation thus generated is allowed to react with a nucleophile in the flow system.

Introduction

Reactions of Organic Cations in Synthesis

Organic cations (carbocations and onium ions) are important reactive intermediates in organic synthesis. From an experimental point of view, it is noteworthy that the manner in which we carry out reactions of organic cations is different from that for carbanions (Scheme 1). Usually, carbanions are generated and accumulated in a solution in the absence of electrophiles. After the generation process is complete, an electrophile is added to the solution of the pre-formed carbanion to achieve a desired transformation. In contrast, organic cations are usually generated in the presence of nucleophiles. This is probably

because organic cations that are often used in organic synthesis are unstable and transient in conventional reaction media and should be trapped in situ by nucleophiles immediately after their generation. Therefore, reactions of organic cations suffer from the limitation of variation of nucleophiles. Nucleophiles that do not survive under the generation conditions cannot be used.

This comparison is, however, probably unfair, because we usually regard organometallic compounds as carbanions. Organometallic compounds have carbon-metal covalent bonds, although magnitude of the ionic character of the bond depends on the nature of the metal and substituents on the carbon. Organometallic compounds are widely utilized as carbanions equivalents, but ionic carbanions are rarely used in organic synthesis. On the other hand, we do not regard a species that has a covalent bond between carbon and a leaving group as an organic cation. We only regard ionic species that do not have such a covalent bond as carbocations or onium ions.

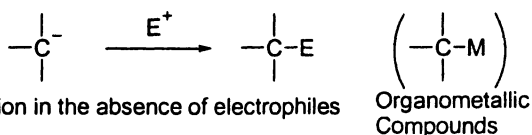
Apart from such arguments, development of a new method that enables generation of organic cations in the absence of nucleophiles is strongly needed for expanding the scope of cation chemistry in organic synthesis. In this vein, we initiated our project on the "cation pool" method and the "cation flow" method, whereby organic cations are generated in the absence of nucleophiles and are used for the subsequent reactions.

Reactions of Carbocations



generation in the presence of nucleophiles

Reactions of Carbanions



generation in the absence of electrophiles

Organometallic
Compounds

Scheme 1.

Methods of Generating Organic Cations

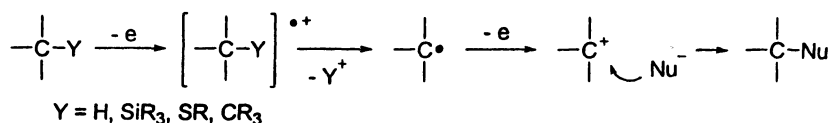
Before discussing the concepts of the "cation pool" method and the "cation flow" method, let us briefly touch on generation methods of organic cations.

Two methods are popular in organic synthesis; the acid promoted method and the oxidative method.

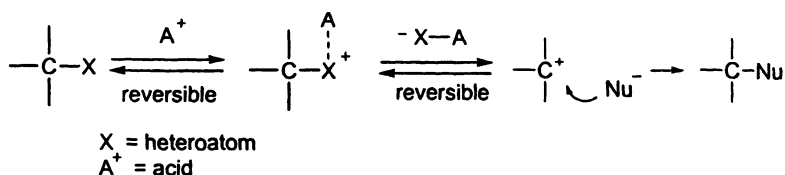
Acid promoted reactions are most commonly used for the generation of organic cations in organic synthesis. In this method, a proton or a Lewis acid is used to activate a leaving group that is covalently bound to a carbon. In the next step, heterolysis of the bond occurs to generate a carbon having a positive charge. These steps are reversible. The equilibrium usually lies toward the starting material. Then, a nucleophile, which is present in the solution, attacks the cationic carbon to give the final product.

In the oxidative generation, a neutral organic molecule is oxidized to generate the corresponding radical cation species. There are several possibilities for the fate of the radical cation.¹ In some cases, elimination of a proton takes place to give a carbon radical. Such a radical species can also be generated via dissociation of a carbon-heteroatom bond or a carbon-carbon bond in the radical cation. Such carbon radical species are often further oxidized under the reaction conditions to give the corresponding cations. These steps are essentially irreversible. Then, a nucleophile attacks the cation to give the final product. The oxidative cation generation is also usually carried out in the presence of nucleophiles because of the instability of organic cations. Therefore, only a nucleophile that has a higher oxidation potential relative to the cation precursor could be used for this type of transformation.

Oxidative generation



Acid promoted generation



Scheme 2.

Principle of the “Cation Pool” Method

Outline of the “Cation Pool” Method

The “cation pool” method is based on the irreversible oxidative generation of organic cations. In the first step, the cation precursor is oxidized via an electrochemical method. An organic cation thus generated is accumulated in the solution in the absence of a nucleophile that we want to introduce onto the cationic carbon. Counter anions which are normally considered to be very weak nucleophiles are used to avoid the nucleophilic attack on the cationic center. In order to avoid thermal decomposition of the cation, electrolysis should be carried out at low temperatures such as $-78\text{ }^{\circ}\text{C}$. After electrolysis is complete, the nucleophile is then added to obtain the desired product. The use of a carbon nucleophile results the direct carbon-carbon bond formation.

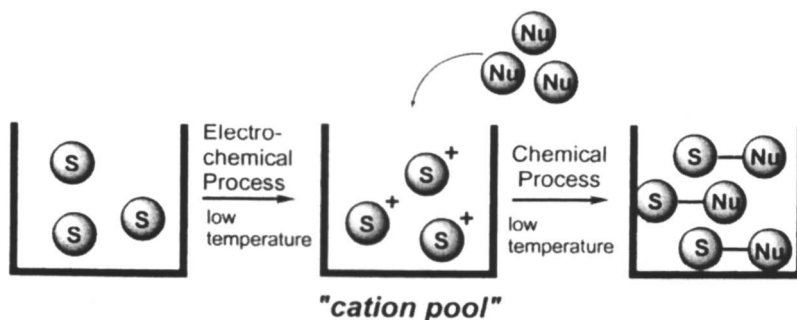


Figure 1. Schematic Diagram for the “Cation Pool” Method.

Low Temperature Electrolysis

When we initiated our study on the “cation pool” method, it was generally considered to be very difficult to carry out preparative electrochemical reactions at such a low temperature because of high viscosity of the solution, which renders the movement of ions in solution to carry charges unfavorable. Conductivity typically decreases when electrolysis temperature is lowered. However, we found that by tuning the reaction conditions such as the solvent and the supporting electrolyte, electrolyses can be accomplished at such low temperature in a preparative scale. The low temperature electrolysis is the key technology for the success of the “cation pool” method. Dichloromethane (CH_2Cl_2) seems to be the best solvent among the solvents examined, presumably because of its low viscosity even at low temperatures. Tetrabutylammonium

tetrafluoroborate ($\text{Bu}_4\text{N}^+\text{BF}_4^-$) is usually used as a supporting electrolyte because of its high solubility, which ensures sufficient conductivity at low temperatures. Therefore, the counter anion of organic cations generated by the “cation pool” method is usually BF_4^- , which is considered to be a very weak nucleophile to cationic carbons.

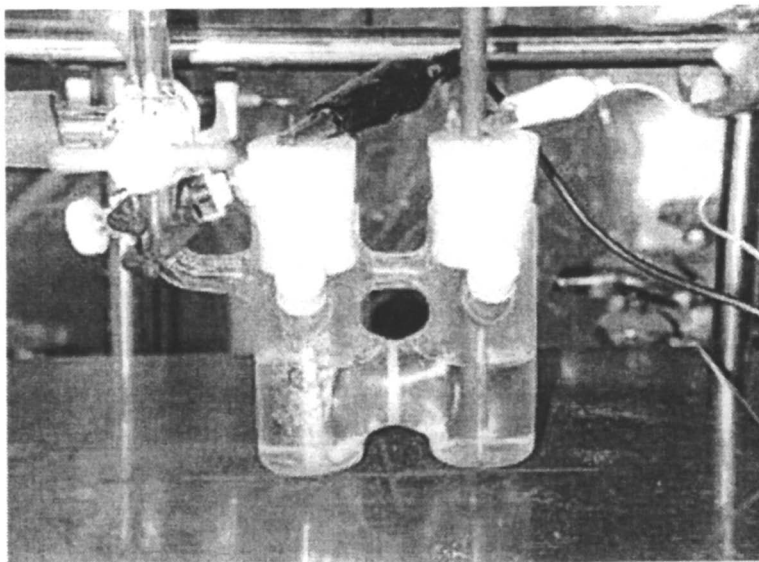
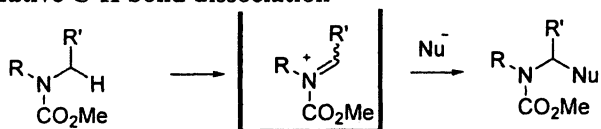
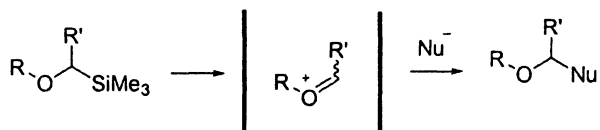
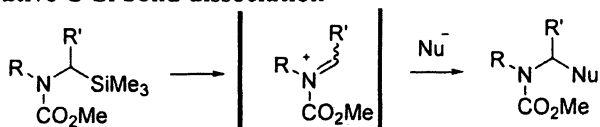
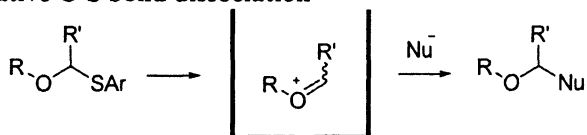
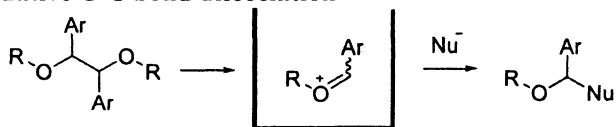


Figure 2. Apparatus for Low Temperature Electrolysis

Methods for the Oxidative Generation of Cations for Use in “Cation Pools”

We focused on two types of organic cations, *N*-acyliminium ions and alkoxy-carbenium ions,² because they are very popular in organic synthesis. A number of reactions involving such onium ions have been developed and widely utilized for the construction of organic molecules.

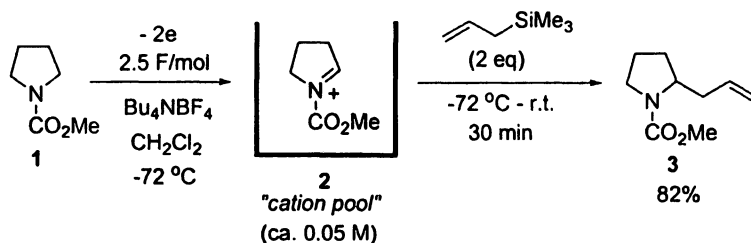
Four methods are used for generating “pools” of these onium ions; oxidative C-H bond dissociation, oxidative C-Si bond dissociation, oxidative C-S bond dissociation, and oxidative C-C bond dissociation (Scheme 3). In the following sections, we will discuss the principles and synthetic applications of these methods.

(1) Oxidative C-H bond dissociation**(2) Oxidative C-Si bond dissociation****(3) Oxidative C-S bond dissociation****(4) Oxidative C-C bond dissociation***Scheme 3.****N*-Acyliminium Ions****Generation of *N*-Acyliminium Ion Pools by C-H Bond Dissociation**

It is well known that oxidation of carbamates leads to the formation of *N*-acyliminium ions via dissociation of the C-H bond *a.* to nitrogen. The electrochemical,⁴ metal-catalyzed,⁵ and chemical methods⁶ have been reported in the literature to accomplish this transformation. The transformation serves as a useful tool for organic synthesis, although only compounds of high oxidation potentials such as methanol and cyanide ion can be used as nucleophile. It

should be noted that *N*-acyliminium ions, which do not have a stabilizing group, have not been detected spectroscopically and that they have been considered to be transient intermediates.

Thus, we first chose to apply the “cation pool” method to generate and accumulate *N*-acyliminium ions.⁷ For example, low-temperature electrolysis of pyrrolidine carbamate **1** gave the corresponding *N*-acyliminium ion **2** as a single species, which was indicated by NMR analysis (¹H NMR: 9.38 ppm due to the methine proton; ¹³C NMR: 193.36 ppm due to the methine carbon) (Scheme 4).⁸ These chemical shifts indicated that there was a strong positive charge at the carbon and that the *N*-acyliminium ion was formed as an ionic species. The addition of allyltrimethylsilane to the solution afforded the corresponding allylated product **3** in 82% yield. It should be noted that the oxidation potential of allyltrimethylsilane is lower than the starting carbamate **1**. Therefore, it should be very difficult to carry out the electrochemical oxidation of **1** in the presence of the more easily oxidized allyltrimethylsilane to obtain **3** selectively.



Scheme 4.

The *N*-acyliminium ion can be characterized by FTIR spectroscopy as well.⁹ The starting carbamate **1** exhibited an absorption at 1694 cm^{-1} due to the carbonyl stretching, while the *N*-acyliminium ion **2** generated by the “cation pool” method exhibited an absorption at 1814 cm^{-1} . The higher wave number observed for the cation is consistent with the existence of a positive charge at the nitrogen atom adjacent to the carbonyl carbon. The shift to higher wave number is also supported by DFT (density functional theory) calculations.

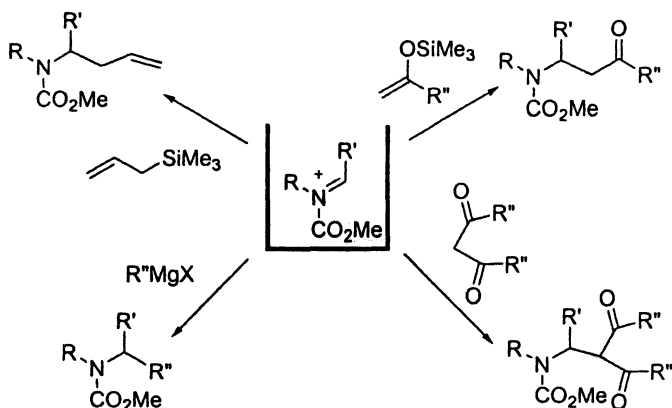
Generation of *N*-Acyliminium Ion Pools by C-Si Bond Dissociation

We have proposed the concept of electroauxiliary,¹⁰ which activates substrate molecules toward electron transfer and controls a reaction pathway that would favor the formation of the desired products. For example, pre-introduction of an electroauxiliary such as a silyl group to a carbon α to nitrogen gives rise to selective introduction of a nucleophile on the carbon to which the auxiliary has been attached. The use of a silyl group as electroauxiliary was

found to be quite effective for the “cation pool” method (Scheme 3).¹¹ The introduction of a silyl group decreases the oxidation potentials of carbamates. Therefore, the electrolysis can be carried out more easily. Control of the regiochemistry by the silyl group is also advantageous if we use unsymmetrical carbamates.

Reactions of *N*-Acylium Ion Pools

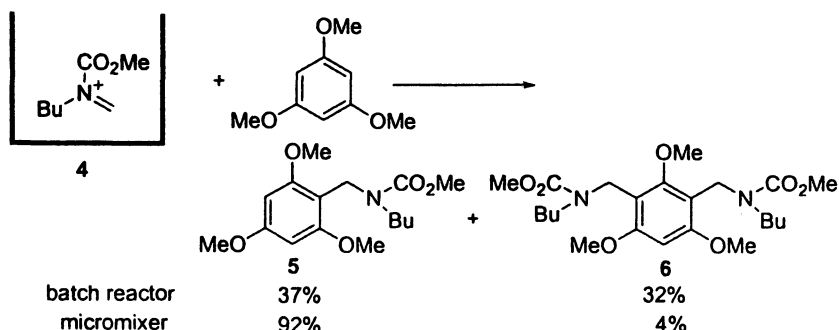
N-Acylium ion pools were found to react with various carbon nucleophiles. Scheme 5 summarizes reactions of the *N*-acylium ion pools with allylsilanes, silyl enol ethers, Grignard reagents, and 1,3-dicarbonyl compounds.¹²



Scheme 5.

Friedel-Crafts Type Reactions of *N*-Acylium Ion

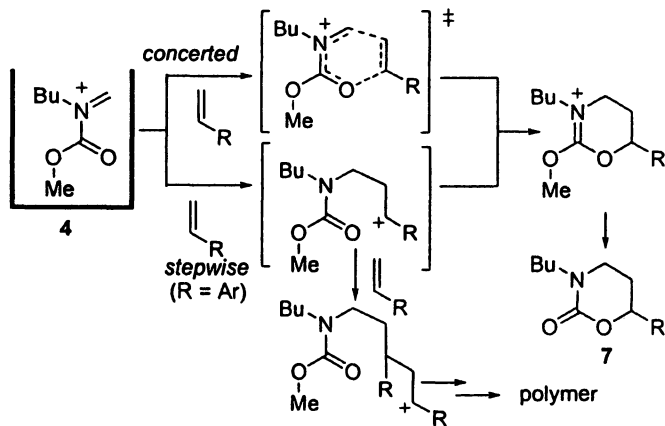
N-Acylium ion pools were also found to react with aromatic and heteroaromatic compounds to give Friedel-Crafts type alkylation products (Scheme 6).¹³ The reaction of *N*-acylium ion pool 4 with electron-rich aromatic compounds such as 1,3,5-trimethoxybenzene is interesting. The reaction was extremely fast and a macroscale batch reaction led to the formation of a significant amount of the dialkylation product 6 together with the monoalkylation product 5, although it was revealed that the second alkylation was slower than the first reaction. Therefore, the observed selectivity can be ascribed to the problem of “disguised chemical selectivity”¹⁴ because of faster reaction relative to mixing rate. The problem was solved by using micromixing, which enables extremely fast mixing by virtue of short diffusion path in the microstructure.



Scheme 6.

[4+2] Cycloaddition of *N*-Acylium Ion with Alkenes

N-Acylium ions are known to serve as electron-deficient 4π components and undergo [4+2] cycloaddition with alkenes and alkynes.¹⁵ The reaction has been utilized as a useful method for the construction of heterocycles and acyclic amino alcohols. The reaction can be explained in terms of an inverse electron demand Diels-Alder type process that involves an electron-deficient hetero-diene with an electron-rich dienophile. *N*-Acylium ions generated by the “cation pool” method were also found to undergo [4+2] cycloaddition reaction to give adduct 7 as shown in Scheme 7.¹⁶ The reaction with an aliphatic olefin seems to proceed by a concerted mechanism, whereas the reaction with styrene derivatives seems to proceed by a stepwise mechanism. In the latter case, significant amounts of polymeric products were obtained as byproducts. The formation of polymeric byproducts can be suppressed by micromixing.

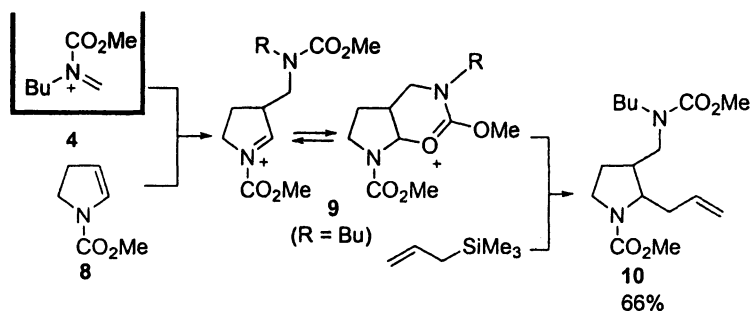


Scheme 7.

Three Component Coupling based on the “Cation Pool” Method

Because of the increasing demand for producing a large number of compounds in a highly time-efficient fashion, integration of chemical transformation is one of the central issues in current organic synthesis.¹⁷ We have developed sequential one-pot multi-component coupling reactions based on the “cation pool” method.¹⁸ The basic concept of the present coupling reaction is as follows: The addition of a “cation pool” with an electron-rich carbon-carbon double bond generates a new “cation pool”, which is allowed to react with a carbon nucleophile. This approach is the *umpolung* of the addition of a carbon nucleophile to an electron-deficient carbon-carbon double bond followed by the trapping of the resulting carbanion with a carbon electrophile.¹⁹

Thus, an *N*-acyliminium ion pool **4** was allowed to react with an enamine derivative **8** (Scheme 8). The addition of the cation to the carbon-carbon double bond generated the second cation **9**, which seemed to exist either as the open form or the cyclic form. In the next step, cation **9** was treated with allyltrimethylsilane to give the final three component coupling product **10**.



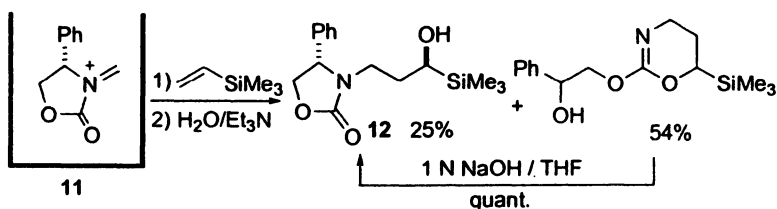
Scheme 8.

Various carbon nucleophiles, such as allylsilanes, allylstannanes, silyl enol ethers, ketene silyl acetals, organoaluminum compounds, and Grignard reagents were effective as carbon nucleophiles.

Cationic Carbohydroxylation of Alkenes

Carbo-oxylation (carbohydroxylation and carboalkoxylation), whereby an organic group and an oxy (hydroxyl or alkoxy) group add across a carbon-carbon double bond or a triple bond, is an important transformation in organic synthesis. We found that the reaction of a “cation pool” with an alkene or alkyne followed by the trapping of the resulting carbocation by water led to the

formation of the corresponding carbohydroxylation product (Scheme 9).²⁰ When vinyltrimethylsilane was used as an alkene for the reaction of cation **11**, the reaction was highly diastereoselective, allowing access to an enantiomerically pure α -silyl- γ -amino alcohol **12**.



Scheme 9.

Carbocationic Polymerization Using a “Cation Pool” as an Initiator

“Cation pools” were found to serve as effective initiators in cationic polymerization of vinyl ethers.²¹ In conjunction with a microsystem, this method effects cationic polymerization in a highly controlled manner without the deceleration inherent in the dynamic equilibrium between active and dormant species, which is essential for conventional living cationic polymerization.²² The molecular weight distribution ($M_w/M_n = 1.14$) can be controlled by extremely fast micromixing, and the polymer end can be used as living reactive species for the follow-up reaction. Extremely fast initiation reaction together with extremely fast mixing by the microsystem seem to be responsible for the high level of molecular weight distribution control.

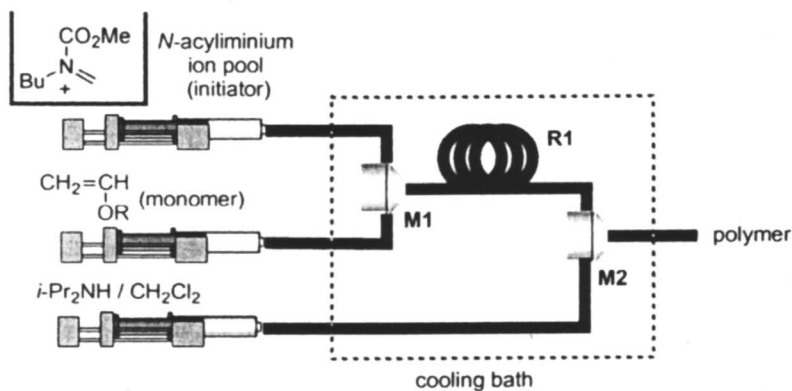
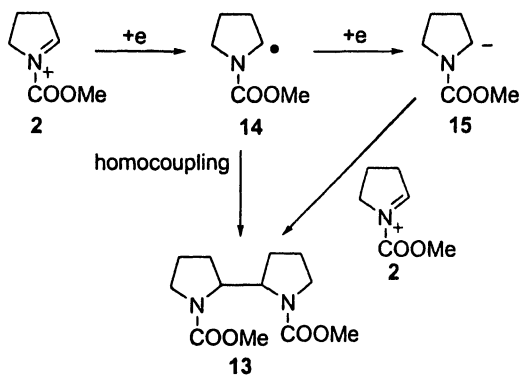


Figure 3. Microsystem for the “cation pool” initiated polymerization of vinyl ethers.

Radical Chemistry Using the “Cation Pool” Method

Carbocations, carbon radicals, and carbanions are important reactive carbon intermediates in organic chemistry and their interconversions could be effected, in principle, by redox processes. With the “cation pool” method at hand, we next examined the redox-mediated interconversions of such reactive carbon species.

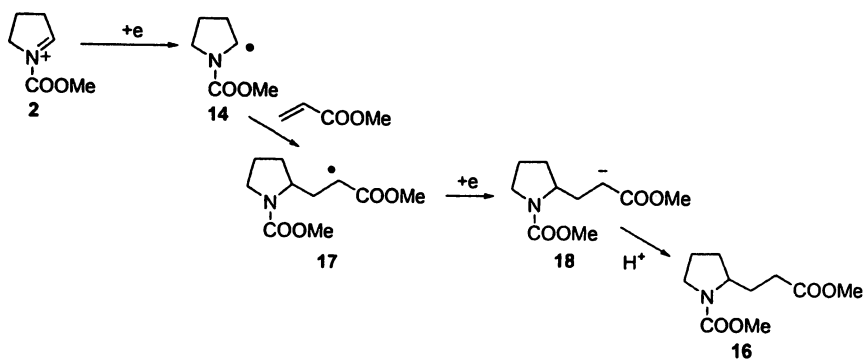
The electrochemical reduction of *N*-acyliminium ion pool **2** gave rise to the formation of the corresponding homo-coupling product **13** (Scheme 8).²³ Presumably, a radical intermediate **14** was generated by one electron reduction of **2** and homo-coupling of the radical led to the formation of the dimer **13**. However, a mechanism involving two-electron reduction to give anion **15** followed by the reaction with cation **2** cannot be ruled out.



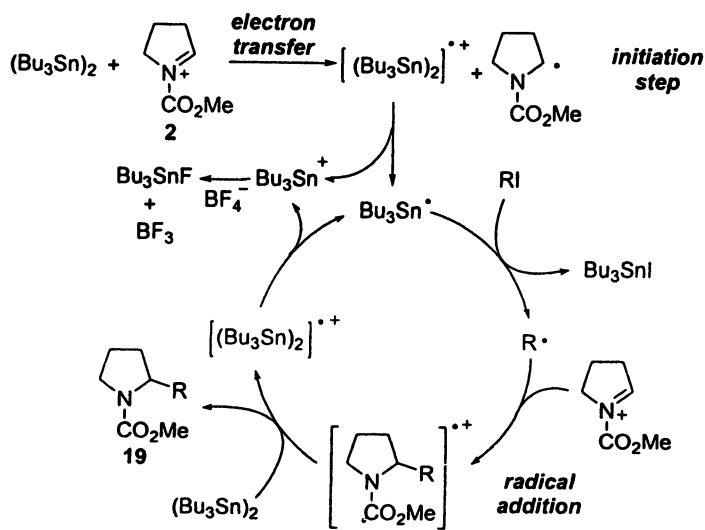
Scheme 10.

Next, we examined the reduction of “cation pools” in the presence of radical acceptors. The radical that is formed by one-electron reduction of the cation is expected to add to a carbon-carbon double bond. The electrochemical reduction of **2** in the presence of methyl acrylate gave the expected addition product **16** (Scheme 9). A mechanism involving addition of radical **14** to the acrylate to generate radical **17** followed by subsequent reduction of anion **18**, which is protonated to give **16** has been suggested.

Radical addition to an *N*-acyliminium ion is also an interesting feature of the “cation pool” chemistry. We found that an alkyl iodide reacted with an *N*-acyliminium ion pool in the presence of hexabutyldistannane to give coupling product **19**.²⁴ A chain mechanism shown in Scheme 10, which involves the addition of the alkyl radical to the *N*-acyliminium ion to form the corresponding radical cation, seems to be reasonable. The present reaction opens a new possibility for radical-cation crossover mediated carbon-carbon bond formation.



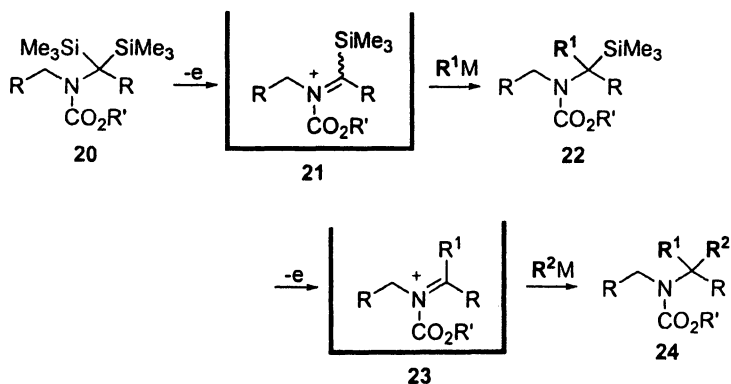
Scheme 11.



Scheme 12.

Sequential Generation of “Cation Pools” Using Two Silyl Groups

The use of two electroauxiliaries on the same carbon enables sequential generation of the “cation pool” as shown in Scheme 13.¹¹ Low temperature electrolysis of **20** generated the first cation **21**, which was allowed to react with first nucleophile to give **22**. The electrolysis of **22** generated the second cation **23**, which was allowed to react with the second nucleophile to give **24**. This methodology was successfully applied to the synthesis of cephalotaxine, which is the parent compound of the antileukemic active harringtonines, a group of uniquely structured pentacyclic alkaloids having a nitrogen containing spiro system.



Scheme 13.

Combinatorial Synthesis Based on the “Cation Pool” Method

The “cation pool” method serves as a powerful tool for parallel combinatorial synthesis.²⁵ Required for successful combinatorial synthesis are reactions of high generality to couple any desired combination of molecules we want. The “cation pool” method seems to be suitable for this purpose, because organic cations generated by this method are usually so highly reactive as to couple with a wide range of nucleophiles.

A typical example of the parallel synthesis based on the “cation pool” method is shown in Fig 4. A solution of a cation generated by low-temperature electrolysis is divided into several portions. To each portion, different nucleophiles are added to obtain products of different coupling combinations.

The procedure can be easily automated²⁶ by a robotic synthesizer equipped with automated syringes and low temperature reaction vessels. The yields of the

products are essentially the same as those obtained by one-pot reactions with manual operation, which are shown in parentheses.

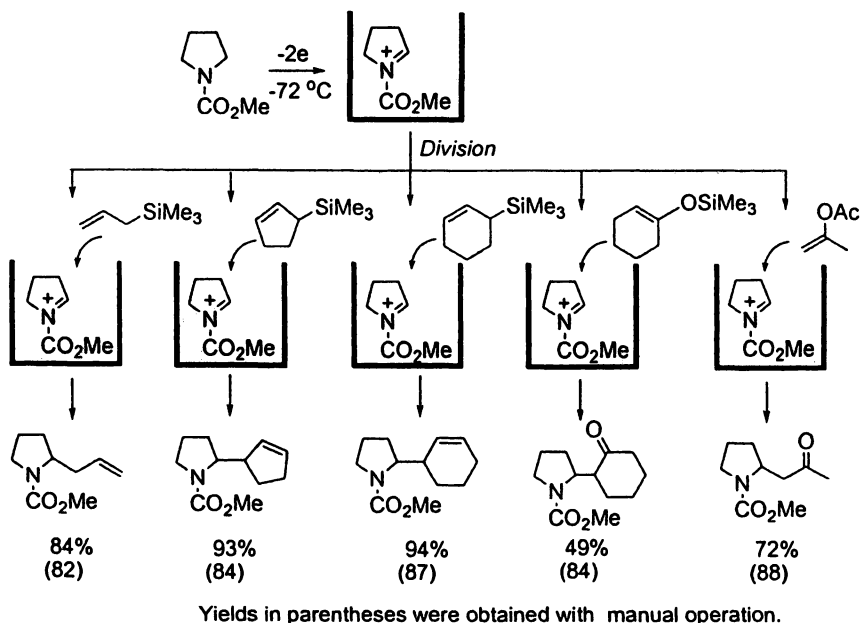


Figure 4. Parallel combinatorial synthesis based on the "cation pool" method.

The "Cation Flow" Method

Outline of the "Cation Flow" Method

The "cation pool" method enables easy manipulation of organic cation intermediates to achieve reactions with various nucleophiles, but its applicability strongly depends on the stability of the cation that is generated and accumulated. In order to solve this problem, the "cation flow" method using a microflow electrochemical system has been developed.^{9,27}

In the "cation flow" method an organic cation is generated continuously by low temperature electrolysis using an electrochemical microflow reactor. The cation thus generated is immediately allowed to react with a carbon nucleophile in the flow system. This method, in principle, enables the manipulation of highly reactive organic cations.

A schematic diagram of the “cation flow” method for generating *N*-acyliminium ion **2** is shown in Fig. 5. A solution of carbamate **1** is introduced into the anodic compartment of electrochemical microflow cell, where oxidation takes place on the surface of a carbon fiber electrode. A solution of trifluoromethanesulfonic acid (TfOH) was introduced in the cathodic compartment, where protons are reduced to generate dihydrogen on the surface of a platinum electrode. *N*-Acyliminium ion **2** thus generated can be analyzed by an in-line FT-IR analyzer to evaluate the concentration of the cation. The solution of the cation is then allowed to react with a nucleophile such as allyltrimethylsilane in the flow system to obtain the desired product **3**.

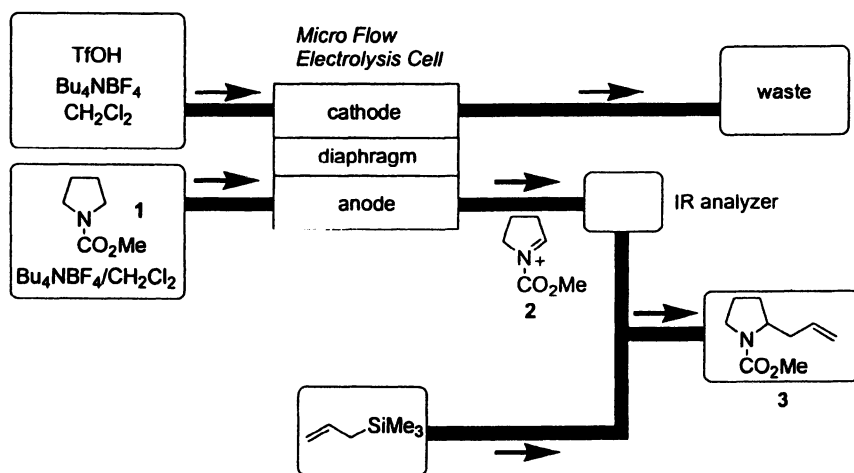


Figure 5. Schematic diagram of the “cation flow” method.

Serial Combinatorial Synthesis Based on the “Cation Flow” Method

An outstanding feature of the “cation flow” method is that the method enables continuous sequential combinatorial synthesis by simple flow switching as shown in Figure 6. In the first step, the cation flow generated from precursor **A1** is allowed to react with nucleophile **B1**. Then, the cation flow is allowed to react with the nucleophile **B2**. In the third step, the cation flow is allowed to react with nucleophile **B3**. Then, the precursor of the cation is switched to **A2**, and the cation flow generated from **A2** is allowed to react with nucleophiles **B1**, **B2**, and **B3** sequentially. Then, the precursor of the cation is switched to **A3**, and the

cation flow generated from **A3** is allowed to react with nucleophiles **B1**, **B2**, and **B3** sequentially.

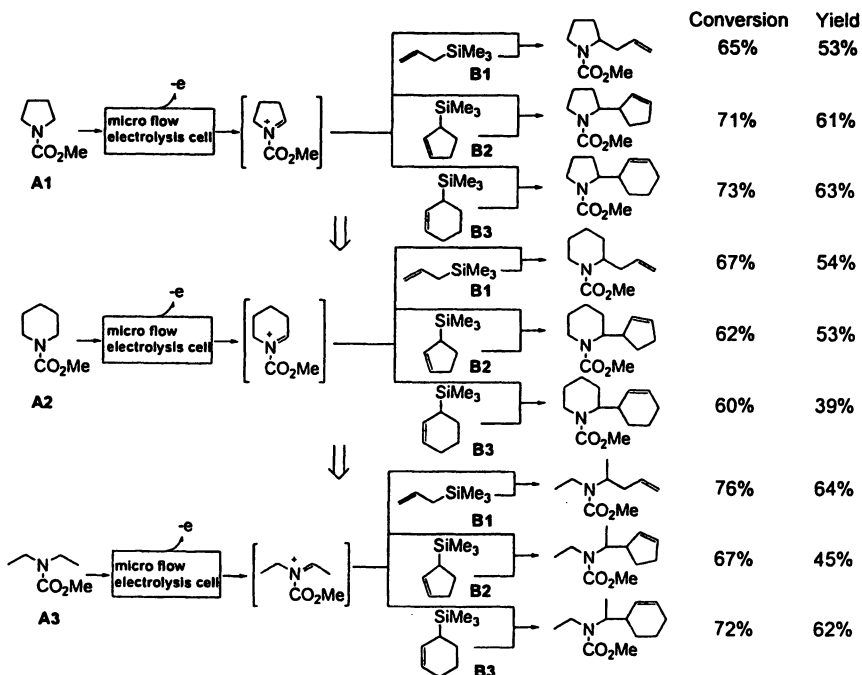


Figure 6. Sequential combinatorial synthesis based on the "cation flow" method.

Alkoxy-carbenium Ion Pools

Generation of Alkoxy-carbenium Ion Pools by C-Si Bond Dissociation

Alkoxy-carbenium ions are important reactive intermediates in modern organic synthesis.²⁸ It should be noted that other names such as oxonium ions, oxocarbenium ions, and carboxonium ions have also been used for carbocations stabilized by an adjacent oxygen atom and that we often draw structures having a carbon-oxygen double bond for this type of cations.² Alkoxy-carbenium ions are often generated from the corresponding acetals by treatment with Lewis acids in the presence of carbon nucleophiles. This type of reaction serves as efficient methods for carbon-carbon bond formation.

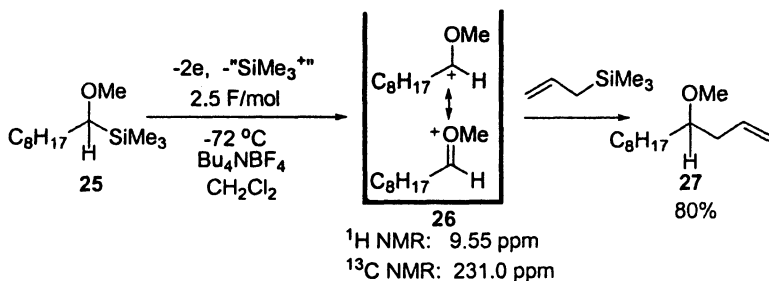
The mechanism of the Lewis acid promoted reaction of acetals has been investigated extensively. For example, Denmark demonstrated the presence of

Lewis acid-acetal complexes in NMR studies, but never detected alkoxy-carbenium ions.²⁹ The absence of alkoxy-carbenium ions in the spectra, however, does not necessarily rule out their intermediacy in the reactions with nucleophiles. Therefore, it was imperative to accomplish the reactions of spectroscopically characterized, nonstabilized alkoxy-carbenium ions with carbon nucleophiles. The cation pool method made it possible and opened a new chapter in the chemistry of alkoxy-carbenium ions.

If we consider the generation of alkoxy-carbenium ions by C-H bond dissociation, ethers should be of our first choice as precursors of alkoxy-carbenium ions by analogy to carbamates. The oxidation potentials of ethers, especially aliphatic ethers, however, are very positive, and therefore, it is rather difficult to oxidize ethers selectively under usual conditions. The regioselectivity is also a problem. Usually a mixture of two regioisomers of products is obtained because two regioisomeric alkoxy-carbenium ions are generated.

The concept of electroauxiliary is quite powerful to solve these problems. The pre-introduction of a silyl group as an electroauxiliary decreases the oxidation potential of dialkyl ethers by virtue of the orbital interaction. As a matter of fact, we demonstrated that the anodic oxidation of α -silyl ether took place smoothly in methanol.³⁰ Selective dissociation of the C-Si bond occurred and the methoxy group was introduced on the carbon to which the silyl group was attached. Therefore, α -silyl ethers seemed to serve as suitable precursors for alkoxy-carbenium ions in the cation pool method.

We therefore initiated a study on the generation of alkoxy-carbenium ion pools from α -silyl ethers by oxidative C-Si bond dissociation.³¹ "The low-temperature electrochemical oxidation of α -silyl ether **25** gave a solution of alkoxy-carbenium ion **26**, which exhibited a ¹H NMR signal at 9.55 ppm due to the methine proton, and a ¹³C NMR signal at 231.0 ppm due to the methine carbon (Scheme 14). These chemical shifts are consistent with those of an alkoxy-carbenium ion generated in superacid, reported by Olah and Forsyth and suggest the presence of a strong positive charge at the carbon."³²



Scheme 14.

Alkoxy-carbenium ion pool **26** was allowed to react with allyltrimethylsilane as a carbon nucleophile to give the corresponding allylated product **27**. The success of the nucleophilic reaction also indicated the presence of the alkoxy-carbenium ion in relatively high concentration in the solution.

The thermal stability of the alkoxy-carbenium ion is noteworthy. When the electrolysis was complete, the cation pool of **26** was allowed to warm up to a second temperature. After being kept there for 30 min, the cation was allowed to react with allyltrimethylsilane. The yield of allylated product **27** was plotted against the temperature. It can be seen from Fig. 7 that alkoxy-carbenium ion **26** is stable at temperatures approximately below $-50\text{ }^{\circ}\text{C}$. Above this temperature, the yield of **27** decreased significantly. Intramolecular coordination of ether functionality seems to be effective for the stabilization of alkoxy-carbenium ions.³³

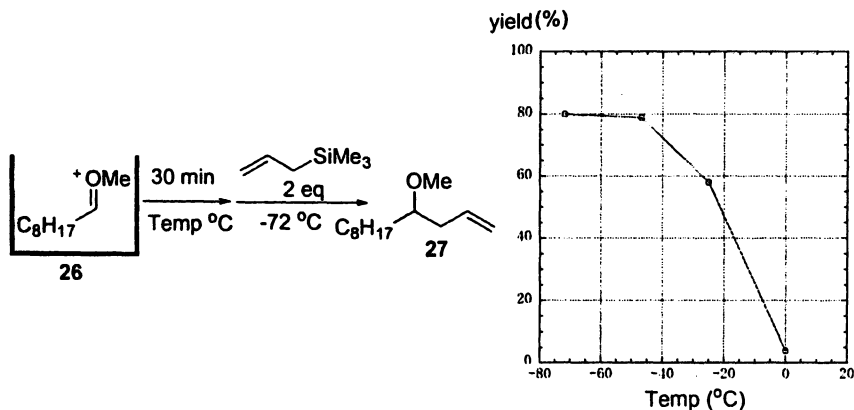
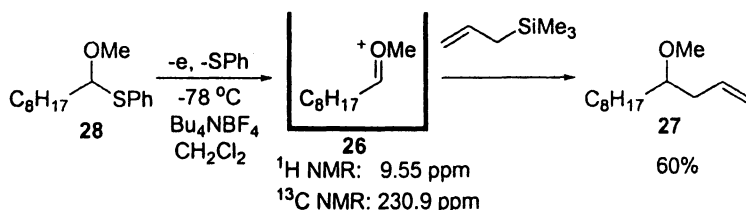


Figure 7. Thermal stability of alkoxy-carbenium ion

The alkoxy-carbenium ions generated by the “cation pool” method react with various carbon nucleophiles such as substituted allylsilanes and enol silyl ethers to give the corresponding coupling products in good yields. It should be noted that the reactions of alkoxy-carbenium ion pools with such nucleophiles are much faster than the Lewis acid promoted reactions of acetals with similar nucleophiles. A higher concentration of the cationic species in the “cation pool” method seems to be responsible.

Generation of Alkoxy-carbenium Ion Pools by Oxidative C-S Bond Cleavage

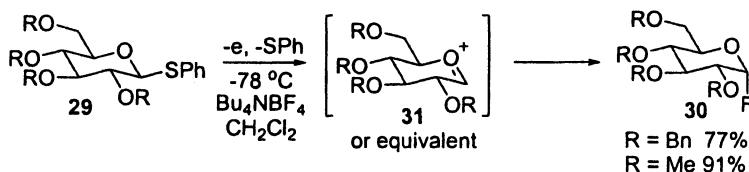
Alkoxy-carbenium ion pools can also be generated by oxidative C-S bond dissociation. We have reported that organothio groups could serve as electroauxiliaries for the electrochemical oxidation of heteroatom compounds.³⁴ The introduction of an organothio group decreases the oxidation potential and the C-S bond is cleaved selectively to generate the corresponding cation. Therefore, we next examined the oxidative C-S bond dissociation for the generation of the cation pool.³⁵



Scheme 15.

The α -phenylthioether **28** was oxidized in the absence of a nucleophile by low temperature electrolysis (Scheme 15). The corresponding alkoxy-carbenium ion pool **26** was formed, which exhibited a single set of signals in ^1H and ^{13}C NMR spectroscopy. The chemical shifts were quite similar to those obtained by the oxidative C-Si bond dissociation described in the previous section. Subsequently, the cation pool was allowed to react with allyltrimethylsilane to obtain the allylated product **27**.

We next attempted to generate the glycosyl cation pools as shown in Scheme 16. Thus, thioglycosides **29** were oxidized under the standard conditions, and solutions thus generated were allowed to react with methanol. However, no methoxylated compounds were obtained. Only glycosyl fluorides **30** were obtained. The glycosyl cations **31** or their equivalent was apparently trapped by fluoride anion derived from BF_4 . The present observations suggested that glycosyl cations are more reactive toward BF_4^- than simple alkoxy-carbenium ions.

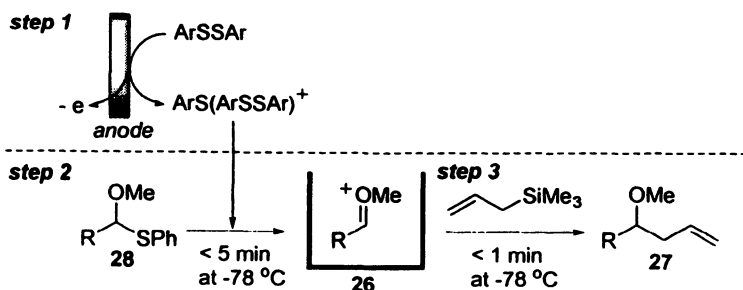


Scheme 16.

Indirect Cation Pool Method

In the “cation pool” method organic cations are generated by low temperature electrochemical oxidation of their precursors. Because electrochemical reactions take place only on the surface of the electrode, the accumulation of cations usually takes several hours. Therefore, the applicability of the method strongly depends on the stability of the cation that is accumulated. In order to solve this problem, we have developed a sequential one-pot indirect method, in which an active reagent is generated and accumulated electrochemically (step 1), and is subsequently allowed to react with a precursor to generate a “cation pool” (step 2). The “cation pool” thus-generated is allowed to react with a nucleophile (step 3).³⁶

We chose to study the generation of alkoxy-carbenium ion **26** from thioacetal **28**. The electrochemically generated $\text{ArS}(\text{ArSSAr})^+$,³⁷ which was well characterized by CSI-MS, was found to be quite effective for the generation of alkoxy-carbenium ions, presumably because of its high thiophilicity (Scheme 17). The conversion of **28** to **26** requires 5 min at -78°C . The alkoxy-carbenium ion pool **26** thus obtained exhibited similar stability and reactivity to that obtained with the direct electrochemical method. The indirect “cation pool” method serves a powerful tool not only for mechanistic studies on highly reactive cations but also for rapid parallel synthesis.

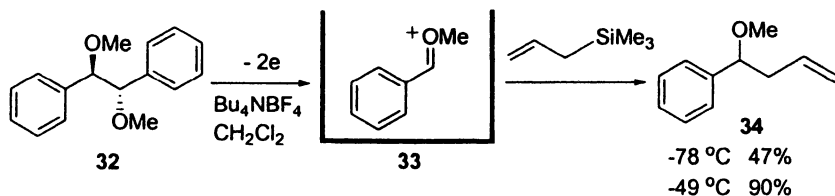


Scheme 17.

Generation of Alkoxy-carbenium Ion Pools by Oxidative C-C Bond Dissociation

Alkoxy-carbenium ion pools can also be generated by oxidative C-C bond dissociation. Oxidative C-C bond dissociation is well known in the literature.³⁸ Thus, the electrochemical oxidation of 1,2-dimethoxy-1,2-diphenylethane **32**

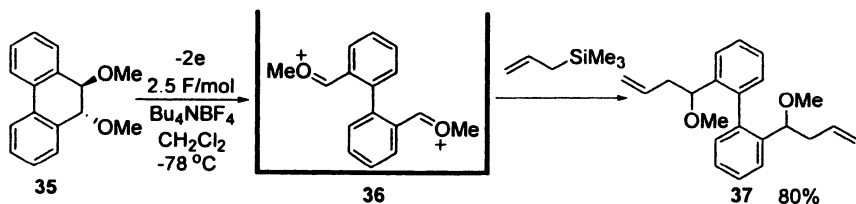
was carried out under these conditions to obtain the “cation pool” of **33**, which was allowed to react with allyltrimethylsilane to obtain **34** (Scheme 18).³⁹ It is important to note that a slightly higher temperature was required for the effective cleavage of the C-C bond. Two diastereomers of the precursor exhibited similar reactivity.



Scheme 18.

A major advantage of the C-C bond dissociation approach is easy generation of dication, ⁴⁰ if we employ cyclic compounds as starting materials. Such dication may provide powerful intermediates for the construction of various molecular architectures.

The anodic oxidation of compound **35** resulted in the formation of dication **36** (Scheme 19). ¹³C NMR indicated that two cationic centers are equivalent. The addition of allyltrimethylsilane to the solution gave rise to the formation of diallylated compound **37** in 80% yield.



Scheme 19.

Summary

The “cation pool” method and the “cation flow” method, which are based on low temperature electrochemical oxidation, have opened up a new chapter in the chemistry of organic cations, which have been considered to be difficult to manipulate in normal reaction media. The indirect “cation pool” method, which

is based on chemical generation of organic cations using an electrochemically generated reagent, has also been developed. By using these methods organic cations are generated and are accumulated in the solution. The cations can be characterized spectroscopically and then submitted to reactions with a variety of carbon nucleophiles to achieve direct C-C bond formation. The successful applications to the reactions of *N*-acyliminium ions and alkoxy-carbenium ions signifies the potentiality of the methods in conventional and combinatorial organic synthesis. Future work will hopefully enable manipulation of various types of unstable organic cations, allowing them to be utilized just like conventional reagents in organic synthesis.

Acknowledgement

This work was partially supported by the Grant-in-Aid for Scientific Research.

References and Notes

1. (a) Schmittel, M.; Burghart, *Angew. Chem. Int. Ed. Engl.* **1997**, *36*, 2550. (b) Baciocchi, E.; Bietti, M.; Lanzalunga, O. *Acc. Chem. Res.* **2000**, *33*, 243.
2. Other names such as oxonium ions, oxocarbenium ions, and carboxonium ions have also been used for oxygen-stabilized carbocations. (a) Mayr, H.; Gorath, G. *J. Am. Chem. Soc.* **1995**, *117*, 7862. (b) Moraes, L. A. B.; Mendes, M. A.; Sparrapan, R.; Eberlin, M. N. *J. Am. Soc. Mass Spectrom.* **2001**, *12*, 14. (c) Romero, J. A. C.; Tabacco, S. A.; Woerpel, K. A. *J. Am. Chem. Soc.* **2000**, *122*, 168.
3. Reviews for the synthetic utility of *N*-acyliminium cations, see: (a) Speckamp, W. N.; Hiemstra, H. *Tetrahedron* **1985**, *41*, 4367. (b) Hiemstra, H.; Speckamp, W. N. In *Comprehensive Organic Synthesis*; Trost, B. M., Fleming, I. Eds.; Pergamon Press: Oxford, 1991; Vol. 2, pp 1047. (c) Zaugg, H. E. *Synthesis* **1984**, 85. (d) Zaugg, H. E. *Synthesis* **1984**, 181.
4. For electrochemical example, see: (a) Shono, T.; Matsumura, Y.; Tsubata, K. *J. Am. Chem. Soc.* **1981**, *103*, 1172.
5. For example using Ru catalyzed oxidation, see: Naota, T.; Nakato, T.; Murahasi, S. *Tetrahedron Lett.* **1990**, *31*, 7475.
6. Chen, C-K.; Hortmann, A. G.; Marzabadi, M. R. *J. Am. Chem. Soc.* **1988**, *110*, 4829.
7. Yoshida, J.; Suga, S.; Suzuki, S.; Kinomura, N.; Yamamoto, A.; Fujiwara, K. *J. Am. Chem. Soc.* **1999**, *121*, 9546.

8. NMR study of iminium cations have been reported: (a) Yamamoto, Y.; Nakada, T.; Nemoto, H. *J. Am. Chem. Soc.* **1992**, *114*, 121. (b) Kodama, Y.; Okumura, M.; Yanabu, N.; Taguchi, T. *Tetrahedron Lett.* **1996**, *37*, 1061. (c) Mayr, H.; Ofial, A. R.; Würthwein, E.-U.; Aust, N. C. *J. Am. Chem. Soc.* **1997**, *119*, 12727 and references therein. It has been reported that the covalent structure exhibits the signal at 7.9 ppm in ^1H NMR spectroscopy: (d) Bose, A. K.; Spiegelman, G.; Manhas, M. S. *Tetrahedron Lett.* **1971**, 3167.
9. Suga, S.; Okajima, M.; Fujiwara, K.; Yoshida, J. *J. Am. Chem. Soc.* **2001**, *123*, 7941.
10. (a) Yoshida, J.; Maekawa, T.; Murata, T.; Matsunaga, S.; Isoe, S. *J. Am. Chem. Soc.* **1990**, *112*, 1962. (b) Yoshida, J.; Nishiwaki, K. *J. Chem. Soc., Dalton Trans.* **1998**, 2589.
11. Suga, S.; Watanabe, M.; Yoshida, J. *J. Am. Chem. Soc.* **2002**, *124*, 14824.
12. Suga, S.; Okajima, M.; Yoshida, J. *Tetrahedron Lett.* **2001**, *42*, 2173.
13. (a) Suga, S.; Nagaki, A.; Yoshida, J. *Chem. Commun.* **2003**, 354. (b) Nagaki, A.; Togai, M.; Suga, S.; Aoki, N.; Mae, K.; Yoshida, J. *J. Am. Chem. Soc.* **2005**, *127*, 11666.
14. (a) Rys, P. *Acc. Chem. Res.* **1976**, *10*, 345; (b) Rys, P. *Angew. Chem. Int. Ed. Engl.* **1977**, *12*, 807.
15. (a) Schmidt, R. R. *Synthesis* **1972**, 333. (b) Zaugg, H. E. *Synthesis*, 1984, 181. (c) Weinreb, S. M.; Scola, P. M. *Chem. Rev.*, **1989**, *89*, 1525.
16. (a) Suga, S.; Nagaki, A.; Tsutsui, Y. Yoshida, J. *Org. Lett.* **2003**, *5*, 945. (b) Suga, S.; Tsutsui, Y.; Nagaki, A.; Yoshida, J. *Bull. Chem. Soc. Jpn.* **2005**, *78*, 1206.
17. For example, (a) Dömling, A.; Ugi, I. *Angew. Chem. Int. Ed.* **2000**, *39*, 3168. (b) Bienaymé, H.; Hulme, C.; Odon, G.; Schmitt, P. *Chem. Eur. J.* **2000**, *6*, 3321. (c) Balme, G.; Bossharth, E.; Monteiro, N. *Eur. J. Org. Chem.* **2003**, 4101. (d) Tietz, L. F. *Chem. Rev.* **1996**, *96*, 115. (e) Parsons, P. J.; Penkett, C. S.; Shell, A. *J. Chem. Rev.* **1996**, *96*, 195. (f) Ho, T.-L. *Tactics of Organic Synthesis*; Wiley: New York, 1994; Chapter 4. (g) Orita, A.; Yaruva, J.; Otera, J. *Angew. Chem., Int. Ed.* **1999**, *38*, 2267. (b) Itami, K.; Nokami, T.; Ishimura, Y.; Mitsudo, K.; Kamei, T.; Yoshida, J. *J. Am. Chem. Soc.* **2001**, *123*, 11577.
18. Suga, S.; Nishida, T.; Yamada, D.; Nagaki, A.; Yoshida, J. *J. Am. Chem. Soc.* **2004**, *126*, 14338.
19. For example, Noyori, R.; Suzuki, M. *Angew. Chem., Int. Ed. Engl.* **1984**, *23*, 847.
20. Suga, S.; Kageyama, Y.; Babu, G.; Itami, K.; Yoshida, J. *Org. Lett.* **2004**, *6*, 2709.
21. Nagaki, A.; Kawamura, K.; Suga, S.; Ando, T.; Sawamoto, M.; Yoshida, J. *J. Am. Chem. Soc.* **2004**, *126*, 14702.

22. (a) Miyamoto, M.; Sawamoto, M.; Higashimura, T. *Macromolecules* **1984**, *17*, 265. (b) Higashimura, T.; Sawamoto, M. *Adv. Polym. Sci.* **1984**, *62*, 49. (c) Sawamoto, M. *Prog. Polym. Sci.* **1991**, *16*, 111. (d) Matyjaszewski, K.; Sawamoto, M. in *Cationic Polymerizations*; Matyjaszewski, K., Ed.; Marcel Dekker: New York, 1996.
23. (a) Suga, S.; Suzuki, S.; Yoshida, J. *J. Am. Chem. Soc.* **2002**, *124*, 30. (b) Suga, S.; Suzuki, S.; Maruyama, T.; Yoshida, J. *Bull. Chem. Soc. Jpn.* **2004**, *77*, 1545.
24. (a) Maruyama, T.; Suga, S.; Yoshida, J. *J. Am. Chem. Soc.* **2005**, *127*, 7324. (b) Maruyama, T.; Suga, S.; Yoshida, J. *Tetrahedron* **2006**, *62*, 6519.
25. For example: (a) Borman, S. *Chem. Eng. News* **1996** (February 12), 28. (b) Thompson, L. A.; Ellman, J. A. *Chem. Rev.* **1996**, *96*, 555. (c) Borman, S. *Chem. Eng. News* **1997** (February 24), 43. (d) Borman, S. *Chem. Eng. News* **1999** (March 3), 33. (e) Dagani, R. *Chem. Eng. News* **1999** (March 3) 51 and references therein.
26. For example: (a) Booth, R. J.; Hodges, J. C. *Acc. Chem. Res.* **1999**, *32*, 18. (b) Gravert, D. J.; Janda, K. D. *Chem. Rev.* **1997**, *97*, 489. (c) Studer, A.; Hadida, S.; Ferritto, R.; Kim, S.-Y.; Jeger, P.; Wipf, P.; Curran, D. P. *Science* **1997**, *275*, 823. (d) Cheng, S.; Commer, D. D.; Williams, J. P. Myers, P. L.; Boger, D. L. *J. Am. Chem. Soc.* **1996**, *118*, 2567 and references therein.
27. Suga, S.; Okajima, M.; Fujiwara, K.; Yoshida, J. *QSAR Comb. Sci.* **2005**, *24*, 728.
28. For example, Santelli, M.; Pons, J.-M. *Lewis Acids and Selectivity in Organic Synthesis*; CRC Press: Boca Raton, 1995; Chapter 4.
29. Denmark, S. F.; Willson, T. M. In *Selectivities in Lewis Acid Promoted Reactions*; Schinzer, D. Ed.; Kluwer Academic Publishers: Dordrecht, 1989; p 247.
30. (a) Yoshida, J.; Murata, T.; Isoe, S. *J. Organomet. Chem.* **1988**, *345*, C23. (b) Yoshida, J.; Matsunaga, S.; Murata, T.; Isoe, S. *Tetrahedron* **1991**, *47*, 615.
31. Suga, S.; Suzuki, S.; Yamamoto, A.; Yoshida, J. *J. Am. Chem. Soc.* **2000**, *122*, 10244.
32. (a) Olah, G. A.; Bollinger, J. M. *J. Am. Chem. Soc.* **1967**, *89*, 2993. (b) Olah, G. A.; Sommer, J. *J. Am. Chem. Soc.* **1968**, *90*, 4323. (c) Forsyth, D. A.; Osterman, V. M.; DeMember, J. R. *J. Am. Chem. Soc.* **1985**, *107*, 818.
33. Suga, S.; Suzuki, S.; Yoshida, J. *Org. Lett.* **2005**, *7*, 4717.
34. (a) Yoshida, J.; Sugawara, M.; Kise, N. *Tetrahedron Lett.* **1996**, *37*, 3157. (b) Yoshida, J.; Sugawara, M.; Tatsumi, M.; Kise, N. *J. Org. Chem.* **1998**, *63*, 5950. See also: Chiba, K.; Uchiyama, R.; Kim, S.; Kitano, Y.; Tada, M. *Org. Lett.* **2001**, *3*, 1245.

35. Suzuki, S.; Matsumoto, K.; Kawamura, K.; Suga, S.; Yoshida, J. *Org. Lett.* **2004**, *6*, 3755.
36. Suga, S.; Matsumoto, K.; Ueoka, K.; Yoshida, J. *J. Am. Chem. Soc.* **2006**, *128*, 7710.
37. (a) Gybin, A. S.; Smit, W. A.; Bogdanov, V. S.; Krimer, M. Z.; Kalyan, J. B. *Tetrahedron Lett.* **1980**, *21*, 383. (b) Bogdanov, V. S.; Gybin, A. S.; Cherepanova, F. G.; Smith, W. A. *Izv. Akad. Nauk SSSR, Ser Khim.* **1981**, 2681. See, also: (c) Moore, C. G.; Porter, M. *J. Chem. Soc.* **1958**, 2890. (d) Pietra, F.; Vitali, D.; *J. Chem. Soc. B.* **1970**, 623. (e) Miller, B.; Han, C. H. *J. Org. Chem.* **1971**, *36*, 1513. (f) Capozzi, G.; Lucchini, V.; Modena, G.; Rivetti, F. *J. Chem. Soc. Perkin II*, **1975**, 900. (g) Weiss, R.; Schlierf, C. *Synthesis* **1976**, 323. (h) Grewal, G.; Kaila, N.; Franck, R. W. *J. Org. Chem.* **1992**, *57*, 2084.
38. Mechanistic studies: (c) Camaioni, D. M.; Franz, J. A. *J. Org. Chem.* **1984**, *49*, 1607. (d) Okamoto, A.; Snow, M. S.; Arnold, D. R. *Tetrahedron* **1986**, *42*, 6175. (e) Camaioni, D. M. *J. Am. Chem. Soc.* **1990**, *112*, 9475. (f) Shaik, S. S.; Dinnocenzo, J. P. *J. Org. Chem.* **1990**, *55*, 3434. (g) Popielarz, R.; Arnold, D. R. *J. Am. Chem. Soc.* **1990**, *112*, 3068. (h) Norrsell, F.; Handoo, K. L.; Parker, V. D. *J. Org. Chem.* **1993**, *58*, 4929. (i) Baciocchi, E.; Bietti, M.; Putignani, L.; Steenken, S. *J. Am. Chem. Soc.* **1996**, *118*, 5952. (j) Freccero, M.; Pratt, A.; Albini, A.; Long, C. *J. Am. Chem. Soc.* **1998**, *120*, 284. Synthetic studies: (k) Shono, T.; Matsumura, Y. *J. Org. Chem.* **1970**, *35*, 4157. (l) Shono, T.; Matsumura, Y.; Hashimoto, T.; Hibino, K.; Hamaguchi, H.; Aoki, T. *J. Am. Chem. Soc.* **1975**, *97*, 2546. (m) Kumar, V. S.; Floreancig, P. F. *J. Am. Chem. Soc.* **2001**, *123*, 3842. (n) Seiders, J. R., II; Wang, L.; Floreancig, P. F. *J. Am. Chem. Soc.* **2003**, *125*, 2406. (o) Aubele, D. L.; Rech, J. C.; Floreancig, P. E. *Adv. Synth. Catal.* **2004**, *346*, 359. (p) Wang, L.; Seiders, J. R., II; Floreancig, P. E. *J. Am. Chem. Soc.* **2004**, *126*, 12596.
39. Okajima, M.; Suga, S.; Itami, K.; Yoshida, J. *J. Am. Chem. Soc.* **2005**, *127*, 6930.
40. The generation of stable ditrityl cations by the oxidative C-C bond cleavage of cyclic compounds has been reported: (a) Suzuki, T.; Nishida, J.; Tsuji, T. *Angew. Chem., Int. Ed. Engl.* **1997**, *36*, 1329. (b) Suzuki, T.; Nishida, J.; Tsuji, T. *Chem. Commun.* **1998**, 2193. See also (c) Wang, H.; Gabbai, F. P. *Org. Lett.* **2005**, *7*, 283. (d) Wang, H.; Webster, C. E.; Perez, L. M.; Hall, M. B.; Gabbai, F. P. *J. Am. Chem. Soc.* **2004**, *126*, 8189. (e) Saitoh, T.; Yoshida, S.; Ichikawa, J. *Org. Lett.* **2004**, *6*, 4563. Saitoh, T.; Ichikawa, J. *J. Am. Chem. Soc.* **2005**, *127*, 9696.

Chapter 11

Fluorenylidene and Indenyliidene Dications: Insights about Antiaromaticity

Nancy S. Mills

Department of Chemistry, Trinity University, San Antonio, TX 78212–7200

Fluorenylidene dications, such as the dications of *p*- and *m*-substituted diphenylmethylenefluorenes, show appreciable antiaromaticity. Evidence of antiaromaticity is demonstrated through ^1H NMR shifts, nucleus independent chemical shifts (NICS), magnetic susceptibility exaltation, Λ , and (anti)aromatic (de)stabilization energies, ASE. Extension of the research to indenylidenefluorene dications shows that, contrary to expectation, the indenyl cation in these dications is less antiaromatic than the fluorenyl cation. The magnitude of the antiaromaticity is evaluated through comparison to the aromaticity of related dianions and reveals that the fluorenylidene dications are more antiaromatic than the fluorenylidene dianions are aromatic.

Introduction

Aromaticity is one of the fundamental principles of organic chemistry, used to predict products from chemical reactions based on the stability of the possible products, as well as to rationalize the stability of transition states, such as the transition state of the Diels Alder reaction (*1*). Aromatic species have $4n + 2\pi$ electrons in a cyclic system that allows complete delocalization of the electrons.

While benzene was the first aromatic system studied, the formulation of Hückel's rule and the theory behind it created an impetus to prepare non-benzenoid species such as the tropylium cation and cyclopentadienyl anion that also obeyed Hückel's rule to see if these species were also aromatic. This required that the properties of aromatic compounds be defined.

Criteria for Aromaticity

The criteria used to evaluate aromaticity were based on the properties of benzene and fall into three general categories, energetic, structural, and magnetic. The *energetic* criteria focused on the greater stability of aromatic compounds compared to localized reference systems. Most commonly, the stability was evaluated through calculation, looking at resonance stability or more generally the aromatic stabilization energy (ASE) (2). In these studies, the stabilization due to the cyclic π -electron delocalization was evaluated by comparison of the energy of the species under examination to that of a localized reference system. The difficulty was in the choice of the appropriate reference system. One of the most frequently used approaches is the evaluation of ASE through isodesmic, homodesmotic reactions in which the reference systems chosen are matched in terms of the number and type of atoms, as the ring and angle strain (3). Experimental verification of the stability related to aromaticity has also been explored through the measurement of heats of reaction (4). If the species examined were a dication or dianion which could be formed by oxidation/reduction of a neutral precursor, comparison of the redox potential for formation of the aromatic di-ion could be compared to that of an analogous precursor (5,6,7).

Structural criteria considered planarity and lack of bond length alternation. Of these two properties, lack of bond length alternation has found the greatest application in the assessment of the aromaticity of benzenoid and non-benzenoid species. Probably the most commonly used method for the evaluation of bond length alternation is the harmonic oscillator measure of aromaticity, or HOMA (8). In this method, the deviation of individual bond lengths from the average bond length of the species is evaluated using the following term, in which the sum of the square of the difference of the individual bond length, R_i from the average bond length, R_{av} is multiplied by a weighting factor which includes the number of bonds in the species under consideration, $[(\alpha/n)\Sigma(R_{av}-R_i)^2]$. This term is considered the geometric term, GEO. Because there are non-aromatic species with little bond length alternation which are not aromatic (9), a second term is included which looks at the deviation of the average bond length, R_{av} , from the optimal bond length of an aromatic compound, R_{opt} . Because a defor-

mation of a bond from its optimal length requires energy, this term is called the energetic term or EN. The combination of the two terms, as shown below, is the HOMA equation.

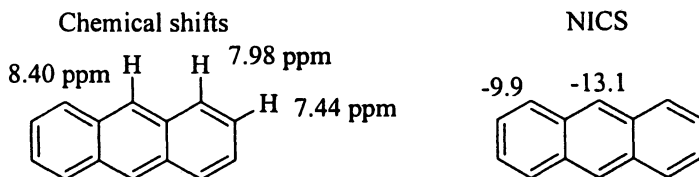
$$\text{HOMA} = 1 - \left[\alpha (\text{R}_{\text{opt}} - \text{R}_{\text{av}})^2 + \frac{\alpha}{n} \sum (\text{R}_{\text{av}} - \text{R}_i)^2 \right] = 1 - \text{EN-GEO}$$

The criterion which is most uniquely associated with aromaticity is the *magnetic* criterion in which properties associated with the presence of a ring current are evaluated. The most commonly used property is the existence of a diatropic shift in the ^1H NMR spectrum (10) although recent studies have emphasized that a diatropic shift may be the result of environmental factors as well as the presence of a ring current (11). Related to the diatropic or downfield shift of the protons on the periphery of an aromatic ring system is the paratropic or upfield shift of protons in the center of an aromatic ring system. This effect was observed in the upfield shifts of protons on the interior of annulenes prepared to test Hückel's rule in non-benzenoid aromatics (12). One can position a dummy atom in the center of a ring system and calculate the chemical shift of this atom. This shift is called the nucleus independent chemical shift or NICS (13). The NICS value for an aromatic species is negative and the magnitude of the value is a measure of relative aromaticity. Since its introduction, the procedure for obtaining the NICS value has undergone some modifications, including evaluating the chemical shift at a distance of 1 Å above the plane of the ring, denoted as NICS(1) (14) to avoid local effects of the sigma system and using the chemical shift tensor perpendicular to the ring system, in the z-axis if the ring is in the x-y plane, NICS_{zz}, to restrict the chemical shift to effects primarily from the π -system (15). Other approaches have been used to restrict the NICS values entirely to effects from the π -system using localized molecular orbitals (LMO) or canonical molecular orbitals (CMO) dissection (16,17) to remove the contributions from the σ -electrons. However, the NICS value calculated perpendicular to the π -system and 1Å above, NICS(1)_{zz}, has been shown to be almost as effective (18). A third property related to the presence of a ring current is the evaluation of magnetic susceptibility exaltation, Λ (19,20). While the magnetic susceptibility of most molecules can be evaluated by summation of the magnetic susceptibility of the bonds and nuclei in the molecule, aromatic molecules possess an enhanced magnetic susceptibility as a result of the ring current created when the molecule is placed in a magnetic field, a magnetic susceptibility exaltation. As was true for the NICS values, Λ for an aromatic species has a negative sign. Magnetic susceptibility can be measured experimentally (21) but is often calculated using, for example, the CSGT (continuous set of gauge transformations) method found in a number of programs, including Gaussian (22). Because the exaltation comes from the

difference in magnetic susceptibility of the aromatic species and the susceptibility of localized bond increments, an appropriate reference system must be defined, raising concerns about that reference system that are similar to concerns raised when resonance energy or aromatic stabilization energies are calculated. In addition, Δ is inversely related to the square of the area of the ring (20), requiring an additional correction.

Problems with the Use of the Criteria

If these criteria measure properties related to aromaticity, it seems as though one could choose the most "accessible" of the criteria and use it to evaluate the aromaticity of a particular species. Unfortunately, the use of the different criteria don't always lead to the same conclusion about relative aromaticity, although they are generally all capable of determining whether a species is aromatic, non-aromatic or antiaromatic. There are a number of examples but the relative aromaticity of the rings of acenes provides a succinct picture of the difficulties. The central ring of anthracene has long been considered as less aromatic than the outer rings because addition reactions such as bromination or Diels-Alder reactions occur preferentially at the central ring, suggesting its diminished aromaticity (23). However, the ^1H NMR shifts for protons of the center ring are further downfield than the outer rings (24) and the NICS values are more negative for the center ring (25), indicating the greater aromaticity of that ring. Similar conclusions can be drawn for other acenes.

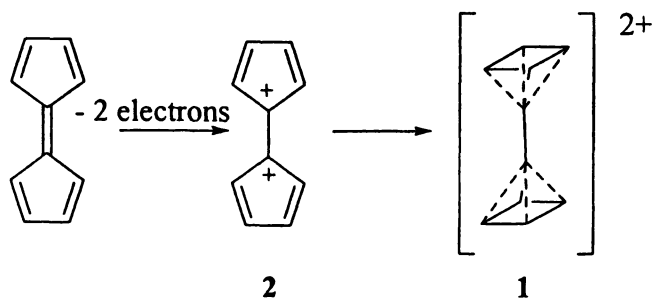


This presents a real problem because when the application of different criteria results in different conclusions about relative aromaticity, our understanding of the phenomenon is obviously incomplete. A number of researchers have attempted to develop a more complete understanding of aromaticity by looking at a variety of aromatic species, but as a recent paper demonstrated (26), even a study that begins with the goal of laying to rest these conflicts can end with the authors agreeing to disagree about the appropriate measure of aromaticity.

We have chosen to examine the problem not by studying more aromatic compounds but instead by looking at antiaromatic species. This approach has been utilized very infrequently (27) because of the perception that antiaromatic species should be so reactive that they would be difficult to study. As we have discovered and will discuss below, antiaromatic dications are very amenable to study.

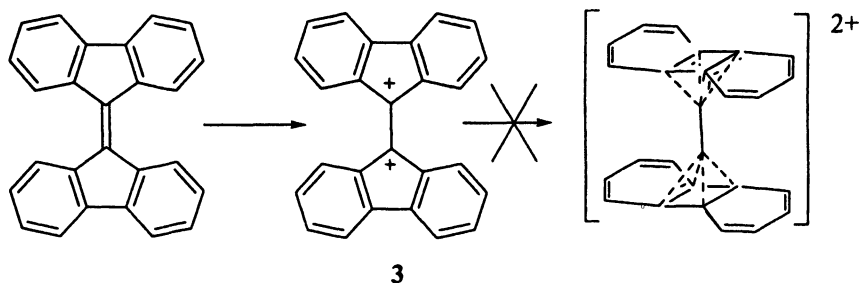
Fluorenylidene Dications as Antiaromatic Species

We were not intending to study antiaromatic species when we began our current research program. We had previously studied unusual forms of aromaticity in hydrocarbon dianions, such as Υ -aromaticity (28) and when we turned our attention to dications, we planned to continue similar studies. We were intrigued by a result of computational studies that suggested that dication **1** might possess three-dimensional aromaticity, because each hypervalent pyramidal cation could be considered as possessing 6 π -electrons holding the capping atom to the cyclobutadienyl ring system. In theory, **1** could be prepared from [5.5]fulvalene by the removal of two electrons to give the antiaromatic dication **2** which would be expected to rearrange to the potentially three-dimensionally aromatic **1** (29). However, [5.5]fulvalene is very difficult to handle

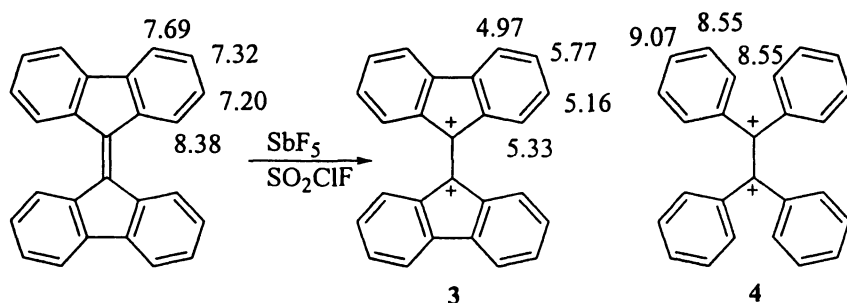


so we decided to begin our explorations with tetrabenzo[5.5]fulvalene. Upon oxidation to the dication **3**, no rearrangement occurred and it was necessary to determine whether **3** was antiaromatic as anticipated.

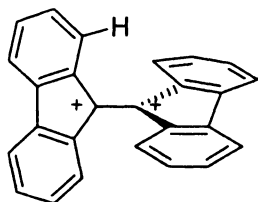
The ^1H NMR spectrum showed the paratropic shift expected of protons in an antiaromatic system. Because it is difficult to evaluate the magnitude of paratropic shift in a charged species, the average shift of protons in **3** were com-

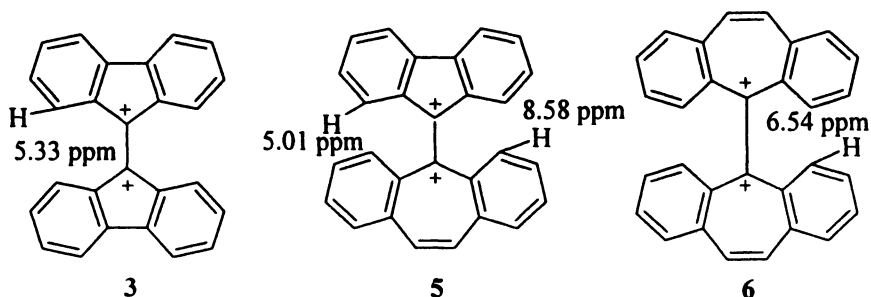


pared to a model system, the dication of tetraphenyl ethylene, **4**. The protons of dication **3** were shifted upfield by 3.34 ppm, compared to the average shift of protons of **4** (29).



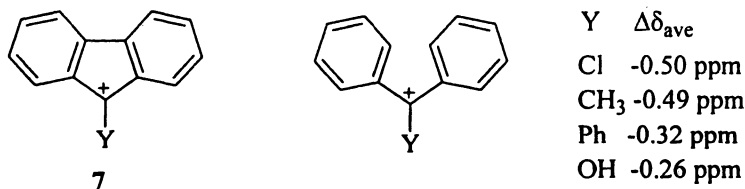
The ^1H NMR shifts showed additional evidence of antiaromaticity. The central double bond of the neutral precursor, tetrabenzo[5.5]fulvalene, is prevented from the optimal planarity by interactions of the ortho hydrogens on the two fluorenyl systems. Upon oxidation, one would anticipate that the steric strain would be released by allowing the two rings to become almost perpendicular. Indeed, the geometry of **3** optimized at the density functional theory level possesses a dihedral angle between the rings of about 60° although the potential energy surface is relatively flat, with the geometry in which the fluorenyl ring systems are perpendicular lying only a couple of kcal/mol higher in energy than the lowest energy conformation (29). This results in a situation in which the ortho protons of one fluorenyl ring system are close to the center of the π -system of the other fluorenyl ring system, as shown below. If the fluorenyl



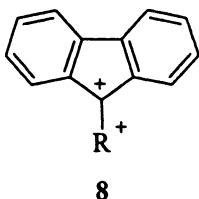


cation ring system was antiaromatic, this would cause a diatropic (downfield) shift of the ortho proton. However, in order to determine that the resonance for the ortho proton has been shifted downfield, it must be compared with the shift of an analogous proton on an appropriate reference system (30). That system could be the dication of tetrabenzo[5.7]fulvalene, 5. The ^1H NMR shifts of the ortho protons on the fluorenyl ring system of 3 resonates at 5.33 ppm, compared to 5.01 ppm for the analogous proton on 5. The shifts are even more dramatic for the protons on the 7-membered rings of 5 and 6, because the larger bond angle in the larger ring forces the ortho protons closer to the π -orbitals of the opposing ring systems. Thus the ortho proton of the tropylium ring system of 5 is shifted substantially further downfield by the antiaromatic fluorenyl ring system than is the analogous ortho proton on the tropylium ring of 6.

Is the behavior of fluorenylidene dications, such as 3 or 5 unusual? Comparison of the average chemical shifts of fluorenyl cations 7 with the analogous diphenylmethyl cations shows minimal antiaromaticity in the monocations, with paratropic shifts of 0.5 ppm or less (29). The dramatic para-



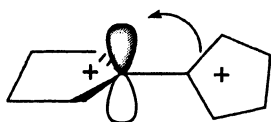
tropic shift for 3 suggested that it might be part of a group of antiaromatic fluorenylidene dications, 8, and that the antiaromaticity of the fluorenyl system might be moderated by changes in the nature of R. This would allow a systematic investigation of antiaromaticity through variation in R from which insights into aromaticity might be gleaned.



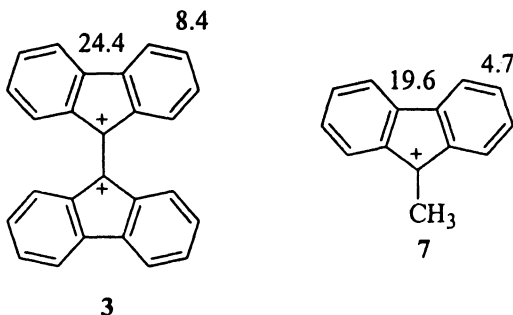
Since antiaromaticity is related to aromaticity, it should be defined by many of the same criteria (31). That is, antiaromatic species should be less stable in comparison to a localized reference system, should demonstrate paratropic shifts in the ^1H NMR spectrum, should have positive NICS values, and positive values of magnetic susceptibility exaltation, Λ . While the presence of enhanced bond length alternation has been considered as evidence of antiaromaticity (31), the deformation of square cyclobutadiene to rectangular cyclobutadiene to reduce its antiaromaticity suggests that the lack of bond length alternation is also a characteristic of antiaromatic compounds.

In the study of **8**, one problem remains. In species like **3** and **5**, the ring systems are not planar, thus the two ring systems can't interact through resonance. If the substituent R is to affect the antiaromaticity of the fluorenyl ring system, how is the effect transmitted to the ring system?

We have considered two potential models for this interaction and the nature of R determines which is operating. Evidence for the first model comes from the ^{13}C NMR shift for C-9 of **3**, 189 ppm, compared to the 9-methylfluorenyl cation, **7** R=CH₃, 228 ppm. The upfield shift for C-9 suggests an increase in electron density, which could be accomplished through a σ donation (32), as shown below. Changes in the electronic nature of the σ -bonds of one ring system can be



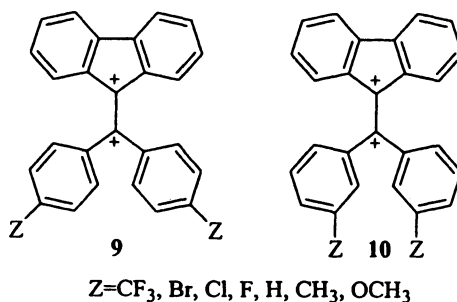
transmitted to the other ring system through hyperconjugation. A second type of interaction was suggested by the NICS(1) values for **3** compared to **7**, R=CH₃, as shown below. The greater antiaromaticity of the 6-membered ring of **3** may



be the result of greater delocalization forced upon the ring system by the positively charged substituent. That is, an increase in the electron deficiency of the substituent on carbon 9 of the fluorenyl cation could result in greater antiaromaticity of the fluorenyl system through greater delocalization. Support for this premise came from examination of the ^{13}C NMR shifts of **3** compared to the four derivatives of **7**, $\text{Y}=\text{CH}_3$, C_6H_5 , Cl , and OH , which demonstrated that the positive charge was delocalized more effectively to the 6-membered ring of **3** than the corresponding ring of **7** (29).

Dications of Diphenylmethylidene fluorene as Antiaromatic Species

Oxidation of *p*- and *m*-substituted diphenylmethylidene fluorenes resulted in the formation of a suite of dications, **9** and **10**, which were shown to be antiaromatic through magnetic and energetic criteria.



Magnetic criteria

Oxidation of *p*-substituted diphenylmethylidene fluorenes with $\text{SbF}_5/\text{SO}_2\text{ClF}$ gave dications **9**, $\text{Z}=\text{CH}_3$, Cl , and F which could be characterized by NMR spectroscopy (33). The ^1H NMR shifts ranged from 4.44 to 5.86 ppm, with the dications with more electron-withdrawing substituents showing the greatest upfield shift. Although ^{13}C NMR shifts are not appropriate to evaluate aromaticity or antiaromaticity, they can be used to evaluate the quality of calculated NMR shifts. Figure 1, a plot of the experimental ^{13}C NMR shifts of **9** vs the shifts calculated with density functional theory methods (B3LYP/6-31g(d)) on geometries optimized at the same level shows very good agreement.

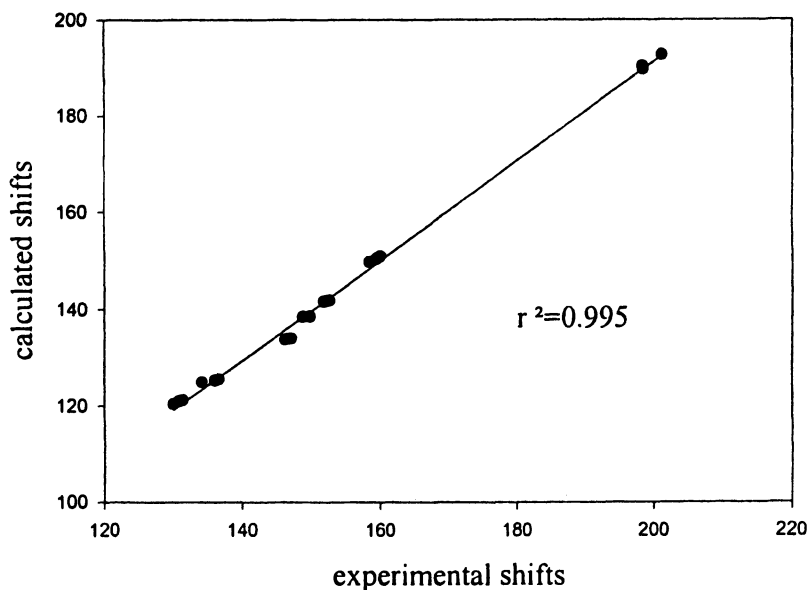


Figure 1. Calculated vs experimental shifts, **9** (Reproduced from reference 34. Copyright 1999 American Chemical Society.)

This provides support for the reliability of the nucleus independent chemical shift values reported in Table I, which are calculated by the same method. These values show that the fluorenyl systems are antiaromatic in **9** and **10**. In addition, the antiaromaticity can be varied by the nature of the substituent and their placement.

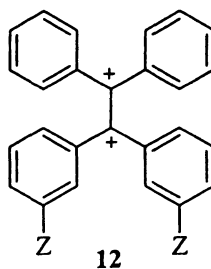
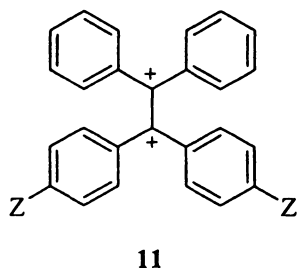
Energetic and structural criteria

The most common evaluation of aromaticity via energetic criteria is done using calculations either a type of isodesmic reaction (34) or comparison of two isomers that differ only through the aromaticity of one (3). We were interested in the possibility of evaluating stability experimentally and the electrochemical formation of dications such as **8** was attractive. In this approach, the redox potential for formation of the dication would be compared to the redox potential for formation of dications which could not be antiaromatic. If **8** was antiaromatic, its redox potential should be larger and more positive than that of the reference system. This approach was applied to the evaluation of the antiaromaticity of **9**

Table I. Nucleus independent chemical shift (NICS(1)) of the fluorenyl systems of 9 and 10

	9			10		
	<i>NICS(1)-</i> 5	<i>NICS(1)-</i> 6	<i>Sum of</i> <i>NICS</i>	<i>NICS(1)-</i> 5	<i>NICS(1)-</i> 6	<i>Sum of</i> <i>NICS</i>
<i>CF</i> ₃	24.0	10.0	44.0	24.4	10.4	45.2
<i>Br</i>	22.6	8.6	39.8	23.7	9.8	43.3
<i>Cl</i>	22.9	8.9	40.7	23.9	10.1	44.1
<i>F</i>	22.9	9.1	41.1	24.1	10.3	44.7
<i>H</i>	23.1	8.9	40.9	23.2	8.9	41.0
<i>CH</i> ₃	22.2	7.5	37.2	22.8	8.6	40.0
<i>OCH</i> ₃	22.2	7.5	37.2	22.6	8.4	39.4

SOURCE: Reproduced from Reference 7. Copyright 2005 American Chemical Society.



and **10** (7). The redox potentials are shown in Table II and it is apparent that the more positive redox potential was for formation of the *m*-substituted **10** rather than *p*-substituted **10**. The redox potentials for formation of the reference compounds **11** and **12** were also obtained and demonstrate that **9/10** are less stable than the reference compounds, which is consistent with antiaromatic behavior.

While the redox potentials for formation of **9** and **10** indicates the greater instability of these dications compared to reference systems, is this instability due to antiaromaticity? The plot of the redox potentials vs the sum of the NICS values for the fluorenyl system, Figure 2, next page, shows a reasonable relationship between these energetic and magnetic measures of antiaromaticity.

The variation in bond length alternation for **9** and **10** was examined using the HOMA approach (8) and it was found that there was relatively little bond length alternation in the fluorenyl systems and that the bond length alternation was affected very little by the substituent (7). Thus, the data suggest that antiaromatic species demonstrate little bond length alternation, but the technique is not sensitive enough to detect the differences seen in NICS values and other measures of antiaromaticity such as magnetic susceptibility exaltation.

Summary of Antiaromaticity of Fluorenylidene Dications

Fluorenylidene dications **8** have been shown to be more antiaromatic than fluorenyl monocations **7**: When the substituent R on **8** has electron-withdrawing

Table II. Redox potentials^a and nucleus independent chemical shifts for **9 and **10****

	<i>Redox potential for 9</i>	<i>Redox potential for 11</i>	<i>Sum of NICS(1) fluorenyl system</i>	<i>Redox potential for 10^a</i>	<i>Redox potential for 12</i>	<i>Sum of NICS(1) fluorenyl system</i>
<i>CF₃</i>	1.54	1.45	44.0	1.53	1.44	45.2
<i>Br</i>	1.33	1.25	39.8	1.44	1.32	43.3
<i>Cl</i>	1.31	1.24	40.7	1.44	1.32	44.1
<i>F</i>	1.26	1.19	41.1	1.41	1.33	44.7
<i>H</i>	1.27	1.20	41.0	1.27	1.20	41.0
<i>CH₃</i>	1.06	1.08	37.2	1.26	1.14	40.0
<i>OCH₃</i>	1.03	0.88	35.2	^b	^b	39.4

^a potentials in V vs ferrocene as internal reference.

^b The cyclic voltammogram was so poorly resolved that the redox potentials for the cation radical and dication couldn't be distinguished.

SOURCE: Reproduced from Reference 7. Copyright 2005 American Chemical Society.

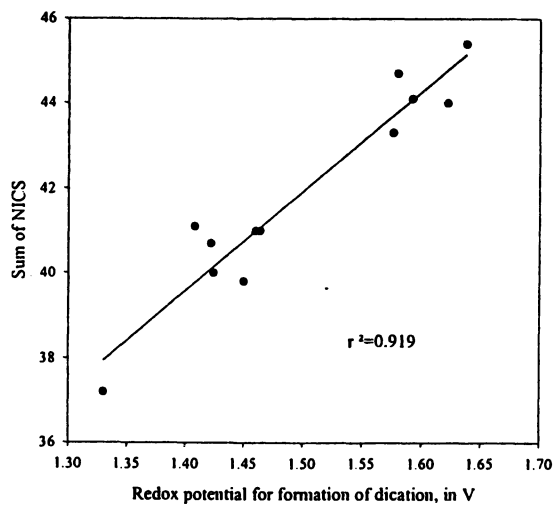
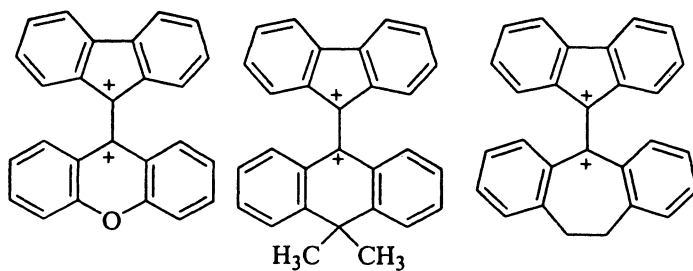


Figure 2. Redox potentials for formation of **9** and **10** vs the sum of NICS values (Reproduced from reference 7. Copyright 2005 American Chemical Society.)

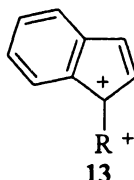


groups, the fluorenyl system becomes more antiaromatic. In the majority of systems studied, it appears that the primary effect of the electron-poor substituent is to force greater delocalization of charge in the fluorenyl system, the second method of interaction proposed for the substituent and the fluorenyl ring system. The first method of interaction proposed, σ to p donation, appears to operate in systems with cyclic substituents, such as **3** and **5** and those shown below(35).

In the majority of the systems examined, the magnetic and energetic criteria used gave similar results, suggesting that either is an effective measure of antiaromaticity in fluorenylidene dications.

Extension of Research to Indenyliidene Dications

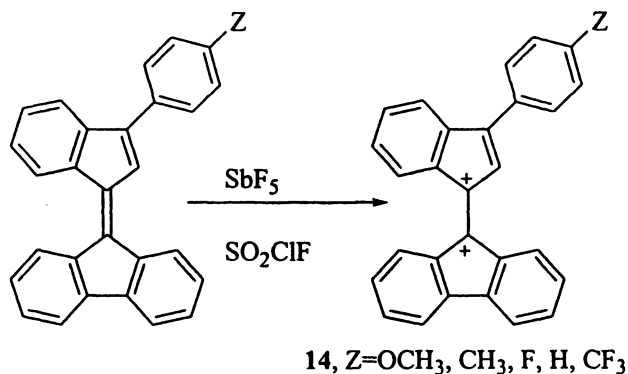
The results from studies on fluorenylidene dications such as **8** demonstrate clearly that species of this type are antiaromatic. However, extension of these studies to indenylidene dications such as **13** has important advantages. The



indenyl cation is known to be more antiaromatic than the fluorenyl cation **7**, Y=H (36) SO it was anticipated that examination of **13** would give results in which the response to the criteria was enhanced, giving a more sensitive measure of the factors that affect antiaromaticity. In addition, the indenyl system has a “probe” proton that would allow assessment of the antiaromaticity of the five-membered ring. In the fluorenylidene dications, the five-membered ring had larger NICS values, suggesting that there was a greater amount of antiaromaticity in that ring. However, the absence of protons on the five-membered ring in the fluorenyl system prevents experimental confirmation of changes in the degree of antiaromaticity. Because two of the positions on the five-membered ring are appropriate for substitution, it should be possible to examine substituent effects on that (potentially) more antiaromatic ring system. Finally, the removal of one benzene ring would allow the five-membered ring to respond more effectively to structural changes caused by changes in antiaromaticity.

Indenylidene fluorene dications

Our investigations of derivatives of **13** began with the oxidation of 3-phenylindenylidenefluorenes to give **14** (*37*). The indenylidenefluorene system would allow us to examine indenyl cations in the context of fluorenyl cations. In



a sense, the fluorenyl system served as an internal calibration of the behavior of the indenyl cations. Because we were concerned about the stability of the indenyl cation, we added a phenyl substituent in the 3-position to add additional stabilization. The phenyl substituent can also be substituted in the *p*-position to provide a method for varying electron density to explore its effect on antiaromaticity.

Oxidation of 3-*p*-substituted-phenyl-indenylidenefluorenes with SbF₅ in SO₂ClF gave **14** for all substituents except OCH₃ which failed to oxidize, presumably because complexation with SbF₅ resulted in a species whose dication was too unstable to form. The dication for **14**, Z=H, is shown in Figure 2. The fluorenyl, indenyl, and phenyl protons are labeled and demonstrate conclusively that the greatest paratropic shift is found for protons on the fluorenyl system. Thus the fluorenyl cation in **14** appears to be more antiaromatic than the indenyl cation.

We were concerned that we had overcompensated for the instability of the indenyl cation with the inclusion of the stabilizing phenyl substituent. That is, did the presence of the phenyl substituent cause a change in the resonance hybrid giving an enhanced contribution of **15** over **16**?

We have not yet prepared the unsubstituted indenylidene fluorene dication **17** but the NICS(1)_{zz} (*18*) values demonstrate that the fluorenyl cation is still more antiaromatic than the indenyl cation, see Table III.

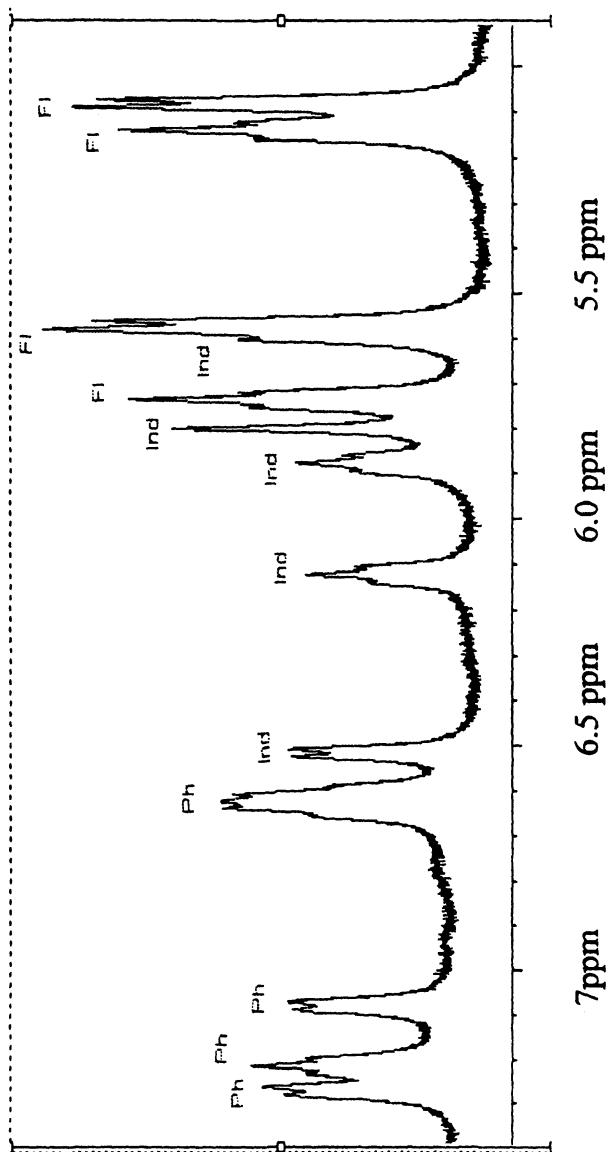


Figure 3. ^1H NMR spectrum of 14, Z=H, in SO_2ClF , referenced to external TMS (Reproduced from reference 38. Copyright 2006 American Chemical Society.)

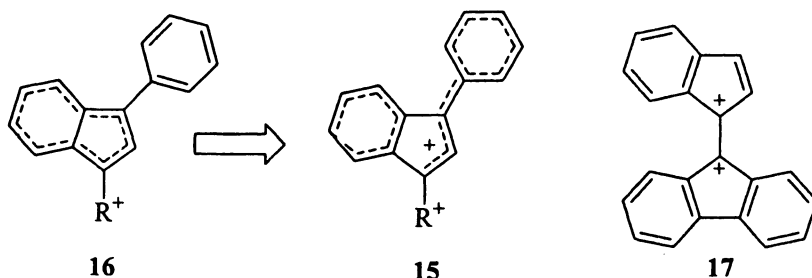


Table III. Nucleus independent chemical shifts^a

	<i>Indenyl ring system</i>		<i>Fluorenyl ring system</i>	
	<i>NICS(1)_{xx}-5</i>	<i>NICS(1)_{zz} 6-1</i>	<i>NICS(1)_{zz} 5-1</i>	<i>NICS(1)_{zz} 6-1</i>
14 , Z=CF ₃	44.61	7.18	70.25	26.88
14 , Z=F	41.71	5.06	69.15	25.71
14 , Z=H	39.04	2.86	68.84	25.21
14 , Z=CH ₃	34.81	-1.62	67.50	23.78
14 , Z=OCH ₃	29.49	-4.38	64.34	20.09
17	89.98	48.71	95.98	61.49

^a The nucleus independent chemical shifts were calculated for ghost atoms placed one Å above and below the center of each ring system. The shifts were calculated with the GIAO method in Gaussian03 (22) at the B3LYP/6-31g(d) level on geometries optimized at the same level. The chemical shift tensor perpendicular to each planar ring system was used for the NICS values.

SOURCE: Reproduced from Reference 38. Copyright 2006 American Chemical Society

Evaluation of Antiaromaticity for Fluorenyl and Indenyl Cations Revisited

Fluorenyl cation

As stated previously, the fluorenyl system of monocations **7** is less antiaromatic than the fluorenyl system in the tetrabenz[5.5]fulvalene dication **3**, as evaluated through NICS values. Table IV gives magnetic susceptibility exaltation values as well as (anti)aromatic (de)stabilization energies for **7** and **3**, demonstrating that by a variety of measures, **3** is more antiaromatic than **7**. Measures of aromaticity such as magnetic susceptibility exaltation are dependent upon the size of the ring (20). Therefore, it is appropriate to consider the values for **3** and for **7** as a function of ring size, to divide the values for **3** by 2 to essentially normalize the data by ring size. When considered this way, **3** is still more antiaromatic than **7**. Schleyer, et. al. (27), have suggested that **7** should be considered as effectively non-aromatic because the aromaticity of the two benzene rings compensates for the antiaromaticity of the cyclopentadienyl ring. While we don't agree with the designation of non-antiaromatic, the diminished antiaromaticity supports this "balancing act."

Indenyl cation

To perform a similar evaluation for the indenyl cation, **18**, we must examine the bis-indenylidene dication, **19**, and the appropriate data for both systems is given in Table IV. While **19** is more antiaromatic than **18** by all measures, the dependence of the measure of aromaticity and presumably antiaromaticity on ring size requires that the values for **19** be divided by 2. When examined in this manner, the indenyl cation **18** is more antiaromatic than **19**, in contrast to the behavior of the fluorenyl system in **7** and **3**.

To better understand the behavior of these antiaromatic cations and dications, it would be nice to be able to use the NICS values to evaluate any differences in the antiaromaticity for individual rings. We need first to establish that the NICS values for each ring system are really representative of some aspect of antiaromaticity. To evaluate that, we examined the relationship of the sum of the NICS values to a global measure of antiaromaticity, magnetic susceptibility exaltation, Λ . While the sum of the NICS values has been suggested as a global measure of aromaticity (14) and has been used as such (38), there has been no study that compares the summation of NICS with global measures of aromaticity. Among concerns expressed is the concern that

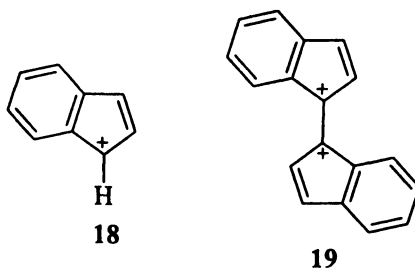


Table IV. Energetic and magnetic measures of antiaromaticity for fluorenyl systems, 7, Y=H, and 3, indenyl systems, 18 and 19, *vide infra*, and indenylidenefluorene dications

	<i>ASE</i>	<i>NICS(1)-5</i>	<i>NICS(1)-6</i>	Σ <i>NICS</i>	<i>A</i>
7	16.3	67.75	20.05	107.85	36.8
3	25.5	74.04	31.41	274.06	95.8
18	26.8	104.69	49.43	154.12	47.4
19	45.5	75.74	45.90	243.26	80.6
17	42.6			356.43	121.3
17-indenyl		89.98	48.71	138.69	
17-fluorenyl		95.98	60.88	217.74	

“double-counting” could occur with a simple summation because bonds are shared within rings. Finally, the relationship for antiaromatic species has not been carefully examined. We show the plot of Λ vs $\Sigma\text{NICS}(1)_{zz}$ for the species in Table IV in Figure 4. It is apparent that the relationship is very good.

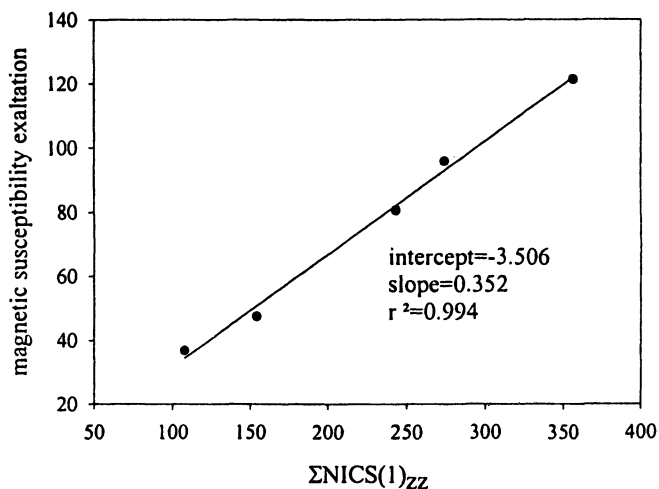


Figure 4. Magnetic susceptibility exaltation Λ vs $\Sigma\text{NICS}(1)_{zz}$

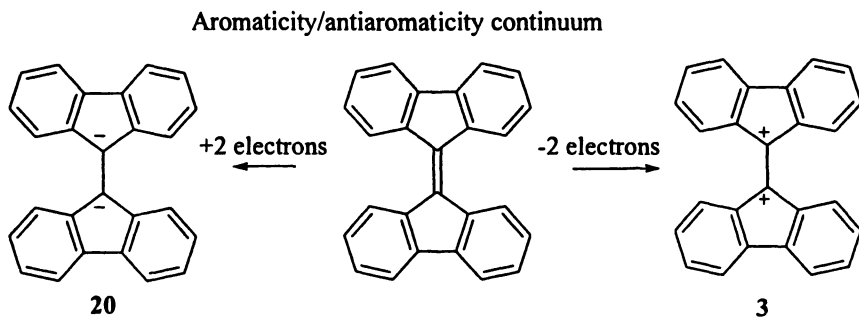
The excellent quality of the relationship suggests that it would be appropriate to evaluate contributions to the overall antiaromaticity through the individual contributions to each ring, as measured by the NICS values for each ring. This approach allows us to suggest that a key difference between **18** and **19** is that the indenyl cation has a greater amount of antiaromaticity in the 5-membered ring and we are currently trying to understand the origin of that effect.

The relationship of the indenyl and fluorenyl rings of **17** can be understood by the approach also. Evaluation of the antiaromaticity of the ring systems in **17** must utilize this method because global measures of antiaromaticity like Λ obscure the contributions from the individual ring systems. When examined in this manner, it is apparent that the indenyl system of **17** is quite similar to the indenyl systems of **18** and **19** in terms of the magnitude of the antiaromaticity of the 6-membered ring and relatively similar in terms of the 5-membered ring. However, both rings of the fluorenyl system of **17** show greatly enhanced antiaromaticity over the analogous rings of **3** and **7**.

Providing a Context for Antiaromaticity; the Aromaticity/antiaromaticity Continuum

The previous sections have demonstrated the antiaromaticity of a variety of indenyl and fluorenyl cations and dications but there has been no attempt to evaluate the degree of antiaromaticity. That is, are these species very antiaromatic or not particularly antiaromatic at all? We need a context for the numbers and the corresponding aromatic dianions provides that context.

That is, just as oxidation of tetrabenzof[5.5]fulvalene resulted in formation of two antiaromatic fluorenyl cations linked by a single bond, reduction should give two aromatic fluorenyl anions, linked by a single bond, **20**. We call this relationship the aromaticity/antiaromaticity continuum and can apply the same measures of aromaticity to **20** as were applied to **3**, to evaluate relative aroma-



ticity/antiaromaticity (**39**). Those relationships are shown in Table V and demonstrate that **20** is aromatic by all measures used while **3** is antiaromatic. Of equal interest is the observation that by all measures used, magnetic and energetic, the antiaromatic dication **3** is more antiaromatic than the aromatic dianion **20** is aromatic. This was of interest to us because the current understanding of antiaromaticity would suggest that an antiaromatic system would find some means to minimize its antiaromaticity, such as the bond deformation shown by cyclobutadiene. We are examining the apparent enhanced antiaromaticity of fluorenylidene and indenylidene dications over the corresponding dianions in our labs.

Conclusions

We have demonstrated that oxidation of fluorenylidenes and indenylidenes results in the formation of dications with appreciable antiaromaticity. The antiaromaticity of these species was examined for a series of dications from

Table V. Comparison of measures of aromaticity/antiaromaticity for 3 and 20

	$\Sigma\text{NICS}(1)^a$	Λ	ASE
3	95.8	38.2	32.7
20	-81.8	-35.2	-24.7

^a NICS(1) values were included in the table rather than NICS(1)_{zz} because those were the values used in Reference 40

SOURCE: Reproduced from Reference 40. Copyright 2006 American Chemical Society

diphenylmethylidene fluorenes. Their antiaromaticity was demonstrated through magnetic properties, including paratropic shifts in the ¹H NMR spectrum, positive nucleus independent chemical shift (NICS) values, and positive values of magnetic susceptibility exaltation, Λ . Energetic criteria, such as (anti)aromatic (de)stabilization energies, ASE, from isodesmic reactions and more positive redox potentials for formation of the dication also supported their antiaromaticity. The antiaromaticity of the fluorenyl system could be altered in a systematic way through variation in the positively charged substituent in position 9. That substituent, although not co-planar with the fluorenyl system, can interact with the fluorenyl system through σ to p donation or by forcing greater delocalization in the fluorenyl system through the magnitude of its positive charge.

The antiaromaticity of indenyl cations was examined in the dication of indenylidene fluorenes. Contrary to expectation, the fluorenyl cation was more antiaromatic than the indenyl cation in these systems. The sum of NICS(1)_{zz} values was linearly related to global measures of antiaromaticity such as Λ , suggesting that they could be used to evaluate antiaromaticity in a local sense, for individual rings.

References

1. Corminboeuf, C.; Heine, T.; Weber, J. *Org. Lett.* **2003**, *5*, 1127-1130.
2. Cyranski, M. K. *Chem. Rev.* **2005**, *105*, 3773-3811.
3. Schleyer, P. v. R.; Puehlofer, F. *Org. Lett.* **2002**, *4*, 2873-2876.
4. Cohen, N.; Benson, S. W. *Chem. Rev.* **1993**, *93*, 2419-2438.
5. Breslow, R.; Murayama, D. R.; Murahashi, S-I.; Grubbs, R. *J. Am. Chem. Soc.* **1973**, *95*, 6688-6699.
6. Mills, N. S.; Benish, M. M.; Ybarra, C. *J. Org. Chem.* **2002**, *67*, 2003-2012.
7. Mills, N. S.; Tirla, C.; Benish, M. A.; Rakowitz, A., J.; Bebell, L. M.; Hurd, C. M. M.; Bria, A. L. M. *J. Org. Chem.* **2005**, *70*, 10709-10716.
8. Krygowski, T. M.; Cyranski, M. K. *Chem. Rev.* **2001**, *101*, 1385-1419.

9. Krygowski, T. M.; Cyranski, M. *Tetrahedron* **1996**, *52*, 1713-1722.
10. Mitchell, R. H. *Chem. Rev.* **2001**, *101*, 1301-1316.
11. Wannere, C. S.; Corminboeuf, C.; Allen, W. D.; Schaefer, H. F., III.; Schleyer, P. v. R. *Org. Lett.* **2005**, *7*, 1457-1460.
12. Sondheimer, F. *Accts. Chem. Res.* **1972**, *5*, 81-91.
13. Schleyer, P. v. R.; Maerker, C.; Dransfeld, A.; Jiao, H.; Hommes, N. J. v. E. *J. Am. Chem. Soc.* **1996**, *118*, 6317-6318.
14. Schleyer, P. v. R.; Manoharan, M.; Wang, Z.-X.; Kiran, B.; Jiao, H.; Puchta, R.; Hommes, N. J. R. v. E. *Org. Lett.* **2001**, *3*, 2465-2468.
15. Steiner, E.; Fowler, P. W.; Jennekens, L. W. *Angew. Chem. Int. Ed. Eng.* **2001**, *40*, 362-366.
16. Kutzelnigg, W. *Isr. J. Chem.* **1980**, *19*, 193-200.
17. Pipek, J.; Mezey, P. G. *J. Chem. Phys.* **1989**, *90*, 4916-4926.
18. Fallah-Bagher-Shaidaei, H.; Wannae, C. S.; Corminboeuf, C.; Puchta, R.; Schleyer, P. v. R. *Org. Lett.* **2006**, *8*, 863-866.
19. Dauben, H. J. J.; Wilson, D. J.; Laity, J. L. *J. Am. Chem. Soc.* **1968**, *90*, 811-813.
20. Gayoso, J.; Ouamerali, O. *Rev. Roum. Chim.* **1981**, *26*, 1035-1040.
21. van Zijl, P. C. M.; Ruessink, B. H.; Bulthuis, J.; MacLean, C. *Accts. Chem. Res.* **1984**, *17*, 172-180.
22. Frisch, M. J.; Trucks, G. W.; Schlegel, H. B.; Scuseria, G. E.; Robb, M. A.; Cheeseman, J. R.; Montgomery, Jr., J. A.; Vreven, T.; Kudin, K. N.; Burant, J. C.; Millam, J. M.; Iyengar, S. S.; Tomasi, J.; Barone, V.; Mennucci, B.; Cossi, M.; Scalmani, G.; Rega, N.; Petersson, G. A.; Nakatsuji, H.; Hada, M.; Ehara, M.; Toyota, K.; Fukuda, R.; Hasegawa, J.; Ishida, M.; Nakajima, T.; Honda, Y.; Kitao, O.; Nakai, H.; Klene, M.; Li, X.; Knox, J. E.; Hratchian, H. P.; Cross, J. B.; Bakken, V.; Adamo, C.; Jaramillo, J.; Gomperts, R.; Stratmann, R. E.; Yazyev, O.; Austin, A. J.; Cammi, R.; Pomelli, C.; Ochterski, J. W.; Ayala, P. Y.; Morokuma, K.; Voth, G. A.; Salvador, P.; Dannenberg, J. J.; Zakrzewski, V. G.; Dapprich, S.; Daniels, A. D.; Strain, M. C.; Farkas, O.; Malick, D. K.; Rabuck, A. D.; Raghavachari, K.; Foresman, J. B.; Ortiz, J. V.; Cui, Q.; Baboul, A. G.; Clifford, S.; Cioslowski, J.; Stefanov, B. B.; Liu, G.; Liashenko, A.; Piskorz, P.; Komaromi, I.; Martin, R. L.; Fox, D. J.; Keith, T.; Al-Laham, M. A.; Peng, C. Y.; Nanayakkara, A.; Challacombe, M.; Gill, P. M. W.; Johnson, B.; Chen, W.; Wong, M. W.; Gonzalez, C.; Pople, J. A.; revision B.03 ed.; Gaussian, Inc.: Pittsburgh PA, 2004.
23. Grandmougin, E. *Compt. rend.* **1921**, *173*, 1176-1178.
24. Hazato, G. *J. Chem. Phys.* **1957**, *27*, 605-606.
25. Schleyer, P. v. R.; Manoharan, M.; Jiao, H.; Stahl, F. *Org. Lett.* **2001**, *3*, 3643-3646.
26. Cyranski, M. K.; Krygowski, T. M.; Katritzky, A. R.; Schleyer, P. v. R. *J. Org. Chem.* **2002**, *67*, 1333-1338.

27. Tidwell, T. *Chem. Rev.* **2001**, *101*, 1333-1348.
28. Mills, N. S.; Shapiro, J.; Hollingsworth, M. J. *Am. Chem. Soc.* **1981**, *103*, 1263-1264.
29. Olah, G. A.; Prakash, G. K. S.; Liang, G.; Westerman, P. W.; Kunde, K.; Chandrasekhar, J.; Schleyer, P. v. R. *J. Am. Chem. Soc.* **1980**, *102*, 4485-4492.
30. Mills, N. S. *J. Am. Chem. Soc.* **1999**, *121*, 11690-11696.
31. Malandra, J. L.; Mills, N. S.; Kadlecck, D. E.; Lowery, J. A. *J. Am. Chem. Soc.* **1994**, *116*, 11622-11624.
32. Krygowski, T. M.; Cyranski, M. K.; Hafelinger, G.; Katritzky, A. R. *Tetrahedron* **2000**, *56*, 1783-1796.
33. Larmertsma, K. *Chem. Intermed.* **1988**, *9*, 141-169.
34. Mills, N. S.; Malinky, T.; Malandra, J. L.; Burns, E. E.; Crossno, P. *J. Org. Chem.* **1999**, *64*, 511-517.
35. Herndon, W. C.; Mills, N. S. *J. Org. Chem.* **2005**, *70*, 8492-8496.
36. Mills, N. S.; Malandra, J. L.; Burns, E. E.; Green, A.; Unruh, K. E.; Kadlecck, D. E.; Lowery, J. A. *J. Org. Chem.* **1997**, *62*, 9318-9322.
37. Jiao, H.; Schleyer, P. v. R.; Mo, Y.; McAllister, M. A.; Tidwell, T. T. *J. Am. Chem. Soc.* **1997**, *119*, 7075-7083.
38. Mills, N. S.; Llagostero, K. B.; Tirla, C.; Gordon, S.; Carpenetti, D., *J. Org. Chem.*, in press.
39. Havenith, R. W. A.; Jiao, H.; Jenneskens, L. W.; van Lenthe, J. H.; Sarobe, M.; Schleyer, P. v. R.; Kataoka, M.; Nacula, A.; Scott, L. T. *J. Am. Chem. Soc.* **2002**, *124*, 2363-2370.
40. Mills, N. S.; Benish, M. A. *J. Org. Chem.* **2006**, *71*, 2207-2213.

Chapter 12

Generation, Stability, and Reactions of Alkylated Fullerene Cations

Toshikazu Kitagawa

Department of Chemistry for Materials, Graduate School of Engineering,
Mie University, Tsu, Mie 514-8507, Japan

Cationic species of fullerenes have long been considered to be difficult to prepare, based on the well-known resistance of C_{60} toward oxidation. However, reliable methods are now available for the preparation of alkylated fullerene cations RC_{60}^+ and RC_{70}^+ as long-lived species, allowing their structures and properties to be investigated in detail. Precise evaluation of their thermodynamic stabilities revealed that these cations have stabilities comparable to the *tert*-butyl cation.

Background

Fullerenes are spherical molecules consisting exclusively of sp^2 carbons that form a three-dimensional π -conjugated system. They are fairly electronegative molecules, which can undergo single- and multi-electron reductions to produce their reduced forms, e.g. C_{60}^{n-} ($n = 1-6$) (1-4). C_{60} typically behaves as an electron-deficient olefin, with a consequence that it readily undergoes addition of nucleophiles (R^-) to one of the 6,6 bonds to form RC_{60}^- anions (5-8). The high stability of these anions has been inferred by the measured high acidities of their conjugate acids: pK_a 4.7 [$R = H$ (9)] and 5.7 [$R = t\text{-Bu}$ (5)].

In contrast to the high stability of anionic species, cations possessing a positive charge on the π -conjugated system of a fullerene cage are uncommon. The chemistry of such cations have remained unexplored for nearly a decade, since C_{60} became available in macroscopic quantities in 1990 (10), in spite of their potential significance in both fundamental and application studies.

The preparation of a stable fullerene cation was first achieved in 1996 by Reed et al. (11) via the single-electron oxidation of C_{76} with the radical cation of tris(2,4-dibromophenyl)amine. They successfully isolated the salt of C_{76}^{2+} using a weakly nucleophilic carborane anion $CB_{11}H_6Cl_6^-$ as the counteranion. The radical cation of C_{60} was similarly prepared in solution by employing an even stronger oxidizing reagent, the hexabromo-*N*-phenylcarbazole radical cation (12), but the isolation of the salt of C_{60}^{2+} was difficult, perhaps because of the bimolecular disproportionation of the radical cation into C_{60}^{2+} and C_{60} at high concentrations.

There are limited number of reports of the observation and isolation of functionalized fullerene cations. The monoalkylated [RC_{60}^+ (13,14), $Cl_2CH-C_{70}^+$ (15), and $(EtO)_2P^+(OH)CH_2-C_{60}^+$ (16)], monoprotonated [HC_{60}^+ (12,17)], and pentaarylated [$Ar_5C_{60}^+$ (18)] fullerene cations have thus far been prepared as stable solutions or isolated as solids (Figure 1).

The RC_{60}^+ cations are carbenium ions (trivalent carbocations), which are formally conjugated with the entire π -system of the fullerene cage. This chapter focuses on recent developments in the author's laboratory regarding the prepara-

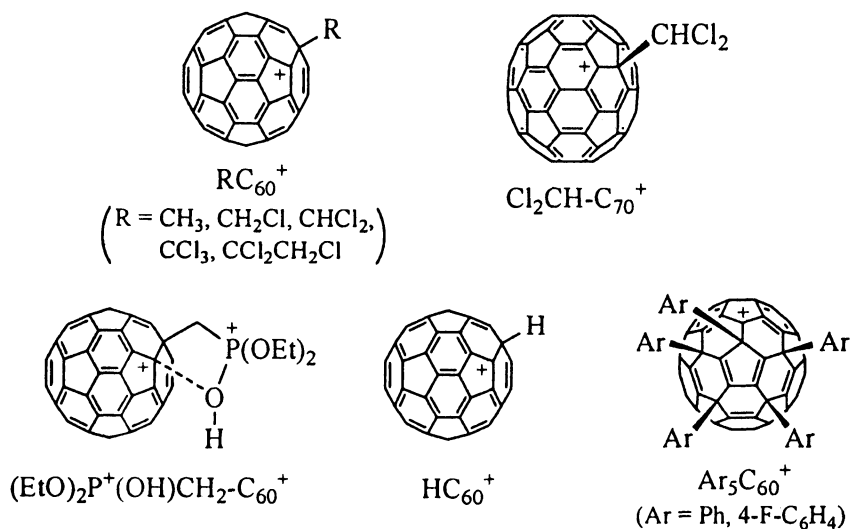


Figure 1. Derivatized fullerene cations.

tion of monoalkylated C_{60} and C_{70} cations as persistent species in solution and in the solid state, as well as reactions proceeding through these cations as an intermediate. Evaluation of their thermodynamic stabilities is also discussed.

Alkylated Fullerene Cations under Stable Ion Conditions

Electrophilic Addition to C_{60}

Although the formation of stable carbanions by nucleophilic addition to C_{60} and higher fullerenes is well known (14,19–21), the addition of electrophiles, which leads to derivatized fullerene cations, is quite rare. When C_{60} is treated with $AlCl_3$ in benzene, a mixture of polyhydrophenylated C_{60} is obtained (Figure 2, [A]) (22–24). In this reaction, a mechanism involving the initial protonation of C_{60} and subsequent phenylation of the intermediate cation HC_{60}^+ was proposed. The electrophilic addition of nitronium ion was proposed for the reaction of C_{60} with $NO_2^+RCO_2^-$ ($R = Ph, p\text{-}BrC_6H_4$), which, after aqueous work-up, gave polyhydroxylated C_{60} (Figure 2, [B]) (25,26).

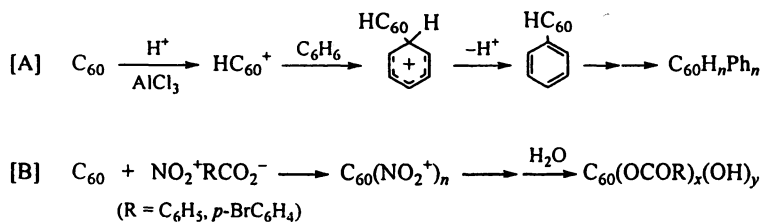


Figure 2. Proposed mechanisms for hydrophenylation and nitration of C_{60} .

While the formation of multiadducts in the above reactions clearly demonstrates the difficulties confronted in terms of controlling the reaction, the issue of whether C_{60} and C_{70} undergo addition by carbon electrophiles is of great interest, because such a reaction would provide a useful method for carbon-carbon bond formation for the derivatization of fullerenes. Initial attempts to test the possibility of electrophilic alkylation of C_{60} with *tert*-butyl chloride and $AlCl_3$ gave only polymeric products, probably formed via isobutene, indicating the insufficient reactivity of C_{60} towards *tert*-butyl cation.

On the other hand, using 1,1,2,2-tetrachloroethane as a source of electrophile and as solvent, an alkylation product RC_{60}Cl ($\text{R} = -\text{CCl}_2\text{CH}_2\text{Cl}$) was obtained in moderate yield (Figure 3) (13). NMR analysis indicated that this product was the isomerically pure 1,4 adduct. It seems that the initially formed cation $^+\text{CHClCHCl}_2$ (or its complex with AlCl_4^-) rearranged to $^+\text{CCl}_2\text{CH}_2\text{Cl}$, which is more stable due to the $p(\pi)$ donation of unshared 3p electrons of the two chlorine atoms (27,28), before the electrophilic attack on C_{60} . A reddish purple color, characteristic to RC_{60}^+ (vide infra), was observed during the reaction, suggesting that the adduct was present in the form of cation RC_{60}^+ , and not RC_{60}Cl . This explains why multiple addition on C_{60} cage did not take place. The intermediate cation was probably coordinated strongly with the counteranion because only the chloride, not an alcohol, was obtained after workup with water.

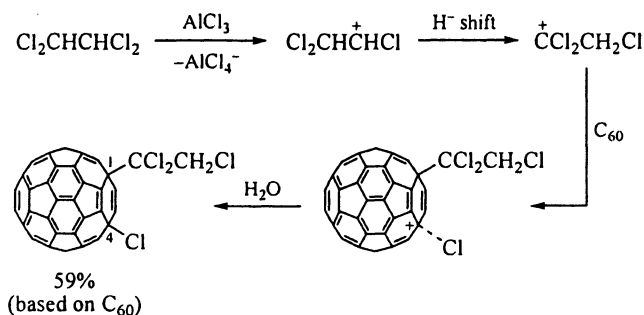


Figure 3. Electrophilic addition of tetrachloroethane to C_{60} .

Similar monoadducts were also obtained, when more simple chloroalkanes such as dichloromethane, chloroform, carbon tetrachloride were used (Figure 4, Table I). In the case of dichloromethane the product was a mixture of the 1,4 and 1,2 adducts. DFT calculations (B3LYP/3-21G*) showed that the 1,2 adduct is slightly more stable than the 1,4 adduct in this case, but becomes less stable when the alkyl group is bulkier, in agreement with the experimental results.

Attempts to alkylate C_{60} with methyl iodide did not give an addition product, probably because of insufficient reactivity of this electrophile system, due to the low electronegativity of iodine. On the other hand, the use of liquified chloromethane at 60 °C in a stainless steel autoclave afforded the methylated product, which consisted of only the 1,2 isomer, as expected from the small steric requirement of the methyl group (29).

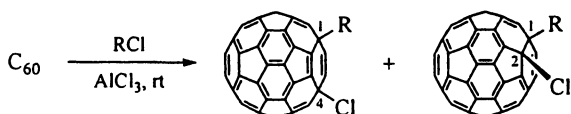


Figure 4. Electrophilic addition of chloroalkanes to C_{60} .

Table I. Electrophilic Addition of Chloroalkanes to C_{60} ^a

Chloroalkane ^b	Time (h)	Product	Yield (%)
CH_3Cl^c	70	1,2- $CH_3-C_{60}-Cl$	33
CH_2Cl_2	46	1,2- and 1,4- $ClCH_2-C_{60}-Cl$ (1:1)	56 ^d
$CHCl_3$	2	1,4- $Cl_2CH-C_{60}-Cl$	60
CCl_4	48	1,4- $Cl_3C-C_{60}-Cl$	58
$Cl_2CHCHCl_2^c$	7	1,4- $ClCH_2CCl_2-C_{60}-Cl$	59

^a $AlCl_3$ (50–100 eq), at room temperature.

^b Used as solvent.

^c At 60 °C in a stainless steel autoclave.

^d Total yield of 1,2 and 1,4 isomers.

A characteristic reaction of the alkylated C_{60} chlorides thus prepared is clean hydrolysis to give fullerlenols in the presence of silica gel. Most simply this could be carried out by passing a solution of the chloride through a column of silica gel. This can be explained via a silica gel-assisted ionization of the chloride and trapping of the intermediate cation by water present in the reaction system. In all cases, the product was the 1,4 isomer (Figure 5).

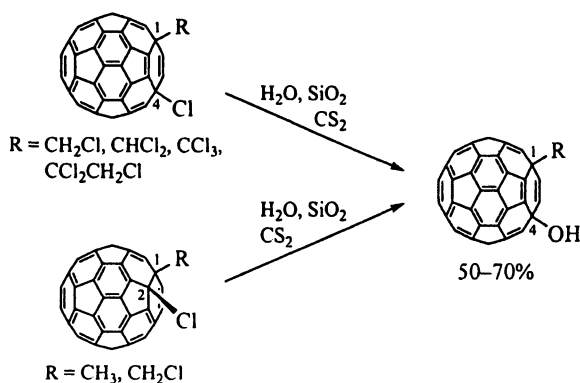


Figure 5. Silica gel-promoted hydrolysis of $RC_{60}Cl$.

Generation of RC_{60}^+ as Long-lived Ion

Fullerenols $RC_{60}OH$ are good precursors for cations RC_{60}^+ under superacidic conditions. Although the ionization of alcohols and halides in superacid media is a powerful method for generating carbenium ions, the use of this method for C_{60} derivatives suffers from undesirable oxidation, since the frequently used superacids are often very strong oxidants. Thus, it is known that the parent C_{60} is oxidized to C_{60}^{++} by strongly oxidizing media such as magic acid (FSO_3H/SbF_5) (22) and oleum (30). Although magic acid is an excellent superacid for generating many carbocations, dissolving $RC_{60}OH$ in FSO_3H/SbF_5 (1:1) resulted in the formation of a dark green, paramagnetic solution, which can be reasonably explained by the formation of C_{60}^{++} via further oxidation of the once formed RC_{60}^+ . On the other hand, trifluoromethanesulfonic acid (CF_3SO_3H), although a weaker acid, is non-oxidizing and is more suitable for the ionization of $RC_{60}OH$. Thus, dissolving these alcohols in CF_3SO_3H gave

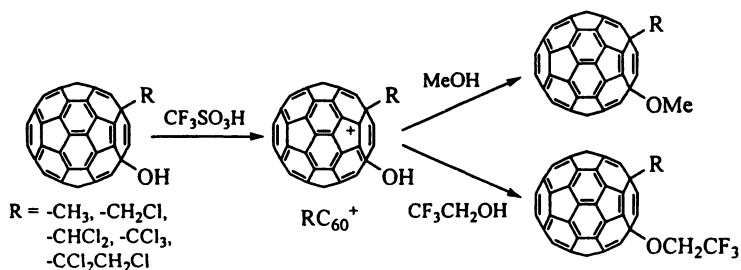


Figure 6. Generation and trapping of alkylated C_{60} cations.

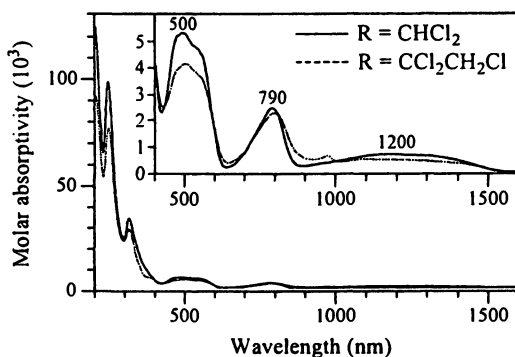


Figure 7. UV-vis-NIR absorption spectra of RC_{60}^+ generated from the corresponding fullerenols in $\text{CF}_3\text{SO}_3\text{H}$ at room temperature. The inset shows the absorptions in the vis-NIR region. (Reproduced from reference 13. Copyright 1999 American Chemical Society.)

reddish purple solutions of RC_{60}^+ (Figure 6), having characteristic absorptions around 500, 790, and 1200 nm (Figure 7). The cations are stable at room temperature in this solvent for at least several weeks. Quenching these solutions with methanol and $\text{CF}_3\text{CH}_2\text{OH}$ led to the regioselective bonding of an alkoxy group to form 1,4- RC_{60}OMe and 1,4- $\text{RC}_{60}\text{OCH}_2\text{CF}_3$, respectively (Figure 6).

The ^{13}C NMR spectra of cations RC_{60}^+ (Figure 8) showed signals corresponding to a cationic center at δ 185.6 ($R = \text{CH}_3$), 180.3 ($R = \text{CH}_2\text{Cl}$), 175.6 ($R = \text{CHCl}_2$), 171.8 ($R = \text{CCl}_3$), and 174.9 ($R = \text{CCl}_2\text{CH}_2\text{Cl}$). In each spectrum, 30 sp^2 carbon signals are observed in the sp^2 carbon region, and the intensity of the signal for the cationic center is about half that of the majority of other sp^2

carbons, indicating that the molecule has C_s symmetry and that the positive carbon is adjacent to the unique sp^3 carbon on the C_{60} cage (Figure 9a). The relatively high-field shift of these signals, compared with the aryl-substituted carbenium ions, Ph_3C^+ (δC^+ 211.6) (31) and 9-phenylfluorenyl cation (δC^+ 224.2) (32), suggests a certain degree of charge delocalization. In addition to the resonance delocalization over the π -system of the C_{60} cage, the intramolecular coordination of the lone pair electrons of the chlorine atom in the R group to the cationic center is conceivable. The latter possibility is supported by the observed high field shifts of the cationic center with increasing number of chlorine atoms attached to the α carbon of the R group (Figure 9b).

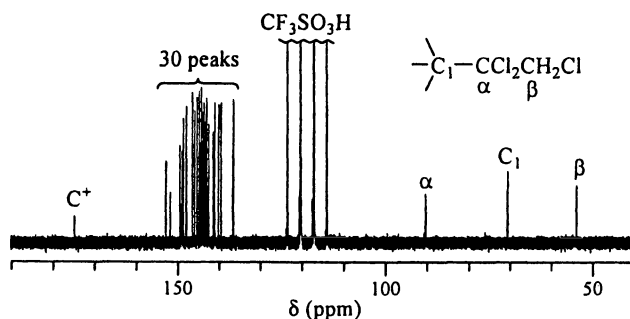


Figure 8. ^{13}C NMR spectrum of $ClCH_2-CCl_2-C_{60}^+$ (rt, 100 MHz, CF_3SO_3H ; cyclohexane- d_{12} was used as an external standard). (Reproduced from reference 13. Copyright 1999 American Chemical Society.)

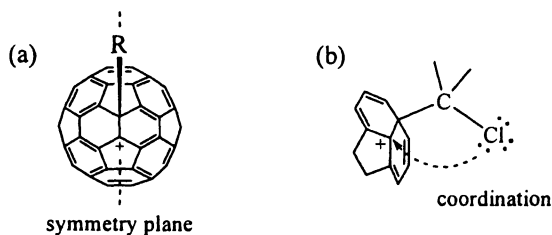


Figure 9. (a) Symmetry of RC_{60}^+ . (b) Coordination of the chlorine lone pair to the cationic center.

The ionization of $\text{Cl}_2\text{CH-C}_{60}\text{OH}$ to $\text{Cl}_2\text{CH-C}_{60}^+$ was also complete in H_2SO_4 . This indicates that alkylated C_{60} cations are so remarkably stable that no superacid is required for their generation. The chemical shifts of the cationic centers were essentially the same in acids with different acidities; [acidity function H_0 ; FSO_3H , -15.1 ; $\text{CF}_3\text{SO}_3\text{H}$, -14.1 ; H_2SO_4 , -12 (33)], showing that $\text{Cl}_2\text{CH-C}_{60}^+$ is free from contact ion pairing with the counteranion.

DFT calculations for $\text{ClCH}_2\text{-C}_{60}^+$ indicated that the chlorine atom is positioned with a 62 degree dihedral angle ϕ (Figure 10). This conformer is more stable than the anti form ($\phi = 180^\circ$) by 0.7 kcal/mol due to an attractive interaction between the cationic center and the chlorine atom. The syn conformation ($\phi = 0^\circ$), with 6.0 kcal/mol higher energy, was found to be a transition state to the rotation of the ClCH_2 group around the $\text{ClCH}_2\text{-C}_{60}$ bond.

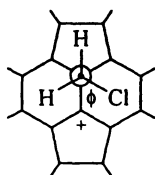


Figure 10. Geometry of $\text{ClCH}_2\text{-C}_{60}^+$ optimized by the DFT method at the B3LYP/3-21G* level. $\phi(\text{Cl-C-C-C}) = 62^\circ$.

Cation $\text{Cl}_2\text{CH-C}_{60}^+$ could also be generated in dichloromethane. Thus, the chloride ion was effectively abstracted from $\text{Cl}_2\text{CH-C}_{60}\text{Cl}$ by silver ion, which was confirmed by UV-vis-NIR and NMR spectroscopies. Due to the low solvent polarity, all visible absorption peaks were blue-shifted by ca. 20 nm, and the chemical shift of the cationic center appeared at lower-field by 12 ppm, compared to $\text{CF}_3\text{SO}_3\text{H}$ solutions. This cation could even be isolated as the SbF_6^- salt by removing AgCl by filtration followed by precipitation by addition of hexane. Alternatively, the chloride ion could be abstracted from $\text{Cl}_2\text{CH-C}_{60}\text{Cl}$ with SbCl_5 in $\text{CS}_2\text{-CH}_2\text{Cl}_2$. In this solvent the salt $\text{Cl}_2\text{CH-C}_{60}^+ \text{SbCl}_6^-$ precipitated as it was formed. The purity of the collected SbF_6^- and SbCl_6^- salts, stable only under vacuum or in a glovebox, was checked by quenching with methanol, which gave the corresponding methyl ether in almost quantitative yields.

Electrophilic Addition to C_{70}

Based on the fact that C_{70} has an oxidation potential of $E_{1/2}^{\text{ox}} = 1.20 \text{ V}$ (vs Fc/Fc^+ , in 1,1,2,2-tetrachloroethane), slightly less positive than that of C_{60}

(1.26 V) (34), the monoalkylated C_{70} cations RC_{70}^+ are also expected to be generated in a similar manner as long lived cations. Unlike the anionic counterpart (35), only one derivatized C_{70} cation, $Cl_2CH-C_{70}^+$, has been reported (15), as a directly observable species. One potential difficulty in its preparation is the possible formation of a mixture of regioisomers due to the presence of five different types of carbons in the C_{70} cage (Figure 11).

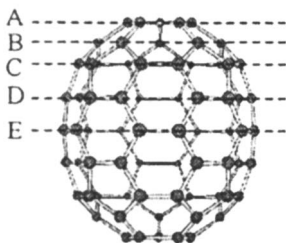


Figure 11. Five types of carbons in the C_{70} framework.

Treatment of C_{70} with $AlCl_3$ in chloroform resulted in the addition of one molecule of chloroform. Separation of unchanged C_{70} (40% recovered) by HPLC gave the $Cl_2CH-C_{70}Cl$ adduct as a major product in 27% yield (Figure 12). The NMR spectra of the adduct indicate that the product is isomerically pure, and that the molecule contains no symmetry elements. Based on these data and on more rigorous discussions of the structure of cation $Cl_2CH-C_{70}^+$ described in the next section, the obtained adduct was assigned as the 23-chloro-7-dichloromethyl derivative, in which the two addends are positioned across a six-membered ring located in a flat region of the C_{70} core.

The observed preferential electrophilic attack on carbon D of C_{70} under Friedel-Crafts conditions ($CHCl_3/AlCl_3$) is consistent with the large HOMO coefficient of this carbon (Figure 13). This is in contrast to the fact that nucleophilic addition (7,35–38) and cycloaddition (38–40) to C_{70} favor carbons A and B, which are most pyramidalized and have large LUMO coefficients (Figure 13).

The chloride $Cl_2CH-C_{70}Cl$ was converted to fulleranol $Cl_2CH-C_{70}OH$ in 63% yield by silica gel-promoted hydrolysis (Figure 12). The hydrolysis is regioselective, producing only a single isomer that shows 68 aromatic carbon signals in the NMR, suggesting that $Cl_2CH-C_{70}OH$ is a structural analogue of $Cl_2CH-C_{70}Cl$.

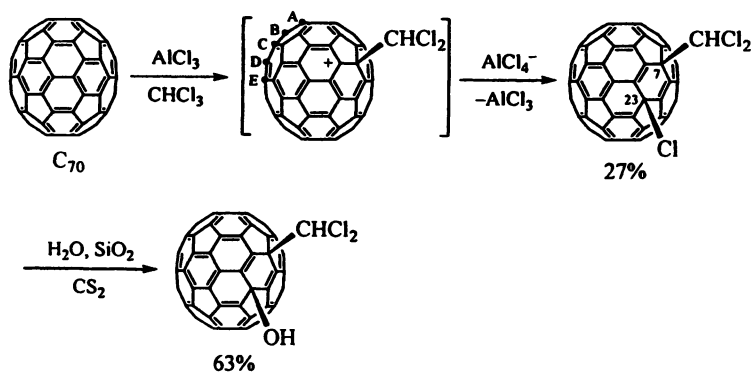


Figure 12. Electrophilic addition of chloroform to C_{70} and the subsequent hydrolysis.

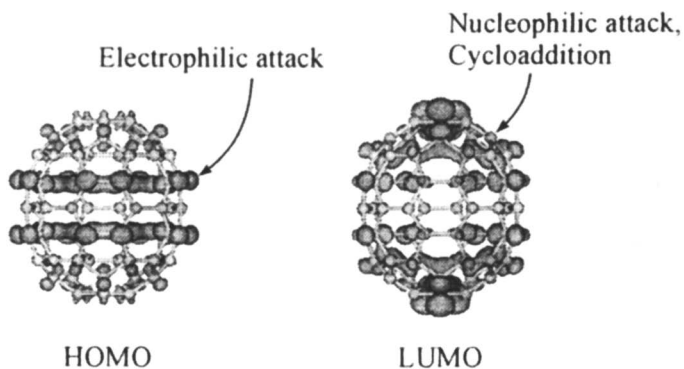


Figure 13. Orbitals of C_{70} calculated by the DFT method at the B3LYP/3-21 level. (Reproduced with permission from reference 15. Copyright 2005 Wiley- VCH.)

Generation of RC_{70}^+ as Long-lived Ion

Fullerenol $\text{Cl}_2\text{CH-C}_{70}\text{-OH}$ was readily soluble in $\text{CF}_3\text{SO}_3\text{H}$, giving a reddish brown solution, which showed characteristic long-wavelength absorptions, as shown in Figure 14. The ^{13}C NMR spectrum of the cation showed the lowest-field signal at δ 198.16, two significantly low-field signals at δ 177.49 and 175.81, and the other 66 sp^2 carbon and two sp^3 carbon signals, indicating the complete formation of a C_1 -symmetric single isomer of the $\text{Cl}_2\text{CH-C}_{70}^+$ cation (Figure 15). The Cl_2CH group should therefore be attached to carbons C or D, otherwise the molecule would have a C_s symmetry. The cation is most likely the D adduct, shown in Figure 16, since it was shown to be the lowest-energy isomer, 2.55 kcal/mol more stable than the C isomer by DFT calculations. Mulliken charges were shown to be mainly distributed on carbons close to the unique sp^3 carbon in the cage, as well as on the carbon atoms in region E, where the pyramidalization of the C–C bonds is relatively small (Figure 17). Quenching this cation with methanol gave the ether $7,27\text{-Cl}_2\text{CH-C}_{70}\text{-OME}$ quantitatively (Figure 16).

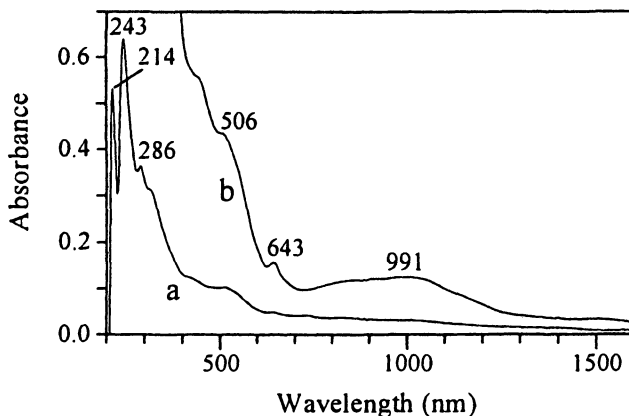


Figure 14. UV-vis-NIR absorption spectra of $\text{Cl}_2\text{CH-C}_{70}^+$ generated from the corresponding fullerenols in $\text{CF}_3\text{SO}_3\text{H}$ at room temperature. Cell length 1 cm. (a) 1017×10^{-5} M. (b) 5.90×10^{-5} M. (Reproduced with permission from reference 15. Copyright 2005 Wiley-VCH.)

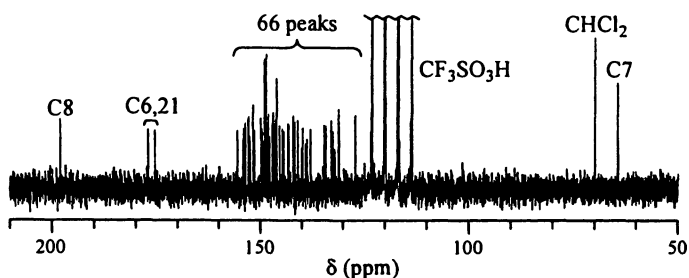


Figure 15. ^{13}C NMR spectrum of $\text{Cl}_2\text{CH-C}_{70}^+$ (rt, 100 MHz, $\text{CF}_3\text{SO}_3\text{H}$; cyclohexane- d_{12} was used as an external standard). (Reproduced with permission from reference 15. Copyright 2005 Wiley-VCH.)

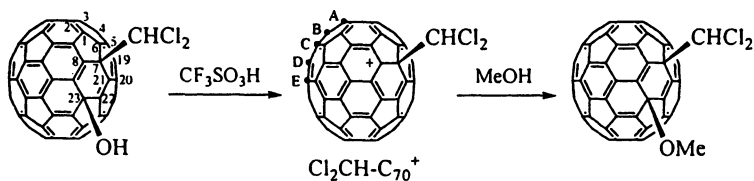


Figure 16. Generation and trapping of $\text{Cl}_2\text{CH-C}_{70}^+$. The plus sign designates the most downfield shifted carbon.

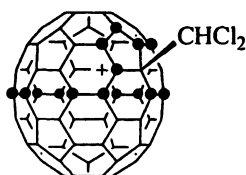


Figure 17. Charge distribution of $\text{Cl}_2\text{CH-C}_{70}^+$. Dots represent carbons possessing a Mulliken charge greater than 0.025 (B3LYP/6-31G*).

Thermodynamic Stabilities of RC_{60}^+ and RC_{70}^+

It would be of interest to evaluate the stabilities of fullerene cations in a quantitative manner. The pK_{R^+} is a stability parameter that is defined as $pK_{R^+} = -\log K_{R^+}$ based on the equilibrium constant for the hydrolysis in solution (Figure 18). Both the RC_{60}^+ cation and the relatively nonpolar neutral fullereneol $RC_{60}OH$ are soluble in mixtures of sulfuric acid and *p*-toluenesulfonic acid ($TsOH \cdot H_2O$). As a result, this mixture serves as an excellent solvent system for the determination of the equilibrium constant. In pure sulfuric acid the fullerenols were completely ionized to the cation, while the addition of a weaker acid, *p*-toluenesulfonic acid, gradually decreased the concentration of the cation due to the shift in the equilibrium to the right hand side (Figure 19). By spectrometrically measuring equilibrium constants in mixtures of various H_2SO_4 - $TsOH$ ratios, the pK_{R^+} values for RC_{60}^+ were determined to be -14.9 to -15.8 (41). These values are comparable to -16.4 (42), -15.5 (43), and -14.7 (44) reported for the *tert*-butyl cation, indicating that the monoalkylated C_{60} cations have approximately the same stability as the *tert*-butyl cation.

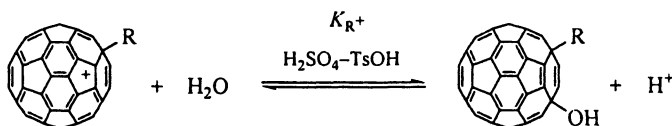


Figure 18. Reversible hydrolysis of RC_{60}^+ .

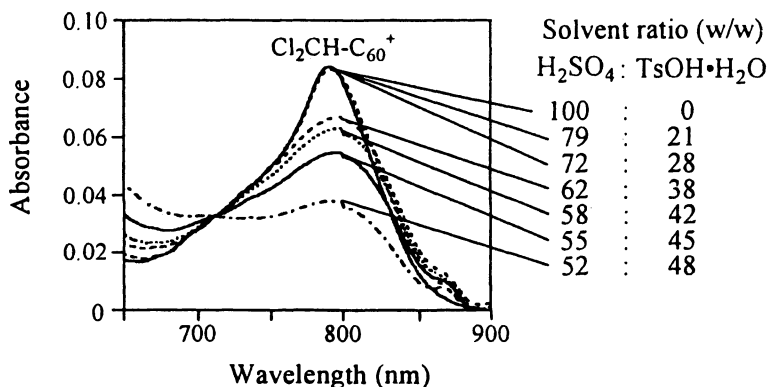


Figure 19. Change in concentration of $Cl_2CH-C_{60}^+$ in H_2SO_4 -*p*-toluenesulfonic acid of different solvent ratios.

Another method for evaluating carbocation stability involves the measurement of solvolysis rates (14,45). Typically, the transition state of the rate-determining step in S_N1 reactions is assumed to closely resemble the intermediate ion pair, on the basis of the Hammond postulate (46). Thus, the free energy of activation for this reaction, ΔG^\ddagger , reflects the relative thermodynamic stabilities of the intermediate carbocations.

Chlorides $RC_{60}Cl$ ($R = CH_3, CH_2Cl, CHCl_2, CCl_3$) and $RC_{70}Cl$ ($R = CHCl_2$) undergo ionization in CF_3CH_2OH -anisole (1:9 v/v) to form RC_{60}^+ and RC_{70}^+ , respectively, as short-lived intermediates, the nucleophilic trapping of which resulted in substitution products shown in Figure 20. Anisole was used as a co-solvent to ensure sufficient solubility for the rate measurements, while it also acted as a nucleophile.

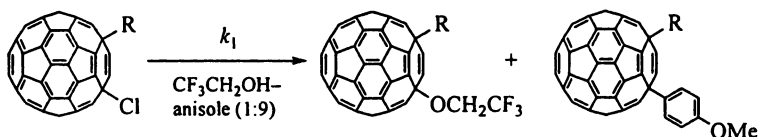


Figure 20. Solvolysis of $RC_{60}Cl$ in CF_3CH_2OH -anisole.

These reactions followed first order kinetics with free energies of activation (ΔG^\ddagger s) summarized in Table II. The ΔG^\ddagger s increased with increasing number of chlorine atoms in group R, suggesting destabilization by the through-bond electron-withdrawing effect of chlorine atoms. No significant difference was observed between $Cl_2CH-C_{60}-Cl$ and $Cl_2CH-C_{70}-Cl$, which have the same addend but different cages. These ΔG^\ddagger s are only slightly lower than that observed for *t*-BuCl under the same conditions (26.9 kcal/mol), in agreement with the results of the pK_R^+ measurements.

Reactions via RC_{60}^+ and RC_{70}^+

Reactions via alkylated C_{60} and C_{70} cation intermediates afford a variety of fullerene derivatives (Figure 21) (45). For example, the treatment of chlorides $RC_{60}Cl$ with $AlCl_3$ in anisole resulted in Friedel-Crafts type substitution at the para position of anisole by fullerenylium cation to give 1,4- $RC_{60}-C_6H_4OMe-p$. A similar transformation can be also performed with an Ag^+ salt. In this case the chloride ion is abstracted by silver ion. An advantage of this method over the reaction with $AlCl_3$ is that the reaction can be carried out in the presence of compounds which contain a hydroxyl group. Thus, addition of $AgBF_4$ to a solution of $RC_{60}Cl$ in anisole, MeOH/PhCN, and $CF_3CH_2OH/Cl_2CHCHCl_2$

Table II. Free Energies of Activation for the Solvolysis in 2,2,2-Trifluoroethanol–Anisole (1:9 v/v)^a

Substrate	Intermediate	$\Delta G^\ddagger_{25^\circ\text{C}}$ (kcal/mol)
1,2-CH ₃ -C ₆₀ -Cl	CH ₃ -C ₆₀ ⁺	23.2
1,2- and 1,4-ClCH ₂ -C ₆₀ -Cl ^b	ClCH ₂ -C ₆₀ ⁺	23.8
1,4-Cl ₂ CH-C ₆₀ -Cl	Cl ₂ CH-C ₆₀ ⁺	24.0
1,4-Cl ₃ C-C ₆₀ -Cl	Cl ₃ C-C ₆₀ ⁺	25.0
7,23-Cl ₂ CH-C ₇₀ -Cl	7-Cl ₂ CH-C ₇₀ ⁺	24.1
(CH ₃) ₃ C-Cl	(CH ₃) ₃ C ⁺	26.9

^a Initial substrate concentration, 0.15–1.4 × 10⁻³ M. 2,6-Lutidine (1.3–6.3 equiv.) was added as a buffer to suppress the reverse reaction.

^b A 1:1 mixture of 1,2 and 1,4 isomers.

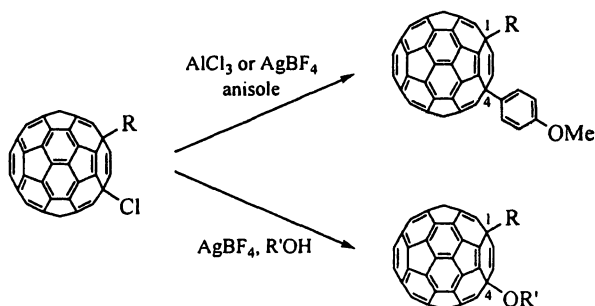


Figure 21. Synthesis of C₆₀ derivatives via an alkylated C₆₀ cation intermediate.

afforded 1,4- $\text{RC}_{60}\text{-C}_6\text{H}_4\text{OMe-}p$, 1,4- RC_{60}OMe , and 1,4- $\text{RC}_{60}\text{OCH}_2\text{CF}_3$, respectively. These reactions proceed under non-acidic conditions and are instantaneous, due to the insolubility of AgCl .

When the nucleophile is an electron-rich molecule, RC_{60}^+ can be reduced via single electron transfer, producing a dimer (47). Thus, electrophilic aromatic substitution normally occurs with substituted benzenes (Figure 22, [A]), but the mode of the reaction is switched if the benzene is strongly activated (Figure 22, [B]).

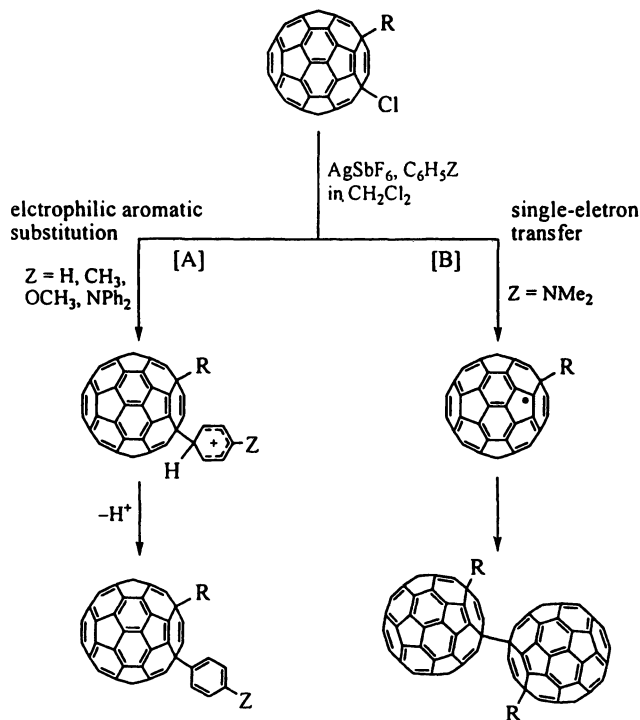


Figure 22. Reactions of RC_{60}^+ intermediate with substituted benzenes.

Reactions of $\text{Cl}_2\text{CH-C}_{70}^+$ with nucleophiles were also regiospecific. The LUMO of this cation is largely distributed on C8, C21, and C23, but the nucleophile attacks only at C23 (Figure 23) (15), because an attack at C8 and C21 would produce sterically unfavorable 1,2-isomers (48–51). The resulting adduct is a derivative of 7,23- C_{70}H_2 , which, based on *ab initio* calculations, is the most stable among the C_{70}H_2 isomers with nonadjacent hydrogens (52–54).

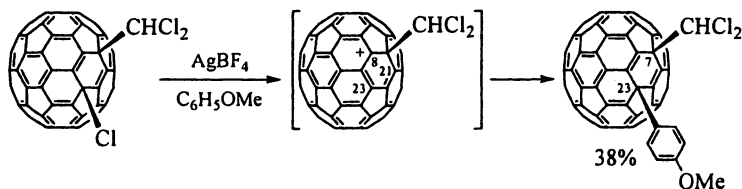


Figure 23. Synthesis of a C₇₀ derivative via an alkylated C₇₀ cation intermediate.

Summary

Although the direct observation and isolation of fullerene cations had previously been considered a challenging task, significant progress has been made in recent years in investigations of this elusive species. It was also found that C₆₀ and C₇₀ are sufficiently nucleophilic to be alkylated by carbenium ions. The resulting cations, RC₆₀⁺ and RC₇₀⁺, are useful for further transformation, which was demonstrated by their formation as reactive intermediates and trapping with a nucleophile, hence providing an efficient method for the synthesis of fullerene derivatives.

References

1. Reed, C. A.; Bolskar, R. D. *Chem. Rev.* **2000**, *100*, 1075.
2. Echevoyen, L.; Diederich, F.; Echevoyen, L. E. in *Fullerenes: Chemistry, Physics, and Technology*; Kadish K. M.; Ruoff, R. S., Eds.; Wiley-Interscience: New York, 2000; chapter 1.
3. Echevoyen, L.; Echevoyen, L. E. *Acc. Chem. Res.* **1998**, *31*, 593.
4. Xie, Q.; Pérez-Cordero, E.; Echevoyen, L. *J. Am. Chem. Soc.* **1992**, *114*, 3978.
5. Fagan, P. J.; Krusic, P. J.; Evans, D. H.; Lerke, S. A.; Johnston, E. *J. Am. Chem. Soc.* **1992**, *114*, 9697.
6. Murata, Y.; Motoyama, K.; Komatsu, K.; Wan, T. S. M. *Tetrahedron* **1996**, *52*, 5077.
7. Hirsch, A.; Grosser, T.; Skiebe, A.; Soi, A. *Chem. Ber.* **1993**, *126*, 1061.
8. Hirsch, A.; Soi, A.; Karfunkel, H. R. *Angew. Chem., Int. Ed. Engl.* **1992**, *31*, 766.
9. Niyazymbetov, M. E.; Evans, D. H.; Lerke, S. A.; Cahill, P. A.; Henderson, C. C. *J. Phys. Chem.* **1994**, *98*, 13093.
10. Krätschmer, W.; Lamb, L. D.; Fostiropoulos, K.; Huffman, D. R. *Nature* **1990**, *347*, 354.

11. Bolskar, R. D.; Mathur, R. S.; Reed, C. A. *J. Am. Chem. Soc.* **1996**, *118*, 13093.
12. Reed, C. A.; Kim, K-C.; Bolskar, R. D.; Mueller, L. J. *Science* **2000**, *289*, 101.
13. Kitagawa, T.; Sakamoto, H.; Takeuchi, K. *J. Am. Chem. Soc.* **1999**, *121*, 4298.
14. Kitagawa, T.; Takeuchi, K. *Bull. Chem. Soc. Jpn.* **2001**, *74*, 785.
15. Kitagawa, T.; Lee, Y.; Masaoka, N.; Komatsu, K. *Angew. Chem. Int. Ed.* **2005**, *44*, 1398.
16. Murata, Y.; Cheng, F.; Kitagawa, T.; Komatsu, K. *J. Am. Chem. Soc.* **2004**, *126*, 8874.
17. Mueller, L. J.; Elliott, D. W.; Kim, K-C.; Reed, C. A.; Boyd, P. D. W. *J. Am. Chem. Soc.* **2002**, *124*, 9360.
18. Avent, A. G.; Birkett, P. R.; Kroto, H. W.; Taylor, R.; Walton, D. R. M. *Chem. Commun.* **1998**, 2153.
19. Hirsch, A.; Brettreich, M. *Fullerenes: Chemistry and Reactions*; Wiley-VCH: Weinheim, 2005; chapter 3.
20. Hirsch, A. *The Chemistry of the Fullerenes*; Thieme: Stuttgart, 1994; chapter 3.
21. Wilson, S. R.; Schuster, D. I.; Nuber, B.; Meier, M. S.; Maggini, M.; Prato, M.; Taylor, R. *Fullerenes: Chemistry, Physics, and Technology*; Kadish, K. M.; Ruoff, R. S., Eds.; Wiley-Interscience: New York, 2000; chapter 3.
22. Olah, G. A.; Bucsi, I.; Aniszfeld, R.; Prakash, G. K. S. *Carbon* **1992**, *30*, 1203.
23. Olah, G. A.; Bucsi, I.; Ha, D. S.; Aniszfeld, R.; Lee, C. S.; Prakash, G. K. S. *Fullerene Sci. Tech.* **1997**, *5*, 389.
24. Olah, G. A.; Bucsi, I.; Lambert, C.; Aniszfeld, R.; Trivedi, N. J.; Sensharma, D. K.; Prakash, G. K. S. *J. Am. Chem. Soc.* **1991**, *113*, 9387.
25. Chiang, L. Y.; Upasani, R. B.; Swirczewski, J. W. *J. Am. Chem. Soc.* **1992**, *114*, 10154.
26. Chiang, L. Y. in *The Chemistry of Fullerenes*; Taylor, R., Ed., World Scientific: Singapore, 1995; chapter 5.
27. Olah, G. A.; Rasul, G.; Heiliger, L.; Prakash, G. K. S. *J. Am. Chem. Soc.* **1996**, *118*, 3580.
28. Frenking, G.; Fau, S.; Marchand, C. M.; Grützmacher, H. *J. Am. Chem. Soc.* **1997**, *119*, 6648.
29. Kitagawa, T.; Ochi, Y.; Komatsu, K. unpublished results.
30. Cataldo, F. *Spectrochim. Acta*, **1995**, *51A*, 405.
31. Abarca, B.; Asensio, G.; Ballesteros, R.; Varea, T. *J. Org. Chem.* **1991**, *56*, 3224.
32. Olah, G. A.; Prakash, G. K. S.; Liang, G.; Westerman, P. W.; Kunde, K.; Chandrasekhar, J.; Schleyer, P. v. R. *J. Am. Chem. Soc.* **1980**, *102*, 4485.
33. Olah, G. A.; Prakash, G. K. S.; Sommer, J. *Superacids*; John Wiley & Sons: New York, 1985.

34. Xie, Q.; Arias, F.; Echegoyen, L. *J. Am. Chem. Soc.* **1993**, *115*, 9818.
35. Sawamura, M.; Iikura, H.; Hirai, A.; Nakamura, E. *J. Am. Chem. Soc.* **1998**, *120*, 8285.
36. Wang, Z.; Meier, M. S. *J. Org. Chem.* **2003**, *68*, 3043.
37. Wang, Z.; Meier, M. S. *J. Org. Chem.* **2004**, *69*, 2178.
38. Thilgen, C.; Herrmann, A.; Diederich, F. *Angew. Chem. Int. Ed. Engl.* **1997**, *36*, 2268 and references cited therein.
39. Bellavia-Lund, C.; Wudl, F. *J. Am. Chem. Soc.* **1997**, *119*, 943.
40. Meier, M. S.; Wang, G.-W.; Haddon, R. C.; Brock, C. P.; Lloyd, M. A.; Selegue, J. P. *J. Am. Chem. Soc.* **1998**, *120*, 2337.
41. Kitagawa, T.; Lee, Y.; Hanamura, M.; Takeuchi, K.; Komatsu, K. unpublished results.
42. Toteva, M. M.; Richard, J. P. *J. Am. Chem. Soc.* **1996**, *118*, 11434.
43. Wayner, D. D. M.; McPhee, D. J.; Griller, D. *J. Am. Chem. Soc.* **1988**, *110*, 132.
44. Arnett, E. M.; Hofelich, T. C. *J. Am. Chem. Soc.* **1983**, *105*, 2889.
45. Kitagawa, T.; Lee, Y.; Hanamura, M.; Sakamoto, H.; Konno, H.; Takeuchi, K.; Komatsu, K. *Chem. Commun.* **2002**, 3062.
46. Smith, M. B.; March, J. *Advanced Organic Chemistry*; John Wiley & Sons: New York, 2001; pp. 432–433.
47. Kitagawa, T.; Yoshida, R.; Lee, Y.; Komatsu, K. unpublished results.
48. Kitagawa, T.; Tanaka, T.; Takata, Y.; Takeuchi, K.; Komatsu, K. *J. Org. Chem.* **1995**, *60*, 1490.
49. Kitagawa, T.; Tanaka, T.; Takata, Y.; Takeuchi, K.; Komatsu, K. *Tetrahedron* **1997**, *53*, 9965.
50. Kitagawa, T.; Tanaka, T.; Murakita, H.; Takeuchi, K. *J. Org. Chem.* **1999**, *64*, 2.
51. Kitagawa, T.; Tanaka, T.; Murakita, H.; Nishikawa, A.; Takeuchi, K. *Tetrahedron* **2001**, *57*, 3537.
52. Karfunkel, H. R.; Hirsch, A. *Angew. Chem. Int. Ed. Engl.* **1992**, *31*, 1468.
53. Henderson, C. C.; Rohlfing, C. M.; Cahill, P. A. *Chem. Phys. Lett.* **1993**, *213*, 383.
54. Henderson, C. C.; Rohlfing, C. M.; Gillen, K. T.; Cahill, P. A. *Science* **1994**, *264*, 397.

Chapter 13

Carbocations on Surfaces: Formation of Bicyclobutonium Cation via Ionization of Cyclopropylcarbinyl Chloride over NaY Zeolite

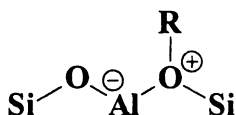
Marcelo Franco, Nilton Rosenbach, Jr., W. Bruce Kover,
and Cláudio J. A. Mota*

Instituto de Química, Universidade Federal do Rio de Janeiro. Cidade
Universitária CT Bloco A, 21949-900, Rio de Janeiro, Brazil

Cyclopropylcarbinyl chloride rearranges to cyclobutyl and allylcarbinyl chlorides over NaY zeolite at room temperature. This result is consistent with ionization of the cyclopropylcarbinyl chloride and formation of bicyclobutonium ion, followed by internal return of the halide. Using a NaY zeolite impregnated with NaBr, besides the rearranged chlorides, formation of cyclopropylcarbinyl bromide, cyclobutyl bromide and allylcarbinyl bromide were also observed, supporting the formation of the bicyclobutonium cation over the zeolite surface. Product distribution was different from that in solution, favoring formation of the allylcarbinyl, instead of cyclopropylcarbinyl bromide. Calculations showed that bicyclobutonium is a minimum over the zeolite structure. The results support the idea that zeolites act as solid solvents, permitting ionization and solvation of ionic species.

Introduction

Zeolites are the main catalyst in the petrochemical industry. The importance of these aluminosilicates is due to their capacity to promote many important reactions. By analogy with superacid media (1), carbocations are believed to be key intermediates in these reactions. However, simple carbocationic species are seldom observed on the zeolite surface as persistent intermediates within the time-scale of spectroscopic techniques. Indeed, only some conjugated cyclic carbocations were observed as long living species, but covalent intermediates, namely alkyl-aluminumsilyl oxonium ions (2) (scheme 1), where the organic moiety is bonded to the zeolite structure, are usually thermodynamically more stable than the free carbocations (3,4).

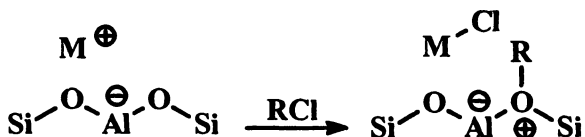


Scheme 1: Structure of alkyl-aluminumsilyl oxonium ions over the zeolite surface.

Numerous studies suggest that alkyl-aluminumsilyl oxonium ions should be the real intermediates in hydrocarbon reactions over zeolite, whereas carbocations should be just transition states (5). Equilibrium between the alkyl-aluminumsilyl oxonium ion and the carbocation, although suggested in some cases, has never been experimentally or theoretically proven, but recent calculations indicated that the *tert*-butyl carbenium ion is an intermediate on some specific zeolite structures (6,7).

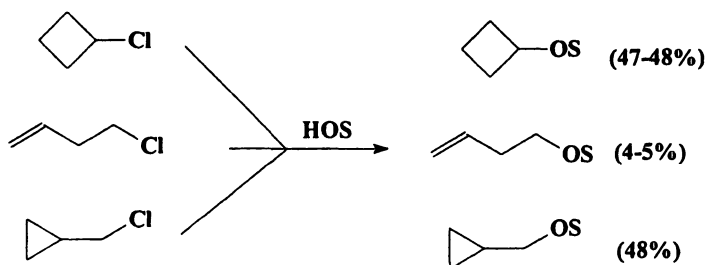
We have recently shown that metal-exchanged zeolites give rise to carbocationic reactions, through the interactions with alkylhalides (8). The metal cation acts as Lewis acid sites, coordinating with the alkylhalide to form a metal-halide species and an alkyl-aluminumsilyl oxonium ion bonded to the zeolite structure, which acts as an adsorbed carbocation (scheme 2). We were able to show that they can catalyze Friedel-Crafts reactions (9) and isobutane/2-butene alkylation (10), with a superior performance than a protic zeolite catalyst.

Nevertheless, the discussion whether the intermediates involved in the reactions of hydrocarbons over zeolite surface is the alkyl-aluminumsilyl oxonium ion or the carbocation could not be answered with these previous studies.



Scheme 2: Reaction of an alkylchloride with a metal-exchanged zeolite.
Formation of alkyl-aluminumsilyl oxonium ion.

The rearrangement of the cyclopropylcarbiny chloride in solution is well known in the literature (11). In polar solvents three products, arisen from the nucleophilic substitution of the solvent to the chloride, are usually detected, which are formed via nucleophilic substitution of chloride by solvent. This chemistry can be explained by the formation of the bicyclobutonium cation (C_4H_7^+), which acts as a tridentated ion, generating the three products shown in scheme 3.



Scheme 3 - Product distribution from solvolysis of cyclopropylcarbiny, cyclobutyl and allylcarbiny derivatives.

The ^{13}C NMR spectrum of the C_4H_7^+ cation in superacid solution shows a single peak for the three methylene carbon atoms (12). This equivalence can be explained by a *nonclassical* single symmetric (three-fold) structure. However, studies on the solvolysis of labeled cyclopropylcarbiny derivatives suggest a degenerate equilibrium among carbocations with lower symmetry, instead of the three-fold symmetrical species (13). A small temperature dependence of the ^{13}C chemical shifts indicated the presence of two carbocations, one of them in small amounts but still in equilibrium with the major species (13). This conclusion was supported by isotope perturbation experiments performed by Saunders and Siehl (14). The *classical* cyclopropylcarbiny cation and the *nonclassical* bicyclobutonium cation were considered as the most likely species participating in this equilibrium.

On the other hand, many theoretical methods have been employed to elucidate the potential energy surface of the $C_4H_7^+$ in gas phase (15,16) and in solution (17). High-level *ab initio* calculations suggest that, in gas phase, there are three $C_4H_7^+$ structures as minima on the potential energy surface (14). These calculations pointed to bicyclobutonium and cyclopropylcarbinyl as the most stable structures.

There are no reported studies of this rearrangement on the zeolite surface and we argued that it could give some clues to the alkyl-aluminumsilyl oxonium ion/carbocation equilibrium. In this work we show experimental and theoretical results on the rearrangement of the cyclopropylcarbinyl chloride over NaY zeolite, aiming at demonstrating the equilibrium between the carbocation and the alkyl-aluminumsilyl oxonium ion.

Experimental and Theoretical Methods

Experimental Part

The rearrangement reactions were studied on NaY (Si/Al = 2.6 and surface area of $704 \text{ m}^2 \cdot \text{g}^{-1}$). To assess the product distribution, a sample of the NaY impregnated with NaBr was prepared by soaking NaY zeolite with an aqueous solution of NaBr and the water was evaporated in a rotary evaporator.

The reaction was carried out in a glass unit with a straight reactor (fixed bed) at room temperature and atmospheric pressure. About 200 mg of the zeolite was initially pretreated at $300 \text{ }^\circ\text{C}$ ($2.5 \text{ }^\circ\text{C} \cdot \text{min}^{-1}$), under an atmosphere of N_2 ($40 \text{ mL} \cdot \text{min}^{-1}$). The reactor was cooled to room temperature and 0.5 mL of cyclopropylcarbinyl chloride (Aldrich) was injected in the N_2 flow, with the use of a syringe. The products were collected at the reactor outlet, using a trap immersed in ice bath. The products were separated by a gas chromatograph (Agilent Instruments) equipped with a HP1 capillary column (cross linked 100% dimethylpolysiloxane, nonpolar, $30 \text{ m} \times 0.32 \text{ mm} \times 0.25 \text{ } \mu\text{m}$ film thickness) and characterized by MS analysis, using a 5973-Network spectrometer (Agilent Instruments) with an ionization voltage of 70 eV, coupled to the CG instrument.

Theoretical Methods

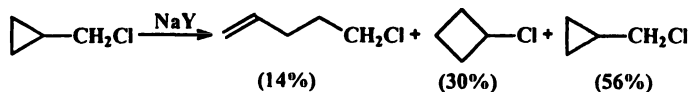
The theoretical studies were carried out employing the ONIOM scheme developed by Morokuma and collaborators (18). This approach can be of great

utility because it allows the study of large molecular system, and thus the study of a particular zeolite structure. In this work, we used a molecular system with 161 atoms ($\text{AlSi}_{45}\text{O}_{69}\text{H}_{46}$), representing the supercage of the zeolite Y. The crystalline structure of the zeolite Y is formed by association of Al and Si tetrahedrons linked by oxygen atoms. The free valences of border aluminum and silicon atoms were saturated with hydrogen atoms, to avoid dangling bonds. The calculations were performed using the ONIOM method available in GAUSSIAN 98 package (19). The molecular system was divided in two layers (Figures 1 to 5). The atoms of the active site of the zeolite Y and the organic moiety (high layer) were treated by the B3LYP functional with 6-31++G(*d*, *p*) orbital basis set, whereas the other atoms (low layer) were treated by the semiempirical MNDO method. Among the possible intermediates (minima on the potential energy surface), we have calculated: carbocations (bicyclobutonium and cyclopropylcarbiny) and alkyl-aluminumsilyl oxonium ions (cyclobutyl, cyclopropylcarbiny and allylcarbiny). The geometry of all species were fully optimized, and characterized as minima on the potential energy surface by the absence of imaginary frequencies, after vibrational analysis of the optimized geometries. Zero-point energies (ZPE) and thermal correction were calculated at the same level. Relative energies were computed and refer to enthalpy differences at 298.15K and 1 atm.

Results and Discussions

Rearrangement of the Cyclopropylcarbiny Chloride

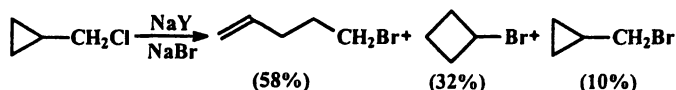
When a gaseous flow of cyclopropylcarbiny chloride is passed over NaY zeolite at room temperature, formation of cyclobutyl chloride and allylcarbiny chloride was observed (scheme 4), as well as cyclopropylcarbiny chloride (product and unreacted starting material). These data are consistent with formation of the C_4H_7^+ cation with internal return of the chloride ion.



Scheme 4: Product distribution from reaction of cyclopropylcarbiny chloride on NaY.

To check this possibility and to exclude any possible concerted rearrangement we used a NaY zeolite impregnated with NaBr, to see if we could observe substitution of the bromide in the organic moiety. After the reaction, besides the chloride products, we also observed the alkylbromides (scheme 5). An interesting point is the relative distribution of the bromides, favoring the allylcarbiny bromide instead of the cyclic bromides, as was found in solution (11).

These results are consistent with ionization of the cyclopropylcarbiny chloride on the zeolite, with formation of the $C_4H_7^+$ cation. Attack of the chloride ion (internal return) might then occur at the three possible positions, giving the rearranged alkyl chlorides. This hypothesis was supported by the data obtained with impregnation of the NaBr on the NaY zeolite. The observation of the three alkylbromides is consistent with a mechanism involving ionization and attack of the external bromide nucleophile.



Scheme 5: Product distribution from reaction of cyclopropylcarbiny chloride on NaY impregnated with 15% of NaBr.

Theoretical Calculations

Figures 1 and 2 show the calculated structure of cyclopropylcarbiny and bicyclobutonium carbocations, respectively, whereas figures 3 to 5 show the calculated structure of allylcarbiny, cyclobutyl and cyclopropylcarbiny aluminumsilyl oxonium ions on the zeolite surface. Analysis of the geometries shows that the carbocations are located on the active site, near the Al atom. This preferential location is due to the neutralization of the negative charge, resulting from the tetracoordination of the aluminum atom in the crystalline structure of the zeolite Y. One can see in figure 2 that the bicyclobutonium ion is stabilized by hydrogen bonding with the zeolite structure, as the C-H...O distance is considerably shorter (1.59 Å) than the same distance in the cyclopropylcarbiny system (2.21 Å). This interaction is responsible for the stretching of the C-H bond (1.15 Å) of the bicyclobutonium relative to the cyclopropylcarbiny cation (1.09 Å). It can also be seen that the Al-O bond of the zeolite framework is slightly larger (1.84 Å) in the case of the bicyclobutonium than in the cyclopropylcarbiny system (1.82 Å), also supporting the hydrogen bonding with the zeolite structure.

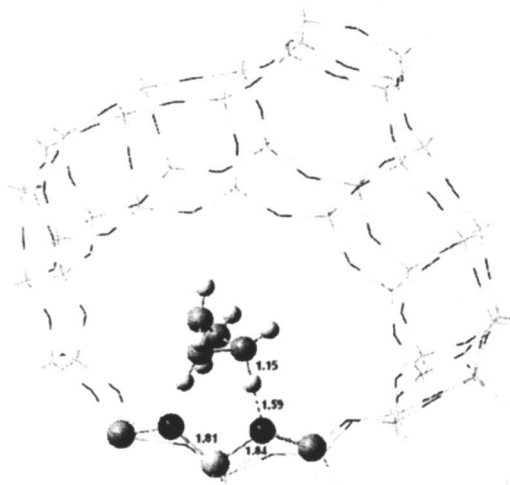


Figure 1: Calculated structure of the cyclopropylcarbinyl carbocation over zeolite Y surface, at B3LYP/6-31++G(d,p):MNDO.

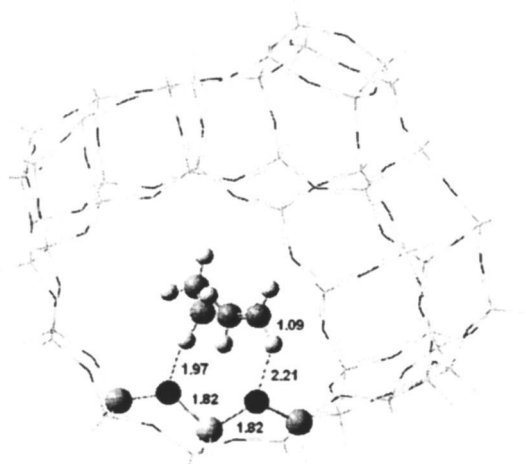


Figure 2: Calculated structure of the bicyclobutonium carbocation over zeolite Y surface at B3LYP/6-31++G(d,p):MNDO.

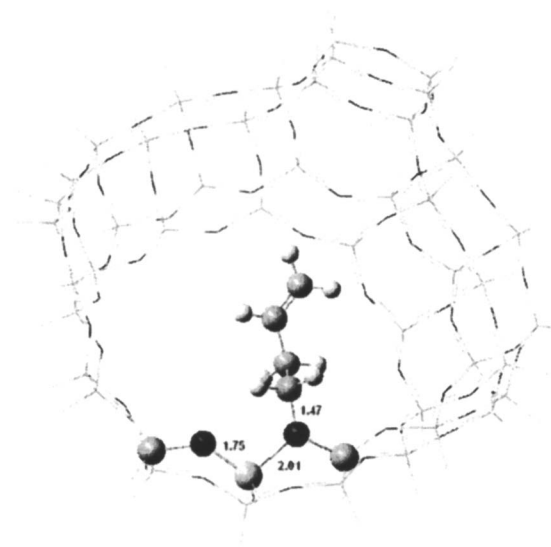


Figure 3: Calculated structure of the allylcarbanyl aluminum-silyl oxonium ion, at B3LYP/6-31++G(d,p):MNDO.

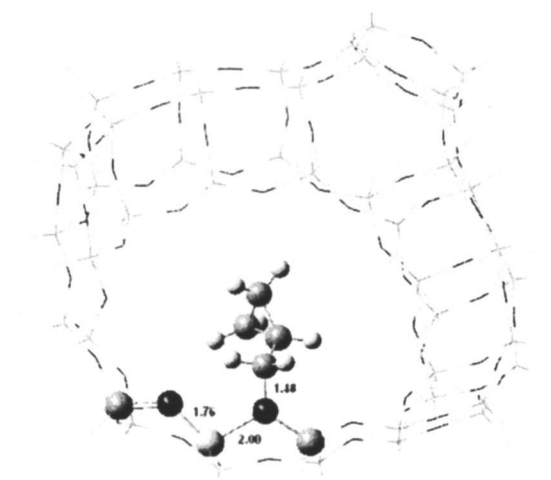


Figure 4: Calculated structure of the cyclopropylcarbanyl aluminum-silyl oxonium ion, at B3LYP/6-31++G(d,p):MNDO.

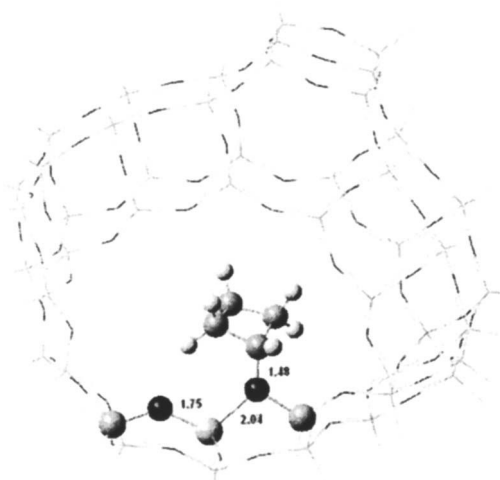


Figure 5: Calculated structure of the cyclobutyl aluminumsilyl oxonium ion, at B3LYP/6-31++G(d,p):MNDO.

Table 1: Relative energy of the calculated alkyl-aluminumsilyl oxonium ions and carbocations, at B3LYP/6-31++G(d,p):MNDO.

<i>Species</i>	<i>Relative Energy (kcal.mol⁻¹)</i>
Allylcarbiny l aluminumsilyl oxonium ion	0.0
Cyclopropylcarbiny l aluminumsilyl oxonium ion	4.5
Allylcarbiny l aluminumsilyl oxonium ion	4.7
Bicyclobutonium cation	36.2
Cyclopropylcarbiny l cation	39.2

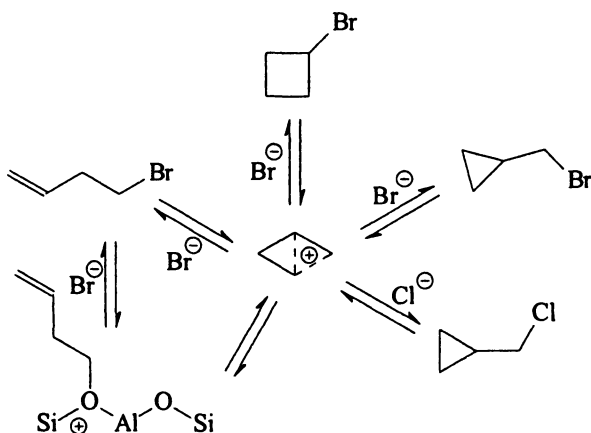
The alkyl-aluminumsilyl oxonium ions are linked to oxygen atom forming a covalent bond. It is interesting to note that the Al-O bond length is considerably stretched, in the range of 2.00 to 2.04 Å, in the alkyl-aluminumsilyl oxonium ions compared with the carbocations. This reflects the tricoordination of the oxygen atom, forming the covalent bond with the alkyl group.

Table 1 summarizes the relative energy for all minima calculated in this study. It can be seen that bicyclobutonium and the cyclopropylcarbinyll ions are minima in the potential energy surface. However, they are higher in energy than the alkyl-aluminumsilyl oxonium ions. The bicyclobutonium is 3.0 kcal.mol⁻¹ lower in energy than the cyclopropylcarbinyll ion, as observed in previous calculations (15). This difference on the zeolite surface might be understood in terms of hydrogen bonding. In fact, hydrogen bonding plays a key role in the adsorption process on zeolite surface, as we suggested elsewhere (20).

The three alkyl-aluminumsilyl oxonium ions are more stable than the carbocations, with the allylcarbinyll aluminumsilyl oxonium ion lying 4.5 and 4.7 kcal.mol⁻¹ lower in energy than cyclobutyl and cyclopropylcarbinyll aluminumsilyl oxonium ions, respectively. This result is in agreement with the thermodynamic stability of the respective chlorides.

The experimental and theoretical results indicated that the bicyclobutonium cation (C₄H₇⁺) is an intermediate on the zeolite surface. The equilibrium between the carbocation and the alkyl-aluminumsilyl oxonium ion might be inferred from the alkylbromide distribution. It has been kinetically shown that the allylcarbinyll bromide is formed in higher percentage than cyclobutyl and cyclopropylcarbinyll bromides over NaY impregnated with NaBr, contrary to what was found in solution, where the cyclic products are formed in larger amounts. The distribution in solution reflects the kinetics of attack of the nucleophile on the bicyclobutonium, as shown by theoretical calculations (17). Formation of allylcarbinyll derivatives is normally preferred under thermodynamical control. To check this possibility we performed experiments with varying flow rate of the carrier gas, but no significant difference in isomer distribution was found, indicating that the distribution over NaY zeolite better reflects the kinetics of the reaction, rather than thermodynamic control. Thus, we suggest that upon ionization the bicyclobutonium might be in equilibrium with the alkyl-aluminumsilyl oxonium ion. It is possible that the allylcarbinyll bromide might be formed either through the interaction of the C₄H₇⁺ ion with the bromide ion or through the interaction of the respective aluminumsilyl oxonium ion with the bromide inside the zeolite cavity (S_N2 type mechanism), explaining its higher distribution on the zeolite surface. The other two alkyl-aluminumsilyl oxonium ions are not susceptible to S_N2 attack, as they would have more sterically demanding transition states than allylcarbinyll aluminumsilyl oxonium ion, nor lead to stable isolated products. This mechanistic proposal is illustrated in scheme 6.

However, this hypothesis does not explain the higher distribution of the cyclobutyl bromide as compared to cyclopropylcarbinyl bromide, since a distribution near 1:1 would be expected, if nucleophilic attack to the bicyclobutonium occurs in the same way as in solution. The different distribution, favoring the cyclobutyl bromide, may suggest that the bromide ion is not uniformly dispersed on the zeolite cavity, preferentially occupying certain positions on the zeolite surface, where it can better attack the bicyclobutonium at one of the three positions.



Scheme 6: Possible mechanistic scheme for cyclopropylcarbinyl chloride rearrangement over NaY/NaBr zeolite.

To check this possibility we performed experiments with different concentrations of NaBr in the NaY zeolite. Table 2 presents the results. It can be seen that upon increasing the amount of NaBr impregnated on NaY, there is preference to formation of the cyclobutyl bromide over allylcarbinyl bromide, indicating that the relative position between the bromide ions and bicyclobutonium governs the product distribution. Hence, zeolites may act as solid solvent, favoring ionization of alkyl halides and nucleophilic substitution reactions. In contrast to liquid solvents, where solvation is mostly uniform, the zeolite surface seems to provide unsymmetrical solvation of the cations, leading to product distribution that is different from solution.

Table 2: Effect of NaBr impregnated on NaY on the distribution of alkyl bromides formed upon ionization of cyclopropylcarbinyl chloride

<i>NaBr impregnated</i>	<i>Allylcarbinyl bromide</i>	<i>Cyclobutyl bromide</i>	<i>Cyclopropylcarbinyl bromide</i>
5	70	20	10
10	63	28	9
15	58	32	10

The concept of zeolite as solid solvent has already been proposed in the literature (21), to account for the ability of zeolites to concentrate the reactants inside their cavities, in terms of partition coefficient, by favoring closer average approximation of the reactants. However, the concept as a solvent to promote ionization and solvation of ionic species seems to arise from the present results, and might be explored in other reaction systems.

Conclusions

Rearrangement of the cyclopropylcarbinyl chloride takes place over NaY zeolite, indicative of the formation of the bicyclobutonium cation. Theoretical calculations show that the bicyclobutonium is an intermediate on the zeolite surface and might be in equilibrium with the alkyl-aluminumsilyl oxonium ion.

Calculations showed that allylcarbinyl aluminumsilyl oxonium ion is the most stable species having 4.5 and 4.7 kcal.mol⁻¹ lower energy than the cyclobutyl and cyclopropylcarbinyl aluminumsilyl oxonium ions, respectively. The bicyclobutonium and cyclopropylcarbinyl ion are 36.2 and 39.2 kcal.mol⁻¹ higher in energy than the allylcarbinyl aluminumsilyl oxonium ion.

The results of cyclopropylcarbinyl chloride rearrangement over NaY impregnated with NaBr suggest that there is an equilibrium between the bicyclobutonium cation and the alkyl-aluminumsilyl oxonium ion, explaining the preferred formation of the allylcarbinyl bromide in the rearranged products. It also suggests that zeolites may act as solid solvents, providing unsymmetrical solvation for the ions inside the cavities.

Acknowledgements

The authors thank CAPES, CNPq and FAPERJ for financial support.

References

1. Olah, G. A.; Prakash, G. K. S.; Sommer, J. *Superacids*; Wiley-Inter-science: New York, NY, 1995.
2. Some authors refer to these species as alkoxides. For more information see: Haw, J. F.; Nicholas, J. B.; Xu, T.; Beck, L. W.; Ferguson, D. B. *Acc. Chem. Res.* **1996**, *29*, 259.
3. Haw, J. F.; Richardson, B. R.; Oshiro, I. S.; Lazo, N.D.; Speed, J.A. *J. Am. Chem. Soc.* **1989**, *111*, 2052.
4. Aronson, M. T.; Gorte, R. J.; Farneth, W. E.; White, D. *J. Am. Chem. Soc.* **1989**, *111*, 840.
5. (a) Kazansky, V. B. *Catal. Today*, **1999**, *51*, 419. (b) Kazansky V. B.; Senchenya, I. N. *J. Molec. Catal.* **1992**, *74*, 257.
6. Tuma C.; Sauer, J. *Angew. Chem. Inter. Ed.* **2005**, *44*, 4769.
7. Boronat, M.; Viruela, P. M.; Corma, A. *J. Am. Chem. Soc.* **2004**, *126*, 3300.
8. Corrêa; R. J.; Mota, C. J. A. *Phys. Chem. Chem. Phys.* **2002**, *4*, 4268.
9. Bidart, A. M. F.; Borges, A. P. S.; Nogueira, L.; Lachter, E. R.; Mota, C. J. A. *Catal. Lett.* **2001**, *75*, 155.
10. Rosenbach Jr. N.; Mota, C. J. A. *J. Braz. Chem. Soc.* **2005**, *16*, 691.
11. Roberts, J. D.; Mazur, R. H. *J. Am. Chem. Soc.* **1951**, *73*, 2509.
12. Olah, G. A.; Kelly, D. P.; Jeuell, C. J.; Porter, R. D. *J. Am. Chem. Soc.* **1970**, *93*, 2544.
13. Starat, J. S.; Roberts, J. D.; Prakash, G. K. S.; Donovan, D. J.; Olah, G. A. *J. Am. Chem. Soc.* **1978**, *100*, 8016.
14. Saunders, M.; Siehl, H. U. *J. Am. Chem. Soc.* **1988**, *102*, 6868.
15. Saunders, M.; Laidig, M.; Wiberg, K. E.; Schleyer, P. v. R. *J. Am. Chem. Soc.* **1988**, *110*, 7652.
16. Koch, W.; Liu, B.; Defrees, D. J. *J. Am. Chem. Soc.* **1988**, *110*, 7225.
17. Casanova, J.; Kent IV, D. R.; Goddard III, W. A.; and Roberts, J. D. *Proc. Nat. Acad. Sci.* **2003**, *100*, 15.
18. Dapprich, S.; Komáromi, I.; Byun, K. S.; Morokuma, K.; Frisch, M. J. *J. Molec. Struct. (THEOCHEM)* **1999**, *1*, 461.
19. Frisch, M. J.; Trucks, G. W.; Schlegel, H. B.; Scuseria, G. E.; Robb, M. A.; Cheeseman, J. R.; Zakrzewski, V. G.; Montgomery, Jr., J. A.; Stratmann, R. E.; Burant, J. C.; Dapprich, S.; Millam, J. M.; Daniels, A. D.; Kudin, K. N.; Strain, M. C.; Farkas, O.; Tomasi, J.; Barone, V.; Cossi, M.; Cammi, R.; Mennucci, B.; Pomelli, C.; Adamo, C.; Clifford, S.; Ochterski, J.; Petersson, G. A.; Ayala, P. Y.; Cui, Q.; Morokuma, K.; Malick, D. K.; Rabuck, A. D.; Raghavachari, K.; Foresman, J. B.; Cioslowski, J.; Ortiz, J. V.; Baboul, A. G. B.; Stefanov, B.; Liu, G.; Liashenko, A.; Piskorz, P.; Komaromi, I.; Gomperts, R.; Martin, R. L.; Fox, D. J.; Keith, T.; Al-Laham, M. A.; Peng,

- C. Y.; Nanayakkara, A.; Gonzalez, C.; Challacombe, M.; Gill, P. M. W.; Johnson, B.; Chen, W.; Wong, M. W.; Andres, J. L.; Gonzalez, C.; Head-Gordon, M.; Replogle, E. S.; Pople, J. A. *Gaussian 98*, Revision A.7, Gaussian, Inc., Pittsburgh PA, 1998.
20. Mota, C. J. A.; Bhering, D. L.; Rosenbach Jr., N. *Angew. Chem. Int. Ed.* **2004**, *43*, 3050.
21. (a) Derouane, E. G. *J. Molec. Catal. A: General* **1998**, *134*, 29. (b) Derouane, E. G.; Crehan, G.; Dillon, C. J.; Bethell, D.; He, H.; Abd-Hamid, S. B. D. *J. Catal.* **2000**, *194*, 410.

Chapter 14

MO Calculations Involving μ -Hydrido Cation Intermediates Relevant to the Heptane to Toluene Dehydrocyclization Reaction

Ted S. Sorensen* and Esther C. F. Yang

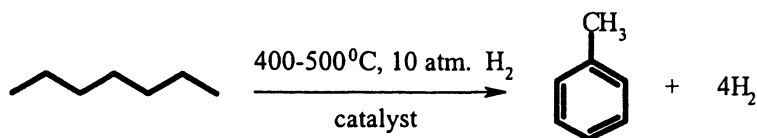
Department of Chemistry, University of Calgary, 2500 University Drive
NW, Alberta T2N 1N4, Canada

*Corresponding author: sorensen@ucalgary.ca

The catalytic dehydrocyclization of alkanes at 400–500°C into aromatics and dihydrogen is a very important petrochemical reaction. Many catalysts have been investigated, but the so-called “dual-function” type catalyst, having both acidic (Al_2O_3) and dehydrogenation (Pt) sites, appear to be superior to those having only a dehydrogenation capacity. The present studies originated from a suggestion by Davis that carbocations may be reactive intermediates in the cyclization part of the overall reaction, with the resulting cycloalkane then dehydrogenated to aromatics by the Pt site. The actual dehydrocyclization reaction of an observable μ -H-bridged cyclodecyl cation is assumed as a reasonable model for how simple linear and branched alkyl cation intermediates could also cyclize. In this work, molecular orbital studies have been performed on both the cyclodecyl cation dehydrocyclization reaction, and on simple n-heptyl and n-octyl cation systems, with the calculations yielding similar ground-state and transition-state structures. An important aspect of commercial dehydrocyclization reactions may involve an alkane isomerization equilibrium which is faster than the dehydrocyclization reaction, and this possibility has also been explored computationally.

Introduction

Catalytic dehydrocyclization (also known as alkane reforming), discovered in 1936, is now an important industrial process that converts alkanes to aromatics (1, 2). This reaction is often shown for the prototypic conversion of heptane to toluene and four moles of hydrogen, although in model studies octanes have played a greater role since there is a larger product diversity possible.

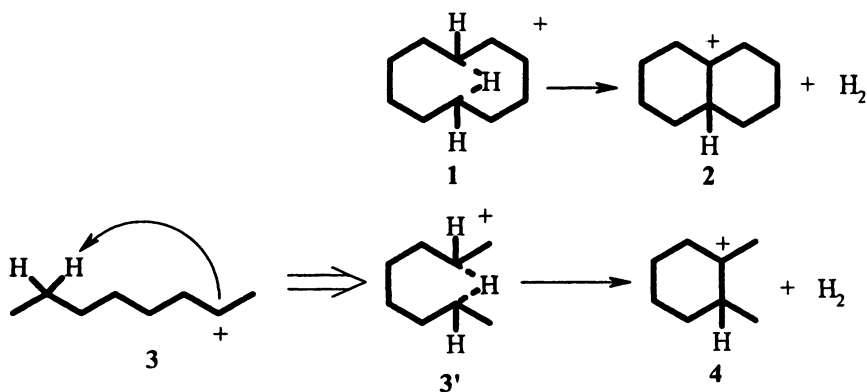


This conversion of alkanes to aromatics greatly improves the octane rating of the fuels and also serves as the most important North American source of aromatics such as benzene, toluene and xylenes (BTX). The earliest catalyst used for this reaction was chromia-alumina ($\text{Cr}_2\text{O}_3/\text{Al}_2\text{O}_3$). However this catalyst had a rather short life-time due to rapid coke build-up which limited its commercial use. In the 1950's, the $\text{Pt}/\text{Al}_2\text{O}_3$ catalyst was introduced and gained rapid commercial success. This $\text{Pt}/\text{Al}_2\text{O}_3$ catalyst is known as a bifunctional catalyst and has both acidic (Al_2O_3) and dehydrogenation (Pt) sites. Promoters are also used to enhance catalytic activity and/or extend catalyst life. Other aspects of this reaction will be discussed subsequently.

There have been numerous laboratory-scale studies designed to probe various aspects of the mechanism(s) by which heptane, and other related alkanes, is converted to aromatics. This background work has been reviewed by Davis (3). These studies can be divided into a number of categories. Many are concerned with catalyst development, optimization of reaction conditions (H_2 pressure, reaction temperature, reaction kinetics, etc). Other studies focus more on "mechanistic" objectives by using single alkane feed stocks, cycloalkanes, and various isotopically-labelled alkanes. Most of these mechanism-probing studies have used monofunctional catalysts (active dehydrogenation catalysts on nonacidic alumina or other neutral supports), e.g. Cr_2O_3 in the older work or Pt, often in conjunction with other metals, e.g. Pt-Sn. It is usually found that a cycloalkane, e.g. methylcyclohexane, is converted to toluene using shorter reaction times, or a lower temperature, than the conditions needed for the heptane conversion, leading to the conclusion that the ring-forming reaction is a ratelimiting process (4). Ring formation can occur readily using monofunctional

catalysts, e.g. Pt, and in recent studies Somerjai (5) has obtained infra-red spectra of some of the adsorbed alkane intermediates on a Pt(111) crystal surface, from which one can obtain cycloalkanes (thought to be mostly cyclopentanes). However in other modeling work, using a bifunctional catalyst, Davis (6-8) has concluded that the cyclization of the alkane feeds under his conditions required the existence of **carbocation intermediates**, formed by reaction of the alkane with acidic sites on the bifunctional catalyst. Thus there appear to be two distinct ways in which cycloalkanes can be formed, and since a dual function catalyst contains both Pt and acidic sites, one would expect both to contribute. However the Davis study is consistent with the carbocation route playing the greater role when one is using these dual function catalysts.

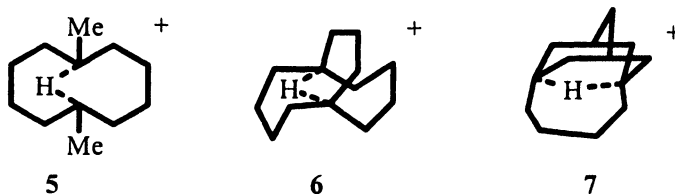
Our interest in the forgoing dehydrocyclization mechanisms stems from some superacid-based studies we carried out some years ago, in which an observable cyclodecyl cation **1** loses H_2 concomitant with C-C bond formation (shown in bold) to give the 9-decalyl cation **2**, and the possible analogy with a 2-octyl cation **3** (as **3'**) giving H_2 and 1,2-dimethyl cyclohexane **4** is shown in Scheme 1. The background to this work is reviewed in the next section.



*Scheme 1: Analogy between the observable dehydrocyclization of **1** under low temperature superacid conditions, and the possible cyclization of a 2-octyl cation in catalytic dehydrocyclizations at 400~500°C. In the μ -H-bridged cations the positive charge is delocalized, so the position of the (+) simply indicates the total charge in these species.*

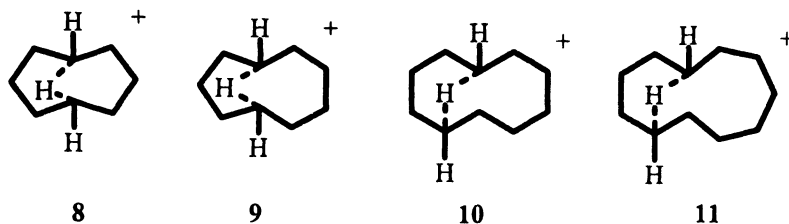
Supercacid Observation and Reactivity of μ -H-Bridged Carbocations

A large number of tertiary alkyl cations have been directly observed by NMR spectroscopy and in some cases by X-ray crystallography (9). An unique subgroup of these cations are those formed in medium-size ring systems, in which a μ -H-bridging structure has been proposed (10, 11, 12), and some examples are shown below:

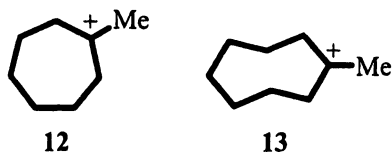


The distinctive feature of these cations is a very high field chemical shift for the bridging (μ -) hydrogen, typically found from ca. δ -4 to -7 ppm. Using moderately low temperature NMR techniques these cations are not difficult to characterize.

In contrast, secondary μ -H-bridged cations are much more fragile, and only the cyclooctyl 8, cyclononyl 9, cyclodecyl 10 and cycloundecyl 11 cations have been characterized.

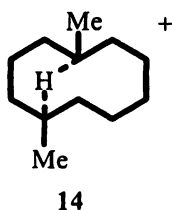


The instability of the cyclooctyl and cyclononyl cations is due to a rapid rearrangement to the lower ring tertiary cation, the 1-methylcycloheptyl 12 and 1-methylcyclooctyl 13 cation, respectively.



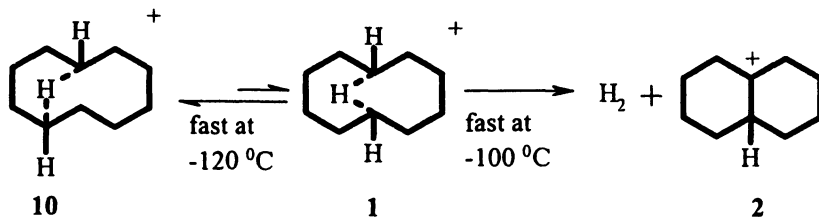
The cyclodecyl system is unique however in undergoing a dehydrocyclization reaction to give the 9-decalyl cation, as was shown in Scheme 1.

When we originally reported the preparation of the μ -H cyclodecyl cation (13), we assigned this a 1,6-bridged structure, in analogy to our previously reported (10) 1,6-dimethyl system 5. However, after preparing the 1,5-dimethylcyclodecyl cation 14, and comparing this with the isomeric 1,6-isomer 5, it was realized that a 1,5- μ -H-bridged (10) structure was a better fit of various NMR parameters than those expected for the secondary 1,6- μ -H-bridged cyclodecyl cation 1, particularly the chemical shift position of the μ -H (14, 15).



Support for this conclusion was provided by several further studies: (1) the 1,5 and 1,6-dimethylcyclodecyl cations 14 and 5 (both bridged structures) underwent equilibration in superacid solution at $-84\text{ }^{\circ}\text{C}$ to give a 2.8/1 mixture favoring the 1,5-structure. (2) theoretical calculations, initially by Galasso (16), and now by us using somewhat higher level methods (B3LYP, MP2/6-31G** with ZPVE correction.), show that the 1,5-secondary cation (10) is slightly more stable than the 1,6-cation (1) (by about 0.8 kcal/mol).

One expects that the TS barrier between these isomeric cations will be substantially less than in the dimethyl case, allowing the following scheme to be written.



Although accurate kinetics have not been obtained experimentally, the ΔG^\ddagger transition-state energy for the above dehydrogenation step has been estimated as 10 ± 1 kcal/mol (15). Since this measurement starts at the energy level of the 1,5-bridged cation, the actual barrier for the second step should be at least 1 kcal/mol lower, e.g. 9 ± 1 kcal/mol.

This introduction brings us back to the structural analogy shown earlier between the cation **1** dehydrocyclization reaction and the plausible connection between this reaction and that for a 2-octyl cation intermediate **3'** (and which could include many other linear alkane carbocation systems with at least six contiguous carbons). Our initial aim therefore was to study computationally the dehydrocyclization of the cyclodecyl cation **1**, to see if one could satisfactorily model this known reaction.

Theoretical Modeling of the Cyclodecyl Cation **1** \rightarrow 9-Decalyl Cation **2** + H₂ Reaction

Olah and coworkers have carried out reactions of alkanes in superacid solution (SbF₅-HF or SbF₅-FSO₃H), leading to observable (by NMR) tertiary alkyl carbocations (17, 18, 19). This reaction is pictured as a protonation of the alkane to give a pentacoordinated intermediate which then loses H₂. Thus, a plausible mechanism for the cyclodecyl \rightarrow 9-decalyl cation reaction could involve loss of the bridging hydrogen (as H⁺) to form decalin, and then reprotonation of the decalin to eventually form H₂ + 9-decalyl cation. However, when the cyclodecyl cation **1** was prepared in SbF₅-FSO₃D solution, there was no evidence of H-D formation in the hydrogen gas that was produced. It was concluded therefore that the H₂ gas must come directly from the carbocation hydrogens without any involvement by the superacid system.

As already mentioned, molecular orbital calculations agree with the experimental finding of μ -H-bridged structures for the secondary and tertiary cyclodecyl cations. Expanding on this work, we were able to obtain ground-state minima (at B3LYP/6-31G**) for the 1,5 *cis*- μ -H-bridged, **10**, and both the 1,6 *cis*- and *trans*- μ -H-bridged stereoisomers (**1**) of the secondary cyclodecyl cation, as shown in Figures 1 and 2.

A transition state (TS) for H₂ loss was easily located in both 1,6- μ -H-structures, and an intrinsic reaction coordinate (IRC) following, shows that each TS is connected to the respective *cis*- or *trans*- 9-decalyl cation + H₂ product. The *cis*-1,5-bridged structure **10** also has a transition-state for H₂ loss, but this is higher in energy than those for the 1,6-analogs since the product tertiary cation

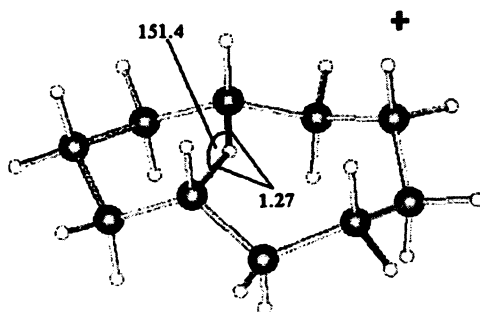


*Figure 1. Optimized 1,5- μ -H-bridged secondary cyclodecyl cation 10, showing bond distance (\AA) and bond angle (degree) at the B3LYP/6-31G** level.*

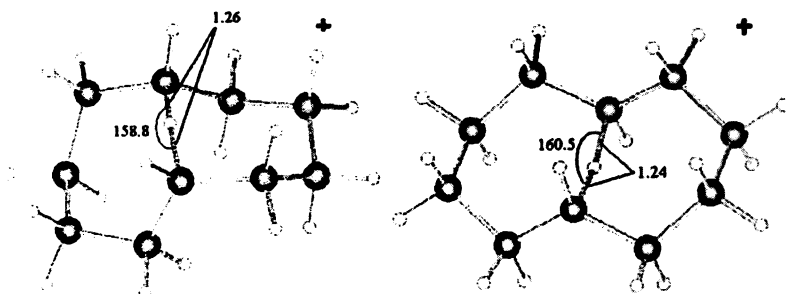


*Figure 2. The cis- and trans-1,6- μ -H-bridged stereoisomers of the secondary cyclodecyl cation 1 showing bond distance (\AA) and bond angles (degree) at the B3LYP/6-31G** level.*

is the considerably more strained 5-7 bicyclic ring system. Note also that these calculated transition-states for H₂ loss cannot be formed from tertiary μ -H-bridged cations because there are no flanking hydrogens.

The transition-state structures for the H₂ loss in *cis* and *trans* **1** are shown in Figure 3, along with some of the key geometric parameters. The transition-state ΔE^\ddagger values at the B3LYP/6-31G** level (corrected for ZPVE with appropriate scaling factor (20)) are 24.6 and 21.2 kcal/mol, respectively, for the *cis*- and *trans*- isomers. At the MP2 level, the corresponding values are 16.3 and 14.4 kcal/mol (18.5 and 15.7 kcal/mol using the recently recommended spin-component-scaled MP2 energies (SCS-MP2) which are obtained when the α - α and β - β components of the second-order perturbation energies are scaled by 1/3 and the α - β components by 6/5 - see reference (21) for further details). Both the B3LYP and MP2 numbers are considerably larger than the experimental ΔG^\ddagger estimate even after taking into consideration the T Δ S term. The experimental rate study for loss of dihydrogen was conducted in an open system (essentially zero back pressure of hydrogen) so this fact can contribute in a small way to a smaller experimental value for ΔG^\ddagger , but another possibility is that some quantum mechanical tunneling may be involved since our modeling does not take this possibility into account.

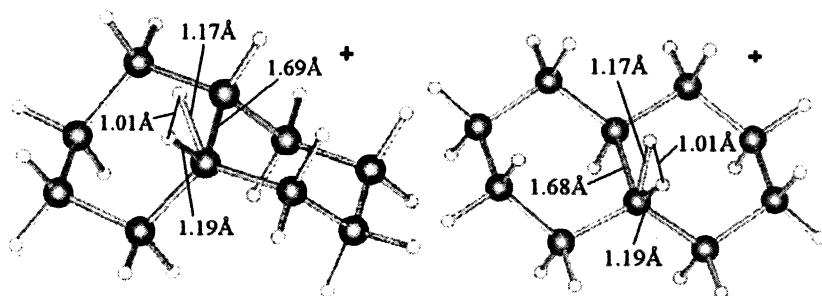
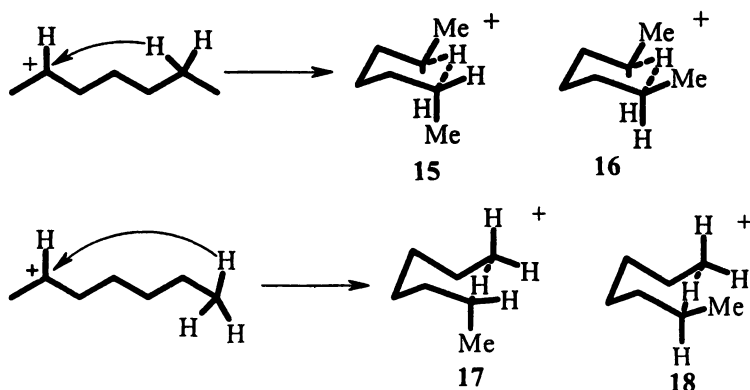


Figure 3. The transition-states for H₂ loss in the *cis*- and *trans* 1-6- μ -H-bridged secondary cyclodecyl cations **1**, showing some of the key geometric parameters at the B3LYP/6-31G** level

These calculations act as a backdrop for the next part of this Chapter, in which we describe calculations of ground-states, transition-states and products, for the loss of H₂ from simple secondary alkyl carbocations, using the cyclodecyl cations as our model.

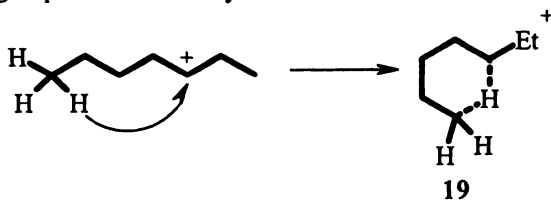
The 2-Heptyl Cation Systems

There are three possible secondary heptyl cations, 2-heptyl, 3-heptyl and 4-heptyl. Calculation at the B3LYP/6-31G** level shows that the 3-heptyl cation is about 1kcal/mol more stable than either the 2- or 4- heptyl cation. The 2-heptyl cation can in principle form a 1,5- μ -H-bridged structure with a methyl group at each termini (isomeric structures 15 and 16) or a 1,6- μ -H-bridge with a primary carbon at one end (isomeric structures 17 and 18), as shown in the following diagrams:



The 1,5- μ -H-bridged structures (15 and 16) have *cis* and *trans*-isomers, and in the 1,6- μ -H-bridged case (17 and 18), the methyl group can adopt a pseudoaxial or equatorial conformation.

The 3- and 4-heptyl cations cannot form a 1,6- μ -H-bridge. The 3-heptyl cation could in principle form a primary-secondary 1,5- μ -H-bridged structure with an ethyl group at the secondary cation terminus.



Primary cations are about 15 kcal/mol less stable than secondary cations and are unlikely to make a significant contribution to the overall reactions, even at high temperatures, and so these have been excluded from consideration. Isomerization between the "normal" extended structures of the 2-, 3-, and 4-

heptyl cations are expected to involve very low energy hydride shift transition-state barriers, or to even exist as 1,2-H- bridged or partially bridged structures. Considerable background information on this subject is available both experimentally (17, 18, 22) and from calculations (23, 24, 25) for the related secondary 2-butyl cation. It should be mentioned in this regard that secondary alkyl carbocations larger than 2-butyl have not been observed under low temperature-superacid conditions, only rearranged tertiary ions are seen. However, these rearrangements are potentially reversible and the implications of this will be part of our later discussion.

Calculations at the B3LYP/6-31G** level on structures 15 to 19 shows that the *cis*- 1,5- μ -H-bridged structure 16 is the global minimum. This result is similar to that found in a recent computational study by Siehl (26). In Table I, the relative energies of 15 to 19 are compared, where the *cis*-1,5- μ -H-bridged structure 16 is set as an arbitrary zero reference point for these energy comparisons.

Table I. The relative energies for 15 to 19 in kcal/mol at B3LYP/6-31G and SCS-MP2/6-31G****

	B3LYP ^a	SCS-MP2 ^a
15	1.16	1.02
16	0	0
17	9.90	9.64
18	8.46	8.96
19	4.19	5.30

^a Corrected for ZPE.

It is gratifying to find that the 1,6- μ -H-bridged primary-secondary structures 17 and 18 are minima, even if they are 7-9 kcal/mol less stable than the 1,5- μ -H-bridged secondary-secondary systems, 15 and 16. The bonding in 17 and 18 is clearly not a symmetrical μ -H bond, as shown by the two different C—H—C distances in the calculated structures 17 and 18 shown in Figure 4. In contrast, the C—H—C bond distance in the 1,5- μ -H bridges (15 and 16) are essentially the same length, as shown in Figure 5. A calculation at the B3LYP/6-31G** level shows however that structure 19, where one tries to form a primary-secondary 1,5- μ -H bond, is only very weakly bridged, as shown in Figure 6. It is worth noting that this 1,5- μ -H-bridged primary-secondary cation 19 behaves quite differently from the corresponding 1,6 systems 17 and 18, where clear evidence of bridging is observed.

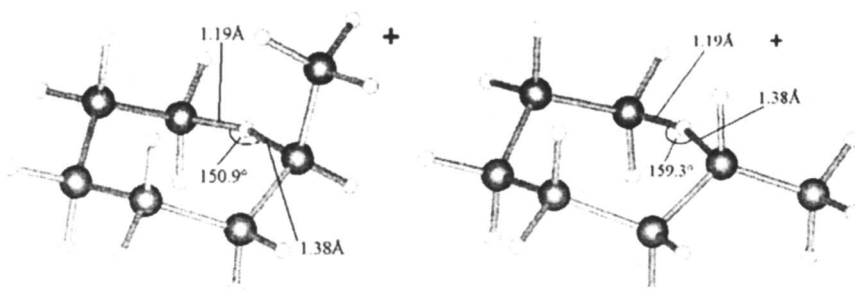


Figure 4. The 1,6- μ -H-bridged stereoisomers (17 and 18) formed from 2-heptyl cation showing bond distance and bond angles at the B3LYP/6-31G** level.

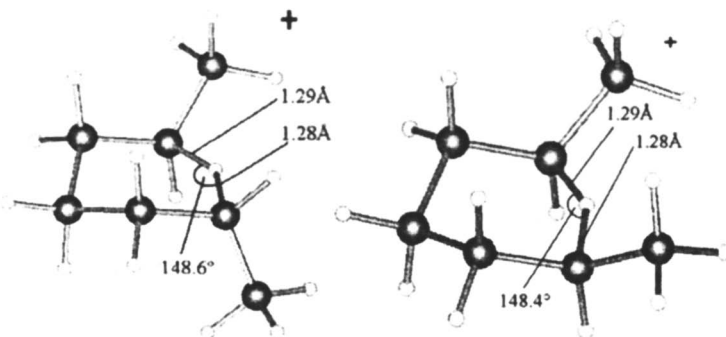


Figure 5. The 1,5- μ -H-bridged stereoisomers (15 and 16) formed from 2-heptyl cation showing bond distance and bond angles at the B3LYP/6-31G** level.

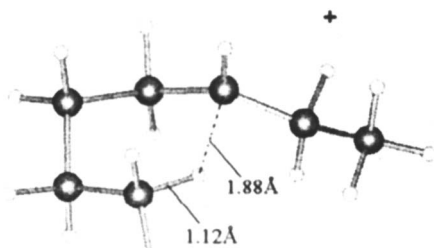


Figure 6. Optimized primary-secondary 1-5- μ -H-bridged structure **19** at the B3LYP/6-31G** level. Notice the long and very weakly bridged μ -H bond.

For the more stable of the two isomers of each type (1,5 and 1,6- μ -H-bridges), cations **16** and **18**, one can locate a transition-state for dehydrocyclization, leading to product ions **20** and **21** respectively, plus molecular hydrogen.



These transition-state structures are shown in Figure 7 and the relative energies of the isomeric transition-states at B3LYP and SCS-MP2/6-31G** level are compared in Table II. One notes that in spite of a 8-9 kcal/mol difference in ground-state energies, the overall transition-state for dehydrocyclization slightly favors the 6 membered ring formation. In the case of the 1,6- μ -H-bridged structure **18** there are in fact two transition-states possible, (the most stable one is that shown in Figure 7), and Figure 8 shows the structure of this second isomer, **22**, where the bridging H combines with a hydrogen on the “primary” side of the original bridge.

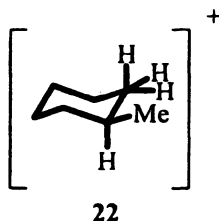


Table II. The relative transition state energies (kcal/mol) at B3LYP and SCS-MP2/6-31G for ground-state structures 16, 18 and 22^a**

	B3LYP	SCS-MP2
TS for 16→19	32.4	26.48
TS for 18→20	30.76	25.33

^a In each case the ground-state energy comparison was to cation 16, the most stable ground-state structure. The data is reported this way because the various ground-states will be in rapid equilibrium, making calculations of individual transition-state energies rather meaningless.

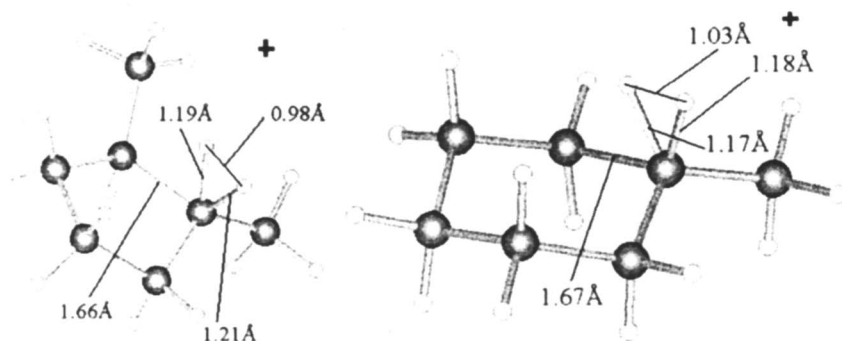
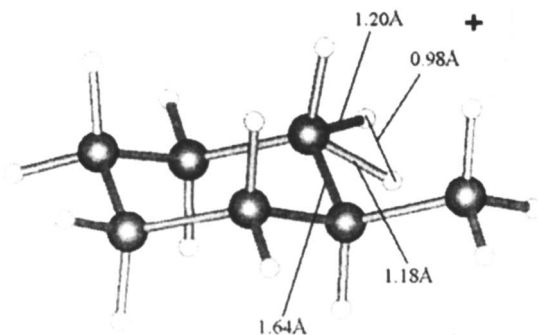


Figure 7. Optimized transition-states for H₂ loss for the 1,5 (16) and 1,6- μ -H-bridged (18) 2-heptyl cations showing some of the key geometric parameters at the B3LYP/6-31G level**

This transition-state, 22, has a calculated energy only slightly higher (0.48 kcal/mol at B3LYP/6-31G**) than the transition-state for isomer 18, and the geometry is also slightly different, for example, a somewhat shorter H—H bond. Loss of dihydrogen from this transition-state will lead to a secondary cation intermediate, and after a 1,2-hydride shift, to the same 1-methylcyclohexyl cation product that is directly produced from the other route.

So far, we have not discussed the overall reactant-product thermodynamics for these dehydrocyclization reactions (based on carbocation intermediates), and these are shown in Table III and Figure 9.



*Figure 8. Alternative optimized transition-state for H₂ loss in 1-6- μ -H-bridged 2-heptyl cation, 22, leading to a cyclized secondary cation intermediate at the B3LYP/6-31G** level.*

Table III. Overall thermodynamics (kcal/mol) for dehydrocyclization via 1-5 and 1-6 μ -H bridged intermediates

	<i>B3LYP</i>	<i>SCS-MP2</i>
16 → TS → 19 + H ₂	3.63	3.03
18 → TS → 20 + H ₂	3.37	2.18

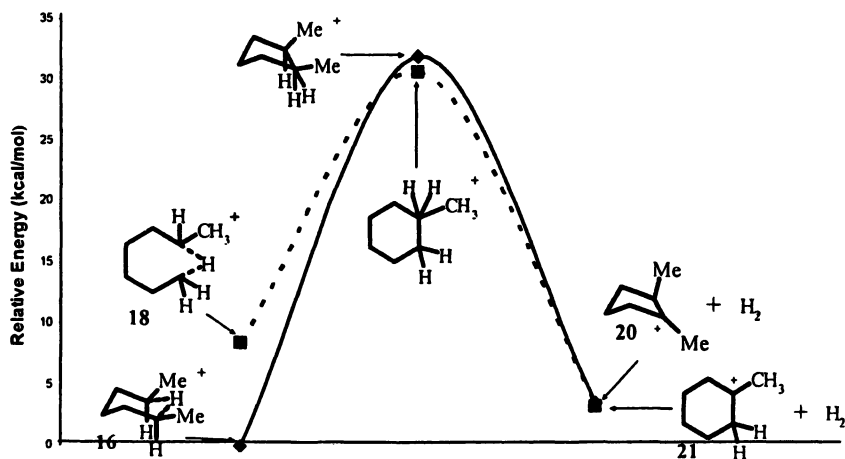


Figure 9. B3LYP/6-31G** Energy profile (ΔE) for 6 ring (---) vs. 5 ring (---) dehydrocyclization in the 2-heptyl cation system. The arbitrary zero reference point is the *cis* 1-5- μ -H-bridged cation 16 (see footnote (a) in Table II). The transition-state structures have been shown in Figure 6. The product ions are the 1-2-dimethylcyclopentyl cation 20 and the 1-methylcyclohexyl cation 21, respectively, and these have almost the same energy at B3LYP/6-31G** level.

For the cyclopentyl cation (20) formation, the reaction is slightly endothermic, while for methylcyclohexyl cation (21), the reaction profile itself is slightly exothermic. However, relative to the most stable 2-heptyl cation, (the 1,5-bridged structure 16) this reaction is also slightly endothermic. Based on calculated ΔG values at 298K, both reaction profiles are exergonic due to a larger entropy contribution for the product side in each case.

One can also verify computationally the connection between a transition-state and the corresponding reactant and product sides by performing an Intrinsic Reaction Coordinate (IRC) calculation. This has been carried out for both the five and six-membered ring formation, as shown in Figure 10 for the latter. It is interesting to note that there is a near inflection point on the product side of the IRC, i.e. a more extreme version of this would lead to a high energy intermediate (a pentacoordinate ground-state). This speculation becomes a reality when we do an IRC calculation on transition-state structure 22. Instead of finding a cyclized secondary cation as a product, the IRC calculation finds a intermediate where the hydrogen molecule is still attached to the carbocation center. A similar observation is also seen in the calculated profile for μ -H $C_2H_7^+$

→ $C_2H_5^+ + H_2$, where at least one high energy pentacoordinate structure is located as an intermediate (minimum on the potential energy surface profile) (27).

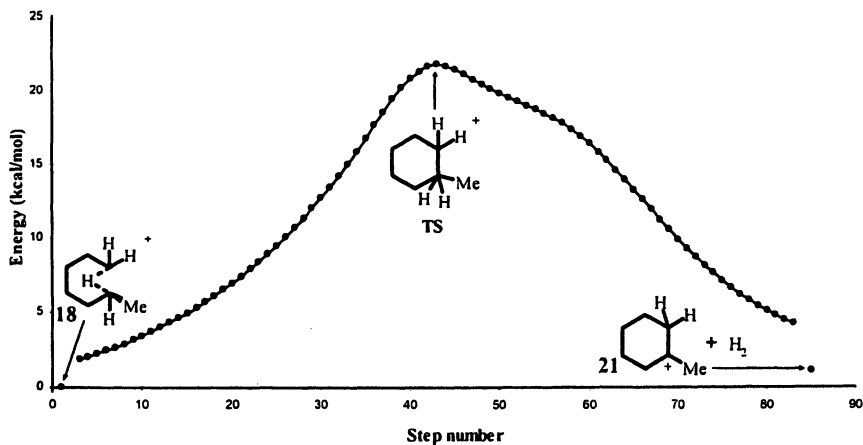
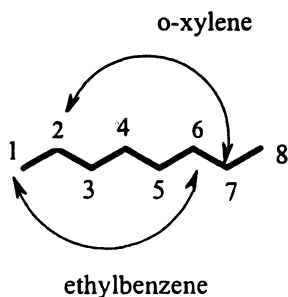


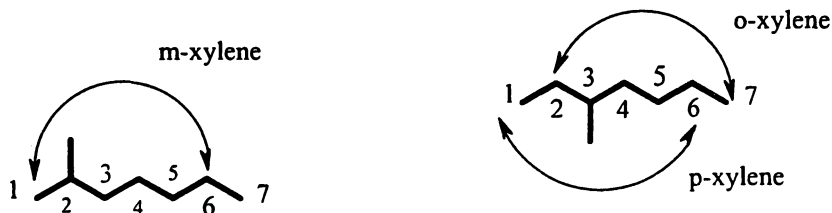
Figure 10. Potential energy diagram for the dehydrocyclization of 18 obtained from an Intrinsic Reaction Coordinate (IRC) calculation at B3LYP/6-31G**. Note that the IRC starts at the TS but does not quite reach either ground-state structure (reactant-products).

Calculations on the 2- and 3-Octyl Cation Systems

In a laboratory scale dehydrocyclization reaction using a dual-function catalyst, Davis (8) reported that the aromatic products were *o*-xylene, *m*-xylene and ethylbenzene in approximately equal amounts (ca. 20-30% each) and *p*-xylene (ca, 15%). The formation of these was assumed to be from a direct 1,6-ring closure, as sketched in the following two diagrams:



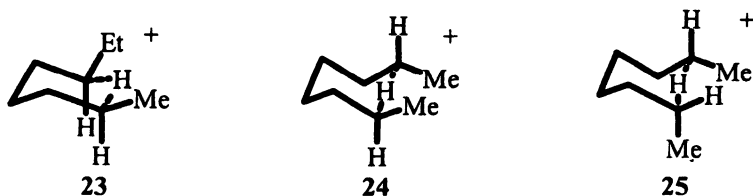
Since there are two different connections possible for n-octane, 1,6 or 3, 8, which could lead eventually to ethylbenzene, there is a statistical entropy factor involved here which is not part of the *o*-xylene route. Therefore, if both closures were equally possible from an enthalpy perspective, one would predict a 2:1 ethylbenzene to *o*-xylene ratio. The formation of the *m*- and *p*-xylene requires prior isomerization of n-octane to 2- and 3-methylheptane, respectively.



In our calculations we will first discuss our results starting with both the 2- and 3- octyl cations (the 4- octyl cation cannot form a 1,6- μ -H-structure). The n-octane conversion to aromatics, as described by Davis (8), is a good test of our proposed mechanisms, for several reasons: (1) his experimental observation would require the formation of approximately equal amounts of 1,2-dimethylcyclohexane (*o*-xylene) and ethylcyclohexane (ethylbenzene), even though in our mechanism the structure of the needed 1,6- μ -H cation intermediates are quite different, and (2) the formation of *m*- and *p*-xylene requires a prior isomerization of n-octane to 2- and 3- methylheptane, and this must be a faster reaction than the dehydrocyclization (or at least competitive with it). If our mechanisms are valid, we should be able to reproduce some aspects of the above results.

Calculations of the 2-Octyl Cation System

Both 1,5- and 1,6- μ -H-bridged structures were found as a ground-states for the 2-octyl cation, the global minimum being the *cis*- 1,5- μ -H-bridged structure **23**, which is 2.60 kcal/mol more stable than both *cis*- and *trans*-dimethyl 1,6- μ -H-bridged structures **24** and **25**.



Only the 1,6- μ -H-bridged structures (24 and 25) are discussed in detail here since these lead to six-membered rings and their transition-states for dehydrocyclization are smaller than for the 1,5- μ -H-bridged 23. However, since 23 is the global minimum for the octyl cation system, it will be used as an arbitrary zero reference point for energy comparison between other isomers.

The bond lengths and the angle of the 1,6- μ -H-bridge in 24 and 25 is shown in Figure 11. Overall these structures have a very similar geometry to those of the cyclodecyl cation (1), as shown by the comparisons in Table IV. The corresponding dehydrogenation transition-states, shown in Figure 12, are also quite similar to those found in the cyclodecyl case, and the geometric data for these are compared in Table V.

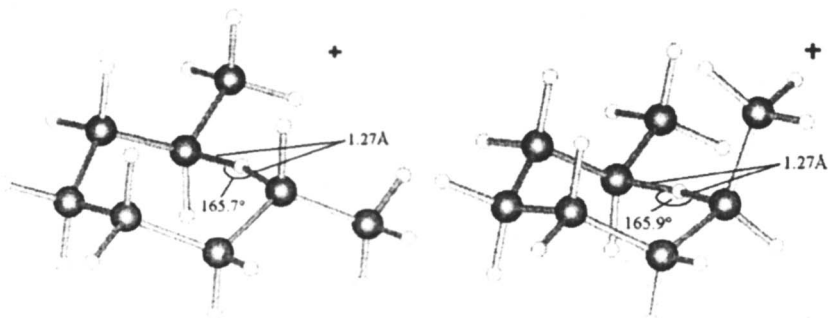


Figure 11. Optimized structure for cis- and trans-dimethyl 1,6- μ -H-bridged 2-octyl cation structures 24 and 25 showing bond distances and bond angles.

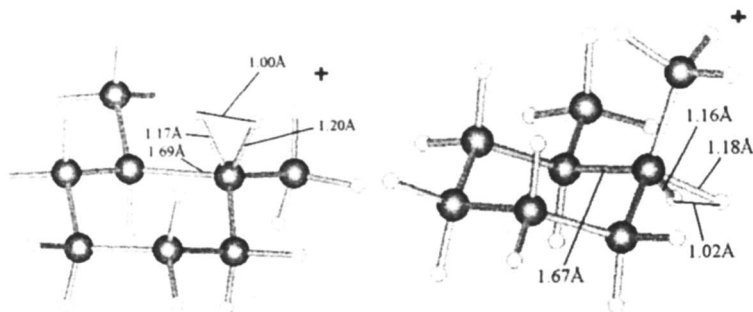
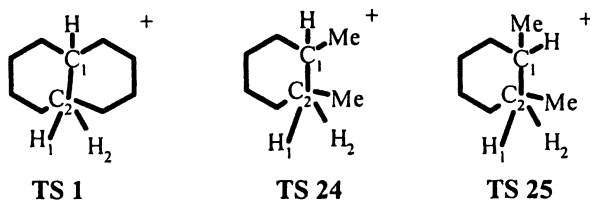


Figure 12. The transition-states for H_2 loss in the cis- and trans-dimethyl 1,6- μ -H-bridged 2-octyl cations **24** and **25**, showing some of the key geometric parameters at the B3LYP/6-31C** level.

Table IV. Geometry comparison between the μ -H-bridged cyclodecyl cation **1** and the 2-octyl cations **24** and **25**

	C_1-H_1 (Å)	H_1-C_2 (Å)	Angle $C_1H_1C_2$ (degree)
1 trans	1.24	1.24	160.5
1 cis	1.26	1.26	158.8
24 (cis)	1.27	1.27	165.7
25 (trans)	1.27	1.27	165.9

Table V. Geometry comparison between the transition states for dehydrocyclization of 1 and 24 and 25



	C_1-C_2 (Å)	H_1-H_2 (Å)	H_1-C_2 (Å)	H_2-C_2 (Å)
TS 1 trans	1.68	1.01	1.19	1.17
TS 1 cis	1.69	1.01	1.19	1.17
TS 24 (cis)	1.69	1.00	1.20	1.17
TS 25 (trans)	1.67	1.02	1.18	1.16

Calculations of the 3-Octyl Cation System

The formation of a 1,6- μ -H-bridged cation in this case requires the existence of primary-secondary termini, as sketched in the structural drawings (26, 27) below:



One might expect those μ -H structures to be considerably less stable than the 2-octyl cation counterparts, where secondary-secondary termini are involved in both 1,6 and 1,5- μ -H bridges, and this was indeed the case. Optimized structures found for 26 and 27 are shown in Figure 13, and their transition states for H_2 loss are shown in Figure 14. The overall energy profile (at B3LYP/6-31G**) for structures 24 to 27, along with their respective transition-states and products are shown in Table VI.

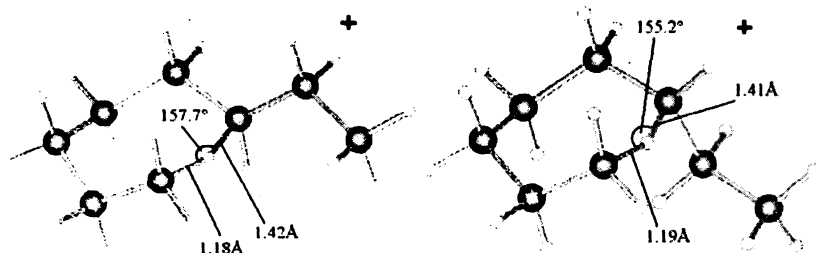


Figure 13. Optimized structure for *cis*- and *trans*- secondary-primary-1,6- μ -H-bridged 3-octyl cations **26** and **27** showing bond distance and bond angle at the B3LYP/6-31G** level.

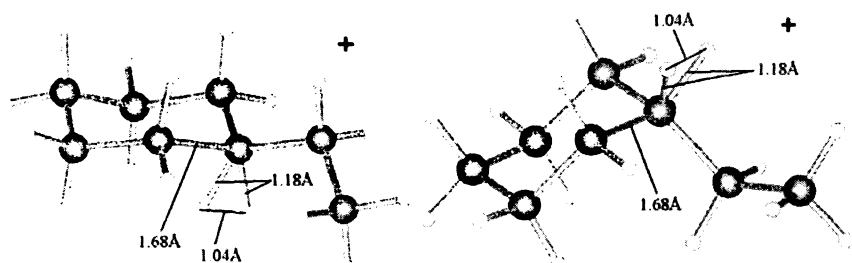


Figure 14. The transition-states for H_2 loss in the *cis*- and *trans*- secondary-primary-1,6- μ -H-bridged 3-octyl cations **26** and **27**, showing some of the key geometric parameters at the B3LYP/6-31G** level.

Table VI. Overall $\Delta E_{\text{reaction}}$ at B3LYP and SCS-MP2/6-31G for the 1,6- μ -H-bridged 2- and 3-octyl cation systems (structures 24 to 27).**

	<i>μ-H-bridged ground state^a</i>		<i>Transition-state</i>		<i>Products (cation + hydrogen)</i>	
	<i>B3LYP</i>	<i>SCS-MP2</i>	<i>B3LYP</i>	<i>SCS-MP2</i>	<i>B3LYP</i>	<i>SCS-MP2</i>
24	2.60	2.20	29.60	23.43	2.49	-0.68
25	3.97	3.31	31.88	24.84	4.24	0.60
26	7.99	8.35	30.99	25.74	3.53	2.60
27	9.47	9.41	32.95	27.12	3.62	1.37

^a Since the various 2- and 3-octyl cations will be in rapid equilibrium, the data in this Table are referenced to the most stable ground-state structure, cation 23.

A graphical energy comparison of the 1,6- μ -H-bridged 2- and 3-octyl cation systems (using the most stable isomers in each case, 24 and 26) is sketched in Figure 15. Although the secondary-secondary transition-state position for the 2-octyl cation is slightly lower than that for the 3-octyl system, the difference is surprisingly small. In the latter cation system we did not try to model the alternative transition-state for the loss of hydrogen, where a primary hydrogen bonds to the μ -H (see discussion of this in the 2-heptyl cation section). However one would expect a very similar alternative transition-state to also exist in this case, making the energy barrier comparison for 24 and 26 even closer.

n-Octane Isomerization

As previously mentioned, Davis (8) has shown that in model dehydrocyclization reactions with a dual function catalyst and an n-octane feedstock, isomerization of the hydrocarbon to 2- and 3-methylheptane is faster than the dehydrocyclization reaction. Although competitive isomerization of an alkane feedstock is commonly observed in model studies using monofunctional (Pt) catalysts, some of the alkanes produced can be rationalized as products of the hydrogenolysis of substituted cyclopentanes, which in turn can be formed on platinum surfaces via free radical-like mechanisms. However, the 2- and 3-methylheptane isomers (out of a total of 18 possible C₈H₁₈ isomers) observed with dual function catalysts are those expected from the rearrangement of n-octane *via* carbocation intermediates. Such acid-catalyzed isomerizations are widely acknowledged to occur *via* a protonated cyclopropane structure (25, 28), in this case one derived from the 2-octyl cation, which can then be the precursor

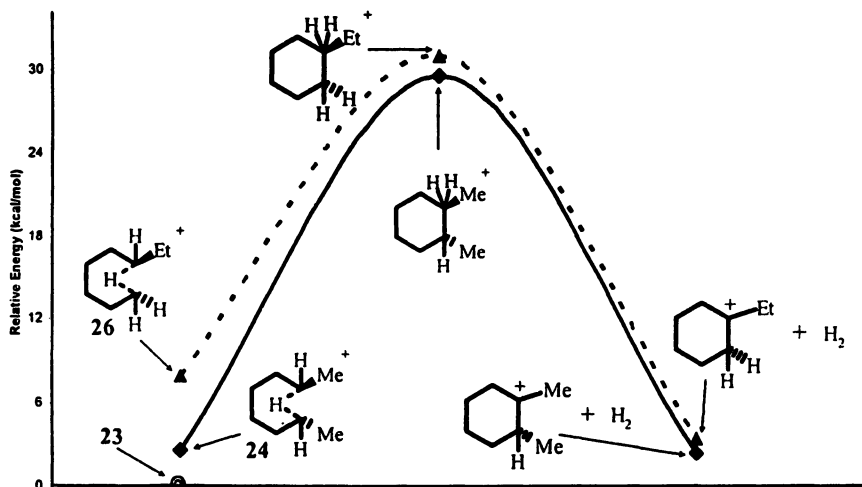


Figure 15. The overall calculated energy profile for the 2- (---) and 3- (- - -) octyl cation systems (24 and 26). The zero reference point is structure 23. The calculated structures for the ground-states and transition-states are shown in Figures 11-14.

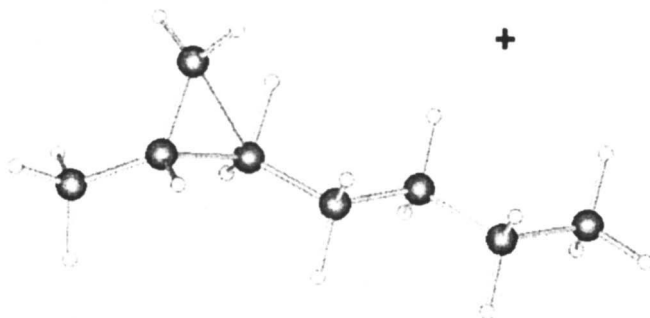


Figure 16. Protonated cyclopropane intermediates 28 from 2-octyl cation.

of both 2- and 3-methylheptane. The calculated structure of the protonated cyclopropane transition-state **28** is shown in Figure 16.

This protonated cyclopropane is found at B3LYP/6-31G** to be 15.99 kcal/mol above the 1,5- μ -H-bridged **23**, the most stable structure of the 2-octyl cation. This transition-state is thus significantly smaller than the calculated transition-states that we have obtained for the dehydrocyclization mechanisms (29.60 kcal/mol for structure **24**), and therefore in at least qualitative agreement with the observation of Davis (8) that an equilibration of n-octane with at least some other iso-octanes is set up prior to significant dehydrocyclization of the feedstock.

Dehydrocyclization of 2- and 3-Methylheptane

We have not carried out calculations starting with secondary cations derived from the title alkanes because at a computational level, these will have ground-states and transition-states similar to heptane itself (previously discussed). This will be true even though the most stable carbocations in these branched alkanes will be the corresponding tertiary ions, which in themselves will not be directly involved in dehydrocyclization processes. However, one has to keep in mind that the thermodynamic ground-states in these "real" catalytic reactions will be the alkanes themselves, and in this regard secondary cations formed from n-octane or 2- (or 3-) methylheptane will not differ much in absolute energy. As shown earlier, a 1,6-closure of 2-methylheptane leads eventually to *m*-xylene, while 3-methylheptane has eventual routes to both *o*- and *p*-xylene.

Formation of Cyclopentanes

Alkyl-substituted cyclopentanes are formed with both monofunctional and dual functional catalyst systems, and some mechanistic proposals for forming six-membered rings even involve a ring expansion of cyclopentanes to cyclohexanes. In our calculations of the 2-heptyl cation system *via* a 1,5- μ -H-bridged structure, one can readily find a transition-state for 1,2-dimethylcyclopentane formation (see previous discussion), and although this transition-state is slightly higher in energy than the six-ring transition-state, both reactions would be competitive at 400~500°C. Note also that we have not calculated all of the possible cyclopentane transition-states which could be involved in the heptane and octane series.

As mentioned, cyclopentanes can be formed with monofunctional catalysts, and so even with dual function catalysts, one would expect some of the cyclopentanes to form via mechanisms associated with the platinum reactivity part of the dual functionality.

Thermodynamics of Dehydrocyclization—A Quick Look

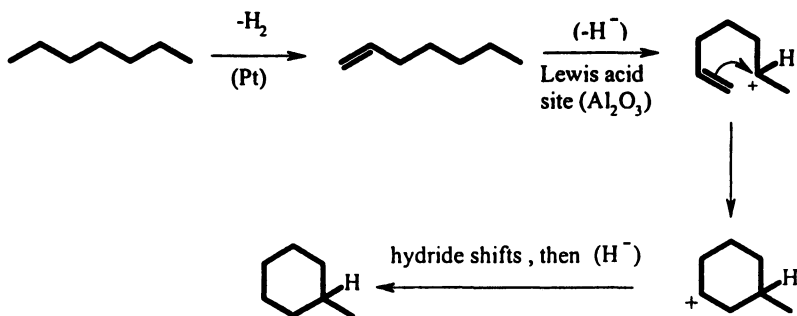
With STP conditions, the hypothetical reaction of heptane to give methylcyclohexane and dihydrogen is endothermic and endergonic. At higher temperatures the $T\Delta S$ term of the overall $\Delta G_{\text{reaction}}$ become increasingly important, but this is off-set in industrial situations by the use of ca. 10 atm of dihydrogen pressure. Given the above, there must be some measure of reversibility for the formation of cycloalkanes from alkanes, particularly for cyclopentanes, because they are generally thermodynamically less stable than cyclohexanes and unlike cyclohexanes they cannot be directly dehydrogenated to aromatics. Cyclopentanes formed under dual function catalyst conditions would have the possibility of reverse addition of hydrogen to a cyclopentyl cation intermediate, to give an alkyl cation intermediate (and eventually an alkane), i.e. the reverse of their proposed formation. Platinum catalyzed hydrogenolysis reactions of cyclopentanes are thought to be important reactions with monofunctional catalysts, and this mechanism could certainly also be operative with the cyclopentanes formed via the carbocation route using the dual function catalysts.

While a majority of laboratory-scale dehydrocyclization studies involve carefully chosen feedstocks, often a single alkane, commercial operators use a naphtha fraction consisting of a complex mixture of hydrocarbons. At least some of these will be incapable of easily undergoing direct dehydrocyclization and need to be isomerized into “reactive” structures if aromatics are to be formed. The work of Davis suggests that the acidity of dual function catalysts is an important added factor in these isomerizations, one which likely complements the different set of isomerizations that may be catalyzed by the platinum function.

Conclusions and Scope for Future Studies

Although there is clear experimental evidence (8) in model dehydrocyclization reactions, using a dual function catalyst, that carbocations are

crucial intermediates in forming cyclic rings from acyclic precursors, there are other speculative ways in which this cyclization could proceed. Perhaps the most obvious one is that shown in Scheme 2: (alkenes are known components of dehydrocyclization reaction mixtures)



Scheme 2. Possible alternative formation of cyclic rings via a carbocation intermediate.

In contrast to this mechanism, the one proposed in our work operates direct from the oxidation state of the alkane feedstock. The **same** alkyl cation intermediate can lead to **both** alkane isomerization (an alkyl cation is widely accepted as the reactive intermediate in these reactions) and we have shown in this paper that a mechanistically viable dehydrocyclization route is feasible starting with the identical cation. Furthermore, the relative calculated barrier for each of the above processes is in accord with the experimental finding of Davis, i.e. that isomerization of a pure alkane feedstock, n-octane, with a dual function catalyst (carbocation intermediate) leads to an equilibration with isooctanes at a faster rate than the dehydrocyclization reaction of these octane isomers (8).

Finally, one has to concede that gas-phase calculations are not the ideal way to model a reaction taking place on a catalyst surface. Computational chemistry developments in this area have been continuing but they are a long way from providing completely realistic models. For example, the overall kinetics for dehydrocyclizations are likely to be rate-limited by the binding of the alkane substrate to catalytically active sites.

Rather large $k_{\text{H}}/k_{\text{D}}$ isotope ratios (29) have been reported in model studies of dehydrocyclization using deuterated vs. normal alkanes, particularly when one considers the high temperatures being used, but the origin of these “effects” is difficult to sort out. In contrast to catalytic dehydrocyclization reactions, the dehydrocyclization reactions of the observable μ -H-bridged cyclodecyl cations are much more amenable to mechanistic studies, albeit difficult because of the low temperatures involved. Examination of the dehydrocyclization transition

states calculated for the cyclodecyl μ -H-bridged structures leaves open the question of whether tunneling through this barrier might be taking place (this could explain the discrepancy between calculated and observed transition-state energies) and a study of the dehydrocyclization of a normal vs. perdeuterated cyclodecyl cation would be very informative in this regard.

Acknowledgements

We thank NSERC (Canada) and the University of Calgary for financial support for this project.

Reference

1. Kazansky, B.A.; Plate, A.F. *Ber.* **1936**, *69*, 1862.
2. Moldvasky, B.L.; Kamisher, H.D. *Compt. Red. Acad. Sci. U.R.S.S.* **1936**, *1*, 355.
3. Davis, B.H. *Catalysis Today* **1999**, *53*, 443-516.
4. Feighan, J.A.; Davis, B.H. *Int. Catalysis* **1965**, *4*, 594.
5. Yang, M.; Somorjai, G.A. *J. Am. Chem. Soc.* **2004**, *126*, 7698.
6. Srinivasan, R.; Sparks, D.; Davis, B.H. *J. Mol. Catal.* **1994**, *88*, 325.
7. Srinivasan, R.; Davis, B.H. *J. Mol. Catal.* **1994**, *88*, 343.
8. Sparks, D.; Davis, B.H. *J. Mol. Catal.* **1994**, *88*, 359.
9. T. Laube, *Accounts of Chemical Research* **1995**, *28*, 399.
10. Kirchen, R.P.; Sorensen, T.S. *J. Chem. Soc., Chem. Commun.* **1978**, 769.
11. McMurry, J.E.; Hodge, C.N. *J. Am. Chem. Soc.* **1984**, *106*, 6450.
12. Sorensen, T.S.; Whitworth, S.M. *J. Am. Chem. Soc.* **1990**, *112*, 8135.
13. Kirchen, R.P.; Sorensen, T.S.; Wagstaff, K. *J. Am. Chem. Soc.* **1978**, *100*, 6761.
14. Kirchen, R.P.; Ranganeyakulu, K.; Rank, A.; Singh, B.P.; Sorensen, T.S. *J. Am. Chem. Soc.* **1981**, *103*, 588.
15. Kirchen, R.P.; Sorensen, T.S.; Wagstaff, K.; Walker, A.M. *Tetrahedron* **1986**, *42*, 1063-1070.
16. Galasso, V. *Int. J. Quantum Chem.* **1998**, *70*, 313.
17. Olah, G.A.; Prakash, G.K.S.; Williams, R.E.; Wade, K. *Hypercarbon Chemistry*; Wiley-Interscience: New York, NY, 1987, 148f.
18. Olah, G.A.; Prakash, G.K.S.; Sommer, J. *Superacids*; Wiley Interscience: New York, 1985, 125f.
19. Olah, G.A. *J. Am. Chem. Soc.* **1972**, *94*, 808-820.
20. Scoff, A.P.; Radom, L. *J. Phys. Chem.* **1996**, *100*, 16502-16513.
21. Grimme, S. *J. Chem. Phys.* **2003**, *118*, 9095-9102.

22. Saunders, M.; Hagen, E.L.; Rosenfeld, J. *J. Am. Chem. Soc.* **1968**, *90*, 6882.
23. Carneiro, J.W.M.; Schleyer, P.R.; Koch, W.; Raghavachari, K. *J. Am. Chem. Soc.* **1990**, *112*, 4046.
24. Buzek, P.; Schleyer, P.R.; Sieber, S.; Koch, W.; Carneiro, J.W.M.; Vancik, H.; Sunko, D.E. *J. Chem. Soc., Chem. Commun.* **1991**, 671
25. Sieber, S.; Buzek, P.; Schleyer, P.R.; Koch, W.; Carneiro, J.W.M. *J. Am. Chem. Soc.* **1993**, *115*, 259-270.
26. Vrcek, V.; Vrcek, I.V.; Siehl, H.U. *J. Phys. Chem. A* **2006**, *110*, 1868-1874.
27. Carneiro, J.W.M.; Schleyer, P.R.; Saunders, M.; Remington, R.; Schaefer, H.F.; Rank, A.; Sorensen, T.S. *J. Am. Chem. Soc.* **1994**, *116*, 3483-3493.
28. Saunders, M.; Hagen, E.L.; Rosenfeld, J. *J. Am. Chem. Soc.* **1968**, *90*, 6882.
29. Price, G.L.; Ismagilov, Z.R.; Hightower, J.W. In *Proc 7th Int. Catal. Congr.*, Seiyama, T.; Tanabe, K., Ed.; Elsevier, Amsterdam, **1981**, 708-723.

Chapter 15

Theoretical Studies on Structure and Dynamics of Carbonium Ions

Pierre M. Esteves¹, Felipe P. Fleming¹, and André G. H. Barbosa²

¹Instituto de Química, Universidade Federal do Rio de Janeiro, Centro de Tecnologia, Bloco A, Cid. Universitária, Rio de Janeiro, Brazil 21949-900
(pesteves@iq.ufrj.br)

²Instituto de Química, Universidade Federal Fluminense, Outeiro de São João Batista, s/n, Niterói, Rio de Janeiro, Brazil 24020-150
(andre@vm.uff.br)

Modern valence bond (VB) theories such as Spin-Coupled theory, together with DFT and Møller-Plesset MO methods, and *ab initio* molecular dynamics, were employed to study structure/dynamics in representative carbonium ions.

Introduction

Carbocations are central to hydrocarbon chemistry (1). Much of this chemistry is based on acid catalysis, which leads to generation of positive ions of carbon. The resulting intermediates are classified as carbenium and carbonium ions, as proposed by Olah (2-4). Carbonium ions are the penta- or higher coordinate carbocations that maintain 8 valence electrons via 2-electron/3-center bonding, quite different from carbenium ions that possess only 6 valence electrons. Figure 1 shows a systematic classification of carbocations.

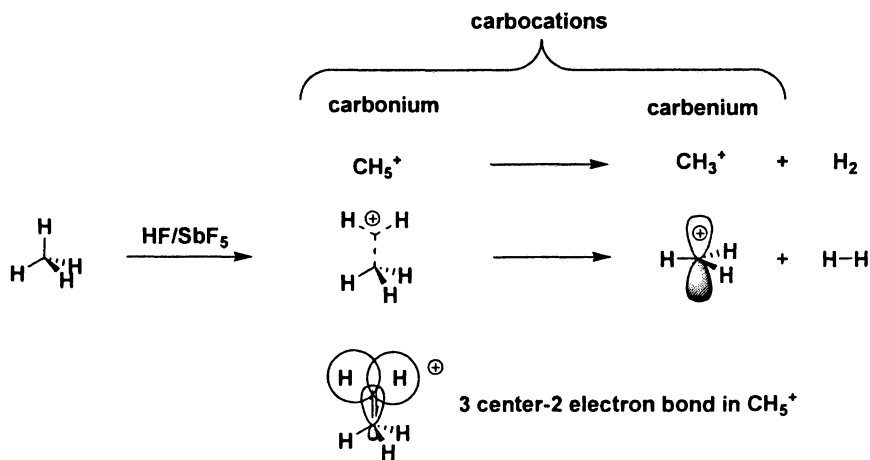


Figure 1. Classification of carbocations into carbonium and carbenium ions, according Olah.²

Methonium ion (CH₅⁺)

The methonium ion (CH₅⁺) is the parent species of all carbonium ions and has attracted a great deal of interest, not only because of its relevance to hydrocarbon chemistry, but also due to its importance in astrochemistry and combustion chemistry. It has an unusual bonding scheme involving a 3-center (nuclei) 2-electron bond (3c2e). Its highly fluxional nature has stimulated active discussion on the nature of the chemical structure for this molecule. Detailed studies concerning the chemical structure of CH₅⁺ could help expand our understanding of the current models for chemical bonding and structure in carbonium ions. Methonium ion is believed to have a C_sI structure as minimum on the potential energy surface, which interconverts into equivalent C_sI isomers after intramolecular bond-to-bond rearrangements. This rearrangement occurs through transition states with C_{2v} symmetry, as shown in Figure 2. Although both C_{2v} and C_sII structures are saddle points on the potential energy surface, their energies are very close to the C_sI minimum. Within the Born-Oppenheimer approximation, a flat energy surface is an indication of molecular fluxionality. This clearly applies to CH₅⁺. Since no single structure can be assigned unambiguously to this ion, any theoretical treatment should include all important structures together. This can be done through a Monte Carlo simulation or directly by *ab initio* molecular dynamics (5-7) treatment of the system. These

calculations demonstrate that on a time average basis, the CH_5^+ has the structure C_sI .

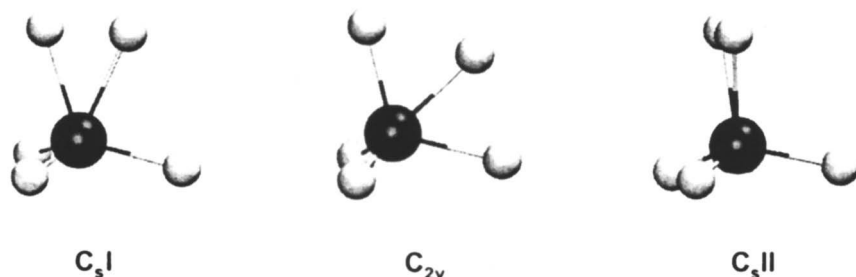


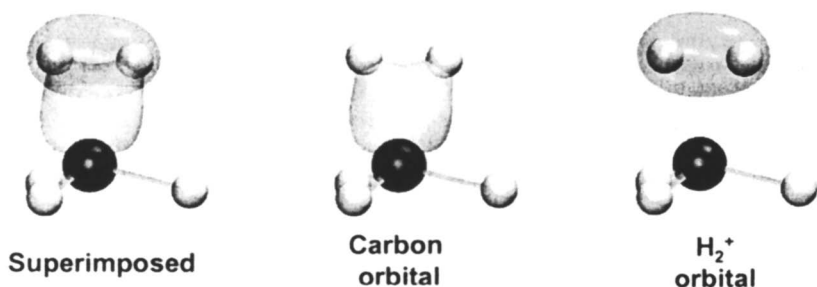
Figure 2. Representation of the three lowest energy stationary configurations of CH_5^+ from the PES. C_sI is the global minimum, C_{2v} is the saddle point to bond to bond rearrangement, and C_sII is the saddle point for rotation of the H_2 moiety.

Quantum mechanics provide many approaches to the description of molecular structure, namely valence bond (VB) theory (8-10), molecular orbital (MO) theory (11,12), and density functional theory (DFT) (13). The former two theories were developed at about the same time, but diverged as competing methods for describing the electronic structure of chemical systems (14). The MO-based methods of calculation have enjoyed great popularity, mainly due to the availability of efficient computer codes. Together with geometry optimization routines for minima and transition states, the MO methods (DFT included) have become prevalent in applications to molecular structure and reactivity.

Many carbonium ions including CH_5^+ (15-22), C_2H_7^+ (23-33), C_3H_9^+ (34-36), $\text{C}_4\text{H}_{11}^+$ (37-41), $\text{C}_6\text{H}_{15}^+$ (42), $\text{C}_8\text{H}_{19}^+$ (43,44), protonated cubane (45), adamantane (46) and numerous μ -hydridobridged carbocations (47,48) were previously studied by MO theory and by density functional theory (DFT) calculations. However, there have been only few studies of carbonium ions employing modern valence bond (VB) methods, such as Spin-Coupled (49-51) or Full Generalized Valence Bond method (52). One major advantage of the VB methods is their ability to give the chemical structure as a direct result of the calculations, giving conceptually useful insights in relation to MO. VB also gives wavefunctions that always result in a lower energy than a Hartree-Fock wavefunction, while yielding an independent particle interpretation. i.e. the wavefunction is defined by one configuration of occupied orbitals. Since both are variational methods, this means that the VB wavefunction is always better than the Hartree-Fock wavefunction at the same basis set.

We have performed Spin-Coupled calculations on a series of selected carbonium ions (53). The Spin-Coupled calculations allow the study of chemical structure of the molecule, since chemical structure and connectivity are central features of VB theory. Spin-Coupled calculations for CH_5^+ in C_s I show the system as bonded by the intuitively proposed 3c2e bond, which connects the carbon atom to two hydrogens, and three ordinary 2c2e bonds between the carbon and the other hydrogens, commonly called the tripod (Figure 3).

3 centers-2 electrons bond



One of the C-H bonds from the "tripod"

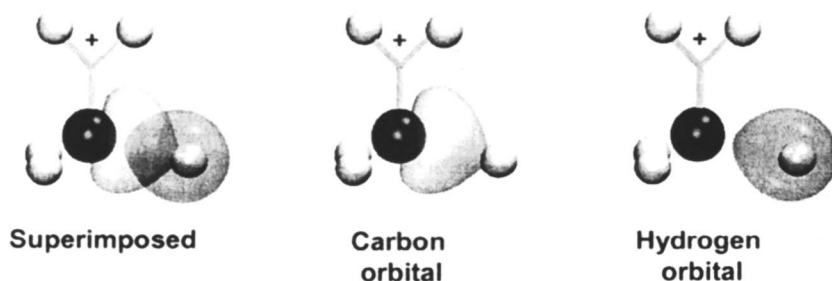


Figure 3. Spin-Coupled orbitals for CH_5^+ .

The dissociation products of CH_5^+ are hydrogen molecule and the classical CH_3^+ carbenium ion. The interpretation of the Spin-Coupled wavefunction is straightforward from the resulting orbitals (Figure 6). The orbitals in VB theory are singly occupied, not having any orthogonality restrictions. The chemical bonds are a result of overlap between these non-orthogonal orbitals within a given spin eigenfunction. Most VB wavefunctions are subject to the variational principle, which means that these wavefunctions, and therefore the orbitals that

are being optimized are always above the exact result. Another aspect of this wavefunction is that it is not written as a single determinant such as the Hartree-Fock wavefunction, which means that the orbitals are uniquely determined and any linear combination between these orbitals will affect the total energy of the wavefunction. Hence, a physical meaning can be associated with these orbitals (52,54,55). The reader should remember that this is not true for the Hartree-Fock wavefunction (56). Technically speaking, the VB orbitals are variationally optimized, singly occupied and non-orthogonal.

For an illustration on the interpretation of the Spin-Coupled results, the orbitals of H_2 and H_2^+ are shown in Figure 4 and CH_4 in Figure 5. It is noticeable that there are two orbitals in the H_2 molecule. Each orbital is populated by one electron and is located mostly over one hydrogen atom. The chemical bond is a result of the overlap between the two orbitals. This overlap is associated with a lowering of the kinetic energy of the electrons which accounts for the rise of the potential energy of bringing two negatively charged particles together in a chemical bond formation (57-60). For the H_2 molecule, this overlap is around 0.80. In the H_2^+ case, the bond is associated only with the lowering of the electron's kinetic energy from the electrostatic interaction with both nuclei. The orbital is no longer localized. This is important, since in modern VB methods such as Spin-Coupled, the localization of the orbitals is no longer a pre-requisite of the wavefunction. The orbitals are only localized when this results in a lower energy for the system.

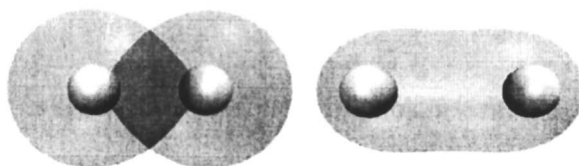


Figure 4. Spin-Coupled orbitals for H_2 (left) and H_2^+ (right).

Methane is formed by four bonds such as the one shown in Figure 5. There are two electrons being shared between the carbon atom and the hydrogen atom. One orbital is localized over the hydrogen (Figure 5, right) and the other over the carbon (Figure 5, middle). Although the carbon orbital closely resembles the classical sp^3 orbital, it is very important to notice that this orbital is an outcome of Spin-Coupled calculation in which no hybridization is imposed!(61) The sp^3 orbitals from the classical VB theory are purely atomic orbitals. In the modern VB approach, the atomic orbitals are combined with every basis function of

every atom and optimized, resulting in orbitals that contains different basis functions from different atoms. This allows the orbital to distort towards the hydrogen atom in order to increase overlap, thus lowering the energy. One should also note that the orbital optimization of the Spin-Coupled wavefunction eliminates the need to consider ionic structures. Their effect is indirectly accounted for through the spatial distortion of the Spin-Coupled orbitals. This is in contrast with the classical VB approach which relies on the superposition of many ionic structures to achieve quantitative accuracy (62).

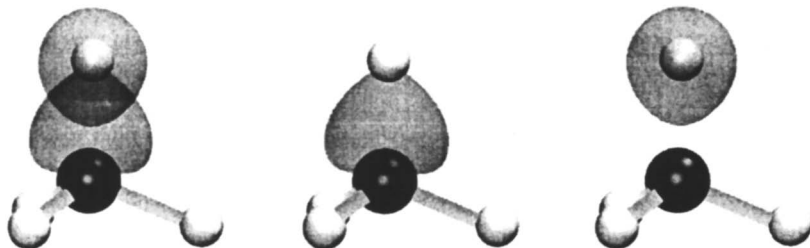
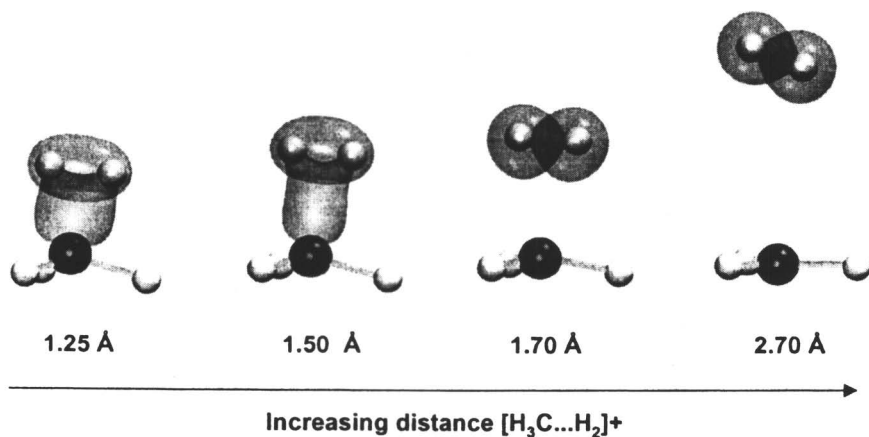


Figure 5. Spin-Coupled orbitals for one of the C-H bonds in CH₄. The two Spin-Coupled orbitals showing their overlap (left), the orbital on carbon (middle) and on hydrogen (right)

The Spin-Coupled results for the dissociation curve of CH₅⁺ into CH₃⁺ and H₂ (Figure 6) indicate that this bond can be pictured as an interaction between a CH₃ radical and H₂⁺, on the regions close to the minimum energy structure C_sI. This can be observed when one compares the orbital surrounding the two hydrogen nuclei in the 3c2e bond and the H₂⁺ orbital. This provides insight into the rotational freedom of this H₂ moiety. Since the carbon is not bound to one or the other hydrogen, but to both at the same time, the forces restricting the free rotation of the H₂⁺ moiety, similar to rotation of CH₃ around the C-C bond in ethane for example, should be small. The other C-H bonds are very similar to the C-H bonds in methane, reflecting the CH₃ radical character. Thus, the intuitive vision of this system through a 3c2e bond is supported by the modern VB theory. Instead of a CH₃⁺ bound to a H₂, the model given by this theory is a CH₃ radical attached to a H₁ species. As the H₂ pulls away from the CH₃ tripod, the orbitals polarize towards the small nuclei, resulting in a hydrogen molecule and methyl cation (Figure 6).



Higher protonated species, such as CH_6^{+2} and CH_7^{+3} have also been proposed (63). Spin-Coupled calculations on CH_6^{+2} confirms the model involving 3c2e bonds (Figure 7) (53). However, these orbitals show that there are two such 3c2e bonds.

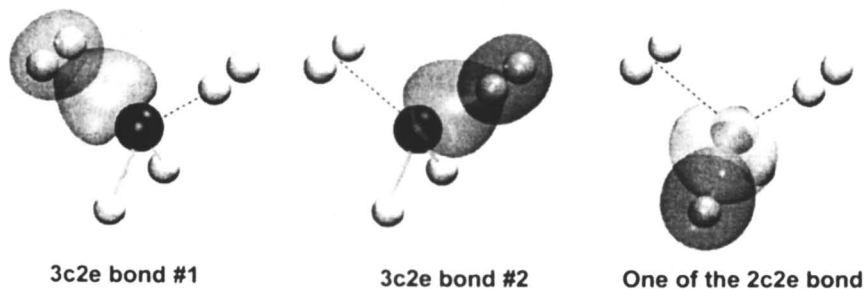


Figure 7. Spin-Coupled orbitals for CH_6^{+2} .

The increase in computing power and recent advances in theory have enabled the study of the dynamics of reactive intermediates, which cannot be properly described by classical force fields due to their unconventional bonding properties. To achieve quantitative accuracy in the study of energetics of

carbonium ions, one needs to use high level quantum chemical calculations. Thus the bond breaking/bond forming process and the unconventional 3c2e bonds, typical from these systems, can be properly described. A complementary technique useful for the study of these systems is known as *ab initio* molecular dynamics (AIMD), which plays a central role in this field (64-66).

Numerous studies concerning the structure and dynamics of the CH_5^+ have been reported (5-7, 16, 18, 67-74). Figure 2 shows the Born-Oppenheimer molecular dynamics (BOMD) calculations for CH_5^+ , calculated at B3LYP/6-31G** level. The structures (a) and (b) correspond to snapshots from the dynamics. Figure 2 (c) shows the superimposed structures from the dynamics, indicating the high fluxionality of CH_5^+ .

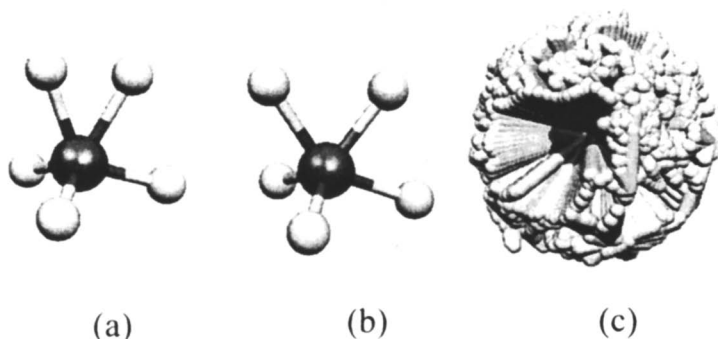


Figure 8. Snapshot of BOMD calculations (a) for CH_5^+ in its close C_sI form, (b) near the transition state for bond-to-bond migration from one 3c2e bond to a C-H from the tripod (C_{2v}), and (c) sum of the superimposed structures, illustrating the fluxional character of the CH_5^+ .

These results are in agreement with other AIMD simulations considering the nuclei as classical particles. Despite fluxionality of CH_5^+ , two types of C-H bonds on average are present: a 3c2e bond and three other conventional 2c2e bonds of a CH_3 moiety, corresponding to a tripod (see Figure 2, left).

Calculations considering proton-tunneling were also performed by AIMD considering the quantum nature of the nuclei, using path-integral techniques (64,75). On a time average) there is a tendency for two protons to form a H_2 moiety, supporting the classical view of a CH_5^+ as corresponding to a $[\text{H}_3\text{C}\dots\text{H}_2^+]$ complex with a 3c2e bond. This structure offers an explanation for

the loss of H₂ by protonation of methane in liquid superacids. For relatively high temperatures, the CH₅⁺ can be thought of as hydrogen atoms moving around a carbon core, the whole system with a positive charge. This has even inspired some researchers to develop a particles-on-the-sphere model for such systems (76). Despite these results from both static and dynamical calculations, some difficulties arise when one attempts to correlate the observed infrared spectrum (6,77). Certain conflicts (78) are found when isotopomers of CH₅⁺, such as CD₄H⁺ and CHD₄⁺ are analyzed. Experimental results (79) for these species indicate that in the absence of intermolecular collisions, CH₄D⁺ and CD₄H⁺ are not scrambling but are relatively stable complexes of [CH₃...HD]⁺ and [CD₃...HD]⁺. This has called to attention deuteration effects on the structure and infrared spectrum of CH₅⁺ (68).

Although the study of CH₅⁺ cation has attracted great attention, higher carbonium ions have not been so intensely studied, especially with molecular dynamics.

Ethonium ion (C₂H₇⁺)

C₂H₇⁺ is the next higher homolog in the series of alkyl carbonium ions, in which a hydrogen atom in CH₅⁺ is substituted by a methyl group. Depending on the hydrogen atom being replaced by a methyl group, two isomers can be formed: (a) the H-ethonium ion, where a hydrogen from the CH₃ moiety (tripod) of CH₅⁺ is replaced, and (b) the C-ethonium, where a hydrogen involved in the 3c2e bond in CH₅⁺ is replaced.

Carneiro *et al.* have shown (31) that the C-ethonium ion is the most stable isomer among various stationary-point conformations found on the MP2/6-31G** potential energy surface for C₂H₇⁺. Further studies added ten other stationary points, by using the same level of theory (24).

Despite lack of studies on higher carbonium ions from a dynamical point of view, the ethonium ion, C₂H₇⁺ has already been studied with AIMD (24). The C₂H₇⁺ ion is predicted to have three isomers at low temperatures: the C-ethonium isomer, the H-ethonium isomer, and a van der Waals complex C₂H₅⁺...H₂, with an H₂ group on top of the bridged proton of C₂H₅⁺ (31). The H-ethonium isomer undergoes rearrangement, and with simulation a qualitative understanding of the experimental infrared spectrum was possible (80). From these results, the species observed in the spectrum of C₂H₇⁺ is likely to be a van der Waals complex C₂H₅⁺...H₂.

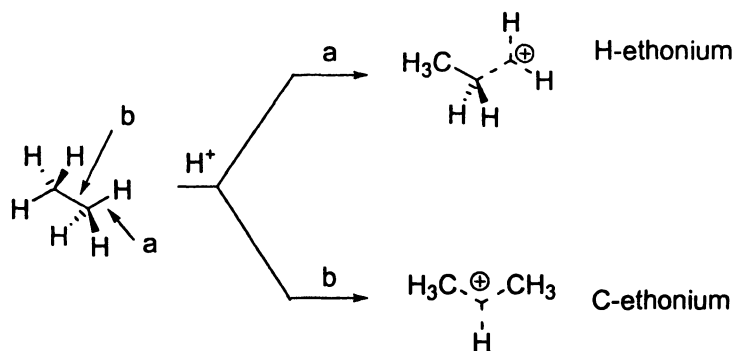


Figure 9. The H- and C-forms of the ethonium ion (C_2H_7^+)

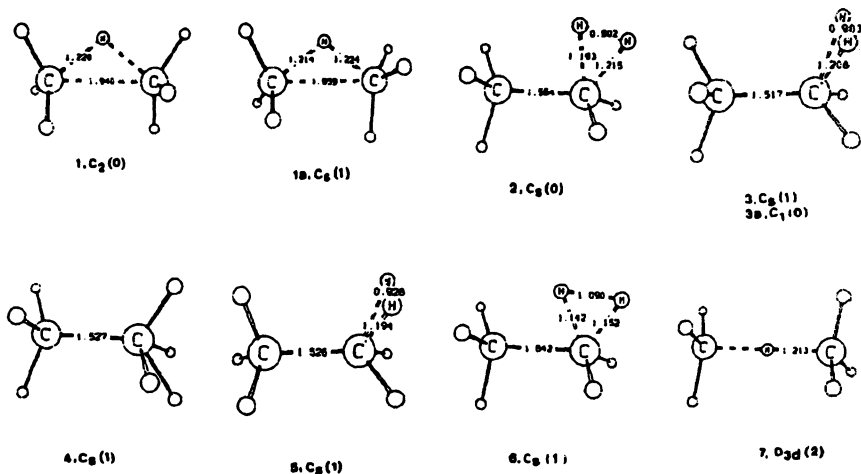


Figure 10. Different structures for the C_2H_7^+ ion (from reference 31). Number of imaginary frequencies are given in parenthesis.

Proponium ions

Proponium ions can be formed via protonation of propane, when CH_3^+ attacks C_2H_6 or C_2H_5^+ attacks CH_4 (34). The protonation outcome could occur at the primary C-H, secondary C-H or the C-C, affording respectively the 1-H-proponium ion, 2-H-proponium ion, or the C-proponium ion (Figure 11). The latter can also be formed when C_2H_5^+ attacks the C-H bond of methane. Propane is an interesting molecule to study, since it is the smallest alkane containing all representative types of bonds present in a linear alkane. Therefore, it is the simplest prototype of linear alkanes.

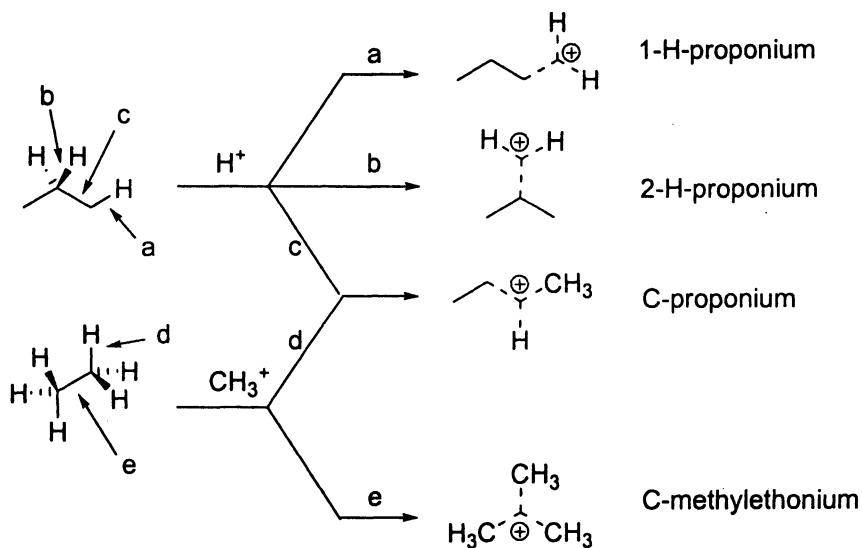


Figure 11. Different ways for the formation of the isomeric proponium ions.

Another possible isomer for C_3H_9^+ is the C-methylethonium cation, which would be hypothetically formed by the attack of CH_3^+ onto the C-C bond of ethane. However, it was shown that the C-methylethonium cation does not represent a minimum on the C_3H_9^+ potential energy surface, and it is thus not a stable intermediate (36). The previously observed ^{13}C scrambling in the reaction of $^{13}\text{CH}_3\text{F}\cdot\text{SbF}_5$ with C_2H_6 must have taken place via the C_3H_9^+ cation and its subsequent cleavage. Actually it is a degenerate second order transition state, lying 46 kcal/mol above the C-proponium cation (global minimum for C_3H_9^+)

(36). Several groups have proposed related species as being intermediates in alkane activation reactions (81).

Ab initio calculations by MP4/6-311++G**//MP2(full)/6-31G** have shown that the most stable structure for $C_3H_9^+$ ion is the C-proponium ion (34,35). This is in agreement with the σ basicity scale (82), which predicts electron richer bonds as being more stabilizing for the carbonium ion. In this case, this cation is even more stable than the van der Waals complexes between a carbenium ion and a neutral molecule. The most stable van der Waals complex is the one involving s- $C_3H_7^+$ and H_2 . This however, is only 0.3 kcal/mol higher in energy than the C-proponium form. The H-proponium ions are significantly higher in energy. The 2-H-proponium is about 7 kcal/mol and the 1-H-proponium about 10 kcal/mol higher than the C-proponium ion. The loss of CH_4 from C-proponium, affording $C_2H_5^+$ is endothermic by 5.0 kcal/mol. The proton affinity calculated for propane affording the C-proponium ion is 149.8 kcal/mol, and correlates quite well with the experimental value of 149.5 kcal/mol (83).

Figure 12 shows the calculated main geometrical parameters for the proponium ions, their corresponding van der Waals complexes and also their relative energies.

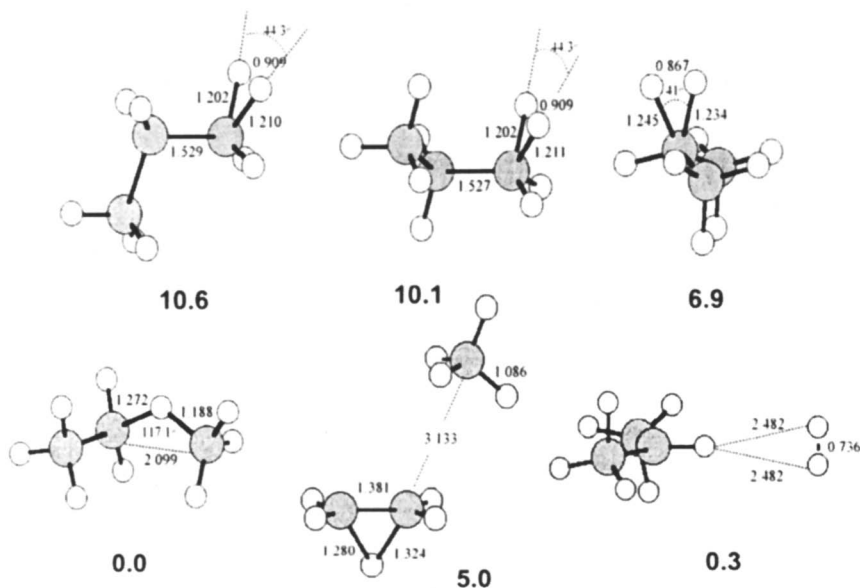


Figure 12. The isomers of the proponium ion. Values on the bottom of the structures correspond to relative energies (ΔH) in kcal/mol obtained at MP4(SDTQ)/6-311++G**//MP2 (full)/6-31G** level.

BOMD calculations on several forms of the proponium ion have been performed at several temperatures (84).

1-H-proponium

BOMD study of the 1-H-proponium ion shows that this species quickly interconverts to the C- proponium ion, after the H₂ moiety involved in the 3c2e bond rotates up toward the C-C bond (Figure 13).

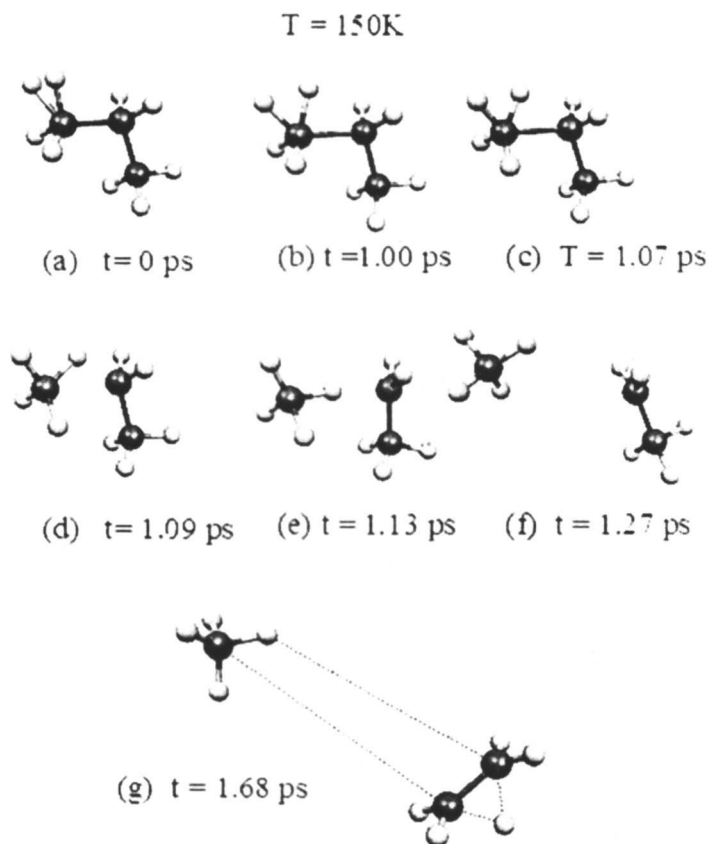


Figure 13. Snapshots of the BOMD of 1-H-proponium cation, its rearrangement to C-proponium cation and further decomposition.

The bond-to-bond rearrangement is faster than C-C insertion and because of the energy released it breaks apart into CH_4 and C_2H_5^+ . Depending on the temperature, it can take more or less time. This dynamical behavior is conceptually interesting, since it means that C-C protonation cannot be taking place directly, once it becomes sterically demanding. Actually, the products that come from C-C protonation could be due to the protonation of the primary C-H bonds, which after rearrangement to the C-proponium, affords its dissociation products.

These results are in line with the earlier MP4 results (34), demonstrating that interconversion, or bond-to-bond rearrangement, among carbonium ions is a fast process. The rearrangement of the 1-H-carbonium to the C-proponium requires only a small energy (0.6 kcal/mol) or no barrier at all, depending on the conformer considered.

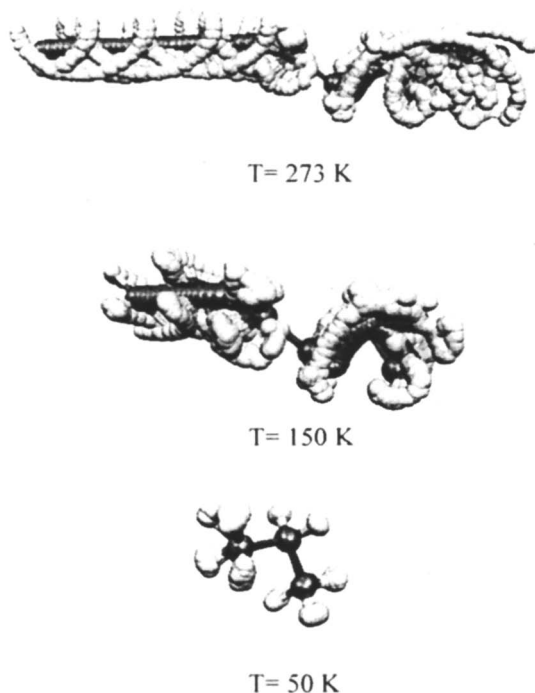


Figure 14. Superimposed structures of the BOMD of the 1-H-proponium cation.

The BOMD study of 2-H-proponium ion shows that it immediately decomposes into the relatively stable $s\text{-C}_3\text{H}_7^+$ and H_2 . Figure 15 shows the decomposition process. Therefore, protonation at the secondary C-H bond in propane should preferentially afford dehydrogenation. *Ab initio* calculations showed that it is actually easier for the secondary carbonium ions, such as the 2-H-proponium ion, to lose H_2 than to rearrange to a C-carbonium ion (34). MP4 results have shown that there is an activation energy of 2.5 kcal/mol for the isomerization of the 2-H-proponium to the C-proponium ion. However, the interconversion of 2-H-proponium in the respective van der Waals complex between H_2 and $s\text{-C}_3\text{H}_7^+$ requires only 0.04 kcal/mol. This reflects the higher stability of the secondary carbenium ion involved in the 3c2e bond, which is more loosely bound to the H_2 moiety, as expressed by its longer C-H bond and shorter H-H bonds involved in the 3c2e bonds in comparison to, for instance, 1-H-carbonium ion (see Figure 12).

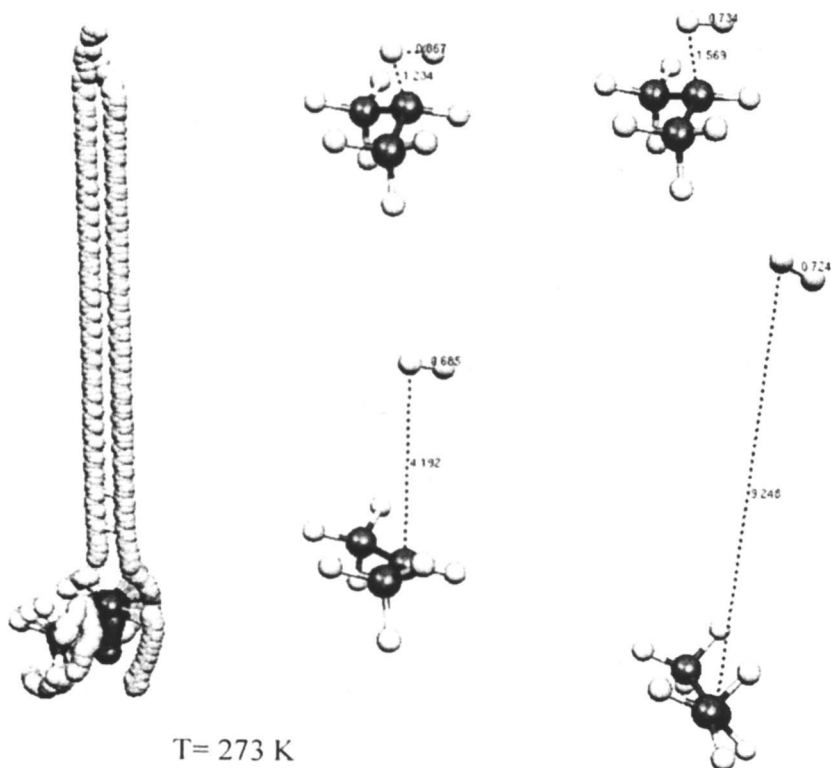


Figure 15. Superimposed structures (left) and snapshots (right) of the BOMD of the 2-H-proponium cation.

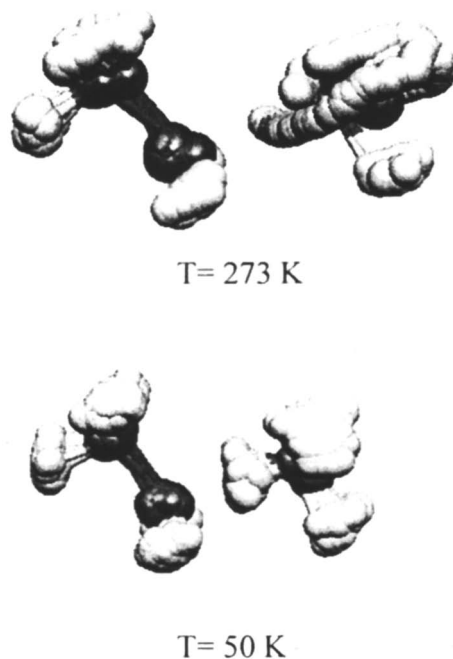


Figure 16. Superimposed structures of the BOMD of the C-proponium cation.

Conversely, the C-proponium ion is dynamically stable (and potentially observable), if formed via insertion of CH_3^+ into a C-H bond in ethane or by electrophilic attack by C_2H_5^+ cation to methane. Figures 16 and 17 show the BOMD results for C-proponium, indicating that the CH_4 moiety is attacked by C_2H_5^+ , at different temperatures. The reaction outcome is interesting as a possible route for generating the C-proponium ion, since it does not involve considerable internal energy release, affording a relatively vibrationally cooled C-proponium ion, which could be potentially observable under proper conditions. This is quite different from attempting to obtain this ion by protonation of propane, which due to exothermicity of H-proponium relative to C-proponium affords vibrationally hot ions, which tend to decompose. Actually, Hiraoka and Kebarle have studied (85-87) the gas-phase reaction between C_2H_5^+ and CH_4 . At temperatures below -60°C , the reaction was exothermic by 6.6 kcal/mol and proceeded without activation energy to form a C_3H_9^+ cation, in agreement with the theoretical results, which predicts its barrierless formation. At temperatures above -60°C , the reaction proceeded with an activation energy of 2.5 kcal/mol to form C_3H_7^+ and H_2 . It is proposed that a C-proponium cation

is initially formed and above $-60\text{ }^{\circ}\text{C}$, it rearranges to a 2-H-proponium cation, which then gives rise to the isopropyl cation and hydrogen. Considering the sum of the enthalpy for C_3H_9^+ formation (-6.6 kcal/mol) and the activation energy of 2.5 kcal/mol , one finds an experimental value of 9.1 kcal/mol for the energy barrier for the rearrangement of the C-proponium cation in the isopropyl cation plus hydrogen system.

Butonium ions ($\text{C}_4\text{H}_{11}^+$)

The ions $n\text{-C}_4\text{H}_{11}^+$ and $i\text{-C}_4\text{H}_{11}^+$ provide good models for comparison among several types of 2e-3c bonding involved in alkanonium ions, since they contain most of the characteristic of 2e-3c bonds of interest in alkane activation, and their structural isomers allow direct energy comparison among the different $\text{C}_4\text{H}_{11}^+$ ions (Figure 18). In particular, isobutane, is an interesting molecule to study, since it is the smallest alkane containing all representative types of bonds in a branched alkane, being the simplest propotype of these compounds.

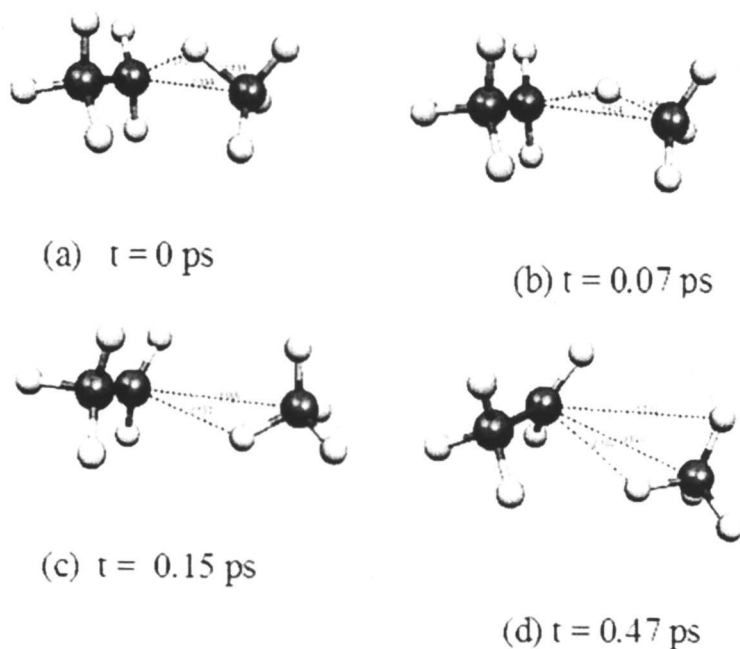


Figure 17. Snapshots of the BOMD of the C-proponium cation.

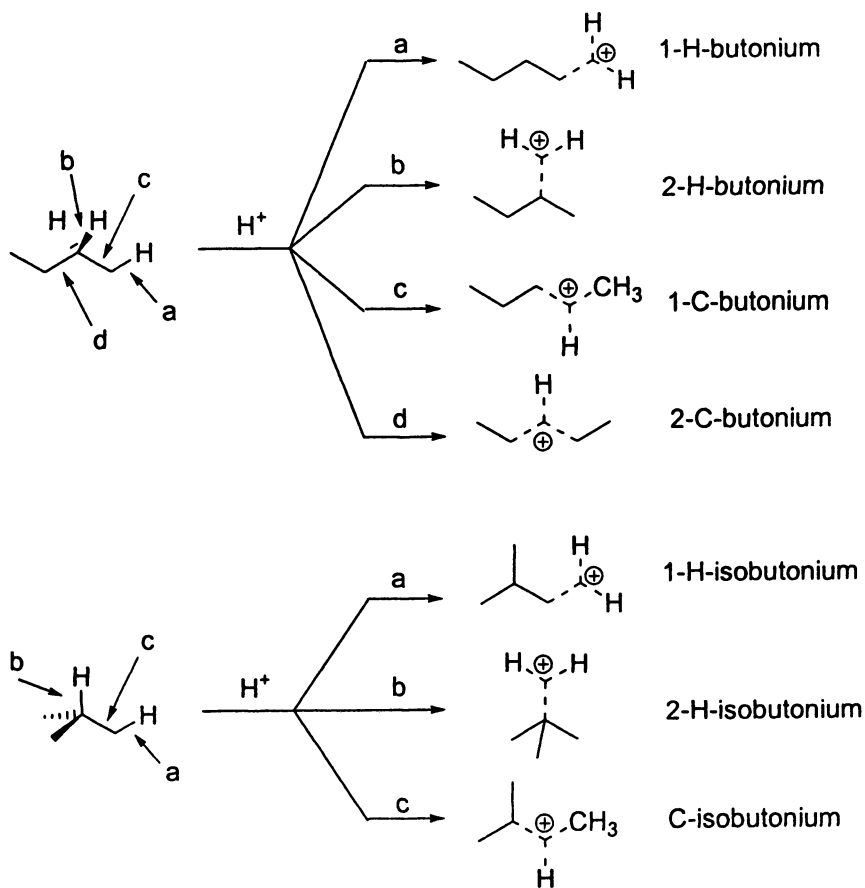


Figure 18. The *n*-butonium (top) and the isobutonium ions (bottom)

Theoretical studies on protonated isobutane revealed that the van der Waals complexes $\text{CH}_4 \dots \text{C}_3\text{H}_7^+$ and $\text{H}_2 \dots t\text{-C}_4\text{H}_9^+$ are actually lower in energy than either H-isobutonium or C-isobutonium cations (Figure 19). The complex $\text{H}_2 \dots t\text{-C}_4\text{H}_9^+$ is the lowest energy species. Among the carbonium ions, the energy increases in the order C-isobutonium < 2-H-isobutonium < 1-H-isobutonium, following the same trend observed for the ethonium and proponium cations, where the C-carbonium ions have lower energy than the H-carbonium.

Relative stabilities of the H-carbonium ions are explained by the extent of H-H bonding in the 3c2e bond. In the 2-H-carbonium, this is stronger than in 2-H-isobutonium, reflecting the greater ability of the carbonium ion, by receiving electrons from the H_2 moiety in the latter case. The lower energy of the C-isobutonium cation in comparison to the H-isobutonium cations is due to a better charge distribution among the atoms of the 3c2e bond. The results indicate low barriers for the conversion of the carbonium ions into the respective van der Waals complexes between hydrogen or methane (Figure 20).

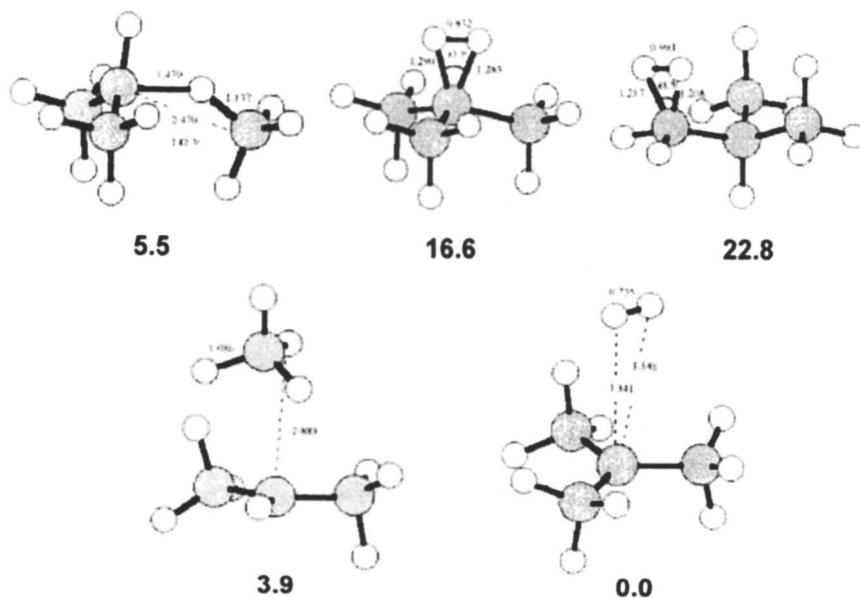


Figure 19: The isobutonium ions. Values on the bottom of the structures correspond to relative energies (ΔH) in kcal/mol.

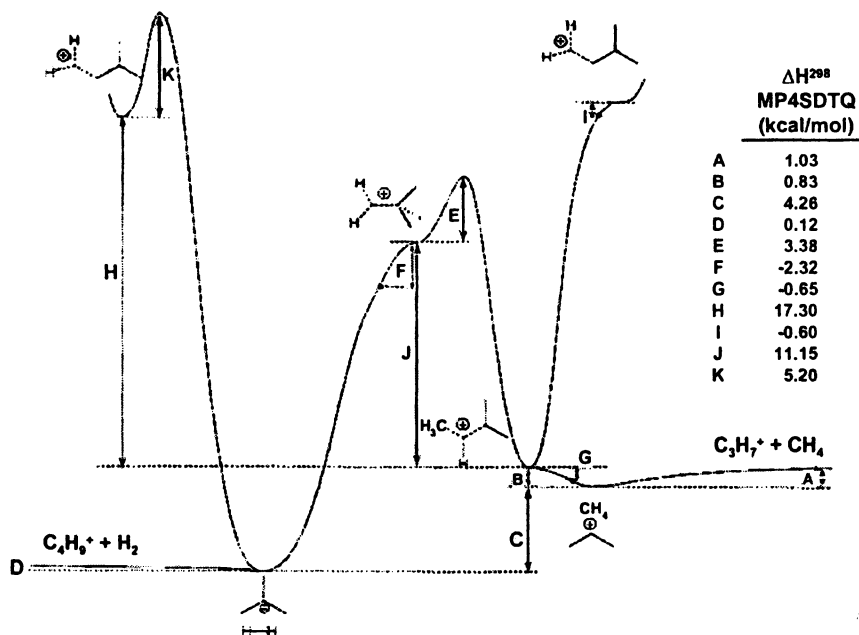


Figure 20. Pictorial representation of the potential energy surface for $C_4H_9^+$.

BOMD calculations on the 1-H-isobutonium ion show that it rearranges into the C-isobutonium ion, as was also observed with 1-proponium ion. Figure 21 illustrates snapshots of BOMD for 1-H-isobutonium ion and its rearrangement (17.3 kcal/mol) and decomposition into the methane and the carbenium ion. Due to the absence of molecules that could withdraw the energy released from this rearrangement, the resulting C-carbenium is vibrationally hot, which leads to its decomposition into CH_4 and $s-C_3H_7^+$, even at low temperatures, such as 5 K. Once again, the sterically demanding C-C protonation process could also be understood as a byproduct of primary C-H protonation, as seen in the case of propane.

Eleven stable structures were located for *n*-butonium ion at MP4SDTQ(fc)/6-311++G**//MP2(full)/6-31G** level (37,38,41), following the stability order 2-C-*n*-butonium > 1-C-*n*-butonium > 2-H-*n*-butonium > 1-H-*n*-butonium (Figure 22). The H-*n*-butonium and the 1-C-*n*-butonium ions are higher in energy relative to the van der Waals complexes between the isopropyl cation and CH_4 , and *tert*-butyl cation plus H_2 . The 1-H-*n*-butonium ion prefers to undergo intramolecular rearrangement to the 1-C-*n*-butonium ion, similar to H-ethonium or 1-H-proponium ions. This seems to be a general trend in the chemistry of the alkanonium ions. On the other hand, the 2-H-*n*-butonium ion prefers to decompose into the van der Waals complex of the *sec*-butyl cation plus H_2 .

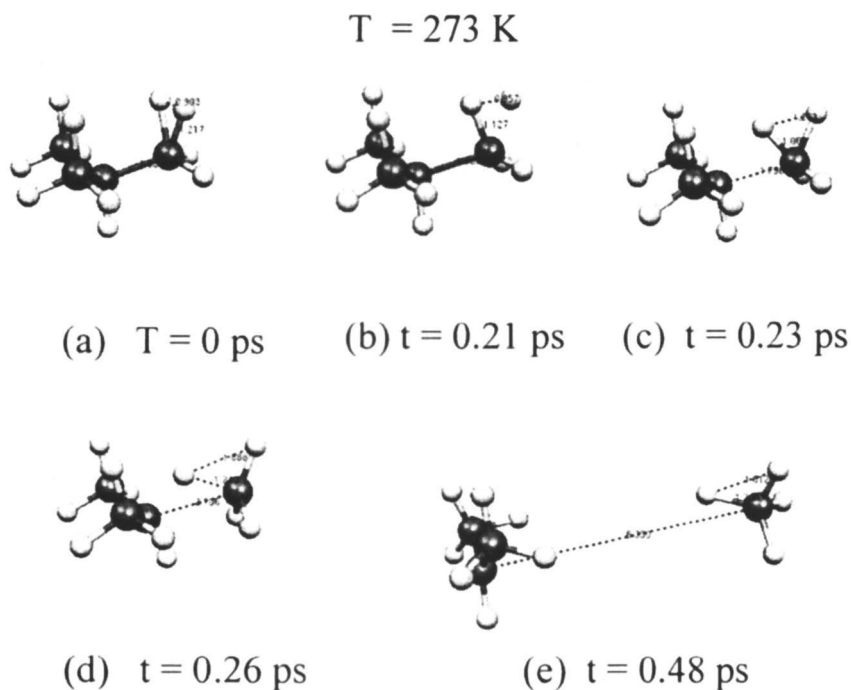


Figure 21. Snapshots of the BOMD of the 1-H-isobutonium cation.

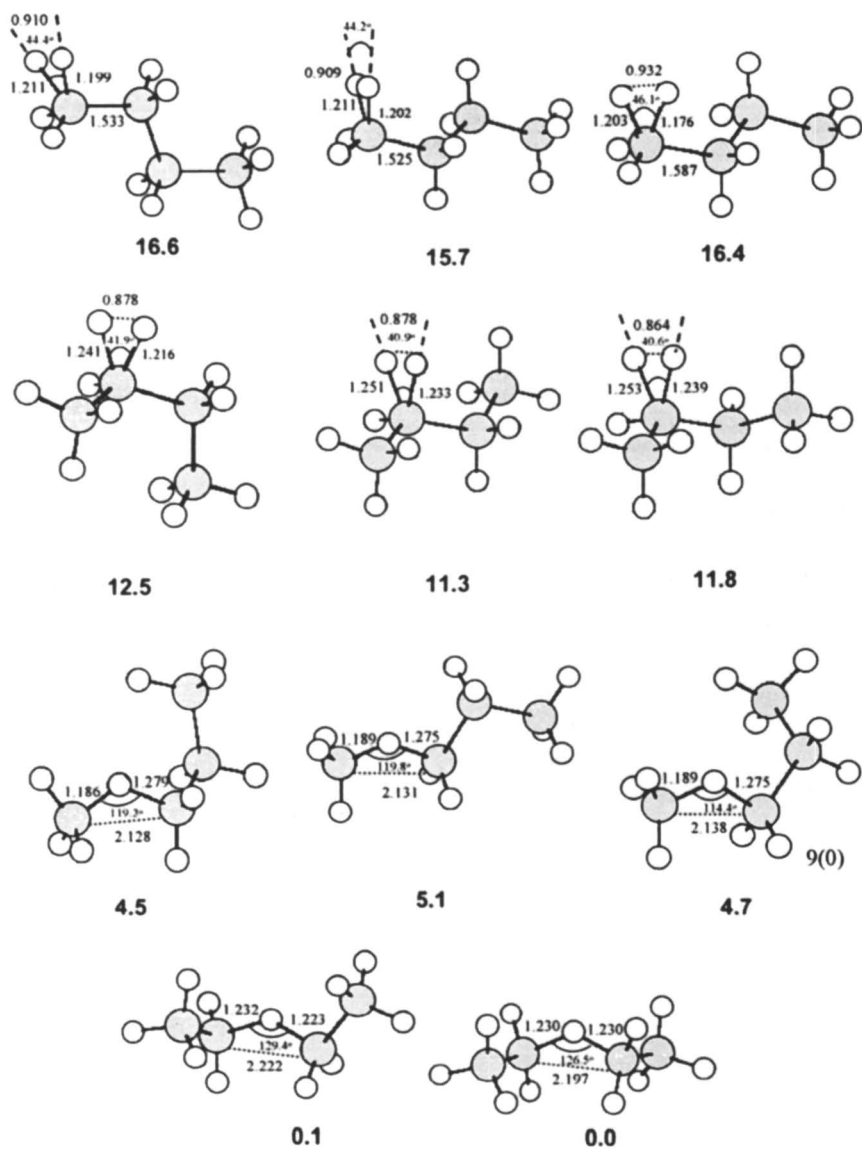


Figure 22. The butonium ions. Values on the bottom of the structures correspond to relative energies (ΔH) in kcal/mol.

Comparison among *n*-butonium and isobutonium ions allows for the interpretation of the effect of structural parameters on the basicity of these alkanes. A scale of basicity for σ bonds of alkanes was proposed based on these results (82).

Figure 23 shows the lowest energy species among the possible conformers for each butonium ion.

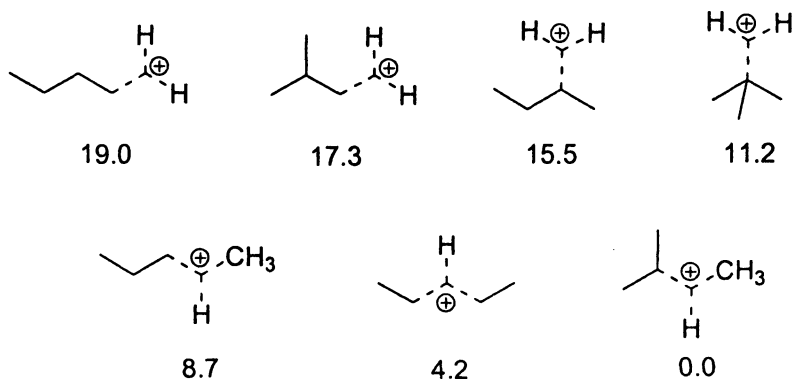


Figure 23. Relative enthalpy (ΔH) for the isomeric butonium cations, calculated by MP4SDTQ/6-311++G**//MP2(full)/6-31G**(82).

The σ basicity scale is different from the empirically based σ reactivity scale previously proposed by Olah *et al.* (88,89). The latter is based on the reactivity of different alkanes in liquid superacids, and affords the following order of reactivity: *tert* C-H > C-C > *sec* C-H > *prim* C-H > CH₄. Actually, Olah's scale is related to kinetics and therefore to energy barriers, whereas the σ -basicity scale refers to chemical equilibria. Basicity is a property related to chemical equilibrium (ΔG), while reactivity is related to chemical kinetics (ΔG^\ddagger). The outcome of the reaction of alkanes with small electrophiles seems to be better correlated by the σ -basicity scale. On the other hand, for reactions in the condensed phase where bulky solvated electrophiles are involved, these are generally driven by kinetics and are better correlated with Olah's reactivity scale, which actually is a kinetic scale. Theoretical calculations support this interpretation (90,91). The 3c2e bonding concept is more intimately related to the basicity of the σ bond itself. The basicity of a σ bond follows the ability of each of the resonance structures to stabilize the positive charge. One can visualize the groups in the three center bond spreading the positive charge, as shown in Figure 24. In the case of H-carbonium ions (R = H), there is only one resonance structure where the positive charge lies over the carbon atom of the alkyl group, while in the C-carbonium ion there are two structures. Hence, less

charge is concentrated on the hydrogens of the three center bond in C-carbonium ions, resulting in a better stabilization. Similarly, the different C-C bond basicities can be understood in the same way. For instance, the C-C bond in isobutane is more basic than the external C-C bond in n-butane, due to greater stability of the carbenium ions involved in the resonance structures of the 3c2e bonds in the former, which are a secondary and a methyl carbenium ions, hence less energetic than the primary and methyl carbenium ions in the latter.

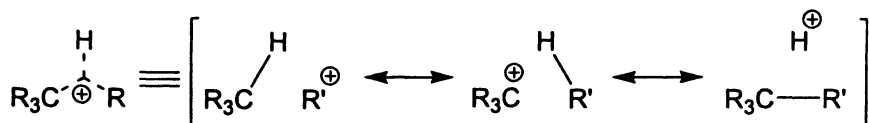


Figure 24. Classical VB canonical structures representing the 3c2e Bonds in carbonium ions

Solvation of Carbonium Ions

Solvation of carbonium ions has also been taken into account. The dynamics of CH_5^+ solvated by H_2 and other molecules have been studied experimentally, and in the case of solvation by H_2 through classical AIMD studies (92-94). The solvation effect on the 3c2e bonds leads to freezing of the scrambling of protons within CH_5^+ , that could be considered due to hydrogen bonding between σ bonds (Figure 25). This solvation leads to a more resolved IR spectrum (93).

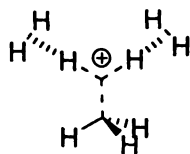


Figure 25. CH_5^+ Solvated by H_2 .

Raugei and Klein (72,95) have studied hydrocarbon protonation by HF/SbF_5 using Car-Parrinello molecular dynamics (CPMD) calculations (65,96). An interesting issue arising from CPMD simulations is the scrambling between hydrogen atoms near the transition state (Figures 26 and 27). This scrambling is

faster for CH_5^+ than for the other hydrocarbons, supporting the idea that even in solvated systems, these systems can undergo bond-to-bond rearrangement. The fluxional transition state is characterized by H-bond-like interactions between the hydrogens of a protonated alkane moiety and the nearby F atoms of the SbF_6^- . These weak bonds continuously break and reform with the average lifetime shorter than 1 ps.

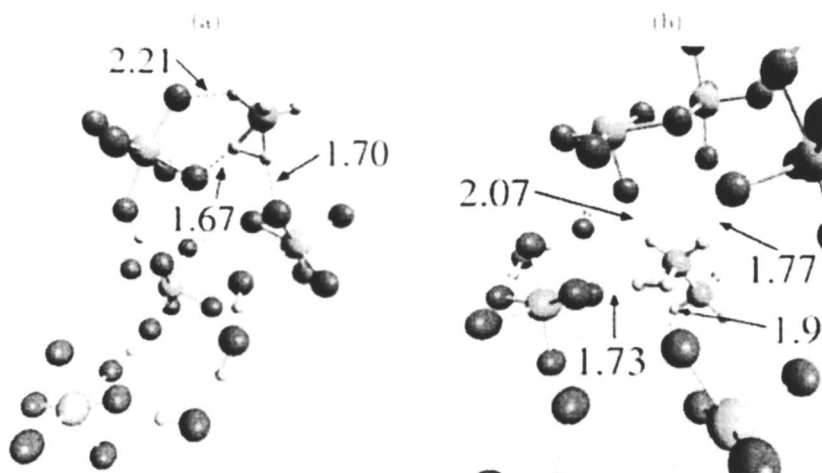


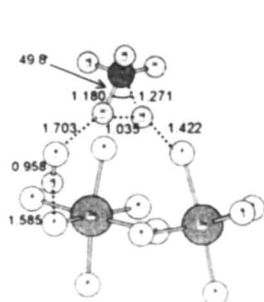
Figure 26 Car-Parrinello Molecular Dynamics of CH_4 (a) and C_2H_6 (b) in SbF_5/HF 50 mol % SbF_5 . (from reference 72)

Study of the C-C protonation of ethane has revealed that from the minimum reaction path, which corresponds to the approach of a proton nearly perpendicular to the C-C bond, the system can easily protonate at C-H, affording a transition state which is H-ethonium like.

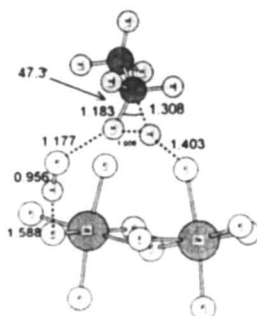
Microsolvation approaches have also been considered toward understanding the role of the primary solvation shell of a carbonium ion (18,90,91,97,98). These ions tend to become transition states whenever strong solvation is taking place (Figure 27).

Solvation by “solid solvents” such as zeolites has also been investigated by several groups, as shown in Figure 29 (99-109). The theoretical results also demonstrate that these actually correspond to carbonium-like transition states.

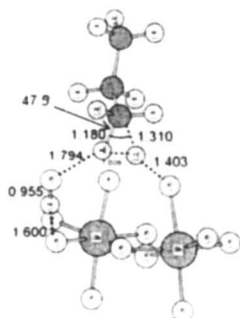
An interesting feature is that, although solvated carbonium ions usually afford transition states when the anions are considered in the calculations, their chemistry could be thought of as being analogous to that of carbonium ions. In many cases, these structures could potentially be transition states with interesting properties, such as scrambling and other processes that are characteristic of weakly solvated carbonium ions.



$\text{CH}_5^+ \cdot \text{Sb}_2\text{F}_{11}^- \cdot \text{HF}$



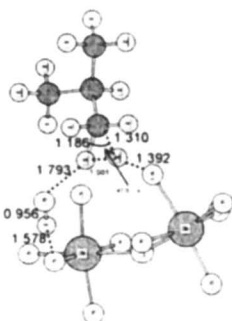
$\text{C}_2\text{H}_7^+ \cdot \text{Sb}_2\text{F}_{11}^- \cdot \text{HF}$



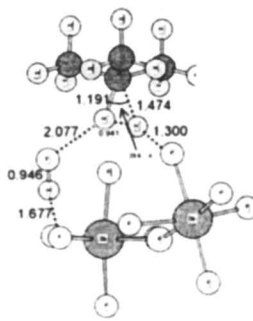
1-H-proponium. $\text{Sb}_2\text{F}_{11}^- \cdot \text{HF}$



2-H-proponium. $\text{Sb}_2\text{F}_{11}^- \cdot \text{HF}$

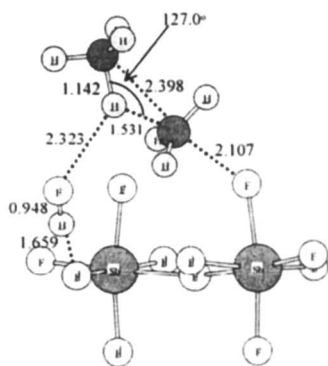


1-H-isobutonium. $\text{Sb}_2\text{F}_{11}^- \cdot \text{HF}$



2-H-isobutonium. $\text{Sb}_2\text{F}_{11}^- \cdot \text{HF}$

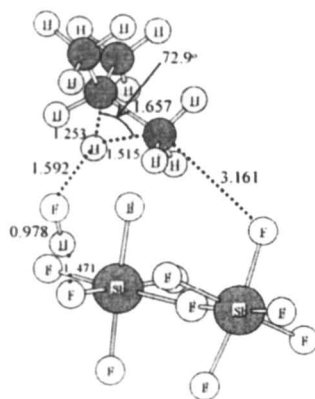
Figure 27. H-carbonium ion-like transition states for methane, ethane, propane and isobutane protonation by HF/SbF₅.



C-ethonium. $\text{Sb}_2\text{F}_{11}^- \cdot \text{HF}$



C-proponium. $\text{Sb}_2\text{F}_{11}^- \cdot \text{HF}$



C-ethonium. $\text{Sb}_2\text{F}_{11}^- \cdot \text{HF}$

Figure 28. C-carbonium ion-like transition states for ethane, propane and isobutane protonation by HF/SbF_5 .

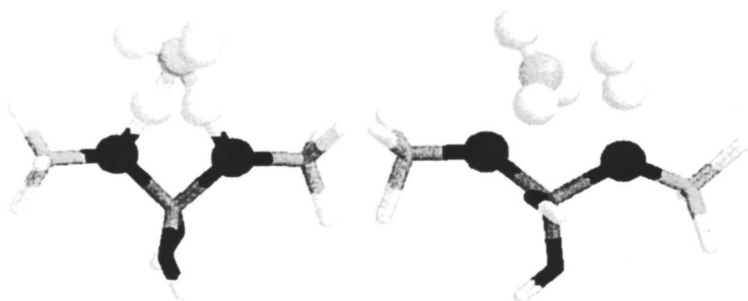


Figure 29. Two modes of interaction of CH_5^- within zeolite structure, leading to H-H exchange (left) and dehydrogenation (right).

Concluding Remarks and Outlook

Aspects of bonding and structure/dynamics in selected carbonium ions were presented and discussed. These representative studies demonstrate the power of structural theory in the development of concepts that could lead to new and efficient processes, especially in the area of hydrocarbon chemistry and catalysis. There is no doubt that as newer theoretical and experimental techniques and models are introduced, they will be applied to the study of carbonium ions. A deeper understanding of structure/dynamics of hypervalent “non-classical” carbonium ions will not only deepen our knowledge of structural theory in chemistry, but could also help in the development of new processes and materials useful in our daily life.

Acknowledgements

We acknowledge the Brazilian agencies (CNPq, FAPERJ, CAPES) for financial support and also thank Dr. Jiabo Li for help with the VB2000 package (110,111).

References

1. Olah, G. A.; Molnar, A. *Hydrocarbon Chemistry*; 2nd ed.; Wiley-Interscience: New York, 2003.
2. Olah, G. A. *J. Am. Chem. Soc.* **1972**, *94*, 808.

3. Olah, G. A. *J. Org. Chem.* **2001**, *66*, 5943-5957.
4. Prakash, G. K. S. *J. Org. Chem.* **2006**, *71*, 3661-3676.
5. Padma, K. P.; Marx, D. *Phys. Chem. Chem. Phys.* **2005**, *8*, 573-586.
6. Asvany, O.; Kumar, P.; Redlich, B.; Hegemann, I.; Schlemmer, S.; Marx, D. *Science* **2005**, *309*, 1219-1222.
7. Marx, D.; Parrinello, M. *Science* **1999**, *284*, 59-+.
8. Heitler, W.; London, F. Z. *Physik* **1927**, *44*, 455.
9. Pauling, L. *The Nature of the Chemical Bond*; Cornell University Press: Ithaca, 1960.
10. Slater, J. C. *Phys. Rev.* **1931**, *37*, 481.
11. Mulliken, R. S. *Chem. Rev.* **1931**, *9*, 347.
12. Hehre, W. J.; Radom, L.; Schleyer, P. v. R.; Pople, J. A. *Ab Initio Molecular Orbital Theory*; Wiley-Interscience: New York, 1986.
13. Kohn, W.; Sham, L. *J. Phys. Rev.* **1965**, *137*, A 1687.
14. Hoffmann, R.; Shaik, S.; Hiberty, P. C. *Acc. Chem. Res.* **2003**, *36*, 750-756.
15. Jin, Z.; Braams, B. J.; Bowman, J. M. *J. Phys. Chem. A* **2006**, *110*, 1569-1574.
16. Thompson, K. C.; Crittenden, D. L.; Jordan, M. J. T. *J. Am. Chem. Soc.* **2005**, *127*, 4954-4958.
17. Kaledin, A. L.; Kuniyeev, S. D.; Taylor, H. S. *J. Phys. Chem. A* **2004**, *108*, 4995-4997.
18. Ahlberg, P.; Karlsson, A.; Goepfert, A.; Lill, S. O. N.; Diner, P.; Sommer, J. *Chem. Eur. J.* **2001**, *7*, 1936-1943.
19. Schreiner, P. R. *Angew. Chem. Int. Ed.* **2000**, *39*, 3239.
20. Muller, H.; Kutzelnigg, W.; Noga, J.; Klopper, W. *J. Chem. Phys.* **1997**, *106*, 1863-1869.
21. Marx, D.; Savin, A. *Angew. Chem. Int. Ed.* **1997**, *36*, 2077-2080.
22. Schleyer, P. V.; Carneiro, J. W. D. *J. Comp. Chem.* **1992**, *13*, 997-1003.
23. Fisher, J. J.; Koyanagi, G. K.; McMahon, T. B. *Int. J. Mass Spectrom.* **2000**, *196*, 491-505.
24. East, A. L. L.; Liu, Z. F.; McCague, C.; Cheng, K.; Tse, J. S. *J. Phys. Chem. A* **1998**, *102*, 10903-10911.
25. Lee, H. S.; Bierbaum, V. M.; DePuy, C. H. *Int. J. Mass Spectrom.* **1997**, *167*, 587-594.
26. Hrusak, J.; Zabka, J.; Dolejssek, Z.; Herman, Z. *Int. J. Mass Spectrom.* **1997**, *167*, 675-687.
27. Frash, M. V.; Solkan, V. N.; Kazansky, V. B. *J. Chem. Soc. Far. Trans.* **1997**, *93*, 515-520.
28. Collins, S. J.; O'Malley, P. J. *J. Chem. Soc. Far. Trans.* **1996**, *92*, 4347-4355.
29. Collins, S. J.; O'Malley, P. *J. Chem. Phys. Lett.* **1994**, *228*, 246-251.
30. Mestres, J.; Duran, M.; Bertran, J. *Theor. Chim. Acta* **1994**, *88*, 325-338.

31. Carneiro, J. W. D.; Schleyer, P. V.; Saunders, M.; Remington, R.; Schaefer, H. F.; Rauk, A.; Sorensen, T. S. *J. Am. Chem. Soc.* **1994**, *116*, 3483-3493.
32. Obata, S.; Hirao, K. *Bull. Chem. Soc. Japan* **1993**, *66*, 3271-3282.
33. Heck, A. J. R.; Dekoning, L. J.; Nibbering, N. M. M. *Int. J. Mass Spectrom Ion Proc.* **1992**, *117*, 145-169.
34. Esteves, P. M.; Mota, C. J. A.; Ramirez-Solis, A.; Hernandez-Lamoned, R. *J. Am. Chem. Soc.* **1998**, *120*, 3213-3219.
35. Okulik, N.; Peruchena, N.; Esteves, P. M.; Mota, C.; Jubert, A. H. *J. Phys. Chem. A* **2000**, *104*, 7586-7592.
36. Goepfert, A.; Sassi, A.; Sommer, J.; Esteves, P. M.; Mota, C. J. A.; Karlsson, A.; Ahlberg, P. *J. Am. Chem. Soc.* **1999**, *121*, 10628-10629.
37. Okulik, N. B.; Sosa, L. G.; Esteves, P. M.; Mota, C. J. A.; Jubert, A. H.; Peruchena, N. M. *J. Phys. Chem. A* **2002**, *106*, 1584-1595.
38. Esteves, P. M.; Alberto, G. G. P.; Ramirez-Solis, A.; Mota, C. J. A. *J. Phys. Chem. A* **2000**, *104*, 6233-6240.
39. Okulik, N.; Peruchena, N. M.; Esteves, P. M.; Mota, C. J. A.; Jubert, A. J. *J. Phys. Chem. A* **1999**, *103*, 8491-8495.
40. Mota, C. J. A.; Esteves, P. M.; Ramirez-Solis, A.; Hernandez-Lamoned, R. *J. Am. Chem. Soc.* **1997**, *119*, 5193-5199.
41. Lobayan, R. M.; Sosa, C. L.; Jubert, A. H.; Peruchena, N. M. *J. Phys. Chem. A* **2004**, *108*, 4347-4356.
42. Hunter, K. C.; Seitz, C.; East, A. L. L. *J. Phys. Chem. A* **2003**, *107*, 159-168.
43. Seitz, C.; East, A. L. L. *J. Phys. Chem. A* **2002**, *106*, 11653-11662.
44. Esteves, P. M.; Araujo, C. L.; Horta, B. A. C.; Alvarez, L. J.; Zicovich-Wilson, C. M.; Ramirez-Solis, A. *J. Phys. Chem. B* **2005**, *109*, 12946-12955.
45. Fokin, A. A.; Tkachenko, B. A.; Gunchenko, P. A.; Schreiner, P. R. *Angew. Chem. Int. Ed.* **2005**, *44*, 146-149.
46. Esteves, P. M.; Alberto, C. C. P.; Ramirez-Solis, A.; Mota, C. J. A. *J. Phys. Chem. A* **2001**, *105*, 4308-4311.
47. Sorensen, T. S. In *Stable Carbocation Chemistry*; Prakash, C. K. S., Schleyer, P. v. R., Eds.; John Wiley & Sons, Inc.: 1997, p 75-136.
48. Boronat, M.; Viruela, P.; Corma, A. *J. Phys. Chem. B* **1999**, *103*, 7809-7821.
49. Gerratt, J.; Cooper, D. L.; Karadakov, P. B.; Raimondi, M. *Chem. Soc. Rev.* **1997**, *26*, 87-100.
50. Cooper, D. L.; Gerratt, J.; Raimondi, M. *Chem. Rev.* **1991**, *91*, 929-964.
51. Gerratt, J. In *Advances in Atomic and Molecular Physics*; Academic Press: New York, 1971; Vol. 7, p 141-222.
52. Ladner, R. C.; Goddard, W. A. *J. Chem. Phys.* **1969**, *51*, 1073-&.
53. Fleming, F. P.; Barbosa, A. C. H.; Esteves, P. M. manuscript in preparation.

54. Goddard, W. A. *Phys. Rev.* **1967**, *157*, 73.
55. Goddard, W. A. *Phys. Rev.* **1967**, *157*, 81.
56. Szabo, A.; Ostlund, N. S. *Modern Quantum Chemistry Introduction to Advanced Electronic Structure Theory*; New Ed edition ed.; Dover Publications: New York, 1996.
57. Ruedenberg, K. *Rev. Mod. Phys.* **1962**, *34*, 326-&.
58. Wilson, C. W.; Goddard, W. A. *Theor. Chim. Acta* **1972**, *26*, 195-&.
59. Goddard, W. A.; Wilson, C. W. *Theor. Chim. Acta* **1972**, *26*, 211-&.
60. Nascimento, M. A. C.; Barbosa, A. C. H. In *Fundamental Aspects of Quantum Chemistry - A Tribute to Per-Olov Löwdin*; Kryachko, E. S., Ed.; Kluwer: Amsterdam, 2003; Vol. 1, p 371.
61. Penotti, F.; Gerratt, J.; Cooper, D. L.; Raimondi, M. *Theochem-Journal of Molecular Structure* **1988**, *46*, 421-436.
62. Coulson, C. A.; Fischer, I. *Phil. Mag.* **1949**, *40*, 386-393.
63. Olah, C. A.; Rasul, C. *Acc. Chem. Res.* **1997**, *30*, 245-250.
64. Marx, D.; Parrinello, M. *J. Chem. Phys.* **1996**, *104*, 4077-4082.
65. Marx, D.; Hutter, J. In *Modern Methods and Algorithms of Quantum Chemistry*; Grotendorst, J., Ed.; NIC: Jülich 2000, p 301-449.
66. Tse, J. S. *Ann. Rev. Phys. Chem.* **2002**, *53*, 249-290.
67. Huang, X. C.; McCoy, A. B.; Bowman, J. M.; Johnson, L. M.; Savage, C.; Dong, F.; Nesbitt, D. J. *Science* **2006**, *311*, 60-63.
68. Huang, X. C.; Johnson, L. M.; Bowman, J. M.; McCoy, A. B. *J. Am. Chem. Soc.* **2006**, *128*, 3478-3479.
69. Gerlich, D. *Phys. Chem. Chem. Phys.* **2005**, *7*, 1583-1591.
70. Brown, A.; McCoy, A. B.; Braams, B. J.; Jin, Z.; Bowman, J. M. *J. Chem. Phys.* **2004**, *121*, 4105-4116.
71. Brown, A.; Braams, B. J.; Christoffel, K.; Jin, Z.; Bowman, J. M. *J. Chem. Phys.* **2003**, *119*, 8790-8793.
72. Raugei, S.; Klein, M. L. *J. Phys. Chem. B* **2002**, *106*, 11596-11605.
73. Shiga, M.; Tachikawa, M.; Miura, S. *J. Chem. Phys.* **2001**, *115*, 9149-9159.
74. Marx, D.; Muser, M. H. *J. Phys. Cond. Matt.* **1999**, *11*, R117-R155.
75. Marx, D.; Parrinello, M. *Nature* **1995**, *375*, 216-218.
76. Deskevich, M. P.; Nesbitt, D. J. *J. Chem. Phys.* **2005**, 123.
77. White, E. T.; Tang, J.; Oka, T. *Science* **1999**, *284*, 135-137.
78. Kramer; M., C.; Oka, T.; White, T., E.; Marx, D.; Parrinello; Michele *Science* **1999**, *286*, 1051a.
79. Heck, A. J. R.; Dekoning, L. J.; Nibbering, N. M. M. *J. Am. Soc. Mass Spectrom.* **1991**, *2*, 453-458.
80. Yeh, L. I.; Lee, Y. T. *J. Am. Chem. Soc.* **1989**, *111*, 5597-5604.
81. Ivanova, II; Pomakhina, E. B.; Rebrov, A. I.; Derouane, E. C. *Top. Catal.* **1998**, *6*, 49-59.
82. Esteves, P. M.; Alberto, C. C. P.; Ramirez-Solis, A.; Mota, C. J. A. *J. Am. Chem. Soc.* **1999**, *121*, 7345-7348.

83. Hunter, E. P.; Lias, S. C. *J. Phys. Chem. Ref Data* **1998**, *27*, 413-656.
84. Esteves, P. M., unpublished results.
85. Hiraoka, K.; Kebarle, P. *J. Am. Chem. Soc.* **1976**, *98*, 6119-6125.
86. Hiraoka, K.; Kebarle, P. *J. Chem. Phys.* **1975**, *63*, 394-397.
87. Hiraoka, K.; Kebarle, P. *Can. J. Chem.* **1975**, *53*, 970-972.
88. Olah, C. A.; Halpern, Y.; Shen, J.; Mo, Y. K. *J. Am. Chem. Soc.* **1973**, *95*, 4960-4970.
89. Goepfert, A.; Sommer, J. *New J. Chem.* **2002**, *26*, 1335-1339.
90. Esteves, P. M.; Ramirez-Solis, A.; Mota, C. J. A. *J. Phys. Chem. B* **2001**, *105*, 4331-4336.
91. Esteves, P. M.; Ramirez-Solis, A.; Mota, C. J. A. *J. Braz. Chem. Soc.* **2000**, *11*, 345-348.
92. Boo, D. W.; Lee, Y. T. *Int. J. Mass Spectrom. Ion Proc.* **1996**, *159*, 209-229.
93. Boo, D. W.; Lee, Y. T. *J. Chem. Phys.* **1995**, *103*, 520-530.
94. Boo, D. W.; Liu, Z. F.; Suits, A. C.; Tse, J. S.; Lee, Y. T. *Science* **1995**, *269*, 57-59.
95. Raugei, S.; Kim, D.; Klein, M. L. *Quant. Struct.-Activ. Rd.* **2002**, *21*, 149-165.
96. Car, R.; Parrinello, M. *Phys. Rev. Letters* **1985**, *55*, 2471.
97. Goepfert, A.; Bhering, D. L.; Sommer, J.; Mota, C. J. A. *J. Phys. Org. Chem.* **2002**, *15*, 869-873.
98. Ahlberg, P.; Karlsson, A.; Goepfert, A.; Lilt, S. O. N.; Diner, P.; Sommer, J. *J. Chem. Eur. J.* **2001**, *7*, 2501-2501.
99. Okulik, N. B.; Diez, R. P.; Jubert, A. H.; Esteves, P. M.; Mota, C. J. A. *J. Phys. Chem. A* **2001**, *105*, 7079-7084.
100. Esteves, P. M.; Nascimento, M. A. C.; Mota, C. J. A. *J. Phys. Chem. B* **1999**, *103*, 10417-10420.
101. Zheng, X. B.; Blowers, P. J. *Mol. Catal. A Chem.* **2006**, *246*, 1-10.
102. Zheng, X. B.; Blowers, P. J. *Mol. Catal. A Chem.* **2005**, *242*, 18-25.
103. Khaliullin, R. Z.; Bell, A. T.; Kazansky, V. B. *J. Phys. Chem. A* **2001**, *105*, 10454-10461.
104. Vollmer, J. M.; Truong, T. N. *J. Phys. Chem. B* **2000**, *104*, 6308-6312.
105. Zheng, X. B.; Blowers, P. J. *J. Phys. Chem. A* **2006**, *110*, 2455-2460.
106. Milas, I.; Nascimento, M. A. C. *Chem. Phys. Lett.* **2006**, *418*, 368-372.
107. Zheng, X. B.; Blowers, P. J. *J. Phys. Chem. A* **2005**, *109*, 10734-10741.
108. Garcia-Serrano, L. A.; Flores-Sandoval, C. A.; Zaragoza, I. P. *J. Mol. Catal. A Chem.* **2003**, *200*, 205-212.
109. Milas, I.; Nascimento, M. A. C. *Chem. Phys. Lett.* **2001**, *338*, 67-73.
110. Li, J.; Duke, B.; McWeeny, R. VB2000 Version 1.8, SciNet Technologies, San Diego, CA, 2005.
111. Li, J.; McWeeny, R. *Int. J. Quantum Chem.* **2002**, *89*, 208.

Chapter 16

Quantum Chemical Studies of Carbocations from Oxidized Metabolites of Aza-Polycyclic Aromatic Hydrocarbons

Gabriela L. Borosky¹ and Kenneth K. Laali^{2,*}

¹Unidad de Matemática y Física, INFIQC, Facultad de Ciencias Químicas,
Universidad Nacional de Córdoba, Ciudad Universitaria, Córdoba 5000,
Argentina

²Department of Chemistry, Kent State University, Kent, OH 44242

Model computational studies aimed at understanding structure-reactivity relationships and substituent effects on carbocation stability for aza-PAHs derivatives were performed by density functional theory (DFT). Comparisons were made with the biological activity data when available. Protonation of the epoxides and diol epoxides, and subsequent epoxide ring opening reactions were analyzed for several families of compounds. Bay-region carbocations were formed via the O-protonated epoxides in barrierless processes. Relative carbocation stabilities were determined in the gas phase and in water as solvent (by the PCM method).

Introduction

Polycyclic aromatic hydrocarbons (PAHs) derived from incomplete combustion of organic matter are widespread environmental mutagens and/or carcinogens (1, 2). In order to exert their biological activity the PAHs require metabolic activation for transformation into oxidized metabolites, namely dihydrodiols (proximate carcinogens) and diol epoxides (ultimate carcinogens) (3, 4). Among them, the bay-region diol epoxides (DEs) exhibit increased mutagenic and carcinogenic properties (5). These studies have led to the development of the so-called bay-region theory (6, 7). The pathway for metabolic formation of the bay-region DEs involves oxidation of a terminal, angular benzo ring of the hydrocarbon to form an arene oxide, hydration of the arene oxide to form a *trans*-dihydrodiol, and subsequent epoxidation of the bay-region double bond of the dihydrodiol. Benzylic carbocations generated from these electrophilic DEs by opening of the O-protonated epoxide ring are capable of forming covalent adducts with the nucleophilic sites in DNA (3, 8), and this is recognized as a key step in chemical carcinogenesis.

Mechanistic studies on the hydrolysis of benzo[*a*]pyrene-DE demonstrated pH dependency and catalysis by DNA and by polynucleotides, showing that protonation must occur either before or during the rate determining step (9, 10). Based on these studies, it was proposed that a physically-bound DE reacts to form a physically bound benzylic carbocation in the rate determining step. The monohydrogen phosphate group on the nucleotide acts as general acid, and stacking interactions between the PAH-DE and the base contribute to catalysis. Moreover, it is likely that electrophilic attack of DNA nucleotides by PAH epoxides is S_N1-like and proceeds through proton-stabilized transition states in which the hydrocarbon exhibits significant carbocationic character (11-13).

Methyl substitution in strategic positions in polyarenes frequently results in notable enhancement of carcinogenic activity. Thus, methyl substitution at a bay region tends to markedly increase the biological activity (14). Moreover, carcinogenic activities of PAHs are often strongly affected by fluorine substitution at proper molecular sites (3, 15).

Under appropriate combustion conditions, incorporation of nitrogen into the aromatic ring systems could lead to the formation of aza-PAHs (16). A number of such aza-aromatic hydrocarbons were found in significant amounts in urban air particulates, gasoline engine exhaust, tobacco smoke, and effluents from coal combustion processes (2, 17-19). Substantial evidence has been obtained suggesting that, like the PAHs, the aza-analogues are also metabolically activated to DEs according to the bay-region theory (20-22). Experimental data have revealed that the position of the nitrogen heteroatom in the aza-PAHs could have a significant effect on the carcinogenic potencies of their dihydrodiol and bay-region DE metabolites.

Quantum-mechanical calculations have been successfully applied to the study of the carcinogenic pathways of PAH and aza-PAH derivatives, and very good correlations have been shown with the available experimental reactivities of these compounds (23-28). Furthermore, modeling studies of biological electrophiles from PAHs by density functional theory (DFT) methods have given proper descriptions of the charge delocalization modes and NMR characteristics of their resulting carbocations (29-33).

Considering the relevance of aza-PAHs in the elucidation of the mechanism of chemical carcinogenesis, our goal was to apply DFT methods to achieve a better understanding of the structural and electronic factors affecting the reactivity of this type of compounds. In this chapter we summarize our recent and ongoing computational studies in this field.

Methods

Quantum chemical DFT calculations were performed with the Gaussian 03 suite of programs (34), employing the B3LYP functional (35-37) and suitable basis, as the 6-31G* and 6-31+G* split-valence shell basis sets. Geometries were fully optimized and minima were characterized by calculation of the harmonic vibrational frequencies. Natural bond orbital population analysis was evaluated by means of the NBO program (38). The solvent effect was estimated by the polarized continuum model (PCM) (39-42). NMR chemical shifts and NICS (nuclear independent chemical shift) (43) values were calculated by the GIAO method (gauge independent atomic orbitals) (44). NMR chemical shifts were referenced to TMS (GIAO magnetic shielding tensor = 182.4656 ppm; this value is related to the GIAO isotropic magnetic susceptibility for ^{13}C) and to CFCl_3 (GIAO magnetic shielding tensor = 179.0548 ppm; value related to the GIAO isotropic magnetic susceptibility for ^{19}F). NICS values were computed at each ring centroid. Semiempirical calculations were carried out with the AM1 method (45).

Charge delocalization modes (positive charge density distribution) in the resulting carbocations were evaluated by GIAO-NMR (via computed $\Delta\delta^{13}\text{C}$ values) and by means of the NPA-derived changes in charges (carbocation minus neutral) for carbon (and overall charges over CH units) and nitrogen. GIAO-NMR chemical shifts for the epoxides and diol epoxides were also computed in water as solvent. Relative aromaticity in various rings in the aza-PAH carbocations was gauged via NICS and ΔNICS .

Benzo [*h*] quinoline, Benzo [*f*] quinoline, and Benzo [*c*]phenanthridine Derivatives

Measurements of the mutagenic activities of several derivatives of benzo[*h*]quinoline (BhQ), benzo[*f*]quinoline (BfQ) and their carbon analogue phenanthrene (Phe) (Figure 1) revealed that the BhQ bay-region DE (with the *anti* isomer being more active than *syn*) was considerably less mutagenic than phenanthrene DE (46). Based on these studies, it was inferred that the BhQ bay-region DE and BhQ-tetrahydroepoxide are considerably more mutagenic than those of BfQ at similar doses (BfQ *anti* isomer was not available for direct evaluation) (46). The differences in bioactivity between the BhQ and BfQ DEs were explained by Hückel and PMO considerations, whereby diminished reactivity of BfQ-7,8-diol-9, 10-epoxide was attributed to the destabilizing effect of placement of a positive charge on the nitrogen heteroatom by resonance of the carbenium ion formed (46, 47).

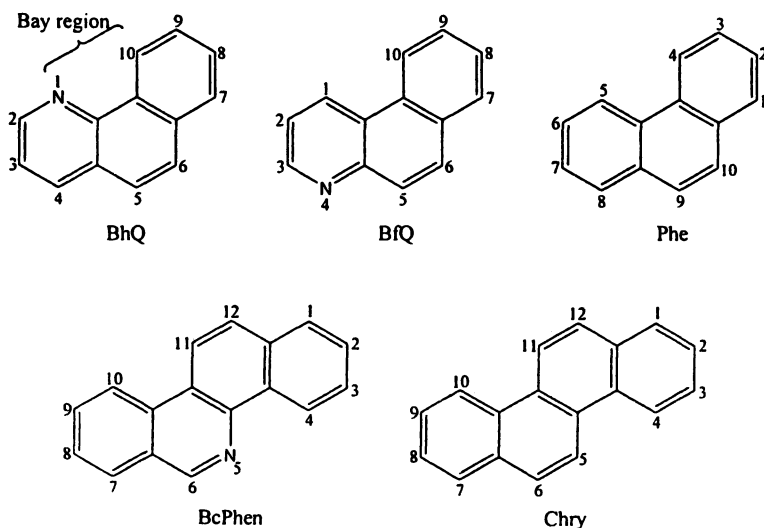
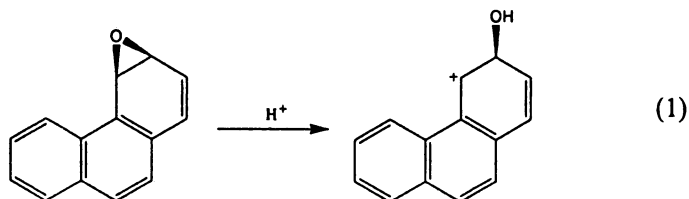


Figure 1. Structures and numbering of benzo[*h*]quinoline (BhQ), benzo[*f*]quinoline (BfQ), Benzo[*c*]phenanthridine (BcPhen) and their carbon analogues phenanthrene (Phe) and Chrysene (Chry). Adapted from Reference 26.

In order to evaluate the influence of the nitrogen atom on reactivity, computations on BhQ and BfQ derivatives were compared with the data obtained for the corresponding carbon analogue (Phe) (26). Both bay-region structures

present the nitrogen atom located at different positions of the fused-ring system. Furthermore, calculations for the related system benzo[*c*]phenanthridine (BcPhen) (Figure 1) were performed and compared with the results for chrysene (Chry) (26). In this way, the structures for the epoxides and the *anti*-DEs derived from Phe, BhQ and BfQ, and those derived from Chry and BcPhen were optimized at the B3LYP/6-31G* level. In every case, epoxide protonation led to the formation of the open carbocations depicted in Figure 2 via a barrierless process, indicating that oxonium ions were not minima on the respective potential energy surfaces. Changes in energy for every ring opening reaction of type 1 are presented in Table 1, as well as some selected NPA-derived charges for the carbocations.



According to the NPA-derived charge distributions, positive charge in the resulting carbocations was delocalized throughout the π -system. Nitrogen substitution did not significantly modify the charge distribution pattern. Computed GIAO ^{13}C NMR chemical shifts and changes in chemical shifts ($\Delta\delta^{13}\text{C}$ values) exhibited essentially the same trends as changes in NPA charges, that is, changes in the chemical shifts to the more positive values (carbocations versus neutral compounds) followed the increments in positive charge for the respective positions in every structure. NICS values revealed that the ring adjacent to the carbocationic center is no longer aromatic, and this applied to both PAHs and aza-PAHs. Therefore, substitution of a carbon atom in a ring for nitrogen did not affect the relative aromaticity of the different rings in the carbocations. Consequently, similar reactivity patterns are expected to be followed by both PAHs and aza-PAHs compounds.

For the three-ring compounds, ΔE_r s in Table 1 show a decrease in the exothermicity of reaction 1 in the sense $1\text{H}^+ > 2\text{H}^+ > 3\text{H}^+$, and also in the series $4\text{H}^+ > 5\text{H}^+ > 6\text{H}^+$. According to these results, the calculated relative ease of formation, that is, the stability of the derived carbocations followed the mutagenic activities observed for the tetrahydro epoxide and the tetrahydro DE derivatives of Phe, BhQ and BfQ (46). The NPA-derived positive charge at the carbocationic center was smaller for 1H^+ than for 2H^+ , suggesting that stabilization by delocalization was larger for 1H^+ , in accord with its greater ease of formation. However, this was not the case for 3H^+ , whose ΔE_r did not correlate with the charge at the carbocationic center and was smaller than for 2H^+ . On the other hand, it could be noted that 3H^+ presented a less negative

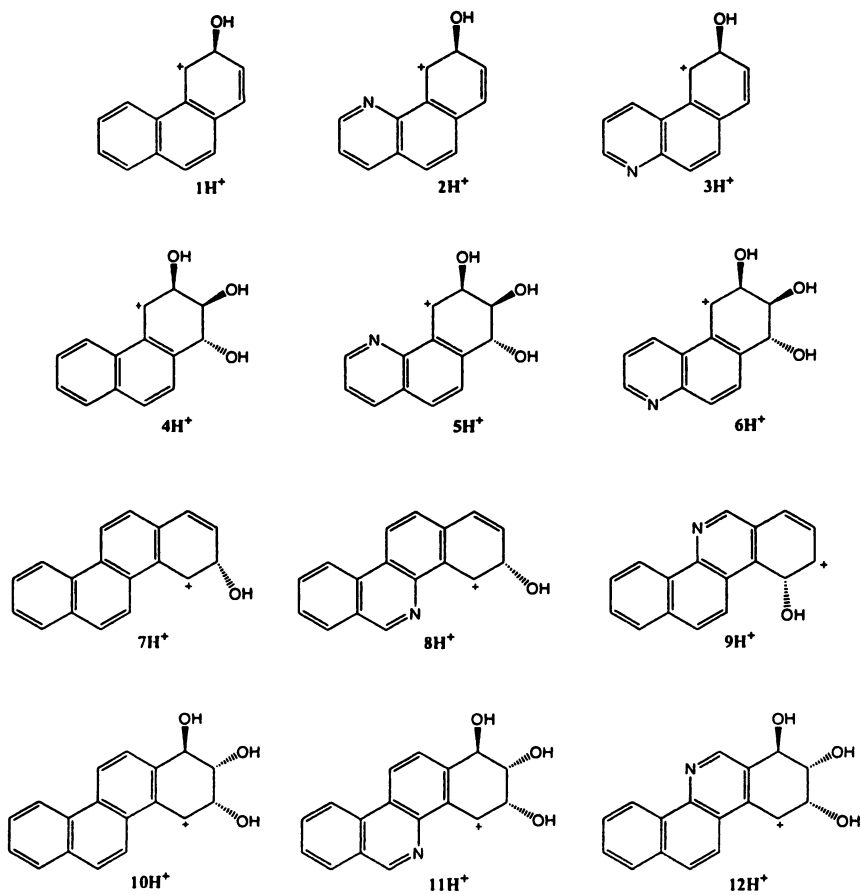


*Figure 2. Studied carbocations from PAHs and Aza-PAHs.
Figure adapted from reference 26.*

Table I. B3LYP/6-31G* Calculations for the Carbocations in Figure 2^a

Cation	ΔE_r (kcal/mol) ^b	$\Delta \bar{E}_r$ (kcal/mol) ^c	NPA Charge ^d	NPA Charge at N	GIAO-NMR $\delta^{13}C^e$ (ppm)
1H ⁺	-234.18 (-165.51)	-227.06	0.243 (0.271)	-	167.6 (172.0)
2H ⁺	-231.97 (-163.22)	-224.98	0.308 (0.313)	-0.449 (-0.475)	178.7 (180.4)
3H ⁺	-228.84 (-161.91)	-221.95	0.254 (0.291)	-0.400 (-0.449)	169.9 (177.1)
4H ⁺	-233.53 (-162.07)	-226.15	0.311 (0.313)	-	182.3 (181.5)
5H ⁺	-230.20 (-157.89)	-223.06	0.361 (0.356)	-0.449 (-0.474)	177.3 (177.6)
6H ⁺	-227.90 (-156.49)	-220.85	0.300 (0.330)	-0.393 (-0.439)	165.2 (171.5)
7H ⁺	-236.06 (-164.43)	-228.93	0.243 (0.277)	-	168.7 (174.8)
8H ⁺	-234.95 (-162.73)	-227.92	0.309 (0.319)	-0.468 (-0.485)	181.0 (183.2)
9H ^{†f}	-232.82 (-162.13)	-225.62	0.211 (0.250)	-0.429 (-0.464)	163.1 (171.5)
9H ^{†g}	-224.36	-217.77	0.265	-0.348	
10H ⁺	-236.63 (-159.75)	-229.16	0.272 (0.298)	-	161.9 (166.4)
11H ⁺	-227.24 (-156.58)	-220.63	0.361 (0.361)	-0.468 (-0.485)	180.3 (181.0)
12H ⁺	-222.58 (-147.02)	-215.62	0.320 (0.356)	-0.337 (-0.360)	175.4 (180.4)

^a PCM values in parenthesis (water as solvent).

^b Energy difference between carbocation and the neutral compound (as in reaction 1).

^c Including zero-point energy (ZPE) contribution.

^d At the carbocationic center (carbon plus hydrogen charges).

^e At the carbocationic center.

^f Non bay-region carbocation formed.

^g Bay-region carbocation.

charge at the nitrogen atom than 2H^+ . Going from the epoxide to the carbocation yielded an increase of positive charge density at N of 0.006 for **2**, while in case of **3** this increment was 0.041. The same observations applied to the DEs, that is, 5H^+ was more stable than 6H^+ not because of a greater delocalization of the positive charge but as a consequence of its more negatively charged nitrogen atom. As for Chry and BcPhen derivatives, carbocation formation was more favored in the order $7\text{H}^+ > 8\text{H}^+ > 9\text{H}^+$ and $10\text{H}^+ > 11\text{H}^+ > 12\text{H}^+$.

Selected BcPhen derivatives present the nitrogen heteroatom in the bay region where the benzylic cation is formed (BcPhen-3,4-epoxide **8** and BcPhen-1,2-diol-3,4-epoxide **11**), or in the other bay region, more distant to the carbocationic center (BcPhen-9,10-epoxide **9** and BcPhen-7,8-diol-9,10-epoxide **12**). It was found surprisingly that **9** opened in the non bay-region sense to give the carbocation 9H^+ upon epoxide protonation. The bay-region carbenium ion (9H^{++}) was computed to be ca. 8 kcal/mol less stable. Comparison of NPA charges for both isomeric carbocations showed that in the most stable carbocation (9H^+) the nitrogen had a somewhat greater negative charge, and the positive charge was more delocalized (Figure 3). The same correspondence pertaining to larger negative charge on N and greater stability of the carbocation was found for the corresponding DEs.

Isodesmic reactions **2** and **3** were calculated as a measure of the relative ease of formation of the aza-epoxides, in order to obtain some insight as to the effect of nitrogen atom on metabolic activation of aza-PAHs. It was presumed that formation of the epoxides is not as relevant as carbocation formation in determining the relative reactivities of Phe, BhQ and BfQ, because almost no energy differences were observed for the isodesmic reactions involving these compounds.

Covalent Adducts of Carbocations with Representative Nucleophiles

Calculations of the nucleophilic reactions with MeO^- were performed for the carbocations 4H^+ , 5H^+ and 6H^+ in order to simulate the crucial step of aza-PAH/adduct formation. These reactions were considered as models for evaluation of the reactivity trend for these carbocations toward nucleophiles. Thus, the thermodynamical tendency of each carbocation to react with the nucleophilic sites of DNA was estimated.

Both *syn* and *anti* methoxy adducts were considered (Figure 4). The 6-31+G* basis set was employed to give a proper description of the anions by inclusion of diffuse functions. The corresponding ΔE_r and ΔG_r for these

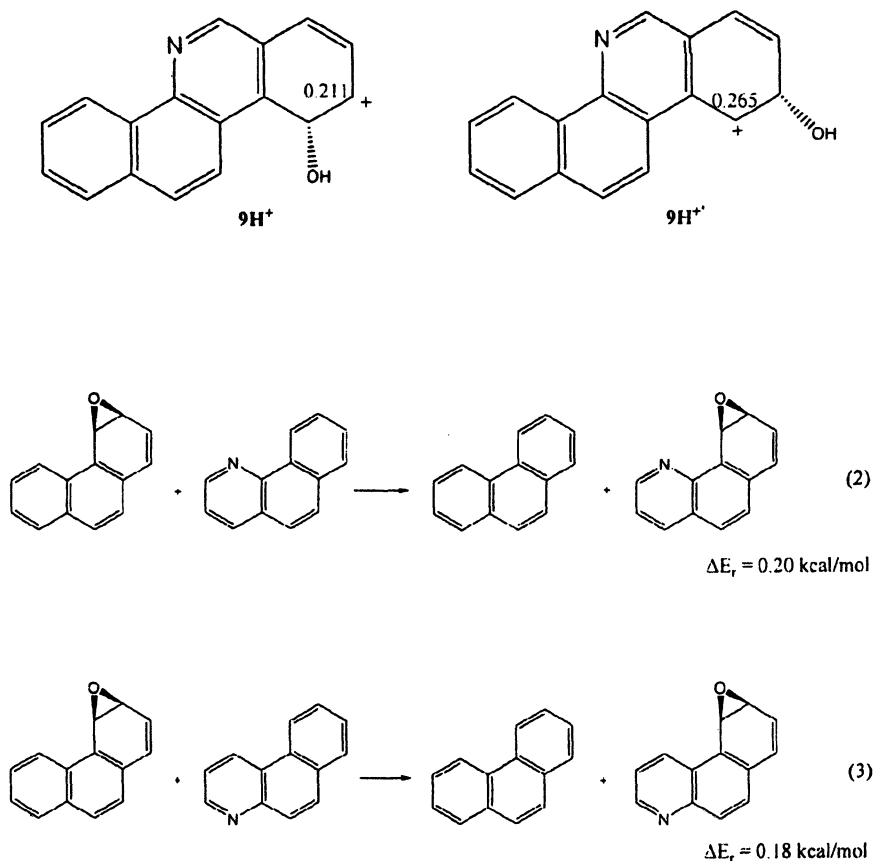


*Figure 3. NPA charges for both isomeric carbocations derived from 9.
Figure adapted from reference 26.*

reactions showed similar trends (see Table 2). Different rotamers in the corresponding adducts resulting from rotation of the C-OMe bond were computed by AM1, allowing for diverse dispositions of the methyl group, and selected conformational isomers were subsequently optimized by DFT.

Both ΔE_r and ΔG_r values for reactions between the carbocations of the Phe derivative and those derived from the aza-PAHs with the nucleophile did not correlate with the known relative experimental activities of these compounds (46). These results reinforce the earlier proposed mechanistic picture that

epoxide ring opening for activation of PAHs could become substantially S_N1 -like or proceed through proton stabilized transition states that present significant carbocationic character (11-13). Thus, the experimental activity order $\text{Phe} > \text{BhQ} > \text{BfQ}$ could be explained by the relative stabilities of their derived carbocations. It was remarkable that inclusion of the solvent effect did not alter these observations. In aqueous phase calculations, the decrease in the exothermicity of the reactions due to the more efficient solvation of the charged reactants was especially noteworthy. Accordingly, the reactivity of this type of compounds would be predominantly governed by the feasibility of carbocation formation.

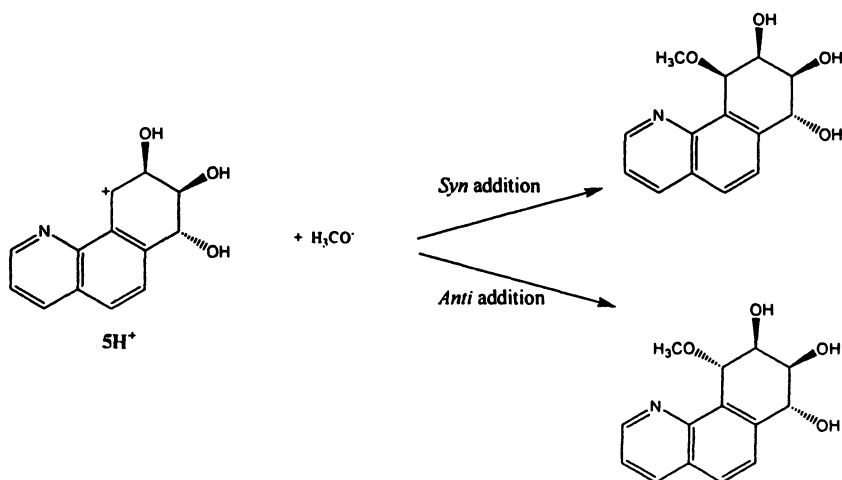


Figure 4. Calculated nucleophilic reactions with MeO.
Adapted from reference 26.

Table II. B3LYP/6-31+G* Calculations for Nucleophilic Additions^a

Cation	Nucleophile	Addition	ΔE_r (kcal mol)	ΔG_r (kcal mol) ^b
4H^+	$\text{H}_3\text{C}-\text{O}^-$	Syn	-175.12 (-59.74)	-157.38
		Anti	-177.73 (-62.88)	-159.62
5H^+	$\text{H}_3\text{C}-\text{O}^-$	Syn	-183.04 (-64.40)	-164.62
		Anti	-176.48 (-63.48)	-158.59
6H^+	$\text{H}_3\text{C}-\text{O}^-$	Syn	-180.78 (-65.93)	-162.84
		Anti	-182.98 (-69.34)	-164.80

^a PCM values in parenthesis (water as solvent).

^b T = 298.15 K, 1 atm.

Furthermore, the adducts of 1H^+ and 2H^+ with guanine were computed at the B3LYP/6-31G* level. It has been established that bay-region diol epoxides derived from PAHs predominantly form stable adducts with DNA by *cis* or *trans* addition to the exocyclic amino groups of deoxyguanosine and deoxyadenosine (48, 49). Moreover, depurinating products that are lost from DNA by cleavage of the glycosidic bond are formed by reaction with the N-7 of guanine, and at N-3 and N-7 of adenine (50). Taking this into account, the adducts arising from reactions with the exocyclic nitrogen and with the N-7 of guanine were calculated for both carbocations. The *trans* products were selected, as this attack mode is preferred for *anti*-diol epoxides (51). The most stable rotamer for each compound was located via AM1 conformational searches by rotation of the generated C-N bond. The lowest energy structures were subsequently optimized by DFT calculations (Table 3, Figures 5 and 6).

Table III. B3LYP/6-31G* Calculations for Guanine Adducts

Carbocation	Reacting Nitrogen of Guanine	Relative Energy (kcal/mol)		$\Delta E_{\text{reaction}}$ (kcal/mol) ^a	
		Gas Phase	Aqueous Phase	Gas Phase ^b	Aqueous Phase
1H^+	Exocyclic	2.38	0.00	214.28 (221.11)	260.36
	N-7	0.00	2.40	211.90 (220.80)	262.76
2H^+	Exocyclic	1.36	0.00	213.63 (220.84)	258.62
	N-7	0.00	2.32	212.27 (220.33)	260.94

^a $\Delta E_{\text{reaction}} = \text{Energy}_{\text{Adduct}} - \text{Energy}_{\text{Guanine}} - \text{Energy}_{\text{Carbocation}}$

^b $\Delta G_{\text{reaction}}$ in parenthesis (T=298.15 K, 1 atm).

Reaction energies for the formation of each type of adduct with both carbocations (measured as the energy difference between the adduct minus guanine and carbocation total energies) were comparable, and the same observation applied to the ΔG_r values. Inclusion of the solvent caused an increase in the endothermicity of the reactions, presumably due to a better solvation of the carbocations. The change in the preferred product of the addition

reactions with guanine due to solvent effect is noteworthy. Whereas the N-7 adducts were most stable in the gas phase, in water as solvent the most stable adducts were those formed by reaction with the exocyclic nitrogen of guanine, in accordance with the experimental observations.

Dibenzo[*a,h*]acridine, Benzo[*a*]acridine, and Benzo[*c*]acridine Derivatives

Several dibenzacridines (DBACRs), including DB[*a,h*]ACR, DB[*a,j*]ACR, and DB[*c,h*]ACR, have been identified as environmental contaminants (52). Among the DBACRs tested, DB[*a,h*]ACR is a highly potent mutagen (53) and carcinogen (54), with a tumorigenic activity similar to its carbon analogue

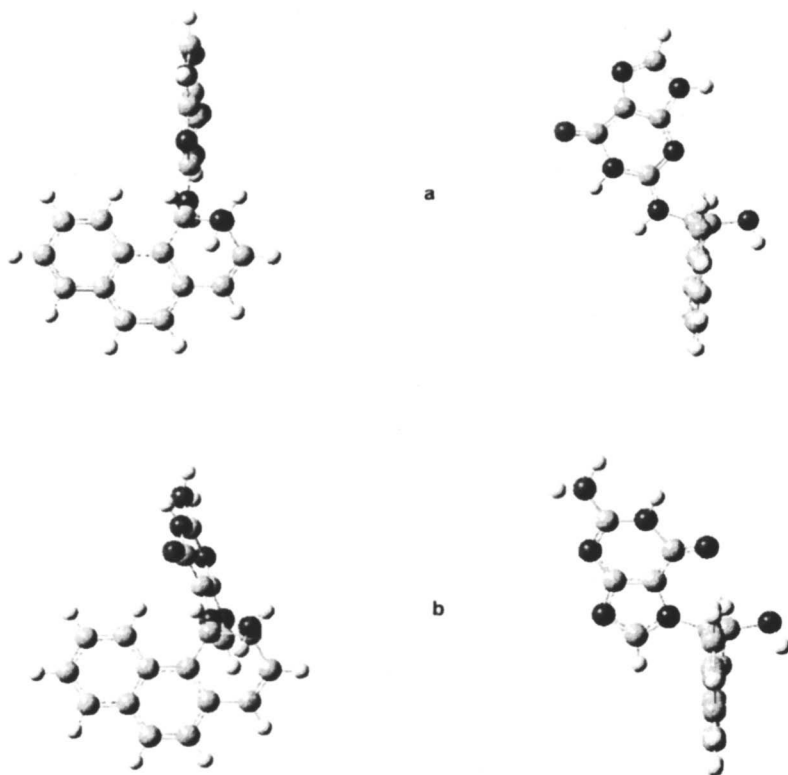


Figure 5. Adducts between guanine and $1H^+$ (a) Exocyclic N. (b) N-7 isomer. Figure adapted from reference 26.

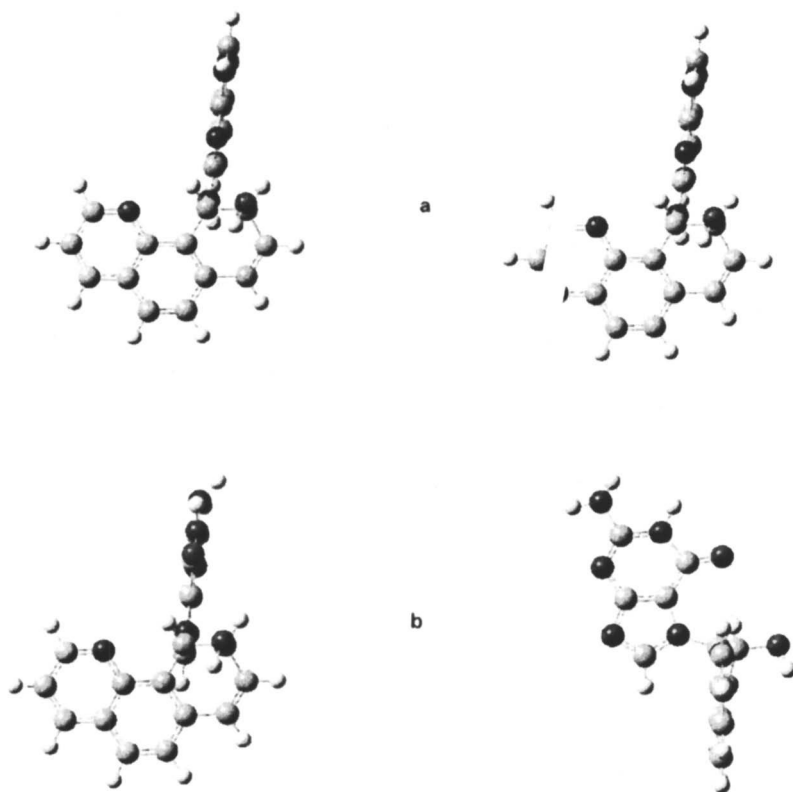


Figure 6. Adducts between guanine and $2H^+$. (a) Exocyclic N. (b) N-7 isomer.
Figure adapted from reference 26.

dibenzo[*a,h*]anthracene (DB[*a,h*]A) (55). In DB[*a,h*]ACR the nitrogen heteroatom at position 7 defines two nonequivalent bay regions: in one of them, nitrogen is located in the bay region; while in the other, nitrogen is distal relative to the bay region (Figure 7). Hence, this compound provides a means to evaluate the impact of the presence and absence of a nitrogen heteroatom in the bay region on the biological activity of the bay-region DEs. It has been reported that bay-region DB[*a,h*]ACR-10,11-diol-8,9-epoxide is more mutagenic and tumorigenic than the isomeric bay-region 3,4-diol-1,2-epoxide (56, 52). Only (+)-DB[*a,h*]ACR-10S,11R-diol-8R,9S-epoxide-2¹ displayed significant tumorigenic activity (54).

¹ The designations 1 and 2 for the diol epoxides indicate that the benzylic hydroxyl group and the epoxide oxygen are *cis* (*syn*) or *trans* (*anti*), respectively.

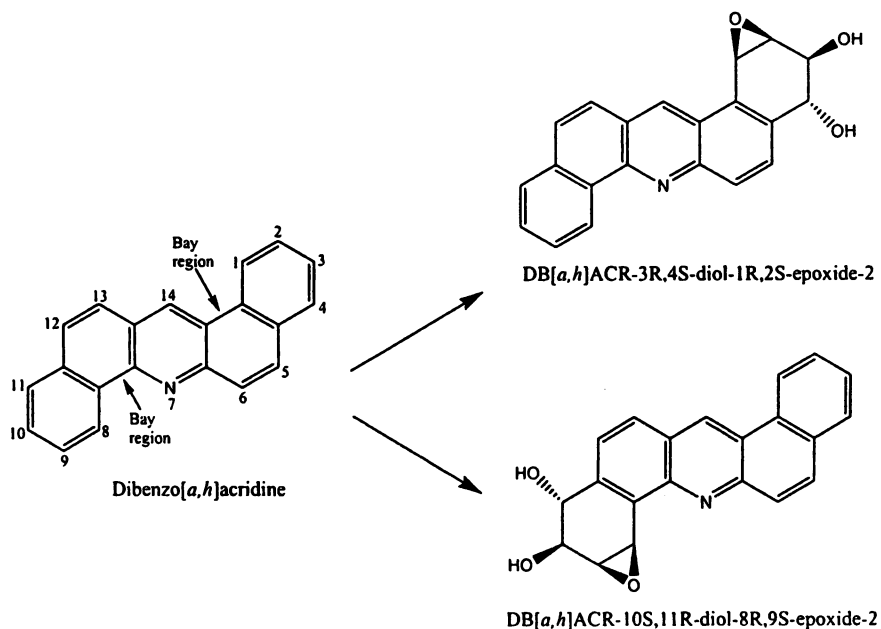


Figure 7. Structure and numbering of dibenzo[*a,h*]acridine and its major metabolites. Figure adapted from reference 27.

As regards the biological activity of methylated DB[*a,h*]ACR derivatives, early studies indicated that the 14-methyl analogue is moderately active (20), the 3-methyl derivative is inactive, and the 8-ethyl compound is moderately active (20). Considering other related compounds, benzo[*a*]acridine (B[*a*]ACR) is noncarcinogenic, while benzo[*c*]acridine (B[*c*]ACR) is generally regarded as inactive or weakly active (20). In contrast, 7-Me-B[*c*]ACR is highly active (20). Bay-region DE formation is the sole pathway reported for acridines (57) and for mutagenic activation of dimethylbenzo[*c*]acridines (58).

Early quantum mechanical calculations at the Hückel, INDO, Gaussian 70 and PMO level were in accord with resonance predictions regarding the relative chemical reactivities of DB[*a,h*]ACR-10,11-diol-8,9-epoxide and the 3,4-diol-1,2-epoxide (47, 59, 60, 20). For the C-1 carbocation formed by ring opening of the bay-region DE of DB[*a,h*]ACR-3,4-diol-1,2-epoxide, these data had shown that delocalization of the positive charge by resonance through the π electron system places a positive charge on the nitrogen heteroatom at N-7, an energetically destabilizing contribution. However, this is not the case for the C-8 carbocation of the 10,11-diol-8,9-epoxide, which could explain the higher activity of this latter derivative.

With the aim of understanding the structural and electronic factors affecting the reactivity of DB[*a,h*]ACR derivatives, changes in energy for epoxide ring opening reactions of the O-protonated DB[*a,h*]ACR-3,4-diol-1,2-epoxide (**13**) and DB[*a,h*]ACR-10,11-diol-8,9-epoxide (**14**) were calculated (27). For comparison purposes, formation of the same carbocations from the respective 1,2- (**15**) and 8,9-epoxides (**16**) were computed (Figure 8). Results were compared with those for the carbon analogue DB[*a,h*]A. B[*a*]ACR (**17**) and B[*c*]ACR (**18**) bay-region epoxide derivatives were also analyzed. Changes in energy for every epoxide opening reaction are presented in Table 4.

Table IV. Calculations for Reactions in Figure 8

<i>Aza-PAH</i>	ΔE_r (kcal/mol)		Charge Density at C ^a (ΔqC) ^b	Charge Density at N-7 (ΔqN) ^b
	<i>Gas Phase</i>	<i>Aqueous Phase</i>		
13	-235.31	-159.75	-0.037 (-0.090)	-0.396 (0.049)
14	-235.19	-160.19	-0.019 (-0.071)	-0.435 (0.022)
DB[<i>a,h</i>]A-1,2- epoxide ^c	-241.85	-167.73	-0.055 (-0.108)	-
15	-237.00	-163.79	-0.040 (-0.091)	-0.403 (0.044)
16	-239.83	-165.46	-0.012 (-0.068)	-0.438 (0.014)
17	-234.80	-163.90	-0.041 (-0.092)	-0.378 (0.058)
18	-232.86	-165.41	0.009 (-0.047)	-0.429 (0.022)

^a Carbocationic center.

^b Change in charge density between the open carbocation and the neutral closed epoxide ($qC_{\text{carbocation}} - qC_{\text{epoxide}}$).

^c Dibenzo[*a,h*]anthracene.

The protonated epoxides, i.e. the oxonium ions, could not be characterized as minima on the respective potential energy surfaces, as in every case the epoxide ring opened by a barrierless process upon O-protonation. Charge delocalization maps are shown in Figure 9, and some selected NPA-derived charges for the carbocations are displayed in Table 4.

Based on the calculated results presented in Table 4, stability of the carbocations generated from oxidized metabolites of DB[*a,h*]A, DB[*a,h*]ACR, B[*a*]ACR and B[*c*]ACR correlate with the available data on their biological activities. According to ΔE_r of the corresponding reactions, carbocation formation at C-8 ($14H^+$) was more favored than at C-1 ($13H^+$), and the carbocation derived from DB[*a,h*]A was more stable than those from DB[*a,h*]ACR. The relative stabilities of the aza-PAH carbocations correlated with the magnitude of the negative charge at N-7, and not with the extent of charge delocalization (measured by the decrease in positive charge density at the carbocation center). In this manner, development of less negative charge at N by resonance results in destabilization of the open carbocationic structures and is a determining factor in their relative stability order. Aqueous phase calculations (PCM method with water as solvent) afforded the same reactivity trend, although the ring opening reactions were less exothermic due to the large solvation energy of proton (despite the greater stabilization of the carbocations as compared to the neutral epoxides). As the same trend was followed by both families of compounds (DEs and epoxides), subsequent calculations in this study were performed only for the epoxide derivatives in order to reduce computational costs.

The effect of fluorine substitution on ΔE_r for the epoxide ring opening reaction, and hence on carbocation stabilities, was analyzed. According to the charge delocalization maps for both bay-region epoxides, substitution at positions 6 and 3 of the 1,2-epoxide would be expected to produce the most noticeable changes, followed by position 12. On the other hand, the 8,9-epoxide should be most strongly affected by substitution at C-13, 10, and 5. Thus, calculations were carried out for the 5-, 6-, 12- and 13-fluorinated derivatives of both isomeric bay-region epoxides. Positions 3 and 10, although exhibited a significant positive charge density in the carbocations derived from the 1,2- and 8,9-epoxide, respectively, were left unsubstituted since these sites are subject to metabolic activation to the corresponding DEs. Fluorination at C-14 was also considered to account for any influence that may be exerted by a fluorine atom located in a bay region. Reactions are displayed in Figures 10 and 11, and calculation results are gathered in Table 5.

Taking into account the ΔE_r s for epoxide ring opening of the fluorinated compounds, it could be noted that the F-6 structure (**20**) was most favored for opening of the 1,2-epoxide, yielding a ΔE_r even more exothermic than the unsubstituted molecule. Therefore, a fluorine atom at a highly positively charged site stabilized the carbocation. Fluorine at positions 12 (**21**) and 14 (**23**) afforded

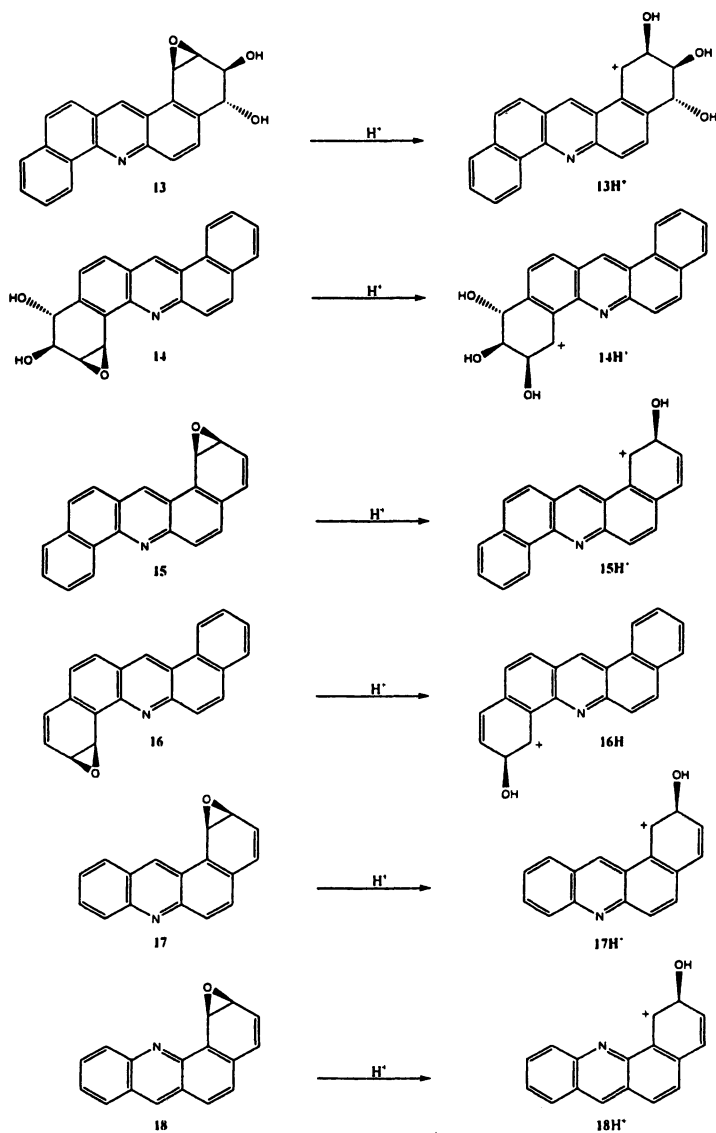


Figure 8. Epoxide ring opening reactions of bay-region diol epoxides and epoxides from dibenzo[*a,h*]acridine, and epoxides from benzo[*a*]acridine and benzo[*c*]acridine. Figure adapted from reference 27.

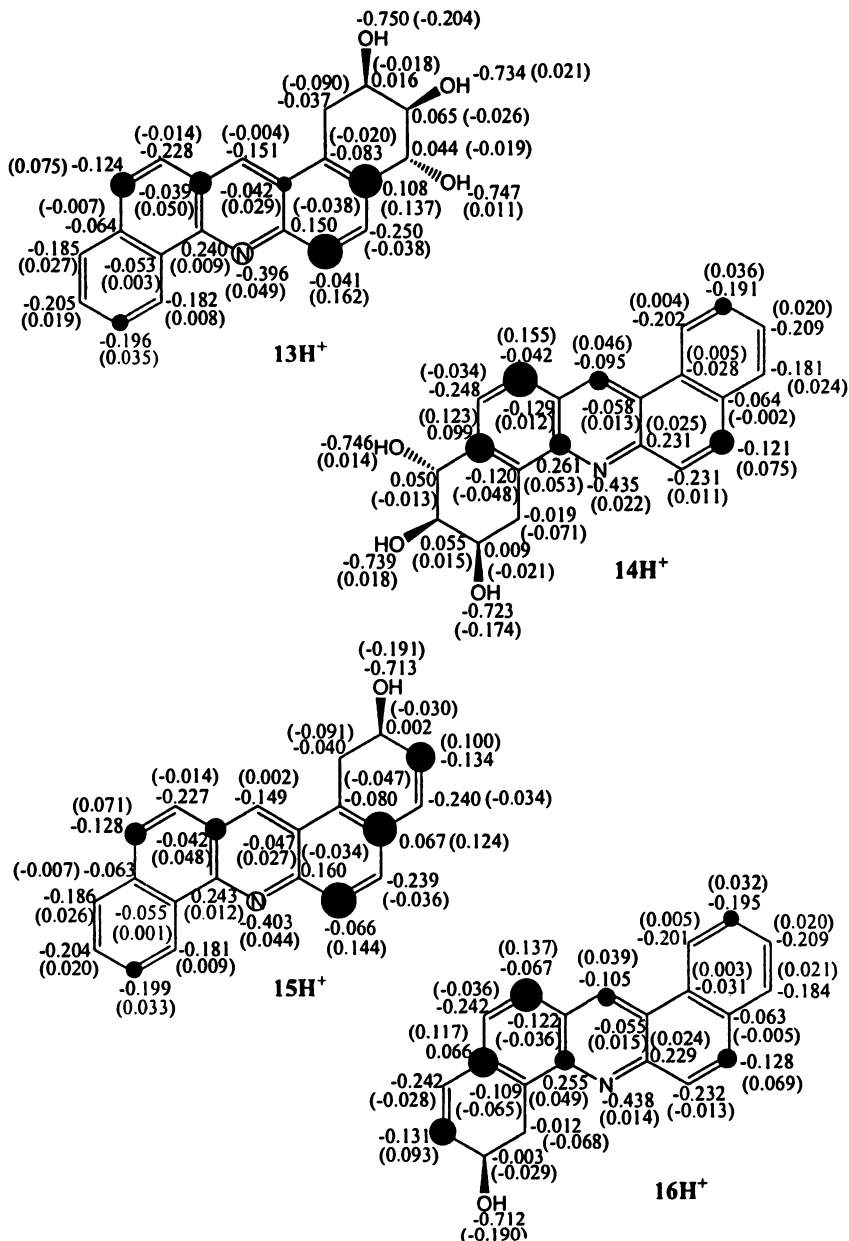


Figure 9. Computed NPA-derived heavy atom charges (Δ charges related to the neutral compound in parentheses) for carbocations. [Dark circles are roughly proportional to the magnitude of C Δ charges, and white circles to N Δ charges; threshold was set to 0.030]. Figure adapted from reference 27.

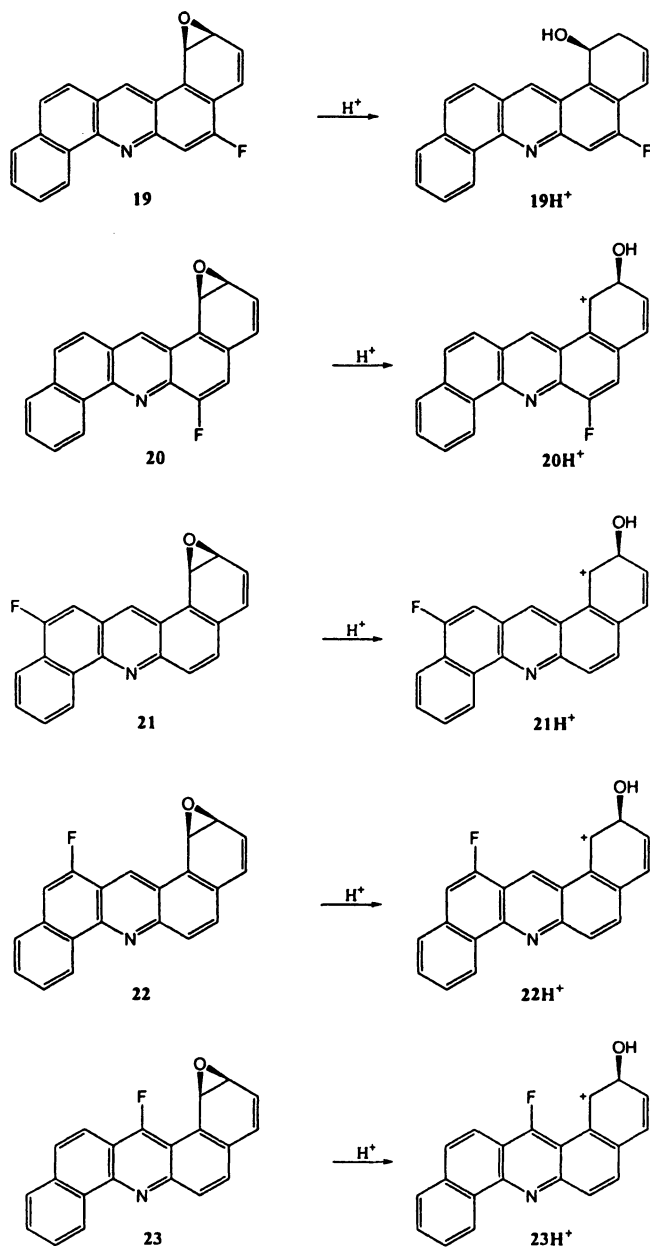


Figure 10. Epoxide ring opening reactions of the fluorinated derivatives of dibenzo[*a,h*]acridine-1,2-epoxide. Figure adapted from reference 27.

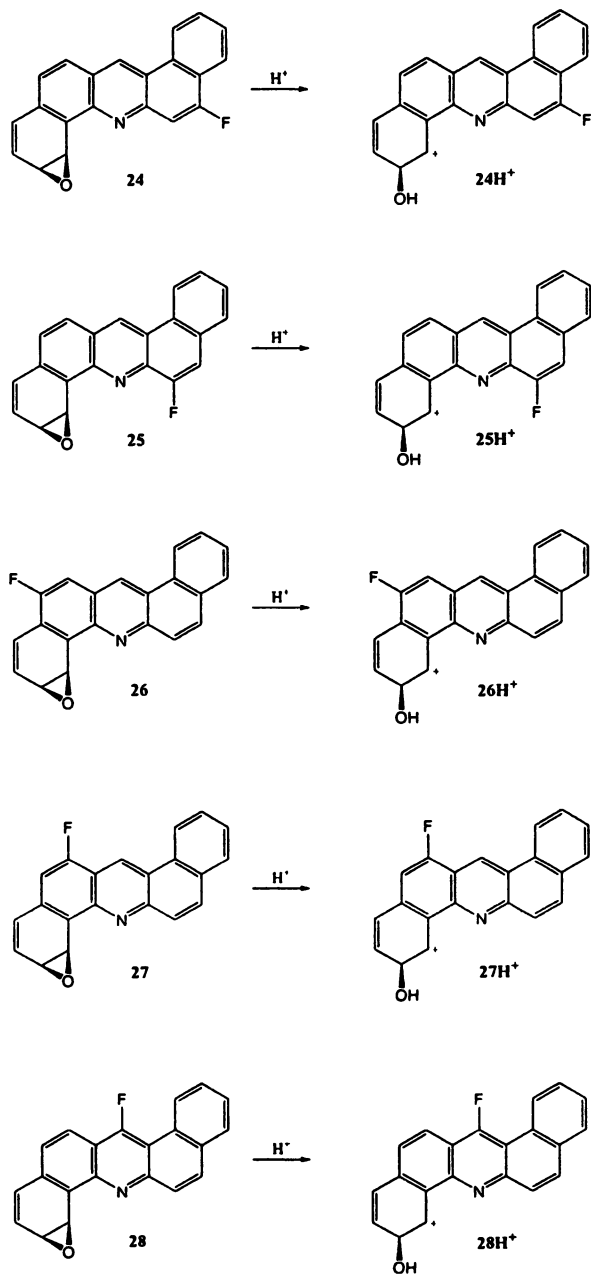


Figure 11. Epoxide ring opening reactions of the fluorinated derivatives of dibenzo[*a,h*]acridine-8,9-epoxide. Figure adapted from reference 27.

Table V. Calculations for Fluorinated Derivatives of DB[*a,h*]ACR-1,2-Epoxyde and DB[*a,h*]ACR-8,9-Epoxyde in Figures 10 and 11

Fluorinated Position (Compound)	ΔE_r (kcal/mol) Gas Phase (Aqueous Phase)	q^a	qF (ΔqF) ^b	GIAO-NMR $\delta^{19}F$ ($\Delta\delta^{19}F$) (ppm)	C-F Bond Length (Angstroms)
DB[<i>a,h</i>]ACR-1,2-epoxyde					
C-6 (20)	-238.30 (-165.21)	0.144	-0.263 (0.054)	-43.4 (79.6)	1.3 134
C-14 (23)	-236.80 (-163.37)	0.002	-0.315 (0.014)	-119.7 (1.5)	1.3448 ^c
C-12 (21)	-236.46 (-163.64)	0.071	-0.300 (0.032)	-88.9 (39.5)	1.3338
C-5 (19)	-235.14 ^d (-162.08)	-0.036	-0.307 (0.024)	-113.4 (10.7)	1.3383
	-232.78 ^e (-160.20)		-0.305 (0.026)	-116.5 (7.6)	1.3386
C-13 (22)	-234.75 (-162.55)	-0.014	-0.320 (0.014)	-128.8 (4.0)	1.3458
DB[<i>a,h</i>]ACR-8,9-epoxyde					
C-13 (27)	-240.59 (-166.46)	0.137	-0.284 (0.049)	-58.6 (70.6)	1.3255
C-S (24)	-239.19 (-165.24)	0.069	-0.300 (0.030)	-86.4 (37.7)	1.3337
C-14 (28)	-238.14 (-164.10)	0.039	-0.305 (0.024)	-104.8 (18.9)	1.3379 ^c
C-6 (25)	-237.70 (-164.33)	-0.013	-0.305 (0.013)	-122.3 (4.0)	1.3354
C-12 (26)	-235.60 (-162.06)	-0.036	-0.307 (0.026)	-121.2 (6.9)	1.3395

^a Change in charge density for the indicated carbon atom in the nonfluorinated compound ($q_{C_{\text{carbocation}}} - q_{C_{\text{epoxyde}}}$).

^b Change in charge density between the open carbocation and the neutral closed epoxyde ($qF_{\text{carbocation}} - qF_{\text{epoxyde}}$).

^c The fluorine atom forms a hydrogen-bond interaction.

^d Non bay-region carbocation.

^e Bay-region carbocation.

ca. the same ΔE_r as the nonfluorinated structure. On the other hand, F-substitution at a position with negative charge density decreased the exothermicity of the opening reaction. A correlation was also noted between exothermicity and the C-F bond length, whereby the C-F bond becomes shorter with increasing stability of the carbocation. This observation corresponded to electron density loss at F, assessed by both NPA-derived charges and $\delta^{19}\text{F}$ NMR deshielding. So, fluorine stabilization of the aza-PAH carbocation correlated with the degree of fluoronium ion character, which can override the unfavorable inductive electron withdrawal of F. Fluorine substitution was previously seen to have a major impact on the charge distribution of protonated PAHs (61, 62) and PAH dications (60). The only exception in the observations made above was the 14-F compound (23), where a hydrogen bond interaction between the fluorine and the hydrogen atom attached to C-1 was stronger in the open carbocation (H/F distance is 2.1164 Å in the epoxide versus 2.1007 Å in the carbocation), thus favoring epoxide ring opening. A hydrogen bond between F and the hydrogen attached at C-4 determined that the 5-F-derivative (19) opened in the non bay-region sense upon O-protonation.

DFT study of the fluorinated DB[*a,h*]ACR-8,9-epoxides lead to the same conclusions regarding fluoronium ion character and stabilization at positively charged sites of the parent DB[*a,h*]ACR, and destabilization via inductive effect at positions bearing negative charge density.

In order to obtain some insight concerning the effect of fluorine on metabolic activation of fluorinated PAHs, isodesmic reactions (Figure 12) were calculated as a measure of the relative ease of formation of the fluorinated epoxides. Almost no energy differences were observed, consequently formation of these intermediates could be assumed not to be as relevant as carbocation formation in determining the relative reactivity of the ultimate metabolites.

The methyl substituent effect on reactivity was considered by computing the reaction energies for ring opening of the epoxides in selected methyl-analogues of DB[*a,h*]ACR (Figures 13 and 14). The 5-, 8-, 12- and 14-methyl-DB[*a,h*]ACR-1,2-epoxide, and 3-, 5-, 12-, and 14-methyl-DB[*a,h*]ACR-8,9-epoxide were selected by considering the biological activities of several derivatives (see 20 and references cited therein) (Table 6). DB[*a,h*]ACR analogues with an isopropyl group at C-14 were included for considering the influence of a bulky substituent at the bay region.

Although very similar values were obtained for each methylated DB[*a,h*]ACR-1,2-epoxide, and for the corresponding methylated DB[*a,h*]ACR-8,9-epoxides, respectively, the methylated analogues exhibited a more exothermic AE, than the corresponding parent molecules. According to NPA charges on the resulting carbocations, the methyl group did not participate in

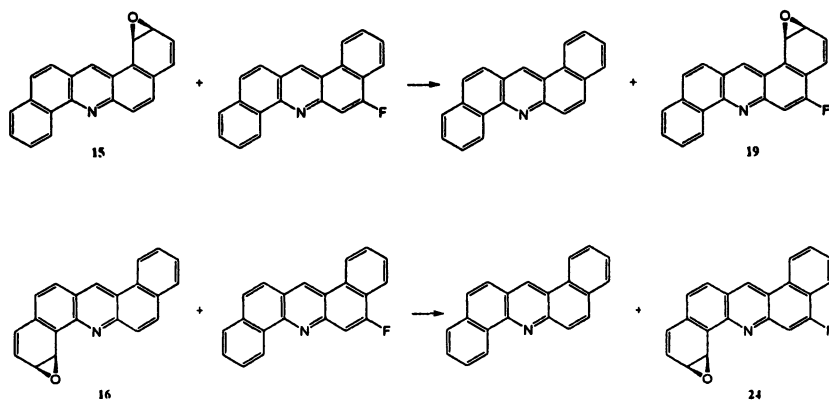


Figure 12. Isodesmic reactions for the formation of the fluorinated epoxides.
Figure adapted from reference 27.

hyperconjugation. At the same time, no important variations in the GIAO NMR chemical shifts for the methyl group were noticed. These observations indicated that the predominant stabilization mode for the carbocations was by inductive effect, contrary to the outcome for the fluorinated derivatives, whereby stronger fluoronium ion character produced larger variations in ΔE_r among the different analogues.

The 14-methyl compound yielded the most favorable ΔE_r for both series of epoxides (32, 36). In these cases, the neutral epoxides exhibited a deviation from planarity of the aromatic system at the bay region due to the steric strain induced by the methyl group. The enhanced carcinogenic activity brought about by methyl substitution at the bay region has been explained by a more favored opening of the epoxide ring (23). This fact stems from instability of the ring closed species, which presents a distorted non-planar structure (63), rather than from stabilization of the open carbocation by methyl substitution. Steric effects at the bay region developed by the isopropyl substituent produced the most exothermic opening reactions (Table 6). Thus, increased strain at the bay region was also evidenced by a progressive deviation of planarity of the aromatic system from unsubstituted DB[*a,h*]ACR epoxides to the 14-methyl and 14-isopropyl analogues.

Epoxide ring opening of 7-Me-B[*c*]ACR was more exothermic than for B[*c*]ACR, in accord with the relative reactivities reported in the literature (20).

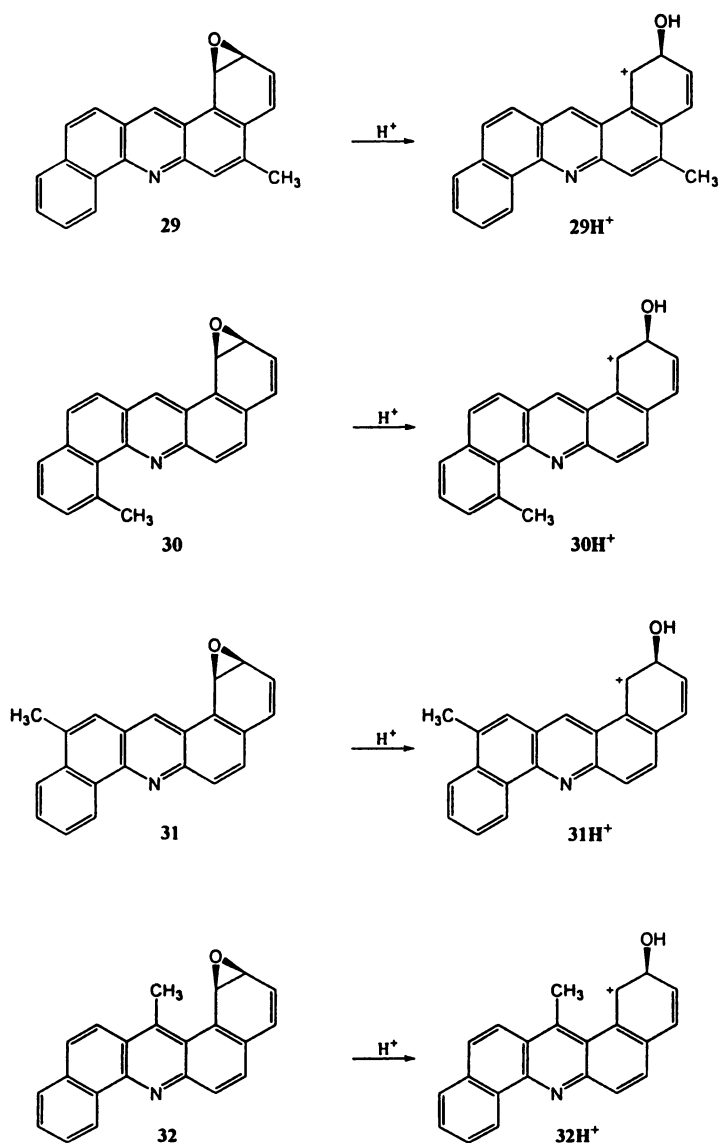


Figure 13. Epoxide ring opening reactions of the methylated derivatives of dibenzo[*a,h*]acridine-1,2-epoxide. Figure adapted from reference 27.

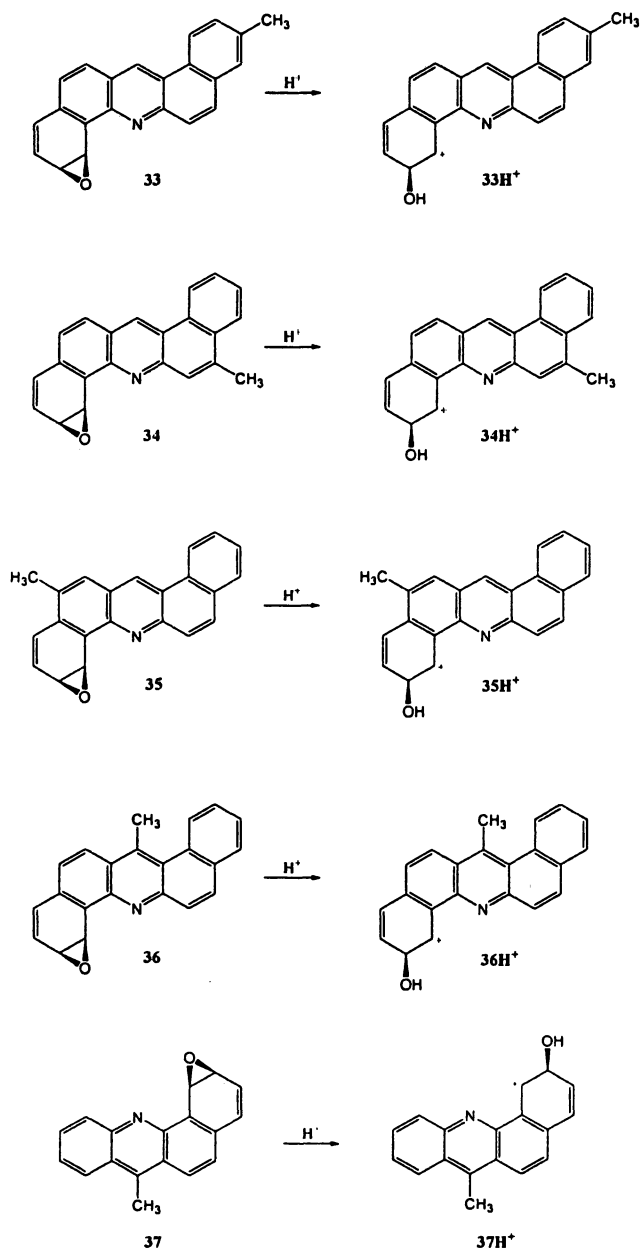


Figure 14. Epoxide ring opening reactions of the methylated derivatives of dibenzo[*a,h*]acridine-8,9-epoxide and benzo[*c*]acridine-1,2-epoxide. Figure adapted from reference 27.

Table VI. Calculations for Alkylated Derivatives of DB[*a,h*]ACR-1,2-Epoxyde, DB[*a,h*]ACR-8,9-Epoxyde, and B[*c*]ACR-1,2-Epoxyde

<i>Methylated Position (Compound)</i>	ΔE_r (kcal/mol) <i>Gas Phase (Aqueous Phase)</i>	q^a	qCH_3 (ΔqCH_3) ^b	<i>GIAO-NMR</i> $\delta^{13}C$ ($\Delta\delta^{13}C$) (ppm) ^c	<i>Biological Activity</i> ^d
DB[<i>a,h</i>]ACR-1,2-epoxyde					
C-14 (32)	-239.09 (-164.49)	0.002	0.067 (0.020)	12.3 (-1.6)	Moderately active
C-12 (31)	-238.61 (-164.15)	0.071	0.074 (0.038)	15.4 (1.3)	
C-5 (29)	-238.12 (-163.62)	-	0.079 (0.040)	12.5 (-2.2)	
C-8 (30)	-237.87 (-164.32)	0.009	0.068 (0.015)	22.1 (-0.6)	Moderately active ^e
C-14 ^f	-239.68 (-164.45)	0.002	0.073 (0.024) ^f	15.2 (-2.3) ^g	
DB[<i>a,h</i>]ACR-8,9-epoxyde					
C-14 (36)	-241.69 (-165.76)	0.039	0.073 (0.030)	14.1 (0.1)	Moderately active
C-5 (34)	-241.41 (-165.83)	0.069	0.074 (0.036)	15.5 (1.2)	
C-3 (33)	-240.90 (-165.60)	0.020	0.066 (0.028)	15.1 (0.1)	Inactive
C-12 (35)	-240.83 (-165.30)	-	0.076 (0.040)	12.4 (-1.9)	
C-14 ^f	-242.78 (-165.83)	0.039	0.082 (0.038)	19.3 (2.3)	
B[<i>c</i>]ACR-1,2-epoxyde					
C-7 (37)	-240.28 (-166.39)	0.055	0.080 (0.037)	7.4 (0.7)	Highly active

^a Change in charge density for the indicated carbon atom in the nonalkylated compound ($q_{C_{carbocation}} - q_{C_{epoxyde}}$).

^b Change in charge density between the open carbocation and the neutral closed epoxyde ($q_{CH_3_{carbocation}} - q_{CH_3_{epoxyde}}$).

^c Carbon atom of the methyl group.

^d Reference 20.

^e Ethyl substituent.

^f Isopropyl group as substituent.

^g Carbon atom of the methyl group with the highest $\Delta\delta$ (isopropyl substituent).

Aza-Benzo[a]pyrene Derivatives

Benzo[a]pyrene (BaP), one of the most highly investigated environmental contaminants, has potent carcinogenicity and mutagenicity (3, 64, 65). Its ultimate active metabolite is the bay-region DE (7,8-dihydrodiol-9,10-epoxide) (6, 66). In contrast, only a few studies have been carried out on the toxicity of azabenzo[a]pyrenes (aza-BaPs). In case of 10-azaBaP, an analogue with a nitrogen atom in the bay region, no bay-region DE could be formed. However, this compound has been reported to be carcinogenic (67), although less mutagenic *in vivo* than BaP (68). Its major metabolite is the 4,5-oxide (69).

In a effort to examine the influence of a nitrogen atom on the reactivity of this system, we performed computations at the B3LYP/6-31G* level on BaP bay-region epoxide (38) and DE (39). Comparisons were made with 4-azaBaP bay-region epoxide (40) and DE (41), and with the K-region 10-azaBaP-4,5-oxide (42) (Figure 15). In every case, epoxide protonation led to the formation of the open carbocations via barrierless processes, indicating that the oxonium ions were not minima on the respective potential energy surfaces. Charge delocalization patterns are shown in Figure 16. Changes in energy for reactions in Figure 15 are presented in Table 7, as well as some selected NPA charges for the carbocations.

According to the results in Table 7, the bay-region derivatives were the most reactive. Formation of the BaP carbocation was more exothermic than formation of the corresponding 4-aza-carbocation. On the other hand, opening of the O-protonated K-region epoxide was a less favored process. This trend in reactivity was in line with the development of negative charge density at the carbocation center, that is, with the degree of delocalization of the net positive charge through the aromatic system (Figure 16). The carbocation derived from the K-region epoxide presented relatively minor charge delocalization, as compared with the highly delocalized bay-region analogues. In this case, the charge density at the nitrogen atom and its change in charge density to the more positive values in going from the epoxide to the carbocation do not appear to be the determining factors for relative carbocation stabilities in the azaBaP systems, as can be seen by comparing the values for 40H^+ and 42H^+ . However, both epoxides are located at different positions of the carbon framework and generate different carbocations, therefore this type of comparison may not be justified. In contrast, the destabilizing influence of the development of positive charge density on nitrogen is evident in comparing 38H^+ with 40H^+ .

Further computational studies on the azaBaP system are currently in progress. We are also evaluating the protonation reactions on different positions of the rings in order to establish the most favored protonation site. The effect of methylation/protonation at nitrogen on epoxide reactivity is also being examined.

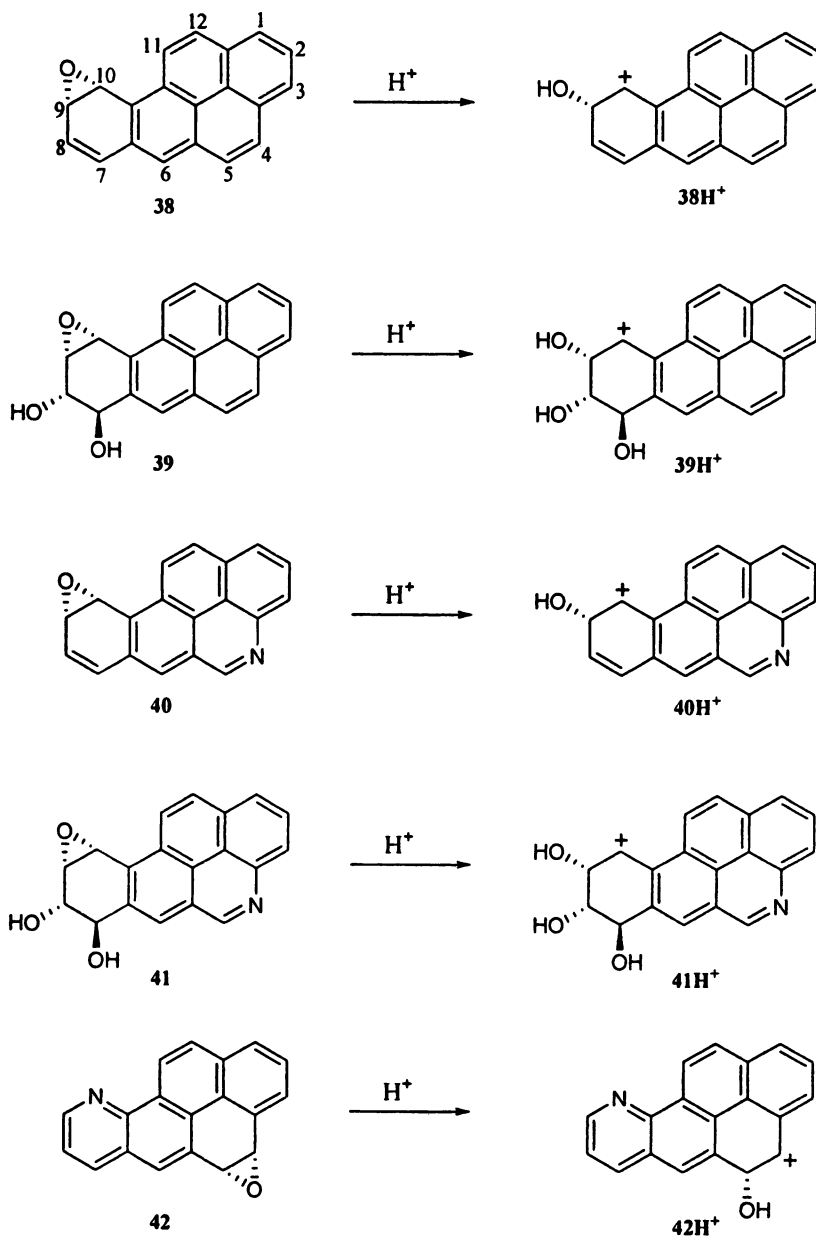


Figure 15. Epoxide ring opening reactions of epoxides and diol epoxides from benzo[a]pyrene, 4-azabenz[a]pyrene and 10-azabenz[a]pyrene.

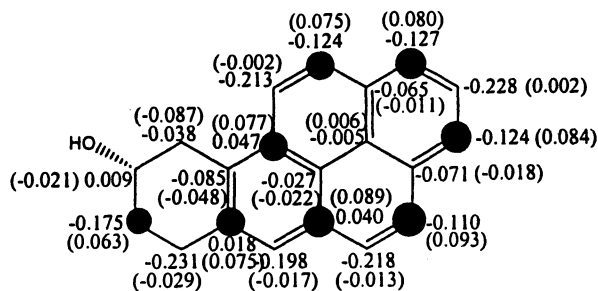
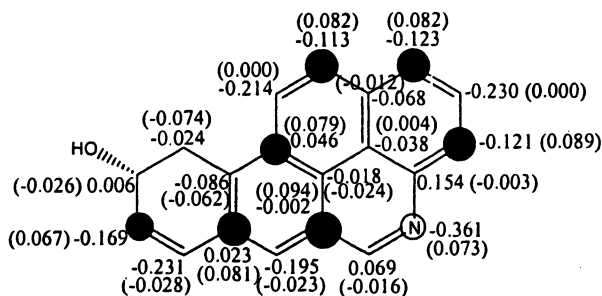
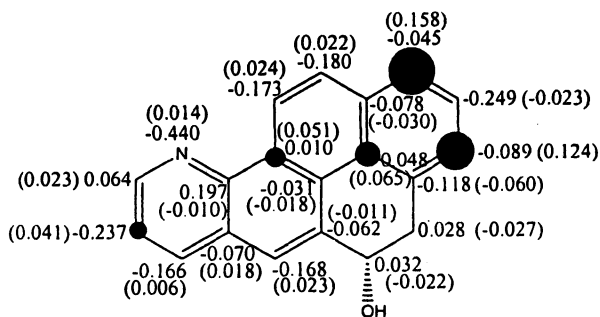
**38H⁺****40H⁺****42H⁺**

Figure 16. Computed NPA heavy atom charges (Δ charges related to the neutral compound in parentheses) for carbocations from BaP and azaBaP. [Dark circles are roughly proportional to the magnitude of C Δ charges, and white circles to N Δ charges; threshold was set to 0.030].

Table VII. Calculations for Reactions in Figure 15

<i>BaP</i> <i>Derivative</i>	ΔE_r (kcal/mol)		<i>Charge</i>	<i>Charge</i>	<i>GIAO-</i> <i>NMR</i> $\delta^{13}C^a$ (ppm)
	<i>Gas</i> <i>Phase</i>	<i>Aqueous</i> <i>Phase</i>	<i>Density at</i> <i>C^a</i> (ΔqC) ^b	<i>Density at N-</i> <i>τ^c</i> (ΔqN) ^d	
BaP-9,10- epoxide (38)	-243.91	-169.67	-0.038 (-0.087)	-	158.8
BaP-7,8-diol- 9,10-epoxide (39)	-241.03	-166.62	-0.063 (-0.117)	-	146.9
4-azaBaP- 9,10-epoxide (40)	-235.84	-163.19	-0.024 (-0.074)	-0.361 (0.073)	163.1
4-azaBaP- 7,8-diol-9,10- epoxide (41)	-232.31	-159.21	-0.045 (-0.098)	-0.356 (0.079)	150.7
10-azaBaP- 4,5-epoxide (42)	-229.07	-157.24	0.028 (-0.027)	-0.440 (0.014)	182.7

^a Carbocationic center.

^b Change in charge density between the open carbocation and the neutral closed epoxide ($qC_{\text{carbocation}} - qC_{\text{epoxide}}$).

^c Open carbocation.

^d Change in charge density between the open carbocation and the neutral closed epoxide ($qN_{\text{carbocation}} - qN_{\text{epoxide}}$).

Summary and Conclusions

According to these results, the calculated relative ease of formation, that is, the relative stabilities of the carbocations, were found to correlate with the available biological activities. The relative stability of the aza-PAH carbocations did not correlate with the extent of charge delocalization (measured by the decrease in positive charge density at the carbocation center) but rather with the magnitude of the negative charge at N. In this way, a larger negative charge on N accounted for a greater stability of the carbocation. Likewise, a larger increase in positive charge density at N as a result of formation of the open carbocation resulted in destabilization, and was a determining factor in the relative stability order. A similar observation could not be made for the azaBaP compounds because the studied structures formed carbocations at different positions of the fused-ring systems.

A fluorine atom at a highly positively charged site stabilized the carbocation. Therefore, fluorine stabilization of the aza-PAH carbocations correlated with the degree of fluoronium ion character, compensates the unfavorable inductive electron withdrawal of F. On the other hand, F-substitution at a position with negative charge density decreased the exothermicity of the opening reaction. A fluorine at the bay region formed hydrogen bond interactions that favored epoxide ring opening.

Methyl substitution effects were consistent with inductive stabilization of the carbocations. These effects produced minor variations in ΔE_r among the different derivatives as compared to fluorine substitution. Steric effects brought about by bay-region substitution led to the most exothermic ring opening reactions. Hence, the neutral epoxides exhibited deviation from planarity of the aromatic system due to steric strain induced by a methyl group at the bay region. Increased strain was evidenced by a progressive deviation of planarity of the aromatic framework in going from unsubstituted DB[*a,h*]ACR epoxides to the 14-methyl and 14-isopropyl analogues.

Acknowledgement

Support of our work under "Reactive Intermediates of Carcinogenesis of PAHs" by the NCI of NIH (2R15-CA078235-02A) is gratefully acknowledged. G.L.B thanks CONICET and the Secretaría de Ciencia y Tecnología de la Universidad Nacional de Córdoba (Secyt) for financial support.

References

1. *Polycyclic Aromatic Compounds, Part 1, Chemical Environmental and Experimental Data*; International Agency for Research on Cancer Monographs on the Evaluation of the Carcinogenic Risks to Humans 32; IARC: Lyon, France, 1983.
2. Hoffmann, D.; Wynder, E. L. In *Air Pollution*, 3rd ed.; Stern, A. C., Ed.; Academic Press: New York, 1977; Vol. 2, pp 361-455.
3. Harvey, R. G. *Polycyclic Aromatic Hydrocarbons, Chemistry and Carcinogenicity*; Cambridge University Press: Cambridge, UK, 1991.
4. Nordquist, M.; Thakker, D. R.; Yagi, H.; Lehr, R. E.; Wood, A. W.; Levin, W.; Conney, A. H.; Jerina, D. M. In *Molecular Basis of Environmental Toxicity*; Bhatnagar, R. S., Ed.; Ann Arbor Science Publishers: Ann Arbor, MI, 1980; pp 329-357.
5. Wood, A. W.; Chang, R. L.; Levin, W.; Ryan, D. E.; Thomas, P. E.; Croisy-Delcey, M.; Ittah, Y.; Yagi, H.; Jerina, D. M.; Conney, A. H. *Cancer Res.* **1980**, *40*, 2876-2883 and references therein.

6. Jerina, D. M.; Yagi, H.; Lehr, R. E.; Thakker, D. R.; Schafer-Ridder, M.; Karle, J. M.; Levin, W.; Wood, A. W.; Chang, R. L.; Conney, A. H. In *Polycyclic Hydrocarbons and Cancer*; Gelboin, H. V.; T'so, P. O. P., Eds.; Academic Press: New York, 1978; Vol. 1, pp 173-188.
7. Wood, A. W.; Levin, W.; Chang, R. L.; Yagi, H.; Thakker, D. R.; Lehr, R. E.; Jerina, D. M.; Conney, A. H. In *Polycyclic Aromatic Hydrocarbons*; Jones, P. W., Leber, P., Eds.; Ann Harbor Science Publishers, Inc.: Ann Harbor, MI, 1979; pp 531-55 1.
8. Harvey, R. G.; Geacintov, N. E. *Acc. Chem. Res.* **1988**, *21*, 66-73 and references therein.
9. Islam, N. B.; Whalen, D. L.; Yagi, H.; Jerina, D. M. *J. Am. Chem. Soc.* **1987**, *109*, 2108-2111.
10. Gupta, S. C.; Islam, N. B.; Whalen, D. L.; Yagi, H.; Jerina, D. M. *J. Org. Chem.* **1987**, *52*, 3812-3815.
11. Nashed, N. T.; Bax, A.; Loncharich, R. J.; Sayer, J. M.; Jerina, D. M. *J. Am. Chem. Soc.* **1993**, *115*, 1711-1722.
12. Nashed, N. T.; Balani, S. K.; Loncharich, R. J.; Sayer, J. M.; Shipley, D. Y.; Mohan, R. S.; Whalen, D. L.; Jerina, D. M. *J. Am. Chem. Soc.* **1991**, *113*, 3910.
13. Nashed, N. T.; Rao, T. V. S.; Jerina, D. M. *J. Org. Chem.* **1993**, *58*, 6344-6348.
14. Hecht, S. S.; Melikian, A. A.; Amin, S. In *Polycyclic Aromatic Hydrocarbon Carcinogenesis: Structure-Activity Relationships*; Yang, S. K.; Silverman B. D., Eds.; CRS Press: Boca Raton, FL, 1988; Vol 1, pp 95-128.
15. Hecht, S. S.; Amin, S.; Melikian, A. A.; LaVoie, E. J.; Hoffman, D. In *Polycyclic Hydrocarbons and Carcinogenesis*; Harvey, R. G., Ed.; ACS Symposium Series 283; American Chemical Society: Washington, DC, 1985; Ch. 2, pp 85-105.
16. *Biological Effects of Atmospheric Pollutants*; Committee on Biologic Effects of Atmospheric Pollutants, Particulate Polycyclic Organic Matter; National Academy of Sciences: Washington, DC, 1972.
17. Dong, M.; Locke, D. D.; Hoffmann, D. *Environ. Sci. Technol.*, **1997**, *11*, 612-618.
18. *Certain Polycyclic Aromatic Hydrocarbons and Heterocyclic Compounds*; International Agency for Research on Cancer Monographs on the Evaluation of the Carcinogenic Risks to Humans; LARC: Lyon, France, 1972; Vol. 3.
19. Dong, M.; Schmeltz, I.; LaVoie, E.J.; Hoffman, D. In *Carcinogenesis: Polynuclear Aromatic Hydrocarbons*; Jones, P. W.; Freudenthal, R. I., Eds.; Raven Press: New York, 1978; Vol. 2, pp 97-108.
20. Lehr, R. E.; Wood, A. W.; Levin, W.; Conney, A. H.; Jerina, D. M. In *Polycyclic Aromatic Hydrocarbon Carcinogenesis: Structure-Activity Relationships*; Yang, S. K.; Silverman, B. D., Eds.; CRC Press: Boca Raton, FL, 1988; L. 1, pp 31-58 and references therein.

21. Lang, R. L.; Wood, A. W.; Xie, J. G.; Huang, M. T.; Cui, X.; Kole, P. L.; Sikka, H. C.; Balani, S. K.; Jerina, D. M.; Kumar S.; Conney, A. H. *Proc. Am. Assoc. Cancer Res.* **1996**, *37*, 128.
22. Warshawsky, D. *J. Environ. Sci. Health* **1992**, *C10*, 1-71.
23. Borosky, G. L. *J. Org. Chem.* **1999**, *64*, 7738-7744.
24. Borosky, G. L. *Helv. Chim. Acta* **2001**, *84*, 3588-3599.
25. Borosky, G. L. *J. Comput. Chem.* **2003**, *24*, 601-608.
26. Borosky, G. L.; Laali, K. K. *Org. Biomol. Chem.* **2005**, *3*, 1180-1188.
27. Borosky, G. L.; Laali, K. K. *Chem. Res. Toxicol.* **2005**, *18*, 1876-1886.
28. Borosky, G. L.; Laali, K. K. *Chem. Res. Toxicol.* **2006**, *19*, 899-907.
29. Okazaki, T.; Laali, K. K.; Zajc, B.; Lakshman, M. K.; Kumar, S.; Baird, W. M.; Dashwood, W. -M. *Org. Biomol. Chem.* **2003**, *1*, 1509-1516.
30. Laali, K. K.; Okazaki, T.; Kumar, S.; Galembeck, S. F. *J. Org. Chem.* **2001**, *66*, 780-788.
31. Laali, K. K. In *Carbocation Chemistry*; Olah, G. A.; Prakash, G. K. S., Eds.; Wiley: 2004; Ch. 9.
32. Okazaki, T.; Laali, K. K. *Org. Biomol. Chem.* **2003**, *1*, 3078-3093.
33. Okazaki, T.; Laali, K. K. *J. Org. Chem.* **2004**, *69*, 510-516.
34. Gaussian 03, Revision B.05; Gaussian, Inc.: Wallingford, CT, 2003; Frisch, M. J.; Trucks, G. W.; Schlegel, H. B.; Scuseria, G. E.; Robb, M. A.; Cheeseman, J. R.; Montgomery, Jr., J. A.; Vreven, T.; Kudin, K. N.; Burant, J. C.; Millam, J. M.; Iyengar, S. S.; Tomasi, J.; Barone, V.; Mennucci, B.; Cossi, M.; Scalmani, G.; Rega, N.; Petersson, G. A.; Nakatsuji, H.; Hada, M.; Ehara, M.; Toyota, K.; Fukuda, R.; Hasegawa, J.; Ishida, M.; Nakajima, T.; Honda, Y.; Kitao, O.; Nakai, H.; Klene, M.; Li, X.; Knox, J. E.; Hratchian, H. P.; Cross, J. B.; Bakken, V.; Adamo, C.; Jaramillo, J.; Gomperts, R.; Stratmann, R. E.; Yazyev, O.; Austin, A. J.; Cammi, R.; Pomelli, C.; Ochterski, J. W.; Ayala, P. Y.; Morokuma, K.; Voth, G. A.; Salvador, P.; Dannenberg, J. J.; Zakrzewski, V. G.; Dapprich, S.; Daniels, A. D.; Strain, M. C.; Farkas, O.; Malick, D. K.; Rabuck, A. D.; Raghavachari, K.; Foresman, J. B.; Ortiz, J. V.; Cui, Q.; Baboul, A. G.; Clifford, S.; Cioslowski, J.; Stefanov, B. B.; Liu, G.; Liashenko, A.; Piskorz, P.; Komaromi, I.; Martin, R. L.; Fox, D. J.; Keith, T.; Al-Laham, M. A.; Peng, C. Y.; Nanayakkara, A.; Challacombe, M.; Gill, P. M. W.; Johnson, B.; Chen, W.; Wong, M. W.; Gonzalez, C.; Pople, J. A.
35. Becke, A. D. *J. Chem. Phys.* **1993**, *98*, 5648-5652.
36. Lee, C.; Yang, W.; Parr, R. G. *Physical Review B* **1998**, *37*, 785-789.
37. Miehlich, B.; Savin, A.; Stoll, H.; Preuss, H. *Chem. Phys. Lett.* **1989**, *157*, 200-206.
38. NBO Version 3.1; Glendening, E. D.; Reed, A. E.; Carpenter, J. E.; Weinhold, F.
39. Cancès, M. T.; Mennucci, B.; Tomasi, J. *J. Chem. Phys.* **1997**, *107*, 3032-3041.

40. Mennucci, B.; Tomasi, J. *J. Chem. Phys.* **1997**, *106*, 5151-5158.
41. Mennucci, B.; Cancès, E.; Tomasi, J. *J. Phys. Chem. B* **1997**, *101*, 10506-10517.
42. Tomasi, J.; Mennucci, B.; Cancès, E. *J. Mol. Struct. (Theochem)* **1999**, *464*, 211-226.
43. Schleyer, P. v. R.; Maerker, C.; Dransfeld, A.; Jiao, H.; Hommes, N. J. v. E. *J. Am. Chem. Soc.* **1996**, *118*, 6317-6318.
44. Wolinski, K.; Hinton, J. F.; Pulay, P. *J. Am. Chem. Soc.* **1990**, *112*, 8251-8260.
45. Dewar, M. J. S.; Zoebisch, E. G.; Healy, E. F.; Stewart, J. J. P. *J. Am. Chem. Soc.* **1985**, *107*, 3902-3909.
46. Kumar, S.; Sikka, H. C.; Dubey, S. K.; Czech, A.; Geddie, N.; Wang, C. – X.; LaVoie, E. J. *Cancer Res.* **1989**, *49*, 20-24.
47. Lehr, R. E.; Jerina, D. M. *Tetrahedron Lett.* **1983**, *24*, 27-30.
48. Jerina, D. M.; Chadha, A.; Cheh, A. M.; Schurdak, M. E.; Wood, A. W.; Sayer, J. M. In *Biological Reactive Intermediates IV Molecular and Cellular Effects and Their Impact on Human Health*; Witmer, C. M.; Snyder, R.; Jollow, D. J.; Kalf, G. F.; Kocsis, J. J.; Sipes, I. G., Eds.; Plenum Press: New York, 1991.
49. Dipple, A. In *DNA Adducts: Identification and Biological Significance*; Hemminki, K.; Dipple, A.; Shuker, D. E. G.; Kadlubar, F. F.; Segerbaeck, D.; Bartsch, H., Eds.; IARC Publications: Lyon, France, 1994.
50. Cavalieri, E. L.; Rogan, E. G. In *The Handbook of Environmental Chemistry: PAHs and Related Compounds*; Neilson, A. H., Ed.; Springer: Heidelberg, Germany, 1998; Vol. 3J, pp 81-117.
51. Agarwal, S. K.; Sayer, J. M.; Yeh, H. J. C.; Pannell, L. K.; Hilton, B. D.; Pigott, M. A.; Dipple, A.; Yagi, H.; Jerina, D. M. *J. Am. Chem. Soc.* **1987**, *109*, 2497-2504 and references therein.
52. Dipple, A.; Moschel, R. C.; and Bigger, A. H. (1984) In *Chemical Carcinogens* (Searle, C. E., Ed.) 2nd ed., pp 43-163, American Chemical Society, Washington, DC.
53. Wood, A. W.; Chang, R. L.; Katz, M.; Conney, A. H.; Jerina, D. M.; Sikka, H. C.; Levin, W.; Kumar, S. *Cancer Res.* **1989**, *49*, 6981-6984.
54. Kumar, S.; Chang, R. L.; Wood, A. W.; Xie, J. G.; Huang, M. T.; Cui, X. X.; Kole, P. L.; Sikka, H. C.; Balani, S. K.; Conney, A. H.; Jerina, D. M. *Carcinogenesis* **2001**, *22*, 951-955.
55. Chang, R. L.; Levin, W.; Conney, A. H.; Boyd, D. R.; Balani, S. K.; Yagi, H.; Jerina, D. M.; Wood, A. W. *Proc. Am. Assoc. Cancer Res.* **1989**, *30*, 144.
56. Chang, R. L.; Levin, W.; Wood, A. W.; Shirai, N.; Ryan, A. J.; Duke, C. C.; Jerina, D. M.; Holder, G. M.; Conney, A. H. *Cancer Res.* **1986**, *46*, 4552-4555.

57. Xue, W.; Warshawsky, D. *Toxicol. Appl. Pharmacol.* **2005**, *206*, 73-93.
58. Ye, Y.; Scharping, C. E.; Holder, G. M. *Carcinogenesis* **1995**, *16*, 787-793.
59. Lowe, J. P.; Silverman, B. D. *Cancer Biochem. Biophys.* **1983**, *7*, 53-60.
60. Sawyer, J. M.; Lehr, R. E.; Kumar, S.; Yagi, H.; Yeh, H. J. C.; Holder, G. M.; Duke, C.C.; Silverton, J. V.; Gibson, G.; Jerina, D. M. *J. Am. Chem. Soc.* **1990**, *112*, 1177-1185.
61. Laali, K. K.; Hansen, P. F. *J. Org. Chem.* **1993**, *58*, 4096-4104.
62. Laali, K. K.; Tanaka, M.; Hansen, P. F. *J. Org. Chem.* **1998**, *63*, 8217-8223.
63. Afshar, C. E.; Katz, A. K.; Carrell, H. L.; Amin, S.; Desai, D.; Glusker, J. P. *Carcinogenesis* **1999**, *20*, 1549-1553.
64. Hakura, A.; Tsutsui, Y.; Sonoda, J.; Kai, J.; Imade, T.; Shimada, M.; Sugihara, Y.; Mikami, T. *Mutat. Res.* **1998**, *398*, 123-130.
65. Hakura, A.; Tsutsui, Y.; Sonoda, J.; Tsukidate, K.; Mikami, T.; Sagami, F. *Mutat. Res.* **2000**, *447*, 239-247.
66. Conney, A. H. *Cancer Res.* **1982**, *42*, 4875-4917.
67. Lacassagne, A.; Buu-Hoi, N. P.; Zajdela, F.; Mabile, P. *Compt. Rend.* **1964**, *258*, 3387-3389.
68. Yamada, K.; Suzuki, T.; Kohara, A.; Hayashi, M.; Hakura, A.; Mizutani, T.; Saeki, K. *Mutat. Res.* **2002**, *521*, 187-200 and references therein.
69. Okuda, H.; Shudo, K.; Okamoto, T. *Chem. Pharm. Bull.* **1983**, *31*, 2924-2927 and references therein.

Chapter 17

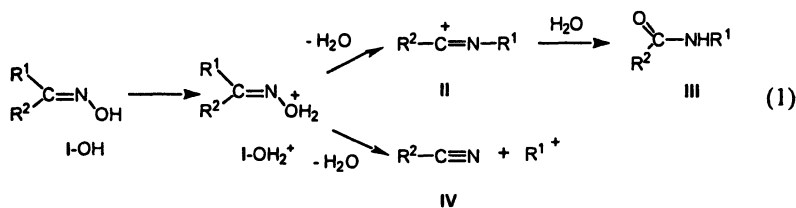
How Does Carbocation Stability Control the Beckmann Rearrangement Reaction?

Salai C. Ammal and Hiroshi Yamataka*

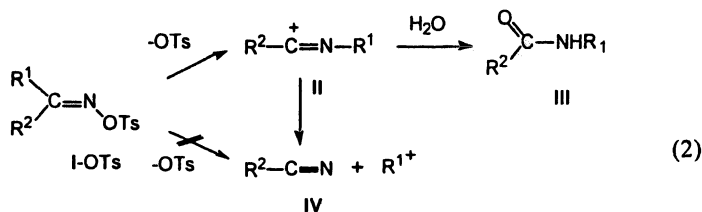
Department of Chemistry, Rikkyo University, Nishi-Ikebukuro,
Toshima-ku, Tokyo 171-8501, Japan

Computational study on borderline Beckmann rearrangement-fragmentation reactions revealed that there is a single transition state either for the rearrangement or the fragmentation pathway, and that the reaction path changes from rearrangement to fragmentation when an electron-donating substituent is introduced to the R¹ group, anti to the leaving group. The overall reactivity nicely follows the Hammett equation, however since the reaction pathway and the product are not the same for all substituted substrates, caution should be exercised in the interpretation of Hammett relationships.

The conversion of oximes into amides, known as the Beckmann rearrangement, is a classical and widely popular reaction in organic chemistry, and its mechanism has been extensively studied for many years (1,2). The reaction involves an initial protonation of an oxime (I-OH) to an oxonium ion (I-OH₂⁺), followed by migration of the group (R¹) anti to the leaving group, and the departure of water molecule giving a nitrilium cation (II), which upon hydrolysis yields the final amide product (III) (eq 1). This Beckmann rearrangement process (I-OH₂⁺ → II) is known to proceed via a concerted mechanism with a higher reactivity for a more electron-donating R¹ group (3,4). Certain oximes, in particular those having an R¹ group that may yield a stable carbocation, are likely to undergo fragmentation to form nitrites (IV, eq 1) instead of amides (1a-d,5). Despite numerous experimental and computational results reported on the reactions of oximes, the mechanistic aspects of these reactions, in particular those dealing with factors that control the product selectivity, remain poorly understood.



Experimental studies have shown that rearrangement of oxime tosylate (I-OTs) in 80% ethanol gave a mixture of the amide and nitrite products and that the product ratio varies depending on R^1 and R^2 (1a). For a series of R^1 , the ratio (%) of fragmentation was reported to be *i*-Pr (0), *t*-Bu (10), and CHPh_2 (80). On the other hand, the overall reactivity varied in the order (relative reactivity). Me (1) < CHPh_2 (40) < Et (60) < Ph (100) < *i*-Pr (810) < *t*-Bu (870). Thus, the ratio of fragmentation to amide formation was not related to the overall reaction rate, but increased with the stability of R^{1+} . These results led the authors to conclude that the reaction of I-OTs gave two types of products via a common intermediate II, rather than via discrete and competitive pathways leading directly to II and IV (eq 2). In the present study, we have carried out ab initio MO calculations on

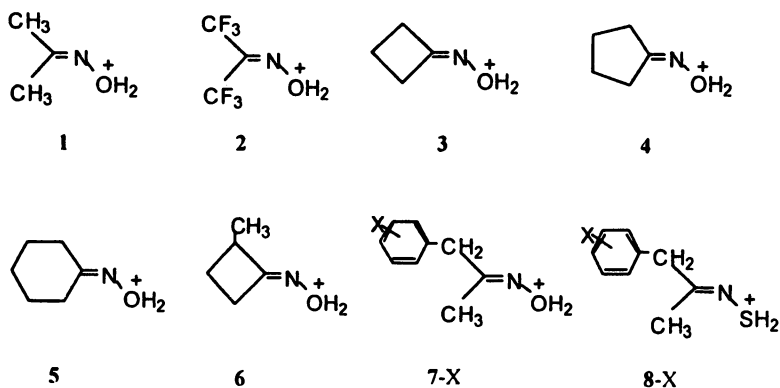


the reactions of a series of ketoximes to address two important mechanistic issues; (a) to understand the factors that control the relative importance of rearrangement and fragmentation routes, and (b) to shed light on how product switching occurs in rearrangement-fragmentation in the case of borderline systems.

Computational Methods

Ab initio calculations were carried out at the HF, B3LYP, and MP2 levels of theory employing different basis sets (6-31G*, 6-31+G*, 6-311+G**) by using the Gaussian98 program (6). Compounds examined are listed in Chart 1. All structures were fully optimized and were verified by means of their Hessian

matrices to be local minima or saddle points. Thermochemical quantities such as entropy, enthalpy and free energy were calculated from harmonic frequencies. Transition states (TSs) were confirmed by the mode of the imaginary frequency and by intrinsic reaction coordinate (IRC) calculations (7).



Results and Discussion

Simple Alkyl Systems

As the first set of calculations, the reactions of five acyclic and cyclic protonated oximes (1 ~ 5) were examined, and the activation barriers calculated at different levels of theory are listed in Table 1. The calculated barrier height depends on the calculation method, but the basic reaction mechanism is the same for the compounds listed in Table 1. In all cases, except $(\text{CF}_3)_2\text{C}=\text{N}-\text{OH}_2^+$ (2), the barriers are rather low, reflecting the extremely high leaving ability of H_2O . As has been reported in the literature (2), all substrates examined gave the corresponding Beckmann rearrangement product via a single reaction pathway upon $\text{N}-\text{OH}_2$ cleavage. The IRC snapshots for the reaction of protonated cyclobutanone oxime (3) are illustrated as an example in Figure 1, which clearly demonstrate that the Beckmann rearrangement takes place in a concerted fashion. The contour energy map for the reaction of protonated acetone oxime (1) in Figure 2 also indicates that there is only one TS for the rearrangement on the potential energy surface. There is no alternative reaction pathway of the $\text{N}-\text{OH}_2$ ionization for these substrates. The results are reasonable since the fragmentation reactions should yield highly unstable primary carbocations.

If a Me group is introduced at the α position, the carbocation that would form via fragmentation will be stabilized, and therefore the fragmentation pathway might be possible. Indeed, protonated 1-methylcyclobutanone oxime (**6**) was found to give the ring-opened fragmentation species as a sole product as shown by its IRC snapshots (Figure 3). Although the computational level is low, the results clearly show that the reaction mechanism changes depending on the substrate structure (i.e. as function of stability of the hypothetical carbocation intermediate that would be formed via the fragmentation pathway).

Aromatic systems

To study more systematically the effect of the substrate electronic structure on the reaction pathway, the reactions of aromatic substrates, p -XC₆H₄CH₂C(CH₃)=NOH₂⁺ (**7-X**) and p -XC₆H₄CH₂C(CH₃)=NSH₂⁺ (**8-X**) were computationally examined by HF/6-31G* and MP2/6-31G*.

The results are summarized in Table 2 and in Figures 4 and 5. The data in Table 2 show that although the barrier height depends on the leaving group (**7** and **8**) the two reaction systems exhibit a common feature; an electron-donating substituent lowers the barrier height, as expected for both rearrangement and fragmentation processes. The calculated small activation energies for **7** indicate that the protonated ketoximes are very reactive species, due to the extremely high leaving ability of water. The calculated activation enthalpies are smaller than the corresponding activation electronic energies for both systems, reflecting smaller zero-point energies for the TSs than for the protonated ketoximes. The smaller activation enthalpies for **7** and even negative one for the p -MeO derivative may suggest that the protonation and the N-O bond cleavage may occur essentially in a concerted manner on the enthalpy surface for **7**. However, since the structures of the protonated ketoximes do not change much with the substituent as described below, the substituent effects for the reactions considered here with the protonated ketoximes as starting materials should reflect the substituent effects for the overall Beckmann rearrangement-fragmentation reactions.

Relative activation enthalpies (ΔH^\ddagger) in Table 2 were converted to $\log(k_X/k_H)$ at 298 K, and were plotted against Hammett σ constants. Here, we used enthalpies, because the size of the entropy and hence the free energy depend much on low frequencies, which are less reliable than higher frequencies, especially for compounds with weak interactions such as TS (**8**). The use of free energy (ΔG^\ddagger) gave similar correlations with more scattered points. As for the Hammett σ constant, we used dual-parameter σ constants in the form of the Yukawa-Tsuno equation (LArSR equation) (**9**) as defined in eq 3. Here, the apparent σ constant (σ_{app}) has a variable resonance contribution parameter (r), which varies depending on the nature of the reaction examined; for t -cumyl

Table 1. Activation Barriers for the Reaction of Protonated Oximes Calculated at Different Levels of Theory.

<i>No</i>	<i>R</i> ¹	<i>R</i> ²	<i>method</i>	ΔE^\ddagger	(ΔH^\ddagger)	$[\Delta G^\ddagger]$
1	CH ₃	CH ₃	B3LYP/6-31G*	11.5	(9.2)	[7.3]
2	CF ₃	CF ₃	B3LYP/6-31G*	18.9	(17.0)	[12.6]
3		(CH ₂) ₃	B3LYP/6-31G*	5.9	(4.5)	[2.6]
			MP2/6-31G*	4.8	(3.2)	[2.4]
4		(CH ₂) ₄	B3LYP/6-31G*	7.7	(5.9)	[3.8]
5		(CH ₂) ₅	B3LYP/6-31G*	5.8	(3.7)	[1.9]

Energies are in kcal mol⁻¹.

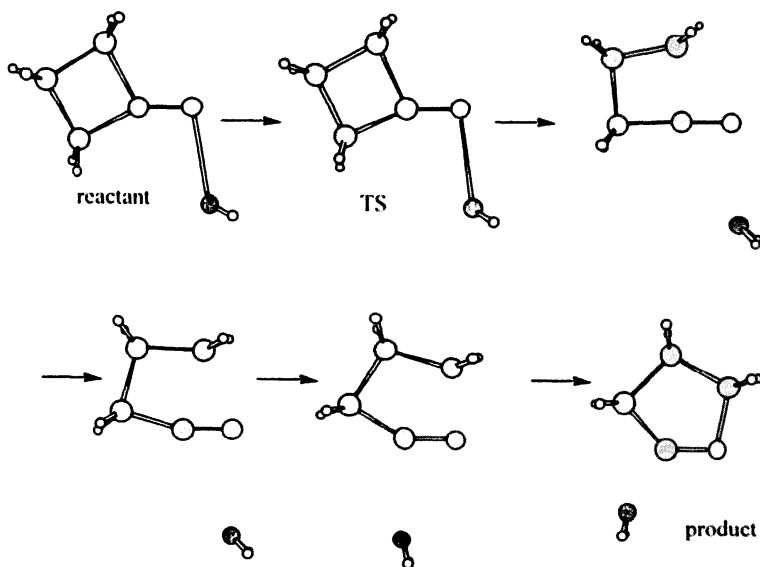


Figure 1. IRC snapshots for the reaction of protonated cyclobutanone oxime (3) calculated at the HF/6-31G level.*

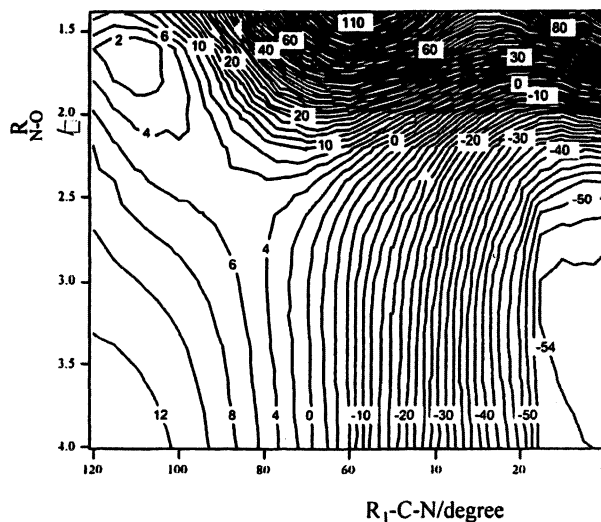


Figure 2. The contour energy map for the reaction of protonated acetone oxime (1) calculated by HF/6-31G*. Numbers on contour lines are relative energies with respect to TS in kcal mol⁻¹.

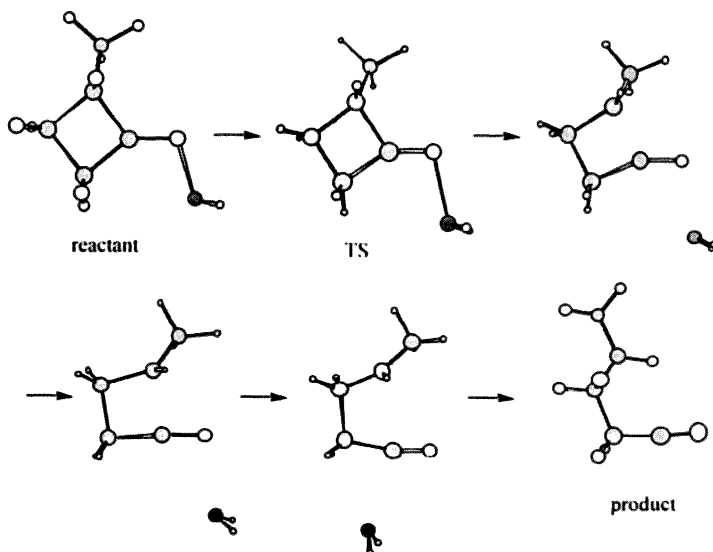


Figure 3. IRC snapshots for the reaction of protonated 1-methylcyclobutanone oxime (6) calculated at the HF/6-31G* level.

Table 2. Activation energies for the reaction of protonated benzyl methyl ketoximes and their sulfur analogous systems calculated by MP2/6-31G*.

substituent	7	8
	ΔE^\ddagger (ΔH^\ddagger) [ΔG^\ddagger]	ΔE^\ddagger (ΔH^\ddagger) [ΔG^\ddagger]
<i>p</i> -MeO	1.4(-0.1) [0.0]	16.9 (13.6) [12.0]
<i>p</i> -Me	2.0 (0.2) [0.3]	---
H	2.5 (0.7) [0.6]	20.4 (17.8) [16.5]
<i>p</i> -CN	3.7 (1.6) [1.8]	23.1 (19.5) [17.2]
<i>p</i> -NO ₂	4.0 (2.1) [1.7]	23.8 (20.2) [17.7]

Energies are in kcal mol⁻¹.

chloride solvolysis, $r = 1.0$ and σ_{app} becomes σ^+ , and for benzoate ester hydrolysis, $r = 0.27$ and then σ_{app} becomes the original Hammett σ .

$$\log(k_X/k_H) = \rho[\sigma^\circ + r(\sigma^+ - \sigma)] = \rho[\sigma + r\Delta\bar{\sigma}_R^+] = \rho\sigma_{\text{app}} \quad (3)$$

The Hammett plots in Figure 4 revealed that the reactivities correlate nicely with the σ_{app} constants, with $r = 0.6$ for the reaction of 7 and $r = 1.0$ for the reaction of 8. The results indicate that certain amount of positive charge is developed on the benzylic carbon of R¹ at the TS for both reactions. The larger r and ρ values for 8 reflect more cationic nature of R¹ at the TSs for 8-X due to their higher barriers and later TSs (10) than for the reactions of 7-X. The linear Hammett plots suggest that the reaction mechanism does not change as a function of the substituent in both reactions.

In Figure 5 are illustrated reactant structures of three selected substituted compounds (7-X) and their corresponding TS structures. It appears in Figure 5 that the reactant structure does not change much with the substituent, whereas the TS structure varies quite smoothly with substituent, being more reactant-like with a more electron-donating substituent. Such a variation in the TS structure is consistent with the Hammond postulate (10), and is commonly observed in computational organic chemistry. The same trend was also found for 8-X. Therefore, both the relative reactivities and the TS structures appear to indicate that the reaction is mechanistically well-behaved, with a single reaction pathway giving a single product.

The nature of the reaction pathway can be unequivocally examined by IRC calculations from each individual TS. Structural variations along IRC at the MP2/6-31G* level are illustrated for five different para-substituted substrates (7-X: X = MeO, Me, H, CN, NO₂) in Figure 6, where the horizontal axis is the

reaction coordinate (RC) in $\text{amu}^{1/2}$ Bohr and the vertical axis is the distance between the benzylic carbon and the nitrogen ($R_{\text{C-N}}$), and only the IRC traces toward the product state are shown. It can be seen that the IRC for all reactions, except for that of *p*-MeO-substituted compound, reached the product state via a short C-N distance, namely the Beckman rearrangement product. On the other hand, the reaction pathway along the IRC for 7-MeO reached the product with a long C-N distance, therefore through the fragmentation mechanism. It is clear in Figure 6 that, as in the case of TS structure, the IRC pathway varies smoothly and continuously with the substituent, from clear fragmentation (*p*-MeO) through borderline fragmentation-rearrangement (*p*-Me and H) to rearrangement (*p*-NO₂ and *p*-CN), whereas the product must be either one of the two, even for the borderline cases. As a result, despite the fact that the nature of the TS in

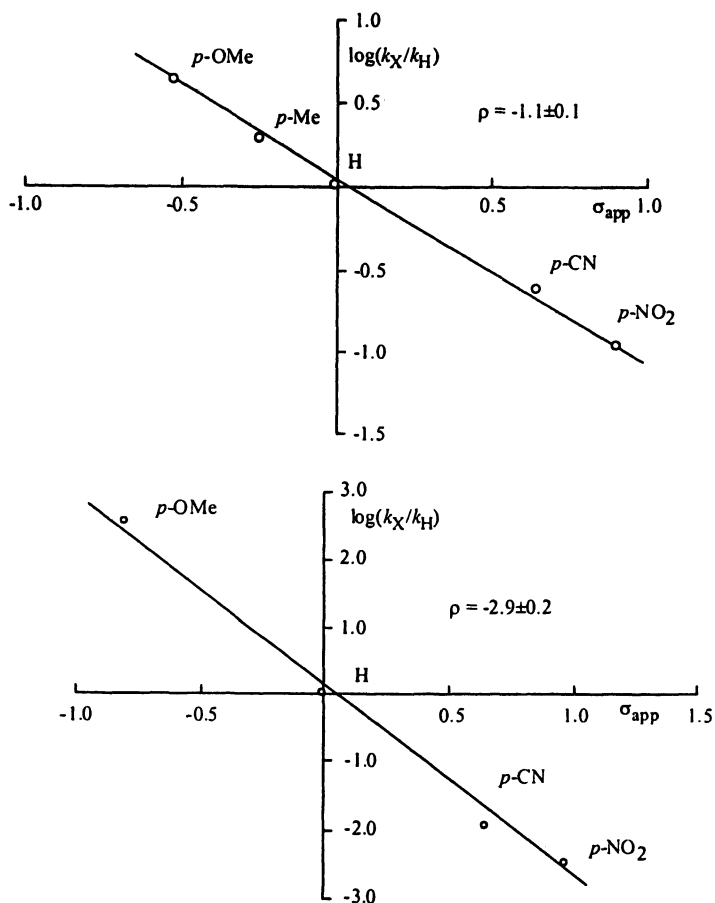


Figure 4. Hammett plots for the reactions of 7 (top) and 8 (bottom). Relative reactivities at 298 K were calculated with the MP2/6-31G* enthalpies.

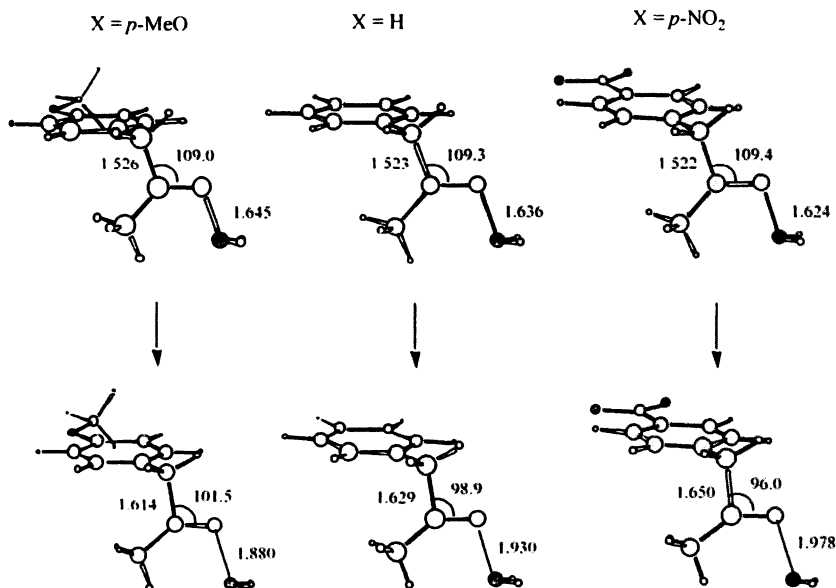


Figure 5. Calculated structures of the reactants (top) and TS (bottom) for 7-X, X = p-MeO, H, and p-NO₂. Distances are in Å amid angles are in degree.

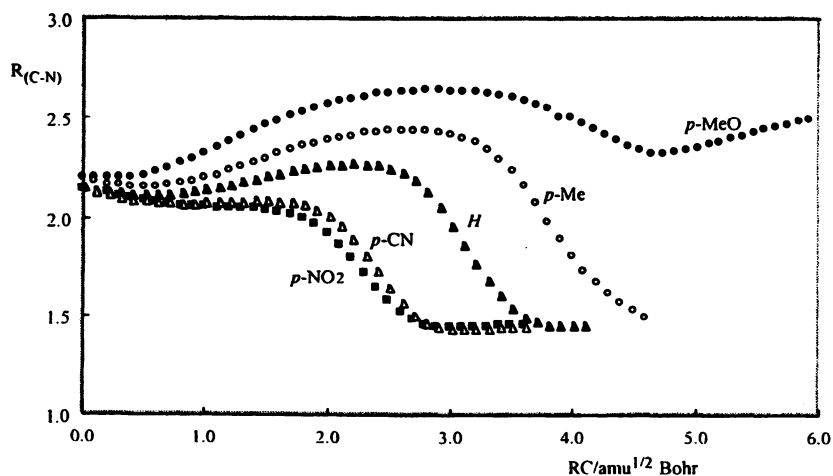


Figure 6. Variations of the atomic distance between the benzylic carbon and nitrogen along IRC for 7-X (X = p-MeO, p-Me, H, p-CN, amid p-NO₂) calculated at MP2/6-3G*.

terms of energy and structure and the IRC pathway vary smoothly with substituent, the reaction product and hence the reaction mechanism exhibit a sharp change as a function of the substituent.

The present findings suggest that mechanistic and reaction product variations are not necessarily accompanied by a clear difference in reactivity and the TS structure, and hence experimentally observable quantities, such as relative reactivities (Hammett equation) and kinetic isotope effects (KIEs), which are commonly considered to be useful means to detect a change in reaction mechanism (11,12), may not always be useful.

It is interesting to point out that for the several reaction systems, including 7-X (13), the two types of products (rearrangement and fragmentation) have been observed for a single reaction (1a). If only a single TS exists for the N-O ionization process as described here, the formation of both rearrangement and fragmentation products should arise from a common intermediate (1a) or via a common TS and path bifurcation (14,15). Studied along this line are under way.

In conclusion, the present computational analysis on the borderline Beckmann rearrangement-fragmentation reactions revealed several mechanistic points; (a) there is a single TS either for the rearrangement or fragmentation routes, and rearrangement/fragmentation product switching occurs as a function of the substituent. The introduction of Me into the cyclobutanone system (3 vs 6) or introduction of a more electron-donating substituent into the Ph ring of aromatic systems (7 and 8) switches the rearrangement route to fragmentation, (b) the overall reactivity increases with a more electron-donating substituent on the Ph ring of 7 or 8 in such a manner that the relative reactivity follows nicely the extended (Yukawa-Tsuno) Hammett equation, (c) the structure of the TS for 7-X and 8-X varies with X in a manner consistent with the Hammond postulate, and (d) the reaction mechanism for 7-X is different for X = *p*-NO₂, *p*-CN, H, and *p*-Me and for X = *p*-MeO. However, despite the findings described here under points (b) and (c) above, measurements of substituent effects and KIEs should be interpreted with care since these experimental means may not always reflect the reaction mechanism.

Acknowledgments: The study was supported by a Grant-in-Aid for Scientific Research from the Ministry of Education, Science, Sports, Culture and Technology, Japan, and by Rikkyo University Frontier Project "Life's Adaptation Strategies to Environmental Changes". SCA thanks CREST project operated by the Japan Science and Technology Agency (JST). The authors thank N. Yoshimura for his assistance.

References and Notes

1. (a) Grob, C. A.; Fischer, H. P.; Raudenbusch, W.; Zergenyi, J. *Helv. Chim. Acta* **1964**, *47*, 1003-1021. (b) Grob, C. A.; Ide, J. *Helv. Chim. Acta* **1974**, *57*, 2562-

2571. (c) Grob, C. A.; Ide, J. *Helv. Chim. Acta* **1974**, *57*, 2571-2583. (d) Huitric, A. C.; Nelson, S. D. Jr. *J. Org. Chem.* **1969**, *34*, 1230-1233. (e) Hudrlik, P. F.; Waugh, M. A.; Hudrlik, A. M. *J. Organomet. Chem.* **1984**, *271*, 69-76. (f) Huisgen, R.; Ugi, I.; Assemi, M. T.; Witten, J. *Ann.* **1957**, *602*, 127-135.
- Raspoet, G.; Nguyen, M. T.; Vanquickenborne, L. G. *Bull. Soc. Chim. Belg.* **1997**, *106*, 691-697. Nguyen, M. T.; Raspoet, G.; Vanquickenborne, L. G. *J. Am. Chem. Soc.* **1997**, *119*, 2552-2562. Yamaguchi, Y.; Yasutake, N.; Nagaoka, M. *J. Mol. Struct. (Theochem)* **2003**, *639*, 137-150. Yamabe, S.; Tsuchida, N.; Yamazaki, S. *J. Org. Chem.* **2005**, *70*, 10638-10644.
 - Chapman, A. W.; Fidler, F. A. *J. Chem. Soc.* **1936**, 448-453. Pearson, D. E.; Ball, F. *J. Org. Chem.* **1949**, *14*, 118-131. Gregory, B. J.; Moodie, R. B.; Schofield, K. *J. Chem. Soc. (B)* **1970**, 33 8-346.
 - Kim, S.-G.; Ando, T.; Yukawa, Y. *Bull. Chem. Soc. Jpn.* **1979**, *52*, 1115-1120.
 - Fischer, H. P.; Grob, C. A.; Renk, E. *Helv. Chim. Acta* **1962**, *45*, 2539-2553. Hassner, A.; Nash, E. G. *Tetrahedron Lett.* **1965**, 525-529.
 - Frisch, M. J.; Trucks, G. W.; Schlegel, H. B.; Scuseria, G. E.; Robb, M. A.; Cheeseman, J. R.; Zakrzewski, V. G.; Montgomery, J. A.; Stratmann, R. E.; Burant, J. C.; Dapprich, S.; Millam, J. M.; Daniels, A. D.; Kudin, K. N.; Strain, M. C.; Farkas, O.; Tomasi, J.; Barone, V.; Cossi, M.; Cammi, R.; Mennucci, B.; Pomelli, C.; Adamo, C.; Clifford, S.; Ochterski, J.; Petersson, G. A.; Ayala, P. Y.; Cui, Q.; Morokuma, K.; Malick, D. K.; Rabuck, A. D.; Raghavachari, K.; Foresman, J. B.; Cioslowski, J.; Ortiz, J. V.; Stefanov, B. B.; Liu, G.; Liashenko, A.; Piskorz, P.; Komaromi, I.; Gomperts, R.; Martin, R. L.; Fox, D. J.; Keith, T.; Al-Laham, M. A.; Peng, C. Y.; Nanayakkara, A.; Gonzalez, C.; Challacombe, M.; Gill, P. M. W.; Johnson, B. G.; Chen, W.; Wong, M. W.; Andres, L.; Head-Gordon, M.; Replogle, E. S.; Pople, J. A. GAUSSIAN 98, Revision A.9: Gaussian Inc., Pittsburgh, PA, **1998**.
 - Fukui, K. *J. Phys. Chem.* **1970**, *74*, 4161-4163. Ishida, K.; Morokuma, K.; Komornicki, A. *J. Chem. Phys.* **1977**, *66*, 2153-2156.
 - Ammal, S. C.; Mishima, M.; Yamataka, H. *J. Org. Chem.* **2003**, *68*, 7772-7778
 - Yukawa, Y.; Tsuno, Y. *Bull. Chem. Soc. Jpn.* **1959**, *32*, 971-981. Yukawa, Y.; Tsuno, Y.; Sawada, M. *Bull. Chem. Soc. Jpn.* **1966**, *39*, 2274-2286. Tsuno, Y.; Fujio, M. *Chem. Soc. Rev.* **1996**, *25*, 129-139.
 - Hammond, G. S. *J. Am. Chem. Soc.* **1955**, *77*, 334-338.
 - Leffler, J. E.; Grunwald, E. *Rates and Equilibria of Organic Reactions*, Wiley, New York, 1963. Hammett, L. P. *Physical Organic Chemistry, Reaction Rates, Equilibria, and Mechanisms*, 2nd Ed., McGraw-Hill, New York, 1970. Shorter, J. *Correlation Analysis on Organic Chemistry*, Clarendon Press, Oxford, 1973. Johnson, C. R. *The Hammett Equation*, Cambridge University Press, New York, 1979.
 - Melander, L.; Saunders, W. H., Jr. *Reaction Rates of Isotopic Molecules*; Wiley-Interscience: New York, 1980; Chapter 4.
 - Preliminary results.
 - Yamataka, H.; Aida, M.; Dupuis, M. *Chem. Phys. Lett.* **2002**, *353*, 310-316.
 - Ussing, B. R.; Hang, C.; Singleton, D. A. *J. Am. Chem. Soc.* **2006**, *128*, 7594-7607, and references cited therein.

Chapter 18

Solvent Effects on the Chemistry of Bromonium and β -Bromocarbenium Ions as Reactive Intermediates

Cinzia Chiappe

Dipartimento di Chimica Bioorganica e Biofarmacia, via Bonanno 33,
Università di Pisa, 56126 Pisa, Italy

The ability of solvent to influence the rate of formation and subsequent evolution of the bromonium ion or the β -bromocarbenium ion as key ionic intermediates formed by bromine addition to alkenes are discussed based on kinetic and stereochemical studies as well as theoretical investigations.

Formation of bromonium ions (or β -bromocarbenium ions) and their role in electrophilic bromination of alkenes is a widely investigated organic textbook problem.⁽¹⁾ During the past fifty years there has been a revival of interest in electrophilic bromination, and the mechanistic aspects of bromine addition to double bonds continue to remain a topic of current intense studies. This continuing interest probably stems from the fact that halogenation mechanisms are sensitive to substituent effects, to geometrical constraints, and to environmental influences, making it difficult to assume or generalize the mechanistic details in many instances.

Indeed, more intermediates are involved in alkenes bromination than were previously considered. The first intermediates formed in the early steps are the alkene-halogen molecular complexes, whose ionization gives the corresponding bromonium or β -bromocarbenium bromide (tribromide) ion pairs. ⁽²⁾ The reversibility of the ionization step has been widely discussed in the last years

and its conclusive demonstration has been a relatively recent achievement. The first studies dealing with the reversibility were based on product studies, demonstrating: (a) the exchange of Br^+ (from solvolytically generated bromonium ions) to scavenger olefins; (b) the formation of alkenes at the expense of dibromides from bromonium bromide ion pairs (produced from bromohydrins and gaseous HBr); or (c) *cis/trans* isomerization during the bromination of *cis*-alkenes. (3) Subsequently, kinetic evidences for rate determination during the nucleophilic step of bromination have been obtained, showing that ion-pair return in electrophilic bromination of double bonds is a common process, not limited to sterically congested alkenes. (4) During the last decade, the initially formed 1:1 Br_2 -alkene complexes have been extensively studied, demonstrating that at least in the case of alkyl-substituted olefins, the formation constant of these transient species is affected by both the ionization potential of the donor and the polarizability of the double bond. (5) However, the presence of a heteroatom within the olefin may induce additional effects. Studies carried out on adamantylideneadamantanes bearing an electron withdrawing substituent on the homoallylic carbon (C-4) showed that OH or the OEt groups affect the complex formation constant through dipole-dipole interactions, whereas with halogens this occurs via dipole-induced dipole interactions. (6) Moreover, the presence of these substituents affects the stability of the corresponding ionic intermediates. In particular, the different ability of the ionic intermediates arising from 4-X-adamantylideneadamantanes (**1**) (4-chloro, 4-bromo, 4-fluoro, 4-hydroxy, 4-ethoxy and 4-acetoxy) to give substitution products or to remain in solution in equilibrium with the reagents, has been attributed to the differences in charge distribution in the cationic moiety of the ionic intermediate. A more pronounced β -bromocarbenium character of the cationic moiety in the intermediate is probably necessary for the intermediate to proceed to product. Theoretical calculations show (6) a larger difference in charge on the two carbons of the bromonium ring of 4-hydroxyadamantylideneadamantane, which gives a substitution product, when compared with 4-chloroadamantylideneadamantane, whose reaction with bromine stops at the stage of the ionic intermediate. A correlation between the increased β -bromocarbenium character and the tendency to give substitution products has been found also with other congested alkenes, having structures strictly correlated to adamantylideneadamantane, such as *trans*-(1-methyl-2-adamantylidene)-1-methyladamantane, **2**, (7) and bicyclo[3.3.1]nonylidenebicyclo[3.3.1]nonane, **3**. (8)

Contrary to the situation in adamantylideneadamantane, the ability of **3** to give a substitution product has been considered a consequence of the lack of bridging of CH_2 groups, thus allowing the fused cyclohexane rings to adopt other conformations, hence allowing proton abstraction and Br^+ shift, Scheme 1. DFT calculations show (8) that the boat conformation of the ionic intermediate arising from **3** is characterized by a significantly high difference of charge on the two carbons of the bromonium ring (Figure 1). This situation does not occur in the bromonium ion arising from adamantylideneadamantane.

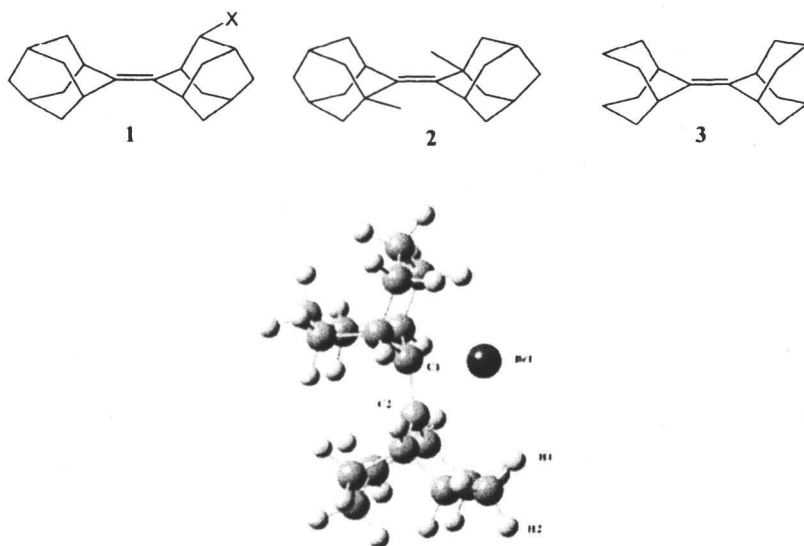
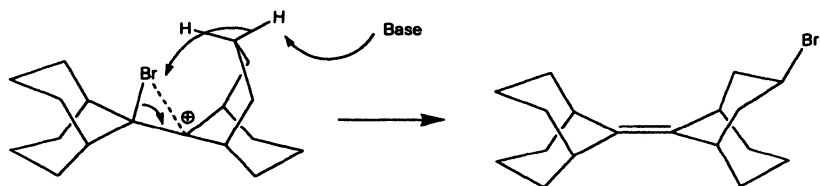


Figure 1. Boat conformation of the ionic intermediate arising from Br_2 addition to 3 in chlorinated solvents.



Scheme 1. Proposed mechanism for product formation in bromination of 3.

In the case of *trans*-(1-methyl-2-adamantylidene)-1'-methyladamantane, **2**, increased bromocarbenium character of the ionic intermediate is a consequence of steric strain present both in the starting olefin and in the corresponding bromonium ion. Introduction of the two *trans*-methyl groups at the allylic carbon atoms markedly increases the strain of the system, inducing significant torsion and out-of-plane bending of the double bond (7).

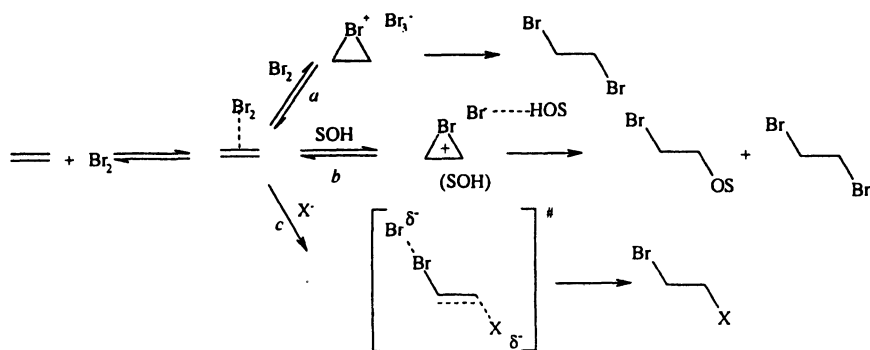
In agreement with the involvement of ionic intermediates for electrophilic halogenation of alkenes, an important role is also exerted by the solvent. Not only the reaction rate is strongly solvent-dependent, but also the stereochemical course of the addition process may be affected by the polarity of the medium. Solvent properties determine:

- the reaction rate
- the overall kinetic order
- the nature of the products
- the stereochemistry of the products

Solvent polarity has a dramatic effect on the overall rate constant, which increases in the case of 1-pentene by more than six orders of magnitude in going from acetic acid to water (1*d*). Moreover, the ability or inability of the solvent to exhibit hydrogen bonding determines the reaction order. The accepted mechanism (1*e*) for bromine addition to alkenes involves the initial formation of a transitory 1:1 substrate-Br₂ π complex, which is in rapid equilibrium with the reagents. In aprotic solvents, such as chloroform, dichloromethane, 1,2-dichloroethane, the rate determining ionization of the π complex is catalyzed by a second molecule of bromine to give a bromonium (or β -bromocarbenium) tribromide ion pair, which then collapses to the corresponding dibromo adduct(s), Scheme 2 path *a*. The addition reaction follows an overall third order rate law (second order in Br₂).

In contrast, in protic solvents and at low bromine concentration, the addition process is characterized by a second order rate law (first order in bromine), Scheme 2, path *b*. In this case, due to the ability of the solvent to provide a specific electrophilic solvation to the leaving bromide ion, the reaction occurs via an S_N1-like unimolecular ionization of the 1:1 π complex to form a bromonium or β -bromocarbenium bromide ion pair. It is worth noting that protic solvents can also give nucleophilic assistance, depending on their specific solvent properties.

Finally, in the presence of halide salts (bromide or chloride, which in low polarity non-protic solvents bind to Br₂ to give a stable trihalide species), the addition reaction proceeds through a rate- and product-determining nucleophilic attack of Br⁻ anion on the 1:1 π complex, Scheme 2 path *c*. No intermediate is formed in this latter reaction: the nucleophilic attack of halide (X⁻) and the Br-Br bond breaking are indeed concerted, although not necessarily synchronous.

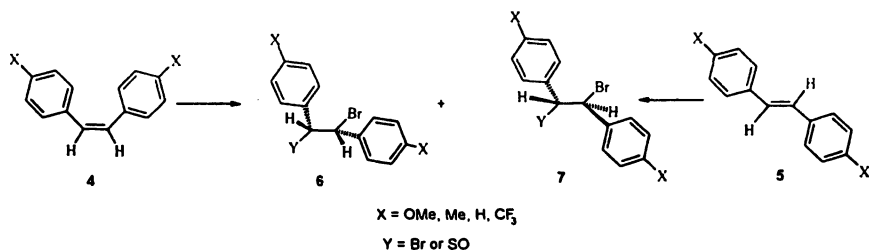


Scheme 2. Mechanisms for alkene bromination in aprotic and protic solvents.

The nature of the solvent also determines the chemoselective outcome in the reaction products. Products arising from the incorporation of one solvent molecule are formed (besides dibromides) in alcohols, acetic acid and acetonitrile (*1d-e*), whereas dibromo derivatives are formed exclusively in chlorinated solvents, nitromethane and in ionic liquids. (9) Chemoselectivity depends on the relative nucleophilicity of the solvent and the counterion, although it is affected also by other phenomena (ion pairing, and ion dissociation); in methanol the addition process gives quasi-exclusively bromomethoxy adducts, whereas in acetic acid dibromides are the main products, formed in addition to smaller amounts of the bromo-acetoxy derivatives. (10)

In agreement with other processes occurring through carbocations, elimination and transposition reactions can compete with the addition process which also depend on solvent. Finally, solvent properties can affect the stereochemical course of the addition reactions: for example, the stereoselectivity of bromine addition to *cis*- and *trans*-stilbenes has been found to be strongly solvent-dependent. (10)

The bromination of *trans*-stilbenes in methanol, trifluoroethanol and in acetic acid leads almost exclusively to the *erythro* adducts via a 100% anti addition, regardless the substituents and the solvent. In contrast, the stereochemistry of the reaction of *cis*-stilbenes exhibits a considerable dependence on the substituents and on the solvents; the reaction of *p*-methoxystilbenes is always stereo-convergent, that of *p,p'*-bis(trifluoromethyl)stilbenes is stereo-specific in all investigated solvents, whereas unsubstituted stilbenes can produce variable stereochemical outcomes ranging from stereo-specific to stereo-convergent in going from methanol to trifluoroethanol as solvent.

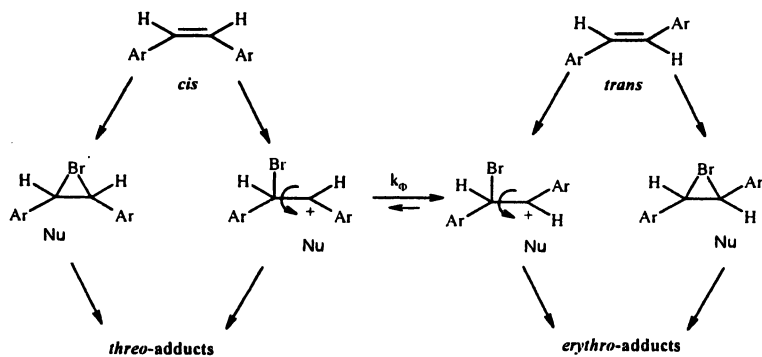


Although the stereochemical behavior of bromine addition to alkenes has been often considered to be the result of differential solvation requirements in the bromonium and carbenium ions in their equilibria, leading to more carbenium character as the solvent polarity increases, more recent kinetic and stereochemical data on bromination of stilbenes in protic solvents provided evidence that the nature of the ionic intermediates is solvent independent (10). Changes in bromine bridging as a function of substituents lead to markedly curved pa plots for arylolefin bromination,(11), but rigorously linear log-log relationships have been found (10) between the rate data for substituted *cis*- and *trans*-stilbenes in methanol and in the other solvents, showing that bromine bridging is not solvent dependent. At least in the case of stilbenes, bridging depends exclusively on the nature of the substituents on the aromatic ring, whereby electron-donating groups (methoxy) favour the formation of open intermediates but electron-withdrawing substituents favour bridged species (bromonium ions). The dependence of stereochemistry on solvent, which characterizes the bromination of some stilbenes may be therefore attributed to the ability of the medium to control the lifetime of the ionic intermediates through pre-association and dissociation phenomena. Open intermediates can react stereospecifically in MeOH, if the usual conformer rotation does not occur before the anti attack by MeOH (Scheme 3). The lifetimes of bromination intermediates may be shorter in nucleophilic solvents as compared to other media: in solvents such as methanol bromination may be nucleophilically assisted, whereas in AcOH and trifluoroethanol other pathways are preferred.

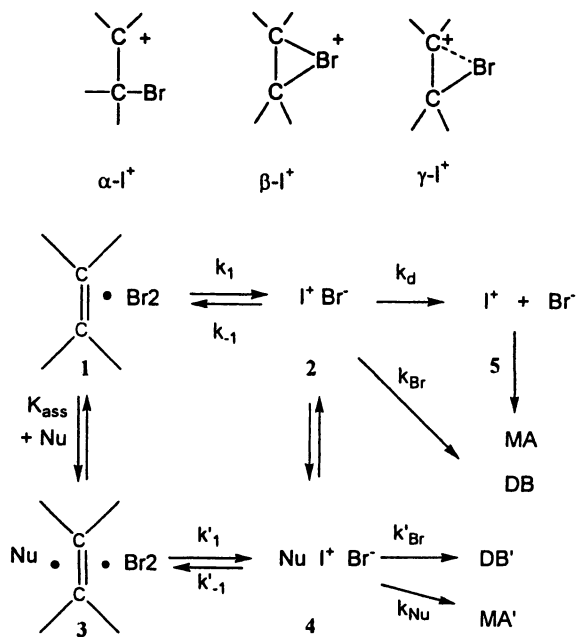
A mechanistic scheme, (Scheme 4) similar to that previously reported (12) for nucleophilic substitution, in which pre-association, free-ion and ion-pairs pathways compete, can therefore also be proposed for bromination. Based on this scheme, the stereochemical behaviour depends on both solvent and substituents. In *trifluoroethanol*, the reaction occurs independently of the substituents on the double bond, via free ions;



fully open bromocarbenium intermediates can equilibrate before trapping to give the expected products in a stereo-convergent manner. In acetic acid, a protic solvent with low polarity, the reaction always occurs through ion pairs;



Scheme 3.

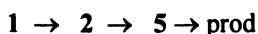


MA or MA' = Solvent incorporating products
 DB or DB' = dibromides

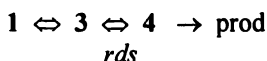
Scheme 4.



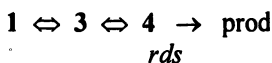
the addition mechanism involves solvent association with the ion pair before product formation. Finally, in *methanol* the reaction pathway is also determined by the nature of substituents. In the case of stilbenes, bearing strongly electron-donating substituents, reaction occurs through open intermediates, which rapidly dissociate to free ions. Formation of these intermediates is the rate-determining step (rds), and the reaction products are formed in a stereo-convergent manner as in trifluoroethanol.



For stilbenes, bearing moderately electron-donating substituents, the reaction occurs through open intermediates, present in solution as ion sandwich, 4. Formation of 4 is the rate determining step:

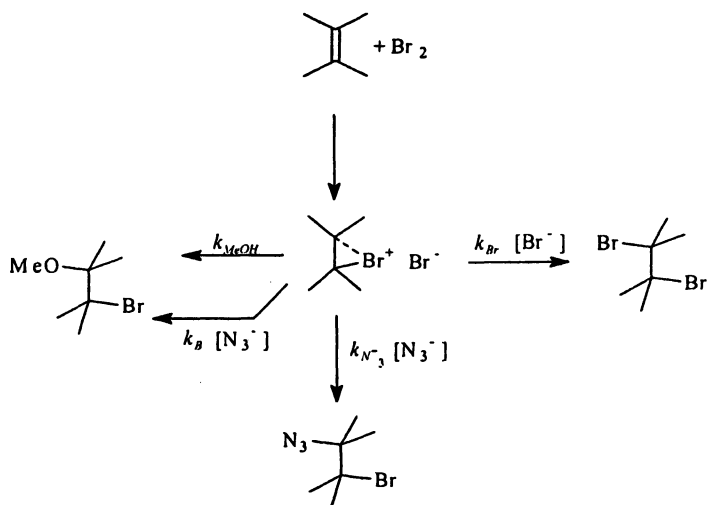


Finally, in the case of stilbenes bearing electron-withdrawing substituents, reaction occurs through bridged intermediates, which are present in solution as ion sandwich, 4. Transformation of 4 to products is the rate determining step. Bromonium ions arising from these olefins can return to reagents and a change in the rate determining step, from the step leading to 4 to the product-forming step can be envisaged, as bromine bridging increases.



Therefore, the lifetime of the intermediates determines the pathway followed under a given set of reaction conditions, establishing the product stereochemistry.

For nucleophilic substitution reactions, the lifetime of the ionic intermediates is generally calculated using the azide clock method; *i.e.* on the basis of the ratio (products incorporating azide)/total products, (f_{az}), determined by performing the reaction in the presence of increasing amounts of NaN_3 (13). Based on the mechanistic picture reported in Scheme 5, this method has been applied more recently to determine the lifetime of ionic intermediates arising from bromine addition to simple alkenes (cyclohexene, cyclopentene, tetramethylethylene and styrene) in methanol (14). (Scheme 5). Since in bromination in methanol the amount of dibromo adducts is generally irrelevant, only the data for bromo-methoxy and bromo-azido derivatives have been used to calculate f_{az} . Applying equation (1),



$$f_{az} = \frac{k_{N_3} [N_3^-]}{k_{Br} [Br^-] + k_{MeOH} + k_{N_3} [N_3^-] + k_B [N_3^-]} \quad (1)$$

which can be rewritten as:

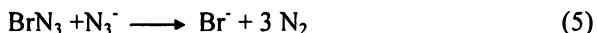
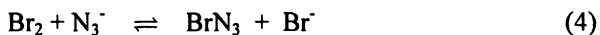
$$\frac{1}{f_{az}} = \frac{k_{N_3} + k_B}{k_{N_3}} + \frac{k_{Br} [Br^-] + k_{MeOH}}{k_{N_3}} \frac{1}{[N_3^-]} \quad (2)$$

the partitioning rate constant ratios can be obtained simply by plotting $1/f_{az}$ vs $1/[N_3^-]$.

Bromination of alkenes in MeOH in the presence of added NaN_3 is quite complex and involves a number of possible competing equilibria, which can generate different brominating species. Bromine addition in methanol gives extensive solvent incorporation into the products, leading to the liberation of bromide ions which are in equilibrium ($K_{MeOH} 177 M^{-1}$) with the tribromide species (3). Although this equilibrium may complicate the kinetic analysis of olefin bromination, in general, Br_2 is a more effective brominating agent than Br_3^- .



However, in the presence of NaN_3 , Br_2 is rapidly transformed into a new species having an absorption maximum around 312 nm. This species is most likely BrN_3 , a material shown (15) originally by Hassner to be capable of ionic electrophilic addition to olefins. It has been demonstrated, (16) at least in neutral aqueous solutions, that BrN_3 reacts with azide ions to give N_2 and Br^- .



Therefore, in order to obtain information about the nature of the brominating species present in the reaction mixture, and on its stability, spectroscopic measurements were carried out in the absence of olefin on methanolic Br_2 solutions containing increasing amount of NaN_3 . (14) When bromine (4.3×10^{-3} M) and methanolic solution of NaN_3 (between 4.7×10^{-2} to 2.37×10^{-1} M) were rapidly mixed in a stopped-flow apparatus, at 25 °C, no kinetic of disappearance of Br_2 could be observed, but only the presence of a new absorption band (λ_{max} 316 nm) and its subsequent decrease could be measured. The disappearance of the absorption band followed a first order rate law. The observed kinetic constants are reported in Table I.

Table I. Rate Constants,^a k (s^{-1}), for the Reaction of Azide with BrN_3 Formed by Mixing Br_2 (0.043 M) and NaN_3 at 25 °C.

$[\text{NaN}_3]$	$k_{\text{pseudo-2}}^{\text{(obsd)}}$ s^{-1}	r
0.0475	0.0106	0.9998
0.0950	0.0192	0.9999
0.1425	0.0276	0.9994
0.1900	0.0320	0.9994
0.2375	0.0370	0.9995

^a Reproducibility, better than $\pm 3\%$

Taking into account the reaction mechanism proposed for the same reaction in water, eq (4) and (5), BrN_3 should be the reactive intermediate formed in a pre-equilibrium step, the rate of consumption of the total bromine is therefore expressed by eq (6). At sufficiently high N_3^- concentration, the BrN_3 concentration is simply given by eq (7) and that of total bromine by eq (8). The introduction of eq (7) and (8) in eq (6) gives eq (9) from which the observed third-order rate constant, measurable by monitoring the free Br_2 and the observed

second-order rate law, measurable by monitoring the BrN_3 , could be obtained, eq (10) and eq (11).

$$-d[\text{Br}_2]_t / dt = k_2 [\text{BrN}_3][\text{N}_3^-] \quad (6)$$

$$[\text{BrN}_3] = K_f [\text{Br}_2]_{\text{free}} [\text{N}_3^-] \quad (7)$$

$$[\text{Br}_2]_t = [\text{Br}_2]_{\text{free}} + [\text{BrN}_3] \quad (8)$$

$$-d[\text{Br}_2] / dt = (k_2 K_f / 1 + K_f [\text{N}_3^-]) [\text{Br}_2] [\text{N}_3^-]^2 \quad (9)$$

$$k_{3(\text{obsd})} = k_2 K_f / 1 + K_f [\text{N}_3^-] \quad (10)$$

$$k_{2(\text{obsd})} = k_2 / 1 + K_f [\text{N}_3^-] \quad (11)$$

The kinetic constants, measured by monitoring the disappearance of the BrN_3 under the experimental conditions, are pseudo order constants, $k_{\text{pseudo-2}(\text{obsd})} = k_{2(\text{obsd})} [\text{N}_3^-]$, eq (12). For eq 12 a linearized form, eq (13), can be written.

$$k_{\text{pseudo-2}(\text{obsd})} = \frac{k_2 [\text{N}_3^-]}{1 + K_f [\text{N}_3^-]} \quad (12)$$

$$\frac{1}{k_{\text{pseudo-2}(\text{obsd})}} = \frac{1}{k_2 [\text{N}_3^-]} + \frac{K_f}{k_2} \quad (13)$$

A plot of $1/k_{\text{pseudo-2}(\text{obsd})}$ vs $1/[\text{N}_3^-]$ yields a straight line, the slope of which ($1/k_2$) refers to the rate constant for BrN_3 disappearance, and the intercept of which (K_f/k_2) refers to its stability constant. On the basis of the data reported in Table I, a k_2 value of 0.25 (0.003) $\text{M}^{-1} \text{s}^{-1}$ can be evaluated while the K_f value is 2.45 (0.15) M^{-1} .

Both these parameters reflect a moderate stability for BrN_3 in methanol. This feature made it impossible to apply the azide clock method to determine the lifetime of the ionic intermediates arising from deactivated alkenes (for example, *p,p'*-bis(trifluoromethyl)stilbenes). Nevertheless, for a couple of *p*-methoxy substituted stilbenes and unsubstituted stilbenes the selectivity ratios reported in Table II have been found. (17)

The values, ranging from 3 to 6 M^{-1} , are seven orders of magnitude smaller than the selectivity observed for activation limited reactions with stable cations, and can be used as evidence that the reaction with azide ion is a diffusion controlled process. Choosing a value for the rate constant for a diffusion-limited

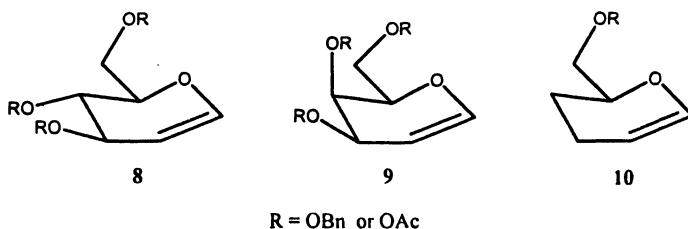
Table II. Partition Constant Ratios for the Reactions of Azide and MeOH with Various Bromonium Ions Formed via Electrophilic Addition of Br₂ to Stilbenes in Methanol at 25 °C.

p,p'-X-stilbene X	k_{N_3} / k_{MeOH} (M ⁻¹)	$(k_{N_3} + k_B) / k_{N_3}$
OCH ₃ , cis	5.78	1.10 (0.05)
OCH ₃ , trans	6.06	1.35 (0.08)
H,H cis	2.98	0.99 (0.05)
H,H trans	3.18	1.01 (0.04)
m,m'-di-Cl trans	47.92	0.96 (0.02)

reaction, and thus for $k_{az} = 1 \times 10^{10} \text{ M}^{-1} \text{ s}^{-1}$, the rate constants for the reaction of the ionic intermediates arising from the investigated stilbenes with methanol ranged from 1.6×10^9 to $3.3 \times 10^9 \text{ s}^{-1}$. In other words, the lifetimes of the corresponding intermediates in methanol ranged from $6.0 \times 10^{-10} \text{ s}$ at $3 \times 10^{-10} \text{ s}$. Similar values (ranging from 2.7×10^{-10} to 9.3×10^{-10}) were reported by Brown for bromonium (β -bromocarbenium) ions arising from cyclohexene, cyclopentene, tetramethylethene and styrene. (14) The nature of the substituents on double bond, and consequently the nature of the intermediates (bromonium or bromocarbenium), seems to have a minor effect on this kinetic property determined by transition-energies associated with the solvent attack, if the values reported above represented always the lifetime of the ionic intermediates. Only in the case of stilbenes bearing two moderate electron-withdrawing groups (metachlorine atoms), we evaluated a $t_{1/2}$ around $5 \times 10^{-9} \text{ s}$. However, the fact that similar values of $t_{1/2}$ have been found for two olefins (*p*-methoxystilbenes and unsubstituted stilbenes), for which kinetic and product distribution data show that the reactions occurs through different reaction pathways, strongly suggests that lifetimes of ionic intermediates formed by bromine addition in methanol, evaluated using the azide clock method, are not able to provide information about the reaction mechanism. At least in the case of stilbenes, a more efficient method to estimate the lifetime of these ionic intermediates is their rate of conformational rotation. The intermediate arising from *p*-methoxystilbenes is surely long lived in MeOH and AcOH, as full rotation is achieved before its trapping by these solvents; by contrast, in the case of unsubstituted stilbenes the lifetime of the corresponding ionic intermediates is short in methanol but very long in TFE.

The determination of the lifetime of the ionic intermediates using the azide-clock method has been however useful in showing that electrophilic addition of Br₂ can occur, even through a fully concerted mechanism, definable as S_N2-like. Bromination of cyclic enol ethers (glycals) **8-10** in methanol in the presence of

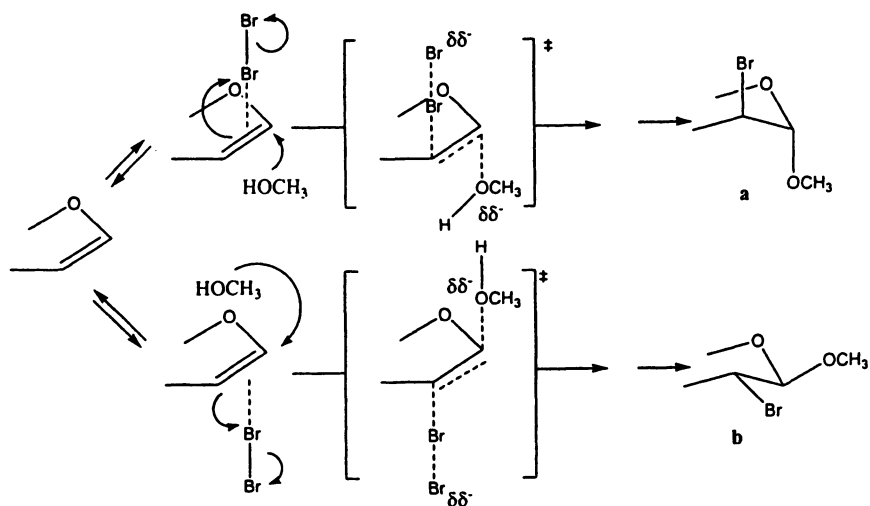
NaN_3 is generally a process characterized (18) by the absence of any azide incorporation product, suggesting that these reactions are concerted and not stepwise.



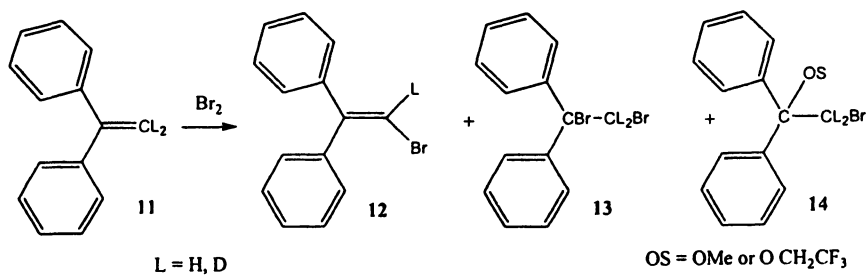
This result agrees fairly well with the observation (19) that nucleophilic substitutions on glycosyl derivatives, a class of carbocation-forming reactions having some common features with bromination, cannot involve carbocationic intermediates in the presence of strong nucleophiles. In this context, the measurable lifetime of the oxocarbenium ion derived from triacetylglucal (8, $R = \text{OAc}$, $t_{1/2} 6 \times 10^{-11}$ s) in which the substituents are acetoxy groups, instead of benzyloxy groups or hydrogen atoms, suggests a shift of the mechanism from concerted to pre-association in going from simple cyclic enoethers or tribenzylglucal to triacetylglucal. The product distribution data are in agreement with this shift of mechanism. The higher diastereoselectivity which characterize the reaction of triacetylglucal with respect to that of tribenzylglucal (a:b; 70:30 with respect 55:45) can be interpreted in terms of a pre-association mechanism in which methanol on one side and bromine on the other pre-associate with the enolic double bond, before ionization within the ternary complex gives a cationic intermediate formed in sandwich complex between leaving bromide and entering methanol (Scheme 6). The selectivity of the methanol attack increases on increasing the carbenium character of the cationic intermediate inside the sandwich species.

It is noteworthy that the nature of the ionic intermediate formed in bromine addition to olefins and the solvent properties also govern the competition between nucleophilic trapping and elimination. Thus 1,1-diphenylethylene, **11**, gives the corresponding dibromide **13** (or solvent incorporated products, **14**) and vinyl bromide, **12**, in a ratio changing from 99:1 to 5:95 depending on solvent and on bromine concentration.(20) (see Table III results)

Since the kinetic constant is independent of the reagent concentration and of the extent of proton loss from the intermediate, the last step is surely not rate limiting and the formation of the intermediate is for this olefin completely rate determining. (20) Consistent with this hypothesis is the lack of a large primary kinetic isotope effect (KIE), $k_H/k_D = 0.97$ (0.01), expected for a slow L^+ loss when the vinyl bromide is the main product. Taking into account that the rate determining step is the formation of a bromocarbenium-tribromide (bromide) ion pair and that the transition state should be closely related to the intermediate,



Scheme 6.



Scheme 7.

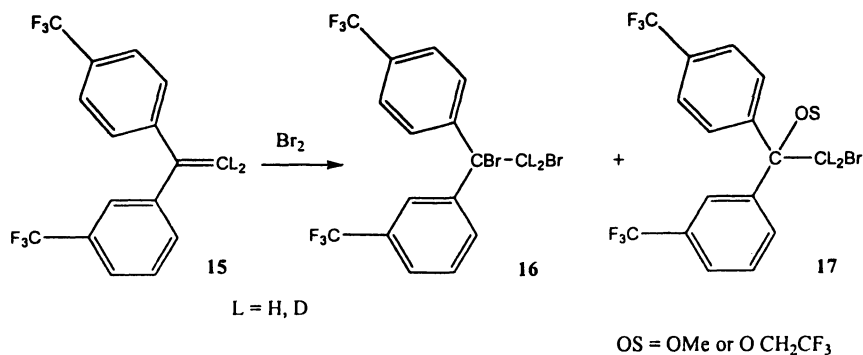
the apparent lack of even a secondary isotope effect has been attributed to a compensation of the inverse KIE produced by hybridization change at the methylene carbon during the ionization step, by a normal effect of comparable magnitude due to the hyperconjugative interaction of the carbenium centre with the β -C-L bonds.

Table III. Product Distribution for bromination of 1,1-diphenylethylene(11) at 25 °C.

[11]	[Br ₂]	Solvent	12	13	14
10 ⁻²	10 ⁻²	DCE ^a	0	100	
5 x 10 ⁻⁴	5 x 10 ⁻⁴		60	40	
10 ⁻²	10 ⁻²	DCM ^a	0	100	
5 x 10 ⁻⁴	5 x 10 ⁻⁴		40	60	
10 ⁻²	10 ⁻²	CHCl ₃ ^a	0	100	
2.5 x 10 ⁻⁴	2.5 x 10 ⁻⁴		15	85	
10 ⁻²	10 ⁻²	TFE	60	10	30
5 x 10 ⁻⁴	5 x 10 ⁻⁴		95		5
10 ⁻²	10 ⁻²	MeOH	5		95
5 x 10 ⁻⁴	5 x 10 ⁻⁴		0		100

^a From ref. 20.

On the contrary, bromination of 1-(3-trifluoromethylphenyl)-1-(4-trifluoromethylphenyl) ethylene (15) gives, in the entire range concentration and solvent investigated, only the corresponding dibromide or the solvent incorporated products



Scheme 8.

Table IV. Product Distribution for bromination of 1-(3-trifluoromethylphenyl)-1-(4-trifluoromethylphenyl) ethylene (15) at 25 °C.

[15]	[Br ₂]	Solvent	16	17
10 ⁻²	10 ⁻²	DCE ^a	100	
5 x 10 ⁻⁴	5 x 10 ⁻⁴		100	
10 ⁻²	10 ⁻²	DCM ^a	100	
5 x 10 ⁻⁴	5 x 10 ⁻⁴		100	
10 ⁻²	10 ⁻²	CHCl ₃ ^a	100	
2.5 x 10 ⁻⁴	2.5 x 10 ⁻⁴		100	
10 ⁻²	10 ⁻²	TFE	68	32
5 x 10 ⁻⁴	5 x 10 ⁻⁴		65	35
10 ⁻²	10 ⁻²	MeOH	6	94
5 x 10 ⁻⁴	5 x 10 ⁻⁴		2	98

^aFrom ref 20.

For this olefin a significant inverse KIE, $k_H/k_D = 0.70$ (0.05), was observed for bromination in DCE (20), suggesting probable involvement of a fully bridged or partially bridged intermediate, susceptible to return to reagents (20). The differing nature of the intermediates arising from 1,1-diphenylethylene **11** and its bis-trifluoromethyl derivative **15** was attributed the different product distribution, *i.e.* open β -bromocarbenium ion, involved in bromination of 1,1-diphenylethylene, could more easily undergo proton loss than the bridged ions. On the other hand, the concentration and solvent effect on the ratio of vinyl bromide/addition product(s), determined for 1,1-diphenylethylene in chlorinated solvents, can be related to the degree of ion pair dissociation. A progressive change from tight to solvent-separated ion pairs and then to free ions may occur in going from CHCl₃ to DCE (21) by decreasing the reagent concentrations. The ion pair dissociation can disfavor the rapid collapse of the counter-anion with the carbocation making the fast removal, of a β proton by a base competitive. It is possible that the geometrical requirements for nucleophilic trapping and elimination are different, and the barrier for the different types of ion pairs is smaller in the solvent separated ion pairs than in the tight ones.

Again, bromination of **11** in methanol shows (21) an inconsistent behavior with reactions found in all the other solvents, and in particular in TFE. Despite the fact that its polarity should favor ion pair dissociation, the reaction gives at all reagent concentrations examined, practically only the bromomethoxy derivative. This behavior may be attributed to the ability of MeOH to provide nucleophilic assistance; a reaction pathway occurring through ion sandwich could account for the absence of the elimination product.

guished. A more efficient approach, at least in the case of stilbenes, is the estimation of ionic intermediates lifetimes on the basis of the rate of conformational rotation of the cationic moiety.

- 4) Finally, in agreement with the behavior characterizing nucleophilic substitution, a highly concerted mechanism not involving ionic intermediates, similar to that occurring in nucleophilic substitution (S_N2 route), can be envisaged in bromination of activated alkenes in methanol.

References

1. (a) de la Mare, P. B. D.; Bolton, R. *Electrophilic Additions to Unsaturated Systems*, 2nd ed.; Elsevier: New York, 1982; pp 136-197. (b) V'yunok, K. A.; Ginak, A. I. *Russ. Chem. Rev. (Engl. Transl.)* **1981**, *50*, 151. (c) Schmid, G. H. *The Chemistry of Double-Bonded Functional Groups*; Patai, S., Ed.; Wiley: New York, 1989; Supplement A, Vol. 3, Part 1, p 699. (d) Ruasse, M. F. *Adv. Phys. Org. Chem.* **1993**, *28*, 207. (e) D. Lenoir, C. Chiappe *Chem Eur. J.* **2003**, *9*, 1036. (f) Brown, R. S. *Acc. Chem. Res.* **1997**, *30*, 131.
2. a) (a) Bennet, A. J.; Brown, R. S.; McClung, R. E. D.; Klobukowski, M.; Aarts, G. H. M.; Santarsiero, B. D.; Bellucci, G.; Bianchini, R. *J. Am. Chem. Soc.* **1991**, *113*, 8532. (b) Bellucci, G.; Bianchini, R.; Chiappe, C.; Lenoir, D.; Attar, A. *J. Am. Chem. Soc.* **1995**, *117*, 6243. (c) Bellucci, G.; Chiappe, C.; Bianchini, R.; Lenoir, D.; Herges, R. *J. Am. Chem. Soc.* **1995**, *117*, 12001. (d) Brown, R. S.; Nagorski, R. W.; Bennet, A. J.; McClung, R. E. D.; Aarts, G. H. M.; Klobukowski, M.; McDonald, R.; Santarsiero, B. D. *J. Am. Chem. Soc.* **1994**, *116*, 2448. (e) Nagorski, R. W.; Slebocka-Tilk, H.; Brown, R. S. *J. Am. Chem. Soc.* **1994**, *106*, 419. (f) Slebocka-Tilk, H.; Motallebi, S.; Nagorski, R. W.; Turner, P.; Brown, R. S.; McDonald, R. *J. Am. Chem. Soc.* **1995**, *107*, 8769. (g) Slebocka-Tilk, H.; Gallagher, D.; Brown, R. S. *J. Org. Chem.* **1996**, *61*, 3458.
3. Brown R. S.; Gedye, R.; Slebocka-Tilk, H.; Buschek, J. M.; Kopecky, K. R. *J. Am. Chem. Soc.* **1984**, *106*, 4515. Bellucci, G.; Chiappe, C.; Marioni, F. *J. Am. Chem. Soc.* **1987**, *109*, 515. Bellucci G.; Bianchini, R.; Chiappe, C.; Marioni, F. Spagna, R. *J. Am. Chem. Soc.* **1988**, *110*, 546. Bellucci, G.; Bianchini, R.; Chiappe, C.; Brown, R. S.; Slebocka-Tilk, H. *J. Am. Chem. Soc.* **1991**, *113*, 8012.
4. Brown R. S.; Slebocka-Tilk, H.; Bennet, A. J.; Bellucci, G.; Bianchini, R.; Ambrosetti, R. *J. Am. Chem. Soc.* **1990**, *112*, 6310. Ruasse, M. F.; Motallebi, S.; Galland, B. *J. Am. Chem. Soc.* **1991**, *113*, 3440. Bellucci, G.; Chiappe, C. *J. Org. Chem.* **1993**, *58*, 7120.

5. Chiappe C.; Detert, H.; Lenoir, D.; Pomelli, C. S.; Ruasse, M. F. *J. Am. Chem. Soc.* **2003**, *125*, 2864.
6. Chiappe, C.; De Rubertis, A.; Jaber, A.; Lenoir, D.; Wattenbach, C.; Pomelli, C. S. *J. Org. Chem.* **2002**, *67*, 7066.
7. Chiappe, C.; De Rubertis, A.; Lemmen, P.; Lenoir, D. *J. Org. Chem.* **2000**, *65*, 1273.
8. Chiappe, C.; Pomelli, C. S.; Lenoir, D.; Carsten W. *J. Mol. Model* **2005**.
9. Bellucci, G.; Bianchini, R.; Chiappe, C. *J. Org. Chem.* **1991**, *56*, 3067; Chiappe C. Capraro, D.; Conte, V.; Pieraccini D. *Org. Lett.* **2001**, *3*, 1061.
10. Ruasse, M. F.; Lo Moro, G.; Galland, B.; Bianchini, R.; Chiappe, C.; Bellucci, G. *J. Am. Chem. Soc.* **1997**, *119*, 12492.
11. Ruasse, M. F.; Dubois, J. F. *J. Org. Chem.* **1972**, *37*, 1770.
12. Jencks, W. P. *Acc. Chem. Res.* **1980**, *13*, 161.
13. Amyes, T. L.; Jencks, W. P. *J. Am. Chem. Soc.* **1989**, *111*, 7888. Amyes, T. L.; Richard, J. P. *J. Am. Chem. Soc.* **1990**, *112*, 9507.
14. Nagorski, R. W.; Brown, R. S. *J. Am. Chem. Soc.* **1992**, *114*, 7773.
15. Boerwinkle, F.; Hassner, A. *J. Am. Chem. Soc.* **1968**, *90*, 216.
16. Vivekanandam, T. S.; Singh, U, C.; Ramachandran, M. S. *Inter. J. Chem. Kinet.* **1981**, *13*, 199.
17. Chiappe, C., Ruasse, M. F. unpublished results.
18. Boschi, A.; Chiappe, C.; De Rubertis, A.; Ruasse, M. F. *J. Org. Chem.* **2000**, *65*, 8470.
19. Amyes, T. L.; Jencks, W. P. *J. Am. Chem. Soc.* **1989**, *111*, 7888. Banait, N. S.; Jencks, W. P. *J. Am. Chem. Soc.* **1991**, *113*, 7951.
20. Bellucci, G.; Chiappe, C. *J. Chem. Soc. Perkin Trans.2* **1997**, 581.
21. Bini, R. Chiappe, C. unpublished results from this laboratory

Chapter 19

Syntheses of the CFY_2^+ ($\text{Y} = \text{Cl}, \text{Br}$) and CX_3^+ ($\text{X} = \text{Cl}, \text{Br}, \text{OTeF}_5$) Cations Employing the Noble-Gas Oxidant, $\text{XeOTeF}_5^+\text{Sb}(\text{OTeF}_5)_6^-$

Hélène P. A. Mercier, Matthew D. Moran, and Gary J. Schrobilgen*

The Department of Chemistry, McMaster University, Hamilton,
Ontario L8S 4M1, Canada

The strong oxidant properties of the noble-gas salt, $\text{XeOTeF}_5^+\text{Sb}(\text{OTeF}_5)_6^-$, have been exploited to synthesize $\text{Sb}(\text{OTeF}_5)_6^-$ salts of trihalomethyl cations by the low temperature oxidation of a halide ligand of the corresponding tetrahalomethane in SO_2ClF solvent. Among the trihalomethyl cations that have been synthesized are CCl_3^+ , CBr_3^+ , CFCl_2^+ , and CFBr_2^+ , as well as $\text{C}(\text{OTeF}_5)_3^+$. The carbocations have been stabilized as salts of the preformed, oxidatively resistant and weakly coordinating $\text{Sb}(\text{OTeF}_5)_6^-$ anion, thus avoiding the use of more strongly coordinating anions derived from strong Lewis acid ligand acceptors such as SbF_5 . The CFCl_2^+ and CFBr_2^+ cations are the only known persistent fluorine-containing trihalomethyl cations, and appear to be the most electrophilic fluorine-containing cations synthesized to date. Evidence has been obtained for transient formation of CF_2Cl^+ , CF_2Br^+ , and CF_3^+ cations but, thus far, their high electrophilicities have precluded isolation.

Earlier Studies of Long-Lived CX_3^+ ($X = Cl, Br, I$) and $CF_nX_{3-n}^+$ ($X = Cl, Br; n = 0-3$) Cations

Trihalomethyl cations, CX_3^+ ($X = Cl, Br, I$), have been the subject of considerable interest. The CCl_3^+ and CBr_3^+ cations have been postulated as superelectrophilic intermediates that catalyze efficient cracking, isomerization, and oligimerization of alkanes and cycloalkanes, as well as facilitating the syntheses of carbocations via hydride abstraction by the CCl_3^+ cation.¹ The CCl_3^+ cation, the first perhalomethyl cation to have been reported, was observed in the gas phase by mass spectrometry² and by ion cyclotron resonance (ICR) mass spectrometry.³ The CCl_3^+ cation has also been isolated in the solid state by ultraviolet or microwave irradiation of $CHCl_3$ and entrapment of the free cation in an argon matrix at 14 K,^{4,5} and by codeposition of CCl_4 and SbF_5 on a CsI window at 77 K followed by warming to 150 K to produce $CCl_3^+Sb_2F_{10}Cl^-$ in an SbF_5 matrix.⁶ In all three cases, CCl_3^+ was characterized by infrared spectroscopy. More recently, the CBr_3^+ and CI_3^+ cations have been generated in the gas phase and observed by ICR mass spectrometry.⁷ The CF_3^+ cation has been observed by mass spectrometry² and ICR mass spectrometry,³ and was first produced in the condensed state by photodecomposition of CF_3X ($X = Cl, Br, I, H$) in argon matrices.⁸ The CF_3^+ cation has also been obtained by photoionization and radiolysis of $^{12/13}CF_3Br$,⁹ by decomposition of an Ar/F_3CNNCF_3 mixture at 14 K that had been codeposited with a beam of microwave-excited neon atoms,¹⁰ and by codeposition of a Ne/CF_4 mixture at 5 K with microwave-excited neon atoms.¹¹ Matrix-isolated CF_3^+ , generated in the aforementioned manners, was characterized by infrared spectroscopy, and the vibrational assignments for CF_3^+ have been confirmed by ab initio calculations.¹²

The mixed, fluorine-containing halomethyl cations, $CFCl_2^+$,¹³⁻¹⁶ CF_2Cl^+ ,^{14,15} $CFBr_2^+$,^{13,15} and CF_2Br^+ ,^{13,15} have been generated in the gas phase by various ionization methods and observed as short-lived cations. The $(CFCl_2^+||Cl^-)_{solv}$ ion pair has been generated as a transient species by pulse radiolysis of $CFCl_3$ in methylcyclohexane.¹⁷

Persistent $CFCl_2^+$ ¹⁸ and CF_2Cl^+ ¹⁹ cations have been generated by matrix radiolysis and photoionization during co-condensation of $CFCl_3$ and CF_2Cl_2 , respectively, with argon at 15 K. Both cations were characterized by infrared spectroscopy, but the assignments of the complex mixture of cationic and radical chlorofluorocarbon species were not corroborated by other means. In another matrix-isolation study, it has been claimed that the $CFCl_2^+ \cdots Cl^-$ ion pair was generated by irradiation of $CFCl_3$ at 77 K with γ -rays from a ^{60}Co source, followed by irradiation with a xenon lamp using a cutoff of 900 nm.²⁰ The proposed ion pair was characterized by UV-visible absorption spectrophotometry. Persistent $CFBr_2^+$ ⁹ has been generated by photoionization and radiolysis of $CFBr_3$ and CF_2Br_2 , whereas $^{12/13}CF_2Br^+$ ⁹ has been generated from CF_2Br_2 and $^{12/13}CF_3Br$, during co-deposition with argon at 15 K. Both cations were characterized by infrared spectroscopy.

The first syntheses of long-lived perhalomethyl cations in solution were achieved by the reactions of CX_4 ($X = Cl, Br, I$) with SbF_5 in SO_2ClF solvent at $-78\text{ }^\circ C$ to give $CX_3^+Sb_nF_{5n}X^-$ ($X = Cl, Br, I; n \geq 1$).²¹ All three cations were characterized by ^{13}C NMR spectroscopy. The CCl_3^+ cation was also generated by reaction of $CCl_3C(O)Cl$, CCl_3SO_2Cl , and $CCl_3C(O)F$ with SbF_5 in SO_2ClF at $-78\text{ }^\circ C$.^{21,22} Similar attempts to generate CF_3^+ by reaction of SbF_5 with CF_4 , $CF_3C(O)F$, and CF_3SO_2Cl in SO_2ClF at $-78\text{ }^\circ C$ were unsuccessful and, in the cases of $CF_3C(O)F$ and CF_3SO_2Cl , yielded CF_4 .^{21,22} The Cl_3^+ cation has been recently synthesized as $Cl_3^+Al(OC(CF_3)_3)_4^-$ by the room temperature abstraction of iodide as AgI from Cl_4 in CH_2Cl_2 solution by use of $Ag^+Al(OC(CF_3)_3)_4^-$ and characterized by X-ray crystallography.²³

Although a considerable number of carbocations structures have been determined,²⁴⁻²⁷ relatively few crystal structures are known for halogen- and oxygen-substituted carbocations. These include $c-(F_2C-S-CF-S)^+$,²⁸ $(CH_3)_2CF^+$,²⁹ $(m-CF_3C_6H_4)(C_6H_5)CF^+$,²⁹ CH_3OCHF^+ ,³⁰ $(o-CIC_6H_4)(C_6H_5)CCl^+$,³¹ $ClCO^+$,³² $(p-CH_3C_6H_4)CO^+$,³³ CH_3CO^+ ,³³ $CH_3CH_2CO^+$,³³ $(3,5-F-4-CH_3-C_6H_2)CO^+$,³³ $Cl_2C^+-NH_2$,³⁴ $ClBrC^+-NH_2$,³⁵ CH_3OCHCl^+ ,³³ $C(OH)_2CH^+$,^{36,37} $HC(OH)_2^+$,³⁸ $(p-CH_3C_6H_4)C(OH)_2^+$,³⁹ $(C_6H_5)C(-OCH_2CH_2O)^+$,⁴⁰ and $(CH_3)C(-OC(CH_3)_2C(CH_3)_2O)^+$.⁴¹ Until the work described in this Review, the Cl_3^+ and $C(OH)_3^+$ cations were the only trihalo- and trioxy-substituted cations to have been characterized by X-ray crystallography.^{23,42}

As a consequence of the relative paucity of solid state structural data for trihalomethyl cations, electronic structure calculations have been heavily relied upon for geometric data and have been used to account for the bonding and chemical properties of these cations. The relative stabilities of the trihalomethyl cations have been assessed in terms of relative degrees of σ and $p(\pi)$ donation from the halogen atom to the carbon center.^{29,32,43} The σ effect, from the perspective of the halogen atoms of CX_3^+ , has been found to be strongly withdrawing in the case of fluorine and weakly donating in the cases of chlorine, bromine and iodine ($I > Br > Cl$). Conversely, $p(\pi)$ back-donation is very weak for fluorine and stronger for the heavier halogens ($I > Br > Cl$). Other properties have been computed for the CX_3^+ series, including ^{13}C chemical shifts,⁴⁴ fluoride ion affinities (as measures of relative Lewis acidities),²³ vibrational frequencies,¹² and atomic charges.^{22,23,29,32,43,45,46} Recently electron pair affinities have been used to quantify Lewis acidities of the $EX_3^{0/+}$ systems ($E = B, C, Al, Si; X = F, Cl, Br, I$).⁴⁷

Prior syntheses of long-lived perhalomethyl cations have been achieved by halide abstraction by use of either a strong Lewis acid (in superacidic or SO_2ClF solvent media) or Ag^+ (vide supra), but no routes to such carbocations through oxidative removal of a halogen bound to carbon were known. The objectives of the current work have been to provide structural and spectroscopic data that, thus far, have been lacking for these systems, and to provide oxidative routes to

the perhalomethyl cations and related pentafluoroorthotellurate (OTeF_5) substituted cations. An oxidative route to carbocations using the strong oxidant salt, $\text{XeOTeF}_5^+\text{Sb}(\text{OTeF}_5)_6^-$, provides an interesting new application of noble-gas compounds to chemical syntheses,⁴⁸⁻⁵⁹ that has led to the solution characterization and isolation to several salts of the trihalomethyl cations and their (OTeF_5) derivatives.

The XeL^+ ($\text{L} = \text{F}, \text{OSeF}_5, \text{OTeF}_5$) Cations and $\text{M}(\text{OTeF}_5)_6^-$ ($\text{M} = \text{As}, \text{Sb}, \text{Bi}$) Anions; General Background

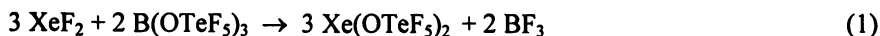
The electronegativity of the OTeF_5 group is comparable to that of fluorine in its ability to stabilize a variety of noble-gas species.^{60,61} Derivatives of the OTeF_5 group are known for the +2, +4, and +6 oxidation states of xenon,⁶²⁻⁶⁹ as well as for the +2 oxidation state of krypton.⁷⁰ The OTeF_5 analogue of the well-known XeF^+ cation, XeOTeF_5^+ , was first obtained as the AsF_6^- salt by reaction of FXeOTeF_5 with AsF_5 .⁶⁴ The $\text{XeOTeF}_5^+\text{Sb}_2\text{F}_{11}^-$ salt was subsequently synthesized from $\text{XeOTeF}_5^+\text{AsF}_6^-$ by AsF_5 displacement in liquid SbF_5 ,⁸ and the XeOTeF_5^+ cation has been characterized in solution by ^{19}F , ^{125}Te , and ^{129}Xe NMR spectroscopy in SbF_5 solvent,⁶⁹ and in the solid state by Raman spectroscopy of $\text{XeOTeF}_5^+\text{AsF}_6^-$ ^{64,65,68} and $\text{XeOTeF}_5^+\text{Sb}_2\text{F}_{11}^-$.⁶⁹ The X-ray crystal structure of $\text{XeOTeF}_5^+\text{AsF}_6^-$ shows that the incomplete primary coordination sphere of XeOTeF_5^+ , like that of XeF^+ , renders it a Lewis acid that interacts with the AsF_6^- anion by means of a fluorine bridge. The $\text{Xe}\cdots\text{F}$ cation-anion distance (2.24(3) Å)⁶⁸ is significantly less than the sum of xenon and fluorine van der Waals radii (3.63 Å)⁷¹ and is similar to that in $\text{XeF}^+\text{AsF}_6^-$ (2.208(3) Å)⁷² and $\text{XeOSeF}_5^+\text{AsF}_6^-$ (2.31(4) Å).⁶⁸

Until recently, no solid state structural data currently exists for salts of the XeF^+ or XeOTeF_5^+ cations in which either XeF^+ or XeOTeF_5^+ , or any other noble-gas cation, may be regarded as "devoid" of interactions with their counter anions. Likely candidates for anions that may prove to be weakly coordinating with respect to XeF^+ and XeOTeF_5^+ are members of the oxidatively resistant $\text{M}(\text{OTeF}_5)_6^-$ ($\text{M} = \text{As}, \text{Sb}, \text{Bi}$) anion series.⁷³ The latter anions effectively disperse a single negative charge over 30 fluorine atoms rather than over six fluorine atoms as in their MF_6^- analogues. In addition to their low basicities, the high effective group electronegativity of the OTeF_5 ligands and their steric requirements in these hexa-coordinate anions may be expected to make the electron lone pairs of the linking oxygen atoms less accessible to attack by strong electrophiles. The $\text{Sb}(\text{OTeF}_5)_6^-$ anion has been shown to resist attack by the strong oxidant cations SbCl_4^+ and SbBr_4^+ ,⁷⁴ leading to the X-ray crystal structure determinations of their $\text{Sb}(\text{OTeF}_5)_6^-$ salts.

The generation of main-group cations by use of xenon cations as oxidants has been limited to salts of the XeF^+ ^{49,56} and $\text{C}_6\text{F}_5\text{Xe}^+$ ⁵⁸ cations and has focused on the oxidation of the central element rather than on the oxidation of a ligand.

Synthesis of $\text{XeOTeF}_5^+\text{Sb}(\text{OTeF}_5)_6^-$

The salt, $\text{XeOTeF}_5^+\text{Sb}(\text{OTeF}_5)_6^-$, provides an example of a synthetically useful low-temperature noble-gas oxidant in which the noble-gas cation is not coordinated to its counter ion (see X-ray Crystal Structure of $\text{XeOTeF}_5^+\text{Sb}(\text{OTeF}_5)_6^- \cdot \text{SO}_2\text{ClF}$). The ability of the neutral precursor, $\text{Xe}(\text{OTeF}_5)_2$, to oxidatively introduce two OTeF_5 groups has been previously exploited in the syntheses of $\text{NR}_4^+\text{Sb}(\text{OTeF}_5)_6^-$ salts ($\text{R} = \text{CH}_3$ or CH_2CH_3) from $\text{NR}_4^+\text{Sb}(\text{OTeF}_5)_4^-$.⁷³ The $\text{XeOTeF}_5^+\text{Sb}(\text{OTeF}_5)_6^-$ salt was first observed in an attempt to synthesize $\text{Sb}(\text{OTeF}_5)_5$ by reaction of equimolar amounts of $\text{Xe}(\text{OTeF}_5)_2$ and $\text{Sb}(\text{OTeF}_5)_3$.⁷⁵ A 2:1 molar ratio of $\text{Xe}(\text{OTeF}_5)_2$ (eq 1) and $\text{Sb}(\text{OTeF}_5)_3$ (eq 2) [$< 1\%$ molar excess of $\text{Xe}(\text{OTeF}_5)_2$] react in SO_2ClF solvent at -20°C in near quantitative yield to form bright yellow to yellow-orange solutions of $\text{XeOTeF}_5^+\text{Sb}(\text{OTeF}_5)_6^-$ (eq 3). Unlike its fluorine analogue,



$\text{XeF}^+\text{SbF}_6^-$, which is insoluble in SO_2ClF at room temperature, the solubility of $\text{XeOTeF}_5^+\text{Sb}(\text{OTeF}_5)_6^-$ in SO_2ClF at -78°C is high, exceeding 2 M. The solid salt, isolated as the pale yellow solvate, $\text{XeOTeF}_5^+\text{Sb}(\text{OTeF}_5)_6^- \cdot \text{SO}_2\text{ClF}$ at -78 to 0°C , is stable to pumping at 0°C for at least 4–5 h. The solid decomposes above 10°C after 4–6 h, in marked contrast with $\text{XeOTeF}_5^+\text{AsF}_6^-$ ^{64,65,68} and $\text{XeF}^+\text{SbF}_6^-$,⁷⁶ which are stable at room temperature. Solutions of $\text{XeOTeF}_5^+\text{Sb}(\text{OTeF}_5)_6^-$ in SO_2ClF show significant decomposition after 30 min to 1 hat -10°C .

Structural Studies of $\text{XeOTeF}_5^+\text{Sb}(\text{OTeF}_5)_6^-$

(a) **Multi-NMR Spectroscopy.** The ^{17}O , ^{19}F , ^{121}Sb , ^{125}Te and ^{129}Xe NMR spectra of $\text{XeOTeF}_5^+\text{Sb}(\text{OTeF}_5)_6^-$ have been recorded at -50°C in SO_2ClF solvent (Table 1). The ^{17}O NMR spectrum was recorded for an enriched [$^{17,18}\text{O}$]- $\text{XeOTeF}_5^+\text{Sb}(\text{OTeF}_5)_6^-$ sample at -15°C , which was prepared according to eq 3 by reaction of natural abundance $\text{Sb}(\text{OTeF}_5)_3$ with a stoichiometric amount of enriched [$^{17,18}\text{O}$]- $\text{Xe}(\text{OTeF}_5)_2$ (^{16}O , 35.4%; ^{17}O , 21.9%; ^{18}O , 42.7%).

Although SO_2ClF is a very weak Lewis base and has been extensively used as a solvent medium for strong Lewis acid fluoride ion acceptors, ^{19}F NMR studies of MF_5 ($\text{M} = \text{As},^{77}\text{Sb}^{78}$) in SO_2ClF and SO_2F_2 solvents have shown that, unlike SO_2F_2 , SO_2ClF is sufficiently basic to form weak donor-acceptor adducts with strong Lewis acid pentafluorides at low temperatures. Although Raman spectroscopy and single-crystal X-ray crystallography (vide infra) of the $\text{XeOTeF}_5^+\text{Sb}(\text{OTeF}_5)_6^- \cdot \text{SO}_2\text{ClF}$ have shown that SO_2ClF solvent is coordinated

Table 1. The ^{19}F , ^{125}Te , ^{129}Xe , ^{17}O , and ^{121}Sb NMR Parameters for $\text{XeOTeF}_5^+\text{Sb}(\text{OTeF}_5)_6^-$ ^a

Species	chem shifts (δ), ppm					coupling constants, Hz		
	$^{19}\text{F}^b$	^{125}Te	^{129}Xe	$^{17}\text{O}^c$	^{121}Sb	$^2J(^{19}\text{F}_A-^{19}\text{F}_X)^b$	$^1J(^{19}\text{F}-^{125}\text{Te})^b$	$^1J(^{19}\text{F}-^{123}\text{Te})$
XeOTeF_5^+	-51.7 (F_A) -40.3 (F_X)	579.9	-1459.5	133		175	3776 (F_A) 3810 (F_X)	^d 3167 (F_X)
$\text{Sb}(\text{OTeF}_5)_6^-$	-42.4 ($F_A \approx F_B$)	548.4		107	-13	^e	3553	2950

^a All NMR spectra were recorded in SO_2ClF solvent at $-50\text{ }^\circ\text{C}$ except the ^{17}O spectrum, which was recorded at $-15\text{ }^\circ\text{C}$. ^b The subscripts A and B/X, denote axial and equatorial fluorine atoms, respectively. ^c The ^{17}O NMR parameters for solvent SO_2ClF at natural abundance were also determined in the present study: doublet at $\delta(^{17}\text{O})$, 227.0 ppm; $^2J(^{17}\text{O}-^{19}\text{F})$, 27.9 Hz. ^d The ^{123}Te satellites were not observed. ^e The $^2J(^{19}\text{F}_A-^{19}\text{F}_B)$ value of 186 Hz has been estimated in SO_2ClF solvent for $\text{N}(\text{CH}_3)_4^+\text{Sb}(\text{OTeF}_5)_6^-$ and verified by computer simulation (ref 73).
SOURCE: Reproduced from reference 73. Copyright 1994.

through an oxygen atom to the xenon of the XeOTeF_5^+ cation in the solid state (see X-ray Crystal Structure of $\text{XeOTeF}_5^+\text{Sb}(\text{OTeF}_5)_6^-\text{SO}_2\text{ClF}$), the ^{19}F NMR spectrum provides no direct evidence for coordinated SO_2ClF . The absence of a cation-anion interaction is attributed to the lability of the $\text{Xe}\cdots\text{O}$ donor-acceptor bond in solution, resulting in rapid chemical exchange between the bulk SO_2ClF solvent molecules and coordinated SO_2ClF at temperatures as low as -80°C .

(b) X-ray Crystal Structure of $\text{XeOTeF}_5^+\text{Sb}(\text{OTeF}_5)_6^-\text{SO}_2\text{ClF}$. The structure of $\text{XeOTeF}_5^+\text{Sb}(\text{OTeF}_5)_6^-\text{SO}_2\text{ClF}$ ⁷⁹ consists of well-separated XeOTeF_5^+ cations and $\text{Sb}(\text{OTeF}_5)_6^-$ anions in which each XeOTeF_5^+ cation is oxygen-coordinated to an SO_2ClF molecule (Figure 1).

The XeOChF_5^+ ($\text{Ch} = \text{Se}, \text{Te}$) cations have been characterized in their AsF_6^- salts, where all bond lengths and bond angles of the XeOChF_5^+ cations were affected by four-fold orientational disorders.⁶⁸ The XeOChF_5^+ cations were, however, shown to be strongly ion paired with their AsF_6^- anions by means of fluorine bridges between the cations and the anions, a structural feature that is also encountered in XeF^+ salts.^{68,72,80} In contrast, the XeOTeF_5^+ cation in $\text{XeOTeF}_5^+\text{Sb}(\text{OTeF}_5)_6^-\text{SO}_2\text{ClF}$ is neither coordinated to the anion nor disordered. Rather, the xenon atom of XeOTeF_5^+ is coordinated through an oxygen atom of the weak Lewis base solvent molecule, SO_2ClF , forming the adduct-cation, $\text{XeOTeF}_5^+\text{SO}_2\text{ClF}$. The difference in solid state coordination behavior is attributed to the weakly-coordinating nature of the $\text{Sb}(\text{OTeF}_5)_6^-$ anion relative to those of the AsF_6^- , SbF_6^- , $\text{Sb}_2\text{F}_{11}^-$ and related anions derived from strong Lewis acid pentafluorides (vide infra). The only other published examples of crystal structures in which SO_2ClF is coordinated to a Lewis acid center are $\text{Fe}(\text{OTeF}_5)_3\cdot 3\text{SO}_2\text{ClF}$ ⁸¹ and $\text{C}(\text{OTeF}_5)_3^+\text{Sb}(\text{OTeF}_5)_6^-\cdot 3\text{SO}_2\text{ClF}$. In the latter instance, two of the SO_2ClF molecules in the formula unit are oxygen-coordinated to the carbon atom along the pseudo three-fold axis of the $\text{C}(\text{OTeF}_5)_3^+$ cation⁸² [see X-ray Crystal Structure of $\text{C}(\text{OTeF}_5)_3^+\text{Sb}(\text{OTeF}_5)_6^-\cdot 3\text{SO}_2\text{ClF}$].

The gas-phase complexation energies calculated at the SVWN/(SDB)cc-pVTZ level are exothermic for the $\text{Xe}\cdots\text{F}\cdots\text{M}$ ($\text{M} = \text{As}, \text{Sb}$) bridged ion pairs $\text{XeF}^+\text{AsF}_6^-/\text{XeF}^+\text{SbF}_6^-$ ($-624.3/-610.0$ kJ mol^{-1}) and $\text{XeOTeF}_5^+\text{AsF}_6^-/\text{XeOTeF}_5^+\text{SbF}_6^-$ ($-557.7/-543.9$ kJ mol^{-1}) and for the considerably more weakly coordinated and $\text{Xe}\cdots\text{O}$ bonded donor-acceptor adduct $\text{XeOTeF}_5^+\text{SO}_2\text{ClF}$ (-116.3 kJ mol^{-1}). The ion-pairing energies are greater for XeF^+ than for XeOTeF_5^+ for both MF_6^- salts, and the donor-acceptor interaction between XeOTeF_5^+ and SO_2ClF is only ca. 20% that of the fluorine-bridge bond energies in the AsF_6^- and SbF_6^- salts and ca. 50% of the complexation energy for $\text{F}\cdots\text{Xe}\cdots\text{OH}_2^+$ (-216.3 kJ mol^{-1}). At the opposite end of the scale, the complexation energy for XeF^+ and naked F^- ion (-1086.6 kJ mol^{-1}), which leads to XeF_2 formation, is nearly double that of the aforementioned ion pairing energies.

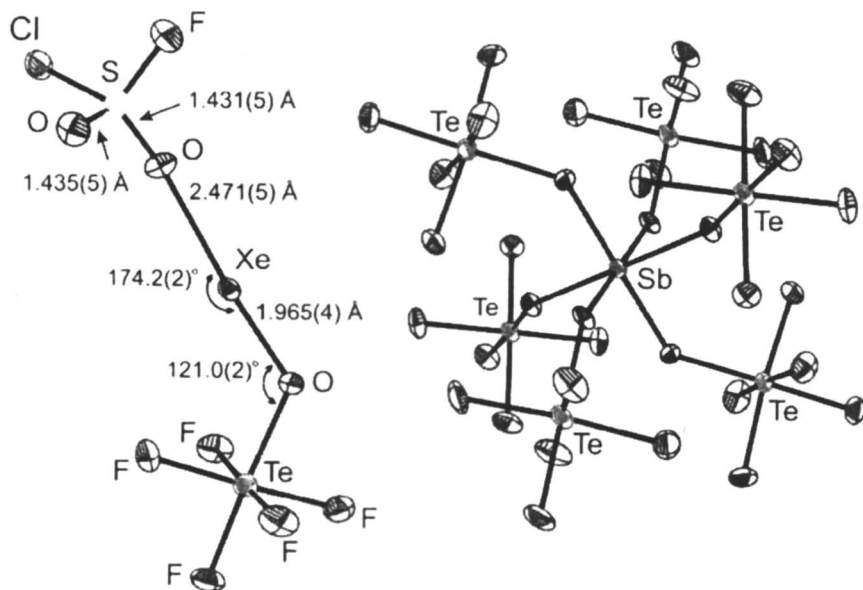
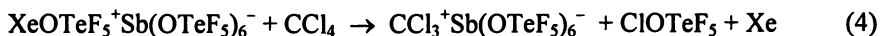


Figure 1. Crystal structure of $XeOTeF_5^+ Sb(OTeF_3)_6^- \cdot SO_2ClF$ with key bond lengths and bond angles given for the $F_5TeOXe^+ \cdot SO_2ClF$ unit.⁷⁹

Syntheses and Solution Characterization by ^{19}F and ^{13}C NMR Spectroscopy of $\text{CCl}_3^+\text{Sb}(\text{OTeF}_5)_6^-$, $\text{CBr}_n(\text{OTeF}_5)_{3-n}^+\text{Sb}(\text{OTeF}_5)_6^-$ ($n = 0-3$), $\text{Br}(\text{OTeF}_5)_2^+\text{Sb}(\text{OTeF}_5)_6^-$, and $\text{C}(\text{OTeF}_5)_4$

The products of reactions 4–9 have been characterized in SO_2ClF solution by ^{13}C and ^{19}F NMR spectroscopy (Table 2). All solid products and their SO_2ClF solutions were stable indefinitely at temperatures approaching $-20\text{ }^\circ\text{C}$.

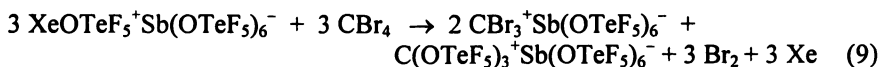
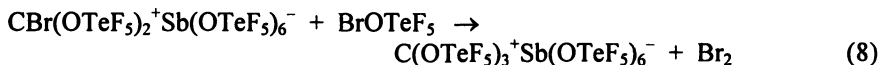
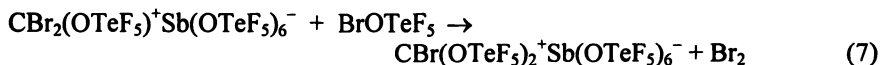
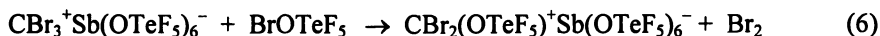
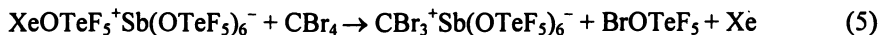
The salt $\text{XeOTeF}_5^+\text{Sb}(\text{OTeF}_5)_6^-$ rapidly oxidizes stoichiometric amounts of CCl_4 at $-78\text{ }^\circ\text{C}$ to yield clear, colorless solutions of $\text{CCl}_3^+\text{Sb}(\text{OTeF}_5)_6^-$ according to eq 4. Removal of SO_2ClF under vacuum at



$-78\text{ }^\circ\text{C}$ gives colorless, crystalline $\text{CCl}_3^+\text{Sb}(\text{OTeF}_5)_6^-$.

The ^{13}C NMR spectrum (SO_2ClF solvent, $-80\text{ }^\circ\text{C}$) of the products resulting from eq 4 give rise to a sharp singlet (237.1 ppm) assigned to $\text{CCl}_3^+\text{Sb}(\text{OTeF}_5)_6^-$, which is in agreement with the previously reported value (236.3 ppm).²¹ The ^{13}C chemical shift of CCl_3^+ is significantly deshielded relative to CCl_4 [$\delta(^{13}\text{C})$, 96.4 ppm; SO_2ClF , $-80\text{ }^\circ\text{C}$], which is consistent with carbocation formation. The ^{19}F NMR spectrum shows the very strongly coupled AB_4 pattern that typifies the $\text{Sb}(\text{OTeF}_5)_6^-$ anion⁷³ and a well-resolved AB_4 pattern for ClOTeF_5 (Table 2).⁸³

The reaction of stoichiometric amounts of CBr_4 with $\text{XeOTeF}_5^+\text{Sb}(\text{OTeF}_5)_6^-$ in SO_2ClF is initially rapid at $-78\text{ }^\circ\text{C}$, giving a deep red-brown solution which lightens to red-orange over a period of several hours at ca $-50\text{ }^\circ\text{C}$ (eq 5). The color change corresponds to the further reaction of the CBr_3^+ cation with BrOTeF_5 to produce Br_2 and the mixed carbocations, $\text{CBr}_2(\text{OTeF}_5)^+$, $\text{CBr}(\text{OTeF}_5)_2^+$ and, ultimately, $\text{C}(\text{OTeF}_5)_3^+$ according to eq 6–8, with the overall reaction being represented by eq 9. The $\text{CBr}_3^+\text{Sb}(\text{OTeF}_5)_6^- \cdot \text{SO}_2\text{ClF}$ and



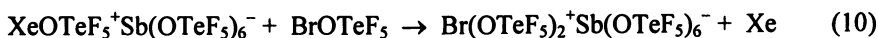
$\text{C}(\text{OTeF}_5)_3^+\text{Sb}(\text{OTeF}_5)_6^- \cdot 3\text{SO}_2\text{ClF}$ salts have been characterized by single-crystal X-ray diffraction (vide infra).

Table 2. The ^{13}C and ^{19}F NMR Parameters^a for $\text{C}(\text{OTeF}_5)_4$ and $\text{CBr}_n(\text{OTeF}_5)_{3-n}$ ($n = 0-3$), and Products Resulting from the Reaction of $\text{XeOTeF}_5^+ \text{Sb}(\text{OTeF}_5)_6^-$ with CCl_4 and CBr_4

Species	chem shifts (δ), ppm ^b				coupling constants, Hz			
	^{13}C	$^{19}\text{F}_\text{B}$	$^{19}\text{F}_\text{A}$	$^2J(^{13}\text{C}-^{125}\text{Te})$	$^2J(^{19}\text{F}_\text{A}-^{19}\text{F}_\text{B})$	$^1J(^{19}\text{F}_\text{B}-^{123/125}\text{Te})$	$^1J(^{19}\text{F}_\text{A}-^{123/125}\text{Te})$ ^c	
CCl_3^{+c}	237.1							
CBr_3^{+c}	209.7							
$\text{CBr}_2(\text{OTeF}_5)^{+c}$	201.1 ^d	-19.9	-61.3		156	^e /4099		
$\text{CBr}(\text{OTeF}_5)_2^{+c}$	187.6	-24.4	-59.3		162	3343/4029	^e /(4075)	
$\text{C}(\text{OTeF}_5)_3^{+c}$	168.8	-31.6	-57.6	69	164	3337/4025	^e /4012	
$\text{C}(\text{OTeF}_5)_4$	115.8	-41.5	-49.9	64	180	3120/3758	3029/3653	
$\text{Br}(\text{OTeF}_5)_2^{+c}$		-24.4	-58.2		164	3324/4013	(3350)/(4047)	
BrOTeF_5^f		-53.8	-47.0		180	3140/3786	^e /3419	
ClOTeF_5		-54.0	-49.2		178	^e /3852	^e /3474	
$\text{Sb}(\text{OTeF}_5)_6^{-c}$			-42.6			^e /3563		

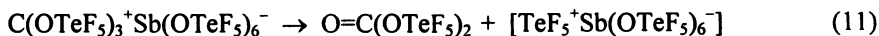
^a Nuclear magnetic resonance spectra were obtained for $\text{SO}_2\text{-ClF}$ solutions at -80°C . ^b The symbols, F_A and F_B , denote axial and equatorial fluorine atoms, respectively. ^c The anion parameters apply to all carbocation salts and to the $\text{Br}(\text{OTeF}_5)_2^+$ salt of $\text{Sb}(\text{OTeF}_5)_6^-$; also see ref 73. ^d Predicted from pairwise additivity parameters as described in the Chemical Shifts and Coupling Constant Trends section. ^e See ref 84 and 85. ^f The ^{123}Te satellites were not observed.

The ^{13}C NMR spectrum of $\text{CBr}_3^+\text{Sb}(\text{OTeF}_5)_6^-$ in SO_2ClF at $-80\text{ }^\circ\text{C}$ is a singlet (209.7 ppm), in good agreement with the previously reported value (207 ppm).²¹ As in the case of CCl_3^+ , the ^{13}C resonance of CBr_3^+ is significantly deshielded with respect to that of its parent molecule, CBr_4 [$\delta(^{13}\text{C})$, -29.7 ppm; SO_2ClF , $-80\text{ }^\circ\text{C}$], and is again characteristic of carbocation formation. The ^{19}F NMR spectrum shows a very strongly coupled AB_4 pattern corresponding to the $\text{Sb}(\text{OTeF}_5)_6^-$ anion (Table 2), similar to that obtained for $\text{CCl}_3^+\text{Sb}(\text{OTeF}_5)_6^-$. The ^{19}F NMR spectrum of pure BrOTeF_5 dissolved in SO_2ClF at $-80\text{ }^\circ\text{C}$ (Table 2) was also obtained and demonstrated that BrOTeF_5 formed in eq 5 was not present. The absence of BrOTeF_5 is consistent with the formation of mixed Br/OTeF_5 -substituted methyl cations and the oxidation of BrOTeF_5 by $\text{XeOTeF}_5^+\text{Sb}(\text{OTeF}_5)_6^-$ to give the new $\text{Br}(\text{OTeF}_5)_2^+$ cation (eq 10). The



formation of $\text{Br}(\text{OTeF}_5)_2^+$ was confirmed, in a separate experiment, by the reaction of BrOTeF_5 with $\text{XeOTeF}_5^+\text{Sb}(\text{OTeF}_5)_6^-$ in SO_2ClF at $-78\text{ }^\circ\text{C}$.⁸⁶

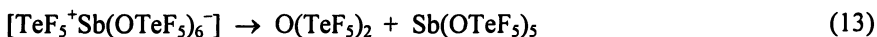
The formation of the $\text{CBr}_n(\text{OTeF}_5)_{3-n}^+$ ($n = 0-2$) cations and their NMR assignments were confirmed by addition of BrOTeF_5 at $-20\text{ }^\circ\text{C}$ to the reaction products of eq 9, in a 3:1 molar ratio relative to the initial amounts of $\text{XeOTeF}_5^+\text{Sb}(\text{OTeF}_5)_6^-$ and CBr_4 . This resulted in increased amounts of the OTeF_5 -containing carbocations and Br_2 as outlined in eq 6-8 (Table 2). The ^{13}C NMR spectrum indicated that a small quantity of $\text{CBr}_3^+\text{Sb}(\text{OTeF}_5)_6^-$ remained unreacted (7% based on integration of all ^{13}C resonances), with $\text{C}(\text{OTeF}_5)_3^+\text{Sb}(\text{OTeF}_5)_6^-$ as the major product (70%; $\delta(^{13}\text{C})$, 168.8 ppm). Of the mixed $\text{CBr}_n(\text{OTeF}_5)_{3-n}$ ($n = 1, 2$) cations, only $\text{CBr}(\text{OTeF}_5)_2^+$ was detected by ^{13}C NMR spectroscopy [10%; $\delta(^{13}\text{C})$, 187.6 ppm], whereas the ^{13}C chemical shift of $\text{CBr}_2(\text{OTeF}_5)^+$ was predicted by use of empirical (pairwise additivity) trends [$\delta(^{13}\text{C})$, 201.1 ppm].^{87,88} A singlet was also observed [13%; $\delta(^{13}\text{C})$, 124.7 ppm] that is tentatively assigned to $\text{O}=\text{C}(\text{OTeF}_5)_2$ based on the similarity of its ^{13}C chemical shift to that of $\text{O}=\text{CE}_2$ (134.2 ppm),⁸⁹ and may arise from the formal loss of the TeF cation from $\text{d}(\text{OTeF}_5)$ according to eq 11.



Alternatively, $\text{O}=\text{C}(\text{OTeF}_5)_2$ may prove to be unstable, decomposing to CO_2 [$\delta(^{13}\text{C})$, 124.2 ppm]⁹⁰ and $\text{O}(\text{TeF}_5)_2$ [$\delta(^{19}\text{F}_\text{B})$, -41.4 ppm; F_A was not observed because of overlap with F_A of $\text{C}(\text{OTeF}_5)_3^+$; $^2J(^{19}\text{F}_\text{A}-^{19}\text{F}_\text{B})$, 164 Hz] according to eq 12. The TeF_5^+ cation presumably is not observed because of its high



electrophilicity, which leads to OTeF_5^- abstraction from $\text{Sb}(\text{OTeF}_5)_6^-$, forming $\text{O}(\text{TeF}_5)_2$ according to eq 13 and/or F^- abstraction to form TeF_6 [$\delta(^{19}\text{F})$, -52.6



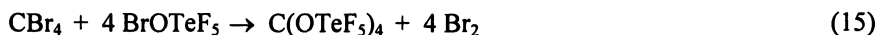
ppm; $^1J(^{19}\text{F}-^{125}\text{Te})$, 3747 Hz; $^1J(^{19}\text{F}-^{123}\text{Te})$, 3095 Hz] according to eq 14. The



proposed Sb(V) species, $\text{Sb}(\text{OTeF}_5)_5$, which is known to be unstable,^{75,91} and $\text{F}_4\text{TeOSb}(\text{OTeF}_5)_5$ have not been further investigated.

The formation of the $\text{C}(\text{OTeF}_5)_3^+$ cation was confirmed by the presence of a satellite doublets in the ^{13}C NMR spectrum that arise from spin-spin coupling of ^{13}C to natural abundance ^{123}Te (0.87%) and ^{125}Te (6.99%) [$^2J(^{13}\text{C}-^{125}\text{Te})$, 69 Hz].⁹² Separate integrations of ^{123}Te and ^{125}Te satellites were not possible as a result of their relatively broad line widths ($\nu_{1/2} \approx 5$ Hz), thus, the ^{123}Te satellites only appear as shoulders. Because ^{123}Te and ^{125}Te are low abundance, spin- $1/2$ nuclei, only a superposition of subspectra arising from the most abundant isotomers, $^{13}\text{C}(\text{O}^0\text{TeF}_5)_3^+$ (singlet) and $^{13}\text{C}(\text{O}^{123/125}\text{TeF}_5)(\text{O}^0\text{TeF}_5)_2^+$ (doublet) (where ^0Te represents all spin-inactive isotopes of tellurium) are observed. Taking into account the natural isotopic abundances, multiplicities, and statistical distributions of tellurium isotopes among three sites, the experimental combined $^{123/125}\text{Te}$ integrated satellite peak/central peak area ratios of 0.111 : 1.000 : 0.123 in the ^{13}C NMR spectrum were used to confirm coupling to three equivalent tellurium atoms when compared with the calculated relative intensity ratios (0.000 : 0.0054 : 0.1268 : 1.0000 : 0.1268 : 0.0054 : 0.0001). Tellurium satellites could not be observed for $\text{CBr}(\text{OTeF}_5)_2^+$ owing to the low concentration of this species (10%).

In order to compare the NMR parameters of $\text{C}(\text{OTeF}_5)_3^+$ with those of the unknown neutral parent, $\text{C}(\text{OTeF}_5)_4$, CBr_4 was allowed to react with a stoichiometric amount of BrOTeF_5 at -78 °C according to eq 15. The ^{13}C NMR

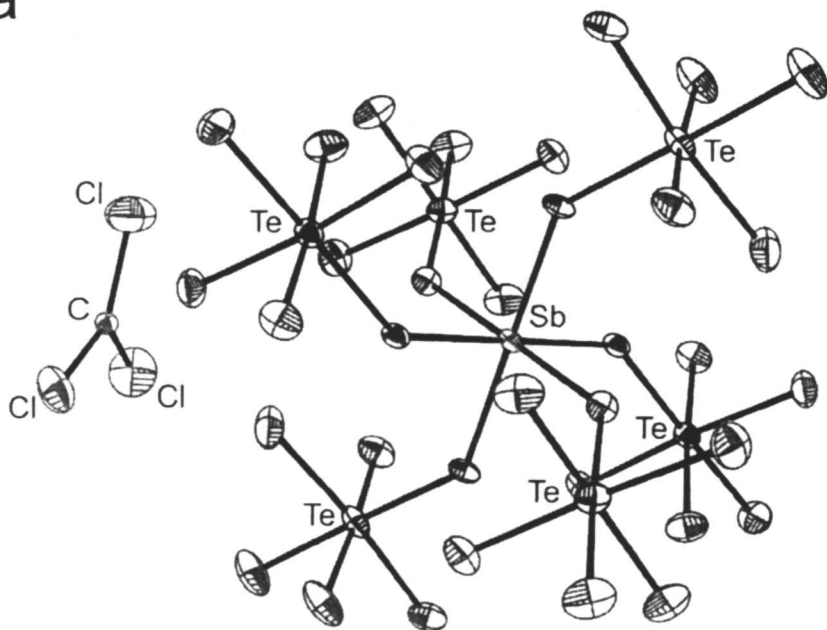


resonance of $\text{C}(\text{OTeF}_5)_4$ is a singlet at 115.8 ppm, accompanied by tellurium satellites. As expected, the ^{13}C chemical shift of $\text{C}(\text{OTeF}_5)_4$ in SO_2ClF solvent is significantly shielded with respect to that of the $\text{C}(\text{OTeF}_5)_3^+$ cation. As in the case of $\text{C}(\text{OTeF}_5)_3^+$, the formation of $\text{C}(\text{OTeF}_5)_4$ was confirmed by the relative intensities of the overlapping $^{123/125}\text{Te}$ satellites [$^2J(^{13}\text{C}-^{125}\text{Te})$, 64 Hz] in its ^{13}C NMR spectrum.⁹³

X-ray Crystal Structures of $\text{CCl}_3^+\text{Sb}(\text{OTeF}_5)_6^-$, $\text{CBr}_3^+\text{Sb}(\text{OTeF}_5)_6^- \cdot \text{SO}_2\text{ClF}$, and $\text{C}(\text{OTeF}_5)_3^+\text{Sb}(\text{OTeF}_5)_6^- \cdot 3\text{SO}_2\text{ClF}$

Key bond lengths and bond angles for the CCl_3^+ , CBr_3^+ , and $\text{C}(\text{OTeF}_5)_3^+$ cations and secondary contacts to $\text{Sb}(\text{OTeF}_5)_6^-$ and SO_2ClF are provided in Figures 2–4.

a



b

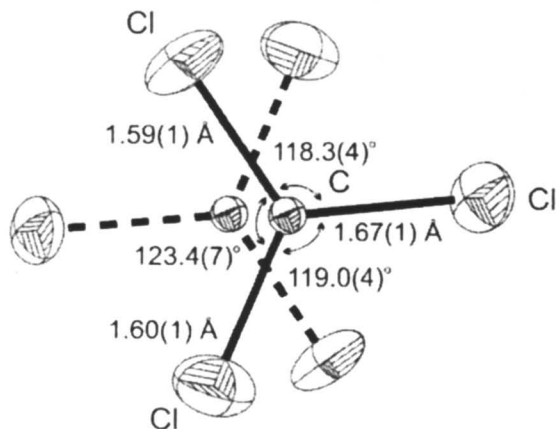
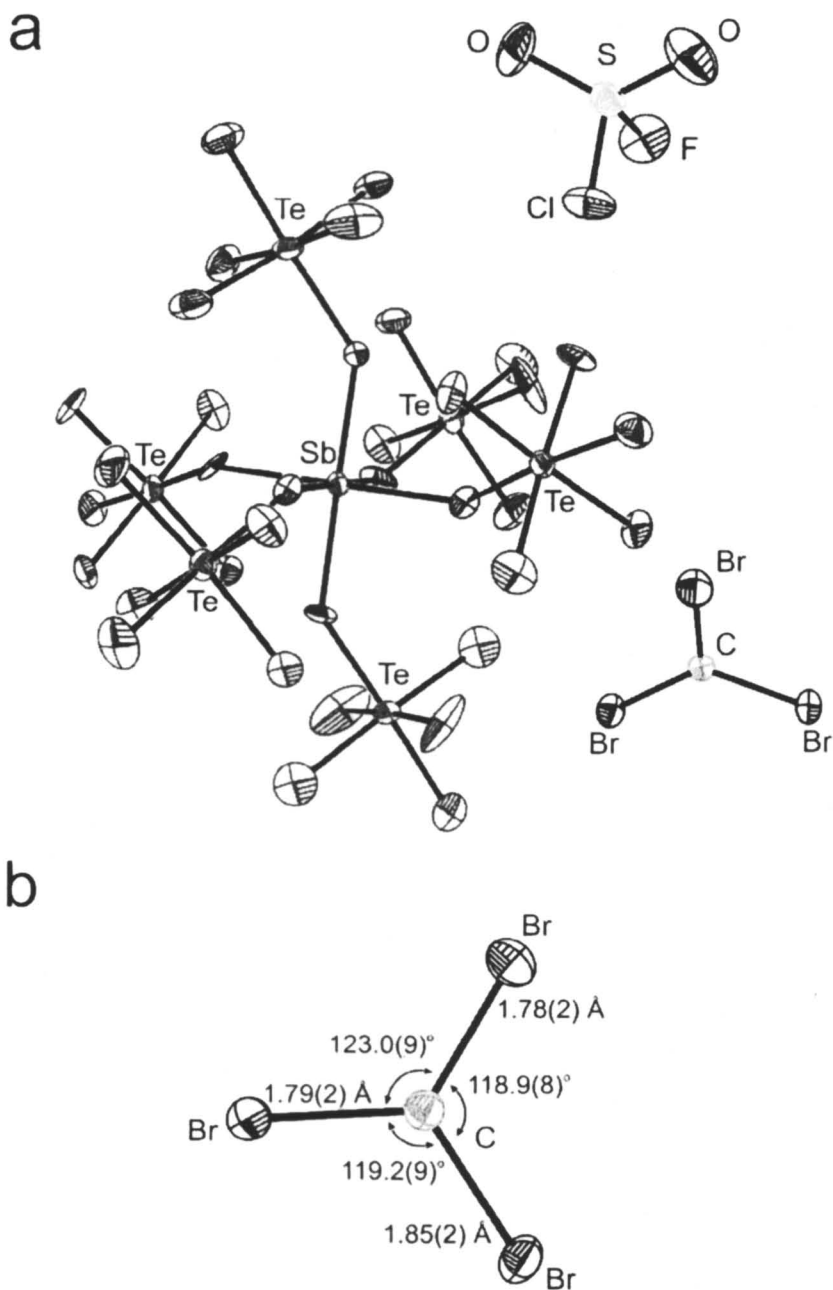


Figure 2. (a) Crystal structure of $\text{CCl}_3^+\text{Sb}(\text{OTeF}_5)_6^-$. (b) A view of the CCl_3^+ cation, with key bond lengths and bond angles, showing the two-fold positional disorder around the crystallographic inversion center.⁸²



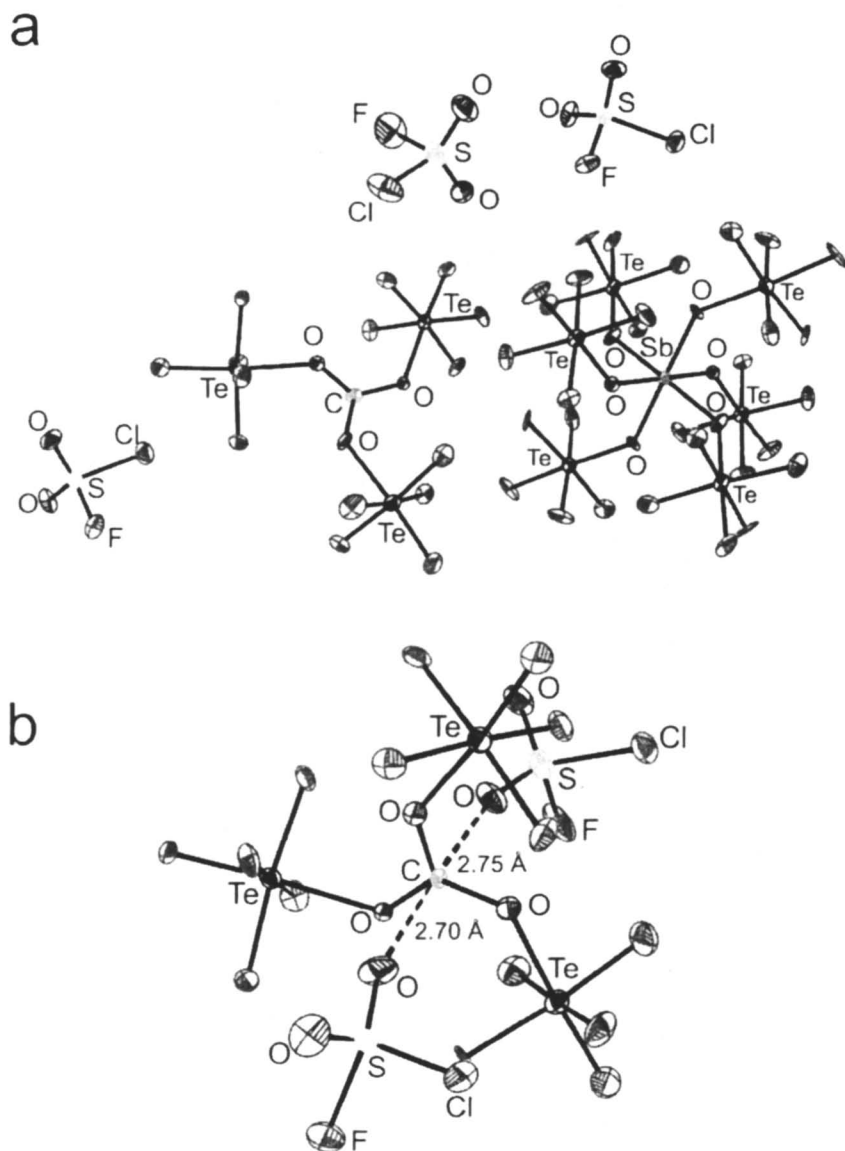


Figure 4. (a) Crystal structure of $C(O\text{TeF}_3)_3^- \text{Sb}(O\text{TeF}_3)_6^- \cdot 3\text{SO}_2\text{ClF}$. The key geometric parameters for $C(O\text{TeF}_3)_3^-$ are: $C-O$, 1.258(15)–1.313(16) Å; $\angle O-C-O$, 119(1)–121(1)°; $\angle C-O-Te$, 125.5(7)–132.7(9)°. (b) A view of the $C(O\text{TeF}_3)_3^-$ cation, showing the contacts between the carbon atom and an oxygen atom from each of two SO_2ClF molecules in the crystal lattice.⁸²

(a) $\text{CCl}_3^+\text{Sb}(\text{OTeF}_5)_6^-$ and $\text{CBr}_3^+\text{Sb}(\text{OTeF}_5)_6^- \cdot \text{SO}_2\text{ClF}$. The trigonal planar CCl_3^+ cation in $\text{CCl}_3^+\text{Sb}(\text{OTeF}_5)_6^-$ is positionally two-fold disordered about the crystallographic inversion center (Figure 2), but its geometry is unaffected by the disorder. In contrast, the CBr_3^+ cation in $\text{CBr}_3^+\text{Sb}(\text{OTeF}_5)_6^- \cdot \text{SO}_2\text{ClF}$ is not disordered (Figure 3). In both cases, the three halogen atoms are crystallographically independent and carbocation planarity is not imposed by symmetry. The C–X bond lengths of each cation are all equal within $\pm 3\sigma$ and the X–C–X angles are all equal to the ideal trigonal planar value within $\pm 3\sigma$, giving the expected D_{3h} symmetry. The C–Cl and C–Br bond lengths are found to be shorter than in CCl_4 [1.751(13) Å],⁹⁴ CFCl_3 [1.75(1) Å]⁹⁵ and CBr_4 (1.91(4) Å)⁹⁶ by ca. 0.15 Å, 0.13 Å, and 0.10 Å, respectively, as expected for positively charged species [also see calculated Charge and Bonding in $\text{CF}_n\text{X}_{3-n}^+$ (X = Cl, Br; $n = 0-3$) and $\text{C}(\text{OTeF}_5)_3^+$]. In both the CCl_3^+ and CBr_3^+ salts, one short cation-anion C···F contact [2.962(9) Å and 3.09(2) Å, respectively; cf. the sum of the carbon and fluorine van der Waals radii, 3.10,⁹⁷ 3.30⁷¹ Å] occurs and approaches the carbon at angles of 3° (CCl_3^+) and 8° (CBr_3^+) with respect to the C_3 symmetry axis. Additionally, longer C···F contacts [CCl_3^+ , 3.464(9), 3.574(11) and 3.574(11) Å; CBr_3^+ , 3.39(2) Å] approach above and below the CX_3 -plane at angles of 4, 13 and 37° (CCl_3^+) and 8° (CBr_3^+), respectively. The bond length and bond angle trends are consistent with the previously noted trend of decreasing contact angle with decreasing contact distance in a number of carbocation structures.²⁴ The structures indicate that the $\text{Sb}(\text{OTeF}_5)_6^-$ anions are very weakly coordinated to the carbon centers. The occurrence of cation-anion contacts is a common feature, and the C···F contact distances are comparable to those observed in $\text{Cl}_3^+\text{Al}(\text{OC}(\text{CF}_3)_3)_4^-$ ²³ (the shortest is 3.26 Å) and in $(m\text{-CF}_3\text{C}_6\text{H}_4)(\text{C}_6\text{H}_5)\text{CF}^+\text{As}_2\text{F}_{11}^-$ [3.01(2) and 3.07(2) Å].²⁹ The chlorine and bromine atoms also interact with the fluorine atoms of the anion and, in the case of the CBr_3^+ salt, with the oxygen atoms of SO_2ClF [$\text{Cl}\cdots\text{F}$: 2.833(5) – 3.022(5) Å; $\text{Br}\cdots\text{F}$: 2.977(9) – 3.301(11) Å; $\text{Br}\cdots\text{O}$: 2.778(13), 2.839(12) Å] (Figure 5). These interactions are shorter than or are at the limit of the sum of the halogen-fluorine (oxygen) van der Waals radii ($\text{Cl}\cdots\text{F}$, 3.15,⁹⁷ 3.22⁷¹ Å; $\text{Br}\cdots\text{O}$, 3.35,⁹⁷ 3.37⁷¹ Å; $\text{Br}\cdots\text{F}$, 3.30,⁹⁷ 3.32⁷¹ Å) and are apparently a consequence of the positive charges on the halogen atoms [also see calculated charge Distributions in CCl_3^+ , CBr_3^+ , and $\text{C}(\text{OTeF}_5)_3^+$ and Correlations with Their Solid State coordination]. The $\text{Br}\cdots\text{O}$ contacts, which occur with the oxygen atoms of two SO_2ClF solvent molecules, are shorter than the secondary C···F cation-anion contacts in the CCl_3^+ and CBr_3^+ salts and are likely responsible for the absence of disorder in the CBr_3^+ structure.

(b) $\text{C}(\text{OTeF}_5)_3^+\text{Sb}(\text{OTeF}_5)_6^- \cdot 3\text{SO}_2\text{ClF}$. The crystal structure of $\text{C}(\text{OTeF}_5)_3^+\text{Sb}(\text{OTeF}_5)_6^- \cdot 3\text{SO}_2\text{ClF}$ consists of $\text{Sb}(\text{OTeF}_5)_6^-$ anions that are well separated from the cations and the solvent molecules, while two of the three SO_2ClF solvent molecules are oxygen coordinated to the carbon atom of the cation (Figure 4). There are no noticeable differences between the geometric

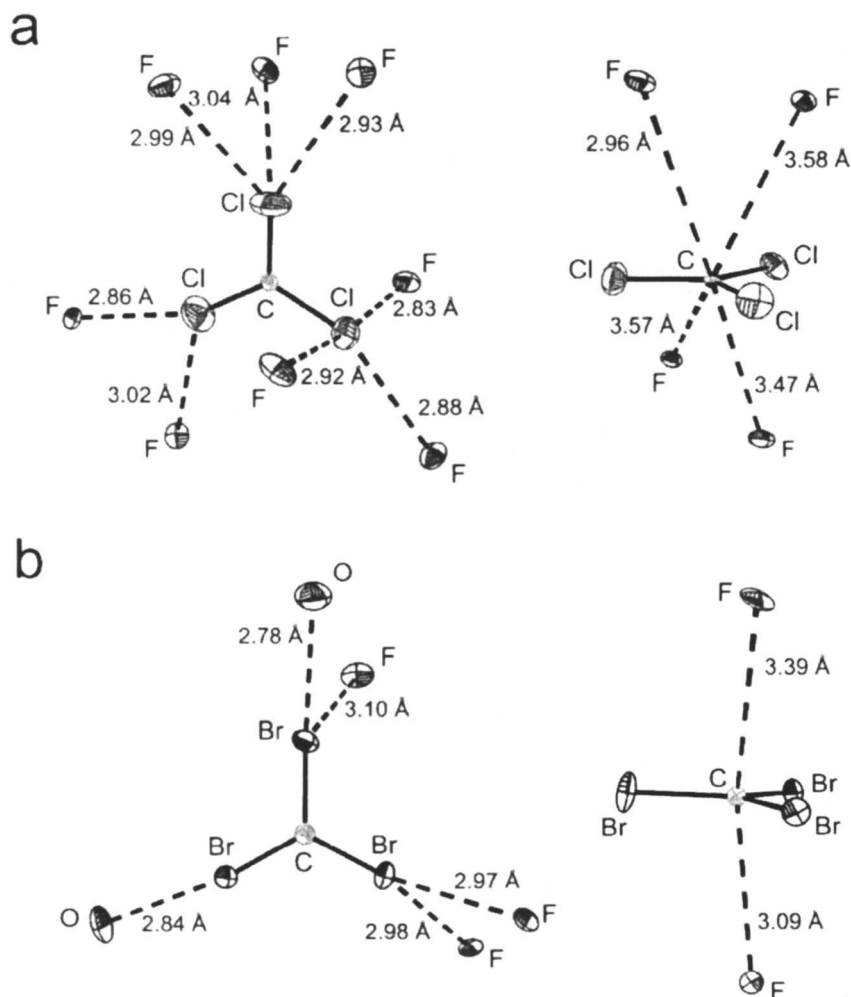


Figure 5. Diagrams showing the halogen-fluorine/oxygen and carbon-fluorine/oxygen contacts for the X-ray crystal structures of (a) CCl_3^+ in $\text{CCl}_3^+\text{Sb}(\text{OTeF}_5)_6^-$ and (b) CBr_3^+ in $\text{CBr}_3^+\text{Sb}(\text{OTeF}_5)_6^- \cdot \text{SO}_2\text{ClF}$.⁴⁷

parameters of the two coordinated and one non-coordinated SO_2ClF molecule in the $\text{C}(\text{OTeF}_5)_3^+\text{Sb}(\text{OTeF}_5)_6^-\cdot 3\text{SO}_2\text{ClF}$ structure.

The $\text{C}(\text{OTeF}_5)_3^+$ cation is isoelectronic and isostructural with the known $\text{B}(\text{OTeF}_5)_3$ molecule.⁹⁸ The $\text{C}(\text{OTeF}_5)_3^+$ cation is only the second example of a trioxy-substituted carbocation to have been isolated and characterized in the solid state by X-ray crystallography, the first being the AsF_6^- salt of the trigonal planar acidium ion of carbonic acid, $\text{C}(\text{OH})_3^+$.⁴² The O–C–O angles of the $\text{C}(\text{OTeF}_5)_3^+$ cation are equal, within $\pm 3\sigma$, to the ideal 120° angle expected for a trigonal planar arrangement. Unlike $\text{B}(\text{OTeF}_5)_3$ and $\text{C}(\text{OH})_3^+$, which have BO_3 and CO_3 arrangements that are planar by symmetry (C_{3h} point symmetry), the planarity of the CO_3 moiety of $\text{C}(\text{OTeF}_5)_3^+$ is not forced by symmetry, and the three OTeF_5 groups bonded to the central carbon atom are crystallographically independent. Despite the low local crystallographic symmetry of $\text{C}(\text{OTeF}_5)_3^+$ (C_1), the conformational geometry of the cation is very close to the optimized C_{3h} gas-phase geometry of this cation and the known solid state⁹⁸ and calculated gas-phase geometries of $\text{B}(\text{OTeF}_5)_3$.⁸² The tellurium and axial fluorine atoms are slightly out of plane and lie to one side of the CO_3 plane by 0.087 and 0.149 Å, respectively. The C–O bond lengths are similar to those in $\text{C}(\text{OH})_3^+$ [1.231(4) Å],⁴² $\text{CH}_3\text{C}(\text{OH})_2^+$ [1.265(6), 1.272(6) Å,³⁶ 1.261(7), 1.273(7) Å³⁷], and $\text{HC}(\text{OH})_2^+$ (1.239(6), 1.255(5) Å).³⁸ As expected for a positively charged isoelectronic species, the C–O bond lengths are shorter than the B–O bond lengths of $\text{B}(\text{OTeF}_5)_3$ [1.358(6) Å]⁹⁸ and the C–O–Te bond angles, which range from $125.7(7)$ to $132.4(9)^\circ$, are similar to those in $\text{B}(\text{OTeF}_5)_3$ [$132.3(4)^\circ$].⁹⁸ The bond lengths and bond angles in the OTeF_5 groups are in good agreement with those observed for the OTeF_5 groups of the $\text{Sb}(\text{OTeF}_5)_6^-$ anion and other OTeF_5 derivatives.^{73,74}

The $\text{C}(\text{OTeF}_5)_3^+$ cation has two C···O contacts [2.690(17) and 2.738(18) Å] with two SO_2ClF solvent molecules (Figure 4), which are both nearly perpendicular to the trigonal CO_3 plane, approaching the carbon atoms at angles of 1 and 3° with respect to the pseudo three-fold symmetry axis of the cation. The contact distances are shorter than the sum of carbon and oxygen van der Waals radii (3.15,⁹⁷ 3.20⁷¹ Å) and the C···F contacts in $\text{CCl}_3^+\text{Sb}(\text{OTeF}_5)_6^-$ and $\text{CBr}_3^+\text{Sb}(\text{OTeF}_5)_6^- \cdot \text{SO}_2\text{ClF}$; but are similar to the C···F contacts observed in $(\text{CH}_3)_2\text{CF}^+\text{AsF}_6^-$ [2.66(1), 2.78(1) Å] and in $(m\text{-CF}_3\text{C}_6\text{H}_4)(\text{C}_6\text{H}_5)\text{CF}^+\text{AsF}_6^-$ [2.78(1), 2.79(1) Å].³² These interactions with the weak Lewis base, SO_2ClF , reflect the high positive charge borne by the carbon atom and its substantial electrophilicity.

(c) Calculated Charge Distributions in CCl_3^+ , CBr_3^+ , and $\text{C}(\text{OTeF}_5)_3^+$ and Correlations with Their Solid State Coordination Environments. In the X-ray crystal structures of $\text{CCl}_3^+\text{Sb}(\text{OTeF}_5)_6^-$ and $\text{CBr}_3^+\text{Sb}(\text{OTeF}_5)_6^- \cdot \text{SO}_2\text{ClF}$,⁸² the chlorine and bromine atoms of the CCl_3^+ and CBr_3^+ cations interact with the fluorine atoms of the anion and, in the case of the CBr_3^+ salt, with the oxygen atoms of SO_2ClF as shown in Figures 2, 3, and 5. These interactions are shorter than or are at the limit of the sum of the accepted halogen···fluorine/oxygen van

der Waals radii (Cl...F, 3.15,⁹⁷ 3.22⁷¹ Å; Br...O, 335,⁹⁷ 337⁷¹ Å; Br...F, 3.30,⁹⁷ 3.32⁷¹ Å; I...F, 3.50,⁹⁷ 3.45⁷¹ Å). These contacts are consistent with the positive charges that have been allocated to the halogen atoms of these cations in computational studies.⁴⁷ The I...F contacts in $\text{Cl}_3^+\text{Al}(\text{OC}(\text{CF}_3)_3)_4^-$ ²³ range from 3.29 to 3.58 Å and suggest less cation-anion interaction through the halogen ligands despite the net positive charges allocated to the iodine atoms may, in part, be a consequence of the diffuse nature of the positive charges on the larger iodine ligands.

The $\text{Sb}(\text{OTeF}_5)_6^-$ salts also exhibit long contacts between the carbon atoms of CCl_3^+ [2.962(9)–3.574(11) Å] and CBr_3^+ [3.09(2), 3.39(2) Å]⁸² and the fluorine atoms of the anions which are at the limit of or longer than the sum of the carbon and fluorine van der Waals radii (3.10,⁹⁷ 3.30⁷¹ Å). The long C...F contacts of these structures are comparable to those observed in $\text{Cl}_3^+\text{Al}(\text{OC}(\text{CF}_3)_3)_4^-$ ²³ (3.26, 3.69, 3.76 Å) and are consistent with the negative charges that have been allocated to the carbon centers of all three trihalomethyl cations.⁴⁷ [also see calculated charge Distributions and Bonding in $\text{CF}_n\text{X}_{3-n}^+$ (X = Cl, Br; $n = 0-3$) and $\text{C}(\text{OTeF}_5)_3^+$]. With the exception of the shortest C...F contact distance in $\text{Cl}_3^+\text{Al}(\text{OC}(\text{CF}_3)_3)_4^-$, no other C...F contacts approach the carbocation center of Cl_3^+ along the pseudo three-fold axis of its vacant p orbital.

The coordination behaviors of the CX_3^+ (X = Cl, Br, I) cations in their presently known salts contrast with the C...F contact distances and contact angles in (*m*- $\text{CF}_3\text{C}_6\text{H}_4$)(C_6H_5) $\text{CF}^+\text{As}_2\text{F}_{11}^-$ [3.01(2), 3.07(2) Å], (*m*- $\text{CF}_3\text{C}_6\text{H}_4$)(C_6H_5) $\text{CF}^+\text{AsF}_6^-$ (2.78(1), 2.79(1) Å), and $(\text{CH}_3)_2\text{CF}^+\text{AsF}_6^-$ [2.66(1), 2.78(1) Å].²⁹ All three salts exhibit carbocation environments in which the trigonal planar cation interacts with fluorine ligands of neighboring AsF_6^- or $\text{As}_2\text{F}_{11}^-$ anions along the trajectory of the vacant p orbital of carbon to give trigonal bipyramidal coordination at the carbocation center. Moreover, the C...F contact distances are significantly shorter than the sum of the carbon and fluorine van der Waals radii (vide supra). The study notes that the coordination behaviors of these monofluorinated carbocations are consistent with positive charges at the carbocation center. The substantial positive charge on carbon was confirmed by calculations⁴⁷ for $(\text{CH}_3)_2\text{CF}^+$ at the MP2/cc-pVTZ level of theory, which also provided geometric parameters that are in good agreement with those of the experimental structure. The experimental geometric parameters for $(\text{CH}_3)_2\text{CF}^+$ are taken from ref 29 and the calculated values⁴⁷ are given in square brackets: C–C, 1.413(13), 1.450(13) Å [1.431 Å]; C–F, 1.285(11) Å [1.319 Å]; $\angle\text{C–C–C}$, 126.1(8)° [130.3°]; $\angle\text{F–C–C}$, 116.5(8), 117.3(8)° [114.8°]. NBO natural charges; methyl C (–0.740), central C (0.922), F (–0.192). Valencies; methyl C (3.956), central C (4.000), F (1.836). Ionic bond orders: C–C (0.127), C–F (1.131).

The coordination behaviors of the CX_3^+ (X = Cl, Br, I) cations also contrast with that of the $\text{C}(\text{OTeF}_5)_3^+$ cation in the crystal structure of $\text{C}(\text{OTeF}_5)_3^+\text{Sb}(\text{OTeF}_5)_6^- \cdot 3\text{SO}_2\text{ClF}$ (Figure 4).⁸² In this instance, the carbon atom

is coordinated to two oxygen ligands of two SO_2ClF molecules which again results in trigonal bipyramidal coordination around the central carbon atom, with $\text{C}\cdots\text{O}$ contacts [2.69(2), 2.74(2) Å] that are significantly less than the van der Waals radii sums for the oxygen and carbon atoms (3.15,⁹⁷ 3.20⁷¹ Å). The $\text{C}\cdots\text{O}$ contact distances and coordination around carbon are again consistent with the calculated positive charge on carbon (1.30) at the HF/(SDB)-cc-pVTZ level of theory. Moreover, this charge is similar to those predicted for CF_3^+ (1.57), BF_3 (1.56) and $\text{B}(\text{OTeF}_5)_3$ (1.45) at the HF/(SDB)-cc-pVTZ level of theory.⁸² It is worth noting that the homologous series of $\text{H}_{3-n}\text{C}(\text{ChH})_n^+$ (Ch = O, S, Se, Te) cations has been investigated by quantum mechanical calculations (natural population analysis calculations at the MP2(full)/LANL1DZ + P' level).⁹⁹ The carbon atom is positively charged for $\text{C}(\text{OH})_3^+$ (1.212), whereas the charges on carbon for the remaining members of the series are all negative, with the negative charge increasing upon descending group 16. This trend agrees well with that determined for the CX_3^+ (X = F, Cl, Br, I) series.⁴⁷

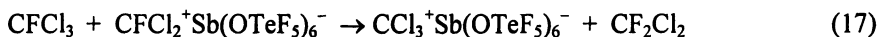
Fluorine-Containing Trihalomethyl Cations

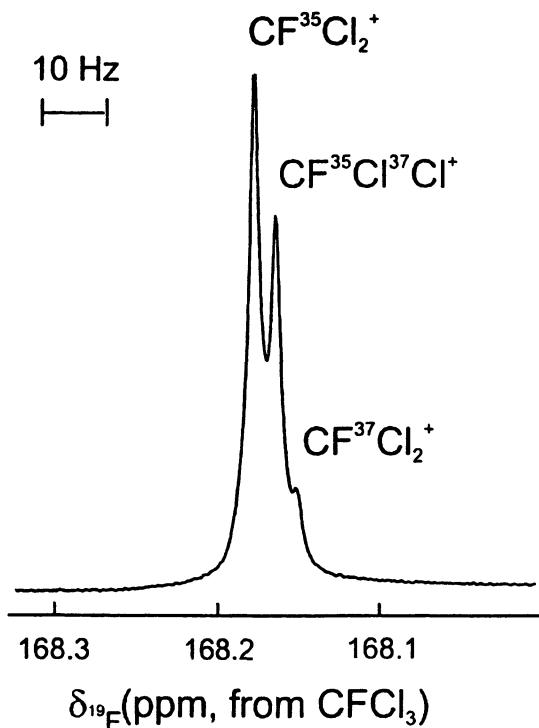
Preliminary studies have revealed that the chlorofluorocarbons (CFCs) CFCl_3 (Freon-11) and CF_2Cl_2 (Freon-12) are oxidized, albeit more slowly, by $\text{XeOTeF}_5^+\text{Sb}(\text{OTeF}_5)_6^-$ in SO_2ClF at -78°C but that CF_3Cl (Freon-13) and COClF are not oxidized at temperatures approaching room temperature. Thus far, the CFCl_2^+ cation has been synthesized (eq 16) and characterized by ^{13}C



and ^{19}F NMR spectroscopy. The ^{19}F (168.6 ppm) and ^{13}C (214.3 ppm) chemical shifts are significantly deshielded with respect to those of its parent, CFCl_3 [$\delta(^{19}\text{F})$, -1.1 ppm; $\delta(^{13}\text{C})$, 117.1 ppm; $^1J(^{19}\text{F}-^{13}\text{C})$, 335 Hz; SO_2ClF solvent at -80°C]. The large increase in $^1J(^{19}\text{F}-^{13}\text{C})$ coupling in going from CFCl_3 (335 Hz) to CFCl_2^+ (429 Hz) is consistent with the increase in s-character in going from sp^3 -hybridization to sp^2 -hybridization at the carbon center. The CFCl_2^+ cation is unambiguously established by observation of the secondary isotope shift on the ^{19}F resonance arising from ^{35}Cl and ^{37}Cl , which gives three peaks in the correct intensity ratios corresponding to the isotopomers $\text{FC}^{35}\text{Cl}_2^+$, $\text{FC}^{35}\text{Cl}^{37}\text{Cl}^+$, and $\text{FC}^{37}\text{Cl}_2^+$ (Figure 6).

It was shown by ^{13}C and ^{19}F NMR spectroscopy that the CFCl_2^+ cation undergoes ligand exchange with CFCl_3 at -50°C over a period of several hours to give $\text{CCl}_3^+\text{Sb}(\text{OTeF}_5)_6^-$ and CF_2Cl_2 (eq 17). Furthermore, the highly electrophilic CFCl_2^+ cation and ClOTeF_5 react, with redox elimination of chlorine, to give the $\text{CFCl}(\text{OTeF}_5)^+$ cation (eq 18) which has also been





	δ , ppm		1J , Hz	Isotope Shift, ppm
	^{19}F	^{13}C	$^{19}\text{F}-^{13}\text{C}$	$^2\Delta^{19}\text{F}(^{37/35}\text{Cl})$
CFCl_3	-1.1	117.1	334.6	-0.0079
CFCl_2^+	168.2	213.2	429.3	-0.0137

Figure 6. The ^{19}F NMR spectrum (470.665 MHz) and ^{19}F and ^{13}C (125.770 MHz) NMR parameters for CFCl_2^+ generated by the reaction of CF_2Cl_2 with $\text{XeOTeF}_5^+\text{Sb}(\text{OTeF}_5)_6^-$ and recorded at -78°C in SO_2ClF solvent.⁸⁶



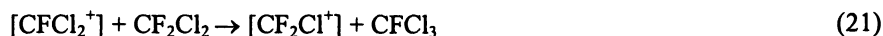
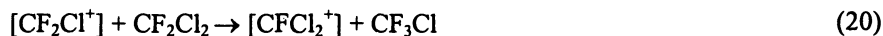
unambiguously characterized by ^{13}C and ^{19}F NMR spectroscopy [$\delta(^{13}\text{C})$ doublet, 175.4 ppm, $^1J(^{13}\text{C}-^{19}\text{F}) = 399.3$ Hz; $\delta(^{19}\text{F})$ quintet, 90.0 ppm, for fluorine bonded to carbon, $^4J(^{19}\text{F}-^{19}\text{F}_e) = 9.7$ Hz; the quintet pattern arising from coupling to the equatorial fluorines, F_e , of the OTeF_5 group shows a secondary isotope shift, $^2\Delta^{19}\text{F}(^{37/35}\text{Cl}) = -0.0099$ ppm, arising from one chlorine atom bound to carbon].

Evidence for the existence of the CFCl_2^+ cation in the solid state has been obtained from Raman spectroscopy.⁸⁶ The Raman spectrum of $\text{CFCl}_2^+\text{Sb}(\text{OTeF}_5)_6^-$, synthesized in SO_2ClF solvent at -78 °C according to eq 16 and isolated as a white solid, was obtained at -160 °C. The study provided the vibrational frequencies for CFCl_2^+ (C_{2v}) [$\nu_1(\text{A}_1)$, not observed; $\nu_3(\text{B}_2)$, 1224 cm^{-1}] $\nu_2(\text{A}_1)$, 649 cm^{-1} ; $\nu_4(\text{B}_1)$, 618 cm^{-1} ; $\nu_6(\text{B}_2)$, 448 cm^{-1} ; $\nu_3(\text{A}_1)$, 337 cm^{-1}] which were assigned with the aid of electronic structure calculations and are in good agreement with the calculated values [MP2/cc-pVTZ; $\nu_1(\text{A}_1)$, 1409; $\nu_3(\text{B}_2)$, 1191 cm^{-1} ; $\nu_2(\text{A}_1)$, 678 cm^{-1} ; $\nu_4(\text{B}_1)$, 618 cm^{-1} ; $\nu_6(\text{B}_2)$, 455 cm^{-1} ; $\nu_3(\text{A}_1)$, 338 cm^{-1}].

The reaction of CF_2Cl_2 and $\text{XeOTeF}_5^+\text{Sb}(\text{OTeF}_5)_6^-$ at -78 °C in SO_2ClF has also been studied by NMR spectroscopy (eq 19). It is proposed that the



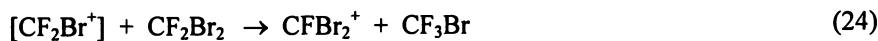
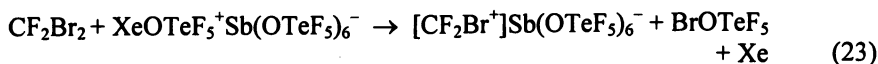
CF_2Cl^+ cation is generated, but is not observed because it rapidly undergoes halogen exchange reactions to generate CFCl_2^+ , CCl_3^+ , CFCl_3 , and CF_3Cl according to eq 20–22. This result is not unexpected as CF_2Cl^+ is destabilized



with respect to CFCl_2^+ and CCl_3^+ by virtue of the greater inductive effect of fluorine²⁹ [see calculated charge Distributions and Bonding in $\text{CF}_n\text{X}_{3-n}^+$ ($\text{X} = \text{Cl}, \text{Br}; n = 0-3$) and $\text{C}(\text{OTeF}_5)_3^+$].

Nuclear magnetic resonance spectroscopy has also been used to study the formation of the mixed bromofluoromethyl cation CFBr_2^+ . Generation of this cation has proven more difficult than CFCl_2^+ because halogen exchange is more facile in the case of bromine, and because the product, BrOTeF_5 , is more reactive towards the CFBr_2^+ cation with respect to redox elimination of Br_2 . Thus, it is proposed that the reaction of CF_2Br_2 with $\text{XeOTeF}_5^+\text{Sb}(\text{OTeF}_5)_6^-$ in

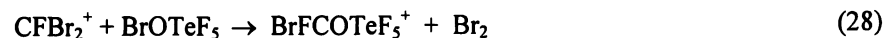
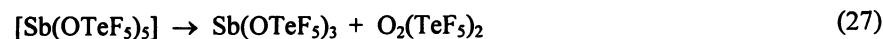
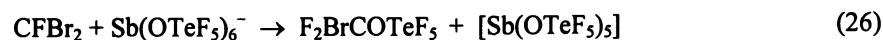
SO₂ClF at -78 °C initially yields CF₂Br⁺, which rapidly undergoes halogen exchange with CF₂Br₂ to give CFB₂⁺, CBr₃⁺, and CF₃Br (eq 23–25). Although



the reactivity of CE₂Br⁺ has precluded its direct detection by NMR spectroscopy, the CFB₂⁺ cation persists for several hours at -80 °C. As with CFC₂⁺, the ¹⁹F (207.9 ppm) and the ¹³C (208.4 ppm) chemical shifts are significantly deshielded with respect to those of its parent, CFB₃ [$\delta(^{19}\text{F})$, 7 ppm; $\delta(^{13}\text{C})$, 45.9 ppm; $^1J(^{19}\text{F}-^{13}\text{C})$, 372 Hz],¹⁰⁰ with a $^1J(^{19}\text{F}-^{13}\text{C})$ coupling (471 Hz) that is again indicative of an sp²-hybridized carbon center.

The ¹⁹F NMR spectrum also showed that BrOTeF₅ was not present in solution, but reacted with both CF₃Br and CF₂Br₂ to generate F₃COTeF₅ and F₂BrCOTeF₅. While the former is known,¹⁰¹ the latter is the first example of a mixed bromofluoro-teflate of carbon.

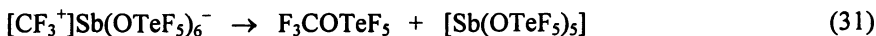
Attempts to grow crystals of CFB₂⁺Sb(OTeF₅)₆⁻ at -50 °C over several hours yielded SbBr₄⁺Sb(OTeF₅)₆⁻ instead by the following proposed reaction pathway (eq 26-29):



The SbBr₄⁺Sb(OTeF₅)₆⁻·SO₂ClF was characterized by single crystal X-ray diffraction, and the parameters determined for the cation and anion proved to be in excellent agreement with those obtained from the crystal structure of SbBr₄⁺Sb(OTeF₅)₆⁻.⁷⁴

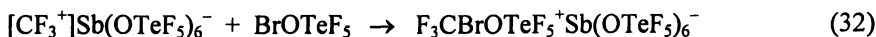
Attempts to generate persistent CF₃⁺ in solution failed, likely because of the high electrophilicity of CF₃⁺. The reaction between CF₃Br and XeOTeF₅⁺Sb(OTeF₅)₆⁻ presumably generates insipient [CF₃⁺]Sb(OTeF₅)₆⁻, which then abstracts F⁻ or OTeF₅⁻ to give CF₄ and F₃COTeF₅, respectively (eq 30 and 31). The resulting neutral antimony species are, themselves, unstable (see





eq 12 and 13).

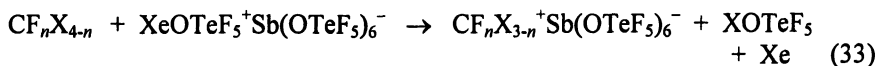
Indirect evidence for CF_3^+ as a reactive intermediate is also indicated by the formation of the $\text{F}_3\text{CBrOTeF}_5^+$ cation (eq 32) which has been



characterized by ^{13}C and ^{19}F NMR spectroscopy [$\delta(^{19}\text{F})$, -12.0 ppm; $\delta(^{19}\text{F}_{\text{eq}})$, -44.6 ppm; $\delta(^{19}\text{F})$, -48.1 ppm; $^1J(^{13}\text{C}-^{19}\text{F})$, 323 Hz; $^2J(^{19}\text{F}_{\text{eq}}-^{19}\text{F}_{\text{ax}})$, 177 Hz; $^4J(^{19}\text{F}-^{19}\text{F}_{\text{eq}})$, 4.3 Hz].

Gas-Phase Thermodynamics of Reactions of XeOTeF_5^+ with $\text{CF}_n\text{X}_{4-n}$ ($\text{X} = \text{Cl, Br}; n = 0-3$)

The calculated standard gas-phase enthalpies (ΔH°) and Gibbs free energies (ΔG°) corresponding to eq 33 are given in Scheme 1. The spontaneity



with which $\text{CF}_n\text{Cl}_{4-n}$ and $\text{CF}_n\text{Br}_{4-n}$ ($n = 0-3$) are oxidized decreases dramatically with each successive addition of a fluorine ligand. This trend is in agreement with the experimental findings. For example, CF_3Cl and $\text{XeOTeF}_5^+\text{Sb}(\text{OTeF}_5)_6^-$, are unreactive at temperatures as high as 0°C in SO_2ClF solvent,⁸⁶ with $\Delta H^\circ = -5.41$ and $\Delta G^\circ = -34.06$ kJ mol^{-1} indicating that the reaction is only slightly favored in the gas phase at 298.15 K. In contrast, the corresponding reaction with CCl_4 occurs rapidly at -78°C in SO_2ClF solvent,⁸² with $\Delta H^\circ = -158.4$ and $\Delta G^\circ = -191.9$ kJ mol^{-1} . Standard heats of reaction leading to the formation of the $\text{CF}_n\text{Br}_{3-n}^+$ cations are $55-65$ kJ mol^{-1} more favorable than their $\text{CF}_n\text{Cl}_{3-n}^+$ analogues, in accord with the anticipated relative ease of oxidation of a bromine ligand versus a chlorine ligand.

Calculated Charge Distributions and Bonding in $\text{CF}_n\text{X}_{3-n}^+$ ($\text{X} = \text{Cl, Br}; n = 0-3$) and $\text{C}(\text{OTeF}_5)_3^+$

Several prior studies have assessed the bonding and relative stabilities of the CX_3^+ ($\text{X} = \text{F, Cl, Br, and I}$) cations in terms of relative degrees of σ and $p(\pi)$ donation from the halogen atom to the carbon center.^{29,32,43} The Natural Bond Orbital (NBO) analyses have shown that the σ effect is strongly withdrawing in the case of fluorine and weakly donating in the cases of chlorine, bromine, and iodine ($\text{I} > \text{Br} > \text{Cl}$), with the $p(\pi)$ back-donation trend following the order $\text{I} > \text{Br} > \text{Cl} > \text{F}$, and are mirrored NBO charge analyses (Figure 7).

Figure 8 provides analogous assessments of charge distributions and σ and $p(\pi)$ donation for the mixed fluoro-chloro and fluoro-bromo trihalomethyl

	ΔH°	ΔG°
$\text{CCl}_4 + \text{XeOTeF}_5^+ \longrightarrow \text{CCl}_3^+ + \text{ClOTeF}_5 + \text{Xe}$	-158.4	-191.9
$\text{CFCl}_3 + \text{XeOTeF}_5^+ \longrightarrow \text{CFCl}_2^+ + \text{ClOTeF}_5 + \text{Xe}$	-121.3	-153.0
$\text{CF}_2\text{Cl}_2 + \text{XeOTeF}_5^+ \longrightarrow \text{CF}_2\text{Cl}^+ + \text{ClOTeF}_5 + \text{Xe}$	-73.3	-106.5
$\text{CF}_3\text{Cl} + \text{XeOTeF}_5^+ \longrightarrow \text{CF}_3^+ + \text{ClOTeF}_5 + \text{Xe}$	-5.4	-34.1
$\text{CBr}_4 + \text{XeOTeF}_5^+ \longrightarrow \text{CBr}_3^+ + \text{BrOTeF}_5 + \text{Xe}$	-223.2	-263.3
$\text{CFBr}_3 + \text{XeOTeF}_5^+ \longrightarrow \text{CFBr}_2^+ + \text{BrOTeF}_5 + \text{Xe}$	-188.3	-220.1
$\text{CF}_2\text{Br}_2 + \text{XeOTeF}_5^+ \longrightarrow \text{CF}_2\text{Br}^+ + \text{BrOTeF}_5 + \text{Xe}$	-140.1	-173.2
$\text{CF}_3\text{Br} + \text{XeOTeF}_5^+ \longrightarrow \text{CF}_3^+ + \text{BrOTeF}_5 + \text{Xe}$	-61.1	-89.6

Scheme 1. Gas-phase values of ΔH° and ΔG° (kJ mol^{-1}) for the reactions of XeOTeF_5^+ with $\text{CF}_n\text{X}_{4-n}$ ($\text{X} = \text{Cl, Br}$; $n = 0-3$) (MP2/cc-pVTZ).

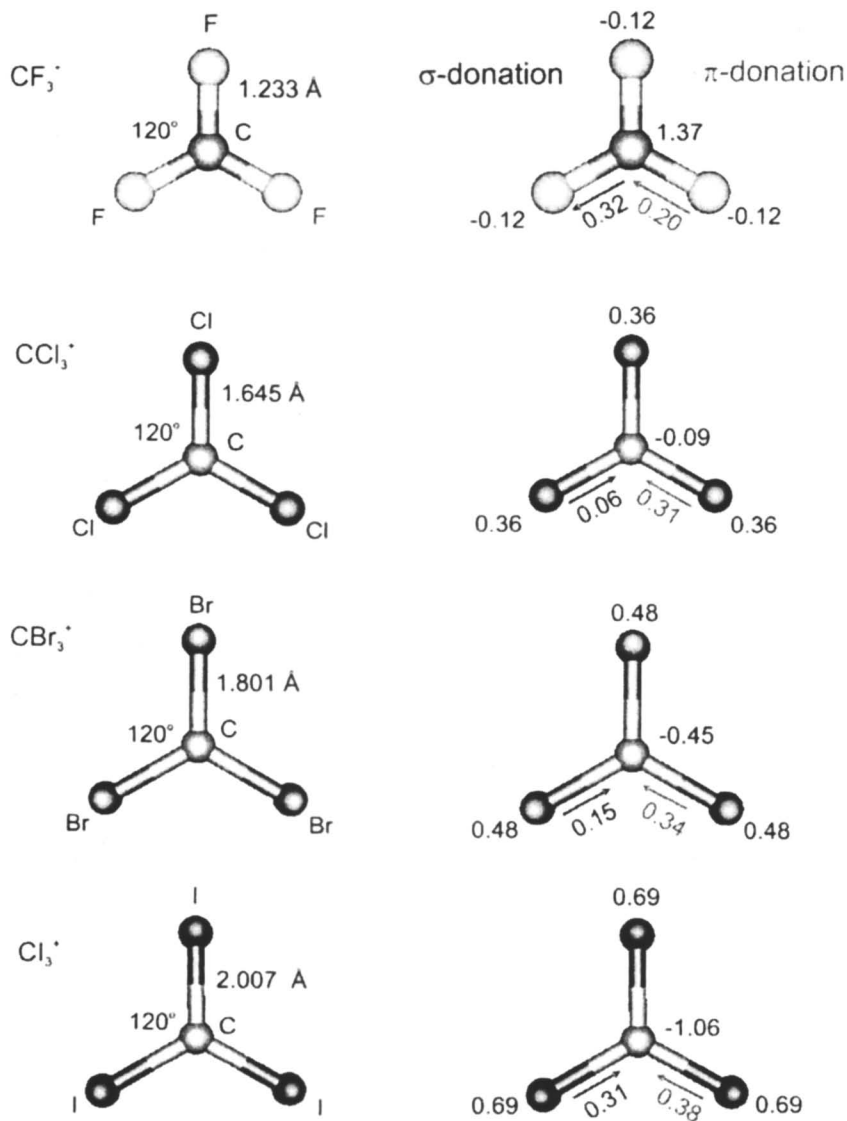


Figure 7. Calculated geometries and natural (NBO) charges for CX_3^+ ($X = F, Cl, Br$; MP2/cc-pVTZ//MP2/cc-pVTZ) and Cl_3^+ [MP2/(SDB)-cc-pVTZ//MP2/(SDB)-cc-pVTZ].

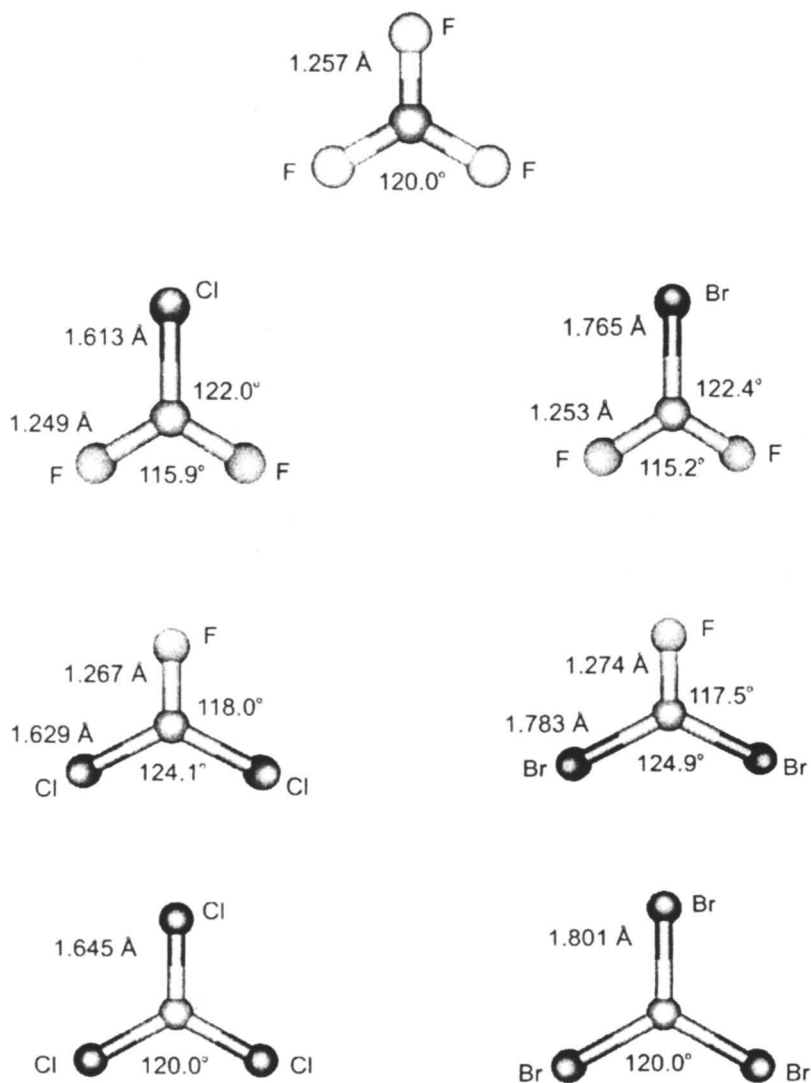


Figure 8a. Calculated geometries for $CF_nX_{3-n}^-$ ($X = Cl, Br$; MP2/cc-pVTZ).

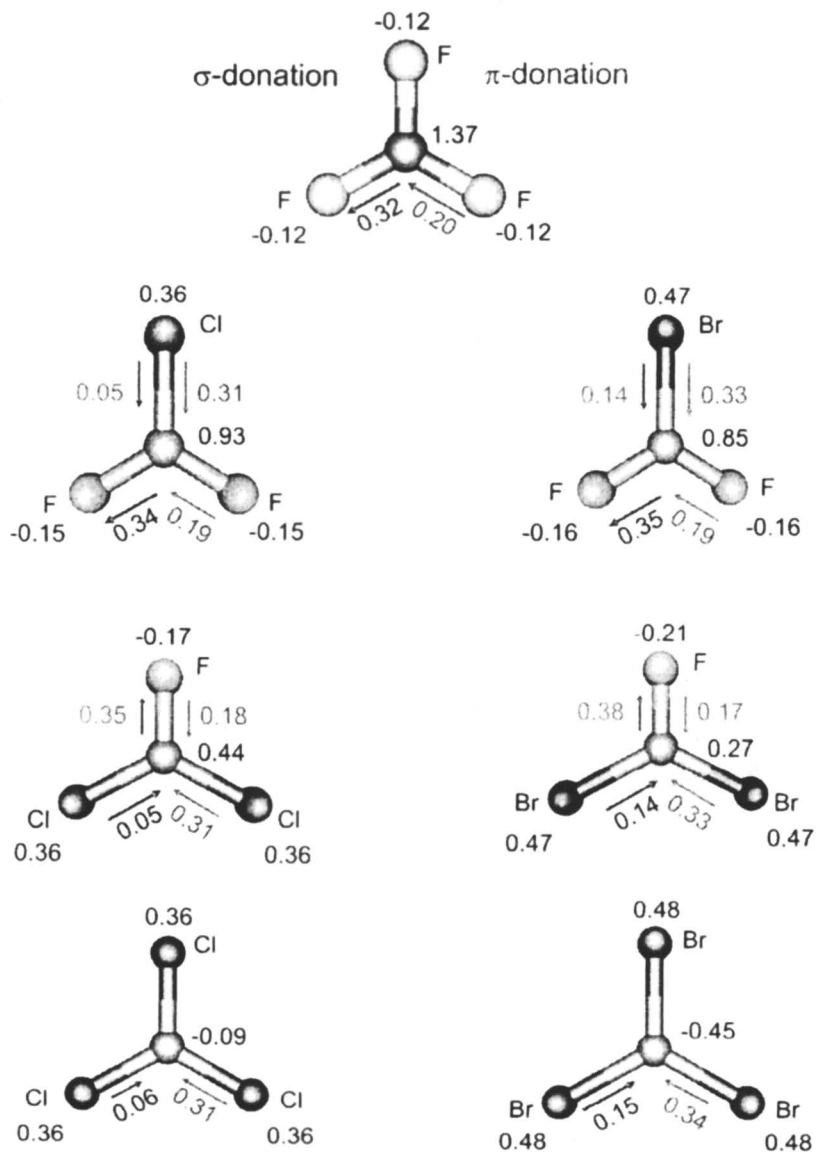


Figure 8b. Calculated natural (NBO) charges for $\text{CF}_n\text{X}_{3-n}^+$ ($X = \text{Cl}, \text{Br}$; $\text{MP2/cc-pVTZ//MP2/cc-pVTZ}$).

cations with CF_3^+ , CCl_3^+ , and CBr_3^+ included for comparison. The individual σ - and π - components are relatively constant throughout the series. The C–F σ -contribution is withdrawing but opposite to the C–F $p(\pi)$ contribution which, like all C–X contributions, are donating with respect to carbon. In all cases the π -donation, which increases along the series $\text{F} < \text{Cl} < \text{Br} < \text{I}$, serves to stabilize the positive carbon center and dominates the σ -contribution, which also increases in the same direction for Cl, Br, and I. With the exception of negative charges on the fluorine ligands, the halogen ligands are always positively charged (see Calculated charge Distributions in CCl_3^+ , CBr_3^+ , and $\text{C}(\text{OTeF}_5)_3^+$ and correlations with Their Solid State coordination Environments) and the charge on carbon becomes significantly more positive with each additional fluorine ligand that is added. Based on calculated carbon charges, the CFCl_2^+ and CFBr_2^+ cations are, thus far, the most electrophilic trihalomethyl cations that have been shown to persist. While rapid halogen exchange involving the more electrophilic CF_2Cl^+ and CF_2Br^+ cations may preclude their isolation, the isolation and characterization of a stable salt of the SO_2ClF -solvated $\text{C}(\text{OTeF}_5)_3^+$ cation, which has a carbon charge and σ - and π -components, in the absence of solvation, that are similar to those of CF_3^+ , suggests that CF_3^+ may still be attainable as a persistent entity.

Conclusions and Outlook

The present studies provide a new oxidative route to carbocations and the first solid state characterization of the previously reported CCl_3^+ and CBr_3^+ cations as well as the novel $\text{C}(\text{OTeF}_5)_3^+$ cation. The cations have been stabilized as salts of the preformed oxidatively resistant and weakly coordinating $\text{Sb}(\text{OTeF}_5)_6^-$ anion, which avoids the use of more strongly coordinating anions derived from strong Lewis acid ligand acceptors, such as SbF_5 . Despite the anticipated high electrophilicity of their cations, these salts are stable up to at least -20°C , with $\text{CCl}_3^+\text{Sb}(\text{OTeF}_5)_6^-$ being stable at room temperature for indefinite periods of time. In addition, the $\text{CBr}(\text{OTeF}_5)_2^+$ and $\text{Br}(\text{OTeF}_5)_2^+$ cations, and the neutral precursor to $\text{C}(\text{OTeF}_5)_3^+$, $\text{C}(\text{OTeF}_5)_4$, have been characterized by ^{13}C and ^{19}F NMR spectroscopy.

X-ray crystallographic studies show, in all cases, that the carbocation center is planar in the absence of symmetry constraints imposed by the crystal lattice. Despite the strong Lewis acidities predicted for perhalomethyl cations, the CCl_3^+ and CBr_3^+ cations are well isolated in their respective crystal lattices and possess only long secondary $\text{C}\cdots\text{F}$ contacts to fluorine atoms of the $\text{Sb}(\text{OTeF}_5)_6^-$ anion that do not significantly exceed the sum of the van der Waals radii of carbon and fluorine. Secondary $\text{X}\cdots\text{F}$ and $\text{X}\cdots\text{O}$ ($\text{X} = \text{Cl}, \text{Br}$) contacts that are close to the sums of the van der Waals radii of the halogen and an oxygen atom of co-crystallized SO_2ClF or a fluorine atom of the anion exist for CCl_3^+ and CBr_3^+ that are in accord with the calculated positive charges on the halogen atoms of both cations.

Computational studies reproduce the experimental geometric parameters of CCl_3^+ , CBr_3^+ and $\text{C}(\text{OTeF}_5)_3^+$, and the vibrational frequencies of CCl_3^+ and CBr_3^+ , and have been extended to their OTeF_5 derivatives.⁸² Contrasting with the CCl_3^+ and CBr_3^+ cations, the $\text{C}(\text{OTeF}_5)_3^+$ cation possesses two short $\text{C}\cdots\text{O}$ contacts to the oxygen atoms of two weakly basic, co-crystallized SO_2ClF molecules, which is consistent with the high positive charge on carbon predicted by electron structure calculations and which approximates that of the highly electrophilic CF_3^+ cation.

Nuclear magnetic resonance spectroscopy has also been used to great advantage to establish the existence of CCl_3^+ , CBr_3^+ , CFCl_2^+ , CFBr_2^+ and $\text{C}(\text{OTeF}_5)_6^-$ as persistent cations in SO_2ClF at low temperatures, as well as to monitor carbocation formation, ligand substitution by means of redox elimination, and decomposition pathways in these systems and in on-going studies.

Attempts to obtain evidence for persistent CF_2Cl^+ , CF_2Br^+ , and CF_3^+ have met with limited success. The study has presently been limited by the $\text{Sb}(\text{OTeF}_5)_6^-$ anion and the OTeF_5 ligand, which provide sufficiently strong nucleophilic sites that can be attacked by these extremely strong electrophiles. While the use of $\text{XeOTeF}_5^+\text{Sb}(\text{OTeF}_5)_6^-$ has proven successful in providing an oxidative routes to CCl_3^+ , CBr_3^+ , and $\text{C}(\text{OTeF}_5)_3^+$ in the solid state and solution, the only examples of persistent mixed chlorofluoro- and bromofluoro-cations that have been characterized in the course of these studies are the monofluorinated CFCl_2^+ and CFBr_2^+ cations. Although both cations are sufficiently long-lived to permit their low temperature characterization in solution by NMR spectroscopy, the only fluorine-containing trihalomethyl cation to have been isolated in the solid state is the CFCl_2^+ which, thus far, has been characterized by low-temperature Raman spectroscopy. Prospects for stabilizing CF_2Cl^+ , CF_2Br^+ , and CF_3^+ will hinge upon the use of a more weakly-coordinating, less nucleophilic, anion that is resistant to oxidative attack by the noble-gas cation, as well as to electrophilic attack by the fluoro-carbocation, and the formation of other reaction products that are not susceptible to electrophilic attack by the fluoro-carbocation.

Acknowledgement

We thank the donors of the Petroleum Research Fund, administered by the American Chemical Society, for support of this work under ACS-PRF No. 40959-AC3.

References

1. Olah, G. A.; Rasul, G.; Yudin, A. K.; Burrichter, A.; Prakash, G. K. S.; Chistyakov, A. L.; Stankevich, I. V.; Akhrem, I. S.; Gambaryan, N. P.; Vol'pin, M. E. *J. Am. Chem. Soc.* **1996**, *118*, 1446-1451 and references therein.

2. Martin, R. H.; Lampe, F. W.; Taft, R. W. *J. Am. Chem. Soc.* **1966**, *88*, 1353–1357.
3. Lias, S. G.; Eyler, J. R.; Ausloos, P. *Int. J. Mass Spectrom. Ion Phys.* **1976**, *19*, 219–239.
4. Jacox, M. E.; Milligan, D. E. *J. Chem. Phys.* **1971**, *54*, 3935–3950.
5. Jacox, M. E. *Chem. Phys.* **1976**, *12*, 51–63.
6. Vančik, H.; Percač, K.; Sunko, D. E. *J. Am. Chem. Soc.* **1990**, *112*, 7418–7419.
7. Abboud, J.-L. M.; Castaño, O.; Herreros, M.; Elguero, J.; Jagerovic, N.; Notario, R.; Sak, K. *Int. J. Mass Spectrom. Ion Processes* **1998**, *175*, 35–40.
8. Prochaska, F. T.; Andrews, L. *J. Am. Chem. Soc.* **1978**, *100*, 2102–2108.
9. Prochaska, F. T.; Andrews, L. *J. Phys. Chem.* **1978**, *82*, 1731–1742.
10. Jacox, M. E. *Chem. Phys.* **1984**, *83*, 171–180.
11. Forney, D.; Jacox, M. E.; Irikura, K. K. *J. Chem. Phys.* **1994**, *101*, 8290–8295.
12. Maclagan, R. G. A. R. *J. Mol. Struct. (Theochem)* **1991**, *235*, 21–24.
13. Langford, M. L.; Harris, F. M. *Int. J. Mass Spectrom. Ion Processes* **1990**, *96*, 111–113.
14. Sheng, L.; Qi, F.; Gao, H.; Zhang, Y.; Yu, S.; Li, W.-K. *Int. J. Mass Spectrom. Ion Processes* **1997**, *161*, 151–159.
15. Seccombe, D. P.; Tuckett, R. P.; Fisher, B. O. *J. Chem. Phys.* **2001**, *114*, 4074–4088.
16. Lee, M. S.; Park, M.; Chung, Y. *J. Korean Phys. Soc.* **2003**, *42*, 493–498.
17. Domazou, A. S.; Quadir, M. A.; Buehler, R. E. *J. Phys. Chem.* **1994**, *98*, 2877–2822.
18. Prochaska, F. T.; Andrews, L. *J. Chem. Phys.* **1978**, *68*, 5568–5576.
19. Prochaska, F. T.; Andrews, L. *J. Chem. Phys.* **1978**, *68*, 5577–5586.
20. Truszkowski, S.; Ichikawa, T. *J. Phys. Chem.* **1989**, *93*, 4522–4526.
21. Olah, G. A.; Heiliger, L.; Prakash, G. K. S. *J. Am. Chem. Soc.* **1989**, *111*, 8020–8021.
22. Olah, G. A.; Rasul, G.; Heiliger, L.; Prakash, G. K. S. *J. Am. Chem. Soc.* **1996**, *118*, 3580–3583.
23. Krossing, I.; Bihlmeier, A.; Raabe, I.; Trapp, N. *Angew. Chem., Int. Ed. Engl.* **2003**, *42*, 1531–1534.
24. Laube, T. *Chem. Rev.* **1998**, *98*, 1277–1312.
25. Müller, T.; Juhasz, M.; Reed, C. A. *Angew. Chem., Int. Ed. Engl.* **2004**, *43*, 1543–1546.
26. Kato, T.; Reed, C. A. *Angew. Chem., Int. Ed. Engl.* **2004**, *43*, 2908–2911.
27. Kato, T.; Stoyanov, E. S.; Geier, J.; Grützmacher, H.; Reed, C. A. *J. Am. Chem. Soc.* **2004**, *126*, 12451–12457.
28. Antel, J.; Klaus, H.; Jones, P. G.; Mews, R.; Sheldrick, G. M.; Waterfeld, A. *Chem. Ber.* **1985**, *118*, 5006–5008.
29. Christe, K. O.; Zhang, X.; Bau, R.; Hegge, J.; Olah, G. A.; Prakash, G. K. S.; Sheehy, J. A. *J. Am. Chem. Soc.* **2000**, *122*, 481–487.

30. Minkwitz, R.; Reinemann, S.; Blecher, O.; Hartl, H.; Brüdgam, I. *Inorg. Chem.* **1999**, *38*, 844–847.
31. Laube, T.; Bannwart, E.; Hollenstein, S. *J. Am. Chem. Soc.* **1993**, *115*, 1731–1733.
32. Christe, K. O.; Hoge, B.; Boatz, J. A.; Prakash, G. K. S.; Olah, G. A.; Sheehy, J. A. *Inorg. Chem.* **1999**, *38*, 3132–3142.
33. Davlieva, M. G.; Lindeman, S. V.; Neretin, I. S.; Kochi, J. K. *J. Org. Chem.* **2005**, *70*, 4013–4021.
34. Minkwitz, R.; Meckstroth, W.; Preut, H. *Z. Anorg. Allg. Chem.* **1992**, *617*, 136–142.
35. Minkwitz, R.; Meckstroth, W.; Preut, H. *Z. Naturforsch., B: Chem. Sci.* **1992**, *48*, 19–22.
36. Jönsson, P.-G.; Olovsson, I. *Acta Crystallogr.* **1968**, *B24*, 559–564.
37. Kwick, Å.; Jönsson, P.-G.; Olovsson, I. *Inorg. Chem.* **1969**, *8*, 2775–2780.
38. Minkwitz, R.; Schneider, S.; Seifert, M. *Z. Anorg. Allg. Chem.* **1996**, *622*, 1404–1410.
39. Lindeman, S. V.; Neretin, I. S.; Davlieva, M. G.; Kochi, J. K. *J. Org. Chem.* **2005**, *70*, 3263–3266.
40. Caira, M. R.; De Wet, J. F. *Acta Crystallogr.* **1981**, *B37*, 709–711.
41. Paulsen, H.; Dammeyer, R. *Chem. Ber.* **1973**, *106*, 2324.
42. Minkwitz, R.; Schneider, S. *Angew. Chem., Int. Ed. Engl.* **1999**, *38*, 714–715.
43. Frenking, G.; Fan, S.; Marchand, C. M.; Grützmacher, H. *J. Am. Chem. Soc.* **1997**, *119*, 6648–6655.
44. Kaupp, M.; Malkina, O. L.; Malkin, V. G. *Chem. Phys. Lett.* **1997**, *265*, 55–59.
45. Robinson, E. A.; Johnson, S. A.; Tang, T.-H.; Gillespie, R. *J. Inorg. Chem.* **1997**, *36*, 3022–3030.
46. Robinson, E. A.; Heard, G. L.; Gillespie, R. *J. Mol. Struct.* **1999**, *485-486*, 305–319.
47. Mercier, H. P. A.; Moran, M. D.; Schrobilgen, G. J.; Suontamo, R. *J. Fluorine Chem.* **2004**, *125*, 1563–1578.
48. Lehmann, J. F.; Mercier, H. P. A.; Schrobilgen, G. *J. Coord. Chem. Rev.* **2002**, *233-234*, 1–39.
49. Minkwitz, R.; Bäck, B. In *Inorganic Fluorine Chemistry, Toward the 21st Century*; Thrasher, J. S., Strauss, S. H., Eds.; ACS Symposium Series 555; Washington, DC, 1994; Chapter 6, pp 90–103.
50. Minkwitz, R.; Nowicki, G. *Angew. Chem., Int. Ed. Engl.* **1990**, *29*, 688–689.
51. Minkwitz, R.; Molsbeck, W. *Z. Anorg. Allg. Chem.* **1992**, *607*, 175–176.
52. Minkwitz, R.; Bernstein, D.; Preut, H.; Sartori, P. *Inorg. Chem.* **1991**, *30*, 2157–2161.
53. Hartl, H.; Nowicki, J.; Minkwitz, R. *Angew. Chem., Int. Ed. Engl.* **1991**, *30*, 328–329.

54. Clegg, M. J.; Downs, A. J. *J. Fluorine Chem.* **1989**, *45*, 13.
55. Stein, L. *J. Fluorine Chem.* **1982**, *20*, 65–74.
56. Brown, D. R.; Clegg, M. J.; Downs, A. J.; Fowler, R. C.; Minihan, A. R.; Norris, J. R.; Stein, L. *Inorg. Chem.* **1992**, *31*, 5041–5052.
57. Drews, T.; Seppelt, K. *Angew. Chem., Int. Ed. Engl.* **1997**, *36*, 273–274.
58. Frohn, H.-J.; Klose, A.; Henkel, G. *GIT Fachz. Lab.* **1993**, *37*, 752–755.
59. Frohn, H.-J.; Klose, A.; Henkel, G. In *11th Winter Fluorine Conference*; St. Petersburg, FL, January 1993; Paper 58.
60. Lentz, D.; Seppelt, K. *Angew. Chem., Int. Ed. Engl.* **1978**, *17*, 355–356.
61. Birchall, T.; Myers, R. D.; de Waard, H.; Schrobilgen, G. *J. Inorg. Chem.* **1982**, *21*, 1068–1073.
62. Sladky, F. O. *Monatsh. Chem.* **1970**, *101*, 1559–1570.
63. Sladky, F. O. *Monatsh. Chem.* **1970**, *101*, 1571–1577.
64. Sladky, F. O. *Monatsh. Chem.* **1970**, *101*, 1578–1582.
65. Sladky, F. O. *Angew. Chem., Int. Ed. Engl.* **1970**, *9*, 375–376.
66. Lentz, D.; Seppelt, K. *Angew. Chem., Int. Ed. Engl.* **1978**, *17*, 356–361.
67. Lentz, D.; Seppelt, K. *Angew. Chem., Int. Ed. Engl.* **1979**, *18*, 66–67.
68. Fir, B. A.; Mercier, H. P. A.; Sanders, J. C. P.; Dixon, D. A.; Schrobilgen, G. J. *J. Fluorine Chem.* **2001**, *110*, 89–107.
69. Keller, N.; Schrobilgen, G. J. *Inorg. Chem.* **1981**, *20*, 2118–2129.
70. Sanders, J. C. P.; Schrobilgen, G. J. *J. Chem. Soc., Chem. Commun.* **1989**, 1576–1578.
71. Bondi, A. J. *Phys. Chem.* **1964**, *68*, 441–451.
72. Elliott, H. S. A.; Lehmann, J. F.; Schrobilgen, G. J., unpublished results.
73. Mercier, H. P. A.; Sanders, J. C. P.; Schrobilgen, G. J. *J. Am. Chem. Soc.* **1994**, *116*, 2921–2937.
74. Casteel, W. J.; Kolb, P.; LeBlond, N.; Mercier, H. P. A.; Schrobilgen, G. J. *Inorg. Chem.* **1996**, *35*, 929–942.
75. Syvret, R. G.; Mitchell, K. M.; Sanders, J. C. P.; Schrobilgen, G. J. *Inorg. Chem.* **1992**, *31*, 3381–3385.
76. Selig, H.; Holloway, J. H., In *Topics in Current Chemistry*; Boschke, F. L., Ed.; Springer-Verlag: Berlin, 1984; Vol. 124, pp 33–90.
77. Brownstein, M.; Gillespie, R. J. *J. Am. Chem. Soc.* **1970**, *92*, 2718–2721.
78. Dean, P. A. W.; Gillespie, R. J. *J. Am. Chem. Soc.* **1969**, *91*, 7260–7264.
79. Mercier, H. P. A.; Moran, M. D.; Sanders, J. C. P.; Schrobilgen, G. J.; Suontamo, R. J. *Inorg. Chem.* **2005**, *44*, 49–60.
80. Holloway, J. H.; Hope, E. G. *Adv. Inorg. Chem.* **1998**, *46*, 51–100.
81. Drews, T.; Seppelt, K. *Z. Anorg. Allg. Chem.* **1991**, *606*, 201–207.
82. Mercier, H. P. A.; Moran, M. D.; Schrobilgen, G. J.; Steinberg, C.; Suontamo, R. J. *J. Am. Chem. Soc.* **2004**, *126*, 5533–5548.
83. Seppelt, K. *Z. Anorg. Allg. Chem.* **1973**, *399*, 65–72.
84. Seppelt, K. *Chem. Ber.* **1973**, *106*, 1920–1926.
85. Gerken, M.; Kolb, P.; Wegner, A.; Mercier, H. P. A.; Borrmann, H.; Dixon, D. A.; Schrobilgen, G. J. *Inorg. Chem.* **2000**, *39*, 2813–2824.

86. Mercier, H. P. A.; Moran, M. D.; Schrobilgen, G. J., unpublished results.
87. Vladimiroff, T.; Malinowski, E. R. *J. Chem. Phys.* **1967**, *46*, 1830–1841.
88. Hartman, J. S.; Schrobilgen, G. J. *Inorg. Chem.* **1972**, *11*, 940–951.
89. Gombler, W. *Spectrochim. Acta., Part A* **1981**, *37*, 57–61.
90. Timoshkin, A. Y.; Suvorov, A. V.; Bettinger, H. F.; Schaefer, H. F. I. *J. Am. Chem. Soc.* **1999**, *121*, 5687–5699.
91. Lentz, D.; Seppelt, K. *Z. Anorg. Allg. Chem.* **1983**, *502*, 83–88.
92. The ${}^2J({}^{13}\text{C}-{}^{123}\text{Te})$ coupling of 57 Hz was calculated using the relationship ${}^nJ_{\text{AB}} = (\gamma_{\text{A}}^n J_{\text{AB}} / \gamma_{\text{A}'}^n)$, where $\text{A} = {}^{123}\text{Te}$ $\text{B} = {}^{13}\text{C}$, and γ_{A} and $\gamma_{\text{A}'}$ are the gyromagnetic ratios of ${}^{123}\text{Te}$ and ${}^{125}\text{Te}$, respectively.
93. The calculated value of ${}^2J({}^{13}\text{C}-{}^{123}\text{Te})$ is 53 Hz (see ref 92).
94. Cohen, S.; Powers, R.; Rudman, R. *Acta. Crystallogr.* **1979**, *B35*, 1670–1674.
95. Cockcroft, J. K.; Fitch, A. N. *Z. Kristallogr.* **1994**, *209*, 488–490.
96. More, M.; Baert, F.; Lefebvre, J. *Acta. Crystallogr.* **1977**, *B33*, 3681–3684.
97. Pauling, L., *The Nature of the Chemical Bond*. 3rd ed.; Cornell University Press: Ithaca, New York, 1960, p 260.
98. Sawyer, J. F.; Schrobilgen, G. J. *Acta. Crystallogr.* **1982**, *B38*, 1561–1563.
99. Ohlmann, D.; Marchand, C. M.; Grützmacher, H.; Chen, G. S.; Farmer, D.; Glaser, R.; Currao, A.; Nesper, R.; Pritzkow, H. *Angew. Chem., Int. Ed. Engl.* **1996**, *35*, 300–303.
100. Muller, N.; Carr, D. T. *J. Phys. Chem.* **1963**, *67*, 112–115.
101. Schack, C. J.; Christe, K. O. *J. Fluorine Chem.* **1990**, *47*, 79–87.

Chapter 20

Organoxenonium Salts: Synthesis by “Xenodeborylation”, Reactivities, and NMR Spectroscopic Properties

H.-J. Frohn^{1*} and V. V. Bardin²

¹Department of Chemistry, Inorganic Chemistry, University of Duisburg-
Essen, Duisburg, Germany

²N. N. Vorozhtsov Novosibirsk Institute of Organic Chemistry, SB RAS,
Novosibirsk, Russia

Organoxenonium(II) salts [R_{Xe}]Y are synthesized by the reaction of XeF₂ with the corresponding organodifluoroboranes, RBF₂. This general method was successful in case of R = aryl, alkynyl, and alkenyl. Extended to XeF₄, it allowed the synthesis of [C₆F₅XeF₂][BF₄]. The reactivity of organoxenonium salts is mainly based on the electrophilic nature on the cation. Typical examples of reactivities with different types of nucleophiles (negatively charged, neutral π- and n-nucleophiles) are reported. Multinuclear NMR spectroscopic properties for [R_{Xe}]Y and [C₆F₅XeF₂][BF₄] salts in acidic and basic solvents are presented and discussed.

Syntheses of Organoxenonium Salts

Only the thermodynamically stable binary xenon fluorides, XeF_2 , XeF_4 , and XeF_6 (1), present a realistic source of organoxenonium salts. Starting from the fluorides having a valence electron decet, dodecet, and quadruccet, respectively, the general synthetic strategy used to form organoxenonium salts entails substitution of one fluorine atom by an appropriate organo group and abstraction of a second fluorine by a Lewis acid, fluoride acceptor (EF_n), to give the $[\text{EF}_{n+1}]$ anion.

How many Types of Organoxenonium Cations may be considered?

At least three types of organoxenonium salts have to be considered, namely, $[\text{RXe}][\text{EF}_{n+1}]$, $[\text{RXeF}_2][\text{EF}_{n+1}]$, and $[\text{RXeF}_4][\text{EF}_{n+1}]$. In case of Xe(IV and VI) polyfluoro(polyorgano)xenonium salts, $[\text{R}_m\text{XeF}_{3-m}][\text{EF}_{n+1}]$, and $[\text{R}_k\text{XeF}_{5-k}][\text{EF}_{n+1}]$ ($m = 2, 3$, $k = 2-5$), may also prove possible, but have not been explored. The actual scope of known organoxenonium salts presently spans two types, namely $[\text{RXe}][\text{EF}_{n+1}]$ and $[\text{RXeF}_2][\text{EF}_{n+1}]$. A preliminary attempt to obtain the first organo derivative of XeF_6 , $[\text{RXeF}_4][\text{BF}_4]$, failed (2).

The First Decade of C-Xe Chemistry: Fundamental Aspects of the Syntheses of Organoxenonium Salts

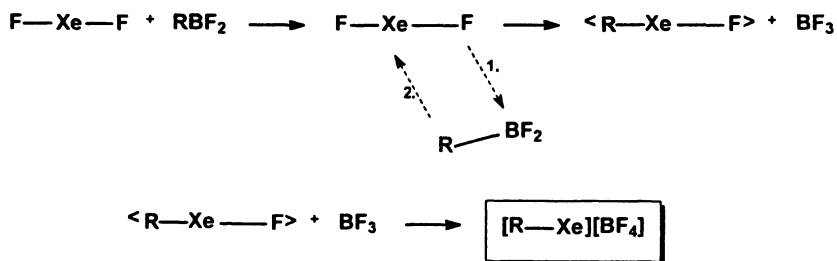
The preparative chemistry of organoxenon compounds was established in 1989 when Naumann and Tyrra (3), and Frohn and Jakobs (4) independently reported the first synthesis of organoxenonium(II) compounds, $[\text{C}_6\text{F}_5\text{Xe}][(\text{C}_6\text{F}_5)_n\text{BF}_{4-n}]$ ($n = 1, 3$). Thereafter, a variety of organoxenonium(II) salts $[\text{RXe}]\text{Y}$ ($\text{R} = \text{aryl, alkenyl, cycloalkenyl, and alkynyl}$) and molecular organoxenon compounds, such as arylxenonacyloxy, -halogen, or -pseudo-halogen compounds, R-Xe-X , and di(aryl)xenon(II) compounds, Ar-Xe-Ar' were prepared. The first organoxenonium(IV) salt, $[\text{C}_6\text{F}_5\text{XeF}_2][\text{BF}_4]$, was reported in 2000 (5).

In 2001–2002, comprehensive reviews (6–8) on the preparation and reactivity of carbon-xenon compounds have been published covering the literature until 2000–2001. The objective of this chapter is to highlight the progress that was achieved during the first decade, to discuss more recent progress, and to identify areas that are open for further investigation.

Topics related to the synthesis and reactivity of organoxenonium compounds are therefore in the foreground. In case of the analytical characterization of C-Xe

compounds we focus on multinuclear NMR spectroscopic properties. Thus, the scope of the present review is primarily geared to those readers who are particularly interested in the preparative aspects of organoxenon chemistry. Consequently, C-Xe chemistry in the gas phase (9), in the matrix (10), and by radiochemical methods (β decay of C- ^{131}I compounds) (11) are excluded.

The nucleophilic substitution of fluorine in xenon fluorides XeF_n ($n = 2, 4, 6$) by an organo group R is an obvious approach to RXeF_{n-1} molecules. Before discussing practical solutions, it is useful to summarize the most important factors that influence this reaction. Because of the lower oxidation state of xenon, XeF_2 is the most promising candidate for F vs. R substitution reactions among the three xenon fluorides. Xenon difluoride possesses a higher fluoride donor strength than XeF_4 as a result of the lower positive partial charge on Xe(II). Despite the high polarity of the Xe-F bond, the linear molecule XeF_2 with its hypervalent 3c-4e bond possesses no permanent dipole moment, which is kinetically not advantageous in polar reactions. The oxidation potential of XeF_2 does not allow the application of a direct nucleophilic substitution by carbanions or related species with strongly reducing properties. By contrast, moderate Lewis acidic boranes, BR_3 , R_2BF , and RBF_2 constitute unique reagents that fulfill two important requirements: a) they are able to polarize the 3c-4e F-Xe-F bond without complete abstraction of fluoride and generation of the strongly oxidizing $[\text{FXe}]^+$ cation and thereby they increase the electrophilicity on Xe(II) and open a route to the successful F vs. R substitution, b) the fluoroboranes, R_2BF , RBF_2 , or BF_3 , formed in the first step, can abstract a fluoride anion from the intermediate product, R-Xe-F, yielding the onium salts, $[\text{RXe}][\text{R}_2\text{BF}_2]$, $[\text{RXe}][\text{RBF}_3]$, or $[\text{RXe}][\text{BF}_4]$. The approach of the formal substitution of the BX_2 group in RBX_2 by Xe^+ derived from XeF_2 is characterized as “xenodeborylation” and illustrated in Scheme 1.

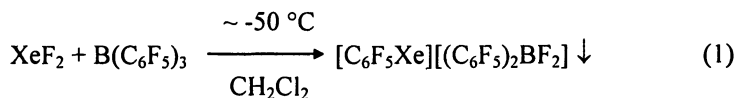


Scheme 1. Reaction of XeF_2 with organodifluoroboranes leading to organoxenonium tetrafluoroborates.

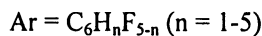
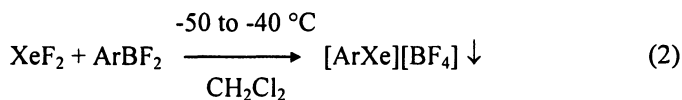
The first step, the interaction of the fluorobase XeF₂ (fluoride donor) with a fluoroacid, e.g., RBX₂ (X = R, F), (fluoride acceptor) increases the electrophilicity of Xe(II), as described above, and in parallel the nucleophilicity of the *ipso*-carbon of R. The latter arises from an increase in the p-orbital contribution at boron (change from sp² to sp³ hybridization of boron) as a result of the acid-base interaction. In parallel, the nature of the reagent changes from borane to borate anion. In part, negative charge of the anion is shifted to the organo group R which, in turn, increases its nucleofugality.

All attempts to substitute trigonalplanar boranes for moderately strong Lewis acids having tetrahedral or trigonalbipyramidal configurations in the acid-assisted F vs. R substitution in XeF₂ have failed thus far. Consequently, the reaction of XeF₂ with boranes will be the subject of discussion here.

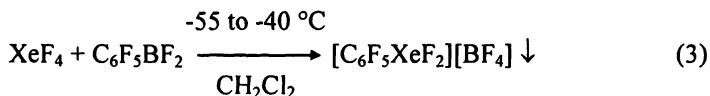
The initial preparations of arylxenonium salts were performed by reacting XeF₂ with BAr₃ (Ar = aryl) in CH₂Cl₂ which was the favored solvent in the low temperature reaction. The desired arylxenonium salts precipitated and thus could easily be isolated. Here the gain in lattice energy is one of the main driving forces and an important stabilizing factor for the intrinsically unstable products. All known arylxenonium salts contain electron-withdrawing substituents (F, (12–15) CF₃, (12, 13) Cl, (15, 16) NO₂ (17)) on the phenyl group. However, the application of BAr₃ in CH₂Cl₂ has two disadvantages: only one third of the aryl groups can be introduced into the xenonium cation, two thirds remain in the anion, [Ar₂BF₂]⁻ (eq 1) (18). The presence of aryl groups in the anion increases its nucleophilicity and lowers the thermal stability of the arylxenonium salt.



All three aryl groups can be transferred onto the Xe(II) moiety when XeF₂ is reacted with B(C₆F₅)₃ in anhydrous HF (aHF) (19). The resulting [C₆F₅Xe]⁺ salt contains [BF₄]⁻ and [HF₂]⁻ anions in the ratio 1 : 2. Protodeborylation of B(C₆F₅)₃ in aHF is suppressed because of the electron-poor nature of the aryl groups. In 1999 important progress in the synthesis of arylxenonium salts was achieved. The ready availability of ArBF₂, produced by fluoride abstraction from the corresponding K[ArBF₃] salts, offered a generally applicable approach to arylxenonium salts (eq 2). (20)



The same method was also applied to synthesize the first, and until now, the only example of a Xe(IV)-containing arylxenonium salt, $[\text{C}_6\text{F}_5\text{XeF}_2][\text{BF}_4]$ (eq 3) (5).



In order to obtain pure $[\text{C}_6\text{F}_5\text{XeF}_2][\text{BF}_4]$, it is important to avoid any excess of $\text{C}_6\text{F}_5\text{BF}_2$ during the preparation, otherwise an admixture of the reduction product, $[\text{C}_6\text{F}_5\text{Xe}][\text{BF}_4]$, is formed. The $[\text{C}_6\text{F}_5\text{XeF}_2]^+$ cation was also detected by multinuclear NMR spectroscopy when XeF_6 was reacted with $\text{C}_6\text{F}_5\text{BF}_2$ in SO_2ClF (2).

Current Progress in the Syntheses of Organoxenonium Salts

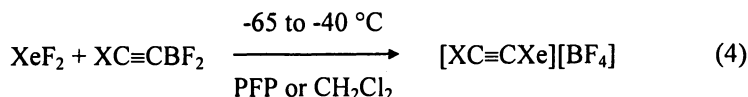
In the following section two aspects are discussed: a) the syntheses of fluorinated and non-fluorinated alkynylxenonium salts, $[\text{XC}\equiv\text{CXe}][\text{BF}_4]$, and b) the syntheses of polyfluoroalkenylxenonium salts $[\text{XCF}=\text{CFXe}][\text{BF}_4]$ and $[\text{CF}_2=\text{CXXe}][\text{BF}_4]$. These topics will provide further insight into the fundamental aspects regarding xenon-carbon bond formation.

The reaction of XeF_2 with perfluorinated and non-fluorinated alk-1-yn-1-yl difluoroboranes

Alkynyl difluoroboranes, $\text{XC}\equiv\text{CBF}_2$, like aryl difluoroboranes do not possess a substituent in addition to the BF_2 group at C-1 and their fluoride affinities of prototypical species vary from 68.9 ($\text{X} = \text{CH}_3$) to 89.0 ($\text{X} = \text{CF}_3$), while the fluoride affinity of $\text{C}_6\text{F}_5\text{BF}_2$ is 85.1 kcal mol^{-1} (21). The greater Lewis acidity of $\text{XC}\equiv\text{CBF}_2$ results in a remarkable enhancement in the competing reaction of XeF_2 with CH_2Cl_2 solvent. Therefore, commercially available hydrofluorocarbons such as 1,1,1,3,3-pentafluoropropane (PEP) (mp < -100 °C, bp 15 °C) and 1,1,1,3,3-pentafluorobutane (PFB) (mp ~ -35 °C, bp 40 °C) were substituted as solvents (22).

A representative series of alk-1-yn-1-ylxenonium tetrafluoroborates were synthesized (eq 4). Perfluoroorganoethynylxenonium tetrafluoroborates, $[\text{R}_\text{F}\text{C}\equiv\text{CXe}][\text{BF}_4]$, were isolated in 30–98 % yield, and non-fluorinated organo-

ethynylxenon(II) salts $[\text{C}_4\text{H}_9\text{C}\equiv\text{CXe}][\text{BF}_4]$ (23) and $[(\text{CH}_3)_3\text{CC}\equiv\text{CXe}][\text{BF}_4]$ (23, 24) were obtained in 20–40 % yield. It is important to note that these latter salts display sufficient solubility in the weakly coordinating solvents CH_2Cl_2 and PFP, whereas poly- and perfluorinated aryl-, alkenyl-, and alkynylxenonium tetrafluoroborates are insoluble.

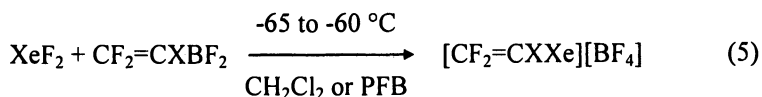


$\text{X} = \text{CF}_3, \text{C}_3\text{F}_7, (\text{CF}_3)_2\text{CF}, \text{cis-}, \text{trans-}\text{CF}_3\text{CF}=\text{CF}, \text{C}_6\text{F}_5, \text{C}_4\text{H}_9, (\text{CH}_3)_3\text{C}$

The reaction of XeF_2 with polyfluoroalk-1-en-1-yl difluoroboranes

All three types of isomeric X-difluorovinyl difluoroboranes, $\text{CF}_2=\text{CXBF}_2$, *cis*- and *trans*- $\text{XCF}=\text{CFBF}_2$, were involved in the reaction with XeF_2 . This feature enabled the study of the influence of electronic and steric factors of substituent X at both positions, C-1 and C-2, on the xenodeborylation reaction.

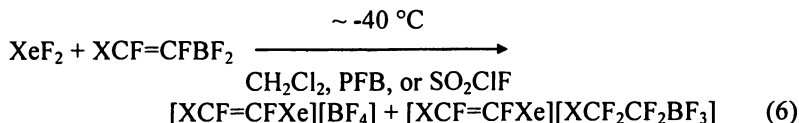
The reaction of $\text{CF}_2=\text{CXBF}_2$ with XeF_2 in PFB or PFP occurred readily at -65 to -60 °C and the corresponding alkenylxenonium tetrafluoroborates (25) precipitated (eq 5).



$\text{X} = \text{H}, \text{Cl}, \text{CF}_3$

The experimental result that no fluorine addition across the C=C double bond was observed in case of the reaction of XeF_2 with $\text{CF}_2=\text{C}(\text{CF}_3)\text{BF}_2$ (fluoride affinity 84.3 kcal mol⁻¹) is astonishing at first glance (see discussion of eqs 7 and 8) if one considers the increased inductive effect of CF_3 relative to F (26). A plausible explanation for the negligible influence on the acidity by the CF_3 group may be an agostic interaction of the CF_3 group with the acidic boron center in geminal position.

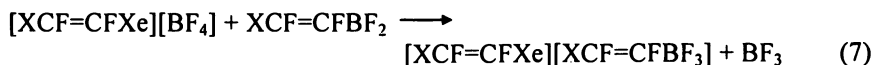
The trifluorovinylxenonium salt (22, 27) and a series of *cis*-X-1,2-difluoroalkenylxenonium salts were successfully synthesized and isolated in 30–60% yields (22). It is noteworthy that the xenodeborylation reaction of highly acidic boranes, $\text{CF}_2=\text{CFBF}_2$ (fluoride affinity 80.3 kcal mol⁻¹) and *cis*- $\text{C}_n\text{F}_{2n+1}\text{CF}=\text{CFBF}_2$ (fluoride affinity 90.0 kcal mol⁻¹ for $n = 1$) is accompanied by their partial conversion into perfluoroalkyltrifluoroborates, whereas in case of $\text{X} = \text{Cl}$ the anion, $[\text{ClCF}_2\text{CF}_2\text{BF}_3]^-$ was not observed (eq 6).



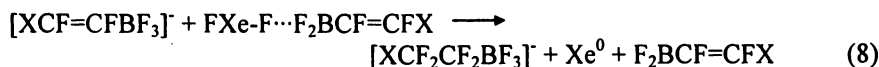
X = F, *cis*-CF₃, *cis*-C₂F₅,

X = *cis*-Cl, *trans*-Cl, *trans*-H, no admixture of [XCF=CFXe][XCF₂CF₂BF₃]

How are fluorinated alkyltrifluoroborate anions formed? The high acidity of XCF=CFBF₂ affords the possibility to abstract fluoride from [BF₄]⁻ as in case of the xenonium salt (eq 7).



The C=C double bond in [XCF=CFBF₃]⁻ is more easily accessible to oxidation (fluorine addition) than that of XCF=CFBF₂ (28). The oxidation is initiated by polarized XeF₂, formed in a channel parallel to the xenodeborylation, by the interaction of XeF₂ and the strong Lewis acid, XCF=CFBF₂ (eq 8).



Consequently, the relative contribution of xenodeborylation to fluorine addition across the C=C double bond and the ratio of the [BF₄]⁻ to [XCF=CFBF₃]⁻ anions depends on the electron-withdrawing character of X (acidity of the borane) and the actual ratio of XeF₂ (fluoride donor) to XCF=CFBF₂ (fluoride acceptor).

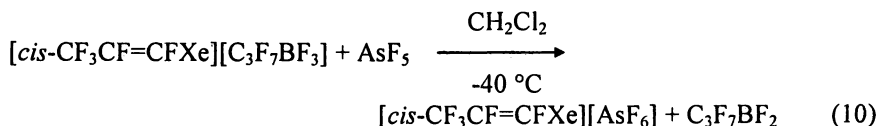
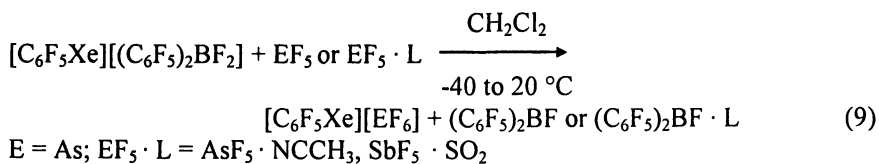
While *trans*-HCF=CFBF₂ and *trans*-ClCF=CFBF₂ reacted with XeF₂ yielding the corresponding alkenylxenonium tetrafluoroborates (eq 6), boranes *trans*-XCF=CFBF₂ (X = C₄H₉, Et₃Si) were consumed without formation of the desired xenonium salts. A slow formation of the corresponding perfluoroalkane and perfluoroalkyldifluoroborane was observed in the reaction of *trans*-C_nF_{2n+1}CF=CFBF₂ (n = 1, 4) with XeF₂. The last result was unexpected, because the fluoride affinities of *cis*- and *trans*-C_nF_{2n+1}CF=CFBF₂ are closely related (90.0 and 89.0 kcal mol⁻¹, respectively). Steric arguments were offered as a possible explanation (22). In the transition state of the xenodeborylation, it was assumed that the steric interaction of the substituent X *trans* to the BF₂ group with one fluorine atom of XeF₂ reduces the rate of xenodeborylation of *trans*-XCF=CFBF₂ relative to that of *cis*-XCF=CFBF₂. Very recently, this explanation was supported by the reaction of XeF₂ with C₄F₉CF=CFBF₂ (*cis* : *trans* 1 : 1)

where a 3 : 1 molar mixture of [*cis*- and *trans*-C₄F₉CF=CFXe][BF₄] was obtained (29).

Reactivity of Organoxenonium Salts

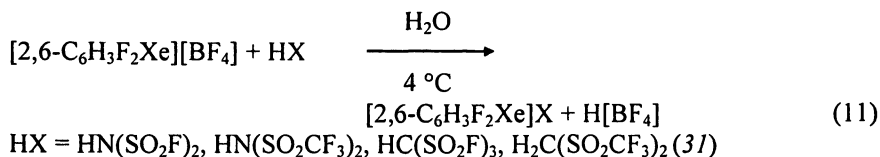
Reactions with Lewis Acids

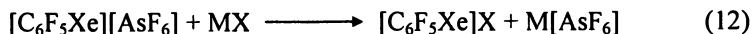
Reactions of organoxenonium salts [RXe][EF_{n+1}] with Lewis acids do not result in transformation of the organo group of the cation [RXe]⁺ (6), but rather give rise to fluoride abstraction from the counteranion [EF_{n+1}]⁻. For example, organoxenonium fluoroborates were converted into [EF₆]⁻ salts by using arsenic or antimony pentafluoride or their adducts, EF₅ · L (eqs 9, 10) (22, 30).



Reaction with Negatively Charged Nucleophiles, X⁻

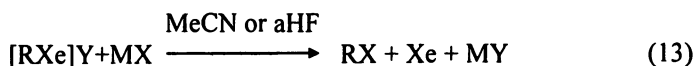
The reactivity of organoxenonium salts [RXe]Y towards anions X⁻ is determined by the nucleophilicity of the latter and nature of solvent. When X⁻ is a weakly nucleophilic anion, anion exchange (metathesis) occurs in polar solvents forming the corresponding [RXe]X salts in high yields (eqs 11, 12).





MX = Li[C(SO₂F)₃] in MeCN, H₂O (0 °C) or SO₂ (-78 °C),
Cs[C(SO₂F)₃] in MeNO₂ (20 °C), Cs[OSO₂CF₃] in CF₃CH₂OH (32),
[Me₄N][(C₆F₅)₄B] in 1,2-C₂H₄Cl₂ (-30 °C) (33)

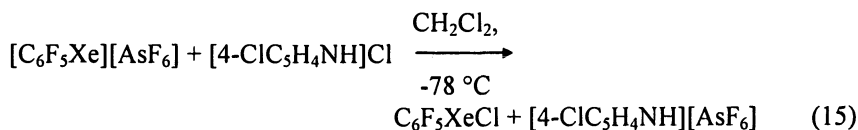
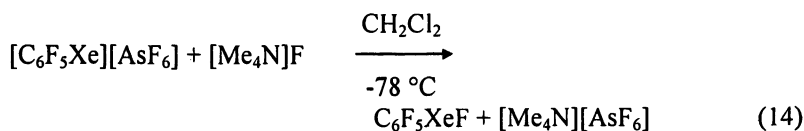
It is noteworthy that the reaction of [C₆F₅Xe][AsF₆] with CsOCOC₆F₅ in water resulted in the covalent compound, C₆F₅XeOCOC₆F₅ (34). This example is the exception rather than the rule because anions of high nucleophilicity react with organoxenonium salts in polar solvents under carbon-xenon bond cleavage. Thus, the action of bromide and iodide anions on aryl-, alkenyl-, and cycloalkenylxenonium salts in basic MeCN as well as in superacidic aHF results in the fast reductive elimination of xenon and formation of the corresponding organobromo or -iodo compounds, respectively (eq 13) (35–40, 12). However, the mechanism is ambiguous and could involve an intermolecular redox process as well as a decomposition of the unstable intermediate RXeX.



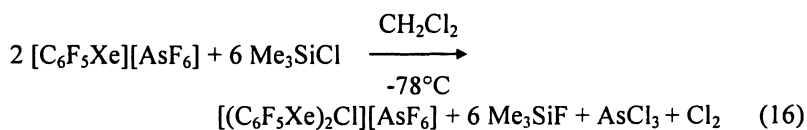
R = C₆H_nF_{5-n}, R'CF=CF (R' = F, H, C₄F₉), cyclo-1,4-C₆F₇, cyclo-C₆F₉; Y = BF₄, AsF₆; X = Br, I

In case of “hard” nucleophiles like F⁻ and Cl⁻, the reaction route depends on the properties of the polar solvent. For example, both [C₆F₅Xe][AsF₆] and nonafluorocyclohexen-1-ylxenonium hexafluoroarsenate do not react with KF or [Me₄N]Cl in aHF solution at 20 °C over several days (36). This arises from the high degrees of protonation of the fluoride and chloride anions in aHF, which significantly diminish the nucleophilicities of F⁻ and Cl⁻ by formation of [F(HF)_n]⁻ and HCl, respectively. On the other hand, in basic MeCN, both salts were easily converted into the corresponding organochloro compounds when reacted with [Me₄N]Cl (36) whereas the reactions with the “hardest” nucleophile, fluoride, proceeded along peculiar pathways. The treatment of [C₆F₅Xe][AsF₆] with CsF in CH₃CN yielded C₆F₅H and C₁₂F₁₀ (5.6 : 1) while the reaction with [Me₄N]F or [Me₄N][HF₂] gave these compounds in addition to C₆F₆ (40). Probably, this reaction proceeds via the intermediate, C₆F₅XeF, which decomposes into the pentafluorophenyl and the FXe radicals under the reaction conditions. A quite different reaction product, perfluoro-3-methylenecyclopentene, was obtained when nonafluorocyclohexen-1-ylxenonium hexafluoroarsenate was treated with NaF in MeCN (41). The result was rationalized in terms of a preferential attack of the “hard” nucleophile F⁻ at the “hard” electrophilic C-2 site, rather than at the “soft” electrophilic xenon(II) site.

In contrast, a series of arylxenon(II) halogen species with covalent Xe-Hal bonds was obtained in reactions with fluoride and chloride in weakly coordinating dichloromethane. Thus, C_6F_5XeF was prepared from $[C_6F_5Xe][AsF_6]$ and $[Me_4N]F$ in CH_2Cl_2 and isolated in 70% yield (eq 14) (42, 43). Under similar conditions, the first xenon(II) chlorine compound, C_6F_5XeCl , was synthesized in good yield (85%) (eq 15) (44).



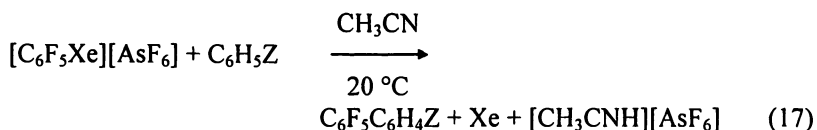
An advantage of this reaction is that both starting substrates and the byproduct ($[Me_4N][AsF_6]$ or $[4-ClC_5H_4NH][AsF_6]$) are practically insoluble in CH_2Cl_2 , whereas the desired products C_6F_5XeF and C_6F_5XeCl are soluble and can be extracted at low temperature from the reaction mixture and isolated in pure form. Remarkably, $[C_6F_5Xe][AsF_6]$ reacts with Me_3SiCl in CH_2Cl_2 to form a dinuclear cation. The salt, $[(C_6F_5Xe)_2Cl][AsF_6]$, was insoluble and was isolated in 91% yield. It seems that its formation occurs via polarization of the anion $[AsF_6]$ by the electrophilic pentafluorophenylxenonium cation and replacement of the bridged fluoride in $[C_6F_5Xe \cdots F \cdots AsF_5]$ by chloride (44).



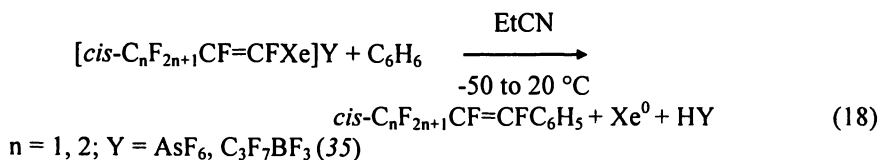
Alternatively, the slow reaction of $[2,6-C_6H_3F_2Xe][BF_4]$ with Me_3SiOTf in CH_2Cl_2 (-20 °C) yielded $[2,6-C_6H_3F_2Xe][OTf]$, BF_3 and Me_3SiF (45).

Reactions with Neutral π - and n -Nucleophiles

Aromatic compounds are the only type of π -nucleophiles involved in reactions with organoxenonium salts. While pentafluorobenzenes, C_6F_5Z ($Z = H, F, CN, SiMe_3$), are not reactive towards $[C_6F_5Xe][AsF_6]$ in MeCN at 20 °C, a series of 2,3,4,5,6-pentafluorobiphenyls was obtained from monosubstituted benzene derivatives, C_6H_5Z , under these conditions. The reaction rates diminish in the sequence $Z = CH_3 > F > CF_3 \sim CN > NO_2$, which is consistent with the electrophilic nature of the process. Nevertheless, the isomer distribution in the $C_6F_5C_6H_4Z$ products shows unambiguously the radical character of the pentafluorophenylation reaction (eq 17) (46).



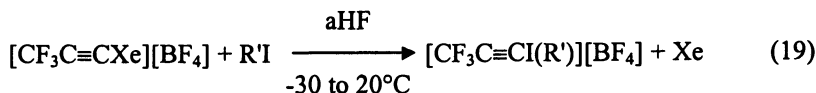
Perfluorinated alkenylxenonium and cycloalkenylxenonium salts react with benzene in a similar manner (eq 18) (35, 39).



Reactions of arylxenonium salts with neutral O-, S-, N-, P-, and As-nucleophiles in MeCN were discussed in the previous review (6). A special case is the reaction of organoxenonium salts with iodo compounds R'I. The fast reaction of $[C_6F_5Xe][AsF_6]$ and C_6H_5I in MeCN (20 °C) gives C_6F_5I (major product) in addition to $C_6F_5C_6H_4I$, C_6F_5H , and $C_6F_5C_6H_5$. These compounds were also obtained in the radical pentafluorophenylation of iodobenzene starting from $C_6F_5NH_2$ and $C_5H_{11}ONO$. Alternatively, iodopentafluorobenzene did not react with $[C_6F_5Xe][AsF_6]$ (MeCN, 20 °C, 70 h; MeCN, 80 °C, 4 h; CH_2Cl_2 , 80 °C, 4 h) (46, 47) nor with $[C_6F_5Xe][C_6F_5BF_3]$ (MeCN, -30 °C) (4), but formed $[(C_6F_5)_2I][C_6F_5)_3BF]$ with $[C_6F_5Xe][C_6F_5)_3BF]$ (MeCN, 20 °C) (3). This apparent contradiction can be explained by the decomposition of $[C_6F_5Xe][C_6F_5)_3BF]$ at room temperature, assuming a reactive intermediate which converts C_6F_5I to $(C_6F_5)_2IF$. Fluoride abstraction of the latter by $(C_6F_5)_3B$ results in the corresponding iodonium salt $[(C_6F_5)_2I][C_6F_5)_3BF]$. C_6F_5I was inert to $[2,4,6-C_6F_3H_2Xe][BF_4]$ in MeCN at 20 °C over a period of 20 h, while at 60

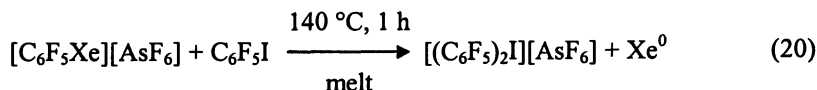
°C the iodonium salt $[(2,4,6\text{-C}_6\text{F}_3\text{H}_2)(\text{C}_6\text{F}_5)\text{I}][\text{BF}_4]$ was formed besides 1,3,5- $\text{C}_6\text{F}_3\text{H}_3$ and $\text{C}_6\text{F}_5\text{H}$ (48).

The reactivity of arylxenonium and alkenylxenonium salts towards iodo compounds in aHF is not yet reported although perfluoroalkynylxenonium tetrafluoroborates show excellent alkynylating properties in reactions with alkyl, trifluorovinyl, pentafluorophenyl, and 3-fluorophenyl iodides (eq 19) (49).

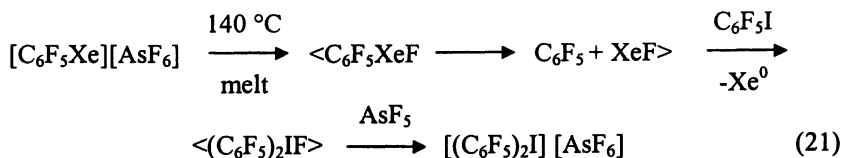


$\text{R} = \text{CF}_3\text{CH}_2, \text{CF}_2=\text{CF}, \text{C}_6\text{F}_5, 3\text{-FC}_6\text{H}_4$

So far the salt, $[\text{C}_6\text{F}_5\text{Xe}][\text{AsF}_6]$, is thermally the most stable organoxenon compound, melting (102°C) without decomposition to form a viscous liquid. It decomposes slowly above 125°C to yield C_6F_6 , AsF_5 , and xenon (30). The reaction of the molten salt $[\text{C}_6\text{F}_5\text{Xe}][\text{AsF}_6]$ with $(\text{C}_6\text{F}_5)_2\text{S}$ and $(\text{C}_6\text{F}_5)_3\text{E}$ ($\text{E} = \text{P}, \text{As}$) at $130\text{--}150^\circ\text{C}$ results in the formation of the corresponding phosphonium, arsonium, and sulfonium salts $[(\text{C}_6\text{F}_5)_{n+1}\text{E}][\text{AsF}_6]$ ($n = 2$ and 3 , respectively) in good yields (6, 50). Even the pentafluorophenylation of $\text{C}_6\text{F}_5\text{I}$ was successfully performed in the viscous melt of $[\text{C}_6\text{F}_5\text{Xe}][\text{AsF}_6]$ at 140°C (eq 20) (47).



When the method was extended to $\text{C}_6\text{F}_5\text{Br}$, the bromonium salt, $[(\text{C}_6\text{F}_5)_2\text{Br}][\text{AsF}_6]$, was isolated in only 6% yield. Formation of the corresponding chloronium salt, $[(\text{C}_6\text{F}_5)_2\text{Cl}][\text{AsF}_6]$, was not established in the reaction of $\text{C}_6\text{F}_5\text{Cl}$ under the above conditions (47). Despite the formal description of the electrophilic pentafluorophenylation via an addition of the $[\text{C}_6\text{F}_5]^+$ cation, it seems more probable to assume the intermediate formation of $\text{C}_6\text{F}_5\text{XeF}$. When this molecule decomposes, the C-Xe bond cleaves homolytically. Formal addition of C_6F_5 and F radicals to $\text{C}_6\text{F}_5\text{I}$ or $\text{C}_6\text{F}_5\text{Br}$ is followed by fluoride ion abstraction by the Lewis acid which is present, resulting in the formation of halonium salt (eq 21).



Multinuclear NMR Spectroscopic Properties of Organoxenonium Salts

NMR spectroscopy is a key tool for the identification and characterization of organoxenonium salts in solution. The convenience of ^{129}Xe NMR spectroscopy is based on the high NMR sensitivity and natural abundance (26.44%) of the ^{129}Xe isotope ($I = \frac{1}{2}$). The considerable magnitude of the spin-spin coupling ${}^nJ(^{129}\text{Xe}, A)$ ($A = {}^1\text{H}$, ^{13}C , and ^{19}F), where the nuclei A are part of the organic group, provides useful information regarding the structures of organoxenon compounds. In case of very dilute samples and of low stability of solutions of organoxenon compounds ^{129}Xe NMR is preferred relative to ^{13}C NMR spectroscopy because of the relatively short time needed to acquire spectra. The overall range of $\delta(^{129}\text{Xe})$ values is approximately 6200 ppm whereas the range of ^{129}Xe resonances of the presently known organoxenon(II) species covers only approximately 800 ppm. In earlier publications, ^{129}Xe NMR chemical shifts were often referenced to the signal of XeF_2 dissolved in various solvents, sometimes with undefined concentrations, and measured at different temperatures. To have a reliable process for referencing, Schrobilgen et al. (51) suggested the use of XeF_2 in MeCN (extrapolated to zero concentration) as a secondary standard with a ^{129}Xe NMR chemical shift equal to -1813.28 ppm at 24 °C. This suggestion was based on the absolute frequency of pure liquid XeOF_4 to 27.810184 MHz at 24 °C, relative to a ${}^1\text{H}$ frequency of exactly 100 MHz of neat $(\text{CH}_3)_4\text{Si}$ at 24 °C. Later XeOF_4 was recommended by IUPAC as standard reference for ^{129}Xe NMR spectroscopy (52). Recently, the dependence of the ^{129}Xe NMR chemical shift of XeE_2 as well as of a representative series of organoxenonium(II) salts $[\text{R}\text{Xe}]\text{Y}$ on temperature and concentration was determined in a prototypic variety of media, in acidic anhydrous HF (aHF), weakly polar aprotic (dichloromethane), and basic (CD_3CN - EtCN, 1 : 3 v/v) solvents (53). This allows the direct comparison of ^{129}Xe NMR chemical shifts measured at various temperatures in these solvents, and for convenience, all $\delta(^{129}\text{Xe})$ values discussed below were extrapolated to -30 °C using these data (53).

NMR Spectra in Anhydrous HF

The choice of an appropriate solvent is determined by the ionic character of organoxenonium salts, $[\text{R}\text{Xe}]\text{Y}$, and their reactivity. One of the most suitable solvents is aHF because it possesses a high solvating ability and chemical stability towards oxidizing compounds. The salts $[\text{R}\text{Xe}]\text{Y}$ exist in aHF solution

as “non-solvated” cations and strongly solvated (protonated) anions. In this sense, the NMR spectra of $[\text{RXe}]\text{Y}$ in aHF characterize a nearly “naked” organoxenonium cation with respect to solutions in basic n-electron donor solvents like MeCN or SO_2 where the interaction of the positively charged xenon center with the solvent is relevant.

The ^{129}Xe NMR signals of $[\text{RC}\equiv\text{CXe}][\text{BF}_4]$ in aHF are singlets located between -3600 and -3790 ppm (Figure 1). The most shielded xenon atom is observed in $[(\text{CH}_3)_3\text{CC}\equiv\text{CXe}][\text{BF}_4]$ (δ -3788). The replacement of $\text{R} = (\text{CH}_3)_3\text{C}$ by $\text{R} = \text{C}_4\text{H}_9$, C_6F_5 , and $\text{CF}_3\text{CF}=\text{CF}$ leads to deshielding of the xenon nucleus and the ^{129}Xe signals move to -3782, -3669, and -3620 ppm, respectively. A remarkably high frequency shift (deshielding) of the xenon atom is observed also when fluorine atoms F in $[\text{CF}_3\text{C}\equiv\text{CXe}]^+$ are replaced by perfluoroalkyl groups): $\delta = -3643$ ($\text{R} = \text{CF}_3$) < -3616 ($\text{R} = \text{CF}_3\text{CF}_2\text{CF}_2$) < -3607 ppm ($\text{R} = (\text{CF}_3)_2\text{CF}$) (-30 °C) (23).

The ^{13}C NMR spectra of $[\text{RC}\equiv\text{CXe}][\text{BF}_4]$ salts contain resonances of carbon C-1 at unusually low frequencies (8 to -24 ppm). The deshielding of C-1 of alkenylxenonium(II) salts in aHF solution bearing either hydrocarbon or perfluorocarbon groups occurred in the same sequence as the deshielding of the xenon atom, that means from $\text{R} = (\text{CH}_3)_3\text{C}$ ($\delta(\text{C}-1)$ -24) to $\text{R} = \text{CF}_3\text{CF}=\text{CF}$ ($\delta(\text{C}-1)$ 7 ppm). The $\delta(\text{C}-2)$ values undergo an opposite shift from 80 to 107 ppm, respectively, parallel to a decreasing of the ^{13}C - ^{129}Xe coupling $^2J(\text{C}-2, \text{Xe})$ from 76 to 60 Hz. The corresponding coupling constants $^1J(\text{C}-1, \text{Xe})$ increase from ca. 265 Hz ($\text{R} = \text{C}_4\text{H}_9$, $(\text{CH}_3)_3\text{C}$) to 308 Hz ($\text{R} = \text{C}_6\text{F}_5$) and ca. 345 Hz ($\text{R} = \text{perfluoroalkyl}$) (23(b)) (Figure 1).

The presence of Xe^+ has no effect on ^1H and ^{19}F chemical shifts or on the coupling constants $J(\text{H}, \text{H})$ and $J(\text{F}, \text{F})$ in the organic moiety R of $[\text{RC}\equiv\text{CXe}][\text{BF}_4]$ with respect to the parent molecules $\text{RC}\equiv\text{CH}$. In some cases long-range couplings ^{19}F - ^{129}Xe were observed. For example, the signal F^3 in $[(\text{CF}_3)_2\text{CFC}\equiv\text{CXe}][\text{BF}_4]$ contains ^{129}Xe satellites with $^4J(\text{F}^3, \text{Xe}) = 8$ Hz. A similar coupling constant $^4J(\text{F}^3, \text{Xe}) = 6$ Hz was found in the spectrum of $[\text{trans-CF}_3\text{CF}=\text{CFC}\equiv\text{CXe}][\text{BF}_4]$, whereas in the spectrum of the *cis*-isomer this splitting was absent, but the signal F^4 of the *cis*-isomer displayed ^{129}Xe satellites with $^5J(\text{F}^4, \text{Xe}) = 17$ Hz. No couplings $^nJ(\text{H}, \text{Xe})$ and $^nJ(\text{F}, \text{Xe})$ were detected in the ^1H and ^{19}F NMR spectra of the other salts, $[\text{RC}\equiv\text{CXe}][\text{BF}_4]$ ($\text{R} = (\text{CH}_3)_3\text{C}$, C_4H_9 , CF_3 , C_3F_7 , C_6F_5).

On the other hand, the presence of the xenon atom can be unambiguously deduced in the ^1H and ^{19}F NMR spectra of polyfluorinated alkenylxenonium and cycloalkenylxenonium salts because of the magnitudes of the $^nJ(\text{H}, \text{Xe})$ and $^nJ(\text{F}, \text{Xe})$ couplings. For example, the ^{19}F NMR spectrum of $[\text{CF}_2=\text{CFXe}][\text{AsF}_6]$ (aHF, -10 °C) displayed resonances at -82.1 (d, $^2J(\text{F}^{2\text{trans}}, \text{F}^{2\text{cis}}) = 41$ Hz; d,

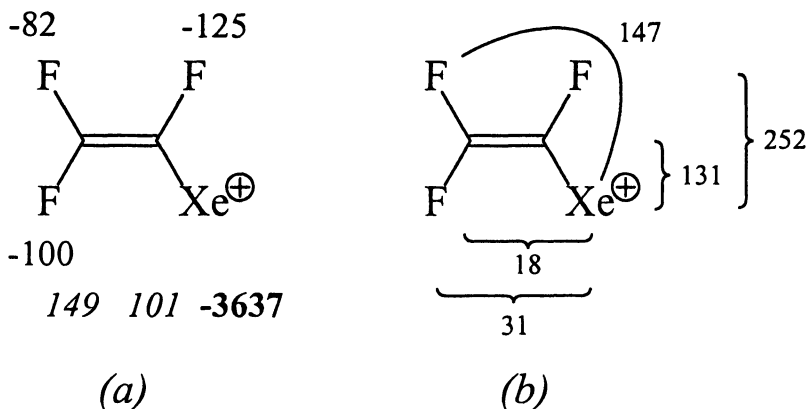


Figure 2. ^{13}C , ^{19}F , and ^{129}Xe NMR spectral data of the trifluoroethenyl-xenonium (II) cation (aHF, $-30\text{ }^\circ\text{C}$): (a) chemical shifts: ^{13}C (italic), ^{19}F (plain), and ^{129}Xe (bold); (b) $J(^{129}\text{Xe}, ^{13}\text{C})$ and $J(^{129}\text{Xe}, ^{19}\text{F})$ couplings [$J(^{13}\text{C}, ^{19}\text{F})$ and $J(^{19}\text{F}, ^{19}\text{F})$ couplings are omitted].

The $^3J(\text{F}_3\text{C}, \text{Xe})$ and $^3J(\text{F}_2\text{C}, \text{Xe})$ couplings in the spectra of both salts, $[\text{CF}_2=\text{C}(\text{CF}_3)\text{Xe}][\text{BF}_4]$ (54) and $[\text{cyclo-C}_6\text{F}_9\text{Xe}][\text{AsF}_6]$ (39), were too small to be observed as well as the $^4J(\text{F}^3, \text{Xe})$ value in the spectra of the latter salt and related cycloalkenylxenonium derivatives (39, 37, 38). Less information is available concerning the $^nJ(\text{H}, \text{Xe})$ couplings relative to the corresponding $^nJ(\text{F}, \text{Xe})$ values. These coupling constants vary from $^2J(\text{H}, \text{Xe}) = 54\text{ Hz}$ ($[\text{CF}_2=\text{CHXe}]^+$ (54)) to $^3J(\text{H}, \text{Xe}) = 22\text{ Hz}$ ($[\text{trans-HCFE}=\text{CFXe}]^+$ (54)), and $^3J(\text{H}, \text{Xe}) = 15\text{ Hz}$ (2-hydroctofluorocyclohexen-1-ylxenonium cation (37)).

The ^{129}Xe NMR spectrum of $[\text{CF}_2=\text{CFXe}][\text{AsF}_6]$ in aHF displayed a doublet of doublets of doublets at δ -3637 (Figure 2) (22). Replacement of one fluorine atom by chlorine caused a deshielding of xenon and moved the signal to $-3550 \pm 15\text{ ppm}$ in the spectra of the isomers $[\text{ClCF}=\text{CFXe}]\text{Y}$ (*cis* and *trans*) and $[\text{CF}_2=\text{CClXe}]\text{Y}$ (22, 54). In contrast, the spectra of the salts without α -fluorine atom, $[\text{CF}_2=\text{CRXe}]\text{Y}$ ($\text{R} = \text{H}, \text{CF}_3$), as well as of the corresponding cycloalkenyl salts, nonafluorocyclohex-1-en-1-ylxenon(II) (Table I), 2-hydrohexafluorocyclohexa-1,4-dien-1-ylxenon(II) (δ -3779), 2-hydroctofluorocyclohex-1-en-1-ylxenon(II) (δ -3721) (37), 3-oxopentafluorocyclohexa-1,4-dien-1-ylxenon(II) (δ -3912) (53, 38) displayed a significant shielding of the xenon atom. This is probably the result of a strong "through-space" electronic interaction of the xenon atom with the vicinal fluorine atom F^2 (*cis* to Xe^+) whereas the salts, $[\text{cis-C}_n\text{F}_{2n+1}\text{CF}=\text{CFXe}]\text{Y}$ ($n = 1, 2$) with F^2 *trans* to Xe^+ , showed the opposite shift of the ^{129}Xe resonance to -3420 ppm (Table I) (22).

Table I. Selected ^{13}C and ^{129}Xe NMR Spectral Data of Organoxenon Compounds $[\text{RXe}]\text{Y}$ and RXeR'

Compound	Solvent	t , °C	$\delta(\text{Xe})$, ppm ^a	$\delta(\text{C}-1)$, ppm	$^1J(\text{C}-1, \text{Xe})$, Hz	$^nJ(\text{Xe}, \text{F})$, Hz	Refs
$[\text{CF}_3\text{C}\equiv\text{CXe}][\text{BF}_4]$	aHF	-60	-3636	-5.2 ^c	343		(23)
$[\text{C}_4\text{H}_9\text{C}\equiv\text{CXe}][\text{BF}_4]$	aHF	-30	-3783	-24.0 ^d	264		(53, 23)
$[\text{C}_4\text{H}_9\text{C}\equiv\text{CXe}][\text{BF}_4]$	CH_2Cl_2	-60	-3698	-16.7 ^e	288		(23)
$[\text{cis}-\text{CF}_3\text{CF}=\text{CFXe}][\text{C}_3\text{F}_7\text{BF}_3]$	aHF	-10	-3431	-3420		$^2J = 154$, $^3J = 183$, $^4J = 38$	(22)
$[\text{cyclo-1-C}_6\text{F}_9\text{Xe}][\text{AsF}_6]$	aHF	-30	-2295	96.2	114	$^3J = 70$	(39)
$[\text{trans-HCF}=\text{CFXe}][\text{BF}_4]$	aHF	-40	-3693	-3689		$^2J = 206$, $^3J = 60$	(22)
$[\text{CF}_2=\text{CHXe}][\text{BF}_4]$	aHF	-60	-4059	-4064		$^3J = 155$, ^{f,8}	(54)
$[\text{CF}_2=\text{C}(\text{CF}_3)\text{Xe}][\text{BF}_4]$	aHF	-60	-3856	-3861		$^3J = 144$, ^f	(53, 54)
$[\text{CF}_2=\text{C}(\text{CF}_3)\text{Xe}][\text{BF}_4]$	EtCN	-60	-3741	-3752		$^3J = 139$, ^f	(54)
$[2\text{-FC}_6\text{H}_4\text{Xe}][\text{BF}_4]$	MeCN	-30	-2039	-3852	105.5		(60)
$[3\text{-FC}_6\text{H}_4\text{Xe}][\text{BF}_4]$	RCN ^h	-80	-1875	-3700	78		(12)
$[4\text{-FC}_6\text{H}_4\text{Xe}][\text{BF}_4]$	MeCN	-30	-1896	-3709	104		(60)
$[4\text{-FC}_6\text{H}_4\text{Xe}][\text{BF}_4]$	RCN ^h	-80	-1915	-3739			(12)
$[3,5\text{-C}_6\text{H}_3\text{F}_2\text{Xe}][\text{BF}_4]$	RCN ^h	-60	-3606	-3612			(20)
$[2,6\text{-C}_6\text{H}_3\text{F}_2\text{Xe}][\text{BF}_4]$	MeCN	-30	-2115	-3928	88.8		(60)
$[3,4,5\text{-C}_6\text{H}_2\text{F}_3\text{Xe}][\text{BF}_4]$	MeCN	-30	-3607	-3607	99		(20)
$[2,4,6\text{-C}_6\text{H}_2\text{F}_3\text{Xe}][\text{BF}_4]$	MeCN	-30	-2073	-3886	104		(60)
$[2,3,4,5\text{-C}_6\text{HF}_4\text{Xe}][\text{BF}_4]$	MeCN	-30	-3712	-3712		$^3J = 63$	(20)
$[\text{C}_6\text{F}_5\text{Xe}][\text{BF}_4]$	aHF	-10	-3941	-3938	85	$^3J = 59$ $^4J = 7$ $^5J = 4$	(20)

$[C_6F_5Xe][BF_4]$	MeCN	-30	-3786	-3786	84.5	118	$^3J = 67$ $^4J = 9$ $^5J = 4$	(20) (56) (56)
$[C_6F_5Xe][PF_6]$	MeCN	24	-3799	-3781	83.9	<i>i</i>	$^3J = 67$	(32)
$[C_6F_5Xe][HF_2]$	MeCN	-40	-3780	-3784	83.0	136	$^3J = 71$	(19)
$[C_6F_5Xe][AsF_6]$	MeCN	-30	-2010	-3798	82.2	117	$^3J = 69$	(40)
$[C_6F_5Xe][AsF_6]$	SO ₂	-40	-3903				$^3J = 64$	(30)
$[C_6F_5Xe][AsF_6]$	H ₂ O	24	-3862				$^3J = 69$	(30)
$[(C_6F_5Xe)_2Cl][AsF_6]$	MeCN	-40	-3938	-3942	92.9	195	$^3J = 81$	(44)
$[C_6F_5XeF_2][BF_4]$	CD ₃ CN	-40	-1706	-1710	121.9	<i>i</i>	$^1J = 3892$	(5)
$[C_6F_5XeF_2][BF_4]$	aHF	-80	-1766	-1780			$^1J = 3894$	(61)
C_6F_5XeF	CD ₂ Cl ₂	-78	-3789	-3820 ^j	86.4	111 ^k	$^1J = 4014$, $^3J = 81$	(42)
C_6F_5XeF	CD ₂ Cl ₂	-30	-1994	-3816			$^1J = 4036$, $^3J = 80$	(62)
C_6F_5XeF	MeCN	-30	-2004	-3826			$^1J = 4100$, $^3J = 82$	(62)
C_6F_5XeCl	CD ₂ Cl ₂	-60	-4117	-4136 ^j	101.6	208		(44)
$C_6F_5XeC_6F_5$	CD ₂ Cl ₂	-78	-4152	-4183 ^j	123.2	315		(42)
$C_6F_5XeC_6F_5$	(CD ₃) ₂ CO	-58	-2376	-4189	123.2 ^l	320	$^3J = 45$, $^4J = 35$, $^5J = 10$	(62)
$C_6H_5C\equiv CXeF$	CH ₂ Cl ₂	-78	-1887	-3730 ^j	29.8 ^m	336		(63)

^a The reported ¹²⁹Xe NMR chemical shifts. Values in italic were referenced to XeF₂ in MeCN as primary standard.

^b The ¹²⁹Xe NMR chemical shifts were referenced to XeOF₄ (24 °C) and extrapolated to -30 °C if measured at other temperature (53).

^c ¹³C NMR: δ 81.2 (d, ²J(C-2,Xe) = 69 Hz, C-2).

^d ¹³C NMR: δ 101.6 (d, ²J(C-2,Xe) = 69 Hz, C-2).

Continued on next page.

^e ¹³C NMR: δ 98.7 (d, ²J(C-2,Xe) = 75 Hz, C-2).

^f ³J(Xe,F^{2trans}).

^g ²J(Xe,H) = 55 Hz.

^h In CD₃CN - EtCN (1 : 3 v/v).

ⁱ The coupling ¹³C-¹²⁹Xe was not observed because of a too low intensity of the parent signal.

^j Extrapolated to -30 °C using Δδ(Xe)/ΔT = -0.64 ppm K⁻¹ obtained for XeF₂ in CD₂Cl₂ (53).

^k ²J(C-1,XeF) = 115 Hz.

^l ²J(C-2,Xe) = 148 Hz.

^m ¹³C NMR: δ 87.6 (d, ²J(C-2,Xe) = 98 Hz, C-2).

The resonances of the carbon atoms C-1 and C-2 in the $^{13}\text{C}\{^{19}\text{F}\}$ NMR spectrum of $[\text{CF}_2=\text{CFXe}]\text{Y}$ (aHF, $-30\text{ }^\circ\text{C}$) were located at 100.6 and 148.8 ppm, respectively (Figure 2). For comparison, the resonance of the carbon atom C-1 in the ^{13}C NMR spectrum of nonafluorocyclohex-1-en-1-yl)xenon(II) hexafluoroarsenate (aHF, $-10\text{ }^\circ\text{C}$) occurred at 96.3 ppm and $^3J(\text{C-1},\text{Xe})$ was 114 Hz (39).

Important NMR data of the pentafluorophenylxenonium cation in aHF are presented in Figure 3. The resonances of the fluorine atoms $\text{F}^{2,6}$ contained well separated ^{129}Xe -satellites (20). The $^4J(\text{Xe},\text{F})$ and $^5J(\text{Xe},\text{F})$ coupling had to be determined from the ^{129}Xe NMR signal. It is worth mentioning, that the coupling constant $^1J(\text{C-1},\text{Xe})$ in aHF (85 Hz) is remarkably smaller than in MeCN (113 Hz).

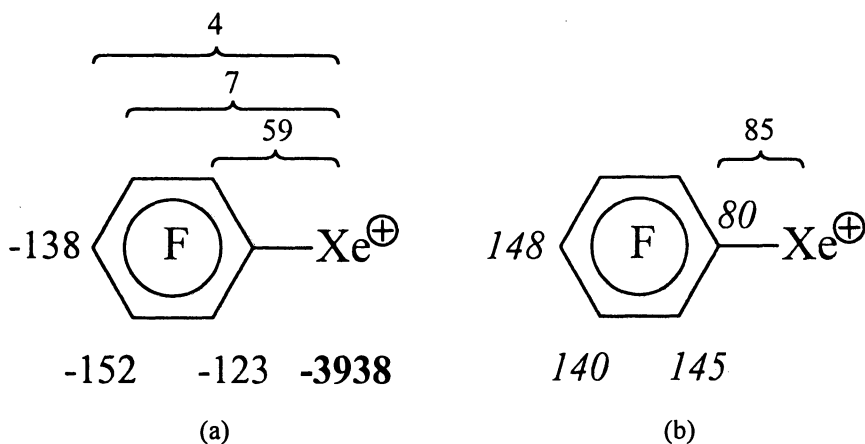


Figure 3. ^{13}C , ^{19}F , and ^{129}Xe NMR spectral data of the pentafluorophenylxenonium(II) cation: (a) ^{19}F (plain), ^{129}Xe (bold) chemical shifts, and $J(^{129}\text{Xe}, ^{19}\text{F})$ coupling; (b) ^{13}C (italic) chemical shifts and $J(^{13}\text{C}, ^{129}\text{Xe})$ coupling (aHF, $-30\text{ }^\circ\text{C}$) [$J(^{19}\text{F}, ^{19}\text{F})$ and $J(^{13}\text{C}, ^{19}\text{F})$ couplings are omitted].

The transitions to the less fluorinated arylxenonium tetrafluoroborates, $[2,3,4,5\text{-C}_6\text{HF}_4\text{Xe}][\text{BF}_4]$, $[3,4,5\text{-C}_6\text{H}_2\text{F}_3\text{Xe}][\text{BF}_4]$, and $[3,5\text{-C}_6\text{H}_3\text{F}_2\text{Xe}][\text{BF}_4]$, were accompanied by high-frequency shifts of the ^{129}Xe resonances of 100, 236, and 232 ppm, respectively (20). The coupling constants $^3J(\text{Xe},\text{F}) = 55\text{--}59\text{ Hz}$ and $^3J(\text{Xe},\text{H}) = 16\text{--}19\text{ Hz}$ did not change remarkably in this series.

NMR spectra in other solvents

The NMR spectra of $[\text{C}_4\text{H}_9\text{C}\equiv\text{CXe}][\text{BF}_4]$ and $[(\text{CH}_3)_3\text{CC}\equiv\text{CXe}][\text{BF}_4]$ in the weakly coordinating solvents CH_2Cl_2 and PFP are noticeably different from the spectra in aHF. Thus, the ^{129}Xe NMR signals in CH_2Cl_2 solution are shifted to high frequencies by 66 and 77 ppm, respectively. The signal of carbon C-1 of both salts was shifted by 8 ppm in the same direction, and the resonance of the atoms C-2 moved by 2 ppm in the opposite direction. Remarkable changes were observed in the ^{19}F NMR signal of the $[\text{BF}_4]^-$ counteranion, which was located at -143 to -145 ppm (in CH_2Cl_2), -139 to -141 ppm (in PFP), and at -148 ppm (in aHF). For comparison, solutions of $[\text{Bu}_4\text{N}][\text{BF}_4]$ in CH_2Cl_2 (24 °C), PFP (-10 °C), and aHF (-20 °C), display ^{19}F signals at -151.8, -148.4, and -148.3 ppm, respectively. In case of the alkynylxenonium salts, the observation is associated with a significant cation-anion interaction in their CH_2Cl_2 and PFP solutions (borderline description as tight ion pair) in contrast to their solutions in aHF where in both salts the counteranion is strongly solvated (23(b)).

All presently known polyfluoroalkenylxenonium salts are insoluble in the weakly coordinating solvents, CH_2Cl_2 and PFB. Some of them were measured in the basic solvents, MeCN or EtCN. The strong donor-acceptor interaction between the trifluoroethenylxenon(II) cation and EtCN (base) caused significant changes in the NMR spectra with respect to the spectra in aHF. The ^{129}Xe NMR signal of $[\text{CF}_2=\text{CFXe}][\text{BF}_4, \text{C}_2\text{F}_5\text{BF}_3]$ (EtCN, -40 °C) was located at δ -3511 (d, $^2J(\text{Xe}, \text{F}^1) = 197$ Hz; d, $^3J(\text{Xe}, \text{F}^{2\text{cis}}) = 27$ Hz; d, $^3J(\text{Xe}, \text{F}^{2\text{trans}}) = 136$ Hz). The ^{19}F NMR spectrum consists of resonances at δ -85.0 (d, $^2J(\text{F}^{2\text{trans}}, \text{F}^{2\text{cis}}) = 46$ Hz; d, $^3J(\text{F}^{2\text{trans}}, \text{F}^1) = 90$ Hz; d*, $^3J(\text{F}^{2\text{trans}}, \text{Xe}) = 139$ Hz 1F $\text{F}^{2\text{trans}}$] -103.4 (d, $^3J(\text{F}^{2\text{cis}}, \text{F}^1) = 124$ Hz; d, $^2J(\text{F}^{2\text{cis}}, \text{F}^{2\text{trans}}) = 46$ Hz; d*, $^3J(\text{F}^{2\text{cis}}, \text{Xe}) = 29$ Hz, 1F, $\text{F}^{2\text{cis}}$], -137.8 (d, $^3J(\text{F}^1, \text{F}^{2\text{cis}}) = 124$ Hz; d, $^3J(\text{F}^1, \text{F}^{2\text{trans}}) = 90$ Hz; d*, $^2J(\text{F}^1, \text{Xe}) = 191$ Hz, 1F, F^1), -149.6 ([BF_4]), and -83.3 (m, 3F, F^2), -136.9 (q, $^2J(\text{F}^1, \text{B}) = 19$ Hz, 2F, F^1), -153.8 (q 1: 1: 1: 1: 1, $^1J(\text{F}, \text{B}) = 41$ Hz, 3F, [$\text{C}_2\text{F}_5\text{BF}_3$]) (55). Cooling to -70 °C resulted in increased shielding of fluorine atom F^1 and a decrease in $^2J(\text{F}^1, \text{Xe})$ to 188 Hz, presumably due to favorable cation-anion interactions relative to cation-EtCN interactions: δ -84.1 (d, $^2J(\text{F}^{2\text{trans}}, \text{F}^{2\text{cis}}) = 46$ Hz; d, $^3J(\text{F}^{2\text{trans}}, \text{F}^1) = 88$ Hz; d*, $^3J(\text{F}^{2\text{trans}}, \text{Xe}) = 136$ Hz, 1F, $\text{F}^{2\text{trans}}$), -102.6 (d, $^2J(\text{F}^{2\text{cis}}, \text{F}^{2\text{trans}}) = 46$ Hz; d, $^3J(\text{F}^{2\text{cis}}, \text{F}^1) = 123$ Hz; d*, $^3J(\text{F}^{2\text{cis}}, \text{Xe}) = 28$ Hz, 1F, $\text{F}^{2\text{cis}}$), -138.3 (ddd*, 1F, F^1) (22).

The multinuclear NMR spectra of $[2,6\text{-C}_6\text{H}_3\text{F}_2\text{Xe}]\text{Y}$ in MeCN (24 °C) (Y are counteranions of low nucleophilicity such as BF_4 , OSO_2CF_3 (45), $\text{N}(\text{SO}_2\text{F})_2$, $\text{C}(\text{SO}_2\text{F})_3$ (31)) do not differ from each other and are characterized by the ^{129}Xe signal at δ -3930 and coupling constant $^3J(\text{F}, \text{Xe}) = 52\text{--}55$ Hz. The NMR spectra of $[\text{C}_6\text{F}_5\text{Xe}]\text{Y}$ salts in MeCN were also independent of the counteranion Y = BF_4 , AsF_6 , SbF_6 , and PF_6 . The ^{19}F signals of the pentafluorophenyl group were

located at δ -125.5 ($F^{2,6}$), -142.3 (F^4), and -155.0 ($F^{3,5}$) and were shielded with respect to aHF solutions. Coordination of MeCN to the cation is accompanied by an increase of the ^{19}F - ^{129}Xe coupling $^3J(F^{2,6},\text{Xe})$ from 58 to 69 Hz. The longer range coupling constants $^4J(F^{3,5},\text{Xe})$ and $^5J(F^4,\text{Xe})$ remained practically unaffected (18 and 4–5 Hz, respectively) as well as the $^nJ(\text{F},\text{F})$ values of the C_6F_5 group (3, 4, 20). The ^{129}Xe NMR spectrum of $[\text{C}_6\text{F}_5\text{Xe}][\text{BF}_4]$ in CD_3CN showed a triplet $^3J(\text{Xe},\text{F}) = 67$ Hz at δ -3786, whereas both smaller coupling constants could not be measured in the past because of broadening of the signal ($\Delta\nu_{1/2} \sim 30$ Hz) (20). Very recently the re-examination of the ^{129}Xe NMR spectrum of $[\text{C}_6\text{F}_5\text{Xe}][\text{BF}_4]$ in MeCN at 24 °C at 7.0463 T revealed all three $^nJ(\text{Xe},\text{F})$ coupling constants as triplet of triplets of doublets ($^3J(\text{Xe},\text{F}) = 67$ Hz, $^4J(\text{Xe},\text{F}) = 9$ Hz, $^5J(\text{Xe},\text{F}) = 4$ Hz) (56), which means that $^4J(\text{Xe},\text{F})$ previously obtained from the ^{19}F NMR spectrum was incorrect (3, 4, 20).

The replacement of the *ortho* and *para* fluorine atoms in $[\text{C}_6\text{F}_5\text{Xe}][\text{BF}_4]$ by hydrogen resulted in a deshielding of the xenon atom. The opposite change occurred after replacement of the *meta* fluorine atoms by hydrogen (Table I). Consequently, the ^{129}Xe chemical shifts of 2-, 3-, and 4-fluorophenylxenonium tetrafluoroborates were -3852, -3700, and -3709 to -3739 ppm, respectively (Table I). The ^{13}C NMR spectrum of $[\text{C}_6\text{F}_5\text{Xe}]\text{Y}$ in MeCN consisted of resonances at 144.8 (C-4), 143.4 (C-2,6), 137.8 (C-3,5), and 82.2 (C-1) ppm. The latter displayed ^{129}Xe -satellites (d^* , $^1J(\text{C}-1,\text{Xe}) = 117$ to 119 Hz) (40, 57). In the series of $[\text{2,4,6-C}_6\text{H}_2\text{F}_3\text{Xe}]^+$, $[\text{2,6-C}_6\text{H}_3\text{F}_2\text{Xe}]^+$, $[\text{2-C}_6\text{H}_4\text{FXe}]^+$ the signal $\delta(\text{C}-1)$ moved to high frequency and in parallel the coupling constant $^1J(\text{C}-1,\text{Xe})$ was diminished from 117 to 78 Hz (Table I).

The influence of bases on the NMR spectra of $[\text{C}_6\text{F}_5\text{Xe}][\text{AsF}_6]$ in solutions was also studied. Thus, the addition of substituted pyridines to a solution of $[\text{C}_6\text{F}_5\text{Xe}][\text{AsF}_6]$ in MeCN caused a remarkable shielding of the fluorine atoms and an increase in the $^3J(F^{2,6},\text{Xe})$ values, from 68 (without addition of base) to 84 Hz (1 equiv of 2,6-dimethylpyridine) (58). A different picture emerged for solutions of $[\text{C}_6\text{F}_5\text{Xe}][\text{AsE}_6]$ in SO_2 and H_2O , where the coordination of oxygen on the organoxenonium cation was weaker than the coordination of nitrogen in case of MeCN (Tables I, II).

Increasing nucleophilicity of the counteranion Y in $[\text{C}_6\text{F}_5\text{Xe}]\text{Y}/\text{MeCN}$ solutions favors the cation-anion interaction and is accompanied by replacement of MeCN with Y in the coordination sphere of the organoxenonium cation. In this sense, the salts $[\text{C}_6\text{F}_5\text{Xe}][\text{HF}_2]$ (19) and $[(\text{C}_6\text{E}_5\text{Xe})_9\text{Cl}][\text{AsF}_6]$ (44) are of particular interest. All ^{19}F NMR shift values of the former salt (MeCN, -40 °C) appear at lower frequencies when compared with $[\text{C}_6\text{F}_5\text{Xe}][\text{AsF}_6]$, but at higher frequencies when compared with the covalent compound $\text{C}_6\text{F}_5\text{XeF}$ (CH_2Cl_2 , -78 °C) (Table II). The spectroscopic result indicates a strong cation-anion contact for solutions of $[\text{C}_6\text{F}_5\text{Xe}][\text{HF}_2]$. It is worth mentioning that in addition the coupling $^1J(\text{C}-1,\text{Xe}) = 135$ Hz is significantly larger than that of $[\text{C}_6\text{F}_5\text{Xe}][\text{AsF}_6]$

Table II. Selected ¹H and ¹⁹F NMR Spectral Data of Organoxenon Compounds [RXe]Y and RXeR'

Compound	Solvent	<i>t</i> , °C	$\delta(F)$, ppm ^a	<i>J</i> , Hz	Refs
[CF ₃ C≡CXe][BF ₄]	aHF	-20	-52.1 (F ³)	All ³ J(H,H) = 7	(23)
[C ₄ H ₉ C≡CXe][BF ₄] ^b	aHF	-30		All ³ J(H,H) = 7	(23)
[C ₄ H ₉ C≡CXe][BF ₄] ^c	CH ₂ Cl ₂	-60		³ J(F ² ,F ³) = 22.5, ⁴ J(F ² ,F ⁴) = 5,	(39)
[cyclo-1-C ₆ F ₉ Xe][AsF ₆]	aHF	-30	-83.0 (F ²), -99.0 (F ^{6,6}), -115.3 (F ^{3,3}), -127.7 (F ^{5,5}), -131.3 (F ^{4,4})	⁴ J(F ² ,F ⁶) = 9.4	
[<i>cis</i> -CF ₃ CF=CFXe][C ₃ F ₇ BF ₃]	aHF	-10	-65.4 (F ³), -77.4 (F ¹), -122.9 (F ²)	⁴ J(F ³ ,Xe) = 40, ⁴ J(F ¹ ,F ³) = 7, ³ J(F ¹ ,F ²) = 71, ² J(F ¹ ,Xe) = 153, ³ J(F ² ,F ³) = 9, ³ J(F ² ,Xe) = 183	(22)
[<i>trans</i> -HCF=CFXe][BF ₄] ^d	aHF	-40	-106.3 (F ¹), -148.2 (F ²)	³ J(H,F ¹) = 5, ² J(H,F ²) = 68, ³ J(H,Xe) = 22, ³ J(F ¹ ,F ²) = 115, ² J(F ¹ ,Xe) = 209, ³ J(F ² ,Xe) = 58	(22)
[CF ₂ =CHXe][BF ₄] ^e	aHF	-60	-60.2 (F ^{2_{cis}}), -67.3 (F ^{2_{trans}})	³ J(H,F ^{2_{cis}}) = 18, ² J(H,Xe) = 54, ² J(F ^{2_{cis}} ,F ^{2_{trans}}) = 7.5, ³ J(F ^{2_{trans}} ,Xe) = 156	(54)
[CF ₂ =C(CF ₃)Xe][BF ₄]	aHF	-60	-47.2 (F ^{2_{cis}}), -51.5 (F ^{2_{trans}}), -56.5 (CF ₃)	² J(F ^{2_{cis}} ,F ^{2_{trans}}) = 23, ⁴ J(F ^{2_{cis}} ,CF ₃) = 8, ³ J(F ^{2_{cis}} ,Xe) = 4, ⁴ J(F ^{2_{trans}} ,CF ₃) = 18, ³ J(F ^{2_{trans}} ,Xe) = 144	(53, 54)
[CF ₂ =C(CF ₃)Xe][BF ₄]	EtCN	-60	-49.8 (F ^{2_{cis}}), -55.3 (F ^{2_{trans}}), -57.1 (CF ₃)	² J(F ^{2_{cis}} ,F ^{2_{trans}}) = 17, ⁴ J(F ^{2_{cis}} ,CF ₃) = 9, ⁴ J(F ^{2_{trans}} ,CF ₃) = 17,	(53, 54)

[2-FC ₆ H ₄ Xe][BF ₄]	MeCN	-30	-100.6 (F ²)	³ J(F ² _{arms} ,Xe) = 138
[3-FC ₆ H ₄ Xe][BF ₄]	RCN ^f	-30	-108.7 (F ³)	³ J(F ² ,Xe) = 48
[4-FC ₆ H ₄ Xe][BF ₄]	RCN ^f	-80	-106.4 (F ⁴)	(12)
[3,5-C ₆ H ₃ F ₂ Xe][BF ₄] ^g	RCN ^f	-60	-101.2 (F ^{3,5})	(20)
[2,6-C ₆ H ₃ F ₂ Xe][BF ₄]	MeCN	-30	-99.6 (F ^{2,6})	(60)
[2,4,6-C ₆ H ₂ F ₃ Xe][BF ₄]	MeCN	35	-96.3 (F ^{2,6}), -96.0 (F ⁴)	(60)
[3,4,5-C ₆ H ₂ F ₃ Xe][BF ₄] ^h	MeCN	-30	-125.9 (F ^{3,5}), -150.4 (F ⁴)	(20)
[2,3,4,5-C ₆ HF ₄ Xe][BF ₄] ⁱ	MeCN	-30	-122.5 (F ²), -147.3 (F ³), -144.4 (F ⁴), -132.1 (F ⁵)	(20)
[C ₆ F ₃ Xe][BF ₄]	MeCN	-30	-125.5 (F ^{2,6}), -142.3 (F ⁴), -155.0 (F ^{3,5})	(20)
[C ₆ F ₅ Xe][BF ₄]	aHF	-10	-123.3 (F ^{2,6}), -137.9 (F ⁴), -151.5 (F ^{3,5})	(20)
[C ₆ F ₃ Xe][HF ₂]	MeCN	-40	-127.1 (F ^{2,6}), -144.6 (F ⁴), -156.1 (F ^{3,5})	(19)
[C ₆ F ₃ Xe][AsF ₆]	MeCN	-40	-125.1 (F ^{2,6}), -141.5 (F ⁴), -154.3 (F ^{3,5})	(40)
[C ₆ F ₃ Xe][AsF ₆]	H ₂ O	35	-126.5 (F ^{2,6}), -142.5 (F ⁴), -154.7 (F ^{3,5})	(30)

Continued on next page.

Table II. Continued.

Compound	Solvent	t , °C	$\delta(F)$, ppm ^a	J , Hz	Refs
[C ₆ F ₅ Xe][AsF ₆]	SO ₂	0	-124.6 (F ^{2,6}), -139.6 (F ⁴), -152.8 (F ^{3,5})	³ J(F ^{2,6} ,Xe) = 64	(30)
[(C ₆ F ₅ Xe) ₂ Cl][AsF ₆]	MeCN	-40	-128.2 (F ^{2,6}), -144.3 (F ⁴), -155.5 (F ^{3,5})	³ J(F ^{2,6} ,Xe) = 81, ⁴ J(F ⁴ ,F ^{2,6}) = 4, ³ J(F ⁴ ,F ^{3,5}) = 20	(44)
[C ₆ F ₅ XeF ₂][BF ₄]	CD ₃ CN	-40	-125.5 (F ^{2,6}), -135.0 (F ⁴), -153.4 (F ^{3,5}), -29.5 (XeF ₂ ⁺)	¹ J(F,Xe) = 3893, ³ J(F ⁴ ,F ^{3,5}) = 20	(5, 61)
[C ₆ F ₅ XeF ₂][BF ₄]	aHF	-80	-123.6 (F ^{2,6}), -129.0 (F ⁴), -150.4 (F ^{3,5}), -33.1 (XeF ₂ ⁺)	¹ J(F,Xe) = 3891, ⁴ J(F ⁴ ,F ^{2,6}) = 9, ³ J(F ⁴ ,F ^{3,5}) = 18, ⁶ J(F ⁴ ,XeF) = 9	(61)
C ₆ F ₅ XeF	MeCN	-30	-129.3 (F ^{2,6}), -148.4 (F ⁴), -157.8 (F ^{3,5}), 4.5 (XeF)	¹ J(F,Xe) = 4100, ³ J(F ^{2,6} ,Xe) = 82	(62)
C ₆ F ₅ XeF	CD ₂ Cl ₂	-78	-129.3 (F ^{2,6}), -146.9 (F ⁴), -156.5 (F ^{3,5}), -3.5 (XeF)	¹ J(F,Xe) = 4013, ³ J(F ^{2,6} ,Xe) = 81, ³ J(F ⁴ ,F ^{3,5}) = 20, ⁴ J(F ^{2,6} ,XeF) = 19	(42, 43)
C ₆ F ₅ XeCl	CD ₂ Cl ₂	-60	-130.8 (F ^{2,6}), -146.2 (F ⁴), -155.5 (F ^{3,5})	³ J(F ^{2,6} ,Xe) = 94, ³ J(F ⁴ ,F ^{3,5}) = 21, ⁴ J(F ⁴ ,F ^{2,6}) = 3	(44)
C ₆ F ₅ XeC ₆ F ₅	CD ₂ Cl ₂	-78	-128.2 (F ^{2,6}), -144.3 (F ⁴), -155.5 (F ^{3,5})	³ J(F ⁴ ,F ^{3,5}) = 21, ³ J(F ^{2,6} ,Xe) = 43	(42, 43)
C ₆ F ₅ XeC ₆ F ₅	(CD ₃) ₂ C O	-58	-131.4 (F ^{2,6}), -153.4 (F ⁴), -158.4 (F ^{3,5})	³ J(F ^{2,6} ,Xe) = 45, ⁴ J(F ^{3,5} ,Xe) = 35, ⁵ J(F ⁴ ,Xe) = 9.5	(62)
C ₆ H ₅ C≡CXeF	CH ₂ Cl ₂	-78	-23.1 (XeF)	¹ J(F,Xe) = 4301	(63)

^a Without the signals of the counteranion Y.

^b ¹H NMR: δ 2.68 (H³), 1.66 (H⁴), 1.46 (H⁵), 0.95 (H⁶).

^c ¹H NMR: δ 2.59 (H³), 1.55 (H⁴), 1.35 (H⁵), 0.87 (H⁶).

^d ¹H NMR: δ 7.75.

^e ¹H NMR: δ 7.56.

^f In CD₃CN - EtCN (1 : 3 v/v).

^g ¹H NMR: δ 7.94 (H^{2,6}), 7.59 (H⁴).

^h ¹H NMR: δ 8.05.

ⁱ ¹H NMR: δ 8.11.

(117 Hz), although the difference in the $\delta(\text{C})$ values is negligible (Table I). The enhanced contribution of covalent character in $[(\text{C}_6\text{F}_5\text{Xe})_2\text{Cl}][\text{AsF}_6]$ (MeCN, -40 °C) is displayed in the ^{13}C , ^{19}F , and ^{129}Xe NMR spectra (Tables I, II) and can be outlined by the significant shielding of carbon C-1, xenon, and the fluorine atoms as well as by larger coupling constants $^1J(\text{C-1,Xe})$ (195 Hz) and $^3J(\text{F}^{2,6},\text{Xe})$ (81 Hz).

When Y is a highly nucleophilic anion like F^- , Cl^- , CN^- , or $\text{C}_6\text{F}_5\text{CO}_2^-$, the organoxenon compound RXeY has covalent character (δ). Although the chemical, spectroscopic, and structural characterizations of these compounds are outside the scope of this review, a several sets of typical NMR spectroscopic data for covalent pentafluorophenylxenon derivatives $\text{C}_6\text{F}_5\text{XeR}'$ ($\text{R}' = \text{F}, \text{Cl}, \text{C}_6\text{F}_5$) are included in Tables I and II for comparison.

NMR Spectra of $[\text{C}_6\text{F}_5\text{XeF}_2][\text{BF}_4]$

The salt, $[\text{C}_6\text{F}_5\text{XeF}_2][\text{BF}_4]$, is the only known organoxenon(IV) derivative (5). Its ^{19}F NMR spectrum in MeCN (-40 °C) consists of resonances at -29.5 (XeF_2^+), -125.5 ($\text{F}^{2,6}$), -135.0 (F^4), -153.4 ($\text{F}^{3,5}$), and -149.0 ppm ($[\text{BF}_4]^-$). The XeF_2 resonance shows satellites corresponding to a one-bond scalar coupling to ^{129}Xe with $^1J(\text{F,Xe}) = 3893$ Hz. This 1J value is comparable to that of XeF_4 itself ($^1J(\text{F,Xe}) = 3908$ Hz), but the fluorine atoms bonded to xenon are more shielded than that of XeF_4 (-19.1 ppm) (MeCN, -40 °C). The ^{129}Xe NMR spectrum of $[\text{C}_6\text{F}_5\text{XeF}_2][\text{BF}_4]$ in MeCN (-40 °C) consists of a triplet at δ -1706 ppm ($^1J(\text{Xe,F}) = 3892$ Hz) located at significantly lower frequencies relative to that of XeF_4 (δ 317 ppm, $^1J(\text{Xe,F}) = 3895$ Hz) (MeCN, 24 °C) (59). The difference in ^{129}Xe chemical shifts between $[\text{C}_6\text{F}_5\text{XeF}_2][\text{BF}_4]$ and XeF_4 is of the same magnitude as that between $[\text{C}_6\text{F}_5\text{Xe}][\text{BF}_4]$ (δ -3787) and XeF_2 (δ -1788) (both in MeCN, -30 °C). This comparison demonstrates the effect of the formal substitution of two fluoride anions by one carbanion. The ^{13}C NMR spectrum of the same solution at -40 °C shows resonances at δ 121.9 (C-1), 143.3 (C-2,6), 138.3 (C-3,5), and 148.5 (C-4) (5). The solution of $[\text{C}_6\text{F}_5\text{XeF}_2][\text{BF}_4]$ in aHF (-80 °C) displays the expected deshielding of the carbon-bonded fluorine atoms with respect to that in MeCN, whereas the signal of the XeF_2^+ moiety moves in the opposite direction, from -29.5 to -33.1 ppm (Table II). In the ^{129}Xe NMR spectra the distinctions caused by both solvents are less than that observed for $[\text{C}_6\text{F}_5\text{Xe}][\text{BF}_4]$: the $\Delta\delta(\text{Xe})$ values are -72 and -152 ppm, respectively. The coupling constant $^1J(\text{Xe,F})$ is not noticeably influenced by either solvent (Table I).

References

1. Žemva, B. Noble Gases: Inorganic Chemistry. In *Encyclopedia of Inorganic Chemistry*; King, R. B. (Ed.) Vol. 5, Wiley, New York, 1994; pp 2660–2680.

2. Christe, K. O. *Angew. Chem. Int. Ed.* **2001**, *40*, 1419-1421, ref. 15.
3. Naumann, D.; Tyrra, W. *J. Chem. Soc. Chem. Commun.* **1989**, 47-50.
4. Frohn, H.-J.; Jakobs, S. *J. Chem. Soc. Chem. Commun.* **1989**, 625-627.
5. Frohn, H.-J.; LeBlond, N.; Lutar, K.; Žemva, B. *Angew. Chem. Int. Ed.* **2000**, *39*, 391-393.
6. Frohn, H.-J.; Bardin, V. V. *Organometallics* **2001**, *20*, 4750-4762.
7. Tyrra, W.; Naumann, D. Organoxenon compounds. In *Inorganic Chemistry Highlights*; Meyer, G.; Naumann, D.; Wesemann, L. (Eds.) Wiley-VCH, Weinheim, 2002; pp. 297-316.
8. Brel, V. K.; Pirguliyev, N. Sh.; Zefirov, N. S. *Usp. Khim.* **2001**, *70*, 262-298; *Russ. Chem. Rev.* **2001**, *70*, 231-264.
9. (a) Holtz, D.; Beauchamp, J. L. *Science* **1971**, *173*, 1237-1238. (b) Hovey, J. K.; McMahan, T. B. *J. Am. Chem. Soc.* **1986**, *108*, 528-529.
10. Pettersson, M.; Lundell, J.; Räsänen, M. *Eur. J. Inorg. Chem.* **1999**, 729-737.
11. (a) Carlson, T. A.; White, R. M. *J. Chem. Phys.* **1962**, *36*, 2883-2887. (b) Nefedov, V. F.; Toropova, M. A.; Levchenko, A. V. *Radiokhim.* **1967**, *9*, 138-139; *Sov. Radiochem.* **1967**, *9*, 166-167. (c) Toropova, M. A.; Nefedov, V. F.; Levchenko, A. V.; Saikov, Y. P. *Radiokhim.* **1968**, *10*, 611-613; *Sov. Radiochem.* **1968**, *10*, 601-603. (d) Toropova, M. A.; Nefedov, V. F.; Levchenko, A. V.; Matveev, O. G. *Radiokhim.* **1968**, *10*, 613; *Sov. Radiochem.* **1968**, *10*, 604. (e) Toropova, M. A.; Nefedov, V. F.; Levchenko, A. V.; Saikov, Y. P. *Radiokhim.* **1968**, *10*, 616-619; *Sov. Radiochem.* **1968**, *10*, 608-611.
12. Frohn, H.-J.; Rossbach, C. *Z. Anorg. Allg. Chem.* **1993**, *619*, 1672-1678.
13. Frohn, H.-J.; Jakobs, S.; Rossbach, C. *Eur. J. Solid State Inorg. Chem.* **1992**, *29*, 729-738.
14. Naumann, D.; Butler, H.; Gnann, R.; Tyrra, W. *Inorg. Chem.* **1993**, *32*, 861-863.
15. Butler, H.; Naumann, D.; Tyrra, W. *Eur. J. Solid State Inorg. Chem.* **1992**, *29*, 739-758.
16. Naumann, D.; Tyrra, W.; Pfolk, D. *Z. Anorg. Allg. Chem.* **1994**, *620*, 987-992.
17. Naumann, D.; Tyrra, W.; Gnann, R.; Pfolk, D. *J. Chem. Soc. Chem. Commun.* **1994**, 2651-2653.
18. Frohn, H.-J.; Jakobs, S.; Henkel, G. *Angew. Chem. Int. Ed.* **1989**, *28*, 1506-1507.
19. Frohn, H.-J.; Schroer, T. *J. Fluorine Chem.* **2001**, *112*, 259-264.
20. Frohn, H.-J.; Franke, H.; Bardin, V. V. *Z. Naturforsch.* **1999**, *54B*, 1495-1498.
21. Abo-Amer, A.; Frohn, H.-J.; Steinberg, C.; Westphal, U. *J. Fluorine Chem.*, in press.
22. Frohn, H.-J.; Adonin, N. Yu.; Bardin, V. V. *Z. Anorg. Allg. Chem.* **2003**, *70*, 2499-2508.

23. (a) Frohn H.-J., Bardin V. V., *Chem. Commun.* **2003**, 2352–2353. (b) Frohn, H.-J.; Bardin, V. V.; *Eur. J. Inorg. Chem.*, in press.
24. Zhdankin, V. V.; Stang, P. J.; Zefirov, N. S. *J. Chem. Soc. Chem. Commun.* **1992**, 578–579.
25. Frohn, H.-J.; Bardin, V. V. *Z. Anorg. Allg. Chem.* **2003**, 629, 2465–2469.
26. Hansch, C.; Leo, A.; Taft, R. W. *Chem. Rev.* **1991**, 91, 165–195.
27. Frohn, H.-J., Bardin, V. V., *Chem. Commun.*, **1999**, 919–920.
28. Frohn, H.-J.; Bardin, V. V. *Z. Anorg. Allg. Chem.* **2002**, 628, 1853–1856.
29. Frohn, H.-J.; Bardin, V. V.; publication in preparation.
30. Frohn, H.-J.; Klose, A.; Schroer, T.; Henkel, G.; Buss, V.; Opitz, D.; Vahrenhorst, R. *Inorg. Chem.* **1998**, 37, 4884–4890.
31. Yagupolskii, Yu. L.; Tyrra, W.; Gnann, R.; Maggiorosa, N.; Naumann, D. *J. Fluorine Chem.* **2002**, 113, 143–146.
32. Franke, H. Doctoral Dissertation, University of Duisburg, Duisburg, Germany, 2000.
33. Schroer, T. Doctoral Dissertation, University of Duisburg, Duisburg, Germany, 1996.
34. Frohn, H.-J.; Klose, A.; Henkel, G. *Angew. Chem. Int. Ed.* **1993**, 33, 99–100.
35. Frohm, H.-J.; Bardin, V. V. *Z. Anorg. Allg. Chem.* **2004**, 630, 1022–1024.
36. Frohn, H.-J.; Bardin, V. V. *Z. Anorg. Allg. Chem.* **1996**, 622, 2031–2034.
37. Frohn, H.-J.; Bardin, V. V. *Z. Naturforsch.* **1998**, 53B, 562–564.
38. Frohn, H.-J.; Bardin, V. V. *Z. Naturforsch.* **1996**, 51B, 1011–1014.
39. Frohn, H.-J.; Bardin, V. V. *J. Chem. Soc. Chem. Commun.* **1993**, 1072–1074.
40. Frohn, H.-J.; Klose, A.; Bardin, V. V.; Kruppa, A. I.; Leshina, T. V. *J. Fluorine Chem.* **1995**, 70, 147–154.
41. Frohn, H.-J.; Bardin, V. V. *Mendeleev Commun.* **1995**, 114–115.
42. Frohn, H.-J.; Theissen, M. *J. Fluorine Chem.* **2004**, 125, 981–988.
43. Frohn, H.-J.; Theissen, M. *Angew. Chem. Int. Ed.* **2000**, 39, 4591–4593.
44. Frohn, H.-J.; Schroer, T.; Henkel, G. *Angew. Chem. Int. Ed.* **1999**, 38, 2554–2556.
45. Naumann, D.; Gnann, R.; Padelidakis, V.; Tyrra, W. *J. Fluorine Chem.* **1995**, 72, 79–82.
46. Frohn, H.-J.; Klose, A.; Bardin, V. V. *J. Fluorine Chem.* **1993**, 64, 201–215.
47. Helber, J.; Frohn, H.-J.; Klose, A.; Scholten, T. *Arkivoc*, **2003**, N 6, 71–82. <http://www.arkat-usa.org/ark/journal/2003/Varvoglis/AV-682A/682.pdf>
48. Butler, H.; Naumann, D.; Tyrra, W. *Eur. J. Solid State Inorg. Chem.* **1992**, 29, 739–v758.
49. Frohn, H.-J.; Bardin, V. V. Organoethynylxenon(II) Tetrafluoroborates [RC~CXe] [BE₄]. In Abstracts, 18th International Symposium on Fluorine Chemistry, Bremen, Germany, Jul 30–Aug 4, 2006; p 92.

50. Frohn, H.-J.; Klose, A.; Henkel, G. *GJTFachz. Lab.* **1993**, *37*, 752–755.
51. Schumacher, G. A.; Schrobilgen, G. J. *Inorg. Chem.* **1984**, *23*, 2923–2929.
52. NMR nomenclature. Nuclear spin properties and conventions for chemical shifts. *Pure Appl. Chem.* **2001**, *73*, 1795–1818.
53. Bardin, V. V.; Frohn, H.-J. *Magn. Res. Chem.* **2006**, *44*, 648–650.
54. Frohn, H.-J.; Bardin, V. V. *Z. Anorg. Allg. Chem.* **2003**, *629*, 2465–2469.
55. As a convention the multiplicities of the ^{19}F NMR signals caused by couplings with the ^{129}Xe nucleus (satellites) are denoted by (*).
56. Koppe, K. Doctoral Dissertation, University of Duisburg-Essen, Duisburg, Germany, 2005.
57. Frohn, H.-J.; Jakobs, S.; Henkel, G. *Angew. Chem. Int. Ed.* **1989**, *28*, 1506–1507.
58. Frohn, H.-J.; Schroer, T.; Henkel, G. *Z. Naturforsch.* **1995**, *50B*, 1799–1810.
59. Christe, K. O.; Curtis, E. C.; Dixon, D. A.; Mercier, H. P.; Sanders, J. C. P.; Schrobilgen, G. J. *J. Am. Chem. Soc.* **1991**, *113*, 3351–3361.
60. Naumann, D.; Butler, H.; Gnann, R.; Tyrra, W. *Inorg. Chem.* **1993**, *32*, 861–863.
61. Koppe, K.; Frohn, H.-J.; Mercier, H. P. A.; Schrobilgen, G. J. Difluoropentafluorophenylxenon (IV) Tetrafluoroborate, $[\text{C}_6\text{F}_5\text{XeF}_2][\text{BF}_4]$, an Improved Synthesis and Detailed Structural Study. In *Abstracts*, 18th International Symposium on Fluorine Chemistry, Bremen, Germany, Jul 30–Aug 4, 2006; p 219.
62. Maggiorosa, N.; Naumann, D.; Tyrra, W. *Angew. Chem. Int. Ed.* **2000**, *39*, 4588–4591.
63. Schmidt, H.; Scherer, H.; Tyrra, W.; Hahn, J.; Naumann, D. *Inorg. Chem.* **2004**, *43*, 1837–1839.

Chapter 21

Halogen Transfer Reactions from *bis*-Amino Halonium Ions to Acceptor Olefins: Mechanism and Strategies for Chiral Halogenation

R. Stan Brown, Alexei A. Neverov, C. Tony Liu,
and Christopher I. Maxwell

Department of Chemistry, Queen's University, Kingston, Ontario K7L 3C1,
Canada

Studies of the transfer of Br^+ and I^+ from amine-coordinated halonium ions to acceptor 1- ω -alkenols have been undertaken to determine the mechanism in an effort to assist in the development of chiral transfer reagents. Transfer of Br^+ and I^+ from two commercially available dimeric hydroquinine and hydroquinidine ligands ((DHQ)₂PHAL and (DHQD)₂PHAL) to various 1, ω -alkenols and 1, ω -alkenoic acids is shown to provide enantiomeric excesses of 4-47% depending on the acceptor alkene.

Transfer of a halonium ion to 1, ω -alkenols or 1, ω -alkenoic acids which are capable of undergoing halocyclization is a key method to generate 4-, 5- and 6-membered heterocyclic rings via the so-called halocyclization processes (1,2,3,4,5,6,7). This synthetic method would be far more valuable if the halogen transfer to an achiral alkene could be conducted in a chiral fashion (exemplified in Figure 1) as it would produce optically active heterocycles that could be further functionalized through manipulation of the halomethyl group.

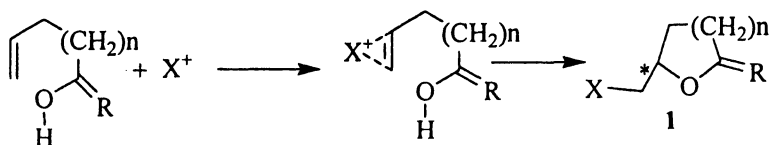
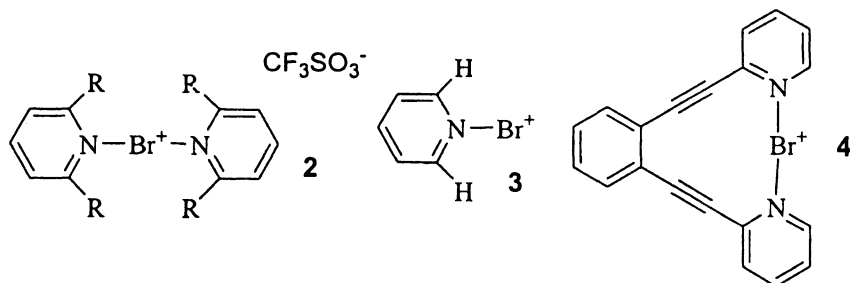


Figure 1. Generalized scheme for halocyclization of a 1, ω -alkenol or 1, ω -alkenoic acid, R=O, H₂, n=1-3.

There are presently four viable approaches to induce an asymmetric environment for the Br⁺ addition to an alkene: a) halogenation inside crystalline cyclodextrin complexes (8,9); b) reactions in solution using chiral ammonium bromides/tribromides or chiral N-bromoamides as Br⁺-transfer agents (10,11); and c) Br₂-addition to olefins or enolates containing a temporarily attached chiral auxiliary (12,13,14,15). More recently, chiral 1,2-dibromides have been synthesized with very high enantioselectivities using chiral mono- and bi-metallic Pd(II) and Cu(II) catalysts (16). The first two approaches suffer from limited substrate selectivity and low e.e.'s, while the third requires that the substrate have a functional group to which the chiral auxiliary can be attached. For the fourth approach, the available evidence indicates that the highest enantioselectivities (95%) occur with terminal olefins, but lower enantioselectivities of 14-84% occur with internal olefins.

A more general approach involves development of reagent-controlled catalysts for X⁺-transfer, defined as having a chiral reagent that directs the addition of the electrophilic X⁺ to one face of the π -bond, but only a limited number of reports of these exists (17,18,19,20) including our own work (21,22,23). In one completed study (21) we investigated the transfer of Br⁺ from



the *bis*(pyridine) bromonium complexes, **2**, where the pyridine 2- and 6-substituents were varied from H to CH₃, cyclopentyl, cyclohexyl, and 2(-)-menthyl. However, very small enantiomeric excesses were observed for the bromocyclization of 4-penten-1-ol and 4-pentenoic acid mediated by *bis*(2(-)-menthylpyridine) bromonium triflate (**21**). Further work (**24**) on the mechanism of Br⁺-transfer from the parent *bis*(pyridine) bromonium ion pointed to a possible source of the lack of chiral induction. The overall process involves a dissociation of **2** (R=H) into **3** (R=H) which is subsequently captured by the alkene (via a π -complex) to give cyclized product **1**. Interestingly the relative rate constants for capture of **3** by a variety of mono, di, tri and tetrasubstituted alkenes were far less sensitive to the nature of the alkene than is the case for electrophilic bromination using Br₂. Moreover, in the bis-complex (**4**) (**24**) the analogous dissociated form (involving rotation of a single pyridine out of complexation) reacted with all acceptors at or near the diffusion limit. This points out an obvious, but often overlooked key concept in designing chiral reagents for X⁺-transfer: the intermediates cannot be so reactive that there is no chemical barrier to their reaction with acceptors otherwise there can be no chiral discrimination.

In what follows we describe some key experiments upon which our current understanding of the mechanism of transfer of Br⁺ and I⁺ from amine complexed halonium ions to acceptor olefins in order to determine the possible origins of enantiomeric selectivity. All the background kinetic work was performed with *bis*(pyridine) and *bis*(substituted-pyridine) halonium triflates in dichloroethane at 25 °C. Triflate counterion was chosen as a poorly nucleophilic counterion which would not interfere with the primary process of X⁺-transfer from the pyridine-X⁺ which we subsequently show is an obligatory intermediate for all these reactions. We will attempt to put these findings into the appropriate physical organic framework for thinking about the requirements for achieving chiral induction. Subsequently, we will turn our attention to experiments aimed at achieving enantiomeric excess for transfer of X⁺ from the *in situ*-generated halonium ion of two commercially available chiral dimeric cinchona-based ligands to some 1, ω -alkenols and alkenoic acids.

General mechanism for transfer of X⁺ from *bis*-amino halonium ions to acceptor olefins.

Before we start with the discussion of the transfer of X⁺ from nitrogen to the alkene, one might consider the somewhat pedagogical question of whether the charge on the starting halo-N complex is localized on the halogen, or on the amine, and thus whether the starting complex is better represented as and X⁺-

amine (which we have chosen to do for the remainder of the chapter) or X-ammonium ion (25). Simple Lewis structures give the impression that the formal charge should be largely borne by the N and its constituent C-H units (an N-halo ammonium ion). The question is not as settled as one would like and to our knowledge, relatively little computational data are available from which one could ascertain the charge densities on the various atoms. In the case of the N-fluoropyridinium ion, *ab initio* calculations (RHF/DZ+P; (9,5,1)/[3,2,1] basis sets for C and F, (4,1)/[2,1] basis sets for H) give Mulliken populations of -0.155, +0.232 and 0.004 on F, N and the adjacent C₁ respectively (26), indicating the halogen carries no (+) in this case. However, to our knowledge, high level calculations have not been performed on the corresponding N-bromo or -iodo pyridines although these would be extremely valuable, and given that the Pauling electronegativities of the various atoms fall in the order of F(4.0) > N(3.0) > Br(2.8) > I(2.5), it is possible that the halogen will become more positively charged than the nitrogen as we move down the periodic table.

Adamantylideneadamantane (Ad=Ad) as an acceptor olefin.

Ad=Ad is a unique olefin which we have shown forms stable bromonium (27) and iodonium (28) ions, both of which are stable enough to be characterized by X-ray crystallography. The alkene structure is such that X⁺ can be transferred to the olefin unit but no further addition or elimination reactions are possible due to the steric hindrance to backside attack and the lack of an appropriately aligned allylic H for elimination to form a double-bond rearranged allylic halide. Since the reaction of Ad=Ad with *bis(sym-collidine)-Br⁺* is subject to a common species rate depression in added [collidine], the mechanism given in Figure 2 is implied from which can be derived various forms of the kinetic expression given in eq 1 (22). By determining the observed rate constant (*k*_{obs}) for disappearance of the *bis(sym-collidine)-Br⁺* as a function of both added [Ad=Ad] and [collidine], one can determine its dissociation rate constant (*k*_d) and partitioning ratio (*k*₂/*k*_d) for the intermediate mono(*sym-collidine*)-Br⁺ ion of 205 s⁻¹ and 0.38 respectively. Of note is the fact that the final product (5) has the Br⁺ coordinated by Ad=Ad and one collidine, so the free bromonium ion of the alkene does not appear to be a thermodynamically stable form, although it is certainly a kinetically important intermediate for transfer of Br⁺ from one Ad=Ad to another alkene (29,23). In the same vein, the Br⁺ from *bis(sym-collidine)-Br⁺* can be transferred to reactive 1,ω-alkenols (22), although these reactions are slightly more complex than transfer to Ad=Ad because of the subsequent ring-closure. The mechanism for this reaction is given in Figure 3

and is consistent with the observation of a common species rate depression in added [collidine].

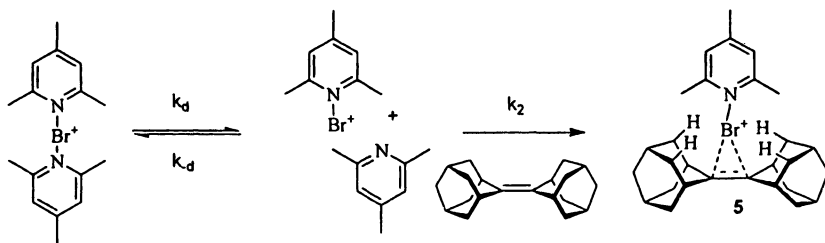


Figure 2. Mechanism for transfer of Br^+ from *sym(collidine)* bromonium ion to $\text{Ad}=\text{Ad}$.

$$k_{\text{obs}} = \frac{k_d k_2 [\text{Ad} = \text{Ad}]}{k_{-d} [\text{col}] + k_2 [\text{Ad} = \text{Ad}]} = \frac{k_d [\text{Ad} = \text{Ad}]}{\frac{k_{-d}}{k_2} [\text{col}] + [\text{Ad} = \text{Ad}]} = \frac{\frac{k_d k_2}{k_{-d}} [\text{Ad} = \text{Ad}]}{[\text{col}] + \frac{k_2}{k_{-d}} [\text{Ad} = \text{Ad}]} \quad (1)$$

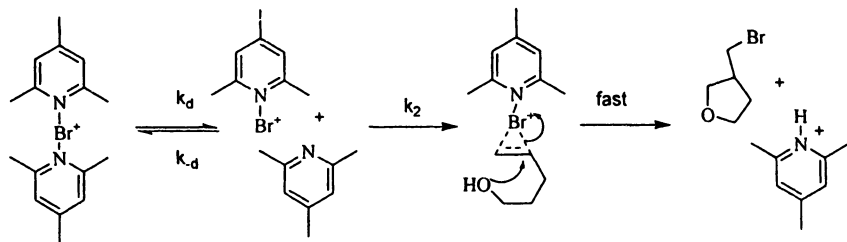


Figure 3. Mechanism for Br^+ transfer from *sym(collidine)* bromonium ion to 4-penten-1-ol, from reference (22).

Detailed kinetic analysis (22) provided the following constants: k_d 205 s^{-1} , $k_{-d} = 3.4 \times 10^6 \text{ M}^{-1}\text{s}^{-1}$ and k_2/k_{-d} 0.015. From the fact that the partitioning ratio (k_2/k_{-d}) is far smaller (about 25-fold) than in the case of reaction of (*sym*-collidine)- Br^+ with $\text{Ad}=\text{Ad}$, it is clear that there is some sensitivity of the partitioning ratio to the alkene structure, although not nearly as great as there is in a normal electrophilic addition of Br_2 to an alkene, where the addition of each subsequent alkyl group on an alkene gives a 15- to 90-fold increase in the reaction rate constant (30). The decrease in the partitioning ratio also means that the initial dissociation of *bis(sym-collidine)*- Br^+ is a true equilibrium process and

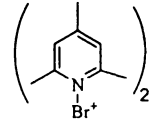
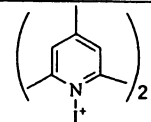
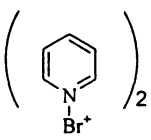
allows one to calculate an equilibrium constant of $K_{\text{eq}} = 6 \times 10^{-5} \text{ M}$, and a k_2 reaction rate constant of the (*sym*-collidine)- Br^+ intermediate with the alkene of $5.1 \times 10^4 \text{ M}^{-1}\text{s}^{-1}$.

Interestingly, subsequent study (31) of the reaction of the *bis*(*sym*-collidine)-iodonium ion with 4-penten-1-ol, 4-hexen-1-ol and Ad=Ad indicated that the iodonium ion also reacts by the same dissociative two-step mechanism as given in Figure 3, but the k_d rate constant is 0.75 s^{-1} (about 250-fold less than the corresponding bromonium ion). The k_2/k_d partitioning ratio is 0.045 and 0.043 respectively for the two alkenols, the two values being ~ 3 -fold greater than with the bromonium ion. However, when the *bis*(*sym*-collidine)-iodonium ion was reacted with Ad=Ad, the same dissociation constant $k_d = 0.75 \text{ s}^{-1}$ was observed, but the k_2/k_d partitioning ratio is 0.0031, at least 100-times less than with the corresponding bromonium ion (0.38). This very large discrimination must stem from a larger sensitivity of the iodine to the restricted space about the double bond of the Ad=Ad as shown in **5** and points out an interesting trade-off between electronic effects and steric effects which strongly retard the reaction with Ad=Ad in the case of the I-analogue.

Further study of the transfer of Br^+ from the *bis*(pyridine)- Br^+ (**2**, R=H) revealed that its overall mechanism is the same as with *bis*(*sym*-collidine)- Br^+ , but there is an interesting insensitivity of the partitioning ratio to the structure of the acceptor alkene (**24**). The k_{obs} values for the reaction of **2**, R=H with four representative alkenes (Ad=Ad, cyclohexene, 4-penten-1-ol and 4-pentenoic acid) each show a common species rate depression in the presence of added pyridine, and a saturation behavior in the presence of increasing [olefin]. Analysis of all the kinetic data provides dissociation rate constant (k_d) for **2**, R=H and partitioning ratios (k_2/k_d) for the intermediate monopyridinium bromonium ion shown in Table 1 below, along with the available constants from our previously published studies. There are two important features of note: first, the k_d dissociation rate constant observed with all these alkenes is, within experimental uncertainty, constant at $\sim 13 \pm 2 \text{ s}^{-1}$ as one expects for a mechanism where the dissociation step is independent of acceptor alkene. This k_d value for **2**, R=H is some 16-times slower than that for dissociation of the *bis*(*sym*-collidine)- Br^+ complex (205 s^{-1}) indicating that the generation of pyridine- Br^+ species from **2**, R=H has a higher activation energy than does dissociation of the *bis*(*sym*-collidine)- Br^+ to generate of *sym*-coll- Br^+ . Perhaps this is due to the methylation of the latter's rings providing an increased ability to accommodate greater (+)-charge development in the coll- Br^+ and/or a steric effect where the 2,6-dimethyl groups on each collidine partner are buttressed against the Br^+ which is relieved by dissociation. The second point of note is the relative insensitivity of the partitioning ratio, k_2/k_d , for the monopyridine- Br^+ to the nature of the alkene which varies by only a factor of four in the Ad=Ad, (0.11); cyclohexene, (0.21); 4-penten-1-ol (0.17); and 4-pentenoic acid (0.05) series.

This contrasts the behavior of the *bis(sym-collidine)-Br⁺* system (22), where the relative reactivity of Ad=Ad, cyclohexene, 4-penten-1-ol toward coll-Br⁺ is 24, 3, and 1, and even more-so the situation for transfer of Br⁺ from the Ad=Ad-Br⁺ to Ad=Ad, cyclohexene, 4-penten-1-ol, and 4-pentenoic acid where the respective reactivities are 2×10^7 , 1.1, 3.4 and 7.6×10^{-2} (32). The reactivity difference between the coll-Br⁺ and Ad=Ad-Br⁺ ions can be rationalized by the fact that the transfer from coll-Br⁺ to the alkene is largely exothermic, having an early TS with little charge development on the alkene. Conversely, the transfer from Ad=Ad-Br⁺ to the alkene is thermoneutral (in the case of Ad=Ad) or largely endothermic with other less substituted olefins, and in the latter cases must proceed through a late TS with a large degree of charge on the alkene. The same explanation applies for pyr-Br⁺ which must be even higher in energy and more reactive than coll-Br⁺ and therefore less selective in its reaction with alkenes. This points to an interesting dilemma in designing pyridine based Br⁺-transfer agents that will discriminate between alkenes with a possible eye to chiral or diastereoselective synthesis: any appropriate transfer agent cannot produce an intermediate so reactive that it reacts with all alkenes at similar rates.

Table 1. Dissociation rate constants and partitioning ratios for reactions of various *bis*(pyridine)-halonium ions with acceptor olefins in ClCH₂CH₂Cl, T=25°C.^a

Halonium ion	k_d (s ⁻¹)	k_2/k_{-d} 4-penten-1-ol	k_2/k_{-d} cyclohexene	k_2/k_{-d} 4-hexen-1-ol	k_2/k_{-d} Ad=Ad
	205	0.015	0.045		0.38
	0.75	0.045		0.043	0.0031
	13.2	0.17	0.21		0.11

a. Data from ref.s (22, 23, 24).

Energy considerations for chiral induction.

Our attempts at using the pyridine and substituted-pyridine based bromonium ions to induce chirality were not encouraging. As exemplified by the process shown in Figure 4, the enantiomeric excesses (e.e.) in the bromocyclized products formed on reaction of the *bis*(2-(-)-menthylpyridine) bromonium ion **6** with both 4-penten-1-ol and 4-pentenoic acid were only 2.4% and 4.8% respectively (21). The exact reasons for the poor e.e.'s observed could be

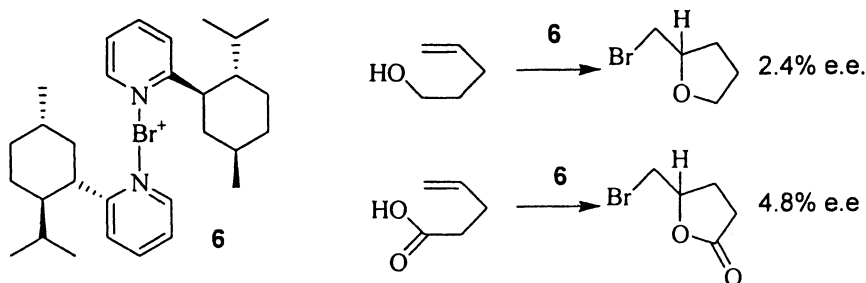
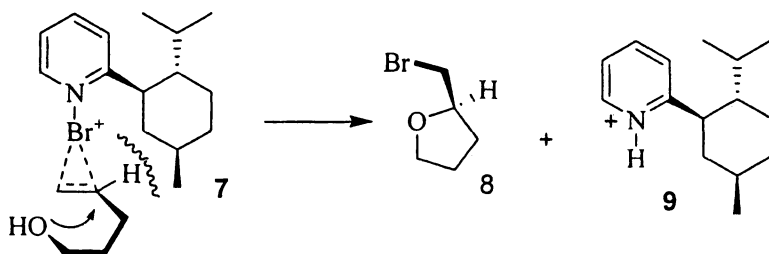


Figure 4. Enantiomeric excesses in bromocyclized products of the reaction of **6** with 4-penten-1-ol and 4-pentenoic acid

related to two main effects. First, and most obvious, there could be a weak steric effect where there is ineffective stereochemical contact between the chiral part of the 2-menthylpyridine-Br⁺ intermediate and the π -complexed alkene (**7**). Second,



the kinetic effect discussed above could be operative where the 2-menthylpyridine-Br⁺ intermediate (**7**) is so reactive there is little selectivity in the ability of different olefins to react with the intermediate. Correspondingly, there must be a small difference in energy between the diastereotopic transition structures required to produce the R- and S-enantiomers of 2-bromomethyltetrahydrofuran (**8**). In all likelihood both effects are extant and

may be linked, so it might be difficult to predict in a given case which is the more important. Addressing the steric effect requires synthesizing carefully constructed X^+ -sources where the halogen resides in a sterically restricted space so as to allow a strong discrimination for the complexation of one π -face of the alkene relative to the other. Such a species requires the X^+ to reside in a rather deep cavity extending far enough past the $N-X^+$ bond that it influences the approach of the π -system. On the other hand, if the kinetic effects result from a highly reactive intermediate, these might be overcome by stabilizing the intermediate halonium ion so its reactivity is reduced, allowing more steric interactions to come into play in determining the chiral induction.

A free energy/reaction coordinate analysis of the problem considers that the reactions described so far proceed via a reversibly-formed and unstable monoamine- X^+ ion intermediate that quickly intercepts the alkene on its pro-R or pro-S face to produce a π_R - or π_S -complex which subsequently proceeds to either the R- or S-cyclized product. Due to the observed instability of the monoamino- X^+ ions, the π -complexes must be lower in energy, so the two kinetic processes leading away from these complexes must have some activation energy to either give product or reform the monoamino- X^+ ion and free olefin. In principle the overall process must adhere to the Curtin-Hammett principle (33,34) and has two limiting cases which are accommodated by the general process shown in Figure 5 for the cyclization of a 1, ω -alkenol. In either scenario the reaction proceeds through intermediate π_S and π_R complexes reminiscent of 7.

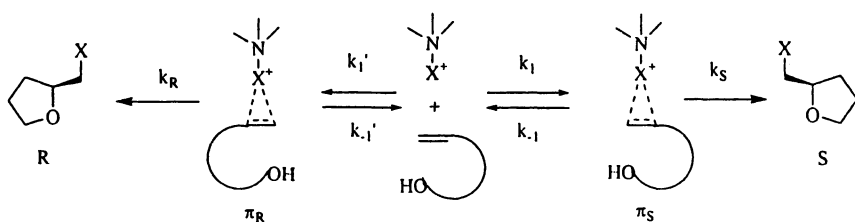


Figure 5. Stylized representation of the reaction of a monoamine halonium intermediate with a 1, ω -alkenol proceeding to R and S halocyclized products.

In Case 1 both the ring closure steps (with rate constants k_S and k_R) are faster than dissociation of the π -complexes to reform the alkenol and $N-X^+$ species. Here the [S]/[R] product ratio is determined only by the difference in the activation energy leading to the π_S - and π_R -complexes because immediately after these are formed the cyclization occurs. Thus, the chirality is set by the approach of the alkene to the halonium ion.

In Case 2, if the ring closure is slower than the reversion of the π -complex, both the π_R - and π_S -complexes are at equilibrium and freely dissociable before

the cyclization (i.e. k_1 and $k_{1'} \gg k_R$ or k_S) and the chirality is set by a combination of the $\Delta\Delta G_{R,S}$ for formation of the two possible π -complexes, and the $\Delta\Delta G_{R,S}^\ddagger$ for their ring closure as shown in Figure 6. Quantitatively, the ratio of the $[R]/[S]$ products is given in eq 2, from which it

$$\frac{d[S]/dt}{d[R]/dt} = \frac{k_S[\pi_S]}{k_R[\pi_R]} = \frac{k_S K_S [ol][NX^+]}{k_R K_R [ol][NX^+]} = \frac{(kT/h) e^{-\Delta G_S^\ddagger/RT} e^{-\Delta G_S/RT}}{(kT/h) e^{-\Delta G_R^\ddagger/RT} e^{-\Delta G_R/RT}} \quad (2)$$

is seen that the $[S]/[R]$ product ratio is given as:

$$\frac{[S]}{[R]} = e^{(\Delta G_R^\ddagger + \Delta G_R) - (\Delta G_S^\ddagger + \Delta G_S)/RT} \quad (3)$$

which indicates the product ratio is determined only by the difference in energy of the k_S and k_R transition states.

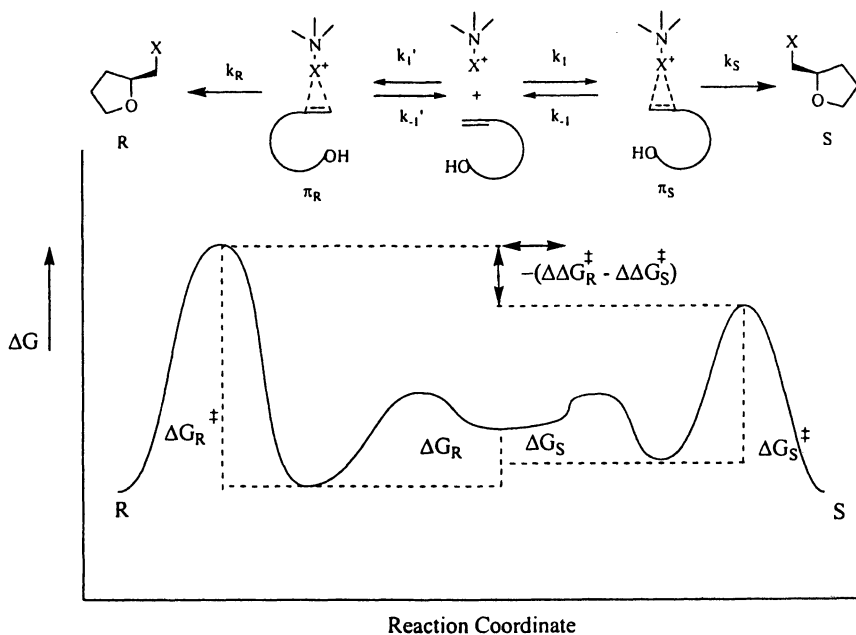


Figure 6. Reaction coordinate diagram for Case 2 of the reaction of the monoamine- X^+ ion with alkenol through π_S and π_R -complexes forming S , and R halocyclized products.

Quinuclidine halonium ions.

One of the possible ways to stabilize the amine-halonium complexes is to increase the basicity of the amine, bearing in mind that an appropriate one must also not have easily removable β -hydrogens which will lead to oxidation of the amine and formation of an imine. Quinuclidine (pK_a of quinuclidinium ion is 11.3 (35)) is 10^5 - 10^6 -fold more basic than the pyridines and both the bromonium (**10** (36)) and iodonium (**11** (37)) BF_4^- salts have been made and characterized by X-ray crystallography. Interestingly, although the reaction must generally occur as outlined in Figure 7, neither of these ions shows any observable reaction

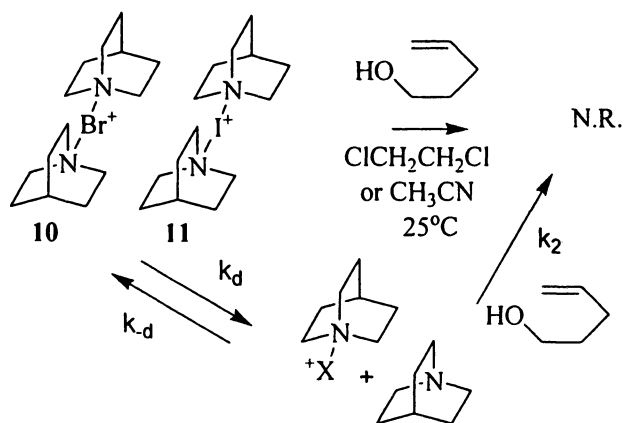


Figure 7. The quinuclidine bromonium and iodonium ions are not reactive with 4-penten-1-ol.

with 4-penten-1-ol in dichloroethane or acetonitrile for reasons that are related to the rate constant for dissociation and the very small partitioning constant (k_2/k_d) of the intermediate N-haloquinuclidinium ion. This is a consequence of the far larger nucleophilicity of the quinuclidine than the alkene and suggests that reaction could be promoted by the addition of an acid which should protonate the nascent quinuclidine and remove it from the equilibrium. Indeed, as shown in Figure 8, when either of **10** or **11** is introduced into solution with pyridinium ion, one can easily determine the rate constant for dissociation of the quinuclidine and the formation of the mixed quinuclidine pyridine- X^+ complex **12**. Two series of experiments were conducted. First, in the presence 0.1 to 2.0 mM of added 4-penten-1-ol, a kinetic investigation of the dissociation of **10** or **11** (0.03 mM in dichloroethane or acetonitrile) indicated that the k_{obs} values were independent

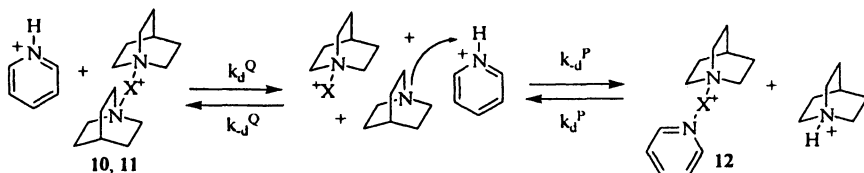


Figure 8. Scheme for trapping the *N*-haloquinuclidinium species formed from dissociation of 10, or 11 by added pyridinium ion.

of added [pyridinium ion] between 0.3 and 3 mM. This shows that at these concentrations the reaction rate does not depend on the alkene or pyridinium ion, and, $k_d^P \gg k_d^Q$, which identifies the k_d^Q step as the rate-limiting one. Given in Table 2 are the so-obtained rate constants in both solvents. Notable in the constants given in Table 1. is the fact that, for a given halonium ion, the k_d^Q dissociation rate constants are ~18-80-fold larger in the more polar acetonitrile than in dichloroethane which is consistent with development of a greater concentration of charge on fewer atoms in the TS.

Table 2. Rate constants pertaining to the processes shown in Figure 8 for reactions of the bromonium or iodonium ions 10, and 11.

Constants (↓) Solvents (→)	10 (Br^+)		11 (I^+)	
	CH_3CN	$CICH_2CH_2Cl$	CH_3CN	$CICH_2CH_2Cl$
k_d^Q (s^{-1})	0.120±0.003	(1.45±0.03) $\times 10^{-3}$	(4.3±0.5) $\times 10^{-3}$	(2.5±0.2) $\times 10^{-4}$
k_d^P (s^{-1})	0.120±0.005		0.120±0.005	
(k_2/k_d^P) 12(Br^+) ^a	16.7±2.3		1.7±0.2	
(k_2/k_d^P) 12(I^+) ^b	12.5±2.2		1.3±0.2	

a. Partitioning ratio for the reaction of the mixed pyridine quinclidine bromonium ion 12(Br^+) with 4-penten-1-ol with added pyridine.

b. Partitioning ratio for the reaction of the mixed pyridine quinclidine bromonium ion 12(I^+) with 4-hexene-1-ol with added pyridine.

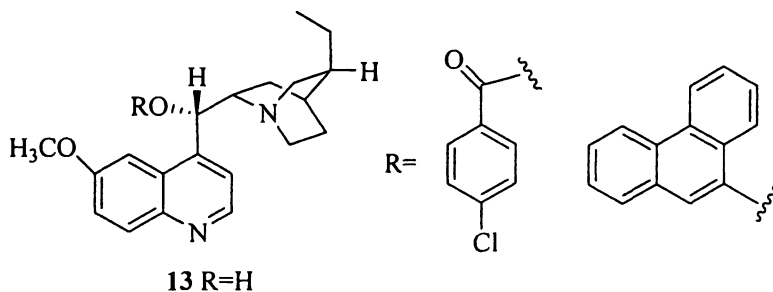
A second set of experiments were performed after the treatment of 10 or 11 with added pyridinium ion whereby the mixed quinuclidine pyridine halonium ion (12) that was created *in situ* was subsequently treated with a varying [4-penten-1-ol] or [4-hexene-1-ol] in the presence of a varying [pyridine]. Inspection of the process shown in Figure 8 suggests that, once having made 12

in situ, one should be able to react that species with the alkenols in a manner completely analogous to what is presented in Figures 2 and 3. This process, if attributable to capture of the intermediate quinuclidineN-X⁺ by the alkene in competition with reformation of **12**, should be subject to a common species rate depression with added [pyridine]. Indeed, this turns out to be the case, and analysis of all the kinetic data according to a kinetic expression analogous to what is given in eq 1 provides the k_2/k_d partitioning ratios given in Table 2. The main feature of note is the partitioning ratio is larger for the bromonium ion than the iodonium ion, but for a given ion does not change markedly between 4-penten-1-ol and 4-hexen-1-ol, suggesting that the rate constant for capture of the monoquinuclidine-X⁺ is insensitive to the substitution on the alkene, at least for the limited examples presented. It is notable that when the data in Table 1 and 2 are compared, the monoquinuclidine-X⁺ ions have at least 30- to 100-fold larger ratios for a given alkene than in the case of the corresponding pyridine-X⁺ ion. Since the k_2/k_d ratio referred to in Figure 8 is for the monoquinuclidine-Br⁺ being captured by pyridine, strictly speaking, the most appropriate comparison in Table 1 would be with the monopyridine-Br⁺ which is far more reactive with pyridine than with 4-pentene-1-ol, the opposite being true for the monoquinuclidine-Br⁺. The reasons for this anomaly are not obvious at this time.

Chiral induction for the reaction of chiral quinuclidine-X⁺ with 1, ω -alkenols

a. Hydroquinidine derivatives.

An electrophilic Br⁺ or I⁺ can be successfully transferred to hydroquinidine (**13**) and two of its commercially available derivatives (4-chlorobenzoate and 9-phenanthryl ether hydroquinidines) simply by mixing two equivalents of the hydroquinidine with one equivalent of *sym*(collidine)₂-X⁺ perchlorate in methylene chloride or acetonitrile. ¹H NMR studies (31) showed that the iodonium ion was associated with the nitrogen at the quinuclidine portion of the hydroquinidine instead of the aromatic nitrogen and also that all of the *sym*-collidines were removed from the X⁺ since only free collidine and no collidine-I⁺ peaks were observed. The (hydroquinidine)₂-halonium ion is stable in solution for more than 30 minutes at room temperature: these ions (and their parent amines) are more soluble in methylene chloride than in acetonitrile, and having R group other than hydrogen also improves the solubility.



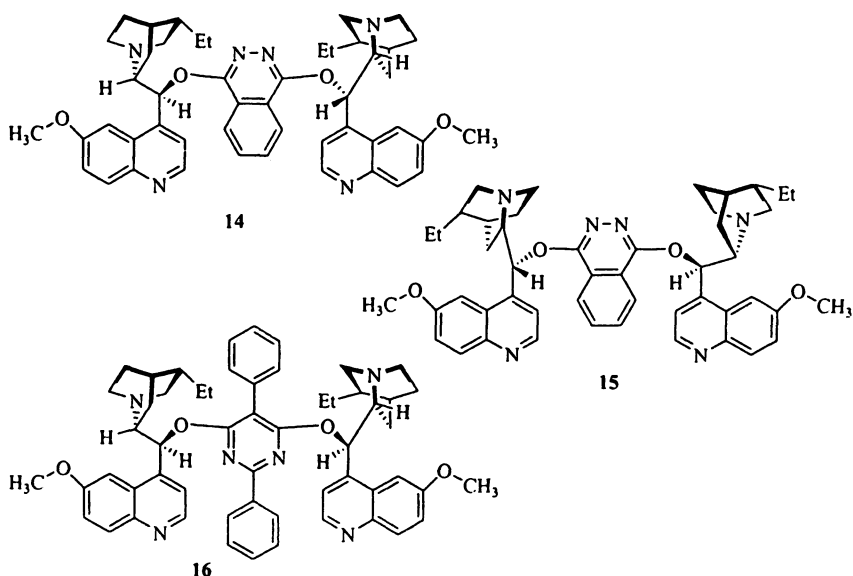
The cyclization reactions were conducted *in situ* in two steps by first transferring the X^+ from 0.36 mM solution of $(\text{collidine})_2\text{-X}^+$ in 10 ml. of dry CH_2Cl_2 to the two equivalents of hydroquinidine, cooling the mixture to 0°C or -78°C and allowing to stir for 15 minutes, followed by adding one equivalent of the 1, ω -alkenol or alkenoic acid and allowing the reaction mixture to come to room temperature over the course of 1 hour. Workup consisted of washing with 2 x 20 ml. of dilute aq. HCl followed by extraction with 3 x 15 ml. of pentane or ether in the case of the acids. The organic layer was then washed three times with 20 ml. of deionized water H_2O , dried over MgSO_4 and the volatiles removed to give an oil that was analyzed by chiral g.c. (column: CP 7502, chirasil-dex GB 25m X 0.25mm, WCOT fused silica 25m x 0.2 5mm, coating CP chirasil-dex GB DF=.25, isothermal conditions at 145°C).

Even though the putative $(\text{hydroquinidine})_2\text{-X}^+$ ion was able to cyclize 4-penten-1-ol and trans-3-hexen-1-ol, neither cyclization was particularly stereoselective. No enantiomeric excess was found for the iodocyclization reactions when these were conducted at -78°C , and there was only a modest 3-4% enantiomeric excess of the bromocyclized products. Assuming the mechanism for this reaction parallels what we have determined for the pyridine and quinuclidine bromonium and iodonium ions above, this indicates that the hydroquinidine- X^+ ion, once complexed to the alkenol, cannot induce enough discrimination between the diastereotopic transition states for ring closure to induce chirality. Interestingly, this finding corroborates that made by Grossman and Trupp (17) for the iodocyclization of some 1, ω -alkenoic acids promoted by 13 where the e.e.'s ranged from 7-15%.

b. Halocyclization promoted by the halonium ions of hydroquinidine 1,4-phthalazinediyl diether (14); hydroquinine 1,4-phthalazinediyl diether (15); and hydroquinidine 2,5-diphenyl-4,6-pyrimidinediyl diether (16).

The hydroquinidine and hydroquinine dimers $(\text{DHQD})_2\text{PHAL}$ (14), $(\text{DHQ})_2\text{PHAL}$ (15) and $(\text{DHQD})_2\text{Pyr}$ (16) are commercially available metal

complexing agents that have seen considerable use in the asymmetric Sharpless epoxidation. The iodonium and bromonium ions of each can be made *in situ* according to a simplified protocol whereby the X^+ ion is transferred from one equivalent of *bis(sym-collidine)-X^+* to one equivalent of **14-16** in CH_2Cl_2 , cooling the solution to $-78\text{ }^\circ\text{C}$, adding one equivalent of the $1,\omega$ -alkenol or $1,\omega$ -alkenoic acid and allowing the mixture to come to room temperature over a period of 2-3 hours. Workup comprised the same acid extraction steps and washing steps as described above for the hydroquinidine promoted cyclizations, followed by removal of the solvent and analysis of the residual oil by chiral phase gas chromatography. Given in Table 3 are the results in terms of the e.e.'s obtained for a variety of substrates.



All the results in the Table obtained using chiral g.c. were analyzed by isothermal gas chromatography. While we do not know the absolute configuration of any of these materials at this time, for these runs, the (-) designation in column 5 of Table 3 means that the second peak is larger than the first, while the (+) designation means that the first peak is larger than the second. However, for the halocyclizations of 4-(*p*-chlorophenyl)-4-pentenoic acid, we follow Wirth's assignments (18) of the S:R enantiomeric excesses where the first peak that elutes on the chiral Chiracel OD-H HPLC column is the S enantiomer. As can be judged from the data presented, the halocyclizations conducted in this way give poor to modest enantiomeric excesses, and in no cases do these exceed 50%.

Table 3. Enantiomeric excesses obtained from halocyclizations of various 1, ω -alkenols or 1, ω -alkenoic acids with halonium ions of dimeric hydroquinidine or dimeric hydroquinine species 14, 15, 16.

<i>Substrate</i>	<i>X⁺ - source</i>	<i>Solvent</i>	<i>T(°C)</i>	<i>e.e.(%)</i>
4-penten-1-ol	14-I ⁺	CH ₂ Cl ₂	-78	5±1
4-penten-1-ol	14-Br ⁺	CH ₂ Cl ₂	-78	-10±1
<i>trans</i> -3-hexen-1-ol	14-I ⁺	CH ₂ Cl ₂	-78	31±3
<i>trans</i> -3-hexen-1-ol	14-Br ⁺ CH ₂ Cl ₂	-78	-12±2	
<i>trans</i> -3-hexen-1-ol	14-I ⁺ CH ₂ Cl ₂	25	17±1	
5-hexen-1-ol	14-I ⁺	CH ₂ Cl ₂	-78	-26±2
5-hexen-1-ol	14-Br ⁺	CH ₂ Cl ₂	-78	-27±3
5-hexenoic acid	14-I ⁺	CH ₂ Cl ₂	-78	-22±2
4-pentenoic acid	14-I ⁺	CH ₂ Cl ₂	-78	-17±2
<i>trans</i> -3-hexenoic acid	14-I ⁺	CH ₂ Cl ₂	-78	47±1
<i>trans</i> -3-hexenoic acid	14-Br ⁺	CH ₂ Cl ₂	-78	-27±2
<i>trans</i> -3-hexenoic acid	15-I ⁺	CH ₂ Cl ₂	-78	-13±2
<i>trans</i> -3-hexenoic acid	16-I ⁺	CH ₂ Cl ₂	-78	-6±1
4-(<i>p</i> -chlorophenyl)-4-pentenoic acid	14-I ⁺	CH ₂ Cl ₂	-78	-5±2 ^a
4-(<i>p</i> -chlorophenyl)-4-pentenoic acid	14-Br ⁺	CH ₂ Cl ₂	-78	-18±2 ^a
4-(<i>p</i> -chlorophenyl)-4-pentenoic acid	15-I ⁺	CH ₂ Cl ₂	-78	-6±1 ^a
4-(<i>p</i> -chlorophenyl)-4-pentenoic acid	15-Br ⁺	CH ₂ Cl ₂	-78	+21±4 ^a

^a defined as the S:R enantiomeric excess; identification of enantiomers follows assignments given in ref (18), determined using chiral HPLC Chiracel OD-H column, 1:9 isopropanol:hexanes, 15-2.0 mL/min.

Summary

In the foregoing, we have summarized our findings that chiral amine-halonium ions can induce some enantiomeric excess to the halocyclization processes with 1, ω -alkenols and alkenoic acids. The enantiomeric excesses observed with the substrates used range from 0 to about 47% in the best cases. The reasons for the modest e.e.'s are not immediately obvious at this time, but we have provided kinetic evidence that in some cases with pyridinium-X⁺ a too highly reactive intermediate may be to blame as it reacts with all substrates so quickly that no chiral induction is observed. The concept of stabilizing the halonium ion to reduce the reaction rate with the alkenes has been explored with some modest improvement in the e.e.'s. It now seems apparent that future work to make a reagent based X⁺-transfer agent to induce chirality in electrophilic addition to an alkene will have to concentrate on placing the chiral appendages from the reagent closer to the halogen:alkene active space to induce a facial selectivity in the first binding step, with maintaining the selectivity during the cyclization process.

Acknowledgements

The authors gratefully acknowledge the financial support for this research by the Natural Sciences and Engineering Research Council of Canada. Tony Liu and Chris Maxwell thank the Student Work Experience Program at Queen's University for financial support during the summer of 2005. We acknowledge Farhad Nowrouzi for synthesis of a precursor to 4-chlorophenyl -4-pentenoic acid and for preliminary measurements of the e.e. for the reaction of 14- Br⁺ with some 1, ω -alkenols and alkenoic acids.

References and Footnotes

1. Homsí, F.; Rousseau, G. *J. Org. Chem.* **1999**, *64*, 81.
2. Homsí, F.; Rousseau, G. *Tetrahedron Lett.* **1999**, 1495.
3. Evans, R. D.; Magee, J. W.; Schlauble, J. H. *Synthesis*, **1988**, 862, and references therein.
4. Roux, M.; Paugam, R.; Rousseau, G. *J. Org. Chem.* **2001**, *66*, 4304.
5. Albert, S.; Robin, S.; Rousseau, G. *Tetrahedron Lett.* **2001**, *42*, 2477.
6. Robin, S.; Rousseau, G. *Eur. J. Org. Chem.* **2000**, 3007.
7. Rousseau, G.; Robin, S. *Tetrahedron Lett.* **2000**, *41*, 8881.

8. Tanaka, Y.; Sakuraba, H.; Nakanishi, H. *J. Chem. Soc. Chem. Commun.* **1983**, 947.
9. Sakuraba, H.; Kaneko, T.; Nagashima, R. *Kenkyu Hokoku - Kanto Gakuin Daigaku Kogakubu* **1999**, 43(1), 35. Chem Abst. 133:30374.
10. Belluci, G.; Berti, G. Bianchini, R. *Gazz. Chim. Ital.* **1987**, 116, 77.
11. Duhamel, L.; Plé, G.; Angibaud, P. Desmurs, J. R. *Synth. Commun.* **1993**, 23, 2423.
12. Giordano, C.; Coppi, L.; Ristilli, A. *J. Org. Chem.* **1990**, 55, 5400; b) Evans, D. A.; Britton, T. C.; Ellman, J.; Dorrow, R. L. *J. Am. Chem.*
13. Evans, D. A.; Britton, T. C.; Ellman, J.; Dorrow, R. L. *J. Am. Chem. Soc.* **1990**, 112, 4011.
14. Duhamel, L.; Angibaud, P.; Desmurs, J. R.; Valnot, J. Y. *Synlett.* **1991**, 807.
15. Hernanz, D.; Camps, F.; Gurrero, A.; Delgado, A. *Tetrahedron: Asymmetry*, **1995**, 6, 2291.
16. El-Qisairi, A. K.; Qaseer, H. A.; Katsigras, G.; Lorenzi, P.; Trivedi. U.; Tracz, S.; Hartmand, A.; Miller, J. A.; Henry, P. M. *Org. Lett.* **2003**, 5, 439.
17. Grossman, R. B.; Trupp, R. J. *Can. J. Chem.* **1998**, 76, 1233.
18. Haas, J.; Piguel, S.; Wirth, T. *Org. Lett.* **2002**, 4, 297.
19. El-Qisairi, A. K.; Qaseer Hanan A.; Katsigras G.; Lorenzi P.; Trivedi U.; Tracz S.; Hartman A.; Miller J. A.; Henry, P. M. *Org. Lett.* **2003**, 5, 439.
20. Wang, M.; Gao, L. X.; Mai, W. P.; Xia, A. X.; Wang, F.; Zhang, S. B. *J. Org. Chem.* **2004**, 69, 2874.
21. Cui, D. X-L.; Brown, R. S. *J. Org. Chem.* **2000**, 65, 5653.
22. Neverov, A. A.; Brown, R. S. *J. Org. Chem.* **1998**, 63, 5977.
23. Neverov, A. A.; Muise, T.; Brown, R. S. *Can. J. Chem.* **1997**, 75, 1844.
24. Neverov, A. A.; Feng, X.; Hamilton, K.; Brown, R. S. *J. Org. Chem.* **2003**, 68, 3802.
25. We thank Prof. George Olah for pointing out this interesting problem.
26. Umemoto, T.; Tomizawa, G.; Hachisuka, H.; Kitano, M. *J. Fluorine Chem.* **1996**, 77, 161.
27. Slebocka-Tilk, H.; Ball, R. G.; Brown, R. S. *J. Am. Chem. Soc.* **1985**, 107, 4504.
28. Brown, R. S.; Nagorski, R. W.; Bennet, A. J.; McClung, R. E. D.; Aarts, G. H. M.; Klobukowski, M.; McDonald, R.; Santarsiero, B. D. *J. Am. Chem. Soc.* **1994**, 116, 2448.
29. Neverov, A. A.; Brown, R. S. *J. Org. Chem.* **1996**, 61, 962-968.
30. Dubois, J.-E.; Mouvier, G. *Bull. Soc. Chim. Fr.* **1968**, 1426.
31. Liu, C. T.; Neverov, A.A.; Brown, R. S. unpublished observations.
32. Neverov, A. A.; Brown, R. S. *J. Org. Chem.* **1996**, 61, 962.
33. Carey, F. A.; Sundberg, R. J. *Advanced Organic Chemistry. Part A: Structure and Mechanisms*. Kluwer Academic: New York, N.Y., 2000, pp220-222.

34. Seeman, J. I. *Chem. Rev.* **1983**, *83*, 83.
35. Aggarwal, V. K.; Emme, I.; Fulford, S. Y. *J. Org. Chem.* **2003**, *68*, 692.
36. Blair, L. K.; Parris, K. D.; Hii, P. S.; Brock, C. P. *J. Am. Chem. Soc.* **1983**, *105*, 3649.
37. Brock, C. P.; Fu, Y.; Blair, L. K.; Chen, P.; Lovell, M. *Acta Cryst. Section C: Crystal Struct. Commun.* **1988**, *C44(9)*, 1582.

Chapter 22

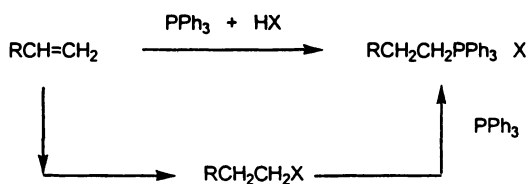
Synthesis of Phosphonium Salts by Metal-Catalyzed Addition Reaction

Mieko Arisawa and Masahiko Yamaguchi*

Department of Organic Chemistry, Graduate School of Pharmaceutical Sciences, Tohoku University, Aoba, Sendai 980-8578, Japan

Phosphonium salts can be synthesized by the transition-metal-catalyzed addition reaction of triaryphosphines and acids to unsaturated compounds. The reaction of PPh_3 , $\text{CH}_3\text{SO}_3\text{H}$, and alkynes in the presence of a palladium or rhodium catalyst gave alkenylphosphonium salts. Although $\text{Pd}(\text{PPh}_3)_4$ directed the C-P bond formation at the internal carbon atom of aliphatic 1-alkynes (Markovnikov mode), $[\text{RhCl}(\text{cod})]_2$ reversed the regioselectivity (*anti*-Markovnikov mode). The $\text{Pd}(\text{PPh}_3)_4$ -catalyzed addition of the phosphine and $\text{CH}_3\text{SO}_3\text{H}$ to allenes stereoselectively gave allylphosphonium salts: (*E*)-Allylphosphonium salts were the thermodynamic product, and (*Z*)-salts the kinetic product. 3-Alkenylphosphonium salts were obtained by the $\text{RhH}(\text{PPh}_3)_4$ -catalyzed stereospecific addition of PPh_3 and $\text{CF}_3\text{SO}_3\text{H}$ to 1,3-dienes. From these results, the catalyzed addition to unactivated alkenes was achieved. The treatment of ethylene at atmospheric pressure, PPh_3 , and Tf_2NH in the presence of $\text{Pd}_2(\text{dba})_3\text{CHCl}_3$ gave an ethylphosphonium salt. 1-Alkylphosphonium salts were obtained by *anti*-Markovnikov addition to 1-alkenes.

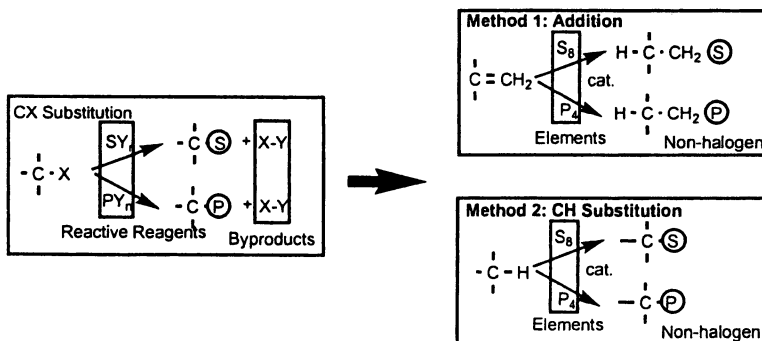
Quaternary phosphonium salts are organophosphorous compounds used as Wittig olefination reagents, phase transfer catalysts, electrolytes, ionic liquids, and as surface active reagents. Their preparation involves the C-P bond formation in tertiary phosphines.¹ We envisaged that addition of phosphines to unsaturated compounds should be preferable as compared to the conventional method using a substitution reaction of organohalogen compounds (Scheme 1). In this chapter, we describe our recent study on this subject.



Scheme 1.

This is part of our program to develop novel synthetic methods for organoheteroatom compounds, compounds of phosphorous, sulfur, selenium, and other elements.² The syntheses of these compounds involve the process of bond formation between carbon and a heteroatom, and conventional methods in general employ a substitution reaction of organohalogen or organosulfonate compounds with heteroatom nucleophiles (Scheme 2). The use of highly reactive leaving groups is essential for this synthesis. Leaving groups are introduced in organic molecules typically by the activation of an alcohol, followed by replacement of heteroatom reagents. The method, however, has serious drawbacks from the standpoint of efficiency. The introduction of leaving groups requires multistep transformations, and such groups are eventually wasted, because they are not incorporated in the product. We considered the addition of heteroatom reagents from carbon-carbon multiple bonds to be preferable (Method I in Scheme 2), because a) unsaturated compounds are inexpensive and readily available compared with organohalogen compounds; b) the method does not waste leaving groups; c) unsaturated groups are generally inert under the conditions for various organic transformations, in which organohalogen compounds might be affected. Many heteroatom reagents, however, are inert to unsaturated carbon-carbon bonds, and catalysts are required for such transformation. Thus, we selected transition-metal complexes for this purpose. It has been thought that transition metals form strong complexes with heteroatom reagent, and are not suitable for the catalysis of heteroatom manipulation. We show here that rhodium and palladium complexes are effective for the addition reaction of heteroatom reagents.² As a further extension of such organoheteroatom synthesis, we are also interested in the conversion of carbon-hydrogen bonds to carbon-heteroatom bonds (Method 2).³

In the phosphonium salt synthesis, the addition reaction of tertiary phosphines to activated alkenes has been reported (Scheme 3). PPh₃ is added to electron-deficient alkenes such as enones or enals at the β-position in the presence of acids.⁴ The reaction of styrenes with phosphine has recently been reported by Okuma, which gave Markovnikov adducts.⁵ Although no catalyzed reactions of



Scheme 2.

unactivated alkenes are known, stoichiometric reactions have been reported. Reaction of alkenes and PPh_3 in the presence of MeSSMe_2 salt gave thiophosphonium salts;⁶ the electrochemical activation of alkenes in the presence of the phosphine provided alkenylphosphonium salts;⁷ the reaction of methallyl alcohol with $\text{RuHCl}(\text{CO})(\text{PPh}_3)_3$ gave hydroxyphosphonium salt.⁸ We have developed an addition reaction for triarylphosphines with unactivated unsaturated compounds catalyzed by a transition metal.

We initially observed an addition reaction of tertiary phosphines to unactivated alkynes. The method was then applied to reactive alkenes, allenes and 1,3-dienes, and finally to unactivated alkenes (Scheme 4). Such a step-up methodology turned out to be effective in this study.

1. Addition Reaction of Phosphine to Alkynes

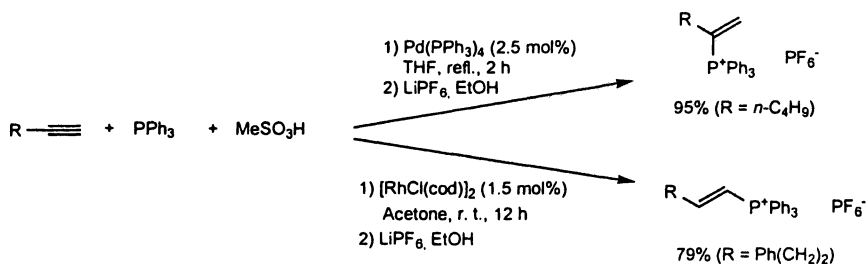
Several years ago, we were studying aromatic vinylation reactions using stoichiometric amounts of main element Lewis acids; for example, phenols were *o*-vinylated with acetylene in the presence of SnCl_4 and Bu_3N .⁹ As an extension, we started to examine catalytic phenol alkylation, in which allenes were found to dimerize in the presence of palladium and phenol catalysts (Scheme 5).¹⁰ When 1,2-undecadiene was treated with $\text{Pd}_2(\text{dba})_3$ (5 mol%), $(p\text{-tol})_3\text{P}$ (15 mol%), and *p*-nitrophenol (10 mol%) in refluxing THF for 12 h, (9*E*, 12*E*)-10-methyl-11-methylene-9,12-icosadiene was obtained in quantitative yield (Scheme 5). The added phenol played an important role, and no reaction took place in its absence. This reaction was effectively promoted by phenol having an electron-withdrawing group, *p*-nitrophenol; however, the yield decreased when phenol, alkylphenol, or methoxyphenol was used. Because acetic acid also promoted the reaction, phenol was considered to function as Brønsted acid.

Cross-conjugated trienes have attracted interest in polymer chemistry and theoretical chemistry as well as in synthetic chemistry.¹¹ Although a palladium complex catalyzed 1,2-propadiene dimerization in the presence of water or an amine produced hydroxylated or aminated 2,3-dimethyl-2,3-butadiene,¹² the method was not applied to the synthesis of cross-conjugated trienes. Another interesting feature

of this reaction is the critical role of phenol as an acid, which led us to examine the effect of added acid on the transition metal catalyzed reaction.

During our investigation, PPh_3 and $\text{CH}_3\text{SO}_3\text{H}$ were found to add to unactivated alkynes in the presence of a palladium or rhodium complex.¹³ The regiochemistry and stereochemistry could be controlled by a judicious selection of the metal catalyst. Alkenylphosphonium salts have various applications in synthetic chemistry,¹⁴ and the present method enables an easy access to the organophosphorous compounds using readily available starting materials.

1-Hexyne was treated with equimolar amounts of PPh_3 and $\text{CH}_3\text{SO}_3\text{H}$ in the presence of $\text{Pd}(\text{PPh}_3)_4$ (2.5 mol%) in refluxing THF for 2 h. The counteranion was substituted for PF_6^- , and recrystallization gave a (1-hexen-2-yl)phosphonium salt in a quantitative yield (Scheme 6). The phosphine attacked the internal carbon of 1-hexyne regioselectively (Markovnikov mode). The palladium complex and $\text{CH}_3\text{SO}_3\text{H}$ were essential, and no reaction occurred in the absence of either. With this catalyst, a turnover number of 1000 could be attained. The effect of the acid structure was small, and PhSO_3H , *p*- tolSO_3H , *p*- $\text{ClC}_6\text{H}_4\text{SO}_3\text{H}$, $\text{CF}_3\text{SO}_3\text{H}$, camphorsulfonic acid, and even H_2SO_4 could be used equally as well. The catalytic activities of several palladium complexes were compared: $\text{Pd}_2(\text{dba})_3\text{CHCl}_3$ (99%), and $\text{Pd}(\text{OAc})_2$ (84%) were active, whereas $\text{PdCl}_2(\text{PPh}_3)_2$ was inactive.

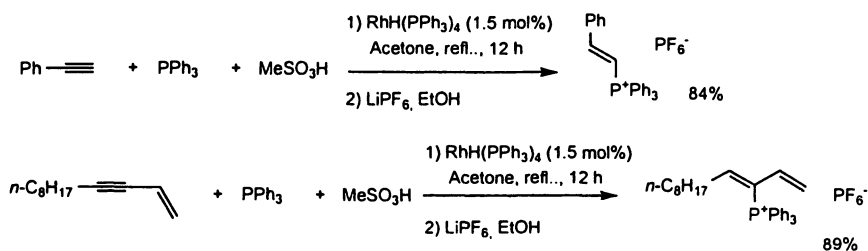


Scheme 6.

Scheme 6 shows a novel C-P bond forming reaction, in which the ligand coupling of an alkyne and a tertiary phosphine on palladium metal occurs. It was also considered very important that a C-P bond could be formed by the addition of a phosphorous reagent to unsaturated compounds.

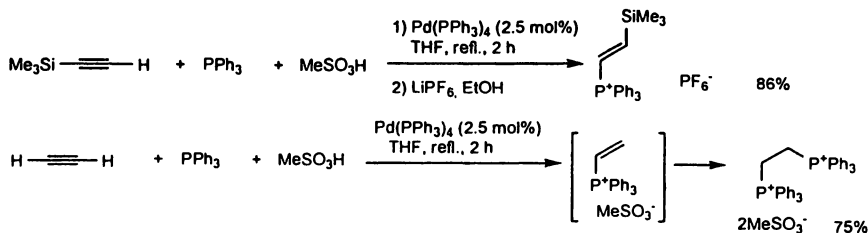
When the rhodium catalyst $[\text{RhCl}(\text{cod})]_2$ ($\text{cod} = 1,5\text{-cyclooctadiene}$) or $\text{RhCl}(\text{PPh}_3)_3$ was used, the observed regioselectivity of the reaction was opposite to that of the palladium-catalyzed reaction (*anti*-Markovnikov mode). The treatment of an equimolar mixture of 4-phenyl-1-butyne, PPh_3 , and $\text{CH}_3\text{SO}_3\text{H}$ with $[\text{RhCl}(\text{cod})]_2$ (1.5 mol%) in acetone at room temperature for 12 h yielded predominantly (*E*)-(4-phenyl-1-butenyl)phosphonium salt with a small amount of the regioisomer in a ratio of 10:1. The pure (*E*)-product was obtained by recrystallization of the PF_6^- salt in 79% yield (Scheme 6). The regioselectivity was shown to be under kinetic control: (4-Phenyl-1-butenyl)phosphonium salt did not isomerize to its internal derivative when treated with $\text{CH}_3\text{SO}_3\text{H}$ in the presence of either $[\text{RhCl}(\text{cod})]_2$ under acetone reflux or $\text{Pd}(\text{PPh}_3)_4$ under THF reflux.

The reactivity of the conjugated alkynes differed slightly from that of the aliphatic 1-alkynes. The addition of PPh_3 to arylacetylenes was effectively catalyzed by $\text{RhH}(\text{PPh}_3)_4$ (Scheme 7), whereas $\text{Pd}(\text{PPh}_3)_4$ and $[\text{RhCl}(\text{cod})]_2$ were not effective. The reaction was applicable to phenylacetylenes with either electron-donating or electron-withdrawing groups giving *anti*-Markovnikov (*E*)-adducts. $\text{RhH}(\text{PPh}_3)_4$ catalyzed the addition to 1-undecen-3-yne yielding the Markovnikov adduct.



Scheme 7.

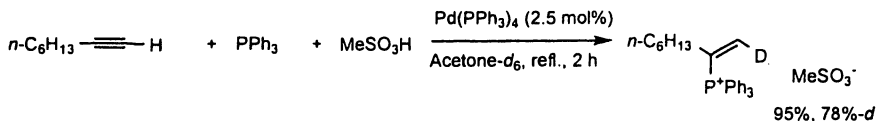
In the presence of a palladium complex, trimethylsilylacetylene was converted to β -silylethenylphosphonium salt in 86% yield (Scheme 8). Phosphine attacked the terminal carbon in this case. When acetylene was used, 1,2-bis(triphenylphosphino)ethane was obtained, which may be formed by the conjugate addition of PPh_3 to the initially generated ethenylphosphonium salt.



Scheme 8.

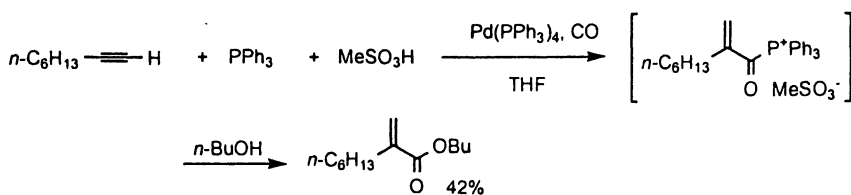
The addition of a proton and a phosphine generally proceeded via *cis*-addition. When 1-octyne was treated with $\text{CH}_3\text{SO}_3\text{H}$ and PPh_3 in acetone- d_6 in the presence of $\text{Pd}(\text{PPh}_3)_4$, (*Z*)-1-deutero-1-octen-2-ylphosphonium salt was obtained (Scheme 9). An H-D exchange occurred between sulfonic acid and the deuterated solvent generating deuterated sulfonic acid, which transferred deuterium to the alkyne.

Two mechanisms are conceivable for the reaction. One involves the hydrometalation of the metal hydride at alkyne followed by reductive elimination.¹⁵ Alternatively, phosphinometalation followed by protide-metalation can occur.¹⁶ To gain insight into the mechanism, a carbonylation



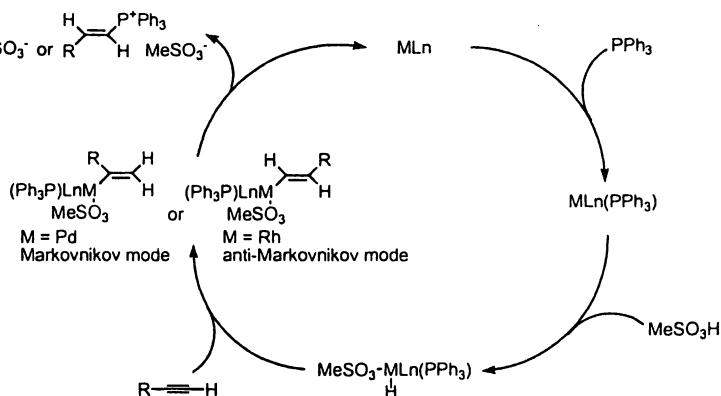
Scheme 9.

reaction was carried out. The reaction of 1-octyne, PPh_3 , and $\text{CH}_3\text{SO}_3\text{H}$ under carbon monoxide atmosphere gave the acylphosphonium salt, which upon treatment with butanol was converted to butyl α -methyleneoctanoate (Scheme 10). Thus, palladium should be attached to the internal carbon of the alkyne, that undergoes carbonylation and phosphonylation. The result is consistent with the hydrometalation mechanism in the Markovnikov mode.



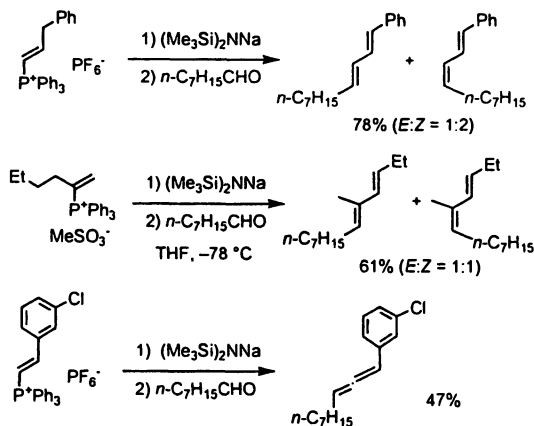
Scheme 10

A possible mechanism therefore can be summarized as follows (Scheme 11). The oxidative addition of an acid to a low-valent metal complex provides a metal hydride, which undergoes hydrometalation with a 1-alkyne. Reductive elimination leads to an alkenylphosphonium salt and a low-valent metal species, which reacts with PPh_3 . Strong electron-withdrawing groups such as CH_3SO_3^- -derived from the acid can facilitate the reductive elimination. The regioselectivity may be controlled at the hydrometalation step: Palladium hydride undergoes Markovnikov addition, whereas rhodium hydride *anti*-Markovnikov addition.



Scheme 11.

Novel alkenylphosphonium salts were subjected to the Wittig reaction (Scheme 12). Allylic deprotonation took place for phosphonium salts possessing such protons, and the olefination proceeded after double bond migration. In cases where such protons were absent, allene formation was observed.

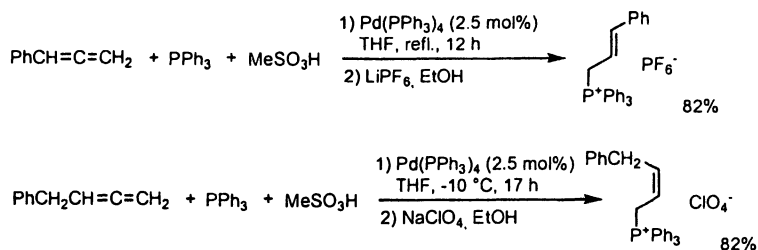


Scheme 12.

Typical Experimental Procedures Under an argon atmosphere, a mixture of $\text{Pd}(\text{PPh}_3)_4$ (2.5 mol%, 29 mg), PPh_3 (1 mmol, 262 mg), 1-hexyne (1 mmol, 0.12 mL), and $\text{CH}_3\text{SO}_3\text{H}$ (1 mmol, 96 mg) in THF (2 mL) was heated at reflux for 2 h. The solvent was removed under reduced pressure, and the residue was washed with ether. After dissolving the crude product in ethanol (2 mL), LiPF_6 (1.5 mmol, 228 mg) was added, and the mixture was stirred at room temperature for 1 h. The precipitated solid was collected by filtration and was dissolved in CHCl_3 followed by filtration. The solution was concentrated, and the residue was recrystallized from CHCl_3 and ether (3:1) yielding (1-hexen-2-yl)triphenylphosphonium hexafluorophosphate (468 mg, 96%) as a colorless solid. Mp 148.5–149.0 °C.

2. Addition Reaction of Phosphine to Allenes

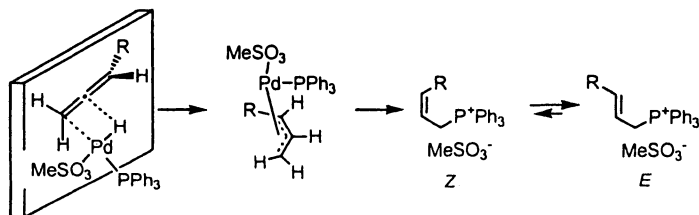
Under the conditions where alkynes reacted, alkenes were inert. To extend this methodology to the less reactive substrate, the reaction of an activated olefin, allene, was examined.¹⁷ 1-Phenyl-1,2-propadiene was treated with equimolar amounts of PPh_3 and $\text{CH}_3\text{SO}_3\text{H}$ in the presence of $\text{Pd}(\text{PPh}_3)_4$ (2.5 mol%) in refluxing THF for 12 h. The counteranion was exchanged with LiPF_6 , and recrystallization gave (*E*)-(3-phenyl-2-propenyl)triphenylphosphonium hexafluorophosphate in 82% yield (Scheme 13). The phosphine attacked at the terminal carbon atom of the allene regioselectively. The palladium complex and $\text{CH}_3\text{SO}_3\text{H}$ were again essential for the addition reaction, and no reaction occurred in their absence.



Scheme 13.

When the reaction was conducted at -10°C , the observed stereoselectivity of the reaction was opposite to that under refluxing conditions. The treatment of an equimolar mixture of 4-phenyl-1,2-butadiene, PPh_3 , and $\text{CH}_3\text{SO}_3\text{H}$ with $\text{Pd(PPh}_3)_4$ (1.5 mol%) in THF at -10°C for 17 h yielded predominantly (*Z*)-4-phenyl-2-butenylphosphonium salt with a small amount of the (*E*)-isomer in a ratio of 13:1. The isomerically pure (*Z*)-compound was obtained by recrystallization of the perchlorate salt in 82% yield. An isolated (*Z*)-product isomerized to the (*E*)-compound when treated with $\text{CH}_3\text{SO}_3\text{H}$ and $\text{Pd(PPh}_3)_4$ under THF reflux.

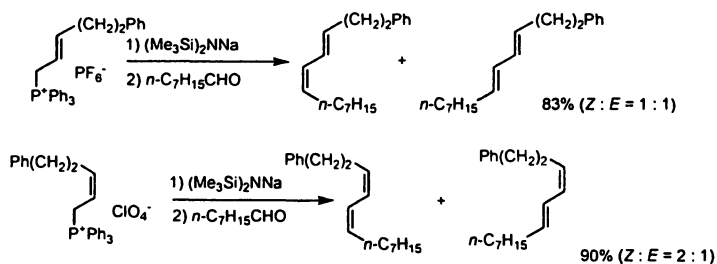
The mechanism of this reaction was considered on the basis of hydropalladation (Scheme 14). To minimize steric repulsions, the palladium hydride complex approaches the $\text{C}=\text{CH}_2$ moiety of the allene in the *anti*-Markovnikov mode from the opposite side of the substituent. This addition gives a π -allyl palladium complex with the (*Z*)-configuration,¹⁸ which is converted to the (*Z*)-product by C-P bond formation, with regeneration of the $\text{Pd}(0)$ catalyst.



Scheme 14.

Allylphosphonium salts are synthesized by substitution of allyl halides with PPh_3 . The use of allyl alcohol, allyl acetate, or nitropropene with a palladium catalyst has also been reported.¹⁹ It is shown in this study that the organophosphorous compounds can be obtained by a palladium-catalyzed addition to an allene. A notable aspect of this method is that it can control the stereochemistry of the phosphonium salt, and that (*Z*)-allylphosphonium salts have been obtained in pure form for the first time.

The Wittig reaction of (*E*)-allylphosphonium salts is notorious for not being stereoselective,²⁰ and in accordance with this, the reaction of an (*E*)-allylphosphonium salt with sodium hexamethyldisilazide in THF followed by octanal gave 1:1 mixtures of (*E,E*)-isomers and (*E,Z*)-isomers (Scheme 15). It was considered interesting to compare the reaction of (*Z*)-isomers. The (*Z*)-allylphosphonium salt gave a similar mixture of (*Z,E*)-isomer and (*Z,Z*)-isomers. The Wittig reaction of (*E*)- and (*Z*)-allylphosphonium salts exhibited similar behavior under the present reaction conditions. Although the stereochemistry of allylphosphonium salt was retained, a mixture of isomers was obtained with respect to the newly formed double bond.



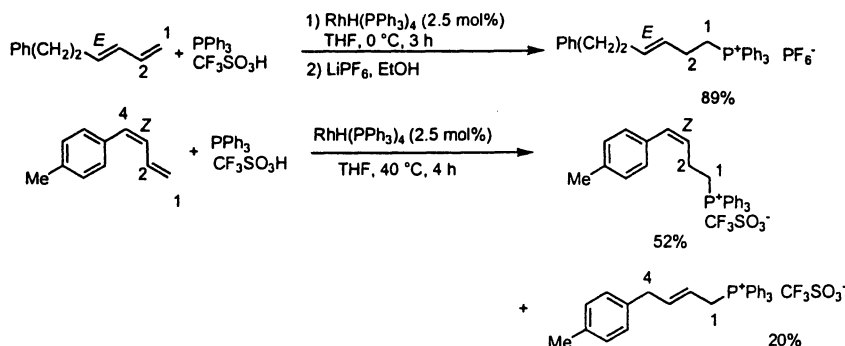
Scheme 15.

Typical Experimental Procedures Under an argon atmosphere, a mixture of Pd(PPh₃)₄ (18 mg, 1.5 mol%), PPh₃ (262 mg, 1 mmol), 4-phenyl-1,2-butadiene (1 mmol, 130 mg), and CH₃SO₃H (96 mg, 1 mmol) in THF (2 mL) was stirred at -10 °C for 12 h. After stirring with a small amount of decolorizing charcoal for 30 min, insoluble materials were removed by filtration. The solution was concentrated under reduced pressure, and the residue was washed with ether. The crude product was dissolved in ethanol (2 mL), to which NaClO₄ (2 mmol, 244 mg) was added. The mixture was stirred at room temperature for 1 h, and the precipitated solid was collected by filtration. CHCl₃ was added to the solid, and insoluble CH₃SO₃Li was removed by filtration. The solution was concentrated, and the residue was recrystallized from acetone and ether (2:1) yielding (*Z*)-(4-phenyl-2-butenyl)triphenylphosphonium salt (403 mg, 82%) as colorless solid. Mp. 180.0-181.0°C.

3. Addition Reaction of Phosphine to 1,3-Dienes

Before examining the reaction of deactivated alkenes, the phosphonium salt synthesis was applied to 1,3-dienes.²¹ When (*E*)-6-phenyl-1,3-hexadiene was treated with equimolar amounts of PPh₃ and CF₃SO₃H in the presence of RhH(PPh₃)₄ (2.5 mol%) in THF at 0 °C for 3 h, (*E*)-(6-phenyl-3-hexenyl)triphenylphosphonium salt was obtained in 89% yield after anion exchange with LiPF₆ and recrystallization (Scheme 16). The addition of phosphine and hydrogen occurred at the 1- and 2-carbon atoms of the 1,3-diene, respectively. The reaction of (*7*)-1,3-dienes was then performed for comparison.

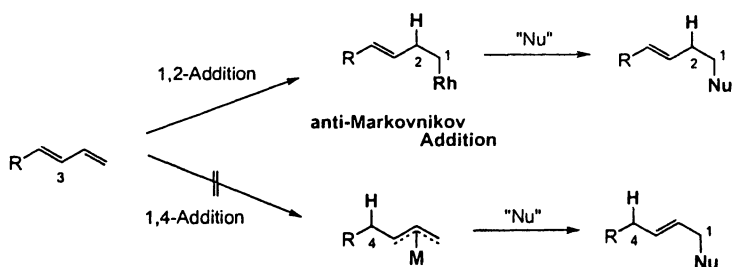
The treatment of (*Z*)-4-(*p*-tolyl)-1,3-butadiene with PPh₃ and CF₃SO₃H at room temperature for 5 h gave a 1,2-adduct, (*Z*)-4-(*p*-tolyl)-3-butenylphosphonium salt, in 52% yield, which was accompanied by the formation of a 1,4-adduct (20%).



Scheme 16.

(*E*)-1,3-Dienes reacted considerably faster than the (*Z*)-isomers, and this feature was utilized to separate the (*Z*)-isomer from the stereoisomeric mixture. When 6-phenyl-1,3-hexadiene (*E/Z* = 50/50) was treated with 0.6 molar amounts of PPh₃ and CF₃SO₃H at 0 °C for 6 h, the (*E*)-phosphonium salt (53%) was formed. The unreacted (*Z*)-1,3-diene could be separated by ether extraction in 41% yield. This procedure provides easy access to (*Z*)-1,3-dienes.²²

In general, transition metal-catalyzed addition reactions to 1,3-dienes gave 1,4-adducts via π -allyl metal intermediates.²³ The *anti*-Markovnikov 1,2-addition mode of this reaction is therefore unusual (Scheme 17). It was noted that the configuration of the 3-olefin was retained with either (*E*)- or (*Z*)-1,3-dienes. The observation that the 3-olefin was unimportant for this reaction strongly suggests that the method could be applicable to “unactivated” alkenes.



Scheme 17.

The difference between palladium and rhodium catalyses regarding regioselectivity is also noteworthy. The palladium complex provided Markovnikov

products in the reaction of aliphatic 1-alkynes and allenes, and *anti*-Markovnikov products were obtained via the rhodium-catalyzed reaction of aliphatic 1-alkynes and 1,3-dienes. This is a novel metal effect on regiochemistry. The phenomenon, however, has exceptions as exemplified by the reaction of “unactivated” 1-alkenes (*vide infra*): Both complexes gave *anti*-Markovnikov adducts.

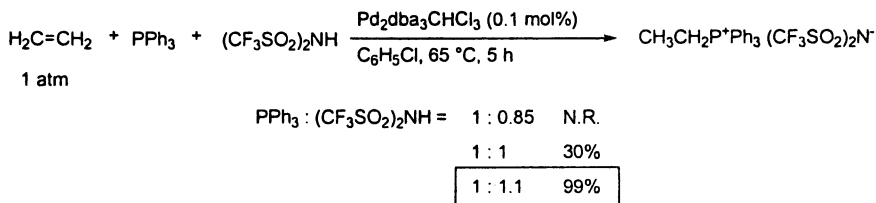
Typical Procedures for Separation of (*Z*)-1,3-Diene. Under an argon atmosphere, a mixture of RhH(PPh₃)₄ (290 mg, 2.5 mol%), PPh₃ (6 mmol, 1.57 g), 6-phenyl-1,3-hexadiene (10 mmol, 1.58 g, *E/Z* = 50/50), and CF₃SO₃H (0.53 mL, 6 mmol) in THF (20 mL) was stirred at 0 °C for 6 h. A small amount of activated charcoal was added, and the mixture was stirred for 30 min to adsorb the metal complex. Insoluble materials were removed by filtration, and the solution was concentrated under reduced pressure (53% yield of (*E*)-6-phenyl-2-hexenylphosphonium salt by ¹H-NMR). The residue was washed with ether, and the ether solution was washed with saturated NaHCO₃ and brine. After drying over MgSO₄ the solution was concentrated, and flash chromatography (hexane) over silica gel gave (*Z*)-6-phenyl-1,3-hexadiene (650 mg, 41%). The residue obtained by ether washing was dissolved in ethanol (10 mL), and LiPF₆ (10 mmol, 1.52 g) was added to the resulted solution. After stirring at room temperature for 1 h, the precipitated solid was collected by filtration. CHCl₃ was added to the solid, and insoluble CF₃SO₃Li was removed by filtration. The solution was concentrated, and the residue was recrystallized from ethanol to give the (*E*)-phosphonium salt (586 mg, 21%) as a colorless solid. Mp. 124.0-125.0 °C.

4. Addition Reaction of Phosphine to Alkenes

From the results of the 1,3-diene addition reaction, the metal-catalyzed reaction of “unactivated” alkenes was examined, and it was found that the palladium complex effectively catalyzed the *anti*-Markovnikov addition of triarylphosphines and bis(trifluoromethanesulfonyl)imide (Tf₂NH).²⁴

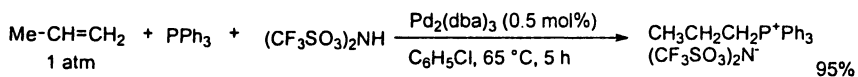
Ethylene at atmospheric pressure (balloon) was treated with PPh₃ and Tf₂NH (1.1 eq.) in the presence of Pd₂(dba)₃CHCl₃ (dba = dibenzylideneacetone) (1.25 mol%) in chlorobenzene at 65 °C for 5 h, and the ethyltriphenylphosphonium salt was obtained in 99% yield after recrystallization (Scheme 18). Tf₂NH gave a better result than CF₃SO₃H. Catalyst loading could be reduced to 0.1 mol% without affecting the yield of the product. The use of a slight excess of Tf₂NH over phosphine (molar ratio = 1.1:1) was critical, which suggests that the acid was not only a “proton source” required to add to 1-alkenes but also an activator of the palladium complex. RhH(PPh₃)₄ was less effective under the conditions used, and required a higher catalyst loading (10 mol%) for effective conversion. In addition, the Rh catalyzed reaction competed with phosphine oxidation to the oxide, presumably caused by a trace amount of dissolved oxygen.

The reaction was applicable to 1-alkenes (Scheme 19). When propene at atmospheric pressure (balloon) was treated with PPh₃ and Tf₂NH (1.1 eq.) in the



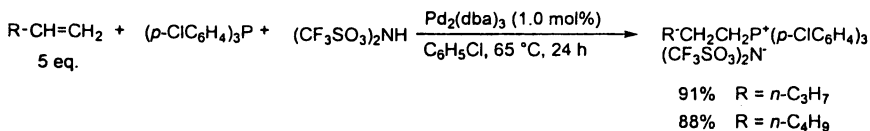
Scheme 18.

presence of $\text{Pd}_2(\text{dba})_3\text{CHCl}_3$ (0.5 mol%) in chlorobenzene at 65 °C for 5 h, 1-propyltriphenylphosphonium salt was obtained in 95% isolated yield. The *anti*-Markovnikov adduct was obtained exclusively, which indicates the essential role of metal catalysis rather than acid catalysis in C-P bond formation. The reaction of 1-butene (20 eq), PPh_3 , and TF_2NH (1.1 eq.) in the presence of $\text{Pd}_2(\text{dba})_3\text{CHCl}_3$ (1.0 mol%) in chlorobenzene at 65 °C for 8 h gave 1-butyltriphenylphosphonium salt in 92% yield. The recovered butenes contained mainly 2-butene and a very small amount of 1-butene (2-butene:1-butene > 20:1). Such equilibration of butenes was attained within 30 min under the conditions used, and a small amount of 1-butene must have reacted with PPh_3 , which indicates a high activity of the catalyst.



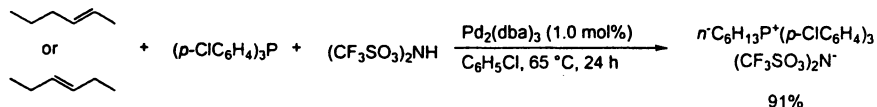
Scheme 19.

Higher 1-alkenes reacted more effectively with $(p\text{-ClC}_6\text{H}_4)_3\text{P}$ than with PPh_3 or $(p\text{-tolyl})_3\text{P}$. The reaction of 1-pentene (5 eq), TF_2NH (1.1 eq), and $(p\text{-ClC}_6\text{H}_4)_3\text{P}$ in the presence of the palladium complex (1.0 mol%) gave the 1-pentylphosphonium salt in 91% yield (Scheme 20). The use of 5 eq of 1-pentene was sufficient for this reaction, despite the volatile nature of this compound (bp 30 °C), and the rapid olefin migration to form a very small amount of 1-pentene. The reaction of 1-hexene also proceeded effectively giving the 1-hexylphosphonium salt in 88% yield.



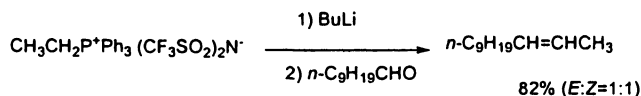
Scheme 20.

Because olefin migration was very rapid under the conditions used, internal alkenes could be used. Thus, treatment of (*E*)-2-pentene or (*E*)-3-pentene with Tf₂NH (1.1 eq) and (*p*-ClC₆H₄)₃P in chlorobenzene at 65 °C for 24 h both gave the 1-pentylphosphonium salt in 91% yields (Scheme 21). The use of mixtures of alkene regioisomers and stereoisomers for the reaction may have a synthetic advantage.



Scheme 21.

It was confirmed that the Wittig reaction proceeded using the Tf₂N phosphonium salt (Scheme 22).



Scheme 22.

Typical Experimental Procedures In a two-necked flask equipped with a reflux condenser were placed PPh₃ (5 mmol, 1.31 g), Pd₂dba₃•CHCl₃ (0.1 mol%, 5.2 mg), and Tf₂NH (5.5 mmol, 1.55 g) in chlorobenzene (6 mL) under an argon atmosphere. After substituting an argon balloon for ethylene, the solution was heated at 65 °C for 5 h. It was then concentrated, and the residue was washed with ether/hexane. Recrystallization from ethanol gave the ethylphosphonium salt (2.79 g, 98%) as a colorless solid. Mp 97.0–97.5 °C.

5. Conclusion

Phosphonium salts can be synthesized from unsaturated compounds by addition of a triarylphosphine and an acid in the presence of a palladium or rhodium catalyst. Transition metal catalysis turned out to be effective for the synthesis of organophosphorous compounds.

Acknowledgments

This work was supported by JSPS (Nos. 16109001 and 17689001). M. A. expresses her thanks to the Grant-in-Aid for Scientific Research on Priority Areas, “Advanced Molecular Transformation of Carbon Resources” from MEXT (No. 18037005).

References

1. *Methoden der Organischen Chemie, Band El, Organische Phosphorverbindungen I*; Regitz, M., Ed.; Georg Thieme: Stuttgart, 1982; p 491. Also see, Beletskaya, I. P.; Kazankova, M. A. *Zh. Org. Khim.*, **2002**, *38*, 1447.
2. Arisawa, M.; Yamaguchi, M. *Org. Lett.* **2001**, *3*, 763. Arisawa, M.; Yamaguchi, M. *J. Am. Chem. Soc.* **2003**, *125*, 6624. Arisawa, M.; Suwa, A.; Fujimoto, K.; Yamaguchi, M. *Adv. Synth. Cat.* **2003**, *345*, 560. Arisawa, M.; Kozuki, Y.; Yamaguchi, M. *J. Org. Chem.* **2003**, *68*, 8964.
3. Arisawa, M.; Ashikawa, M.; Suwa, A.; Yamaguchi, M. *Tetrahedron Lett.* **2005**, *46*, 1727. Arisawa, M.; Tanaka, K.; Yamaguchi, M. *Tetrahedron Lett.* **2005**, *46*, 4797. Arisawa, M.; Ono, T.; Yamaguchi, M. *Tetrahedron Lett.* **2005**, *46*, 5669. Arisawa, M.; Sugata, C.; Yamaguchi, M. *Tetrahedron Lett.* **2005**, *46*, 6097. Arisawa, M.; Fujimoto, K.; Morinaka, S.; Yamaguchi, M. *J. Am. Chem. Soc.* **2005**, *127*, 12226. Arisawa, M.; Suwa, A.; Yamaguchi, M. *J. Organomet. Chem.* **2006**, *691*, 1159. Arisawa, M.; Onoda, M.; Hori, C.; Yamaguchi, M. *Tetrahedron Lett.* **2006**, *47*, 5211.
4. For example, Hoffmann, H. *Chem. Ber.* **1961**, *94*, 1331. Kozikowski, A. P.; Jung, S. H. *J. Org. Chem.* **1986**, *51*, 3400. Takanami, T.; Suda, K.; Ohmori, H. *Tetrahedron Lett.* **1990**, *31*, 677. Cristau, H.-J.; Vors, J.-P.; Christol, H. *Synthesis* **1979**, 538. Stewart, I. C.; Bergman, R. G.; Toste, F. D. *J. Am. Chem. Soc.* **2003**, *125*, 8696.
5. Okuma, K.; Izaki, T. *Bull. Chem. Soc. Jpn.* **2005**, *78*, 1831.
6. Okuma, K.; Koike, T.; Yamamoto, S.; Takeuchi, H.; Yonekura, K.; Ono, M.; Ohta, H. *Bull. Chem. Soc. Jpn.* **1992**, *65*, 2375.
7. Ohmori, H.; Takanami, T.; Masui, M. *Tetrahedron Lett.* **1985**, *26*, 2199. Ohmori, H.; Takanami, T.; Masui, M. *Chem. Pharm. Bull.* **1987**, *35*, 4960.
8. Hiraki, K.; Nonaka, A.; Matsunaga, T.; Kawano, H. *J. Organomet. Chem.* **1999**, *574*, 121.
9. Yamaguchi, M.; Hayashi, A.; Hiramata, M. *J. Am. Chem. Soc.* **1995**, *117*, 1151. Yamaguchi, M.; Arisawa, M.; Omata, K.; Kabuto, K.; Hiramata, M. Uchimarui, T. *J. Org. Chem.* **1998**, *63*, 7298.
10. Arisawa, M.; Sugihara, T.; Yamaguchi, M. *J. Chem. Soc., Chem. Commun.* **1998**, 2615.
11. A review: Hopf, H. *Angew. Chem., Int. Ed.* **1984**, *23*, 948. Also see for examples, Bailey, W. J.; Economy, J.; Hermes, M. E. *J. Org. Chem.* **1962**, *27*, 3295. Kanemasa, S.; Sakoh, H.; Wada, E.; Tsuge, O. *Bull. Chem. Soc. Jpn.* **1986**, *59*, 1869. Kaupp, G.; Frey, H.; Behmann, G. *Chem. Ber.* **1988**, *121*, 2127. Cadogan, J. I. G.; Craddock, S.; Gillam, S.; Gosney, I. *J. Chem. Soc., Chem. Commun.* **1991**, 114. Trahanovsky, W. S.; Koeplinger, K. A. *J. Org. Chem.* **1992**, *57*, 4711.
12. Coulson, D. R. *J. Org. Chem.* **1973**, *38*, 1483. Inoue, Y.; Ohtsuka, Y.; Hashimoto, H. *Bull. Chem. Soc. Jpn.* **1984**, *57*, 3345.

13. Arisawa, M.; Yamaguchi, M. *J. Am. Chem. Soc.* **2000**, *122*, 2387.
14. For examples; Posner, G. H.; Lu, S.-B. *J. Am. Chem. Soc.* **1985**, *107*, 1424. Okada, Y.; Minami, T.; Yahiro, S.; Akinaga, K. *J. Org. Chem.* **1989**, *54*, 974. Lee, P. H.; Kim, J. S.; Kim, Y. C.; Kim, S. *Tetrahedron Lett.* **1993**, *34*, 7583. Byrley, I. Hewson, A. T. *Tetrahedron Lett.* **1994**, *35*, 7099. Clerici, F.; Gelmi, M. L.; Pocar, D.; Rondena, R. *Tetrahedron* **1995**, *51*, 9985. Bitterer, F.; Kucken, S.; Stelzer, O. *Chem. Ber.* **1995**, *128*, 275. Okuma, K.; Ikari, K.; Ono, M.; Sato, Y.; Kuge, S.; Ohta, H.; Machiguchi, T. *Bull. Chem. Soc. Jpn.* **1995**, *68*, 2313. Shen, Y.; Yao, J. *J. Org. Chem.* **1996**, *61*, 8659. Miedaner, A.; Noll, B. C.; DuBois, D. L. *Organometallics* **1997**, *16*, 5779. Hanamoto, T.; Kiguchi, Y.; Shindo, K.; Matsuoka, M.; Kondo, M. *J. Chem. Soc., Chem. Commun.* **1999**, 151.
15. Schweizer, E. E.; Wehman, A. T.; Nycz, D. M. *J. Org. Chem.*, **1973** *38*, 1583. Hinkle, R. J.; Stung, P. J.; Kowalski, M. H. *J. Org. Chem.* **1990**, *55*, 5033. Huang, C.-C.; Duan, J.-P.; Wu, M.-Y.; Liao, F.-L.; Wang, S.-L.; Cheng, C.-H. *Organometallics* **1998**, *17*, 676.
16. Allen, A. Jr.; Lin, W., *Organometallics* **1999**, *18*, 2922.
17. Arisawa, M.; Yamaguchi, M. *Adv. Synth. Cat.* **2001**, *343*, 27.
18. Ahmar, M.; Barieux, J.-J.; Cazes, B.; Gore, J. *Tetrahedron* **1987**, *43*, 513. Cazes, B. *Pure Appl. Chem.* **1990**, *62*, 1867.
19. Moreno-Mañas M.; Trius, A. *Bull. Chem. Soc. Jpn.* **1983**, *56*, 2154. Tsukahara, Y.; Kinoshita, H.; Inomata, K.; Kotake, H. *Bull. Chem. Soc. Jpn.* **1984**, *57*, 3013. Inoue, Y.; Toyofuku, M.; Hashimoto, H. *Bull. Chem. Soc. Jpn.* **1986**, *59*, 1279. Tamura, R.; Kato, M.; Saegusa, K.; Kakihana, M.; Oda, D. *J. Org. Chem.* **1987**, *52*, 4121.
20. For some exceptions using sophisticated (*E*)-allylphosphonium salts, see; Tamura, R.; Saegusa, K.; Kakihana, M.; Oda, D. *J. Org. Chem.* **1988**, *53*, 2723. Ideses R.; Shani, A. *Tetrahedron* **1989**, *45*, 3523. Wang, Q.; Khoury, M. E.; Schlosser, M. *Chem., Eur. J.* **2000**, *6*, 420.
21. Arisawa, M.; Momozuka, R.; Yamaguchi, M. *Chem. Lett.* **2002**, 272.
22. *Comprehensive Organic Synthesis, Vol. 8*; Trost, B. M.; Fleming, I., Eds.; Pergamon Press: New York, 1991, p 417. *Comprehensive Organic Synthesis, Vol. 3*; Trost, B. M.; Fleming, I., Eds.; Pergamon Press: New York, 1991, p 481. Aerssens, M. H. J. P.; Van der Heiden, R.; Heus, M.; Brandsma, L. *Synth. Commun.*, **1990**, *20*, 3421. Miyaura N.; Suzuki, A. *Chem. Rev.* **1995**, *95*, 2457.
23. Tsuji, J. *Palladium Reagents and Catalysts. Innovations in Organic Synthesis*; John Wiley and Sons, Inc.: New York, 1995. For examples, Satoh, M.; Nomoto, Y.; Miyaura, N.; Suzuki, A. *Tetrahedron Lett.* **1989**, *30*, 3789. Miyake H.; Yamamura, K. *Chem. Lett.* **1992**, 507. Xiao, W.-J.; Vasapollo, G.; Alper, H. *J. Org. Chem.* **2000**, *65*, 4138.
24. Arisawa, M.; Yamaguchi, M. *J. Am. Chem. Soc.* **2006**, *128*, 50.

Author Index

- Akimoto, Koji, 160
Ammal, Salai C., 364
Arisawa, Mieko, 477
Barbosa, André G. H., 297
Bardin, V. V., 428
Boltres, Bettine, 51
Borodkin, Gennady I., 118
Borosky, Gabriela L., 329
Brown, R. Stan, 458
Chiappe, Cinzia, 375
Esteves, Pierre M., 297
Fleming, Felipe P., 297
Franco, Marcelo, 254
Frohn, H.-J., 428
Fujita, Morifumi, 68, 88
Ito, Shunji, 160
Juhasz, Mark, 51
Kaiser, Christian, 51
Kitagawa, Toshikazu, 234
Klumpp, Douglas A., 144
Komatsu, Koichi, 32
Kover, W. Bruce, 254
Laali, Kenneth K., 329
Liu, C. Tony, 458
Maier, Rita, 51
Margraf, Dominik, 51
Maxwell, Christopher I., 458
Mercier, H el ene P. A., 394
Mills, Nancy S., 210
Moran, Matthew D., 394
Morita, Noboru, 160
Mota, Claudio J. A., 254
M uller, Thomas, 51
Nasiri, Hamid Reza, 51
Neverov, Alexei A., 458
Okuyama, Tadashi, 68, 88
Prakash, G. K. Surya, 106
Rasul, Golam, 106
Reddy, V. Prakash, 106
Reed, Christopher A., 51
Rosenbach, Nilton, Jr., 254
Schrobilgen, Gary J., 394
Shubin, Vyacheslav G., 118
Siehl, Hans-Ullrich, 1
Sorensen, Ted S., 268
Syha, Yvonne, 51
Yamaguchi, Masahiko, 477
Yamataka, Hiroshi, 364
Yang, Esther C. F., 268
Yoshida, Jun-ichi, 184

Subject Index

A

Ab initio calculations

Beckmann rearrangement, 365–366
proponium ions, 308

Ab initio molecular dynamics (AIMD)

carbonium ions, 304
ethonium ion, 305
proton tunneling and methonium ion, 304–305

Acetals. *See*

Alkylidenecyclopropanone acetals

Acetic acid

bromination of stilbenes, 379–380
reaction through ion pairs, 380, 382
See also Bromination of alkenes

Acid promoted generation, organic cations, 185–186

Activation energies

barriers for reaction of protonated oximes at different levels of theory, 368*t*
reaction of protonated benzyl methyl ketoximes and sulfur analogous systems, 370*t*

N-Acylium ions

[4+2]cycloaddition, with alkenes, 192
Friedel–Crafts type reactions, 191, 192
generation by C–H bond dissociation, 189–190
generation by C–Si bond dissociation, 190–191
radical addition to, 195, 196
reactions of, pools, 191
three component coupling, 193
See also “Cation pool” method

Acyl transfer reactions, cationic groups activating amides in, 151–152

Adamantylideneadamantanes

acceptor olefin, 461–464
bromination, 376, 377
dissociation rate constants and partitioning ratios for reactions of *bis*(pyridine)-halonium ions with, 464*t*
mechanism for transfer of Br⁺ from bromonium ion to, 462*f*
See also Bromination of alkenes

Addition reactions

phosphine to 1,3-dienes, 486–488
phosphine to alkenes, 488–490
phosphine to alkynes, 479–484
phosphine to allenes, 484–486
See also Phosphonium salts

Alkane protonation

C-carbonium ion-like transition states, 323*f*
H-carbonium ion-like transition states, 322*f*

Alkane reforming. *See*

Dehydrocyclization

Alkenes

addition reaction of phosphine to, 488–490
cationic carbohydroxylation of, 193–194
[4+2]cycloaddition of *N*-acylium ion with, 192
See also Bromination of alkenes

Alkoxy-carbenium ion pools

concept of electroauxiliary, 201
generation by C–H bond dissociation, 201
generation by C–Si bond dissociation, 200–202
generation by oxidative C–C bond dissociation, 204–205
generation by oxidative C–S bond cleavage, 203

- indirect "cation pool" method, 204
 thermal stability of
 alkoxycarbenium ion, 202*f*
See also "Cation pool" method
- Alkyl-aluminumsilyl oxonium ions
 calculated structures of, over
 zeolite Y, 261*f*, 262*f*
 formation, 256
 reaction with metal-exchanged
 zeolite, 256
 relative energy, 262*t*
 structure, over zeolite surface, 255
 theoretical calculations, 263
- Alkyl bromides. *See* Carbocations on
 surfaces
- Alkylideneallyl cations
 [4+2] cycloaddition of an, 89
 preparation of
 alkylidenecyclopropanone
 acetals, 90
 reaction selectivity, 103–104
 resonance hybrids, 88, 89
 ring opening of
 alkylidenecyclopropanone
 acetals, 90–96
 solvolysis of vinyl bromide via, 89
See also Alkylidenecyclopropanone
 acetals
- Alkylidenecyclopropanone acetals
 Lewis acid-mediated reaction via
 alkylideneallyl cation, 92
 plausible mechanism for reaction
 with siloxyalkene, 98
 possible pathways for reaction with
 furan, 101, 102
 preparation, 90
 reaction of alkylideneallyl cation
 with methanol, 96
 reaction with benzofuran, 103
 reaction with fluoride ion, 96
 reaction with furans, 99–103
 reaction with hydrogen chloride,
 93–96
 reaction with Lewis acid, 91–93
 reaction with siloxyalkenes, 97–99
 reaction with symmetrical allyl
 anion, 96
 regioselective ring opening, 91
 ring opening, 90–96
 selectivity of acetal cleavage, 93
See also Alkylideneallyl cations
- Alkyl systems, Beckmann
 rearrangement, 366–367
- Alkynes, addition reaction of
 phosphine to, 479–484
- Allenes
 addition reaction of phosphine to,
 484–486
 protonation, 21, 22*f*
- Allyl cations
 formation, 119
See also Persistent organic cationic
 complexes
- Allylphosphonium salts
 synthesis, 485
 Wittig reaction of, 486
See also Phosphonium salts
- Amides
 cationic groups activating, in acyl
 transfer reactions, 151–152
 protonated, activating electrophilic
 centers, 150–151
- Anhydrous HF, nuclear magnetic
 resonance spectra of
 organoxenonium salts in, 440–
 447
- Anthracene
 annelated with bicyclooctene
 (BCO), 37*f*
 aromaticity, 213
 bond lengths of σ -bonds in, and
 radical cation salts, 40*t*
 molecular structure of monomeric
 radical-cation salt, 38*f*
 one-electron oxidation to radical
 cation, 36–37
 two-electron oxidation to dication,
 37, 40
See also Bicyclo[2.2.2]octene
 (BCO) frameworks

- Antiaromaticity**
 aromaticity to, continuum, 230, 231*t*
 dications of
 diphenylmethylenefluorene, 218–221
 evidence for fluorenylidene dications, 215–217
 fluorenylidene dications as, 214–218, 221, 223
 models for ring system interactions, 217–218
See also Fluorenylidene dications
- Anti-Markovnikov addition**
 influencing nucleophilic attack, 152–154
 phosphine addition to alkenes, 488–489
 phosphine addition to alkynes, 482–483
 phosphine addition to allenes, 484–485
 phosphine addition to 1,3-dienes, 486–488
See also Markovnikov addition
- Aromatic hydrocarbons.** *See* Bicyclo[2.2.2]octene (BCO) frameworks
- Aromaticity**
 anthracene, 213
 aromatic stabilization energy (ASE), 211
 criteria, 211–213
 energetic criteria, 211
 fundamentals of organic chemistry, 210–211
 harmonic oscillator measure of, (HOMA), 211, 212
 magnetic criterion, 212–213
 magnetic susceptibility, 212–213
 magnetic susceptibility exaltation, 212
 nucleus independent chemical shift (NICS), 212
 problems with use of criteria, 213–214
 structural criteria, 211–212
See also Antiaromaticity;
 Fluorenylidene dications
- Aromatic stabilization energy (ASE)**
 continuum of
 aromaticity/antiaromaticity, 230, 231*t*
 fluorenyl systems, indenyl systems, and indenylidene fluorene dications, 228*t*
 resonance stability, 211
- Aromatic systems**
 activation energies for reaction of protonated benzyl methyl ketoximes, 370*t*
 Beckmann rearrangement, 367, 370–373
- Arylxenonium salts**
 preparation, 431–432
See also Organoxenonium salts
- As(OTeF₅)₆⁻ anions**
 background, 397
See also XeOTeF₅⁺Sb(OTeF₅)₆⁻
- Automerization reactions,**
 carbocations, 120–121
- Aza-polycyclic aromatic hydrocarbons (aza-PAHs)**
 adducts between carbocation and guanine, 340*f*, 341*f*
 aza-benzo[*a*]pyrene (azaBaP) derivatives, 355
 B3LYP/6-31G calculations for carbocations of PAHs and aza-PAHs, 335*t*
 benzo[*a*]acridine (B[*a*]ACR) and B[*c*]ACR and epoxide derivatives, 342–343
 benzo[*a*]pyrene (BaP), 355
 benzo[*h*]quinoline (BhQ), benzo[*f*]quinoline (BfQ), and benzo[*c*]phenanthridine (BcPhen) derivatives, 332–340

- calculated nucleophilic reactions with MeO^- , 338*f*
- B3LYP/6-31G calculations for guanine adducts, 339*t*
- calculations of dibenzacridines (DBACRs), DB[*a,h*]ACR-1,2-epoxide and DB[*a,h*]ACR-8,9-epoxide, and B[*c*]ACR-1,2-epoxide, 354*t*
- carbocations from PAHs and aza-PAHs, 334*f*
- covalent adducts of carbocations with representative nucleophiles, 336–340
- dibenzacridines (DBACRs), 340–344, 350–351
- epoxide ring opening of bay-region diol epoxides and epoxides from DB[*a,h*]ACR and epoxides from B[*a*]ACR and B[*c*]ACR, 345*f*
- epoxide ring opening reactions, 342–343
- epoxide ring opening reactions for methylated DB[*a,h*]ACR-1,2-epoxide, 352*f*
- epoxide ring opening reactions for methylated DB[*a,h*]ACR-8,9-epoxide and B[*c*]ACR-1,2-epoxide, 353*f*
- epoxide ring opening reactions of epoxides and diol epoxides from BaP, 4-azaBaP, and 10-azaBaP, 356*f*, 358*t*
- epoxide ring opening reactions of fluorinated derivatives of DB[*a,h*]ACR-1,2-epoxide, 347*f*
- epoxide ring opening reactions of fluorinated derivatives of DB[*a,h*]ACR-8,9-epoxide, 348*f*
- fluorinated derivatives of DB[*a,h*]ACR-8,9-epoxide calculations, 349*t*
- fluorine substitution effect on epoxide ring opening reaction, 344, 350
- isodesmic reactions for formation of fluorinated epoxides, 351*f*
- methods, 331
- methyl substitution effect on epoxide ring opening reaction, 350–351
- NPA charges (carbocation minus neutral) for isomeric carbocations from BcPhen-9,10-epoxide (9), 337*f*
- NPA-derived heavy atom charges computed for carbocations, 346*f*
- NPA heavy atom charges computed for carbocations from BaP and azaBaP, 357*f*
- structures and numbering of BhQ, BfQ, BcPhen, and carbon analogues phenanthrene (Phe) and chrysene (Chry), 332*f*
- See also* Polycyclic aromatic hydrocarbons (PAHs)
- Azide clock method
- lifetime of ionic intermediates, 382–383, 386–387
- See also* Bromination of alkenes
- Azulene-substituted methyl cations
- absorption spectra and redox behavior, 167, 168*t*
- cyclopropenylum ion substituted by three guaiazulenes, 163*f*
- polarizability, 162–163
- preparation, 163–164
- preparation of dimethylamino-substituted azulenylmethyl cation salt, 166*f*
- preparation of trimethoxy-substituted azulenylmethyl cation salt, 166*f*
- stabilization of azulenylmethyl cations, 165–167
- structure, 163*f*
- thermodynamic stability, 164–165
- UV-vis spectrum of parent cation, 6-methoxy- and 6-

- dimethylamino- derivatives,
167f
See also Electrochromic materials
- B**
- β -effect
hyperconjugation, 6–7
See also Silyl-substituted
carbocations
- Basicity scale, σ bonds, 319–320
- Beckmann rearrangement
activation barriers for reaction of
protonated oximes calculated at
different levels of theory, 368t
activation energies for reaction of
protonated benzyl methyl
ketoximes and sulfur analogous
systems, 370t
aromatic systems, 367, 370–373
calculated structures for reactants
and transition states (TSs) of
aromatic systems, 372f
computational methods, 365–
366
contour energy map for reaction of
protonated acetone oxime,
369f
experimental studies of oxime
tosylate, 365
Hammett plots for aromatic
substrates, 370, 371f
intrinsic reaction coordinate (IRC),
366
IRC snapshots for reaction of
protonated 1-
methylcyclobutanone oxime,
369f
IRC snapshots for reaction of
protonated cyclobutanone
oxime, 368f
process, 364
simple alkyl systems, 366–367
transition states (TSs), 366
variations of atomic distance
between benzylic C and N along
IRC for aromatic systems, 372f
- Benzenes, reactions of fullerene
cations with, 250
- Benzo[*a*]acridine (B[*a*]ACR)
epoxide derivative, 343–344
epoxide ring opening reactions,
345f
- Benzo[*a*]pyrene (BaP)
aza-BaP derivatives, 355
calculations for carbocations from
BaP and azaBaP, 357f
epoxide ring opening of epoxides
and diol epoxides from azaBaP
derivatives, 356f, 358t
See also Aza-polycyclic aromatic
hydrocarbons (aza-PAHs)
- Benzo[*c*]acridine (B[*c*]ACR)
epoxide derivative, 343–344
epoxide ring opening reactions,
345f
methyl substitution effect on
epoxide ring opening, 353f, 354t
- Benzo[*c*]phenanthridine derivatives.
See Aza-polycyclic aromatic
hydrocarbons (aza-PAHs)
- Benzo[*f*]quinoline (BfQ). *See* Aza-
polycyclic aromatic hydrocarbons
(aza-PAHs)
- Benzo[*h*]quinoline (BhQ). *See* Aza-
polycyclic aromatic hydrocarbons
(aza-PAHs)
- Benzofuran, reaction of
alkylidenecyclopropanone acetal
with, 103
- Benzopentalene skeleton, polycyclic
hydrocarbons, 125
- Benzyl cations
 α -ferrocenyl β -silyl substituted
carbocation, 15
1-phenyl-2-(triisopropylsilyl)ethyl
cation, 8–9, 10f
1-phenyl-2-(trimethylsilyl)ethyl
cation, 10, 11f

- protonation of substituted styrenes, 7–8
- β -silyl effect in, 7–15
- syn*- and *anti*-1-*p*-anisyl-2-(triisopropylsilyl)ethyl cations, 11–12, 14*f*
- See also* β -Silyl-substituted carbocations
- Bi(OTeF₅)₆[−] anions
background, 397
See also XeOTeF₅⁺Sb(OTeF₅)₆[−]
- Bicyclo[2.1.1]hexane-5-methyl tosylate, solvolysis of *endo*- and *exo*-, 109
- Bicyclo[2.2.0]hexane-1-methyl *p*-nitrobenzoate, solvolysis, 108, 109*f*
- Bicyclo[2.2.2]octene (BCO) frameworks
bond lengths of σ -bonds in BCO units in naphthalene, anthracene, biphenylene, and fluorene and their radical-cation salts, 40*t*
- condensed aromatic hydrocarbons annelated with, 36–41
- dications by two-electron oxidation, 37, 40
- dications of tetramer and hexamer oligothiophenes, 47, 48*f*
- dithiins, 43–45
- molecular structure of 1,4-dithiin radical-cation salt by X-ray crystallography, 46*f*
- molecular structures of radical cations of biphenylene and fluorene, 39*f*
- molecular structures of radical cations of naphthalene and anthracene, 38*f*
- naphthalene, anthracene, biphenylene, and fluorene annelated with, 36–37
- oligothiophenes, 45–47
- one-electron oxidation of dimer and trimer to radical cation salts, 46*f*, 47*f*
- one-electron oxidation to radical cations, 36–37
- resonance structure of fluorene dication, 40*f*
- σ -bond lengths of, in σ - π conjugation, 37
- σ - π conjugation with benzenoid π -system with BCO σ -bonds, 39*f*
- spirocyclic arenium-ion salt, 41
- stabilization effect of BCO, 33–34
- sulfur-containing conjugated systems annelated with, 42–47
- thiophene, 42, 43*f*
- transformation from radical cation to arenium ion, 41, 42*f*
- two-electron oxidation of 1,2-dithiin and 1,4-dithiin, 44*f*
- X-ray crystallography of dications of oligothiophenes, 47, 48*f*
- Bicyclo[2.2.2]octenotropylium ions, super-stabilization, 33–34
- Bicyclo[3.2.1]octadienyl carbocations, rearrangements, 124
- Bicyclobutonium ions
2D-*H,H*-COSY NMR spectrum of 3-*endo*-(trialkylsilyl)bicyclobutonium ion, 26*f*
calculated structure of, over zeolite Y, 260*f*
3-*endo*-(trialkylsilyl)bicyclobutonium ion, 24, 25*f*
experimental NMR spectroscopic investigations, 23
intermediates in solvolysis of cyclopropylmethyl and cyclobutyl compounds, 22–23
natural bond orbitals in 3-*endo*-silylbicyclobutonium ion, 27*f*
 γ -silyl effect in, 22–27
structure of 3-*endo*-silylbicyclobutonium ion, 25*f*, 26

- See also* Carbocations on surfaces;
Silyl-substituted carbocations
- Biphenylene**
annulated with bicyclooctene
(BCO), 37*f*
bond lengths of σ -bonds in, and
radical cation salts, 40*t*
molecular structure of monomeric
radical-cation salt, 39*f*
one-electron oxidation to radical
cation, 36–37
two-electron oxidation to dications,
37, 40
See also Bicyclo[2.2.2]octene
(BCO) frameworks
- Born–Oppenheimer molecular
dynamics (BOMD)**
C-proponium cation, 312–313
1-H-isobutonium ion, 316, 317*f*
1-H-proponium ion, 309–310
2-H-proponium ion, 311
methonium ion, 304
- Bromination of alkenes**
1,1-diphenylethylene, 387, 391
adamantylideneadamantane, 376,
377
azide clock method, 382, 386–387
 β -bromocarbenium ion in
bromination of 1,1-
diphenylethylene, 390, 391
boat conformation of ionic
intermediate from Br_2 addition
to
bicyclo[3.3.1]nonylidenebicyclo
[3.3.1]nonane, 376, 377*f*
bromination in methanol with
added NaN_3 , 383–385
bromocarbenium character in
intermediate in *trans*-(1-methyl-
2-adamantylidene)-1'-
methyladamantane, 377, 378
chemoselectivity, 379
cyclic enol ethers (glycols), 386–
387, 388
halide salts and reaction
mechanism, 378
intermediates, 375–376
kinetic analysis, 383–386
lifetime of ionic intermediate for
addition to simple alkenes, 382–
383
lifetime of ionic intermediates
using azide clock method, 386–
387
mechanisms in aprotic and protic
solvents, 379
nucleophilic assistance in
methanol, 380, 381
partition constant ratios for
reactions of azide and methanol
with various bromonium ions,
386*t*
product distribution for
bromination of 1-(3-
trifluoromethylphenyl)-1-(4-
trifluoromethylphenyl) ethylene,
390*t*
product distribution for
bromination of 1,1-
diphenylethylene, 389*t*
proposed mechanism for product
formation in bromination of
bicyclo[3.3.1]nonylidenebicyclo
[3.3.1]nonane, 376, 377
rate constant and solvent polarity,
378
rate constants for reaction of azide
with BrN_3 , 384*t*
reaction through ion pairs for acetic
acid, 380, 382
stereochemical behavior in
trifluoroethanol, 380
trans-stilbenes in methanol,
trifluoroethanol and acetic acid,
379–383
1-(3-trifluoromethylphenyl)-1-(4-
trifluoromethylphenyl) ethylene,
389

- Bromonium ions. *See* Halogen transfer reactions
- Butonium ions
- basicity of σ bond, 319–320
 - Born–Oppenheimer molecular dynamics (BOMD) calculations of 1-H-isobutonium ion, 316, 317*f*
 - comparing 2e-3c bonding types, 313, 315
 - comparing n-butonium and isobutonium ions, 319
 - potential energy surface for $C_4H_9^+$, 316*f*
 - relative energies, 315*f*
 - relative enthalpy for isomeric butonium cations, 319*f*
 - structural isomers of n-butonium and isobutonium ions, 314*f*
 - structures for n-butonium ion, 316, 318*f*
- See also* Carbonium ions
- C**
- C_{60} cations
- derivatized, 235*f*
 - See also* Fullerene cations
- C_{70} cations
- derivatized, 235*f*
 - types of carbon in framework, 243*f*
 - See also* Fullerene cations
- Carbenium ions, carbocation
- classification, 298*f*
- Carboalkoxylation, cationic, of alkenes, 193–194
- Carbocationic polymerization, “cation pool” as initiator, 194
- Carbocations
- classifying into carbonium and carbenium ions, 297, 298*f*
 - reactions in synthesis, 184–185
 - α -silyl substituted, 2–6
- See also* Carbocations on surfaces; Carbonium ions; Electrochromic materials; Fullerene cations; Silyl-substituted carbocations; Vinyl cations
- Carbocations on surfaces
- calculated structure of allylcarbanyl aluminumsilyl oxonium ion, 261*f*
 - calculated structure of bicyclobutonium, over zeolite Y, 260*f*
 - calculated structure of cyclobutyl aluminumsilyl oxonium ion, 262*f*
 - calculated structure of cyclopropylcarbanyl, over zeolite Y, 260*f*
 - calculated structure of cyclopropylcarbanyl aluminumsilyl oxonium ion, 261*f*
 - carbocationic reactions on metal-exchanged zeolites, 255, 256
 - experimental, 257
 - NaBr-impregnated NaY and distribution of allyl bromides, 264, 265*t*
 - possible mechanistic scheme for cyclopropylcarbanyl chloride rearrangement over NaY/NaBr zeolite, 264*f*
 - product distribution from reaction of cyclopropylcarbanyl chloride on NaBr-impregnated NaY, 259
 - product distribution from reaction of cyclopropylcarbanyl chloride on NaY, 258
 - production distribution from solvolysis of cyclopropylcarbanyl, cyclobutyl, and allylcarbanyl derivatives, 256

- rearrangement of
 cyclopropylcarbinyl chloride,
 258–259
- relative energy of alkyl-
 aluminumsilyl oxonium ions and
 carbocations, 262*t*
- structure of alkyl-aluminumsilyl
 oxonium ions over zeolite, 255
- theoretical calculations, 259, 263–
 265
- theoretical methods, 257–258
- Carbohydroxylation, cationic, of
 alkenes, 193–194
- Carbonium ions
- 3c2e bonding concept, 319–320
- BOMD (Born–Oppenheimer
 molecular dynamics)
 calculations for CH_5^+ , 304*f*
- BOMD calculations of 1-H-
 isobutonium ion, 316, 317*f*
- n-butonium and isobutonium ions,
 314*f*
- butonium ions ($\text{C}_4\text{H}_{11}^+$), 313–320
- carbocation classification, 298*f*
- Car–Parrinello Molecular
 Dynamics of CH_4 and C_2H_6 ,
 321*f*
- C-carbonium ion-like transition
 states for ethane, propane and
 isobutane protonation, 323*f*
- CH_5^+ solvated by H_2 , 320*f*
- comparing n-butonium and
 isobutonium ions, 319
- C-proponium ion, 312–313
- ethonium ion (C_2H_7^+), 305–306
- formation of isomeric proponium
 ions, 307*f*
- H- and C-forms of ethonium ion,
 306*f*
- H-carbonium ion-like transition
 states for methane, ethane,
 propane and isobutane
 protonation, 322*f*
- 1-H-proponium, 309–310
- 2-H-proponium ion, 311
- isobutonium ions, 315*f*
- isomers of proponium ion, 308*f*
- methonium ion (CH_5^+), 298–305
- outlook, 324
- potential energy surface for C_4H_9^+ ,
 316*f*
- proponium ions, 307–313
- σ basicity scale, 319–320
- snapshots of BOMD of 1-H-
 proponium cation,
 rearrangement to C-proponium
 cation and decomposition, 309*f*
- solvation of, 320–321
- spin-coupled orbitals for CH_5^+ ,
 300*f*
- spin-coupled orbitals for CH_6^{+2} ,
 303*f*
- spin-coupled orbitals for H_2 and
 H_2^+ , 301*f*
- spin-coupled orbitals for one C–H
 bond in CH_4 , 302*f*
- spin-coupled orbitals from 3c2e
 bond as function of $[\text{H}_3\text{C}\cdots\text{H}_2]^+$
 distance, 303*f*
- stable structures for butonium ions,
 316, 318*f*
- structures of ethonium ion, 306*f*
- superimposed structures of BOMD
 of 1-H-proponium cation, 310*f*
- two modes of interaction of CH_5^+
 within zeolites, 324*f*
- Carbon nucleophiles, reactions of *N*-
 acyliminium ion pools with, 191
- Carboxonium electrophiles
 hydroxylalkylation reaction, 148
 See also Superelectrophilic
 chemistry
- Carboxylic acids, protonated,
 activating electrophilic centers,
 150–151
- Car–Parrinello molecular dynamics
 (CPMD), methane and ethane,
 320–321
- Catalytic dehydrocyclization
 heptane to toluene, 269

- See also* Dehydrocyclization
- “Cation flow” method
 method for generating organic cations, 185–186
 outline, 198–199
 schematic diagram, 199*f*
 serial combinatorial synthesis based on, 199–200
See also “Cation pool” method
- Cationic complexes. *See* Fullerene cations; Persistent organic cationic complexes
- Cationic conjugated systems. *See* Bicyclo[2.2.2]octene (BCO) frameworks
- Cationic nitrogen, enhancing electrophilic character of carbonyl, 146–147
- “Cation pool” method
N-acyliminium ion pools by C–H bond dissociation, 189–190
N-acyliminium ion pools by C–Si bond dissociation, 189, 190–191
 alkoxy-carbenium ion pools by C–S bond cleavage, 203
 alkoxy-carbenium ion pools by C–Si bond dissociation, 200–202
 alkoxy-carbenium ion pools by oxidative C–C bond dissociation, 204–205
 apparatus for low temperature electrolysis, 188*f*
 carbocationic polymerization using “cation pool” as initiator, 194
 cationic carboxylation of alkenes, 193–194
 combinatorial synthesis, 197–198
 [4+2]cycloaddition of *N*-acyliminium ion with alkenes, 192
 Friedel–Crafts type reactions of *N*-acyliminium ion, 191, 192
 indirect, 204
 low temperature electrolysis, 187–188
 method for generating organic cations, 185–186
 methods for oxidative generation of cations for use in, 188, 189
 outline, 187
 oxidative C–C bond dissociation, 189
 oxidative C–H bond dissociation, 189
 oxidative C–S bond dissociation, 189
 oxidative C–Si bond dissociation, 189
 radical chemistry using, 195, 196
 reactions of *N*-acyliminium ion pools, 191
 schematic diagram, 187*f*
 sequential generation of cation pools using two silyl groups, 197
 three component coupling, 193
See also *N*-Acylium ions; Alkoxy-carbenium ion pools; “Cation flow” method
- Cations. *See* “Cation flow” method; “Cation pool” method; $\text{XeOTeF}_5^+\text{Sb}(\text{OTeF}_5)_6^-$
- Chemoselectivity, bromination of alkenes, 379
- Chiral halogenation
 energy considerations, 465–467
See also Halogen transfer reactions
- Chirality probe, primary vinyl cation, 73–76
- Chloroalkanes, electrophilic addition to C_{60} , 237, 238*t*
- Combinatorial synthesis
 “cation flow” method, 199–200
 “cation pool” method, 197–198
- Conformational studies. *See* Cyclobutylmethyl cations
- π -Conjugated cations. *See* Bicyclo[2.2.2]octene (BCO) frameworks

- Coupling, three component, "cation pool" method, 193
- Crystal structures. *See* $\text{XeOTeF}_5^+\text{Sb}(\text{OTeF}_5)_6^-$
- Cyanine–cyanine hybrid
 continuous change in visible spectrum of cation, 173*f*
 cyanine unit at one terminus, 171–172
 di(1-azulenyl)(6-azulenyl)methyl cation, 172*f*
 electrochromic behavior of cation, 172–173
 general structure, 172*f*
 multiple color changes, 170–171
See also Electrochromic materials
- Cyanine–cyanine hybrid, tetracation salt
 continuous changes in visible spectrum, 180*f*
 continuous changes in visible spectrum of tetracation, 178*f*
 di- and monocations synthesized to compare redox properties, 180*f*
 dication example for violene–cyanine hybrid, 177*f*
 first tetracation, 175, 176*f*, 177–178
 monocation as parent compound for multi-charged tetracation, 177*f*
 redox system from cyanine-based hybrid, 173
 schematic of cyanine–cyanine hybrid with cyanine at both termini, 174*f*
 second tetracation connected to thienylacetylene spacers, 178–180
 structure of cyanine–cyanine hybrid with cyanine at both termini, 174*f*
 tetracation improving redox interaction among cationic units, 181*f*, 182
- third tetracation incorporating anthraquinodimethane unit, 180–182
See also Electrochromic materials
- Cyclic enol ethers, bromination, 387, 388
- Cycloaddition [3+2]
 alkylideneallyl cation with 2,3-benzofuran, 102
 alkylideneallyl cation with furan, 101
See also Alkylidenecyclopropanone acetals
- Cycloaddition [4+2]
N-acyliminium ion with alkenes, 192
 alkylideneallyl cation, 89
See also Alkylidenecyclopropanone acetals
- Cyclobutenyl carbocations, long-lived cations, 126
- Cyclobutylmethyl cations
 bent cyclopropyl ring C–C bonds, 107
 density functional theory (DFT) studies of α,α -dicyclopropylcyclobutylmethyl cation, 113–115
 DFT studies of α,α -dimethylcyclobutylmethyl cation, 116
 equilibrating bicyclobutonium ions and bisected cyclopropylmethyl cations, 107*f*
 formation of 1,2-dimethylcyclopentyl cation from ionization of α,α -dimethylcyclobutylmethanol, 113*f*
 formation of 1-bicyclo[4.4.0]dec-1-yl cation from ionization of cyclobutylmethanol, 110, 111*f*
 formation of cyclopentyl cations from ionization of secondary

- cyclobutylmethanols, 111*f*
 generation of persistent, 110
 neighboring group stabilization, 107
 preparation of α,α -
 dicyclopropylcyclobutylmethyl
 cation, 114*f*
 product distribution from solvolysis
 of nopinyl brosylate, 108*f*
 products of acetolysis of
 bicyclo[2.1.1]hexane-5-methyl
 tosylates, 109*f*
 products of solvolysis of
 bicyclo[2.2.0]hexane-1-methyl
p-nitrobenzoate, 109*f*
 ring expansion rearrangement, 109
 rotational barrier for α,α -
 dicyclopropylcyclobutylmethyl
 cation, 115
 secondary, 110–112
 solvolysis of *cis*- and *trans*-2-
 methylcyclobutylmethyl
 brosylates, 109, 110*f*
 solvolytic generation of, 107–109
 stable ion studies, 110–116
 structures of α,α -
 dimethylcyclobutylmethyl
 cation, and *endo*- and *exo*- α -
 methylcyclobutylmethyl cations
 with bond distances, 112*f*
 tertiary, 112–113
 Cyclooctatetraene (COT)
 dications and ring inversion, 36*f*
 super stabilization, 35–36
 Cyclopentanes, dehydrocyclizations,
 292–293
 Cyclopropylcarbinyl carbocations
 calculated structure of, over zeolite
 Y, 260*f*
 relative energy, 262*t*
See also Carbocations on surfaces
 Cyclopropylcarbinyl cations
 formation, 119
See also Persistent organic cationic
 complexes
- Cyclopropylcarbinyl chloride
 rearrangement over NaY zeolite,
 258–259
 solvolysis, 256
See also Carbocations on surfaces
 α -Cyclopropyl substituted
 carbocations, β -silyl effect in, 15–
 17
- ## D
- Degenerate rearrangements
 carbocations, 120–121
 cation undergoing, by 1,2-bridge
 shift, 123–124
 rates for long-lived cations, 122
See also Rearrangements
 Dehydrocyclization
 calculations of 2- and 3-octyl
 cation systems, 283–289
 catalytic, 269
 closure of 2- and 3-methylheptane,
 292–293
 formation of cyclopentanes, 292–
 293
 2-heptyl cation systems, 276–
 283
 mechanisms, 269–270
 n-octane isomerization, 289, 292
 possible alternative formation of
 cyclic rings via carbocation
 intermediate, 293
 scope for future studies, 293–295
 superacid observations and
 reactivity of μ -H-bridged
 carbocations, 271–275
 theoretical modeling of cyclodecyl
 cation to 9-decalyl cation and H₂
 reaction, 273–275
 thermodynamics, 293
See also μ -H-bridged carbocations;
 2-Heptyl cation systems; n-
 Octane isomerization; Octyl
 cation systems

- Density functional theory (DFT)
 α,α -dicyclopropylcyclobutylmethyl cation, 113–115
 α,α -dimethylcyclobutylmethyl cation, 116
 geometry of alkylated fullerene cation $\text{ClCH}_2\text{-C}_{60}^+$, 242*f*
 orbitals of C_{70} calculated by, 244*f*
See also Cyclobutylmethyl cations
- Dibenzacridines (DBACRs)
 epoxide ring opening reactions of diol epoxides and epoxides, 343–344, 345*f*
 fluorine substitution effect on epoxide ring opening, 344, 347*f*, 348*f*, 349*t*
 methyl substitution effect on epoxide ring opening, 350–351, 352*f*, 353*f*, 354*t*
 structure and numbering, 342*f*
See also Aza-polycyclic aromatic hydrocarbons (aza-PAHs)
- Dicationic electrophiles
 enhancing reactivities, 147–148, 157
See also Superelectrophilic chemistry
- Dications. *See* Fluorenylidene dications; Indenylidene dications
- α,α -Dicyclopropylcyclobutylmethyl cation
 density functional theory, 113–115
 rotational barrier for, 115
See also Cyclobutylmethyl cations
- 1,3-Dienes
 addition reaction of phosphine to, 486–488
 typical procedures for separation of (Z)-1,3-diene, 488
- Dieryl cations, β -silyl substituted, 19–21
- α,α -Dimethylcyclobutylmethyl cation, density functional theory, 116
- Diol epoxides. *See* Aza-polycyclic aromatic hydrocarbons (aza-PAHs)
- Dioxirane epoxidations, electrophilic reactivities, 146
- 1,1-Diphenylethene, reaction with superacidic triflic acid, 147
- 1,1-Diphenylethylene
 β -bromocarbenium ion, 390, 391
 bromination, 387, 388
 product distribution of bromination, 389*t*
See also Bromination of alkenes
- Diphenylmethylidenefluorene dications
 energetic and structural criteria, 219–221
 magnetic criteria, 218–219
 nucleus independent chemical shift (NICS) of fluorenyl systems, 220*t*
 redox potentials and NICSs, 221*t*, 222*f*
See also Antiaromaticity
- Diprotonated species, electrophilic reactivities, 145
- Dithiins
 annelation of 1,4-, with bicyclooctene (BCO) units, 44–45
 π -conjugated systems containing sulfur atoms, 43
 molecular structure of radical cation by X-ray crystallography, 45*f*
 molecular structure of radical-cation salt of 1,4-, by X-ray crystallography, 46*f*
 one-electron oxidation of 1,2-dithiin, 43–44
 two-electron oxidation of 1,2- and 1,4-, 44*f*
See also Bicyclo[2.2.2]octene (BCO) frameworks

E

- Electroauxiliaries, sequential generation of cation pools, 197
- Electrochemical oxidation. *See* "Cation flow" method; "Cation pool" method
- Electrochromic materials
- azulene-substituted methyl cations, 162–167
 - cyanine–cyanine hybrid, 170–173
 - preparation of azulene-substituted methyl cations, 163–164
 - stabilization of azulenylmethyl cations, 165–167
 - tetracation salts as novel cyanine–cyanine hybrid system, 173–182
 - thermodynamic stability of azulene-substituted methyl cation, 164–165
 - violene–cyanine hybrid, 161–162
 - violenes, 161
 - Wurster type violene–cyanine hybrid, 162, 168–170
- See also* Azulene-substituted methyl cations; Cyanine–cyanine hybrid; Cyanine–cyanine hybrid, tetracation salt
- Electrochromism, reversible redox systems, 161
- Electrophiles
- addition to C₆₀, 236–239
 - addition to C₇₀, 242–243, 244*f*
 - complexes with C-centered, 119–126
 - complexes with N-centered, 126–139
 - super electrophilic activation, 145
- See also* Persistent organic cationic complexes; Super electrophilic chemistry
- Elimination and participation, vinyl iodonium salts, 81–82
- Energy diagram
- contour energy map for reaction of protonated acetone oxime, 369*f*
 - dehydrocyclization in 2-heptyl cation system, 282*f*
 - overall profile for 2- and 3-octyl cation systems, 289*t*, 290*f*
 - pictorial of potential energy surface for C₄H₉⁺, 316*f*
 - potential, for dehydrocyclization of 2-heptyl cation, 283*f*
- Epoxide ring opening reactions
- epoxides and diol epoxides from benzo[*a*]pyrene (BaP), 4-azabenz[*a*]pyrene (4-azaBaP), 10-azaBaP, 355, 356*f*, 358*t*
 - epoxides from dibenzo[*a,h*]acridine, benzo[*a*]acridine (B[*a*]ACR), and B[*c*]ACR, 345*f*
 - fluorinated derivatives of dibenzo[*a,h*]acridine-1,2-epoxide, 347*f*
 - fluorinated derivatives of dibenzo[*a,h*]acridine-8,9-epoxide, 348*f*, 349*t*
 - fluorine substitution effect on, 344, 350
 - methylated derivatives of dibenzo[*a,h*]acridine-1,2-epoxide, 352*f*, 354*t*
 - methylated derivatives of dibenzo[*a,h*]acridine-8,9-epoxide and B[*c*]ACR-1,2-epoxide, 353*f*, 354*t*
 - methyl substitution effect on, 350–351
 - nucleophilic reactions with MeO[−], 337*f*, 338*t*
 - protonation and formation of open carbocations, 333
- See also* Aza-polycyclic aromatic hydrocarbons (aza-PAHs)
- Ethane protonation
- C–carbonium ion-like transition states, 323*f*

- H-carbonium ion-like transition state, 322*f*
- Ethonium ion
alkyl carbonium ions, 305–306
different structures for, 306*f*
H- and C-forms, 306*f*
See also Carbonium ions
- F**
- α -Ferrocenyl- β -silyl substituted, vinyl cations, 19
- Flow method. *See* “Cation flow” method
- Fluorene
annelated with bicyclooctene (BCO), 37*f*
bond lengths of σ -bonds in, and radical cation salts, 40*t*
molecular structure of monomeric radical-cation salt, 39*f*
one-electron oxidation to radical cation, 36–37
resonance structure of dication, 40*f*
two-electron oxidation to dications, 37, 40
See also Bicyclo[2.2.2]octene (BCO) frameworks
- Fluorenyl cation
antiaromaticity, 227
energetic and magnetic measures of antiaromaticity, 228*t*
- Fluorenylidene dications
antiaromaticity, 221, 223, 227
dications of
diphenylmethylenefluorene as antiaromatic species, 218–221
dication with potential three-dimensional aromaticity, 214
energetic and structural criteria of diphenylmethylenefluorenes, 219–221
evidence of antiaromaticity, 215–217
extending research to indenylidene dications, 223–224
 ^1H NMR spectrum reflecting antiaromatic system, 214–215
magnetic criteria of diphenylmethylenefluorenes, 218–219
nucleus independent chemical shift (NICS) of fluorenyl systems, 220*t*
potential models for ring interactions, 217–218
redox potentials and NICS for fluorenyl systems, 221*t*, 222*f*
research intent, 214
See also Antiaromaticity; Indenylidene dications
- Fluoride ion, reaction of alkylidenecyclopropanone acetal with, 96
- Fluorine-containing halomethyl cations, studies, 395
- Friedel–Crafts type reactions
N-acyliminium ion, 191, 192
electrophilic activation, 152
fullerene cations, 248–250
zeolite catalysts, 255
- Fullerene, three-dimensional π -conjugated system, 234
- Fullerene cations
carbon types in C_{70} framework, 243*f*
charge distribution of $\text{Cl}_2\text{CH}-\text{C}_{70}^+$, 246*f*
chemistry, 235
 ^{13}C NMR spectrum of $\text{Cl}_2\text{CH}-\text{C}_{70}^+$, 246*f*
 ^{13}C NMR spectrum of $\text{ClCH}_2\text{CCl}_2-\text{C}_{60}^+$, 241*f*
coordination of chlorine lone pair to cationic center, 241*f*
derivatized, 235*f*
electrophilic addition of chloroalkanes to C_{60} , 238

- electrophilic addition of chloroform to C_{70} , 244*f*
 electrophilic addition of tetrachloroethane to C_{60} , 237*f*
 electrophilic addition to C_{60} , 236–239
 electrophilic addition to C_{70} , 242–243
 generation and trapping of alkylated C_{60} cations, 240*f*
 generation and trapping of $Cl_2CH-C_{70}^+$, 246*f*
 generation of RC_{60}^+ as long-lived ion, 239–242
 generation of RC_{70}^+ as long-lived ion, 245, 246*f*
 geometry of $ClCH_2C_{60}^+$ optimized by density function theory (DFT), 242*f*
 orbitals of C_{70} by DFT method, 244*f*
 preparation, 235
 proposed mechanisms for hydrophenylation and nitration of C_{60} , 236*f*
 reactions of RC_{60}^+ intermediate with substituted benzenes, 250*f*
 reactions via RC_{60}^+ and RC_{70}^+ , 248–250
 silica gel-promoted hydrolysis of $RC_{60}Cl$, 239*f*
 symmetry of RC_{60}^+ , 241*f*
 synthesis of C_{60} derivatives via alkylated C_{60} cation intermediate, 249*f*
 synthesis of C_{70} derivative via alkylated C_{70} cation intermediate, 251*f*
 thermodynamic stabilities of RC_{60}^+ and RC_{70}^+ , 247–248
 UV-vis-NIR absorption spectra of $Cl_2CH-C_{70}^+$ from corresponding fullerenols, 245*f*
 UV-vis-NIR absorption spectra of RC_{60}^+ from corresponding fullerenols, 240*f*
 Fullerenols
 generation of RC_{70}^+ from, 245
 ionization, 240*f*, 242
 precursors for cations RC_{60}^+ , 239–241
 [5.5]Fulvalene, theoretical dication from, 214
 Furans, reaction of alkylidenecyclopropanone acetal with, 99–103
- G**
- Glycols, bromination, 387, 388
 Guanine, adducts of carbocations with, 339–340, 341*f*
- H**
- Halide salts, bromination reactions, 378
 Halocyclization process
 chiral quinuclidine- X^+ with 1, ω -alkenols, 470–472
 enantiomeric excesses from, 473*t*
 energy considerations for chiral induction, 465–467
 heterocyclic rings, 459–460
 See also Halogen transfer reactions
 Halogenation. *See* Halogen transfer reactions
 Halogen transfer reactions
 adamantylideneadamantane (Ad=Ad) as acceptor olefin, 461–464
 chiral induction for reaction of chiral quinuclidine- X^+ with 1, ω -alkenols, 470–472

- development of reagent-controlled catalysts for X^+ -transfer, 459–460
- dissociation rate constants and partitioning ratios for reactions of bis(pyridine)-halonium ions with acceptor olefins, 464*t*
- enantiomeric excesses from halocyclizations of 1, ω -alkenols or 1, ω -alkenoic acids, 473*t*
- enantiomeric excesses in bromocyclized products of reaction of bromonium ion with 4-penten-1-ol and 4-pentenoic acid, 465*f*
- energy considerations for chiral induction, 465–467
- general mechanism for transfer of X^+ from *bis*-amino halonium ions to acceptor olefins, 460–464
- general scheme for halocyclization, 459*f*
- halocyclization by halonium ions of hydroquinidine and hydroquinidine dimers, 471–472
- halocyclization process, 459
- halonium ion transfer to 1, ω -alkenols and 1, ω -alkenoic acids, 459
- hydroquinidine derivatives, 470–471
- mechanism for transfer of Br^+ from bromonium ion to 4-penten-1-ol, 462*f*
- mechanism for transfer of Br^+ from bromonium ion to Ad=Ad, 462*f*
- quinuclidine bromonium and iodonium ions unreactive with 4-penten-1-ol, 468*f*
- quinuclidine halonium ions, 468–470
- rate constants for reactions of bromonium or iodonium ions, 469*t*
- reaction coordinate diagram for reaction of monoamine- X^+ ion with alkenol, 467*f*
- reaction of monoamine halonium intermediate with 1, ω -alkenol for *R* and *S* halocyclized products, 466*f*
- scheme for trapping *N*-haloquinuclidinium species, 469*f*
- Halomethyl cations, studies of fluorine-containing, 395
- Hammett plots, Beckmann rearrangement of aromatic systems, 370, 371*f*
- Harmonic oscillatory measure of aromaticity (HOMA), bond length alternation, 211
- μ -H-bridged carbocations
- cis*- and *trans*-1,6- μ -H-bridged stereoisomers of secondary cyclodecyl cation, 274*f*
 - examples, 271
 - optimized 1,5- μ -H-bridged secondary cyclodecyl cation, 274*f*
 - rearrangement of cyclooctyl and cyclononyl cations, 271
 - secondary, 271
 - stereoisomers from 2-heptyl cation, 278*t*
 - structure of, 3-octyl cations, 288*f*
 - structures of 2-octyl cation, 285*f*
 - superacid observations and reactivity, 271–275
 - theoretical modeling of cyclodecyl cation to 9-decalyl cation + H_2 , 273–275
 - transition state (TS) for H_2 loss, 273, 275
 - TS for H_2 loss in *cis*- and *trans*-1,6- μ -H-bridged secondary cyclodecyl cations, 275*f*
- See also* Dehydrocyclization; 2-Heptyl cation systems; n-Octane

- isomerization; Octyl cation systems
- 2-Heptyl cation systems
 calculations at the B3LYP/6-31G level, 277
 1,5- μ -H-bridged stereoisomers, 278*f*
 1,6- μ -H-bridged stereoisomers, 278*f*
 alternative optimized transition-state for H₂ loss for 1,6- μ -H-bridged, 281*f*
 energy profile for 6- vs. 5-ring dehydrocyclization, 282*f*
 optimized primary-secondary 1,5- μ -H-bridged structure, 279*f*
 optimized transition-states for H₂ loss for 1,5- and 1,6- μ -H-bridged, 280*f*
 overall thermodynamics for dehydrocyclization via 1,5- and 1,6- μ -H bridged intermediates, 281*t*
 possible secondary heptyl cations, 276
 potential energy diagram for dehydrocyclization, 283*f*
 relative energies, 277*t*
 relative energies of isomeric transition-states, 279, 280*t*
 stability of primary and secondary cations, 276–277
 transition state structures, 279
See also Dehydrocyclization; μ -H-bridged carbocations; n-Octane isomerization; Octyl cation systems
- Heterocyclic aromatic compounds, activating electrophilic functional groups, 148–149
- HF (anhydrous), nuclear magnetic resonance spectra of organoxenonium salts in, 440–447
- Hydride transfer, proposed mechanism for superacid-catalyzed, 145
- Hydrogen chloride, reaction of alkylidenecyclopropanone acetal with, 93–96
- Hydrolysis, fullerene cations, 247
- Hydroquinidine derivatives
 electrophilic Br⁺ or I⁺ transfer, 470–471
 enantiomeric excesses from halocyclizations, 473*t*
 halocyclization by halonium ions of, 471–472
See also Halogen transfer reactions
- Hydroxylalkylation reaction, carboxonium electrophiles, 148
- Hyperconjugation
 β -effect, 6–7
 σ - π conjugation, 33
- I**
- Indenyl cation
 antiaromaticity, 227, 229
 energetic and magnetic measures of antiaromaticity, 228*t*
- Indenylidene dications
 antiaromaticity evaluation, 227, 229
 energetic and magnetic measures of antiaromaticity, 228*t*
 extension of fluorenylidene dication research, 223
¹H NMR spectrum, 225*f*
 indenylidene fluorene dications, 224–226
 magnetic susceptibility exaltation vs. nucleus independent chemical shifts (NICS), 229*f*
 NICS, 226*t*
See also Antiaromaticity; Fluorenylidene dications
- Initiators, “cation pool” as polymerization, 194
- Intrinsic reaction coordinate (IRC) Beckmann rearrangement, 366

- reaction of protonated 1-methylcyclobutanone oxime, 367, 369*f*
- reaction of protonated cyclobutanone oxime, 366, 368*f*
- variations of atomic distance between benzylic C and N along, for aromatic system, 372*f*
- See also* Beckmann rearrangement
- Iodonium ions. *See* Halogen transfer reactions
- Isobutane protonation
- C-carbonium ion-like transition states, 323*f*
- H-carbonium ion-like transition state, 322*f*
- Isobutene, proposed mechanism for superacid-catalyzed hydride transfer, 145
- K**
- Kinetics. *See* Bromination of alkenes
- L**
- Lewis acid
- reaction of alkylidenecyclopropanone acetal with, 91–93
- reactions of organoxenonium salts with, 435
- Living cationic polymerization, “cation pool” as initiator, 194
- M**
- Magnetic susceptibility, calculation, 212–213
- Markovnikov addition
- influencing nucleophilic attack, 152–154
- phosphine addition to alkynes, 482–483
- See also* Anti-Markovnikov addition
- Mechanisms
- addition reaction of phosphine to alkynes, 482–483
- alkene bromination in aprotic and protic solvents, 379
- cyclodecyl to 9-decalyl cation reaction, 273
- influencing anti-Markovnikov and Markovnikov addition, 152–154
- plausible, for reaction of alkylidenecyclopropanone acetal with siloxyalkene, 98–99
- possible pathways for reaction of alkylidenecyclopropanone acetal with furan, 99, 101–102
- proposed, for bromination, 377
- proposed, for hydrophenylation and nitration of C₆₀, 236
- solvent effect on bromination in alkenes, 380–383
- superacid-catalyzed hydride transfer involving isobutene, 145
- Metal-catalyzed addition reaction. *See* Phosphonium salts
- Methane protonation, H-carbonium ion-like transition state, 322*f*
- Methanol
- bromination of stilbenes, 379–380
- substituents determining reaction pathway, 382
- See also* Bromination of alkenes
- Methonium ion
- Born–Oppenheimer molecular dynamics (BOMD) calculations, 304
- lowest energy configurations, 298, 299*f*
- parent species of carbonium ions, 298
- quantum mechanics, 299

- spin-coupled calculations, 300–303
See also Carbonium ions
- Methylheptane, dehydrocyclization of
 2- and 3-, 292–293
- N**
- N*-acyliminium ions
 [4+2]cycloaddition, with alkenes,
 192
 Friedel–Crafts type reactions, 191,
 192
 generation by C–H bond
 dissociation, 189–190
 generation by C–Si bond
 dissociation, 190–191
 radical addition to, 195, 196
 reactions of, pools, 191
 three component coupling, 193
See also “Cation pool” method
- Naphthalene
 annelated with bicyclooctene
 (BCO), 37*f*
 bond lengths of σ -bonds in, and
 radical cation salts, 40*t*
 molecular structure of monomeric
 radical-cation salt, 38*f*
 one-electron oxidation to radical
 cation salt, 36–37
 two-electron oxidation to dications,
 37, 40
See also Bicyclo[2.2.2]octene
 (BCO) frameworks
- Neighboring group participation
 cyclobutylmethyl cations, 107
 vinyl iodonium salts, 76–80
- Nitrenium complexes
 1-amino-1,10-phenanthroline
 mesitylenesulfonate, 136–137
 N-centered electrophiles, 136–
 139
See also Persistent organic cationic
 complexes
- Nitrosonium complexes
 affinity of [2.2]paracyclophane for,
 vs. *para*-xylene, 130–131
 complexes of *N*-heteroaromatic
 compounds, 131–136
 complexes with two-electron
 ligands, 127–129
 correlation between affinity of *N*-
 heteroaromatic compounds for
 NO⁺ cation and proton affinity,
 133*f*
 interaction of pyridine and
 derivatives with NO⁺BF₄⁻, 134
 1-*R*-2-methylacenaphthylenes,
 127–129
 optimized structures of, of
 [2.2]paracyclophane, 131*f*
 [2.2]paracyclophane, 129–131
 persistent cations, 126–136
 rearrangement for, of 1,10-
 phenanthroline, 135–136
 schematic of, of 2,3-dimethyl-2-
 butene, 128*f*
See also Persistent organic cationic
 complexes
- Noble-gas oxidant. *See*
 XeOTeF₅⁺Sb(OTeF₅)₆⁻
- Nopinyl brosylate, solvolysis, 108
- Nucleophiles
 covalent adducts of carbocations
 with, 336–340
 reactions of fullerene cations with,
 250, 251*f*
 reactions of negatively charged,
 with organoxenonium salts,
 435–437
 reactions of neutral π - and *n*-, with
 organoxenonium salts, 438–439
- Nucleus independent chemical shift
 (NICS)
 anthracene, 213
 continuum of
 aromaticity/antiaromaticity, 230,
 231*t*

- fluorenyl systems, 220*t*, 221*t*, 226*t*, 228*t*
 indenylidene fluorene dications, 228*t*
 indenyl systems, 226*t*, 228*t*
 magnetic criterion, 212
See also Antiaromaticity
- O**
- n*-Octane isomerization
 dehydrocyclization of 2- and 3-methylheptane, 292–293
 formation of cyclopentanes, 292–293
 isomerization vs.
 dehydrocyclization reaction, 289, 292
 protonated cyclopropane intermediates from 2-octyl cation, 291*f*
See also Dehydrocyclization; μ -H-bridged carbocations; 2-Heptyl cation systems; Octyl cation systems
- Octyl cation systems
 calculations of 2-octyl cation, 284–285
 calculations of 3-octyl cation, 287, 289
 dehydrocyclization, 283
 energy comparison for 1,6- μ -H-bridged 2- and 3-octyl cation systems, 289*t*, 290*f*
 formation of xylenes, 283–284
 geometry comparison between μ -H-bridged cyclodecyl cation and 2-octyl cations, 286*t*
 geometry comparison between transition states for dehydrocyclization, 287*t*
 optimized structure for *cis*- and *trans*-dimethyl 1,6- μ -H-bridged 2-octyl cation structures, 285*f*
 optimized structure for *cis*- and *trans*-secondary-primary-1,6- μ -H-bridged 3-octyl cations, 288*f*
 protonated cyclopropane intermediates, 291*f*
 transition states for H₂ loss in *cis*- and *trans*-dimethyl 1,6- μ -H-bridged 2-octyl cations, 286*f*
 transition states for H₂ loss in *cis*- and *trans*-secondary-primary-1,6- μ -H-bridged 3-octyl cations, 288*f*
See also Dehydrocyclization; μ -H-bridged carbocations; 2-Heptyl cation systems; *n*-Octane isomerization
- Oligothiophenes
 annelation with bicyclooctene (BCO) units, 46*f*
 cation stabilization, 45–47
 dications of tetramer and hexamer of, 47, 48*f*
 one-electron oxidation of dimer and trimer of, 46*f*, 47*f*
See also Bicyclo[2.2.2]octene (BCO) frameworks
- Onium ions, reactions in synthesis, 184–185
- Organic cationic complexes. *See* Persistent organic cationic complexes
- Organic cations
 methods for generating, 185–186
 oxidative generation of, for use in cation pools, 188, 189
 reactions of, in synthesis, 184–185
See also *N*-Acyliiminium ions; Alkoxycarbenium ion pools; “Cation flow” method; “Cation pool” method
- Organic synthesis, reactive intermediates, 184–185
- Organophosphorus compounds. *See* Phosphonium salts

- Organosilicon compounds. *See* Silyl-substituted carbocations
- Organoxenon compounds [RXe]Y and RXeR'
- ¹³C and ¹²⁹Xe NMR spectral data, 444*t*, 445*t*, 446*t*
 - ¹H and ¹⁹F NMR spectral data, 450*t*, 451*t*, 452*t*, 453*t*
- See also* Organoxenonium salts
- Organoxenonium salts
- arylxenonium salts, 431–432
 - ¹³C, ¹⁹F, and ¹²⁹Xe NMR (nuclear magnetic resonance) spectra data of
 - pentafluorophenylxenonium(II) cation, 447*f*
 - ¹³C, ¹⁹F, and ¹²⁹Xe NMR spectral data of
 - perfluoropentynylxenonium(II) cation and hexynylxenonium(II) cation, 442*f*
 - ¹³C, ¹⁹F, and ¹²⁹Xe NMR spectral data of
 - trifluoroethenylxenonium(II) cation, 443*f*
 - ¹³C and ¹²⁹Xe NMR spectra data of organoxenon compounds [RXe]Y and RXeR', 444*t*, 445*t*, 446*t*
- current progress in syntheses, 432–435
- first decade of C–Xe chemistry, 429–432
- ¹H and ¹⁹F NMR spectral data of organoxenon compounds [RXe]Y and RXeR', 450*t*, 451*t*, 452*t*, 453*t*
- NMR spectra in anhydrous HF, 440–447
- NMR spectra in other solvents, 448–449, 454
- NMR spectra of [C₆F₅XeF₂][BF₄], 454
- nucleophilic substitution of fluorine in XeF_n, 430
- reaction of XeF₂ with organodifluoroboranes, 430
 - reaction of XeF₂ with perfluorinated and non-fluorinated alk-1-yn-1-ylidifluoroboranes, 432–433
 - reaction of XeF₂ with polyfluoroalk-1-en-1-ylidifluoroboranes, 433–435
 - reactions with Lewis acids, 435
 - reactions with neutral π- and n-nucleophiles, 438–439
 - reaction with negatively charged nucleophiles, 435–437
 - reactivity, 435–439
 - types of organoxenonium cations, 429
 - xenodeborylation, 430
- See also* XeOTeF₅⁺Sb(OTeF₅)₆⁻
- Oxidant, noble-gas salt. *See* XeOTeF₅⁺Sb(OTeF₅)₆⁻
- Oxidative generation
- N*-acyliminium ion pools by C–H bond dissociation, 189–190
 - N*-acyliminium ion pools by C–Si bond dissociation, 190–191
 - alkoxycarbenium ion pools by C–C bond dissociation, 204–205
 - alkoxycarbenium ion pools by C–S bond cleavage, 203
 - alkoxycarbenium ion pools by C–Si bond dissociation, 200–202
 - methods for, of cations in cation pools, 188, 189
 - organic cations, 185–186
- See also* “Cation pool” method
- Oximes
- activation barriers for reaction of protonated, 368*t*
 - contour energy map for reaction of protonated acetone oxime, 369*f*
 - conversion into amides, 364
 - reaction of protonated 1-methylcyclobutanone oxime, 367, 369*f*

reaction of protonated
 cyclobutanone oxime, 366, 368*f*
 rearrangement of oxime tosylate,
 365
See also Beckmann rearrangement

P

Parallel combinatorial synthesis,
 "cation pool" method, 197–198

Participation and elimination, vinyl
 iodonium salts, 81–82

4-Penten-1-ol

dissociation rate constants and
 partitioning ratios for reactions
 of *bis*(pyridine)-halonium ions
 with, 464*t*

energy considerations for chiral
 induction, 465–467

mechanism for transfer of Br⁺ from
 bromonium ion to, 462*f*, 463

4-Pentenoic acid, energy
 considerations for chiral induction,
 465

Perhalomethyl cation, studies, 396–
 397

Persistent organic cationic complexes
 affinities of *N*-heteroaromatic
 compounds towards nitrosonium
 cation, 132–133
 affinity of [2.2]paracyclophane for
 nitrosonium cation, 130–131
 automerization reactions, 120–121
 benzopentalene skeleton, 125
 chemical behavior of polycyclic
 aromatic hydrocarbons and
 derivatives, 124–125
 (*cis*-1,2-dimethylvinyl)-9,10-
 dimethylphenanthrenium ion,
 120
 complexes with C-centered
 electrophiles, 119–126
 complexes with N-centered
 electrophiles, 126–139

cyclobutenyl carbocations, 126
 degenerate rearrangements, 120–
 121

formation of 1-amino-1,10-
 phenanthroline
 mesitylenesulfonate, 136–137

interaction of pyridine and
 derivatives with NO⁺BF₄⁻, 134

intermediates in organic
 transformations, 118

isomeric allyl and

cyclopropylcarbinyl cations, 119

1,2-methyl shifts, 120–121

nitrenium complexes, 136–139

nitrosonium complexes, 126–136

nitrosonium complexes of
 [2.2]paracyclophane, 129–131
 nitrosonium complexes of *N*-
 heteroaromatic compounds,
 131–136

nitrosonium complexes with two-
 electron ligands, 127–129

optimized structures of nitrosonium
 complexes of

[2.2]paracyclophane, 131*f*

β-phenyl-substituted carbocations,
 119

rates of 1,2-shifts of vinyl groups in
 cations, 122*t*

rearrangement for nitrosonium
 complex of 1,10-phenanthroline,
 135–136

rearrangements of
 bicyclo[3.2.1]octadienyl
 carbocations, 124

rearrangements of long-lived
 carbocations, 122–123

schematic of nitrosonium
 complexes of 2,3-dimethyl-2-
 butene, 128*f*

slow degenerate rearrangement of
 cation by 1,2-bridge shift, 123–
 124

stability of single-charged π-
 complexes vs. σ-complexes, 130

- β -vinyl-substituted carbocations, 119
- Persistent vinyl cations
- alkyl substituted, 63–64, 65*f*
 - bissilylated arenium ions, 52, 53
 - characteristic nuclear magnetic resonance (NMR) parameters, 55*t*
 - ^{13}C NMR spectra of α -aryl-substituted vinyl cation tetrakis(pentafluorophenyl) borate (TPFPB) salts, 54*f*
 - comparing computed ^{13}C and ^{29}Si NMR chemical shifts with experimental data, 57, 58*f*
 - computed structure of *t*-butyl-substituted vinyl cation, 64, 65*f*
 - σ -delocalization vs. π -conjugation in vinyl cations, 61, 62*f*, 63*f*
 - detection under superacidic reaction conditions, 52
 - Fourier transform infrared (FTIR) spectra of vinyl cation salts of brominated carborane $[\text{CB}_{11}\text{H}_6\text{Br}_6]^+$, 56*f*
 - intramolecular addition of transient silylium ions to $\text{C}\equiv\text{C}$ triple bonds, 53
 - limitations of formation method, 59, 60
 - molecular structure of *t*-butyl-substituted vinyl cation in $[\text{CB}_{11}\text{H}_6\text{Br}_6]^+$ salt, 64*f*
 - occurrence of σ -delocalization by canonical resonance, 61, 62*f*, 63*f*
 - quantum mechanical computations of structure, 56, 57*f*
 - resonance structures of vinyl cations, 60
 - silanorbornyl cations, 52, 53
 - silylated arenium ions, 52, 53
 - silylium ion chemistry, 52
 - β -silyl-substituted carbocations, 52, 53
 - stability and reactivity, 59, 60
 - synthesis of aryl-substituted, 53
 - TPFPB salt of methyl-substituted vinyl cation, 63–64
 - zwitterions, 52, 53
- See also* Vinyl cations
- Phosphine. *See* Phosphonium salts
- Phosphonium cationic center, cationic electrophilic sites, 149–150
- Phosphonium salts
- addition reaction of phosphine to 1,3-dienes, 486–488
 - addition reaction of phosphine to alkenes, 488–490
 - addition reaction of phosphine to alkynes, 479–484
 - addition reaction of phosphine to allenes, 484–486
 - addition reaction of tertiary phosphines to activated alkenes, 478–479, 480
 - allylphosphonium salts, 485
 - conversion of C–H to C–heteroatom bonds, 478, 479
 - experimental procedures, 484, 486, 488, 490
 - preparation including C–P bond formation, 478–479
 - rhodium catalysis, 481–482
 - Wittig reaction of (E)-allylphosphonium salts, 486
- Photosolvolysis
- (E)- and (Z)-2-phenylprop-1-enyl(phenyl)iodonium tetrafluoroborate, 83–84
 - (E)-styryl iodonium salt, 84–85
 - vinyl iodonium salts, 82–86
- Polycyclic aromatic hydrocarbons (PAHs)
- bay-region diol epoxides, 330
 - chemical behavior of, and derivatives, 124–125
 - See also* Aza-polycyclic aromatic hydrocarbons (aza-PAHs)
- Polyelectrochromic materials. *See* Electrochromic materials

- Polymerization, “cation pool” as initiator, 194
- Pool method for cations. *See* “Cation pool” method
- Proline derivative, reaction with superacidic triflic acid, 147
- Propane protonation
 C-carbonium ion-like transition states, 323*f*
 H-carbonium ion-like transition state, 322*f*
- Proponium ions
ab initio calculations, 308
 BOMD (Born–Oppenheimer molecular dynamics) of 1-H-proponium cation, 309*f*, 310*f*
 BOMD study of 2-H-proponium ion, 311
 BOMD study of C-proponium cation, 312–313
 different ways for formation of isomeric, 307*f*
 formation, 307
 geometrical parameters for, 308*f*
 1-H-proponium, 309–310
 isomers, 307–308
See also Carbonium ions
- Protonation
 allenes, 21, 22*f*
 amides and carboxylic acids for activating electrophiles, 150–151
- Q**
- Quantum mechanical computations
 stable vinyl cations, 56, 57*f*
See also Aza-polycyclic aromatic hydrocarbons (aza-PAHs); Persistent vinyl cations
- Quinuclidine halonium ions
 reactivity, 468
 scheme for trapping *N*-haloquinuclidinium species, 469
See also Halogen transfer reactions
- R**
- Radical cation salts. *See* Bicyclo[2.2.2]octene (BCO) frameworks
- Radical chemistry, “cation pool” method, 195, 196
- Reaction selectivity, alkylideneallyl cation, 103–104
- Reactive intermediates, organic synthesis, 184–185
- Reactivity
 salts of vinyl cations, 59, 60
 vinyl iodonium salts, 68
- Rearrangements
 bicyclo[3.2.1]octadienyl carbocations, 124
 long-lived carbocations, 122–123
See also Degenerate rearrangements
- Redox potentials, fluorenyl systems, 221*t*, 222*f*
- Redox systems
 radical chemistry using “cation pool” method, 195, 196
See also Electrochromic materials
- Resonance hybrids, alkylideneallyl cations, 88, 89
- Reversible hydrolysis, fullerene cations, 247
- Ring expansion
cis- and *trans*-2-methylcyclobutylmethyl brosylates, 109, 110*f*
 solvolysis of *endo*- and *exo*-bicyclo[2.1.1]hexane-5-methyl tosylates, 109

Ring opening reactions

- alkylidenecyclopropanone acetals (4), 90–96
- reaction of (4) with fluoride ion, 96
- reaction of (4) with hydrogen chloride, 93–96
- reaction of (4) with Lewis acid, 91–93
- regioselective, at C2–C3 bond of cyclopropane ring of (4), 91
- selectivity of acetal cleavage, 93
- See also* Alkylidenecyclopropanone acetals

Rotational barrier, α,α -

- dicyclopropylcyclobutylmethyl cation, 115

S

Salts. *See* $\text{XeOTeF}_5^+\text{Sb}(\text{OTeF}_5)_6^-$

$\text{Sb}(\text{OTeF}_5)_6^-$ anions

background, 397

See also $\text{XeOTeF}_5^+\text{Sb}(\text{OTeF}_5)_6^-$

Selectivity, alkylideneallyl cation reaction, 103–104

Sequential combinatorial synthesis, “cation flow” method, 199–200

Sequential generation, cation pools, 197

Si-29 nuclear magnetic resonance spectroscopy, β -silylsubstituted carbocations, 15

Siloxyalkenes, reaction of alkylidenecyclopropanone acetal with, 97–99

Silyl effects, carbocations, 27–28

Silylium ion chemistry

stable carbocations, 52

See also Persistent vinyl cations

α -Silyl-substituted carbenium ions, gas-phase studies, 2

Silyl-substituted carbocations

α -silyl substituted, 2–6

β -effect in vinyl cations, 17–21

β -silyl effect in α -cyclopropyl, 15–17

β -silyl effect in benzyl cations, 7–15

β -silyl substituted, 6–17

experimental and computational methods, 27–28

γ -silyl effect in bicyclobutonium ions, 22–27

protonation of allenes, 21, 22*f*

See also Bicyclobutonium ions; Vinyl cations

a-Silyl-substituted carbocations

ab initio calculations, 2

^{13}C NMR chemical shifts for 1-phenyl-1-(trimethylsilyl)ethyl cation (1), cumyl cation, and 1-phenylethyl cation, 3, 5*t*, 6

^{13}C NMR spectrum of 1-phenyl-1-(trimethylsilyl)ethyl cation (1), 4*f*

destabilizing effect of silyl vs. alkyl group, 2

generating 1-phenyl-1-(trimethylsilyl)ethyl cation (1), 3

See also Silyl-substituted carbocations

β -Silyl-substituted carbocations

α -ferrocenyl, 15

β -effect, 6–7

^{13}C NMR spectrum of 1-phenyl-2-(triisopropylsilyl)ethyl cation (12), 9*f*

^{13}C NMR spectrum of *syn*- and *anti*-1-*p*-anisyl-2-(triisopropylsilyl)ethyl cations (18), 12*f*

(E)-1-cyclopropyl-2-(triisopropylsilyl)ethyl cation (22) generation, 15–16

formation of 1-phenyl-2-(triisopropylsilyl)ethyl cation (12), 8–9

- formation of 1-*p*-tolyl-2-(triisopropylsilyl)ethyl cation (15), 11
- formation of mixture of *syn*- and *anti*-1-*p*-anisyl-2-(triisopropylsilyl)ethyl cations (18), 11–12
- geometry of 1-phenyl-2-(trimethylsilyl)ethyl cation (14), 10, 11*f*
- ¹H NMR spectrum of (E)-1-cyclopropyl-2-(triisopropylsilyl)ethyl cation (22), 16*f*
- hyperconjugation, 6–7
- NMR chemical shifts for geometry of *syn*- and *anti*-1-*p*-anisyl-SiH₃-ethyl cation, 15
- protonation of substituted styrenes, 7–8
- quantum chemical calculations for close models of cations (18), 13
- regiospecific formation of β-silyl substituted benzyl cations, 8
- β-silyl effect in α-cyclopropyl substituted carbocations, 15–17
- β-silyl effect in benzyl cations, 7–15
- ²⁹Si NMR chemical shift of (E)-1-cyclopropyl-2-(triisopropylsilyl)ethyl cation (22), 17
- ²⁹Si NMR spectroscopy tool, 15
- ²⁹Si NMR spectrum of 1-phenyl-2-(triisopropylsilyl)ethyl cation (12), 10*f*
- temperature dependence of ¹³C NMR signals of ortho and meta carbons of *syn*- and *anti*-1-*p*-anisyl-2-(triisopropylsilyl)ethyl cations (18), 14*f*
- See also* Silyl-substituted carbocations
- Solvation, carbonium ions, 320–321
- Solvents
- alkene bromination mechanisms, 379
 - polarity and rate constants in bromination, 378
 - reaction of
 - alkylidenecyclopropanone acetal with furan, 101–102
 - See also* Bromination of alkenes
- Solvolysis reactions
- bicyclo[2.2.0]hexane-1-methyl *p*-nitrobenzoate, 108, 109*f*
 - cis*- and *trans*-2-methylcyclobutylmethyl brosylates, 109, 110*f*
 - cyclopropylcarbiny, cyclobutyl and allylcarbiny derivatives, 256
 - (E)-styryl(phenyl)iodonium tetrafluoroborate, 78–79
 - fullerene cations, 248
 - generation of cyclobutylmethyl cations, 107–109
 - nopinyl brosylate, 108
 - 2-phenylprop-1-enyl(phenyl)iodonium tetrafluoroborate, 79, 80
 - photosolvolysis of vinyl iodonium salts, 82–86
 - rearrangement in, of 2,2-dialkylvinyl iodonium salt, 77
 - ring expansion of *endo*- and *exo*-bicyclo[2.1.1]hexane-5-methyl tosylates, 109
 - S_N1 mechanism vinyl iodonium salts, 70–71, 72*f*
 - S_N2 mechanism for vinyl iodonium salt, 73–74
 - vinyl bromide via alkylideneallyl cation, 89
- Spin-Coupled calculations
- dissociation curve for methonium CH₅⁺ into CH₃⁺ and H₂, 302, 303*f*
 - orbitals for CH₆⁺², 303*f*

- orbitals for H_2 and H_2^+ , 301*f*
 orbitals for methonium ion, 300*f*
 orbitals for one C–H bonds in CH_4 ,
 302*f*
- Stabilization**
 azulenylmethyl cations, 165–167
 cyclobutylmethyl cations, 107
 π -conjugated carbocations, 33
 σ -delocalization vs. π -conjugation
 in vinyl cations, 61, 62*f*, 63*f*
 salts of vinyl cations, 59
 vinyl iodonium salts, 68
See also Bicyclo[2.2.2]octene
 (BCO) frameworks; Persistent
 vinyl cations
- Stabilized salts.** *See*
 $XeOTeF_5^+Sb(OTeF_5)_6^-$
- Stilbenes**
 bromination, 379–380
 kinetics of bromination, 385–386
See also Bromination of alkenes
- Styrenes, protonation of substituted,**
 7–8
- Sulfur-containing conjugated systems**
 with bicyclo[2.2.2]octene
 dithiins, 43–45
 oligothiophenes, 45–47
 thiophene, 43, 43*f*
See also Bicyclo[2.2.2]octene
 (BCO) frameworks
- Superacidic reaction conditions, stable**
 vinyl cations, 52
- Superelectrophilic chemistry**
 acyl-transfer reactions, 151–152
 anti-Markovnikov and
 Markovnikov-type products,
 152–154
 application, 145
 carboxonium electrophiles, 148
 cationic nitrogen enhancing
 carbonyl, 146–147
 charge-charge separation as driving
 force, 156
 concept of superelectrophilic
 activation, 145
 conversion and proposed
 mechanism to 5-methyl-
 benzo[*f*]isoquinoline, 156
 dicationic electrophiles, 147–148,
 157
 dioxirane epoxidations, 146
 1,1-diphenylethene vs. proline
 derivative reaction with
 superacidic triflic acid, 147
 distance between charge centers
 and activation of electrophiles,
 154–155
 effects of cationic groups on
 electrophilic reactivities, 146
 examples showing adjacent
 cationic charge centers, 154–155
 hydroxyalkylation reaction, 148
 influencing regiochemistry of
 nucleophilic attack, 152–153
 intermolecular Friedel–Craft-type
 reactions, 152
N-heterocyclic aromatic
 compounds activating
 electrophilic functional groups,
 148–149
 phosphonium cationic center, 149–
 150
 probing mechanisms, 153–154
 products, intermediates, and yields
 from reactions of substituted
 heterocycles with triflic acid and
 benzene, 149*t*
 proposed mechanism for superacid-
 catalyzed hydride transfer
 involving isobutene, 145
 protonated amides and carboxylic
 acids, 150–151
- Super-stabilization**
 cyclooctatetraene (COT) and
 cations, 35–36
See also Bicyclo[2.2.2]octene
 (BCO) frameworks; Persistent
 vinyl cations
- Surfaces.** *See* Carbocations on
 surfaces

T

- Tetracation salt. *See* Cyanine–cyanine hybrid system, tetracation salt
- Tetrachloroethane, electrophilic addition to C₆₀, 237, 238*t*
- Tetrakis(bicyclo[2.2.2]octeno)cyclooctatetraene, super-stabilization, 35–36
- Thermal stability, alkoxy-carbenium ion, 202
- Thermodynamics
dehydrocyclization, 293
gas-phase, of reactions of XeOTeF₅⁺ with CF_nX_{4-n} (X=Cl, Br; n=3–0), 417, 418
- Thermodynamic stabilization
fullerene cations, 247–248
π-conjugated carbocations, 33
- Thiophene
annulation with
bicyclo[2.2.2]octene, 42, 43*f*
possible mechanism for transformation of radical cation, 42, 43*f*
x-ray structure of carbocation salt, 43*f*
See also Bicyclo[2.2.2]octene (BCO) frameworks
- Three component coupling, “cation pool” method, 193
- Transition state (TS)
Beckmann rearrangement, 366, 372*f*
C-carbonium ion-like, for ethane, propane, and isobutane protonation, 323*f*
dehydrocyclization of 2-heptyl cation system, 279, 280*t*, 281*f*
geometry between, for dehydrocyclization of 2-octyl cation, 287*t*
H₂ loss in 1,6-μ-H-bridged 2-octyl cations, 286*f*
H₂ loss in 1,6-μ-H-bridged 3-octyl cations, 288*f*
H₂ loss in cis- and trans-1,6-μ-H-bridged cyclodecyl cations, 273, 275
H-carbonium ion-like, for methane, ethane, propane, and isobutane protonation, 322*f*
See also μ-H-bridged carbocations
- Trifluoroethanol
bromination of stilbenes, 379–380
reaction via free ions, 380
See also Bromination of alkenes
- 1-(3-Trifluoromethylphenyl)-1-(4-trifluoromethylphenyl) ethylene
bromination, 389
product distribution for bromination, 390*t*
See also Bromination of alkenes
- Trihalomethyl cations
calculated charge distributions and bonding in, and C(OTeF₅)₃⁺, 417, 422
early studies of long-lived, 395
fluorine-containing, 413–417
¹⁹F NMR spectrum and ¹⁹F and ¹³C NMR parameters for CFCl₂⁺, 414*f*
gas-phase thermodynamics of reactions of XeOTeF₅⁺ with, 417, 418
See also XeOTeF₅⁺Sb(OTeF₅)₆⁻
- Triphenylene, annelated with bicyclooctene (BCO) units, 41, 42*f*
- Tropylium ions, bicyclo[2.2.2]octeno-, 33–34

V

- Vinyl bromide, solvolysis via alkylideneallyl cation, 89
- Vinyl cations
α-anisyl-β-silyl-substituted, 17, 18

- chirality probe for primary, 73–76
- ¹³C NMR spectrum of 1-trimethylsilyl-4-methyl-1,3-pentadien-2-yl cation (31), 19, 20*f*
- α -ferrocenyl- β -silyl-substituted, 19
- α -mesityl- β -silyl-substituted, 17, 18
- α -phenyl- β -silyl-substituted, 17, 18
- principal reaction paths, 17, 18
- protonation of allenes, 21, 22*f*
- β -silyl effect, 17–21
- β -silyl substituted dienyl cations, 19–21
- 1,1,3,3-tetrakis(trimethylsilyl)-1-propen-2-yl cation (34), 21, 22*f*
- α -tolyl- β -silyl-substituted, 17, 18
- See also* Persistent vinyl cations; Silyl-substituted carbocations; Vinyl iodonium salts
- Vinyl ethers, “cation pool” as polymerization initiator, 194
- Vinyl iodonium salts
 - calculated free energy barrier for 1,2-hydride shift of cyclohept-1-enyl cation, 76*f*
 - chirality probe for primary vinyl cation, 73–76
 - competition between participation and base/nucleophile, 82
 - dec-1-enyl(phenyl)iodonium tetrafluoroborate, 73–74
 - degenerate 1,2-hydride shift of 1,2-dimethylvinyl cation, 77
 - formation of hypervalent adducts, 71, 72
 - free energy barrier for 1,2-hydride shift of 1,2-dimethylvinyl cation, 78*f*
 - initial absorbance and observed rate constants for reaction, 71, 72*f*
 - kinetic measurements for solvolysis, 70, 71*f*
 - kinetic parameters for reaction of *p*-chloro derivative, 73*t*
 - methanolysis of (E)-styryl(phenyl)iodonium tetrafluoroborate (26), 79
 - neighboring group participation, 76–80
 - optically active 4-methylcyclohexylidenemethyl(*p*henyl)iodonium tetrafluoroborate, 74–75
 - participation and elimination, 81–82
 - 2-phenylprop-1-enyl(phenyl)iodonium tetrafluoroborate (31), 79, 80
 - photosolvolysis, 82–86
 - photosolvolysis of (26), 84–85
 - preparation, 68–69
 - product distributions in photosolvolysis of (E)- and (Z)-31, 84*t*
 - product distributions in solvolysis of (31), 80*t*
 - reactions of (26), 78–79
 - reactions of cyclohex-1-enyl iodonium salt, 69–73
 - reactivity and stability, 68
 - rearrangement in solvolysis of 2,2-dialkylvinyl, 77
 - Schiemann-type reaction, 69
 - S_N1 solvolysis mechanism, 70
 - S_N2 solvolysis mechanism, 74
 - solvolysis of 2-methylcyclohexenyl iodonium salt, 70
 - See also* Vinyl cations
- β -Vinyl-substituted carbocations
 - ionization of potential precursors, 119
 - See also* Persistent organic cationic complexes
- Violen–cyanine hybrid redox system, 161–162
- Wurster type, 162, 168–170

See also Electrochromic materials

Violenes

electrochromism, 161

structure, 161*f*

See also Electrochromic materials

W

Wittig reaction

alkenylphosphonium salts, 484

allylphosphonium salts, 486

Wurster type violene–cyanine hybrid

connecting two methylium units,
169*f*, 170*f*

continuous change in visible
spectrum of dication, 171*f*

dication composed of *p*-phenylene
spacer, 168–169

dication composed of thiophenediyl
and thienothiophenediyl spacer,
169–170

general structure, 162

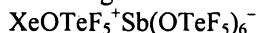
See also Electrochromic materials

X

Xenodeborylation

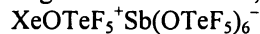
illustration, 430

See also Organoxenonium salts;



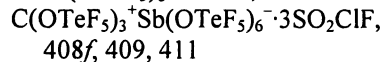
Xenon compounds. *See*

Organoxenonium salts;



$\text{XeOTeF}_5^+\text{Sb}(\text{OTeF}_5)_6^-$

background of XeL^+ cations and
 $\text{M}(\text{OTeF}_5)_6^-$ anions, 397



calculated charge distributions and
bonding in $\text{CF}_n\text{X}_{3-n}^+$ ($\text{X}=\text{Cl}, \text{Br};$
 $n=0-3$) and $\text{C}(\text{OTeF}_5)_3^+$, 417,
422

calculated charge distributions in
 CCl_3^+ , CBr_3^+ , and $\text{C}(\text{OTeF}_5)_3^+$
and correlations with solid state
coordination environments,
411–413

calculated geometries and natural
charge for CX_3^+ ($\text{X}=\text{F}, \text{Cl}, \text{Br}$)
and Cl_3^+ , 419*f*

calculated geometries for $\text{CF}_n\text{X}_{3-n}$
($\text{X}=\text{Cl}, \text{Br}$), 420*f*

calculated natural charges for
 $\text{CF}_n\text{X}_{3-n}$ ($\text{X}=\text{Cl}, \text{Br}$), 421*f*

^{13}C and ^{19}F NMR parameters for
 $\text{C}(\text{OTeF}_5)_4$ and $\text{CBr}_n(\text{OTeF}_5)_{3-n}^+$
($n=0-3$), 403*t*

^{13}C and ^{19}F NMR parameters for
products from
 $\text{XeOTeF}_5^+\text{Sb}(\text{OTeF}_5)_6^-$ with
 CCl_4 and CBr_4 , 403*t*

$\text{CCl}_3^+\text{Sb}(\text{OTeF}_5)_6^-$ and
 $\text{CBr}_3^+\text{Sb}(\text{OTeF}_5)_6^- \cdot \text{SO}_2\text{ClF}$,
406*f*, 407*f*, 409

crystal structure of
 $\text{C}(\text{OTeF}_5)_3^+\text{Sb}(\text{OTeF}_5)_6^-$
 $\cdot 3\text{SO}_2\text{ClF}$, 408*f*

crystal structure of
 $\text{CBr}_3^+\text{Sb}(\text{OTeF}_5)_6^- \cdot 3\text{SO}_2\text{ClF}$,
407*f*

crystal structure of
 $\text{CCl}_3^+\text{Sb}(\text{OTeF}_5)_6^-$, 406*f*

diagrams showing halogen-
fluorine/oxygen and carbon-
fluorine/oxygen contacts, 410*f*

early studies of long-lived CX_3^+
($\text{X}=\text{Cl}, \text{Br}, \text{I}$) and $\text{CF}_n\text{X}_{3-n}^+$
($\text{X}=\text{Cl}, \text{Br}; n=0-3$) cations, 395–
397

^{19}F , ^{125}Te , ^{129}Xe , ^{17}O , and ^{121}Sb
NMR parameters, 399*t*

fluorine-containing trihalomethyl
cations, 413–417

^{19}F NMR spectrum and ^{19}F and ^{13}C
NMR parameters for CFCl_2^+ ,
414*f*

- gas-phase thermodynamics of reactions of XeOTeF_5^+ with $\text{CF}_n\text{X}_{4-n}$ ($\text{X}=\text{Cl}, \text{Br}; n=0-3$), 417, 418
- mixed, fluorine-containing halomethyl cations, 395
- multi-NMR spectroscopy, 398, 400
- outlook, 422–423
- perhalomethyl cations, 396–397
- structural studies, 398–401
- syntheses and solution characterization by ^{19}F and ^{13}C NMR of $\text{CCl}_3^+\text{Sb}(\text{OTeF}_5)_6^-$, $\text{CBr}_n(\text{OTeF}_5)_{3-n}^+\text{Sb}(\text{OTeF}_5)_6^-$ ($n=0-3$), $\text{Br}(\text{OTeF}_5)_2^+\text{Sb}(\text{OTeF}_5)_6^-$, and $\text{C}(\text{OTeF}_5)_4$, 402, 404–405
- synthesis, 398
- trihalomethyl cations, 395
- X-ray crystal structure of $\text{XeOTeF}_5^+\text{Sb}(\text{OTeF}_5)_6^-\cdot\text{SO}_2\text{ClF}$, 400, 401*f*
- X-ray crystal structures of $\text{CCl}_3^+\text{Sb}(\text{OTeF}_5)_6^-$, $\text{CBr}_3^+\text{Sb}(\text{OTeF}_5)_6^-\cdot\text{SO}_2\text{ClF}$, and $\text{C}(\text{OTeF}_5)_3^+\text{Sb}(\text{OTeF}_5)_6^-\cdot 3\text{SO}_2\text{ClF}$, 405–413

Z

Zeolites

- aluminosilicate catalysts, 255
- modes of methonium ion interaction within, 324*f*
- See also* Carbocations on surfaces